

*Edited by*  
*Wolfgang Beckmann*

**Crystallization**

## ***Related Titles***

Chianese, Angelo / Kramer,  
Herman J. (eds.)

### **Industrial Crystallization Process Monitoring and Control**

2012

ISBN: 978-3-527-33173-4

Pollak, P.

### **Fine Chemicals The Industry and the Business**

Second edition

2011

ISBN: 978-0-470-62767-9

Duffar, T. (ed.)

### **Crystal Growth Processes Based on Capillarity Czochralski, Floating Zone, Shaping and Crucible Techniques**

2010

ISBN: 978-0-470-71244-3

Capper, P., Rudolph, P. (eds.)

### **Crystal Growth Technology Semiconductors and Dielectrics**

2010

ISBN: 978-3-527-32593-1

*Edited by Wolfgang Beckmann*

# **Crystallization**

Basic Concepts and Industrial Applications



WILEY-VCH Verlag GmbH & Co. KGaA

#### **The Editor**

**Dr. Wolfgang Beckmann**

Bayer Technology Services  
Crystallization  
Building E41  
Kaiser-Wilhelm-Allee  
51368 Leverkusen

#### **Cover :**

we would like to thank the following  
Companies for their kind permission to use  
the photographic material on the cover:  
Chr. Melches, GEA- Messo  
D. Wieckhusen, Novartis AG  
T. Haag, Bayer AG

All books published by **Wiley-VCH** are carefully produced. Nevertheless, authors, editors, and publisher do not warrant the information contained in these books, including this book, to be free of errors. Readers are advised to keep in mind that statements, data, illustrations, procedural details or other items may inadvertently be inaccurate.

**Library of Congress Card No.:** applied for

#### **British Library Cataloguing-in-Publication Data**

A catalogue record for this book is available from the British Library.

#### **Bibliographic information published by the Deutsche Nationalbibliothek**

The Deutsche Nationalbibliothek lists this publication in the Deutsche Nationalbibliografie; detailed bibliographic data are available on the Internet at <http://dnb.d-nb.de>.

© 2013 Wiley-VCH Verlag GmbH & Co. KGaA,  
Boschstr. 12, 69469 Weinheim, Germany

All rights reserved (including those of translation into other languages). No part of this book may be reproduced in any form – by photoprinting, microfilm, or any other means – nor transmitted or translated into a machine language without written permission from the publishers. Registered names, trademarks, etc. used in this book, even when not specifically marked as such, are not to be considered unprotected by law.

**Print ISBN:** 978-3-527-32762-1

**ePDF ISBN:** 978-3-527-65035-4

**ePub ISBN:** 978-3-527-65034-7

**mobi ISBN:** 978-3-527-65033-0

**oBook ISBN:** 978-3-527-65032-3

**Cover Design** Simone Benjamin, McLeese Lake,  
Canada

**Typesetting** Thomson Digital, Noida, India



## Contents

### List of Contributors XIII

<b>1</b>	<b>Crystallization: Introduction</b>	<b>1</b>
	<i>Wolfgang Beckmann</i>	
<b>2</b>	<b>Mechanisms of Crystallization</b>	<b>7</b>
	<i>Wolfgang Beckmann</i>	
2.1	Crystal Lattice	7
2.1.1	Arrangement of Building Blocks and Symmetries	7
2.1.2	Unit Cell	9
2.1.3	Miller Indices to Describe Crystal Faces	11
2.1.4	Lattice Defects	12
2.1.5	Equilibrium, Growth, and Dissolution Form of Crystals	14
2.1.6	Morphology and Habit	16
2.2	Nucleation of Crystals	17
2.2.1	Mechanism of Primary Nucleation	18
2.2.2	Metastable Zone and Induction Time for Nucleation	20
2.2.3	Form Crystallized: Ostwald's Law of Stages	25
2.3	Growth and Growth Rate of Crystals	25
2.3.1	Kink Position and F, S, and K Faces	26
2.3.2	Growth of Ideal Crystals	27
2.3.3	Growth of Real Crystals	28
2.3.4	Transport Phenomena	32
	Further Reading	33
<b>3</b>	<b>Solubility and Solution Equilibria in Crystallization</b>	<b>35</b>
	<i>Heike Lorenz</i>	
3.1	Phase Equilibria and Phase Diagrams: General Issues	36
3.1.1	Phases, Phase Rule, and Binary Systems	36
3.1.2	Melt and Solution Equilibria	38
3.1.3	Thermodynamic Description of SLE: Liquidus Curve in the Phase Diagram	39
3.1.4	Phase Diagrams of Ternary and Quaternary Systems	42

3.2	Melt Phase Diagrams	44
3.2.1	Types of Phase Diagrams and Their Occurrence	44
3.2.2	Measurement of Melt Phase Diagrams	46
3.2.2.1	Methods	46
3.2.2.2	DSC and How to Measure and Interpret DSC Data	47
3.2.3	Example of a Diastereomeric System	50
3.3	Solution Equilibria	53
3.3.1	Solubility and Concentration Units	53
3.3.2	Solubility Curves of Inorganic and Organic Substances	54
3.3.2.1	Inorganic Substances	55
3.3.2.2	Organic Substances	57
3.3.3	Solvates, Polymorphs, and Cocrystals	58
3.3.4	Influence of Solvents and Impurities	60
3.3.5	Measurement of Solubilities and Corroboration	62
3.3.5.1	Ensuring Equilibrium Conditions	63
3.3.5.2	Excess Method as a Classical Isothermal Method	64
3.3.5.3	Polythermal Measurements	65
3.3.5.4	Prediction and Correlation of Solubilities	67
3.3.6	Oiling-Out	68
3.3.7	Ternary Solution Equilibria: Case of Enantiomers	70
3.3.8	Quaternary Systems: Case of Reciprocal Salt Pairs	72
	References	74
<b>4</b>	<b>Agglomeration during Crystallization</b>	<b>75</b>
	<i>Wolfgang Beckmann</i>	
4.1	Mechanisms and Kinetics of Agglomeration	75
4.1.1	Process of Agglomeration	75
4.1.2	Kinetics of Agglomeration	77
4.2	Parameters Influencing Agglomeration	77
4.3	Agglomeration during Crystallization	80
4.3.1	Agglomeration during Crystallization	80
4.3.2	Spherical Agglomeration	83
4.4	Mechanical Properties of Agglomerates	83
	References	84
<b>5</b>	<b>Polymorphism of Crystalline Systems</b>	<b>85</b>
	<i>Rolf Hilfiker</i>	
5.1	Introduction and Definitions	85
5.2	Occurrence and Properties of Polymorphs and Solvates	86
5.3	Thermodynamics of Polymorphs of Solid-State Forms	87
5.3.1	Basics	87
5.3.2	Energy–Temperature Diagrams	88
5.3.3	Rules to Predict Thermodynamic Relationships	90
5.4	Thermodynamics of Hydrates	91
5.5	Experimental Techniques to Elucidate Thermodynamics	94

5.5.1	DSC	94
5.5.2	Suspension Equilibration	94
5.5.3	Solubility Measurements	95
5.5.4	Other Methods	96
5.6	Formation of Various Polymorphs and Solid-State Forms-Polymorph Screens	97
5.6.1	Principles	97
5.6.2	Crystallization Methods and Choice of Solvent	99
5.6.3	Types of Polymorph Screens	100
5.7	Selection of Optimal Form for Development	101
	Symbols	102
	References	102
<b>6</b>	<b>The Influence of Additives and Impurities on Crystallization</b>	<b>105</b>
	<i>Christiane Schmidt, Matthew J. Jones, and Joachim Ulrich</i>	
6.1	Influence of Additives and Impurities on Crystallization	105
6.1.1	Solubility	105
6.1.1.1	Common Ion Effect	106
6.1.1.2	Thermodynamic Basis of Solubility and the Influence of Additives	106
6.1.1.3	Complex Formation	106
6.1.2	Rate of Nucleation and Crystal Growth	107
6.1.2.1	Nucleation Rates	107
6.1.2.2	Crystal Growth Rates	111
6.1.3	Habit Modification	114
6.2	Influence of Impurities: Modeling	116
6.2.1	Calculating Crystal Habit	116
6.2.1.1	Surface Energy Model	117
6.2.2	Molecular Modeling	118
6.2.3	Modeling of Additives	120
6.3	Tailor-Made Additives	122
6.4	Modeling the Influence of Solvents	122
	References	124
<b>7</b>	<b>Purification by Crystallization</b>	<b>129</b>
	<i>Heike Lorenz and Wolfgang Beckmann</i>	
7.1	Introduction	129
7.2	Mechanisms of Impurity Incorporation and Purification	131
7.2.1	Solubility in the Solid State	132
7.2.2	Fractional Crystallization	133
7.2.3	Inclusion and Surface Adsorption of Impurities	134
7.2.4	Influence of Crystallization Conditions	136
7.2.4.1	Product Yield	136
7.2.4.2	Crystallization Technique and Rate of Crystallization	137
7.2.4.3	Solvent Applied	139
7.2.4.4	Mixing	142

7.2.5	Downstream Processes	142
7.2.5.1	Solid–Liquid Separation and Sweating	143
7.2.5.2	Reslurrying and Washing	144
7.2.6	Workflow to “Manage” Impurities in Process Development	146
	References	147

## **8 Characterization of Crystalline Products 149**

*Rolf Hilfiker*

8.1	Introduction	149
8.2	Characterization of Intrinsic Properties of a Solid	149
8.2.1	Crystal Structure	150
8.2.1.1	X-Ray Powder Diffraction (XRPD)	150
8.2.1.2	Vibrational Spectroscopy (Raman, IR, NIR, THz)	151
8.2.1.3	Solid-State NMR (ssNMR)	152
8.2.2	Thermodynamic Properties	154
8.2.2.1	Differential Scanning Calorimetry (DSC)	154
8.2.2.2	Isothermal Microcalorimetry	157
8.2.3	Composition	158
8.2.3.1	Thermogravimetry (TG, TG-FTIR, and TG-MS)	158
8.2.3.2	Dynamic Vapor Sorption (DVS)	158
8.3	Characterization of Particle Shape and Size	161
8.3.1	Particle Size Distribution: Characteristic Values and Graphs	161
8.3.2	Overview of Available Methods	162
8.3.2.1	Microscopy	163
8.3.2.2	Laser Light Diffraction	163
8.3.2.3	Sieving	165
8.4	Powder Flow Properties	165
8.5	In-Process Characterization	167
8.5.1	Turbidity	167
8.5.2	Raman	168
8.5.3	FBRM and PVM	169
	References	171

## **9 Basics of Industrial Crystallization from Solution 173**

*Wolfgang Beckmann*

9.1	Generation of Supersaturation in a Crystallizer	173
9.2	Mass and Population Balance for Growth from Suspension	176
9.2.1	Mass Balance	176
9.2.2	Population Balance	176
9.3	Operation of a Continuous Crystallizer: Basics	178
9.3.1	Concept and Design of Continuous Crystallizers	178
9.3.2	Mass Balance in a Continuous Crystallizer	178
9.3.3	Population Balance in a Continuous Crystallizer	178
9.3.4	Mean Particle Size	180
9.3.5	Secondary Nucleation	180

9.4	Operation of a Batch Crystallizer: Basics	183
9.4.1	Concept and Design of Batch Crystallizers	183
9.4.2	Mass and Population Balance in a Batch Crystallizer	184
<b>10</b>	<b>Development of Batch Crystallizations</b>	<b>187</b>
	<i>Dierk Wieckhusen</i>	
10.1	Setting Goals	187
10.2	Crystallization of Organic Moieties	188
10.3	Generation of Supersaturation in Batch Crystallizations	189
10.3.1	Cooling	189
10.3.2	Use of Antisolvent	190
10.3.3	Evaporation	191
10.4	Initiation of Crystallization – Nucleation Phase	192
10.5	Seeded Batch Crystallizations	193
10.5.1	Seeding Strategy	194
10.5.2	Designing a Seeding Process	194
10.5.2.1	Quality of Seeds	195
10.5.2.2	Quantity of Seeds	195
10.5.2.3	Preparation of Seeds	196
10.5.2.4	Supersaturation at the Start of Crystallization	197
10.5.2.5	Holding Time After Seeding	197
10.6	Crystallization Period	197
10.7	Scale-Up Considerations	198
10.7.1	Process Time – Rate of crystallization	198
10.7.2	Stirring	199
10.7.3	Operational Aspects	200
10.8	Manipulating Particle Shape	201
<b>11</b>	<b>Continuous Crystallization</b>	<b>203</b>
	<i>Günter Hofmann and Christian Melches</i>	
11.1	Concept and Design of Continuous Crystallizers	204
11.1.1	Importance of Secondary Nucleation	204
11.1.2	Control of Supersaturation	205
11.1.3	Adjustment of the Granulometry – Mean Crystal Size and Crystal Size Distribution	209
11.1.4	Energy Input and Retention Time	212
11.1.5	Which Type of Crystallizer to Select?	215
11.1.6	Seeding of DTB and Oslo Crystallizers	216
11.2	Various Continuous Crystallizers	218
11.2.1	FC Group	218
11.2.2	DTB Group	220
11.2.3	Group of Fluidized Bed Crystallizers	222
11.2.4	Comments on Population Balance and Modeling	223
11.2.5	Manipulation of Crystal Size Distributions	225
11.3	Periphery	226

11.4	Special Features of the Process	229
11.4.1	Surface Cooling Crystallization	229
11.4.2	Vacuum Cooling Crystallization	230
11.4.3	Vacuum Evaporation Crystallization	230
11.5	Adjustment of Suspension Densities	232
	References	233
<b>12</b>	<b>Precipitation</b>	<b>235</b>
	<i>Wolfgang Beckmann</i>	
12.1	Precipitation from Solution by Mixing Two Streams	235
12.1.1	Devices and Mixing Schemes	235
12.2	Semi-Batch Precipitations	236
12.3	Model of Mixing during Precipitation	238
12.4	Precipitations Using Supercritical Fluids	239
12.5	Crystal Issues	241
12.5.1	Polymorphism of Precipitates	241
12.5.2	Crystal Perfection	243
12.5.3	Agglomeration	244
12.6	Particle Size as a Function of Operating Conditions	244
<b>13</b>	<b>Mixing in Crystallization Processes</b>	<b>247</b>
	<i>Bernd Nienhaus</i>	
13.1	Mixing in Batch and Continuous Crystallization Processes	247
13.2	Basic Mixing Tasks – Mixing Tasks in Crystallization	248
13.3	Impellers and Agitation Systems	249
13.3.1	General Overview and Selection Criteria	250
13.3.2	Axial Impellers	250
13.3.2.1	Propeller	250
13.3.2.2	Pitched Blade Turbine	250
13.3.2.3	Helical Ribbon Impeller	252
13.3.3	Radial Impellers	252
13.3.3.1	Flat Blade Disk Turbine	252
13.3.3.2	Disperser Disk	252
13.3.4	Tangential Impellers	253
13.4	Power Consumption of an Impeller System [2]	253
13.4.1	Diameter Ratio	255
13.4.2	Bottom Clearance	256
13.4.3	Filling Level	256
13.4.4	Multistage Impellers	256
13.5	Blending	256
13.5.1	Degree of Homogeneity	256
13.5.2	Turbulent Blending	257
13.5.3	Significance of Circulation Rate	258
13.5.4	Laminar Blending	258
13.6	Suspending	259

13.6.1	Suspending Criteria and Different States of Suspension	259
13.6.2	Power Requirement for the Suspension of Solids	262
13.6.3	Models and Mechanisms for the Suspension of Solids	263
13.6.4	Determination of the Shaft Speed Necessary for Suspending	264
13.6.4.1	Physical Parameters of Liquids and Solids	265
13.6.4.2	Solids Concentration	265
13.6.4.3	Geometry	266
13.6.5	Distribution of Solids	266
13.6.6	Influence on Mass Transfer	267
13.6.7	Influence on Blend Times	267
13.7	Scale-Up of a Crystallization Process	268
13.7.1	Model Tests	269
13.7.2	“Scale-Up” Rules	270
13.7.3	Blending	270
13.7.4	Suspension	270
13.7.5	Dispersing	271
13.7.6	Heat Transfer	272
13.7.7	Special Scale-Up Considerations	272
13.7.8	Summary	273
	References	273
<b>14</b>	<b>Downstream Processes</b>	<b>275</b>
	<i>Dierk Wieckhusen and Wolfgang Beckmann</i>	
14.1	Transfer of Suspension and Filter Cake	275
14.2	Solid–Liquid Separation	275
14.2.1	Cake Forming Filtration	276
14.2.2	Centrifugation	277
14.2.3	Characterization of Filterability in the Laboratory	277
14.2.4	Improving Filterability	278
14.2.5	Washing	280
14.3	Drying	280
14.3.1	Phases of the Drying Process	281
14.3.2	Drying of Hydrates and Solvates	282
14.3.3	Characterizing the Drying Behavior in the Laboratory	284
14.3.4	Amorphization during Drying	284
14.3.5	Effect of Drying on the Particle Size Distribution	285
	References	288
<b>15</b>	<b>Melt Crystallization</b>	<b>289</b>
	<i>Joachim Ulrich and Torsten Stelzer</i>	
15.1	Characteristics of Melt Crystallization	289
15.1.1	Definitions	289
15.1.2	Benefits of Melt Crystallization	290
15.2	Processes of Melt Crystallization	292
15.2.1	Solid Layer Crystallization	292

15.2.2	Suspension Crystallization	294
15.3	Postcrystallization Treatments	295
15.3.1	Sweating	297
15.3.2	Washing	298
15.3.3	Choices	299
15.3.4	Wash Columns	299
15.4	Laboratory Techniques	301
15.4.1	Bottle Test	301
15.4.2	Cold Finger Experiments	301
15.4.3	Zone Melting	303
	References	304
<b>16</b>	<b>Examples of Realized Continuous Crystallization Processes</b>	<b>305</b>
	<i>Günter Hofmann and Christian Melches</i>	
16.1	Choosing the Drain Point in Process Design	305
16.2	Example Crop Crystallization for Organic Compounds	310
16.2.1	Fields of Application for the Crop Principle	310
16.2.2	Definition of Task	311
16.2.3	Selection of the Process Design	312
16.3	Example Crystallization of Table Salt	316
16.3.1	Introduction	316
16.3.2	Performance Requirements	318
16.3.3	Process Design	318
16.3.4	Description of the Plant Function	321
16.4	Results	323
<b>17</b>	<b>Design Examples of Melt Crystallization</b>	<b>325</b>
	<i>Joachim Ulrich and Torsten Stelzer</i>	
17.1	Concepts of Melt Crystallization	325
17.1.1	Solid Layer Crystallization	325
17.1.2	Suspension Crystallization	331
17.2	Outlook	334
	References	335
	<b>Index</b>	<b>337</b>



## List of Contributors

### ***Wolfgang Beckmann***

Bayer Technology Services  
Crystallization  
Building E41  
51368 Leverkusen  
Germany

### ***Rolf Hilfiker***

Solvias AG  
Römerpark 2  
4303 Kaiseraugst  
Switzerland

### ***Günter Hofmann***

GEA Messo GmbH  
Friedrich-Ebert-Str. 134  
47299 Duisburg  
Germany

### ***Matthew J. Jones***

AstraZeneca  
Västra Mälarehamnen 9  
15185 Södertälje  
Sweden

### ***Heike Lorenz***

MPI für Dynamik komplexer technischer Systeme  
Sandtorstr. 1  
39106 Magdeburg  
Germany

### ***Christian Melches***

GEA Messo GmbH  
Friedrich-Ebert-Str. 134  
47299 Duisburg  
Germany

### ***Bernd Nienhaus***

EKATO Rühr- und Mischtechnik GmbH  
Käppelemattweg 2  
79650 Schopfheim  
Germany

### ***Christiane Schmidt***

AstraZeneca  
Västra Mälarehamnen 9  
15185 Södertälje  
Sweden

### ***Torsten Stelzer***

University of Halle  
Zentrum für  
Ingenieurwissenschaften,  
Verfahrenstechnik  
Hoher Weg 7  
06099 Halle (Saale)  
Germany

***Joachim Ulrich***

University of Halle  
Zentrum für  
Ingenieurwissenschaften,  
Verfahrenstechnik  
Hoher Weg 7  
06099 Halle (Saale)  
Germany

***Dierk Wieckhusen***

Novartis AG  
Lichtstr. 35  
4002 Basel  
Switzerland

## 1

**Crystallization: Introduction***Wolfgang Beckmann*

The beauty of crystals can be found in both the naturally appearing minerals such as diamonds or quartzite crystals and the industrial products such as sugar crystals. Crystals that are bound by flat faces intersecting at well-defined angles are characteristic of the substance and give the crop a reproducible appearance. This regular appearance is due to the long-range order of the building blocks of the crystal, be it either atoms or molecules. For example, in sodium chloride, the sodium and chlorine atoms are arranged in a cubic lattice (Figure 1.1). This arrangement maximizes the attractive interactions between the building blocks and thus minimizes the energetic state. The long-range order of its building blocks makes the crystalline state distinct from the gaseous and liquid as well as the amorphous solid state. The long-range order is also the root cause of a number of well-defined properties of the crystals, so these properties can be tailored through the crystallization process.

A further consequence of the well-defined arrangement of the building blocks is the outer shape of the crystals; crystals are limited by flat faces that intersect under well-defined angles determined by the lattice. This can be easily observed for the large crystals of rock sugar (Figure 1.2). For a given substance, ordering is a characteristic. Consequently, the faces and their angles are characteristics of a given substance. All crystals grown under similar conditions will exhibit the same faces and partitioning of the faces.

Though the lattice is characteristic of a given substance, a large number of substances can crystallize following more than one ordering motive, leading to polymorphism. Carbon, for example, can crystallize in two different lattices, as diamond and as graphite. In diamond, the carbon atoms are arranged in two face-centered cubic lattices; in graphite, the carbon atoms are arranged in layers in which the atoms have a hexagonal symmetry (Figure 1.3). With respect to energy and stability, graphite is more stable than diamond at room temperature and ambient pressure, though the barrier for transformation is extremely high.

A further equally important consequence of packing is the well-known purification during crystallization; only molecules of one type are incorporated, while most other molecules are rejected by the growing interface. This is for geometric as well as



**Figure 1.1** Arrangement of the sodium and chlorine atoms in the simple cubic lattice of sodium chloride.



**Figure 1.2** Crystals of rock sugar with large well-developed flat faces, which intersect under certain angles characteristic of the substance; note that the apparent roughness of the faces arises not from the crystallization process, but from the downstream processes like washing.

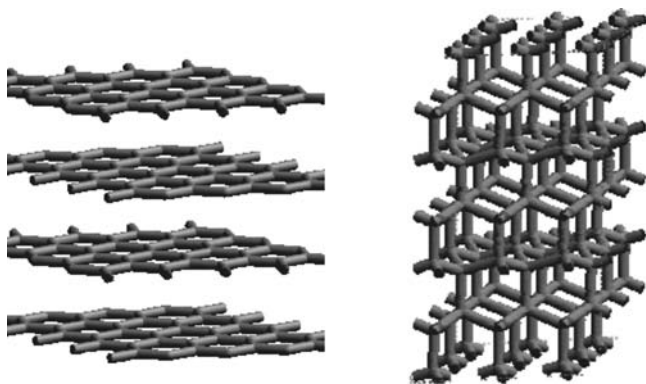


**Figure 1.3** Carbon crystallizing in two different modifications – as graphite and as diamond – having different lattice arrangements.

for energetic reasons as it is energetically favorable to incorporate a proper building block instead of an impurity molecule.

Crystallization belongs to the oldest unit operations known to mankind. Namely, the crystallization of salts can be found through the ages. Early civilizations in coastal areas used large open ponds, salines, to crystallize out the salt, which could then be easily handled, stored, transported, traded, and finally used (Figure 1.4). Salines around the seaport of Ostia are said to have facilitated the development of Roma and the Roman Empire.

However, salt obtained by evaporation of seawater had a number of drawbacks; the purity was limited, mainly due to the high content of inclusions of mother liquor that entrained impurities. Hence, industrial techniques have developed over the time for the industrial crystallization of salt, resulting in the modern continuous vacuum crystallization apparatus.

Today, crystalline products can be found in every aspect of life. Relevant product properties are determined by crystal properties and thus tailored via crystallization. Three examples are shown in Figure 1.5. Sucrose, sugar, is extracted from



**Figure 1.4** Solar ponds in Venezuela (courtesy of Günter Hofmann).



**Figure 1.5** Sugar, table salt, and chocolate as examples of everyday life products, where the properties of the crystalline state determine product properties and where the crystallization is tailored to meet this demand.

plants and crystallized to meet a certain particle size distribution, typically in the range of 700–800  $\mu\text{m}$ , to be free of fines, which allows a free-flowing product that does not agglomerate. Finally, the process arrives at purities of  $>99.5\%$  in an essentially single-step process of a seeded batch crystallization. Table salt also is required to be free flowing and not to agglomerate even in the high relative humidity environment of a kitchen. Here, additives can be employed during the crystallization, which is usually continuously operated evaporation crystallization. Finally, one of the main components of chocolate, cocoa fat has to be crystallized in a certain crystal modification or polymorph to achieve the special mouth taste of chocolate. This modification is unstable at room temperature and achieved via melt crystallization, where the crystals of the desired modification are generated and grown via a temperature program. In addition, additives can be used to stabilize the required modification. The unstable modification of the fatty acid ester can recrystallize to a more stable one, resulting in undesired changes in the appearance of the product.

In a number of cases, mother liquor is the desired product of the crystallization process. The crystallization of ice from aqueous solutions can be used for freeze concentration of aqueous solutions. One example of everyday life is orange

**Table 1.1** Examples for the annual production of crystalline products in various fields.

Product	Produced in	Production (t/a)
Sodium chloride	2001 in the EU	38 350 000
Sugar	2001 in the EU	15 000 000
Caprolactam	2002 worldwide	3 500 000
Ascorbic acid	2009 worldwide	110 000
Acetylsalicylic acid	2008 worldwide	35 000

juice that can be freeze concentrated at low temperatures gently and in an energy-efficient way. The concentration of waste from effluent waters is another application.

The application of crystallization in industry ranges from the isolation of the few milligrams of a substance newly synthesized in the laboratory – where a well-defined melting point is used to both achieve and prove a decent purity of the crop and as an identity check – to a mass crystallization carried out in very diverse industries; some products are listed with their annual production volume in Table 1.1.

The equipment used in the industrial crystallization varies widely, from multi-purpose batch vessels in the life science industry to highly sophisticated dedicated equipment used for some large volume products.

In the following chapters, the basic concepts of the modern understanding of crystallization will be discussed, such as the internal structure of the crystals and their growth mechanisms or the phase diagrams. Attention will be directed to the purification by crystallization and to effects of polymorphism. Next, the basic methods to carry out a crystallization, from both the solution and the melt, are discussed. Finally, the concepts of mass crystallization in continuously operated crystallizers will be shown.

## 2

### Mechanisms of Crystallization

*Wolfgang Beckmann*

One of the most important features of crystals is the long-range order of their building blocks and symmetry of their arrangement. This arrangement maximizes the interaction between the building blocks, stabilizing the crystal. Most macroscopic properties of crystals, such as their shape or the purification during crystallization, are a direct consequence of this arrangement. Thus, the discussion of the mechanisms of crystallizations has first to deal with the symmetry and long-range order in crystals. In the second part, the nucleation and growth mechanisms of crystals are discussed. In both cases, a supersaturated mother phase or a deviation from saturation is necessary. The dependence of the processes on supersaturation and other parameters has to be discussed. The discussion of crystal nucleation has two goals: first, to determine the mechanisms and thus also the prerequisites for nucleation; second, to derive expressions for the dependence on supersaturation.

#### 2.1

##### Crystal Lattice

##### 2.1.1

##### Arrangement of Building Blocks and Symmetries

Crystallization is a phase transformation for which the free enthalpy  $\Delta_{\text{tr}}G$  has to be negative (Equation 2.1). The crystal will be stabilized by minimizing the enthalpy term  $\Delta_{\text{tr}}H$ , which is determined by the interaction of the building blocks. Interactive forces might either be van der Waals or electrostatic forces. In molecular crystals, hydrogen bonding also plays an important role.

The van der Waals forces do have a relatively short-range order, a typical potential is given by  $\Phi = (A/r^{12}) - (B/r^6)$ , where  $r$  is the distance between the interaction bodies. The potential is shown in Figure 2.1. The interaction potential of electrostatic forces decreases via  $\Phi = C/r$ .

$$\Delta_{\text{tr}}G = \Delta_{\text{tr}}H - T\Delta_{\text{tr}}S. \quad (2.1)$$



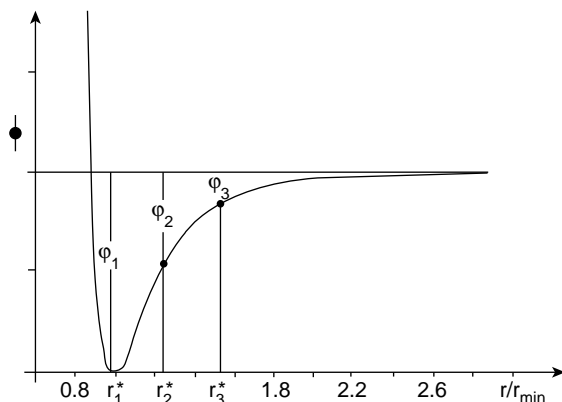


**Figure 2.1** Trend of the pair interaction potential of van der Waals forces. Note that the minimum in the pair interaction at  $r_{\min}$  is slightly different from the equilibrium distance in a crystal. It is apparent that the interaction is mainly determined by the first nearest neighbors.

Due to the rapid decrease of the potential with distance, the nearest-neighbor interactions determine the energetics of the arrangement. Consequently, only well-defined symmetries in the arrangement of the building blocks of a crystal are allowed. This is visualized for a two-dimensional lattice by packing units with different symmetries (Figure 2.2). In part (a), objects with a two-, four-, and sixfold symmetry are packed; in part (b), the units have a five- and sixfold symmetry. The former set of objects allows packing, maximizing the pair interaction of building blocks, while the latter ones lead to suboptimal packing that is subsequently not found in crystals.

The considerations can be applied to the three-dimensional lattice. The packing of spheres in a plane is optimal for a hexagonal arrangement, as shown in Figure 2.3.

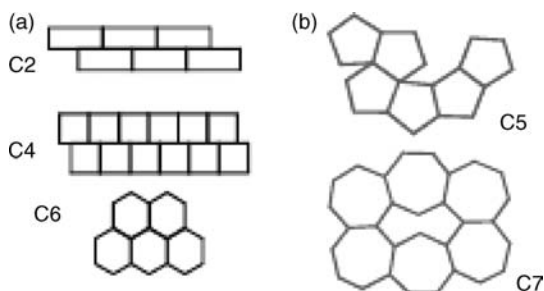


**Figure 2.2** Construction of a 2D lattice by packing units with different symmetries. In part (a), objects with a two-, four-, and sixfold symmetry are packed; in part (b), the units have a five- and sixfold symmetry. While the former set of objects maximizes the interaction between building blocks, the latter ones can only be arranged in a suboptimal packing.

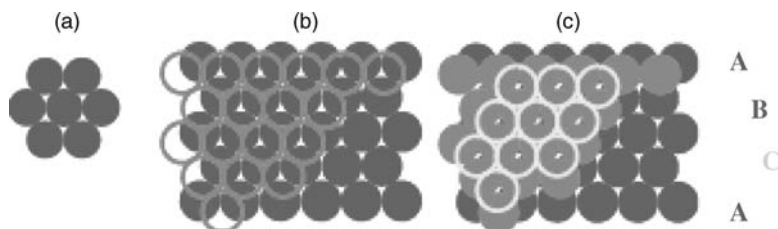


**Figure 2.3** Optimized packing of spheres in (a) in one dimension, followed by the addition of further layers of hexagonally arranged building blocks (b and c). Here, only the case of the cubic closest packing is shown.

Between three building blocks, a concave cavity is formed. In successive layers, the building blocks are also hexagonally arranged. The building blocks of the second layer reside in the cavities formed between the blocks of the first layer. For the packing of the third layer, two possibilities exist. This layer can reside in a different cavity, as shown in Figure 2.3. This leads to the cubic closest-packed lattice, which is a face centred lattice as will be shown later. Alternatively, the layer can be arranged like the first, leading to the hexagonally closest packing. The space filling in both cases is 74%.

In the following, only the face-centered cubic lattice (fcc) will be discussed. For this lattice, a ball-and-stick model is shown in Figure 2.4. The bottom view shows the stacking arrangement in the two different cavities, while the side view shows the **ABCAB . . .** stacking. Some building blocks have been color coded to indicate the unit cell to be discussed in Section 2.1.2.

### 2.1.2

#### Unit Cell

The arrangement of the building blocks in the lattice can be reduced to the smallest unit, the unit cell, from which the lattice can be built by simple displacements in

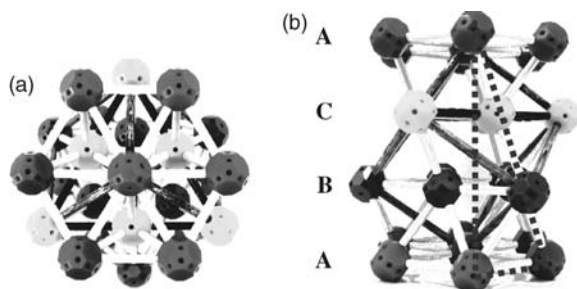


**Figure 2.4** Lattice model for the closest packing of spheres. The bottom view in (a) can be compared with the packing shown in Figure 2.3. Part (b) shows that this packing leads to the **ABCAB . . .** stacking.

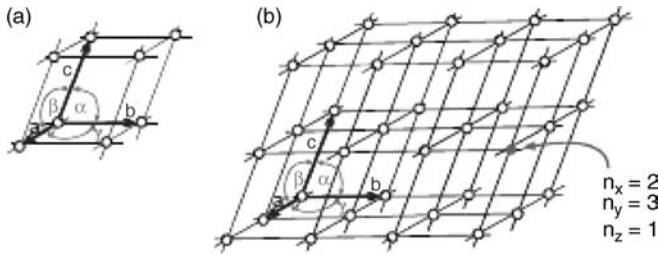


**Figure 2.5** (a) Unit cell as smallest building block of a lattice. (b) By repeating this unit cell in all three directions via translation, the lattice is formed. The size of the unit cell is described by the lattice constants  $a$ ,  $b$ , and  $c$  and the angles  $\alpha$ ,  $\beta$ , and  $\gamma$ .

three dimensions. Figure 2.5 shows such a unit cell and the construction of the lattice by adding successive cells. The unit cell has the dimensions  $a$ ,  $b$ , and  $c$ . The vectors of the unit cell are orthogonal, but not necessarily perpendicular;  $\alpha$  is the angle between the  $y$ - and  $z$ -axes,  $\beta$  is the angle between the  $x$ - and  $z$ -axes; and  $\gamma$  is the angle between the  $x$ - and  $y$ -axes.

As described for a two-dimensional lattice (Figure 2.2), only certain symmetry operations are allowed to build the crystal lattice. These are the seven crystal systems listed in Figure 2.6. For the cubic and monoclinic lattices, the unit cells are also shown.

In certain of the seven crystal systems, the unit cells can contain face- or body-centered building blocks. For the cubic lattice, the body- and face-centered unit cell is shown in Figure 2.7.

For the body-centered cubic lattice (bcc), the addition of a building block is equal to a linear displacement by half a lattice constant in the three lattice directions. For building blocks that do not have a rotational symmetry, an additional rotation of the building blocks can occur; one of the most prominent being a rotation by  $180^\circ$ . This combined displacement and rotation by  $180^\circ$  appears like the movement of a screw.

Cubic	$a = b = c$	$\alpha = \beta = \gamma = 90^\circ$	
Tetragonal	$a = b \neq c$	$\alpha = \beta = \gamma = 90^\circ$	
Monoclinic	$a \neq b \neq c$	$\alpha = \gamma = 90^\circ \neq \beta$	
Triclinic	$a \neq b \neq c$	$\alpha \neq \beta \neq \gamma \neq 90^\circ$	
Orthorhombic	$a \neq b \neq c$	$\alpha = \beta = \gamma = 90^\circ$	
Trigonal	$a = b \neq c$	$\alpha = \beta = \gamma = 120^\circ$	
Hexagonal	$a = b \neq c$	$\alpha = \beta = 120^\circ \neq \gamma = 90^\circ$	

**Figure 2.6** Relation of the lattice constants and angles for the seven crystal systems that are allowed. The simple cubic and monoclinic lattices are drawn.

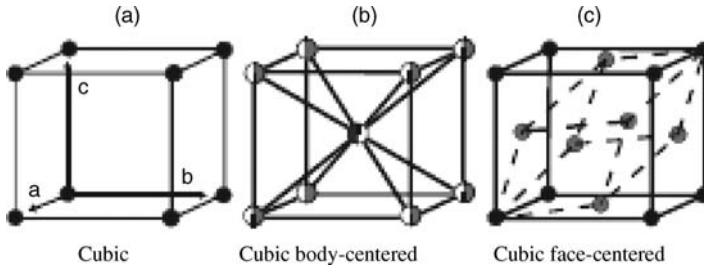


**Figure 2.7** Cubic unit cell with  $a = b = c$  and  $\alpha = \beta = \gamma = 90^\circ$ . The simple cubic cell (a) and the body-centered (b) and face-centered (c) cubic unit cells are to be distinguished.

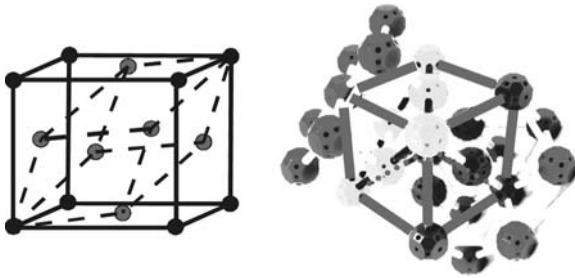


**Figure 2.8** Comparison of the lattice model of closest-packed spheres with the ABCAB . . . stacking with the fcc lattice.

The lattice of closely packed spheres (Figure 2.3) can be reduced to a cubic unit cell with face-centered building blocks, as shown in Figure 2.8.

### 2.1.3

#### Miller Indices to Describe Crystal Faces

The well-defined flat faces limiting a crystal are described by Miller indices. They are denoted  $hkl$  and are independent of the size of the crystal. Using the three axes of the unit cell, a face will intersect these axes at certain distances, for example, for the  $y$ -axis at  $2b$  (Figure 2.9). By referring the intersection to the length of the unit cell in this direction, one arrives at certain multiples for the intersection, that is,  $n_y = y/b$ . The Miller indices  $hkl$  are defined as the reciprocal of the three intersections (Equation 2.2). It is required that  $hkl$  are integers:

$$h : k : l \equiv \frac{a}{x} : \frac{b}{y} : \frac{c}{z} = \frac{1}{n_x} : \frac{1}{n_y} : \frac{1}{n_z}. \quad (2.2)$$

The calculation of the indices is shown in Figure 2.9 for a face at two different growth stages, the small dark face and the larger gray face. Both indices are the same.

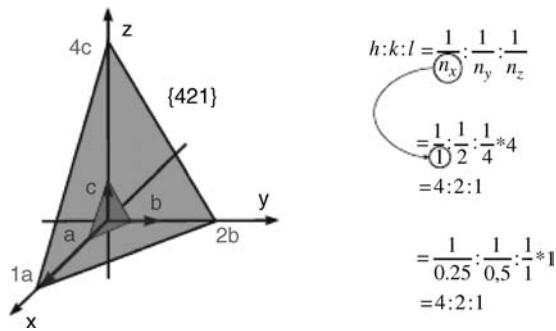


**Figure 2.9** Description of a crystal face by its Miller index  $hkl$ . The large face intersects the three axes at  $x = 1 \cdot a$ ,  $y = 2 \cdot b$ , and  $z = 4 \cdot c$ ; the small face intersects at  $x = (1/4) \cdot a$ ,

$y = (1/2) \cdot b$ , and  $z = 1 \cdot c$ . The calculation is for the larger gray face, top, and the smaller dark face, bottom. Both faces are equal; the index is the same  $(421)$ .

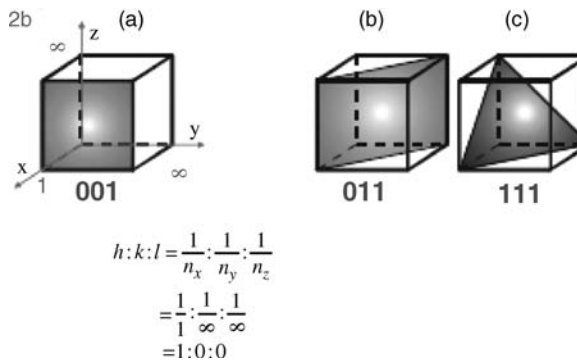


**Figure 2.10** Indexing of the three lowest-indexed faces of the cubic system. In the cubic system, all six faces of the cube are identical, so the indices  $(100)$ ,  $(010)$ , and  $(001)$  are identical (a).

The indices of the three lowest indexed faces of a cubic lattice are shown in Figure 2.10. It should be noted that in a cubic system, all six faces of the cube are identical, so the indices  $(001)$ ,  $(010)$ , and  $(001)$  describe the same faces and can be used arbitrarily. By definition,  $(hkl)$  describe a certain face, while  $\{hkl\}$  describe symmetrically equivalent faces.

#### 2.1.4

##### Lattice Defects

The perfect lattice just described will not be found for real crystals, not even for crystals grown with extreme care. Instead, the crystals will contain a variety of lattice defects with different density. These defects determine the properties of the crystals such as mechanical strength or electric conductivity. Lattice defects also play an

**Table 2.1** Lattice defects ordered by their dimensionality  $D$ .

Defect	$D$	Example
Point	0	Vacancy, interstitial atom
Line	1	Step dislocation, screw dislocation
Surface	2	Twin, small-angle grain/tilt boundary
Volume	3	Inclusion

important role in the growth of the crystals, namely, the screw dislocation (see Section 2.3.3).

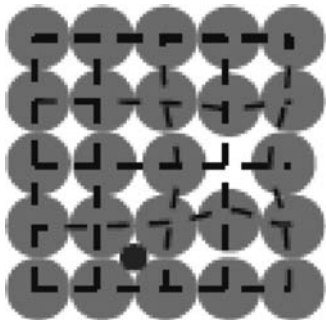
Lattice defects are characterized by their dimensionality  $D$  with which they extend into the lattice. This will be explained by often encountered defects (Table 2.1).

Figure 2.11 shows a two-dimensional lattice with two different defects, a vacancy and an interstitial atom. Both defects are confined to a point and do not extend into the lattice, so their dimensionality is  $D = 0$ .

Screw dislocations are one example for line defects and can be generated by a shearing of the crystal (Figure 2.12). This defect extends in one dimension along the line shown, so that  $D = 1$ .

Twinning is the most prominent example of faults with  $D = 2$ . The fault extends through an entire plane in the crystal (Figure 2.13). For a fcc lattice, twinning can occur by stacking faults; the order of ABCABC . . . is reversed at a certain point to ABCBAC . . . . For the outer shape of the crystal, twinning will appear as an inflection, or forming of a mirror image, a twin. Figure 2.13 also shows a twin of a silver halide crystal. The twin plane is clearly seen.

Finally, volume defects  $D = 3$  can be formed by the inclusion of mother liquor (Figure 2.14). It is interesting to note that the liquid inclusions can be confined by well-expressed low-indexed (negative) faces. Liquid inclusions, for example, occur under high growth rates, for example, for precipitations.



**Figure 2.11** Vacancy and interstitial atoms in a two-dimensional lattice. These lattice defects are confined to a point; thus,  $D = 0$ .

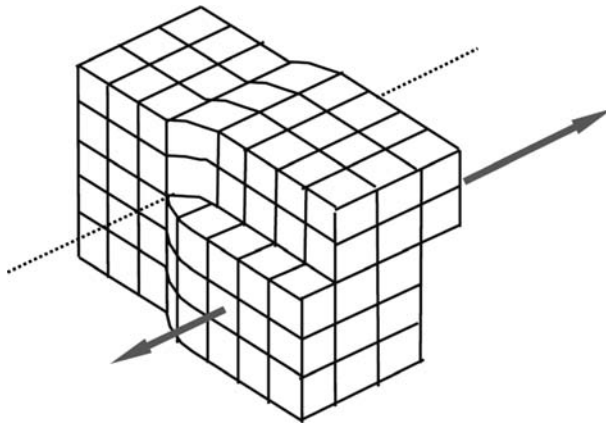


**Figure 2.12** Screw dislocation as, for example, generated by a sheering of the lattice. The defect can be found along the dotted line, resulting in a dimensionality of  $D = 1$ .

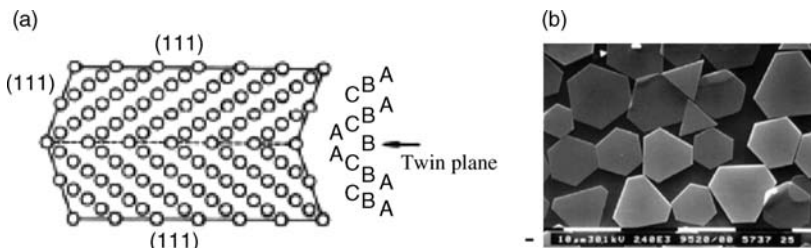


**Figure 2.13** Formation of a twin in an fcc lattice. (a) The stacking ABC is inverted at the twin plane to ABCABACBA. The lattice defect extends in the twinning plane,  $D = 2$ . (b) A twin of a silver halide crystal is shown and the twin plane can be clearly seen.



**Figure 2.14** Formation of volume defects such as liquid inclusion by the overgrowth of mother liquor. These liquid inclusions can be confined by well-expressed low-indexed negative faces,  $D = 3$ .

### 2.1.5

#### Equilibrium, Growth, and Dissolution Form of Crystals

The discussion of crystal shapes has to distinguish between the equilibrium form, which is governed by thermodynamics, and the growth and dissolution form, which is governed by the kinetics of the growth process.

To describe the equilibrium form, the anisotropy in the surface tension of the different faces of a crystal has to be taken into account. The surface tension  $\sigma$  describes the energy required per unit area  $A$  to create a new surface. At constant volume, the free enthalpy of a crystal varies only with the size and surface tension for the formation of the interface (Equation 2.3):

$$\Delta G|_{V=\text{const.}} \propto \sum A_i \sigma_i|_{V=\text{const.}} = \min!. \quad (2.3)$$

In equilibrium, the free energy will acquire a minimum. Carrying out the calculations leads to the requirement that the central distance  $h$ , the distance of the face to the center of the crystal, is proportional to its surface tension (Equation 2.4). The central distance is the length of a line perpendicular to the face to a hypothetical center of the crystal:

$$\frac{h_i}{\sigma_i} = \text{const.} \quad (2.4)$$

The construction is shown in Figure 2.15. Starting from a center, a length corresponding to the central distance is plotted together with the face. The equilibrium form is obtained by drawing the smallest crystal.

The equilibrium form of a crystal is determined by minimizing the free enthalpy, while the growth form is determined by the kinetic effects during crystal growth. It can be constructed in a similar manner. Starting from a polyhedron containing all possible faces, the growth rates of the individual faces are drawn perpendicular to the face and the displacement of the face is regarded after a time  $\Delta t$ . Figure 2.16 shows the construction for a two-dimensional lattice exhibiting both (10) and (11) edges. If the ratio of the growth rates of two edges is  $(v_{11}/v_{10}) \geq \sqrt{2}$ , the (10) edge will start to dominate after  $t = \Delta t$  and will be the only edge after  $t = 2 \times \Delta t$  (Figure 2.16a). The growth form will consist only of (10) edges. Contrarily, if the ratio is within  $\sqrt{2} \geq (v_{11}/v_{10}) \geq (\sqrt{2}/2)$ , both faces will prevail and be part of the growth form (Figure 2.16b). Thus, the slowest growing faces prevail and determine the growth form. Consequently, every parameter influencing the ratio of the growth rates, such as solvents or impurities, will influence the growth form.

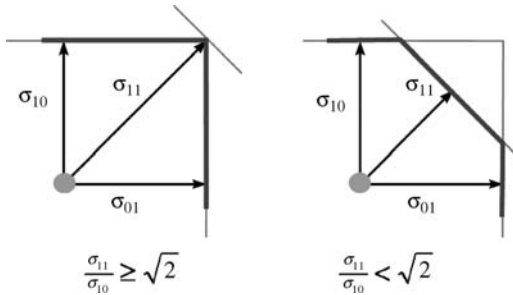


**Figure 2.15** Construction of equilibrium form. Starting from a center, a length corresponding to the central distance is plotted together with the face. The equilibrium form is

obtained by drawing the smallest crystal. Two ratios of the surface tensions are distinguished, leading to squared and octagonal crystals.



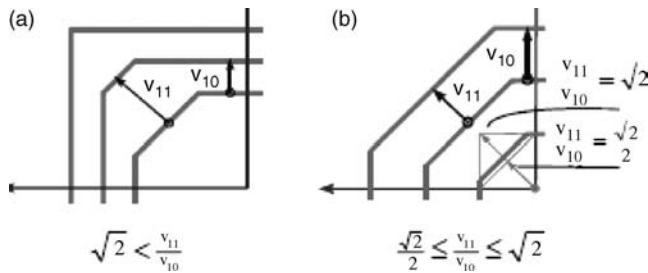


**Figure 2.16** Construction of the growth form of a crystal by starting from a polygonized object. Depending on the ratio of the growth rates of the faces, the fastest growing faces will quickly outgrow the form and vanish (a). The

development is shown in (b) by microscopic images of a crystal first limited by a large variety of faces. In the final state, only the ( $h01$ ) and ( $h10$ ) face remain.

Using the arguments as for growth, it can be shown that the dissolution form of crystals will be limited by the fastest dissolving faces. These faces are the higher indexed faces, so a dissolving crystal will develop a round outer shape.

### 2.1.6

#### Morphology and Habit

The different crystal lattices and variations in the growth rates of the faces lead to a broad variety of morphologies of crystals. These can be differentiated by the elongation of their axes. Often encountered morphologies are summarized in Figure 2.17. The morphology can be altered by processes during crystallization. Changing the solvent or modifying the purity profile can influence the morphology (cf. Chapter 10.8).

Very large difference in growth rates will lead to needlelike crystals (Figure 2.18), also sometimes called whiskers.

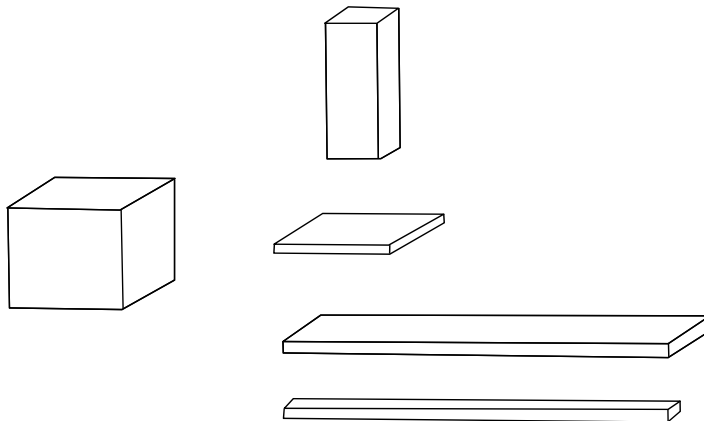


**Figure 2.17** Often encountered morphologies of crystals and their description. A cubic morphology can develop into a columnar crystal when horizontal axis dominates, while tabular

crystals will develop for the horizontal axis to have a low growth rate. Finally, depending on the growth rates of the two horizontal axis, either platelike or acicular crystals will form.

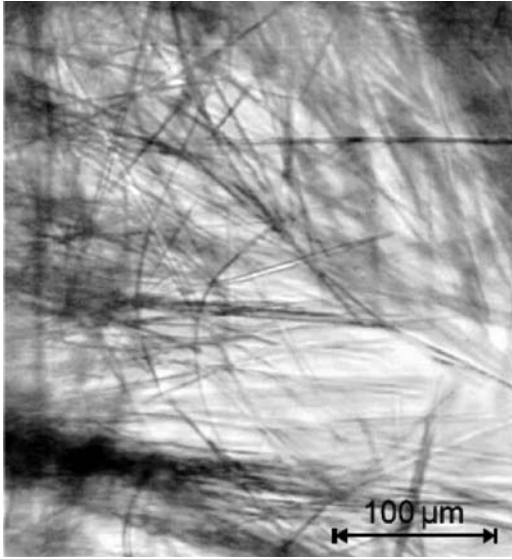


**Figure 2.18** Example of extremely needlelike crystals.

## 2.2

### Nucleation of Crystals

For the nucleation, different processes have to be distinguished (Figure 2.19). Spontaneous nucleation can occur either in the absence of any foreign surface, the so-called homogeneous nucleation, or on foreign surfaces such as dust, the so-called heterogeneous nucleation. This type of nucleation is also called primary nucleation, as it leads to crystalline material *de novo*, and is distinct from secondary nucleation, where the generation of new particles is induced by particles of the solute (cf. Section 9.3.5).

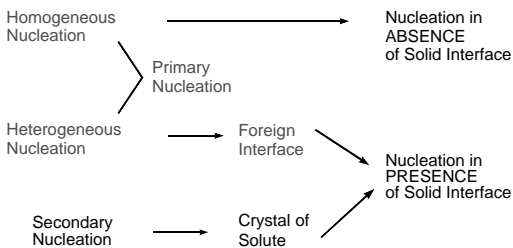


**Figure 2.19** Differentiation of nucleation into spontaneous primary nucleation either in the absence of any foreign surface or on a foreign surface. In addition, nucleation can be induced by crystals of the solute, the so-called secondary nucleation.

## 2.2.1

**Mechanism of Primary Nucleation**

The mechanisms of primary nucleation can best be discussed by using the nucleation of droplets from the vapor phase. Using droplets instead of crystals, the treatment of polyhedral bodies and the differences in interfacial tension of individual faces can be avoided, making the understanding of the treatment easier. The principles can be transferred to polyhedral crystals.

The nucleation process can be regarded as a succession of the addition of growth units to an aggregate. To derive the nucleation rate, the free enthalpy of the formation of a droplet with a radius  $r$ ,  $\Delta_k G_r$ , has to be calculated (Figure 2.20). Two terms contribute to the free enthalpy – the enthalpy of condensation and the enthalpy necessary for creating the new surface (Equation 2.5):

$$\Delta_k G_r = \frac{4\pi}{3} r^3 \Delta_v G - 4\pi r^2 \sigma. \quad (2.5)$$

The enthalpy of condensation is given by the volume of the droplet and the enthalpy of condensation  $\Delta_v G$  per volume of a building block is given by  $\Delta_v G = (RT/\Omega) \ln(p/p_e) = (RT/\Omega) \ln \beta$  with  $\Omega$  as the molar volume. The enthalpy for creation of the new interface is given by the surface area of the droplet and the surface tension  $\sigma$ . The two rhs terms in Equation 2.5 and the resulting  $\Delta_k G_r$  are plotted in Figure 2.20 as a function of radius.

For a droplet to grow, the change in free enthalpy upon adding a building block has to be negative. It is apparent from Figure 2.20 that this is the case only for  $r > r^*$ . For droplets with a size  $r < r^*$ , the addition of a building block is unfavorable, as the free enthalpy increases. Thus, a droplet with a size of  $r = r^*$  has the same probability of adding a growth unit as losing it; it is in equilibrium with the supersaturated mother phase.

As a droplet with size  $r = r^*$  gains one growth unit, the addition of further growth units becomes more and more favorable, as this will further increase the stability of the droplet. The droplets with size  $r = r^*$  are thus the starting point for the nucleation process; the droplets are also called critical nuclei.

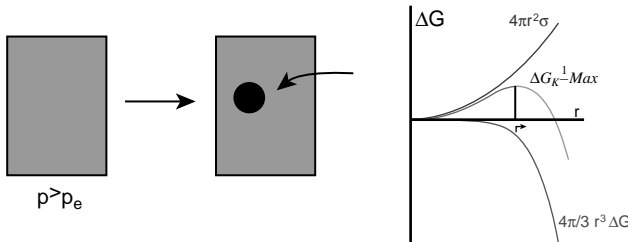


**Figure 2.20** Nucleation of a droplet with size  $r$  from a supersaturated vapor phase. The free enthalpy for the formation of such a droplet is given by the two rhs terms of Equation 2.5 and are sketched together with the resulting free enthalpy of formation of such a droplet.

The nucleation rate  $J$  is given by the density of the nuclei and the rate of addition of one further building block (Equation 2.6):

$$J \equiv \text{Density of nuclei} \times \text{rate of addition of building blocks.} \quad (2.6)$$

The volume density of critical nuclei can be derived using the Boltzmann equation, which relates the concentration of oligomers  $n_i$  to the concentration of monomers,  $n_1$ , to the free enthalpy for the aggregation  $n_i/n_1 = \exp - (\Delta G_i/RT)$ . From Equation 2.5, the size of the critical nucleus,  $r^*$ , can be derived (Equation 2.7):

$$r^* = \frac{2\sigma}{\ln \beta} \cdot \frac{\Omega}{RT}. \quad (2.7)$$

The free enthalpy to form such a critical nucleus, the enthalpy of nucleation, is given by Equation 2.8:

$$\Delta_{r^*} G = \frac{16\pi}{3} \sigma^3 \frac{1}{\Delta_v G^2} = \frac{16\pi}{3} \sigma^3 \left( \frac{1}{(RT/\Omega) \ln \beta} \right)^2. \quad (2.8)$$

Finally, the density of critical nuclei as given in Equation 2.9 is obtained:

$$n^* \propto \exp - \frac{\Delta_{r^*} G}{RT}. \quad (2.9)$$

Thus, the density of critical nuclei depends exponentially on the supersaturation. The second term in Equation 2.6 does only depend linearly on supersaturation, a dependence that can be neglected. Thus, the nucleation rate depends exponentially on supersaturation, as given by Equation 2.10:

$$J \propto \exp - \underbrace{\frac{\Delta G^*}{RT}}_{\propto \frac{1}{\ln^2 \beta}}. \quad (2.10)$$

The qualitative trend of the nucleation rate as a function of supersaturation is depicted in Figure 2.21. The nucleation rate is practically zero below a certain,

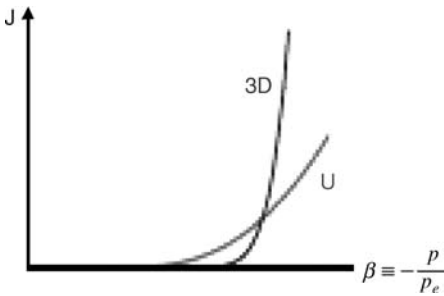


**Figure 2.21** Qualitative dependence of the nucleation rate on supersaturation for primary nucleation via homogeneous, 3D, and by heterogeneous nucleation, U. The exponential nature leads to near negligible nucleation rates below and a steep increase

above a critical supersaturation. The supersaturation necessary for 2D nucleation to occur is drastically lower than for 3D nucleation; however, for high nucleation rates, the number of heterogeneous nuclei can become limiting.

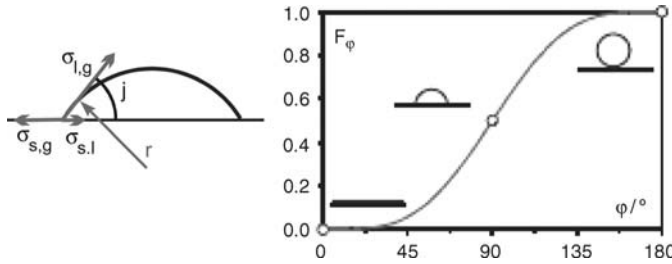


**Figure 2.22** Correction factor  $F_\phi$  for the nucleation of a droplet on a flat surface as a function of the contact angle  $\phi$ . For a contact angle of  $\phi = 180^\circ$ , the liquid will not spread and the foreign surface does not support the nucleation; conversely, for  $\phi = 0^\circ$ , the liquid spreads on the surface and no nucleation is necessary.

critical supersaturation; however, upon reaching this supersaturation, the nucleation rate increases drastically.

Nucleation can also occur on the surface of a foreign particle. The free enthalpy of the formation of a droplet on a surface is decreased. A factor  $F_\phi$  relates the free enthalpy of nucleation on a surface  $\Delta_U G^*$  to that in the volume (Equation 2.11). For a flat surface, the qualitative dependence of  $F_\phi$  on the contact angle is shown in Figure 2.22. For a contact angle of  $\phi = 180^\circ$ , the liquid will not spread and the foreign surface does not support the nucleation; conversely, for  $\phi = 0^\circ$ , the liquid spreads on the surface and no barrier to nucleation has to be overcome.

$$\Delta_U G^* = F_\phi \Delta_{3D} G^*. \quad (2.11)$$

As the factor is always smaller than unity (except for  $\phi = 180^\circ$ ), the nucleation on a surface is energetically favorable to homogeneous nucleation, and will thus have drastically higher rates. This is qualitatively shown in Figure 2.21.

In general, the radius  $r^*$  of the critical nucleus will be much smaller than the radius of most particles in a mother phase, so their surface can be regarded as flat. In effect, the subvisual particles down to the submicrometer range will act as heterogeneous nuclei.

### 2.2.2

#### Metastable Zone and Induction Time for Nucleation

Due to the steep increase of the nucleation rate with supersaturation, primary nucleation in technical system can be differentiated into two categories: *has-not-yet-occurred* and *has-occurred*. Two types of descriptions are used to quantify the effects of nucleation: for a system with a constantly increased supersaturation, the metastable zone width is used; for a system with constant supersaturation, the induction time is used.

The metastable zone describes the zone in the solubility diagram where a mother phase is supersaturated, but has not yet responded with spontaneous nucleation,

within a certain finite time. The two boundaries of the metastable zone are the solubility line and a somewhat hypothetical line at which spontaneous nucleation has occurred. This second line is kinetic value and depends on a number of conditions to be discussed below.

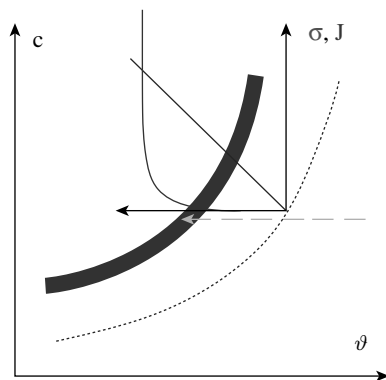
In a cooling crystallization, the system first follows along the path of constant concentration (arrowed line in Figure 2.23). The system crosses the saturation line, dotted line, becomes supersaturated, and the nucleation rate will be greater than zero; the dependence as shown in Figure 2.21 is reproduced as insert. At small supersaturations, the nucleation rate will be practically zero; however, when the supersaturation reaches a value for which the nucleation rate deviates measurably from zero, any further small increase in supersaturation will dramatically increase the nucleation rate, so nucleation will be macroscopically observed.

The width of this metastable zone depends on a number of experimental conditions and is characteristic of the system under considerations.

The most influential parameter is the rate of supersaturating the system, i.e. the rate of cooling, evaporation of solvent or addition of anti-solvent addition. An equally influential parameter is the concentration of additives or impurities in the mother phase (Chapter 6). Another influence is the thermal history of the phase, namely, how long and to which degree has the phase been heated above saturation.

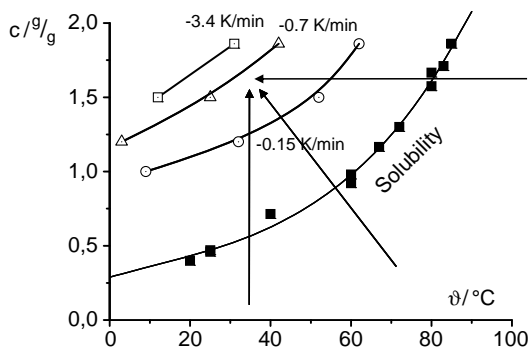
Case is known, where the metastable zone width does not vary between laboratory and plant, while other accounts are also given.

Figure 2.24 shows the width of the metastable zone as a function of cooling rate for a sugar in water. The width is on the order of 10–50 K and strongly depends on the rate of cooling. The subcooling necessary for spontaneous nucleation is plotted



**Figure 2.23** Schematic representation of the width of the metastable zone for the case of a cooling crystallization along the path represented by the arrowed line. The system crosses the saturation line, dotted line, and becomes supersaturated. The nucleation rate will be greater than zero. The dependence

shown in Figure 2.21 is reproduced. When the supersaturation reaches the critical value for nucleation rate to become observable, any small further cooling will dramatically increase the nucleation rate, so that a macroscopically visible nucleation event occurs.



**Figure 2.24** Width of the metastable zone for a sugar in water. It can be seen that the width is relatively large, on the order of 10–50 K, and that the width strongly depends on the rate of cooling.

in Figure 2.25 as a function of the cooling rate. For very low cooling rates, the width tends to 0 K. Conversely, the time the system is actually metastable, that is, the time between crossing the solubility line and spontaneous nucleation, decreases with increasing cooling rate.

The metastable zone width is in case independent of the technique with which the supersaturation is generated. Figure 2.26 shows a system in which the width is nearly the same for a cooling and evaporative crystallization. Note the dispersion between repeated experiments, which is typical for the width of the metastable zone. It should be kept in mind that the nucleation process has a statistical nature and that the rate of the nucleation does depend exponentially on supersaturation.

Usually, aqueous solutions of salts will exhibit a small width of the metastable zone, typically on the order of 1–2 K, but values of 10 K are not an exception. Organic substances dissolved in organic solvents usually have a width of the metastable zone

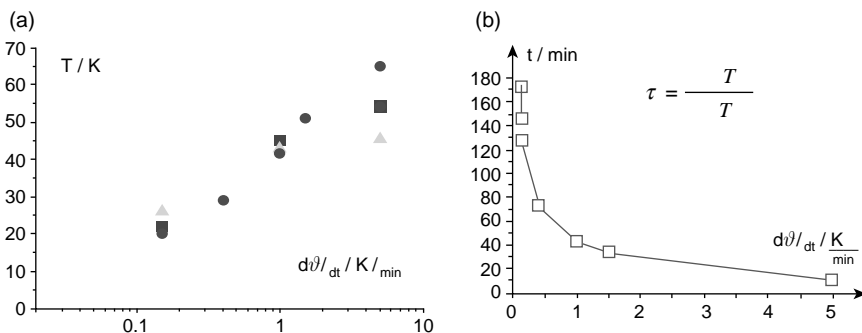


**Figure 2.25** (a) Width of the metastable zone expressed as subcooling  $\Delta T$  for a cooling crystallization of a sugar as function of the cooling rate. (b) For very low cooling rates, the width tends to 0 K. The time the system is actually metastable decreases with the cooling rate.

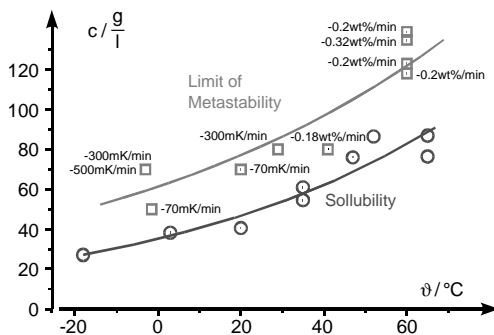


**Figure 2.26** Width of the metastable zone for an organic moiety nucleating in an organic solvent. The width is nearly the same for a cooling and evaporative crystallization. Note, that the cooling rates are given in mK/min and

the rates of evaporation are given in wt-%/min. Note also, that the dispersion between repeated experiments, which is typical for the width of the metastable zone.

on the order of 10 K. Finally, sugars in aqueous solutions exhibit metastability typically on the order of 50 K.

Thus, the supersaturation necessary for spontaneous nucleation can be considerable, which in turn will result in a substantial amount of material to crystallize upon spontaneous nucleation. This crystallization mainly occurs at high supersaturation, which is often undesirable.

For systems with retarded nucleation, the time necessary to build up a certain supersaturation can be short compared to the time necessary for spontaneous nucleation to occur. Thus, nucleation can be observed for constant supersaturation. The time elapsed before nucleation occurs is called induction time  $\tau_{\text{ind}}$  and is given by the time necessary for the formation of nuclei and the time required for the nuclei to reach observable sizes Equation 2.12:

$$\tau \propto \frac{1}{J}. \quad (2.12)$$

By assuming that the number of nuclei necessary for observing the nucleation,  $N$ , is independent of the experimental conditions, the induction time becomes inversely proportional to the nucleation rate (Equation 2.12), that is, the induction time should be indirectly proportional to the supersaturation.

The number of visual and subvisual particles in a solution is known to influence the nucleation process. The induction time of an hexose in water has been measured as a function of supersaturation at room temperature. Solutions prepared from pure sugar and deionized water tend to nucleate within minutes at high supersaturations and within less than an hour at low supersaturations (Figure 2.27). However, filtering the solutions through a 0.2  $\mu\text{m}$  filter into flasks that have been rinsed with particle-free water increases the induction time by one to two orders of magnitude. In addition, the dispersion in the induction times increases considerably.



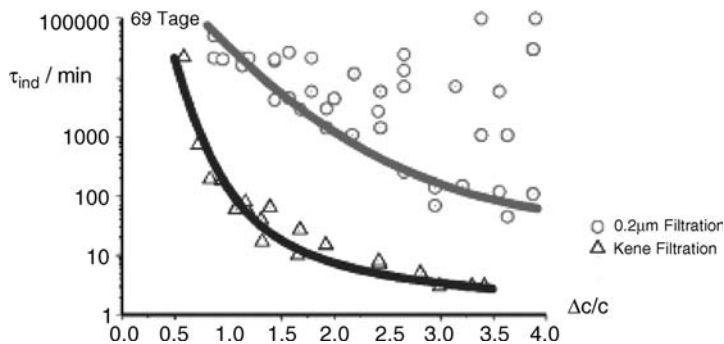


**Figure 2.27** Induction times  $\tau_{\text{ind}}$  for a sugar in water at room temperature. The solutions were used as is ( $\Delta$ ) and filtered using a 200 nm filter ( $\circ$ ).

Crystal nucleation, as crystal growth, involves the transport of building blocks from the bulk of the mother phase to the nucleus. Thus, the nucleation rate is influenced by the viscosity of the mother phase. For the nucleation of citric acid from aqueous solutions, the number of nuclei was counted as a function of supersaturation (Figure 2.28). Two solutions with different concentrations and thus saturation temperatures are compared. The nucleation rate first increases with decreasing temperature and thus increasing supersaturation. However, with decreasing temperature, the viscosity of the solution increases drastically, entailing a drastic decrease in nuclei counted, as the diffusion of building blocks becomes more difficult. The viscosity is also given; note that due to the high solubility of citric acid in water, the viscosity has values on the order of 10 P.

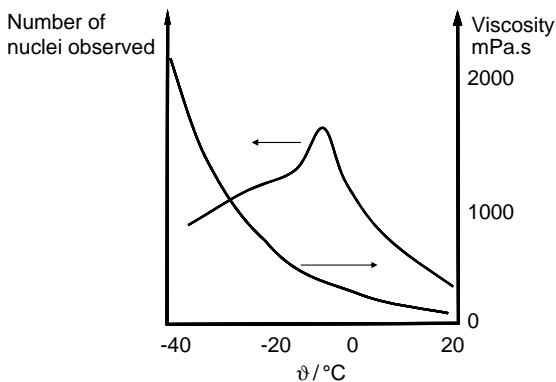


**Figure 2.28** Number of nuclei counted as a function of temperature for two solutions with different saturation temperatures. The nucleation rate first increases with decreasing temperature and thus increasing supersaturation. However, with decreasing temperatures, the viscosity of the solution

increases drastically, entailing a drastic decrease in nuclei counted, as the diffusion of building blocks becomes more difficult. The viscosity is also given; note that due to the high solubility of citric acid in water, the viscosity has values on the order of 10 P.

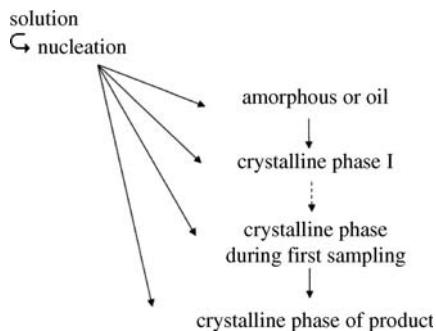


**Figure 2.29** Visualization of Ostwald's law of stages. If a multitude of solid-state forms is possible, the most unstable form will nucleate first. This can either be an unstable crystalline form or even an amorphous solid or oil. As unstable solid-state forms are prone to a (solution-mediated) phase transformation, the unstable form might have transformed into a more stable one before sampling.

### 2.2.3

#### Form Crystallized: Ostwald's Law of Stages

If a system can crystallize in more than one crystalline form and if the substance can form polymorphs (cf. Chapter 5), the instable modifications will develop first – Ostwald's law of stages does say that the “most” unstable modification will nucleate first (cf. Figure 2.29).

If a multitude of solid-state forms is possible, the most unstable form will nucleate first. This can either be an unstable crystalline form or even an amorphous solid or oil. As unstable solid-state forms are prone to a (solution-mediated) phase transformation, the unstable form might have transformed into a more stable one before sampling.

## 2.3

### Growth and Growth Rate of Crystals

The growth of crystals is described by the growth rate  $R$ , which is defined as the rate of displacement of the face under consideration in the direction perpendicular to the plane.

The growth rate of a crystal face is given by the difference of fluxes of growth units onto the surface,  $j_{\text{on}}$ , and leaving the surface,  $j_{\text{off}}$ , that is,  $R = \Omega(j_{\text{on}} - j_{\text{off}})$ . In equilibrium,  $j_{\text{on}} = j_{\text{off}}$  and  $R = 0$ .

It will be shown first that the growth is governed by the growth of flat  $F$  faces and by the generation steps on these faces. Two sources for these steps can be distinguished: First, the steps can be generated by 2D nucleation on the surface or by screw dislocations. Second, the rate of incorporation of the building blocks into the steps at the so-called kink positions will be described.

## 2.3.1

**Kink Position and F, S, and K Faces**

In a cubic lattice, each building block is surrounded by 6 nearest neighbors, via the faces, by 12 second nearest neighbors, over the edges, and by 8 third nearest neighbors over the corner (Figure 2.30). The interaction energy between the neighbors can be taken from the pairwise interaction potential, as depicted in Figure 2.1. From the summation of the pairwise interaction potential, the enthalpy of crystallization can be calculated (Equation 2.13):

$$\Delta_{tr}H \equiv n \cdot \varphi_{1/2} = \frac{N_1}{2} \varphi_1 + \frac{N_2}{2} \varphi_2 + \frac{N_3}{2} \varphi_3 + \dots \quad (2.13)$$

As the interaction potential decreases quickly with distance, only the potential of the nearest neighbors has to be considered (cf. Figure 2.1). For a simple cubic lattice,  $N_1 = 6$ , so the average interaction potential for phase transformation is  $\Delta_{tr}H \approx n \frac{6}{2} \varphi_1 = n 3 \varphi_1|_{\text{cubic lattice}}$ , where  $n$  gives the number of building blocks in the crystal.

For a simple cubic lattice, different positions of building blocks on a face can be differentiated by the number of neighbors they have Figure 2.30. Position A and B are bound by one and two nearest neighbors, respectively, which is less than the average number of three, while position D is bound by five nearest neighbors, which is above average. Thus, at saturation, growth units bound as A and B are more likely to dissolve than to grow, while those in position D are more likely to remain attached. Only building units at position C are bound by three nearest neighbors and are at saturation in equilibrium with the crystal. At the smallest supersaturation, the units are not only stable but newly arriving building growth units will be more easily attached rather to leave the position. Thus, position C, the kink position, will be a center of growth stable. Moreover, attaching a growth unit at C will create the same position again. Position C is called repeatable step and also kink position.

The steps will roughen thermally, forming a number of kink positions. Thus, steps will also start growing at very small supersaturations.

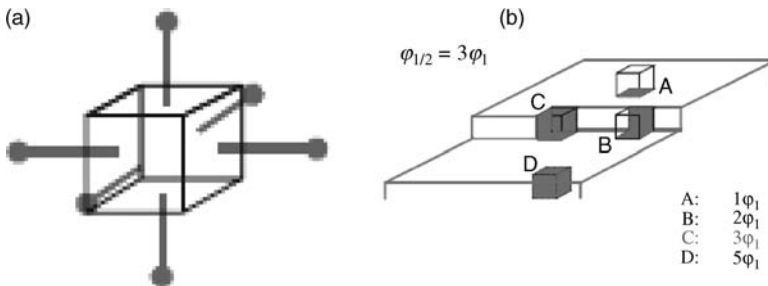


**Figure 2.30** (a) Number of nearest neighbors of building blocks in a simple cubic lattice. (b) Binding of the building blocks to nearest neighbors in different positions in a crystal face.

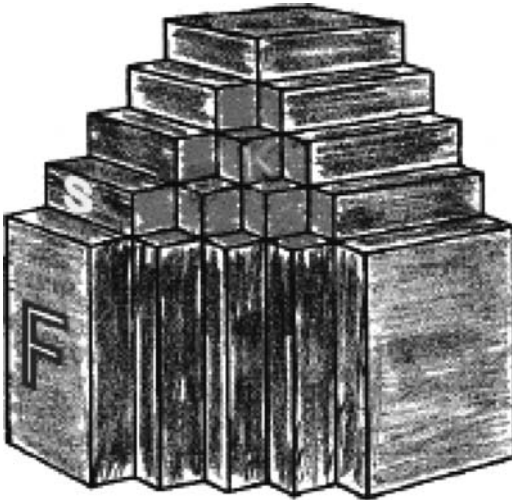


**Figure 2.31** Simple cubic crystal with the three lowest-indexed faces. The faces are flat F, stepped S, and kinks K.

For a simple cubic lattice, three very prominent faces can be distinguished (Figure 2.31). The (001) face is flat, the (101) face is stepped, and the (111) face is kinked.

Each position on a K-face corresponds to a position denoted by C in Figure 2.30. The K-faces will grow at very small supersaturations. The same holds for the S-faces, while the F-faces will not grow. Due to their higher growth rates, the K- and S-faces will not be part of the growth form (Section 2.1.5). The discussion of growth mechanisms can thus be confined to the F-faces and the discussion of the generation of steps on F-faces.

### 2.3.2

#### Growth of Ideal Crystals

Steps on ideal crystals can be formed by 2D nuclei. As discussed before, the supersaturation necessary for nucleation on a surface is significantly lower than the supersaturation necessary for nucleation in the volume. If the surface is a face of the own material, the free enthalpy of nucleation is again lower. Thus, growth via 2D nuclei occurs well below any nucleation in the volume.

Of the three models for the growth via 2D nucleation, only the birth-and-spread model will be discussed here, as it is the most plausible and the free enthalpy of nucleation for this mechanism is the lowest. In this model, 2D surface nuclei are generated on the flat faces. The nuclei are limited by steps that will spread out. It is allowed that new nuclei generate on growing islands (Figure 2.32).

The growth rate is given by the height of the 2D nuclei, usually the height of a building block, and by the time necessary for the islands to have spread over one monolayer; thus,  $R = h/\tau$ . The time  $\tau$  for the filling of one monolayer is given by the rate with which the islands are generated and by the velocity with which the islands spread,  $\tau \propto \nu^{-2/3} J^{-1/3}$ . Both terms depend on supersaturation, however, the

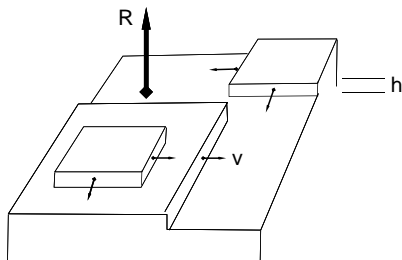


**Figure 2.32** Model for the growth via 2D surface nuclei according to the birth-and-spread model. These 2D nuclei are limited by steps and spread laterally. The nucleation of islands that are still not grown out is allowed.

dependence of the nucleation rate dominates; so the growth depends exponentially on supersaturation (Equation 2.14):

$$R \propto \underbrace{\frac{\Delta G^*}{3RT}}_{\propto \ln \beta} \quad (2.14)$$

Thus, the growth via 2D nucleation will need a certain critical supersaturation to start, upon which the growth rate will increase rapidly, until it is limited by transport phenomena (Figure 2.33).

### 2.3.3

#### Growth of Real Crystals

Screw dislocations, Chapter 2.1.4, Figure 2.12, are a permanent source of steps at which growth will occur. This growth does not require nucleation, the supersaturation necessary for an observable growth is much smaller than that for growth via 2D nuclei. Consequently, this growth mechanism will dominate.

Perpendicular to a screw dislocation, a step is found (Figure 2.12). This step will roughen thermally and grow at low supersaturations. The growth of the step will

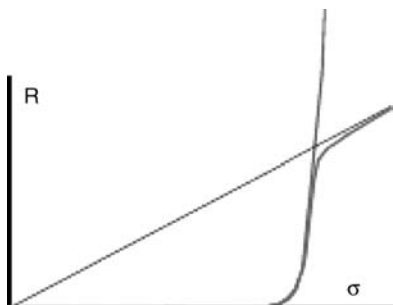


**Figure 2.33** Dependence of the growth rate  $R$  on supersaturation for growth via the birth-and-spread model. Note that a certain supersaturation is necessary for growth to start

and that due to the exponential dependence of the growth rate, the growth rate quickly reaches the limit of diffusion.

generate a further step on that face Figure 2.34. The cycle continues until a growth spiral is formed, which covers the entire crystal face. Thus, a screw dislocation is a permanent source of steps and promotes effectively the growth. Often, one screw dislocation for the growth of the respective face will suffice, although on real crystals, usually more than one screw dislocation is found on a face. These dislocations cooperate and increase the step density.

Such growth spirals have been observed on the surface of a great variety of crystals. Figure 2.34 shows such a spiral on the (001) face of a fatty acid crystal. The step heights observed range from one building block to several tens of that height. It has been observed that the movement of steps is not constant, but rather sometimes behaves like traffic, there are jams and steps can pile up.

The growth rate  $R$  of the face is given by the height  $h$  and distance of the steps and the rate of the displacement of the steps  $v$  (Equation 2.15 and Figure 2.35):

$$R = \frac{vh}{\gamma} \quad (2.15)$$

The distance between steps is determined by the length  $l^*$  a step has to have before it starts to grow. By a simple geometric consideration (Figure 2.34), one finds  $\gamma = 4 \cdot l^*$  for a polygonized growth spiral and  $\gamma = 19r^*$  for a rounded growth spiral.  $l^*$  and  $r^*$  are the length and radius, respectively, of a 2D nucleus. One can derive  $l^* = 2\gamma \cdot f_0(1/\Delta\mu) = 2\gamma \cdot f_0(1/RT \ln \beta)$ , that is, the distance between steps is inversely proportional to the supersaturation.

The rate of displacement of the steps is given by the rate at which growth units arrive at and are incorporated by the step. The steps are a sink for growth units.

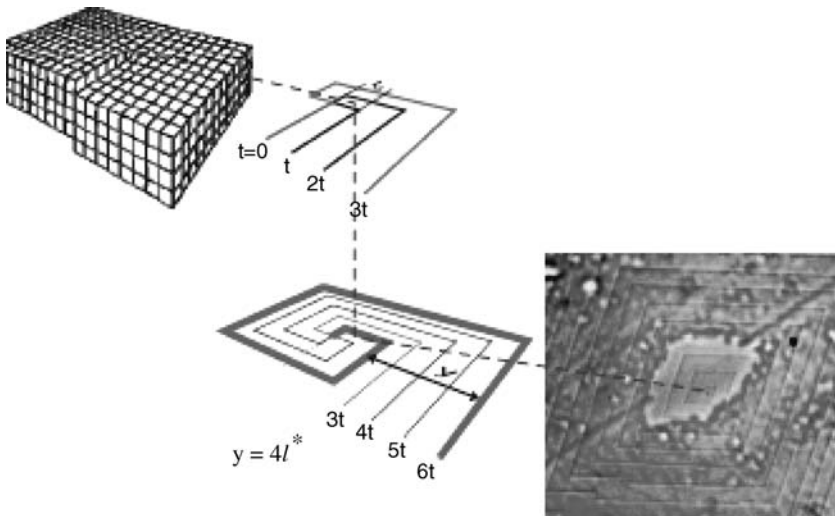


**Figure 2.34** Growth at a screw dislocation. The screw dislocation is a direct source of a step and the growth of the step will generate the next step perpendicular to the first, and so on. Such a growth will lead to growth spirals, either rounded or polygonized, as shown in the micrograph at the right.

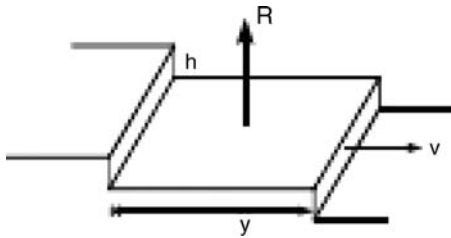


**Figure 2.35** Growth of a face as perpendicular displacement for growth at a screw dislocation. The rate is directly proportional to the distance of the steps, their height, and rate of displacement (Equation 2.15).

Growth units in the bulk of the mother phase adsorb on and desorb from the crystal face. The incorporation of growth units into the steps leads to a concentration gradient on building blocks on the surface of the faces. This is the driving force for a surface diffusion toward the steps (Figure 2.36).

The velocity of the spreading of the steps can be calculated from the sum of the fluxes of building blocks toward the steps, both from the upper and lower terraces.

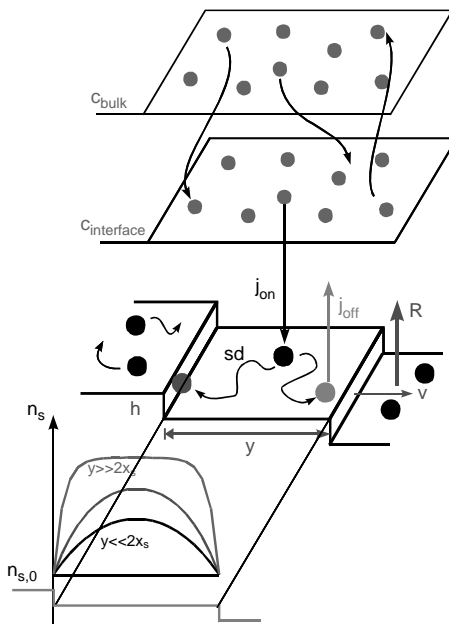


**Figure 2.36** Model for the derivation of the rate of displacement of steps of a screw dislocation. Growth units in the bulk of the mother phase adsorb and desorb on the crystal face. The building blocks do a random walk on the surface. Those building blocks that have

reached a step before they desorb are incorporated into the steps. The sinking of growth units by the steps leads to a concentration gradient on building blocks on the surface of the faces, which is the driving force for surface diffusion toward the steps.

Solving the one-dimensional differential equation, Equation 2.16 is obtained for the rate of displacement of the steps:

$$v \propto f_0 D (\nabla n_s|_{\text{top}} + \nabla n_s|_{\text{bottom}}) = f_0 D \cdot \tanh \frac{\gamma}{2\bar{x}_s}. \quad (2.16)$$

The term  $\bar{x}_s$  is the mean free path for surface diffusion, a building block adsorbed within this distance from a step, will reach the step and will be incorporated. Finally, the growth rate is given by Equation 2.17.  $\sigma^*$  lumps up all constants:

$$R \propto \sigma^2 \tanh \frac{\sigma^*}{\sigma}. \quad (2.17)$$

Depending on the ratio of the distance between steps,  $\gamma$ , and the mean free path for surface diffusion,  $\bar{x}_s$ , the two regimes for the dependence of the growth rate on supersaturation can be distinguished:

- $\gamma \gg 2\bar{x}_s, \quad \sigma \ll \sigma^*$ : For low supersaturations, the mean free path of surface diffusion is much smaller than the distance between the steps; so only a small fraction of building blocks adsorbed reach a step, most desorb before. The growth rate is proportional to the square of the supersaturation.
- $\gamma \ll 2\bar{x}_s, \quad \sigma \gg \sigma^*$ : For high supersaturations, the step density increases, so their distance becomes smaller than the mean free path of surface diffusion; most building blocks adsorbed on a terrace will be integrated into a step. The growth rate varies linearly with supersaturation.

Figure 2.37 schematically shows the dependencies. Linear or quadratic dependencies of the growth rate on supersaturation are commonly found.

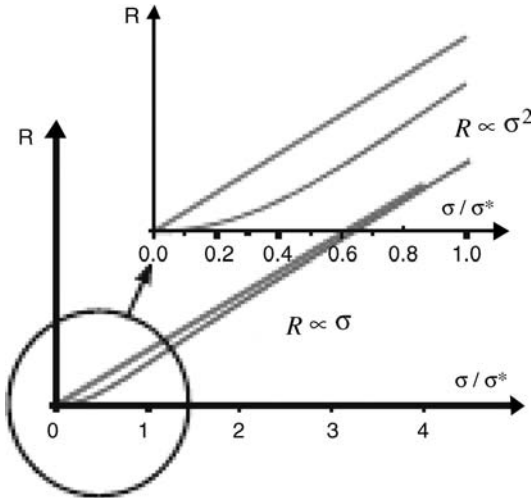


**Figure 2.37** Dependence of the growth rate  $R$  on supersaturation for crystal growth at a screw dislocation as given by Equation 2.17.



## 2.3.4

## Transport Phenomena

Besides being determined by processes at the interface of a crystal, the growth rate can also be determined by transport phenomena in the bulk of the mother phase. In the case of growth from solution, the discussion of transport phenomena can be limited to the transfer of mass. The heat liberated by the crystallization is small compared to the heat conductivity of the mother phase. Conversely, for growth from the vapor phase and from the melt, heat transfer can become limiting.

The transport of mass from the bulk of the mother phase to the interface at the crystal surface requires a certain gradient in concentration, that is, a certain supersaturation. In a first approximation, the crystal can be represented as a sphere with a radius  $r$ . The diffusion layer in a stagnant solution has a thickness of approximately  $r$ . In this case, the mass flux is given by Equation 2.18. The supersaturation necessary for the transport  $\Delta c_{\text{bulk}}$  decreases the supersaturation available for the growth of the interface,  $\Delta c_{\text{int}}$ . Both concentration gradients add up to  $\Delta c = \Delta c_{\text{int}} + \Delta c_{\text{bulk}}$ .

$$\begin{aligned} \dot{m} &= -D \left. \frac{dc_{\text{bulk}}}{dr} \right|_r = -D \frac{\Delta c_{\text{bulk}}}{r} \\ &= k_d \Delta c_{\text{bulk}} \end{aligned} \quad (2.18)$$

The mass transfer by diffusion equals the mass transfer by incorporation of building blocks into the crystal by interfacial processes.

Two regimes can be distinguished, and the concentration gradient is necessary for the mass flux through the bulk of the mother face (Figure 2.38).

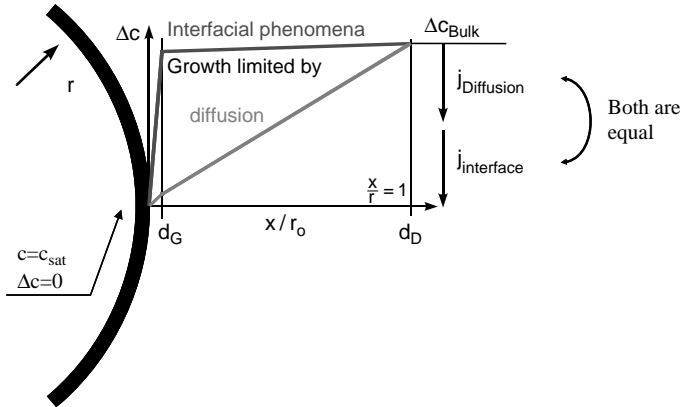


**Figure 2.38** Schematic representation of the steps of diffusion of the building blocks through the bulk of the mother phase to the crystal surface and the incorporation of the building blocks into the crystal lattice. Both fluxes must

be equal. Two cases are distinguished, growth mainly determined by diffusion and growth mainly determined by the processes at the interface.

The effects of mass transport and interfacial kinetics can be differentiated by varying the hydrodynamic conditions in the mother phase, that is, by varying the stirring rate.

### Further Reading

- |  |  |
|--|--|
| Hartmann, P. (1973) <i>Crystal Growth: An Introduction</i> , North Holland.              | Meyer, K. (1968) <i>Physikalisch-Chemische Kristallografie</i> , VEB Grundstoffindustrie.          |
| Hirth, J.P. and Pound, G.M. (1963) <i>Condensation and Evaporation</i> , Pergamon Press. | Mullin, J.W. (1993) <i>Crystallisation</i> , Butterworth-Heinemann.                                |
| Kleber, W. (1990) <i>Einführung in die Kristallografie</i> , Verlag Technik.             | Myerson, A.S., (1995) <i>Crystallization Technology Handbook</i> , Butterworth-Heinemann, 20xx.    |
| Mersmann, A. (1994) <i>Crystallisation Technology Handbook</i> , Dekker.                 | Ohara, M. and Reid, R. (1973) <i>Modelling Crystal Growth Rates from Solution</i> , Prentice Hall. |

## 3

**Solubility and Solution Equilibria in Crystallization***Heike Lorenz*

Equilibria between solid and liquid phases (solid–liquid equilibria (SLE)) are the thermodynamic foundation of all crystallization processes from the melt and solution and thus of fundamental importance for the design of industrial crystallization processes. The informative value of SLE data of a particular substance and thus of the phase diagrams as their graphical representation is miscellaneous, as compiled in Figure 3.1. Besides the general questions, for example, whether a given separation task is feasible by crystallization techniques, much more detailed questions such as the maximum (hypothetical) yield, the purity achievable, and the occurrence of further solid phases (e.g., polymorphs) can be answered. Finally, a crystallization procedure facilitating the separation of the target compound can be derived, which in combination with kinetic data allows systematic process design.

However, often the phase diagrams required are not known in particular for new substances in the fine chemical and pharmaceutical fields. Even more hard to find are ternary solubility phase diagrams that describe equilibria of two substances in a solvent such as the target compound and an impurity in a solvent of choice or the two enantiomers of a chiral system in a solvent. Often one faces a lack of consistent solubility data for the substance of interest. Experimental determination of solubilities is a tedious and time-consuming work and requires a sufficient amount of substance that is often not available in an early stage of development. Also, usually a combination of different analytical techniques is necessary to obtain both the solubility and the identity of the solid phase in equilibrium.

Since the field of solution equilibria is rather extensive, not all aspects can be covered here. The focus is set on determination, understanding, and application of phase diagrams for crystallization purposes. First, general issues of phase equilibria and phase diagrams from thermodynamic viewpoint are discussed. The subsequent sections are concerned with melt and solution equilibria, both comprising typical examples and the measurement of SLE. Alternative techniques are also considered here. Within solution equilibria, the phenomenon of oiling-out, that is, liquid–liquid demixing, that might impair the crystallization process is addressed. Finally, with the examples of enantiomers and reciprocal salt pairs, solution equilibria in ternary and quaternary systems relevant in fine chemistry and mass crystallization applications are briefly treated.

✓ <b>Feasibility of crystallization-based recovery of a target compound (separation, purification)</b>	
✓ <b>How much?</b>	<b>Hypothetical (maximum) yield</b>
✓ <b>Which purity?</b>	<b>Miscibility in solid state (solid solutions)</b>
✓ <b>Further solid phases and their region of stability?</b>	<b>Polymorphs, solvates, and intermediate compounds (stable and metastable phases)</b>
✓ <b>How?</b>	<b>Derivation of the crystallization procedure, quantification, and process design</b>

**Figure 3.1** Informative value of phase diagrams with respect to crystallization: questions that can be answered.

### 3.1

#### Phase Equilibria and Phase Diagrams: General Issues

##### 3.1.1

##### Phases, Phase Rule, and Binary Systems

A phase is a homogeneous part of a system that is uniform throughout the chemical composition and physical state. Phases can be of gaseous, liquid, and solid states and can be a pure substance (pure phase) or a mixture of different substances (mixed phase). For example, oxygen in gaseous state is a pure phase, but a mixture of oxygen, nitrogen, argon, and carbon dioxide as constituents of air is a mixed phase. Any mixture of gases or vapors is a one-phase system. Mixtures of two or more completely miscible liquids or solids are also one-phase systems. On the other hand, mixtures of nonmiscible liquids or solids are heterogeneous systems of two or more phases. As long as a solution of sodium chloride in water is undersaturated, it is a single liquid phase, but when adding sodium chloride to this solution until the solubility at the given temperature is exceeded, a further phase, a solid phase appears. In such a heterogeneous system, the macroscopic properties of the system jump, that is, change unsteadily, at the phase boundary between the phases.

For a system in thermodynamic equilibrium, J.W. Gibbs in 1875 derived the fundamental phase rule that relates the number of independent components,  $N$ , the number of coexisting phases,  $P$ , and the number of degrees of freedom,  $F$ , of the system by the following equation:

$$P + F = N + 2. \quad (3.1)$$

The number of independent components,  $N$ , is the minimum number of chemical species necessary to depict the existing phases completely. It is mathematically given as the difference of the sum of chemical individuals in the system and the sum of restrictive conditions such as chemical equation, electroneutrality, and stoichiometry. Examples with focus on solution equilibria are compiled in Table 3.1. On the basis of the number of independent components, a system is called to be a unary, binary, ternary, quaternary, or quinary system with  $N = 1, 2, \dots, 5$ . For example, the

**Table 3.1** Number of independent components,  $N$ , in different systems.

System	$N$
H <sub>2</sub> O	1
H <sub>2</sub> O + ethanol	2
H <sub>2</sub> O + NaCl	2 (3 – 1)
D-threonine + L-threonine + H <sub>2</sub> O	3
H <sub>2</sub> O + NaCl + KCl	3 (4 – 1)
H <sub>2</sub> O + NaCl + NH <sub>4</sub> HCO <sub>3</sub>	4 (5 – 1)
Na <sup>+</sup> , K <sup>+</sup> , Mg <sup>2+</sup> /Cl <sup>–</sup> , SO <sub>4</sub> <sup>2–</sup> /H <sub>2</sub> O	5 (6 – 1)

last case given in Table 3.1 characterizes the quinary system of the oceanic salts. The ternary system of the threonine enantiomers in water and the quaternary system considered in Table 3.1 are discussed in more detail in Sections 3.3.7 and 3.3.8.

The number of degrees of freedom,  $F$ , characterizes the variance of the system in the given state of equilibrium. It is defined as the number of independent variables (temperature  $T$ , pressure  $p$ , and composition  $x$ ) that can arbitrarily be verified without changing the number of phases present. The number 2 in Equation 3.1 relates to the physical variables pressure and temperature.

The phase rule is universally valid for systems in thermodynamic equilibrium and establishes the theoretical basis for all phase diagrams.

A phase diagram graphically represents (in two or three dimensions) the equilibria between various phases of a system in a wide range of temperature, pressure, and concentration/composition. It specifies the equilibrium conditions ( $T$ ,  $p$ , and  $x$ ) and the corresponding phases present at this state. Thus, in case of SLE, the phase diagram also tells about the solid phases occurring in a system, such as polymorphs, solvates, or intermediate compounds.

Let us now consider solid–liquid equilibria in a binary system. Contrary to phase equilibria between vapor and condensed phases, in the systems comprising solid and liquid phases the pressure as variable can usually be neglected. The behavior of condensed systems does not mostly depend on pressure and thus the appropriate phase diagrams are valid for arbitrary (but not too high) pressures. Thus, phase changes in a binary system can be represented on a temperature–composition diagram as shown in Figure 3.2 for two arbitrary components A and B.

With constant pressure and  $N = 2$  in a binary system, the phase rule follows:  $P + F = 3$ , which means the following:

- The maximum number of phases that can coexist in equilibrium is three, leaving no degree of freedom ( $F = 0$ ), that is, the system is in an invariant state. Temperature and composition are fixed as long three phases coexist. This applies to the eutectic in the phase diagram in Figure 3.2. On heating, a mixture of A and B of eutectic composition melts at the eutectic temperature  $T_{\text{eu}}$ . Three phases coexist at that temperature, solid A, solid B, and the liquid melt. The temperature remains constant as long as all three phases are present and the mixture melts in eutectic

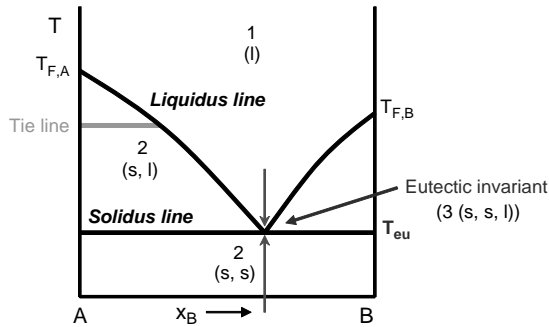


**Figure 3.2** Binary phase diagram of components A and B with  $T$ , temperature,  $x_B$ , mol fraction of B, and  $T_{F,A}/T_{F,B}$ , the melting temperatures of A/B. Numbers refer to the number of phases present and s, l to their state

of aggregation. Below the solidus line, solid phases are present at all compositions in equilibrium; above the liquidus line, the system is liquid.

composition. After melting just one phase remains and the temperature can vary with heating. On cooling, at  $T_{eu}$ , a melt of eutectic composition splits into two solid phases A and B. The eutectic invariant in the phase diagram is represented by a horizontal line connecting the three coexisting phases.

- When two phases are present in equilibrium, one degree of freedom ( $F = 1$ ) is left, that is, the system is in monovariant state. By specifying, for example, temperature, the composition is fixed. Such a situation is illustrated in Figure 3.2 in the two-phase region below the liquidus line of A. A tie line at a certain temperature connects the two coexisting phases, which are a solid and a liquid phase, in fact solid A and a liquid of corresponding composition on the liquidus line. If another temperature is chosen, again the composition of the phases is fixed.
- In case of just one phase, the degree of freedom is two ( $F = 2$ , bivariate state). Temperature and composition can independently be varied to hold the present phase. The one-phase region in Figure 3.2 is the region above the liquidus lines of A and B, being a liquid phase.

For quantification in the phase diagram, the so-called lever rule can be applied: If two phases are in equilibrium, their amount behaves reciprocally to the appropriate part of the tie line.

### 3.1.2

#### Melt and Solution Equilibria

At this point, for clarification purposes, some remarks should be given to the terms melt and solution equilibria. Particularly driven from the application, that is, whether one refers to melt or to solution crystallization (the term “solution” used here to characterize a liquid homogeneous mixture with a classical solvent as one component), it is frequently distinguished between both, what is not mandatory from thermodynamic viewpoint. Generally, a solution is a homogeneous

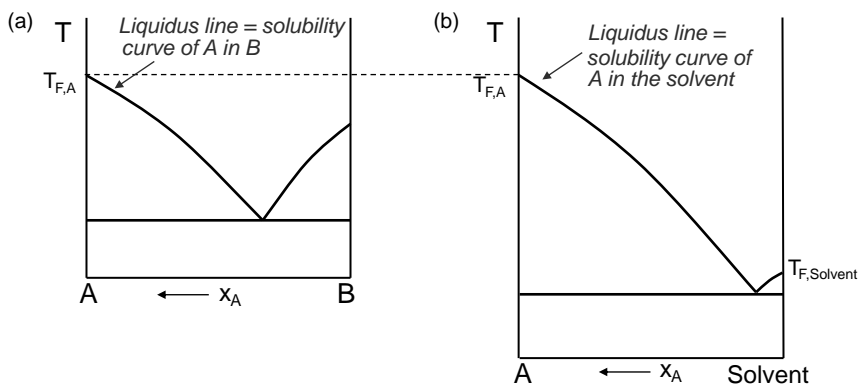


**Figure 3.3** Binary phase diagrams of (a) two compounds A and B and (b) compound A and a solvent demonstrating the formal analogy between melt and solution equilibria.

mixture of two or more substances that can be gaseous, liquid, or solid. In this respect, a melt is a liquid close to its freezing point and, hence, can be treated as a solution. The formal analogy of melt and solution equilibria with respect to the phase diagram is illustrated in Figure 3.3.

Figure 3.3a shows the melt (or melting point) phase diagram of two compounds A and B. The liquidus lines characterize the solubility of one compound in the other. Thus, the marked liquidus line is the solubility curve of A in B. Figure 3.3b presents the phase diagram of compound A and a solvent, and thus the solution equilibria of A in the solvent. The liquidus line of A also starts at the melting temperature of A,  $T_{F,A}$ , and in ideal case is identical to the liquidus line of A in Figure 3.3a since the freezing point depression depends only on composition, not on identity of the second component in the binary system. Thus, both phase diagrams, one representing melt equilibria and the other solution equilibria of a component in a solvent, can be treated in the same way. Moreover, the liquidus line of A in the solvent in Figure 3.3b is nothing else than the “classical” solubility curve of A in this solvent. When rotating the phase diagram in Figure 3.3b by  $90^\circ$  to the right (see Figure 3.4), the typical representation of the solubility curve (concentration/composition as function of temperature) results.

In the following sections, with regard to their application and the differences in determination, melt and solution equilibria will be discussed separately.

### 3.1.3

#### Thermodynamic Description of SLE: Liquidus Curve in the Phase Diagram

The thermodynamic description of the liquidus curve in the phase diagram is based on classical equilibrium considerations, which will not be elaborated in detail here. Only the frequently used simplified final relationship should be briefly derived.

The system to be considered is an arbitrary substance A, where pure A in the solid phase,  $[A]'$ , is in equilibrium with A in the liquid phase,  $[A]''$ .

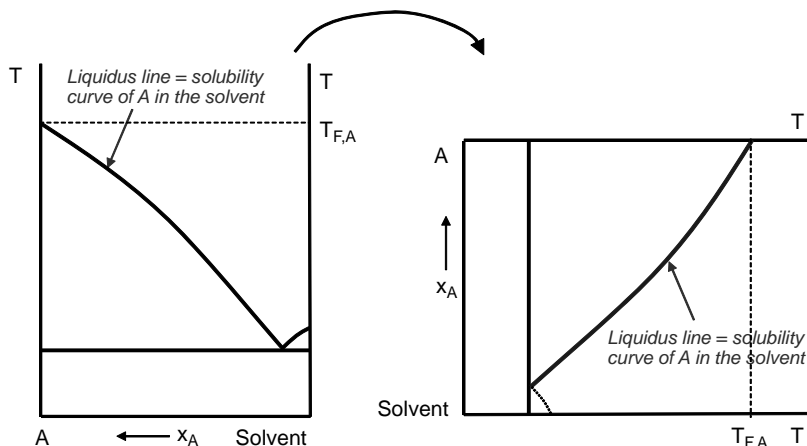


**Figure 3.4** Graphical demonstration of the relationship between the liquidus lines of A in the binary phase diagram A – solvent and the solubility curve of A in the solvent.

$$[A]' \leftrightarrow [A]'' \quad (3.2)$$

Substance A must not dissociate in the liquid state and be fully immiscible with the other component in the solid state. Derived from the formulation of the fundamental equilibrium condition, for such solid–liquid equilibria a special form of the generally valid Clausius–Clapeyron equation applies:

$$\left( \frac{\partial \ln a}{\partial T} \right)_p = \frac{\Delta_F H(T)}{R \cdot T^2}, \quad (3.3)$$

where  $a$  is the saturation activity of A in the liquid phase,  $R$  is the universal gas constant, and  $\Delta_F H$  is the melting enthalpy of A<sup>1)</sup>. This equation describes the temperature dependence of the saturation activity of A in a binary system at constant pressure.

Replacing the activity by the product of the molar fraction,  $x$ , and the activity coefficient,  $\gamma$ , Equation 3.3 becomes

$$\left( \frac{\partial \ln (x \cdot \gamma)}{\partial T} \right)_p = \frac{\Delta_F H(T)}{R \cdot T^2}, \quad (3.4)$$

with the temperature dependence of  $\Delta_F H$  specified by the Kirchhoff relation:

$$\Delta_F H(T) = \Delta_F H_{T_F} + \int_{T_F}^T \Delta_F C_p dT. \quad (3.5)$$

1) Here and in the following the index A characterizing the component is omitted in the formulae for simplification purposes.



In Equation 3.5,  $T_F$  is the melting temperature of the component and  $\Delta_F C_p$  is the molar phase transition heat capacity. The latter is given by the difference of the heat capacities of the liquid and the solid phases which depend on temperature:

$$\Delta_F C_p(T) = C_{p,l}(T) - C_{p,s}(T). \quad (3.6)$$

Assuming further ideality of the binary mixture in the liquid phase, thus setting the activity coefficient  $\gamma$  to 1, and neglecting the temperature dependence of  $\Delta_F C_p$  in Equation 3.6, the well-known Schröder-van Laar equation (Equation 3.7) results, which describes the course of the liquidus line of a component in a binary system:

$$\ln(x(T)) = \frac{\Delta_F H_{T_F}}{R} \left( \frac{1}{T_F} - \frac{1}{T} \right) - \frac{\Delta_F C_p}{R} \left( \ln \frac{T_F}{T} + 1 - \frac{T_F}{T} \right) \quad (3.7)$$

Equation 3.7 is still complex, since beside the melting temperature and the melting enthalpy, heat capacity data are required. Frequently it is found that the second term in Equation 3.7 (containing the heat capacities) is negligible compared to the first term, what (with  $\Delta_F H_{T_F} = \Delta_F H$ ) leads to the simplified version of the Schröder-van Laar equation:

$$\ln(x(T)) = \frac{\Delta_F H}{R} \left( \frac{1}{T_F} - \frac{1}{T} \right) \quad (3.8)$$

Although this equation (due to the simplifications made) just applies to ideal systems, it can be used to predict the liquidus curve as a first approximation from the melting temperature and heat of fusion of the substance which are easily accessible from a DSC measurement. After calculating the liquidus lines for both components of the binary system, the eutectic composition in the phase diagram can be derived from the intersection of the two liquidus lines. To account for deviation from ideality, Equation 3.8 can be modified by re-introducing the activity coefficient  $\gamma$  replacing  $x$  by  $(x \cdot \gamma)$ .

The liquidus line (as demonstrated before) corresponds to the ideal solubility line in an arbitrary solvent and hence, allows the prediction of solubilities only as a very rough estimate.

In general, the total enthalpy of dissolution of an ionic compound in a solvent results from the contributions of the heats of melting, mixing, dissociation and solvation as energetic contributions of successive processes:

$$\Delta_S H = \Delta_F H + \Delta_{mix} H + \Delta_{dissoc} H + \Delta_{solv} H \quad (3.9)$$

However, without dissociation, in an ideal solution at infinite dilution the contributions of the enthalpy of mixing and solvation to the dissolution process can be considered to be negligible, thus giving  $\Delta_F H \sim \Delta_S H$ . Therefore, the Schröder-van Laar equation using the melting enthalpy also for solution equilibria is often a good approximation to estimate the temperature dependence of the solubility of organic substances.

The application of the simplified Schröder-van Laar equation for determination of the ideal solubility curve will be picked up in further detail in Section 3.3.2.

## 3.1.4

## Phase Diagrams of Ternary and Quaternary Systems

Applying the phase rule to a ternary system and neglecting again the pressure as variable in SLE gives  $P + F = 3 + 1$ , that is, a one-phase ternary system has three degrees of freedom. Since it is not possible to represent the effects of three variables in a ternary system on a two-dimensional plot, one often considers conditions with constant temperature. The three components can be graphically represented on a triangular diagram, which might be an equilateral triangle or a right-angled isosceles triangle, as shown in Figure 3.5a. In both cases, the apexes of the triangle represent the pure components A, B, or C. A point on a triangle side characterizes a binary system A/B, B/C, or A/C and each point inside the triangle represents a mixture of all three components A, B, and C. Any convenient concentration unit can be used to scale the axes. Most frequently, weight or mol percent or weight or mol fractions are applied. However, any point in the diagram holds  $A + B + C = 100$  or 1, using percent or fraction units, respectively. The amounts of the components are represented by the distance from the triangle sides, as indicated by the grid lines in the phase diagrams in Figure 3.5a.

Considering now this triangle to be the base of a prism and the axis perpendicular to the triangle to stand for the temperature variable, a three-dimensional representation of the ternary system is provided. Figure 3.5b shows a scheme of such a three-dimensional ternary phase diagram. Here, the three vertical faces of the prism represent the three binary systems A/B, B/C, and A/C, all being of simple eutectic type in this example. Each point below the liquidus lines inside the

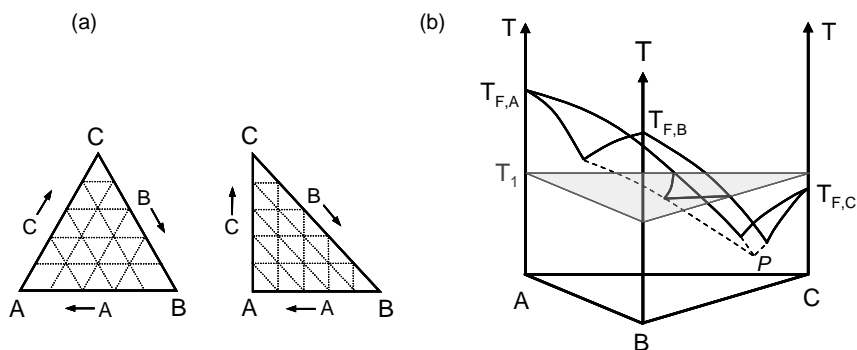


**Figure 3.5** Representation of a ternary system with components A, B, and C. (a) Triangular diagram using an equilateral triangle or a right-angled isosceles triangle. Shown are the construction of grid lines and scales. (b) Three-dimensional representation of a ternary system A, B, and C in the triangular prism. The three vertical faces of the prism characterize the three

binary systems, A/B, B/C, and A/C. The lowest temperature in the system corresponds to the ternary eutectic (P), where four phases are in equilibrium. The shaded area depicts an isothermal section at temperature  $T_1$  representing the ternary phase diagram at a given temperature.

prism represents a mixture of all three components. According to the phase rule, in maximum four phases can coexist in equilibrium leaving the system no degree of freedom. This four-phase invariant is the ternary eutectic characterizing the lowest temperature in the system where the three components as solid phases are in equilibrium with a saturated solution of eutectic composition (point *P*, Figure 3.5b). However, since it is uncomfortable to work with the three-dimensional phase diagrams, often isothermal cuts (as indicated by the shaded area in Figure 3.5b) are used to represent the SLE and their temperature dependence in a ternary system.

Analogous to ternary systems, a quaternary system can be represented in a three-dimensional prism, but having a square as prism base with the four components at the corners. An example is given in Figure 3.6a for four arbitrary components *A*, *B*, *C*, and *D*. Again, only simple eutectic binary systems *A/B*, *B/C*, *C/D*, and *A/D* are assumed. In order to simplify the interpretation of such quaternary phase equilibria, as for ternary systems, usually isothermal slices of the three-dimensional representation of the phase diagram are considered.

A special case of great industrial relevance is the examination of reciprocal salt pairs representing a quaternary system of two salts that do not share a common ion

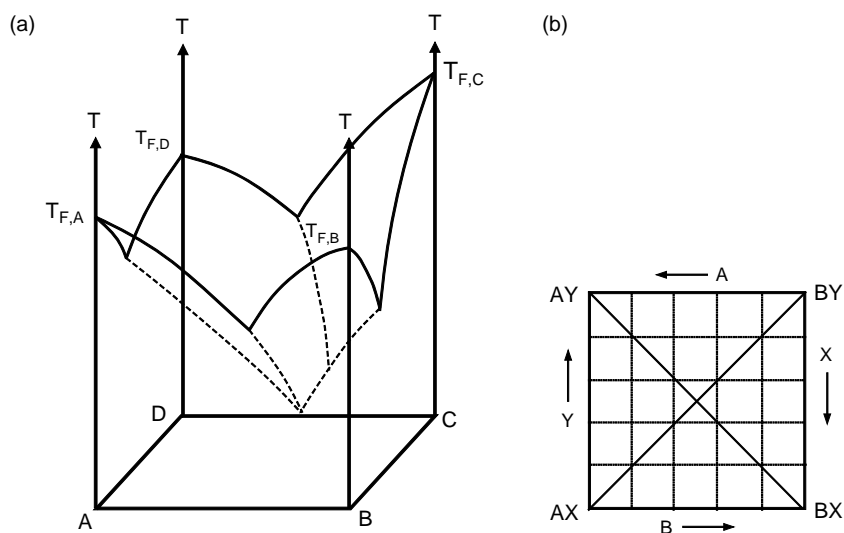


**Figure 3.6** Representation of a quaternary system in the phase diagram. (a) Three-dimensional representation of a quaternary system *A*, *B*, *C*, and *D* in the quadrangular prism (square prism base). The four vertical faces of the prism correspond to the four binary systems, *A/B*, *B/C*, *C/D*, and *A/D*. (b) Square diagram representing the reciprocal salt pairs

*AX*, *BX*, *AY*, and *BY*. Shown are the construction of grid lines and scales. As scale the amount of the particular ions is used. All mixtures of *AX* and *BY* lie on the diagonal line connecting corners *AX* and *BY*. The same applies to mixtures of *BX* and *AY*. (The water content is excluded for simplification purposes.)

in water as solvent. Examples of commercial importance are the systems  $\text{H}_2\text{O}$ ,  $\text{NaCl}$ ,  $\text{NH}_4\text{HCO}_3$  and  $\text{H}_2\text{O}$ ,  $\text{KCl}$ ,  $\text{MgSO}_4$ . Both are composed of five chemical individuals ( $\text{H}_2\text{O}$ ,  $\text{Na}^+$ ,  $\text{Cl}^-$ ,  $\text{NH}_4^+$ ,  $\text{HCO}_3^-$  and  $\text{H}_2\text{O}$ ,  $\text{K}^+$ ,  $\text{Cl}^-$ ,  $\text{Mg}^{2+}$ ,  $\text{SO}_4^{2-}$ ) but electro-neutrality as restrictive condition, thus giving a four-component system. The SLE in such systems are most preferably represented as isothermal cuts of the three-dimensional phase diagram shown schematically in Figure 3.6b. Here, the ions included in the reciprocal salt pairs are generally denoted with A and B (for the cations) and X and Y (for the anions) specifying the salt pairs to be considered as AX, BX, AY, and BY. The four salts occupy the four corners of the square diagram. The diagonal lines represent mixtures of AX and BY or AY and BX. Quantification is feasible using the lever rule.

Much more information regarding the construction of ternary and quaternary phase diagrams and also other possibilities of their representation can be obtained from the monographs [1,2]. Also, Refs [3,4] should be recommended as excellent source of fundamental knowledge on heterogeneous phase equilibria.

In Sections 3.3.7 and 3.3.8 with the cases of enantiomers and the reciprocal conversion, examples of ternary and quaternary solution equilibria of industrial importance will be discussed.

## 3.2

### Melt Phase Diagrams

#### 3.2.1

##### Types of Phase Diagrams and Their Occurrence

Which phase diagrams do occur now in binary systems depicting SLE? When looking in the appropriate literature, there is a diversity of different forms of melt phase diagrams, in particular for inorganic and metallic systems. On the other hand, much less phase diagrams are reported and described for organic substances. However, all (even complicated) phase diagrams can be reduced to a combination or a modification of several fundamental types.

In the context of binary organic mixtures, Figure 3.7 shows main types of phase diagrams together with the related frequency of occurrence.

Generally, one distinguishes between systems exhibiting immiscibility or miscibility in solid state. The first group, which represents with about 86% of the cases the main part of systems, is divided into systems with intermediate compounds (types b and c, Figure 3.7) and systems characterized by simple eutectic behavior (type a, Figure 3.7). The latter is the most frequently occurring type, to which more than half of the systems belong. A simple eutectic system has already been discussed in Section 3.1. Intermediate compounds can occur as congruently (type b) or incongruently (type c) melting compounds characterized by a dystectic invariant (open maximum) in the phase diagram or by a peritectic invariant (concealed maximum), respectively. In contrast to type b, where the

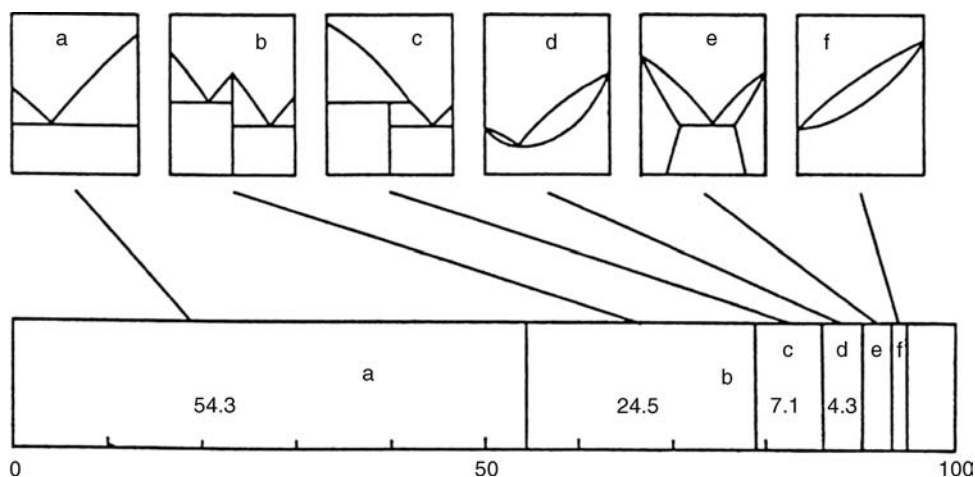


**Figure 3.7** Frequency distribution of SLE of binary organic mixtures according to Matsuoka (reproduced with permission from Ref. [5]).

intermediate compound exists in both the liquid and solid phases, in type c systems, the compound reversibly decomposes before melting giving a new solid phase and a liquid of different composition. In fact, a phase diagram of type b can be considered as a combination of two “type a” cases, both having the intermediate compound as one component in common. In cases where the intermediate compound in the liquid state (reversibly) dissociates into the single components, the peak flattens out forming only a maximum.

Miscibility in solid state, that is, the formation of solid solutions, is less frequent than immiscibility (Figure 3.7). Complete miscibility may be represented in the phase diagram by a melting point minimum (case d), a melting point maximum (not shown), or, as depicted in case f, without an extreme value. In addition, partial miscibility can occur in simple eutectic systems (e.g., type e) and also in systems with intermediate compounds. The number of such phase diagrams reported is rather rare and often partial miscibility in a system is difficult to be recognized. This might be attributed to (i) low levels of miscibility that are hardly detectable and (ii) the low mobility of molecules in solid state making equilibrium measurements almost unattainable. However, the knowledge of partial miscibility in a system is of essential importance for purification purposes since it limits the purity achievable by crystallization techniques. An example is described in Section 3.2.3.

The phase diagrams in Figure 3.7 consider only SLE. In addition, solid–solid equilibria (e.g. polymorphic phase transitions), liquid–liquid equilibria such as a miscibility gap in liquid state (liquid–liquid demixing) and also nonequilibrium phenomena (out-of-equilibrium states) can complicate melt phase diagrams and make their measurement more difficult.

## 3.2.2

**Measurement of Melt Phase Diagrams****3.2.2.1 Methods**

Melt phase diagrams can be determined using different methods of thermal analysis. Here, a substance is subjected to a controlled temperature program and a physical or physicochemical property of this substance is measured as a function of temperature.

Table 3.2 comprises main methods of thermal analysis relevant for melt phase equilibria together with the related properties followed. Apart from techniques of thermooptical analysis (TOA) that allow a qualitative or semiquantitative evaluation of the melting behavior, differential scanning calorimetry (DSC) is the most essential method to establish the binary phase diagram by providing the required detailed quantitative information. Whether one measures temperature ( $\Delta T$ ) or directly energy differences ( $\Delta H$ ) to quantify a thermal effect, one distinguishes between heat flux calorimetry and power compensation calorimetry. The most common technique is heat flux DSC due to its simplicity and its ability to work also with bigger sample amounts, which is preferred for heterogeneous mixtures and heat capacity measurements. Thermogravimetry (TG), favorably coupled with a simultaneous DSC measurement (TG-DSC), is capable to quantify and to assess mass changes of a system as function of temperature and, as TG-DSC version, to assign mass changes to particular thermal effects. Thus, it is possible to clearly identify, for example, phase transitions where the mass remains constant and degradation or dehydration processes that are connected with a mass loss. X-ray powder diffraction (XRPD) is a very powerful tool for solid-phase analysis and as temperature-resolved technique capable to directly relate a phase transition to the solid phases present. It supports the study of melt phase diagrams by gaining direct access to polymorphic transitions, the formation of solid solutions, cocrystals, and in case of solution equilibria to solvates.

**Table 3.2** Main methods of thermal analysis and related properties measured for studying the melting behavior of pure substances and mixtures.

Parameters measured	Methods
Optical properties (e.g. light transmission)	TOA (thermomicroscopy (Kofler hot-stage method), thermophotometry)
$\Delta H$ ( $\Delta T$ )	DSC, TMDSC, Rcal, DTA
Crystal lattice properties	Temperature-resolved XRPD
Mass loss	TG

Coupled techniques are also possible allowing simultaneous measurement of the properties of interest, for example, XRPD-DSC or TG-DSC.

TOA, thermooptical analysis; DSC, differential scanning calorimetry; TMDSC, temperature-modulated DSC; Rcal, reaction calorimetry; DTA, differential thermal analysis; XRPD, X-ray powder diffraction; TG, thermogravimetry.

### 3.2.2.2 DSC and How to Measure and Interpret DSC Data

As DSC is the essential method for quantifying SLE for melt phase diagrams, it should be briefly introduced. DSC provides quantitative information about exothermal and endothermal events occurring within the sample as a function of temperature and/or time. It uses the differential principle, that is, measuring the difference of the heat flux between a sample S and a suitable reference R. In an experiment, S and R are subjected to the same programmed temperature profile, while continuously detecting the temperature difference between them.

With a linear temperature versus time program (Figure 3.8), as long as no thermal event occurs, both the sample and the reference temperature increase with same slope. Due to heat capacity differences of reference and sample, there might be a small but constant deviation between  $T_R$  and  $T_S$ , as shown in Figure 3.8. As reference, an inert material that must not undergo any thermal transformation within the applied temperature range is used, such as alumina or air. Since the reference steadily follows the temperature program, the sample temperature deviates in case a thermal effect occurs. For melting as an endothermal effect, it lags behind the reference temperature (Figure 3.8). After finalized phase transition,  $T_S$  again follows the temperature program. Plotting the temperature difference or the corresponding heat flow, HF, versus time or temperature, a peak characterizing the melting process of the sample arises. As per definition, the peak onset temperature  $T_{on}$  determined from the intersection of the extrapolated (initial) base line and the extrapolated leading edge of the melting effect is taken as the melting temperature  $T_F$  of a substance. From the area enclosed by the DSC curve, the corresponding melting enthalpy can be derived. The peak maximum temperature  $T_{max}$  denotes the

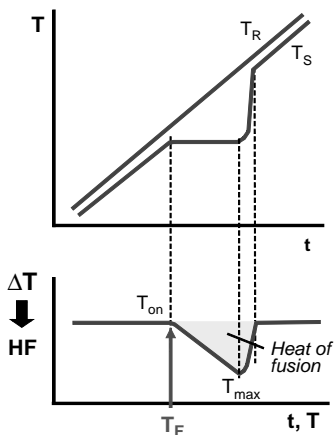


**Figure 3.8** Measurement of DSC curves and derivation of the melting temperature  $T_F$  of a pure substance from the peak onset. The heat flow HF is calculated from the calorimetric

factor  $K$  as provided from the instruments calibration, and the temperature difference  $\Delta T(t) = T_S(t) - T_R(t)$  according to  $HF(t) = K \cdot \Delta T(t)$ .

end of melting, and hence specifies the liquidus temperature  $T_{\text{Liquidus}}$  of a mixture of particular composition.

In the context of a hypothetical binary system, Figure 3.9 illustrates how the liquidus and solidus lines in the phase diagram can be derived from DSC plots of different mixtures of the two components. In the lower part of the figure, the phase diagram of the system is given; in the upper part, the DSC curves of particular compositions are shown together with the derived liquidus line.

Four examples indicated in Figure 3.9 shall demonstrate how such DSC curves can be interpreted. As already discussed, single peaks are always provided from a system in invariant state such as melting of a pure substance or an eutectic phase transition. Such cases are obtained with DSC curves D and E (cases 1 and 2). Since D refers to the lowest temperature measured in the system, it can be related to an eutectic invariant at  $T_{\text{eu},2}$ . DSC curve E characterizes the melting of a single

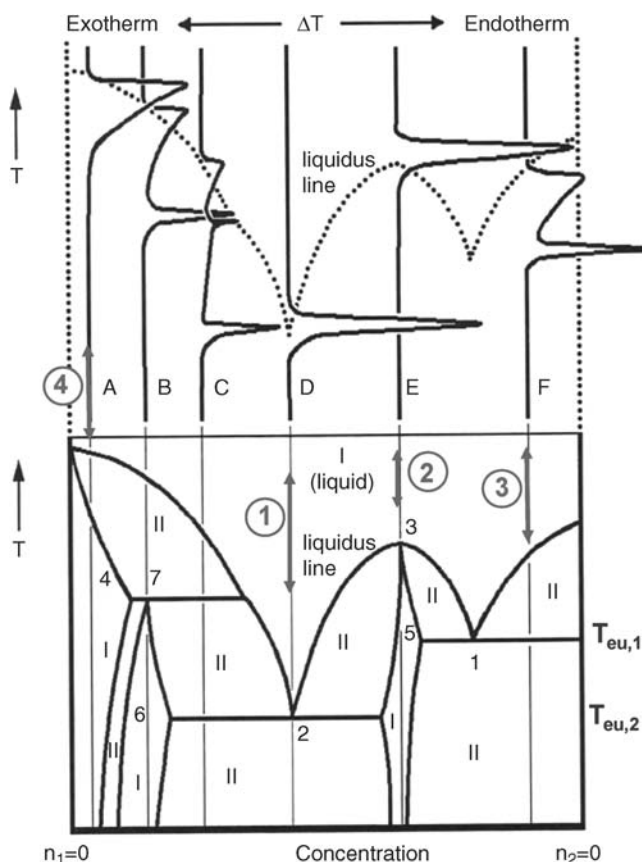


**Figure 3.9** DSC curves providing composition–temperature data to derive the phase diagram for a hypothetical binary system (reproduced with permission from Ref. [6]).



substance, which is the congruent melting of a nonstoichiometric intermediate compound. Case 3 specifies a composition close to pure component 1. The appropriate DSC curve F exhibits first a sharp peak followed by a broad thermal effect. The peak can be assigned to an eutectic at a temperature  $T_{\text{eu},1}$ , the subsequent broad effect to the dissolution of the excess component 1 in the melt, thus giving both  $T_{\text{eu},1}$  and  $T_{\text{Liquidus}}$  for the selected composition. Case 4 in Figure 3.9 represents a mixture close to pure component 2 of the system and just one broad peak is obtained in the DSC curve. It characterizes progressive melting of a solid solution with always two phases present in a binary and thus monovariant system. The onset and the peak maximum of the thermal effect mark the position of the solidus and liquidus lines.

For correct interpretation of DSC curves usually, complementary methods (such as TG, TOA, XRPD, Raman, or IR spectroscopy) must be applied, for example, to recognize decomposition effects and to correctly assign a thermal event to the phases present.

The success of DSC measurements depends on careful sample preparation and selection of adequate measurement conditions. To ensure close-to-equilibrium conditions, low heating rates and low amounts of finely dispersed sample material should be used. To account for thermal lag effects, a separate temperature calibration at each scan rate is recommended. Helium or nitrogen as purge gas at defined flow rate should be applied.

A critical point to be emphasized is the preparation of mixtures, which seems to be easy but in fact is really not a trivial task. Usually, simply grinding the components together in a mortar is not sufficient to provide equilibrated, molecularly dispersed mixtures as required to study phase equilibria. Figure 3.10 exemplarily shows XRPD patterns of differently prepared samples of the tartaric acid enantiomers compared to the pattern of just one enantiomer. For this system, it is known that at the 1 : 1 composition in the phase diagram, an intermediate compound (a so-called racemic compound, see Figure 3.10) is present, which exhibits a different crystal lattice and thus must provide an XRPD pattern different from the enantiomer one. As obvious, the pattern (b) representing a 1 : 1 mixture of the two tartaric acid species grinded together matches the pattern of the enantiomer. Hence, during grinding, no alloying connected with formation of the intermediate compound occurred. Contrarily, sample preparation via dissolution, solvent evaporation, and a final grinding provides the racemic compound (pattern (c)) as expected. Thus, misleading results might be derived from an inadequate sample preparation. The same problem applies to systems with solid solutions.

To our experience, samples should always be prepared via the liquid phase, that is, whether via melting and annealing the solidified melt (preferably close to the phase transition temperature), or via dissolution and recrystallization from an appropriate solvent. Melting is of course feasible only in case the substance does not undergo any degradation. When recrystallizing from a solvent (e.g., by slow evaporation of solvent or freeze-drying), care must be taken with regard to potential solid-state transformations such as solvate formation or polymorphic phase transitions.

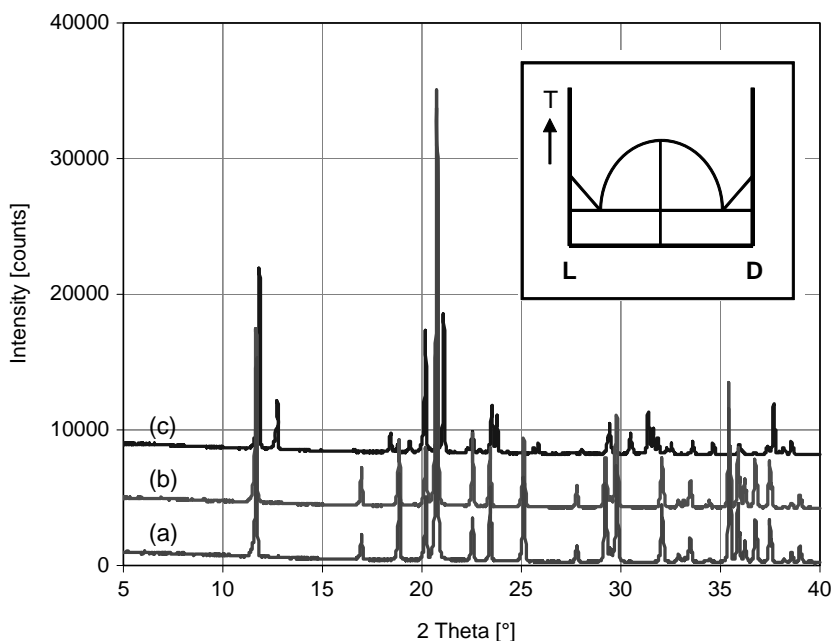


**Figure 3.10** XRPD patterns for differently prepared samples of the tartaric acid enantiomers. The figure illustrates the influence and the importance of an adequate sample preparation procedure for subsequent DSC measurements. (a) L-tartaric

acid, (b) 1:1 mixture of L- and D-tartaric acids grinded together, (c) 1:1 mixture of L- and D-tartaric acids prepared via dissolution and recrystallization from water or acetone as solvent.

### 3.2.3

#### Example of a Diastereomeric System

The example to be represented refers to a binary system of two epimers ( $\alpha$  and  $\beta$ ) of a diastereomeric pharmaceutical intermediate. The epimers are obtained as an 1:1 mixture from chemical synthesis and have to be separated. The chemical formula is not of significance for discussion of the results.

The phase diagram derived from comprehensive DSC measurements is shown in Figure 3.11. The system is of simple eutectic type with an eutectic composition at a mol fraction of about 0.4  $\alpha$ . The melting temperature of 122.1 °C of the  $\alpha$ -epimer exceeds the melting temperature of 110.5 °C of the  $\beta$ -isomer. The same applies to the melting enthalpies obtained with 100.3 and 91.4 J/g, respectively. Symbols indicate measurement data for the liquidus and solidus curves. Furthermore, the liquidus lines were calculated using the simplified Schröder–van Laar equation (Equation 3.8) with the melting data of the  $\alpha$ - and  $\beta$ -epimers. Their intersection does not perfectly match the experimentally determined eutectic temperature. A better agreement is achieved when an average melting enthalpy of 87.8 J/g as obtained for all mixtures on the  $\alpha$ -side is applied (dashed liquidus line in Figure 3.11). This is a simple way of accounting for

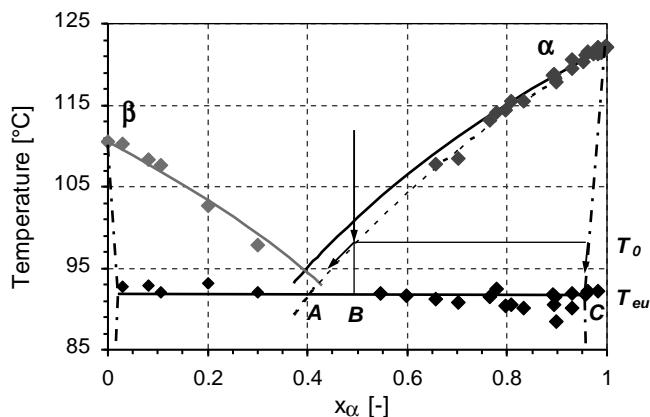


**Figure 3.11** Melt phase diagram of the  $\alpha$ -/ $\beta$ -epimers. Arrows illustrate cooling of a melt of an 1:1 mixture of the epimers. (Reproduced with permission from Ref. [17].)

the temperature dependence of the melting enthalpy (neglected in Equation 3.8) that has often proved to be a more suitable approximation to reality.

Figures 3.12 and 3.13 depict DSC curves and XRPD patterns of selected mixtures of the two epimers close to the  $\alpha$ -side in the phase diagram. The missing eutectic melting in presence of 4.8%  $\beta$  in  $\alpha$  (curve 2, Figure 3.12) indicates partial miscibility in the solid state of  $\beta$  in  $\alpha$ , which is supported by the XRPD results (Figure 3.13). First clear reflections of the  $\beta$ -epimer appear in mixtures containing 7%  $\beta$ , that is, 93%  $\alpha$ . Furthermore, a high-resolution measurement with eight times longer measurement time indicates only trace amounts of the  $\beta$ -phase in the 95.2%  $\alpha$  sample. However, as shown in the phase diagram, sometimes even in presence of less than 5%  $\beta$ , an eutectic effect was observed. Thus, not always perfectly equilibrated solids could be afforded, although all samples were prepared via similar dissolution and slow recrystallization or freeze-drying procedures. A more adequate evaluation of miscibility in solid state can be done via construction of a Tammann graph, plotting the heats of fusion of the eutectic effects in the DSC curves ( $\Delta_F H_{eu}$ ) versus the composition, as shown in Figure 3.14. The  $\Delta_F H_{eu}$  value is highest at the eutectic composition and decreases linearly to both sides of the phase diagram. The intersections with the  $x$ -axis (i.e.,  $\Delta_F H_{eu} = 0$ ) specify the boundaries of solubility in solid state.

Both epimers form solid solutions with the respective other one, with limits of miscibility of  $\sim 5\%$   $\beta$  in  $\alpha$  and  $\sim 3\%$   $\alpha$  in  $\beta$ . These boundaries will limit the depletion of the unwanted component by crystallization.

When cooling a melt of an 1:1 mixture of the epimers, at  $T_0$  (Figure 3.11) first  $\beta$ -rich  $\alpha$ -mixed crystals are formed with a composition defined by the corresponding tie line. On further cooling, the composition of the  $\alpha$ -mixed crystals and the melt alter along the solidus and liquidus lines as indicated by arrows. At the eutectic temperature  $T_{eu}$ , a crystalline phase of composition C and amount A–B will be in equilibrium with a melt having eutectic composition A of amount B–C.

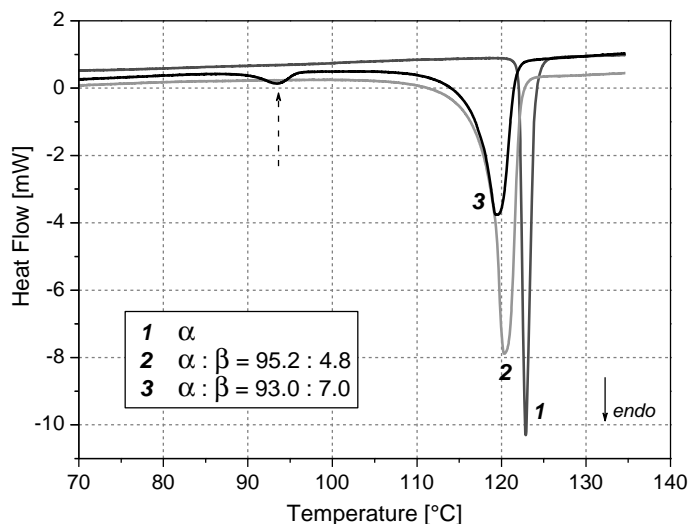


**Figure 3.12** DSC curves of the pure  $\alpha$ -epimer and two mixtures with high  $\alpha$ -content. Shown is the heat flow as function of temperature. The eutectic melting peak is indicated by an arrow (measurement conditions: scan rate 1 K/min, sample mass 7.8/21.4/ 15.6 mg, DSC 111, Setaram). (reproduced with permission from Ref. [17]).

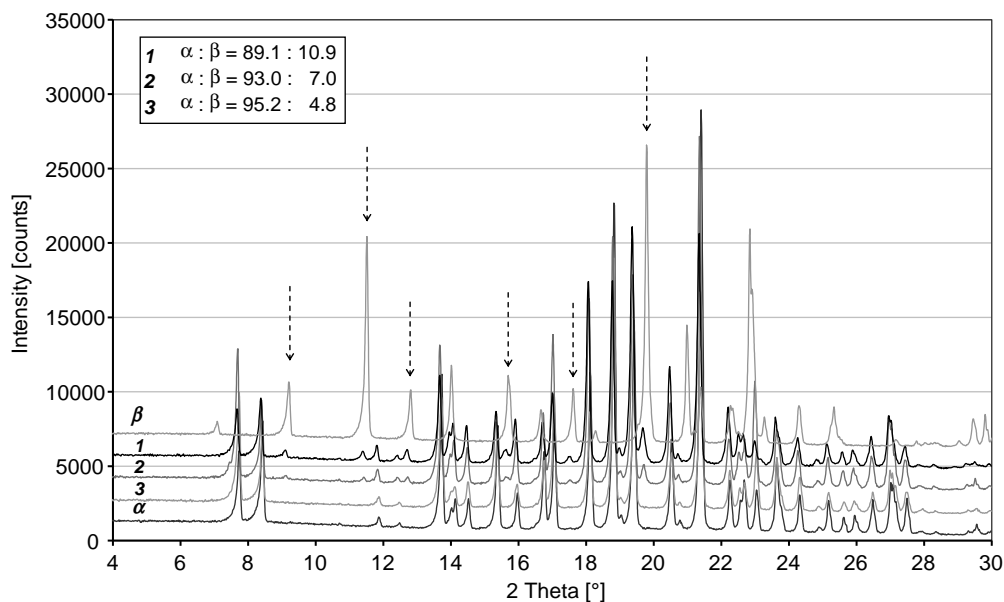


**Figure 3.13** XRPD patterns of the pure epimers and mixtures highly enriched with  $\alpha$ . The samples were prepared by slow crystallization from solution. Arrows indicate typical diffraction peaks of the  $\beta$ -epimer to facilitate their recognition in mixtures

(measurement conditions:  $\sim 10$  mg sample on a background-free sample holder, X'Celerator detector, Cu-K $\alpha$  radiation, step size 0.017°, time per step 50 s, diffractometer X'Pert Pro, PANalytical GmbH). (reproduced with permission from Ref. [17]).

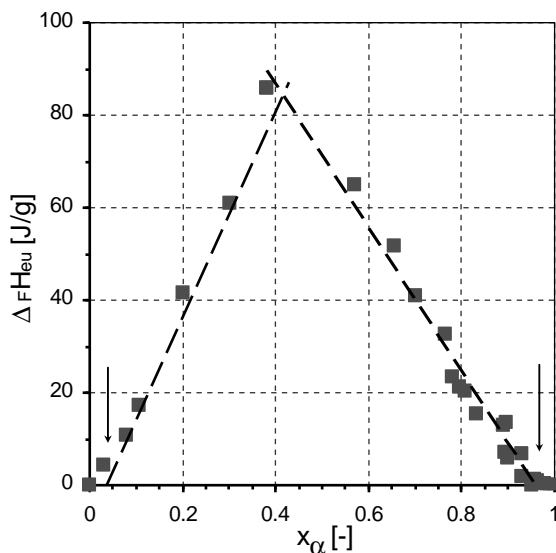


**Figure 3.14** Tammann plot of the heats of fusion of the eutectic effect,  $\Delta_f H_{eu}$ , as function of the composition. Arrows indicate the boundaries of solubility in solid state. (reproduced with permission from Ref. [17]).

Thus, purity demands of  $>99\%$  as often required for fine chemicals cannot be fulfilled here in one crystallization step. As will be described in Chapter 7, fractional crystallization is capable to further (stepwise) deplete the unwanted component in the product to the expense of yield.

### 3.3

#### Solution Equilibria

##### 3.3.1

##### Solubility and Concentration Units

The maximum amount of a solid that can be dissolved in a particular solvent (or solvent mixture) at a given temperature and pressure, that is, the (equilibrium) saturation concentration, is denoted solubility. Since the pressure dependence is usually small, it is normally neglected, as already discussed in Section 3.1.3. A solution is saturated when the solute concentration is at its solubility limit. For clarification purposes, the specific terms connected with the preparation of a solution from a solid and a solvent are illustrated in Figure 3.15.

Different units are in use to express the solubility of a given substance such as weight percent (grams solute in 100 g solution), mass or mol fraction ( $w_i$  or  $x_i$ , grams/mols solute per grams/mols solution), grams solute per 100 g solvent, grams

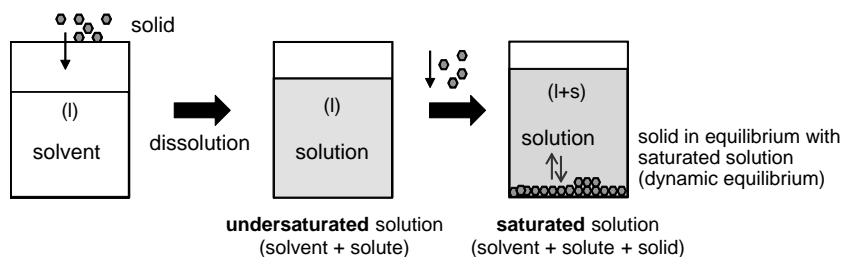


**Figure 3.15** Terms in use for solution equilibria.

solute per volume (liter) solution or solvent, or mol solute per 1000 mol solvent. The choice of the unit often depends on the application, for example, the latter one is often used in connection with hydrates/solvates or reciprocal salt pairs. In general, care should be taken when using data from different sources since the reference medium (solvent or solution) might be different. Furthermore, for interconversion between different composition units, it is recommended to have the density measured at the relevant temperature, in particular when volume-related units are applied. Figure 3.16 gives a measure of the magnitude of potential misinterpretation when mixing different units or not correctly specifying the unit (or solid). The example shows several possibilities to express a solution concentration of 10 g sodium sulfate in 100 g water. When using hydrates (or generally solvates), the solvent content in the solvate has to be considered in preparation of a solution.

### 3.3.2

#### Solubility Curves of Inorganic and Organic Substances

The graphical representation of the temperature dependence of solubility is called solubility curve. It provides information about the solubility of a substance in a particular solvent at different temperatures, and thus is of fundamental importance for development of crystallization processes. For a cooling crystallization, from the solubility difference in the temperature region covered, the possible yield can be determined. As depicted before, the solubility curve of a specific substance A

**Different units to express a solution concentration of 10 g  $\text{Na}_2\text{SO}_4$  in 100 g water**  
(Substance available as anhydrous  $\text{Na}_2\text{SO}_4$  and Glauber's salt ( $\text{Na}_2\text{SO}_4 \cdot 10 \text{H}_2\text{O}$ ))

- 9.1 g  $\text{Na}_2\text{SO}_4$  / 100 g solution = 9.1 wt%
- 12.7 mol  $\text{Na}_2\text{SO}_4$  / 1000 mol  $\text{H}_2\text{O}$
- 0.7 mol  $\text{Na}_2\text{SO}_4$  / 1000 g  $\text{H}_2\text{O}$
- 26 g  $\text{Na}_2\text{SO}_4 \cdot 10 \text{H}_2\text{O}$  / 100 g  $\text{H}_2\text{O}$
- 20.6 g  $\text{Na}_2\text{SO}_4 \cdot 10 \text{H}_2\text{O}$  / 100 g solution

**Figure 3.16** Application of different units to express a certain solution composition.

represents the liquidus line in the binary phase diagram A-solvent. Thus, it also provides information about the possible phases crystallizing at a particular temperature such as solvates or certain polymorphs.

### 3.3.2.1 Inorganic Substances

In Figure 3.17, examples of solubility curves of selected inorganic substances in water as solvent are depicted. As can be seen, different types of solubility-temperature relationships are possible. First, the solubility can strongly increase with temperature as observed for potassium nitrate. Rather smooth increasing solubilities are found for potassium chloride, while the solubility of sodium chloride in water is almost independent of temperature. The absolute solubility values are rather high as expected for those salts in water. However, solubility can vary widely, even over several orders of magnitude. For example, the solubilities of calcium nitrate and calcium chloride respectively are 129 and 74.5 g anhydrous salt per 100 g water (at 20 °C), while calcium sulfate as a sparingly soluble salt has a solubility of 0.2 g per 100 g water (i.e., about 500 times lower).

The solubility behavior of acids, bases, and their salts is characterized by a significant dependence on the pH value. Typical solubility as a function of pH profiles result, which is of particular importance for pharmaceutically relevant salts.

Not all solubility curves behave steadily as observed for sodium carbonate and sodium sulfate (Figure 3.17). At a certain temperature, the slope of the solubility

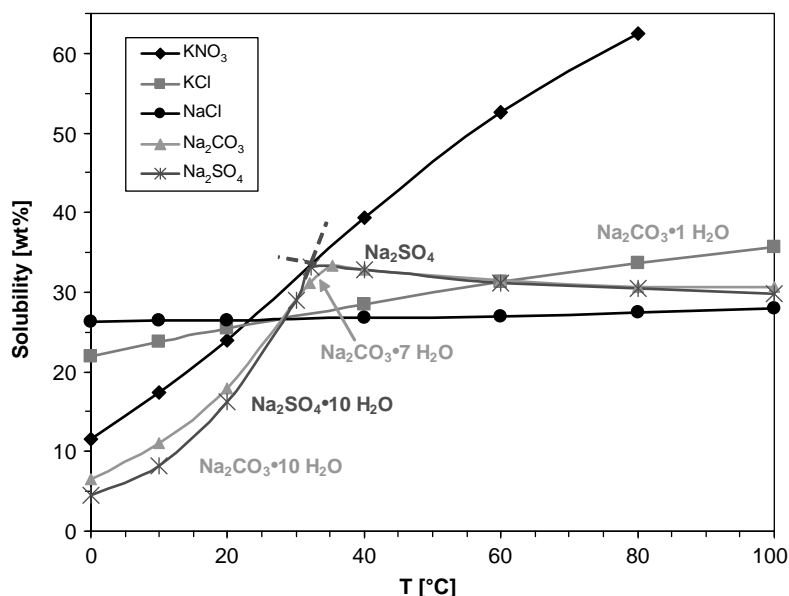


**Figure 3.17** Solubility curves of selected inorganic salts in water. The solubility is given in weight percent. The phases added specify the solid phase in equilibrium with the saturated

solution. Dashed lines exemplarily constructed for the sodium sulfate case represent metastable solubility lines.

curve reverses. While the solubility increases at low temperatures, at higher temperatures the so-called retrograde solubility occurs. A discontinuity in the solubility curve always denotes a phase change caused, for example, by solvate or polymorphic transitions. This means that above and below the phase transition temperature, different solid phases appear. For sodium sulfate, the low-temperature phase is the decahydrate (Glauber's salt). At temperatures exceeding the transition temperature of 32.4 °C, the anhydrate is the stable solid phase crystallizing from aqueous solutions. In the case of sodium carbonate between the decahydrate and the monohydrate, an additional phase, the heptahydrate, exists in the temperature region between the two transition temperatures of 32 °C and 35.3 °C. In fact, the solubility curve depicted for sodium carbonate is not just one, but represents three solubility curves each belonging to a particular solid phase that intersect at the transition temperatures. Extrapolated lines characterize metastable solubility curves that can be of importance for special crystallization processes using metastable equilibria for kinetically driven separations.

The general trend of a solubility curve can be derived from the Le Chatelier's principle considering the dissolution process as a reaction of breaking and forming new bonds, such as breaking ionic bonds in an ionic crystal (of a salt) and formation of (weak) electrostatic ion–dipole interactions due to hydration of the ions, for example, according to



The appropriate reaction enthalpy is the solution enthalpy. In case of an endothermal solution enthalpy, the equilibrium shifts with higher temperature to higher solubilities, and thus results in a positive slope of the solubility curve. On the other hand, an exothermal dissolution process leads to a retrograde solubility behavior. In most cases, the heat of solution is positive, that is, most substances dissolve with absorption of heat. This means that the (positive) lattice enthalpy exceeds the (negative) solvation enthalpy or more energy has to be spent to break the lattice than is evolved by solvation.

As discussed before, the temperature dependence of ideal solubility can be expressed by the simplified Schröder–van Laar equation (Equation 3.8) (Section 3.1.3). It allows the prediction of solubilities only from DSC melting data of the compound of interest. However, often the application of the solution enthalpy in an infinite diluted solution ( $\Delta_s H_\infty$ , the so-called first heat of solution) gives better approximation to the real case. For most inorganic substances, this value is known and can be extracted from databases; for organic compounds, less is reported and measurements are necessary. Since these are time- and substance-consuming, the application of the melting enthalpy quickly available from a DSC scan is always helpful to have a first rough estimate of the solubility curve.

Since Equation 3.8 is a logarithmic function, it is recommended to plot the logarithm of the solubility in mol fraction as a function of the reciprocal temperature, as illustrated in Figure 3.18.



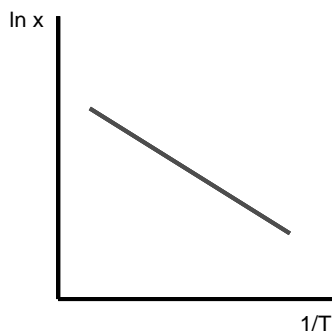


**Figure 3.18** Linearization of the simplified Schröder–van Laar equation (Equation 3.8) to evaluate the temperature dependence of solubility (van't Hoff plot).

Here, the most frequent cases where solubility increases with temperature are shown. It becomes clear that when applying the melting enthalpy in Equation 3.8, a negative slope of the line always results, implying a positive slope of the solubility curve. Thus, retrograde solubility can only be explained with the solution enthalpy that can possess negative values.

To relate now the solution enthalpy to the slope of solubility curves, in Table 3.3 the  $\Delta_s H_\infty$  values are compiled for selected salts included in Figure 3.17. The steep increase of the solubility curve of potassium nitrate correlates with its comparatively high-positive solution enthalpy. Consistently, the weak (positive) temperature dependence of the sodium chloride solubility is expressed by a low (also positive)  $\Delta_s H_\infty$  value. Negative solution enthalpies occur for anhydrides of salts forming stable hydrates at room temperature (such as sodium sulfate and sodium carbonate) where hydration is connected with a strongly exothermal effect.

### 3.3.2.2 Organic Substances

Retrograde solubility also occurs for organic substances. Examples are sulfaguandine and sparteine, a complicated natural product, both in water. Discontinuities in the solubility curve originating from polymorphic phase transitions are observed for enantiotropically related polymorphs. The transformation of one polymorph to the

**Table 3.3** Solution enthalpy in an infinite diluted solution ( $\Delta_s H_\infty$ ) for selected salts in water.

	$\Delta_s H_\infty$ (kJ/mol)
$\text{Na}_2\text{SO}_4$	−1.2
$\text{Na}_2\text{SO}_4 \cdot 10\text{H}_2\text{O}$	78.3
$\text{Na}_2\text{CO}_3$	−23.4
$\text{Na}_2\text{CO}_3 \cdot 10\text{H}_2\text{O}$	67.8
$\text{NaCl}$	3.9
$\text{KNO}_3$	36.0

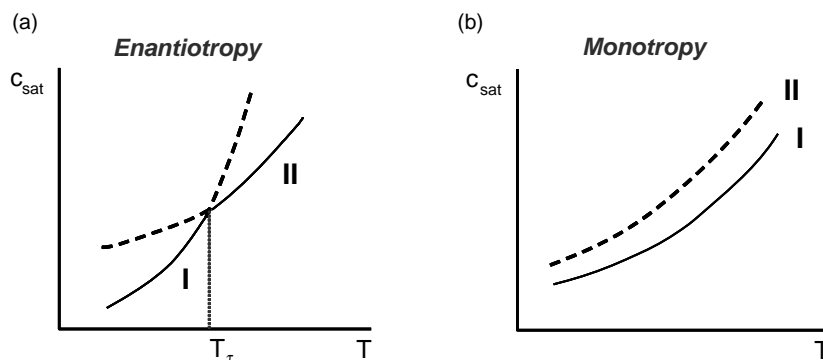


**Figure 3.19** Solubility curves in case of polymorphism. Enantiotropic phase transitions occur reversibly at the phase transition temperature  $T_\tau$  leading to a kink in the solubility curve (a). In case of monotropy (b), one of the

phases is always metastable with respect to the other one (form II with respect to form I), resulting in solubility curves that do not intersect ( $c_{\text{sat}}$ , saturation concentration).

other is reversible and occurs at the phase transition temperature  $T_\tau$  (Figure 3.19a). In contrast, the solubility curves of monotropic forms do not intersect. Independent on temperature one of the two polymorphs is always metastable with respect to the other and thus characterized by higher solubilities (Figure 3.19b). For more details, refer to Chapter 5.

In Figure 3.20, solubility curves of a certain pharmaceutical intermediate in different organic solvents and solvent mixtures are shown. They are presented together with the ideal solubilities in a van't Hoff plot. The linearization is fulfilled, and the R-squared value (or the coefficient of determination) is always  $>0.99$ . Some solubilities exceed the ideal line, some fall below. The solubility in ethylacetate matches almost the ideal values; addition of heptane lowers the solubility successively. The slopes of the real solubility lines seem to deviate not that much from the ideal case. However, the solution enthalpies derived from the curves slope vary between 23.1 and 37.1 kJ/mol compared to 41 kJ/mol for the melting enthalpy of the pure compound.

### 3.3.3

#### Solvates, Polymorphs, and Cocrystals

In solute–solution systems, often solvates occur as solid phases. In solvates, the solvent is part of the crystal structure, that is, coordinated in or accommodated by the crystal structure, thus representing a single phase. According to the differences in the crystal structure, solvates and the appropriate unsolvated solid exhibit different physicochemical properties such as melting point, solubility, dissolution behavior, processability, and stability.

Sometimes the terms solvate and polymorph are mixed, which probably happens due to their behavior with respect to properties. However, both fall in different categories, as shown in Figure 3.21. Polymorphism always occurs in a unary system.

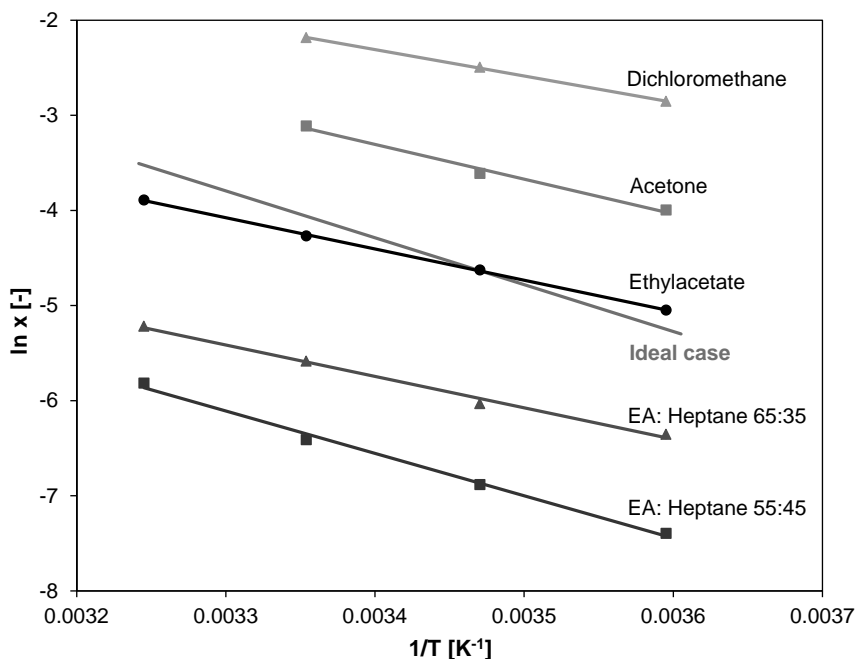


**Figure 3.20** Solubility curves of a pharmaceutical intermediate in different solvents presented as a van't Hoff plot. The ideal solubility curve was

calculated using the simplified Schröder–van Laar equation and the melting data of the substance (EA, ethylacetate).

Different polymorphs are just different crystalline forms of the same chemical compound having same chemical formula. Thus, they are all represented on the pure compound side of the phase diagram (Figure 3.21b). Contrarily, solvates refer to the binary system of a compound and a solvent and, therefore, are represented as intermediate compounds between the pure compound and the solvent in the phase diagram (Figure 3.21a). Hence, they differ in chemical formula. Each solvate may have own polymorphic forms (of same chemical formula), which then again belong to the unary system of the intermediate compound.

As already introduced, phase transitions between different solvates or between a solvate and the unsolvated compound as well as polymorphic transformations can be recognized by discontinuities in the solubility curves. Examples are shown in Figure 3.21 with several hydrates and a couple of enantiotropic phase transitions occurring in the  $\text{Mg}(\text{NO}_3)_2/\text{H}_2\text{O}$  and  $\text{NH}_4\text{NO}_3/\text{H}_2\text{O}$  systems, respectively.

Cocrystals are intermediate compounds of (two or more) discrete neutral molecular species that are, in their pure forms, solids at ambient temperature. This distinguishes cocrystals from solvates where one of the constituents of the intermediate compound is a solvent that is liquid at ambient temperature. As

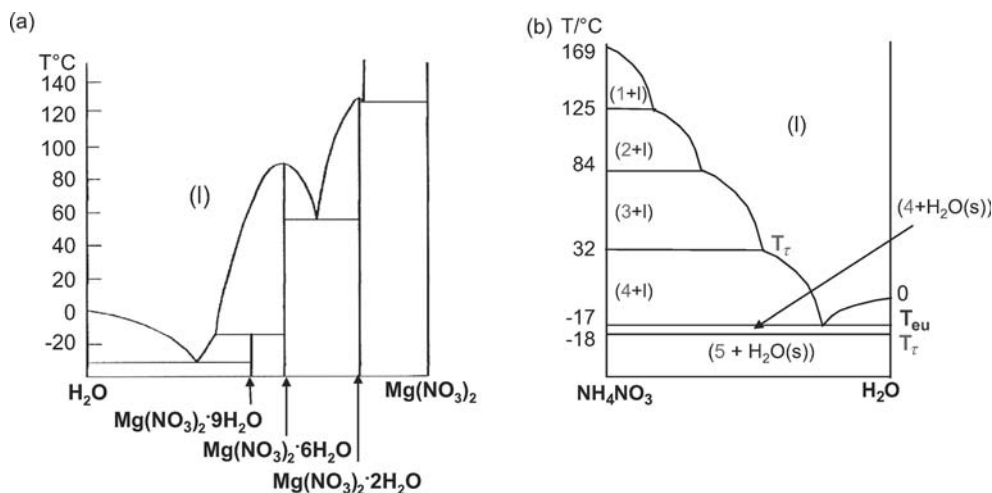


**Figure 3.21** Solvates (a) and polymorphs (b) characterized by their solubility curves in water. The phase diagrams of  $\text{Mg}(\text{NO}_3)_2/\text{H}_2\text{O}$  and  $\text{NH}_4\text{NO}_3/\text{H}_2\text{O}$  are depicted in (a) and (b), respectively. Solvates are indicated by vertical lines in the binary system, thus characterizing intermediate compounds that can melt congruently or incongruently. In the case shown, different hydrates of magnesium nitrate containing 2, 6, and 9 mol water in the crystal

lattice occur. Each hydrate has its own solubility curve represented as the appropriate liquidus line in the phase diagram. Polymorphs have one vertical line in the point of origin in common. The existence regions are bordered by horizontal lines starting from the pure component side specifying the phase transition temperatures of the particular polymorphs,  $T_{\tau}$  (1, 2, . . . 5, polymorphs of ammonium nitrate) (figures according to Refs [3,4]).

intermediate compounds, cocrystals are structurally homogeneous crystalline substances that contain the building blocks in discrete stoichiometric amounts. Thus, they are represented in the phase diagram similar to solvates. Since the building blocks are neutral molecular species, cocrystals are no salts. In the last years, cocrystals as a particular solid-state form have become an increasingly popular issue in the pharmaceutical industry, since they offer an opportunity to improve and tailor the physicochemical characteristics of drugs, such as solubility, shelf life, dissolution rate, and bioavailability. A modification in solubility can, for example, facilitate crystallization at decreased concentration below the solubility of the single components and, therefore, working with cocrystals can be the answer of certain crystallization-based separation problems. An example was recently demonstrated in Ref. [7] with the case of product removal in fermentation processes using cocrystallization as separation technique.

### 3.3.4

#### Influence of Solvents and Impurities

The choice of the solvent plays an important role in crystallization processes. The solute to be crystallized should be readily soluble in the solvent and it should be

easily crystallized from the solution as the desired phase (i.e., polymorph, solvate, or cocrystal). Even if there are many exceptions from the often quoted rule “like dissolves like,” it can generally be used as a rough guide. Based on the kind of intermolecular bonding interactions, solvents can be classified into three main groups: (i) polar protic solvents (such as water and methanol), (ii) dipolar aprotic (e.g., acetonitrile), and (3) nonpolar aprotic solvents (e.g., hexane and benzene). The solvent most often used is water due to its distinct solvent properties and, from application-oriented view, as it is readily available, cheap, and harmless. It is the preferred solvent for crystallization of inorganic compounds and whenever feasible also for organic substances.

Sometimes mixed solvents, that is, mixtures of two or more solvents, show more favorable solution properties for a particular solute than just one solvent. Therefore, like temperature, the solvent composition is a common variable in designing a crystallization process. In antisolvent crystallization, the application of an additional solvent (antisolvent) is targeted to the reduction of the solubility of a substance in order to cause its crystallization.

The solubility characteristics of a given substance in a solvent chosen have considerable influence on the selection of a suitable crystallization technique. In case of a weak solubility–temperature relationship, (as e.g. for NaCl) cooling crystallization is of course not the method of choice. Otherwise, when the solubility curves of two compounds differ significantly, these specific characteristics can be used for separation. For example, in the well-known hot leaching process, potassium chloride as target compound is separated from its mixtures with sodium chloride using the differences in the solubility functions (Figure 3.22).

Impurities can also affect the solubility of a solute of interest. Here, both a solubility enhancement and a solubility decrease occur. When electrolytes are involved, the terms salting-in and salting-out apply. Small impurity contents might be evaluated together with the solvent. In presence of higher impurity contents or in cases where the impurity is readily available in sufficient amounts, it should be considered as a third component in the system. Then, SLE data in the ternary system of the target compound, the impurity, and the solvent/solvent mixture have to be measured and instead of a binary a ternary (solubility) phase diagram applies. The representation and application of ternary SLE will be addressed in Section 3.3.7 on the example of enantiomers.

Solutions containing just one solute are usually “synthetic” solutions, that is, produced by dissolving a pure solid in a pure solvent. Even then measured solubilities can vary since the solid substance could originate from diverse batches and, therefore, be of different purity. Most industrial crystallization processes involve solutions with impurities and both their identity and content might vary, for example, due to alterations in the production process or the heterogeneous composition of ores as starting material. Therefore, it is desirable to know the solubility of a given solute in the actual working solution with the impurities present and it is very unlikely that such data are available in the literature.

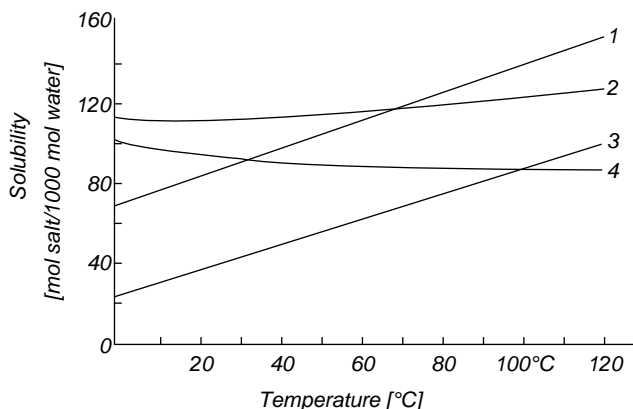


**Figure 3.22** Solubility curves of KCl and NaCl in water (lines 1 and 2) and in saturated solutions of the other salt (KCl in NaCl-saturated solution and NaCl in KCl-saturated solutions (lines 3 and 4)). The figure illustrates both the influence of a further compound (considered as impurity) on solubility of a certain substance and the application of different solubility behaviors for separation purposes. The solubility of both KCl and NaCl decreases in the presence of the other salt. Furthermore, contrary to the solubility curve of

KCl in a NaCl-saturated solution that still increases with temperature, NaCl shows retrograde solubility in KCl-saturated solutions (lines 3 and 4). This particular solubility behavior is used in the so-called hot leaching process to separate KCl and NaCl from sylvinite crude salts. It is obvious from the solubility curves that cooling a solution saturated with both salts (point of intersection of lines 3 and 4 at about 100 °C) leads to selective crystallization of KCl as target compound. (Reproduced with permission from Ref. [8].)

### 3.3.5

#### Measurement of Solubilities and Corroboration

There is no single method that is generally the optimal one for all types of systems. The most suitable method for a given system depends on various subjects such as available amount of substance (which is often a limiting factor during early development stages), kind of solvent (e.g., very viscous solvents cause difficulties with stirring or are hard to evaporate), required analytical techniques, or necessity of additional solid-phase characterization.

Generally, solubility data can be determined in two ways, as illustrated in Figure 3.23:

- 1) The measurement of the saturation concentration ( $c_{\text{sat}}$ ) at constant temperature (a) by successively adding known amounts of solid to the solvent until saturation is achieved (addition method) or (b) by equilibrating and analyzing a solution containing an excess of solid (excess method).
- 2) The measurement of the saturation (solubility) temperature ( $T_{\text{sat}}$ ) by heating a solution of known composition with an initial excess of solid until last particles are dissolved.

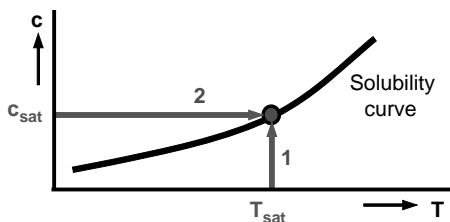


**Figure 3.23** Determination of the saturation concentration  $c_{\text{sat}}$  and the corresponding saturation temperature  $T_{\text{sat}}$  in isothermal (1) and polythermal (2) measurements.

The two approaches differ in the temperature regime applied. In case (1), the sample is analyzed at a constant temperature (isothermal technique); in case (2), the sample is subjected to a slow controlled heating (polythermal technique).

In the following sections, examples of isothermal and polythermal techniques for solubility measurement are presented. Here, advantages and weaknesses of the particular methods as well as the question, how to guaranty equilibrium conditions, are addressed.

#### 3.3.5.1 Ensuring Equilibrium Conditions

Solubility equilibria are characterized by a dynamic equilibrium between a solid and a liquid phase, that is, there is permanent mass transfer between the two phases. Particles from the solid phase pass into the liquid phase and vice versa (Figure 3.15). Here, diffusion resistances in the solution–crystal interface and surface integration resistances have to be overcome. Vigorous, efficient stirring is indispensable to optimize the contact between the phases in order to minimize diffusion resistances. This could be a real obstacle when working with heavily viscous solvents. Achieving equilibrium conditions in solubility equilibria might take a considerable period of time, in particular when the dissolution kinetics is low. Dissolution rates generally become slow close to saturation points. Before starting a solubility measurement, it is therefore recommended to first completely dissolve the solid material by heating above the expected saturation temperature and subsequently recrystallize it by preferably fast cooling in order to produce finely dispersed particles that are well distributed in the saturated solution (the so-called sample pretreatment step).

In isothermal measurements, the time required to establish equilibrium conditions ( $t_{\text{eq}}$ ) can be determined in a simple experiment illustrated in Figure 3.24. The solvent is thermostated at the desired temperature and stirred at moderate rate. After introducing an excess amount of solid into the solvent, samples of clear solution are removed at different times and analyzed for concentration subsequently. When the solution concentration reaches a constant value, saturation is achieved and the minimal equilibration time (for that temperature) can be derived from the concentration–time plot, as given in Figure 3.24.

For polythermal measurements, different heating rates must be checked for the particular system in order to determine the optimal one. The lower the heating rate,

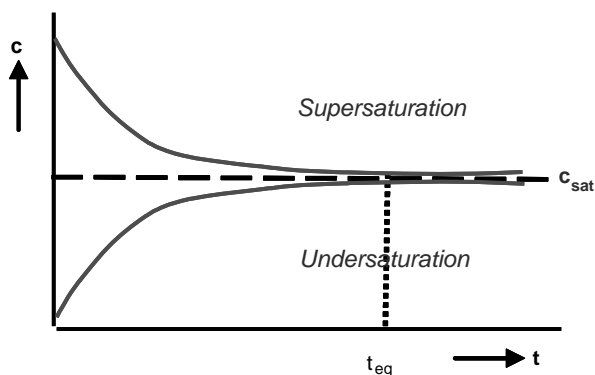


**Figure 3.24** Determination of the time required for achieving equilibrium conditions  $t_{eq}$  at a certain temperature.

the closer the system to equilibrium but weaker the detectability of the phase transition. Often a compromise between a very low heating rate with weak signal strength and a higher heating rate with stronger signal strength (but probably nonequilibrium conditions) has to be made.

### 3.3.5.2 Excess Method as a Classical Isothermal Method

The excess method is a universally applicable and widely used technique. The only limitations are too small amounts of sample that make solid–liquid phase separation and analysis difficult. It involves the following steps:

- 1) Sample preparation and sample pretreatment.

The measurement is performed in a closed sample vessel to prevent loss of solvent by evaporation. The solvent and an excess of the solute (or solutes) are introduced in the sample vial and the stirred solution is subjected to the pretreatment step described in Section 3.3.5.1. From our experience, the solvent volume should not fall much below 1 ml in order to provide sufficient crystal-free saturated solution for subsequent analysis. After recrystallization, the measurement temperature is adjusted.

- 2) Equilibration and stirring at constant temperature for at least  $t_{eq}$ .

The suspension is kept at constant temperature for at least the equilibration time  $t_{eq}$  already determined. Optimal mixing of the suspension should be examined repeatedly during equilibration. Slight inaccuracies of the temperature affect the correctness of the solubility value in particular for strong solubility–temperature relationships.

- 3) Solid–liquid phase separation (preferably isothermally at measurement temperature).
- 4) Analysis of both (a) the liquid phase for concentration or in case of more than one solute for composition and (b) the solid phase for identity.

For the liquid-phase analysis, all possible analytical techniques capable to determine the concentrations of the solution components can be used such as



density and refractive index measurements, HPLC, FT-IR, and gravimetric analysis. The identity of the solid phase should be characterized as fast as possible after solid–liquid separation in order to catch e.g. potential solvates, or polymorphs in equilibrium with the saturated solution. The solid-phase analysis is of significant importance when new or not yet characterized substances are under study, new solvents are introduced in the process, or additional impurities appear in mother liquors. Saturation concentrations measured in solubility experiments always refer to the solid phase that was in equilibrium with the solution analyzed. In case of multicomponent systems, that is, more than one solute in the saturated solution, additional analysis of the solid-phase composition allows to verify the overall mass balance.

Usually it is also feasible to measure multiple  $c_{\text{sat}}-T$  data pairs with one initial suspension (provided the suspension density is not too high). The temperature is stepwise increased after each equilibration and concentration measurement. In addition, the presence and identity of the solid phase have to be ensured and checked, respectively.

For higher throughput of samples, a certain automation of solubility measurements is feasible. For example, the instrument Crystal16<sup>TM</sup> multiple reactor system (Avantium Technologies BV/Amsterdam) is capable to accommodate 16 samples (in standard HPLC glass vials of about 1 ml volume) at the same time and to simultaneously hold them at the same temperature for equilibration purposes. For all vials, electromagnetic stirring is provided. Furthermore, since four vials are always arranged in a separate reactor block, four different temperature levels can also be applied simultaneously.

Even such measurements are often a tedious and time-consuming task, this is compensated by the outstanding features of the excess method:

- static (equilibrium) method,
- high accuracy,
- possibility of solid-phase analysis, and
- applicability to multicomponent systems.

### 3.3.5.3 Polythermal Measurements

Polythermal methods have in common that a suspension containing known amounts of solvent and solute in excess is heated and the temperature where last particles dissolve is detected. For detection, visual observation (e.g., under a microscope), turbidity measurements, particle-detecting inline probes (e.g., FBRM probe (Lasentec<sup>®</sup>, Mettler Toledo GmbH)), or calorimetry may be used. Since it is a dynamic method, the results depend on dissolution kinetics of the particular system. In general, polythermal measurements are easier to automate since just a temperature has to be followed and no special analytical technique is required. The above-mentioned Crystal16<sup>TM</sup> multiple reactor system can also be used to perform such kind of measurements. To detect both the dissolution process for derivation of saturation temperatures (clear points) and the formation of particles (cloud points) for determination of the metastable zone width, the

individual reactors are equipped with turbidity transmission sensors. The disadvantage of such a kind of measurements is that there is no characterization of the solid phase involved. Therefore, separate experiments for solid-phase analysis must be considered to properly reassign the saturation temperatures measured to the appropriate solid phases.

The same applies when using calorimetric detection techniques. Here, on heating, the heat consumed during dissolution of a known amount of solute in a certain amount of solvent is measured. When ensuring close-to-equilibrium experiments, from the thermal dissolution effect, (i) the saturation temperature of the mixture analyzed ( $T_{\text{end}}$ ) (Figure 3.25) and (ii) the solubility curve in the applied temperature region ( $T_1 - T_{\text{end}}$ ) can be derived. The latter requires knowledge of the solubility at  $T_1$ . Such measurements can be performed in reaction calorimeters or classical DSC instruments. Reaction calorimetry usually necessitates higher sample amounts, but allows stirring the mixtures. On the other hand, only some milligrams of material suffice for DSC, but normally no stirring is feasible. Thus, the applicability of calorimetric techniques for solubility determination is limited to systems with sufficient dissolution kinetics and an adequate dependency of solubility on temperature. From previous experiments, heating rates between 0.5 and 1.5 K/min proved to be optimal for most cases. More information may be extracted from literature sources [9,10].

Due to equilibrium constraints, polythermal methods typically do not reach the accuracy achievable with isothermal measurements, but provide first information about the general dissolution and recrystallization behavior of a substance. In addition, the identity of the solid phase for which the solubility is measured cannot

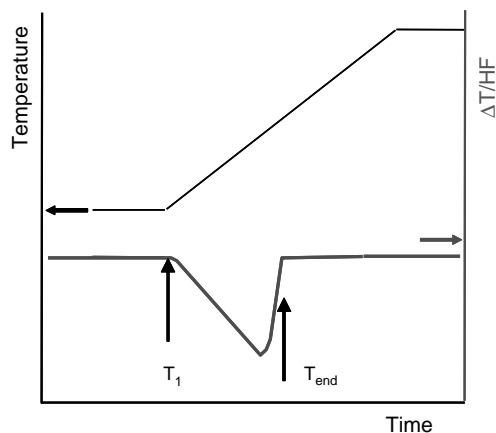


**Figure 3.25** Calorimetric monitoring of a dissolution process. Shown is the heat flow HF measured along a linear heating program. On heating, the solute dissolves in the solvent, and under equilibrium conditions, the amount

dissolved in a certain temperature range corresponds to the course of the solubility curve. The end of the thermal effect ( $T_{\text{end}}$ ) marks the saturation temperature of the mixture studied.

be controlled. Thus, for systems forming either polymorphs or solvates, these techniques do offer some room for error.

#### 3.3.5.4 Prediction and Correlation of Solubilities

At this point, different approaches available and often used for prediction and/or correlation of solubilities should be assembled (Figure 3.26). It is thought to be an entry in this field and, thus, the list of methods given is not exhaustive. The same applies to the references added to extract more information. A more general overview of model development by means of the most frequently applied models in process development is given in Ref. [11].

Often semiempirical  $g^E$  models for determination of the activity coefficients that account for nonideal solution behavior are used. An application-oriented introduction is given in Ref. [12]. Here, several “easy-to-use” approximate calculations for solubility estimation are discussed. In principle, such methods are recommended to be applied as complementary tools to experimental solubility determination that can help to reduce the experimental efforts required.

##### • Predictive models

- Schröder-van Laar equation  
(ideal case or considering real solution behavior by an appropriate activity coefficient relation (see below))
- Group contribution models
  - UNIFAC (UNiversal Functional group Activity Coefficient)
    - (a) Z. Lei, B. Chen, C. Li, H. Liu, *Chem. Rev.* 2008, 108, 1419-1455.
    - (b) I. Hahnenkamp, G. Graubner, J. Gmehling, *Int. J. Pharm.* 2010, 388, 73-81.
  - Modified UNIFAC (Dortmund)
    - (a) U. Weidlich, J. Gmehling, *Ind. Eng. Chem. Res.* 1987, 26, 1372-1381.
    - (b) J. Gmehling et al., *Ind. Eng. Chem. Res.* 1993/1998/2002.
- Quantum chemical approaches
  - COSMO-RS (COnductor like Screening Model for Real Solvents)
    - (a) A. Klamt, *COSMO-RS: From Quantum Chemistry to Fluid Phase Thermodynamics and Drug Design*, Elsevier, Amsterdam, 2005.
    - (b) A. Klamt, In: P. v. R. Schleyer (Ed.), *Encyclopedia of Computational Chemistry*, John Wiley & Sons, Inc. 1998.
    - (c) S. T. Lin, S. I. Sandler, *Ind. Eng. Chem. Res.* 2002, 41, 899-913
  - COSMO-RS (OI)
    - (a) H. Grensemann, J. Gmehling, *Ind. Eng. Chem. Res.* 2005, 44, 1610-1624.
    - (b) I. Hahnenkamp, G. Graubner, J. Gmehling, *Int. J. Pharm.* 2010, 388, 73-81.

##### • Equations of state

- PC-SAFT-equation of state
  - (a) M. Kleiner, F. Tumakaka, G. Sadowski, In: X. Lu, Y. Hu (Eds): *Molecular Thermodynamics of Complex Systems*, Springer, Berlin, 2009.
  - (b) F. Ruether, G. Sadowski, *J. Pharm. Sci.* 2009, 98, 4205-4215.
  - (c) F. Tumakaka, I. V. Prihodko, G. Sadowski, *Fluid Phase Equilib.* 2007, 260, 98-104.

##### • Semiempirical ( $g^E$ ) models for determination of activity coefficients

- Wilson, NRTL (Non-Random Two Liquids), UNIQUAC (UNiversal QUAsi-Chemical)
  - (a) J. Gmehling, B. Kolbe, *Thermodynamik*, Wiley-VCH Verlag GmbH, Weinheim, 1992.
  - (b) H. Renon, J. M. Prausnitz, *AIChE J.* 1968, 14, 135-144.
  - (c) C.-C. Chen, P. A. Crafts, *Ind. Eng. Chem. Res.* 2006, 45, 4816-4824 (NRTL-SAC).

**Figure 3.26** Thermodynamic models for prediction or correlation of solubilities.

As already introduced in Section 3.3.2, it is always advisable to first calculate the ideal solubility curve from the melting data of a substance using the simplified Schröder–van Laar equation (Equation 3.8). The presentation of the ideal values together with a couple of measured solubilities in a van't Hoff plot (Figures 3.18 and 3.20) is a reasonable way to evaluate the solubility behavior of a substance. Deviations between the ideal and real curves slopes e.g. indicate differences between the heat of melting and the heat of solution. Kinks occurring in the van't Hoff plot are an indication of various solid phases of the substance present. Furthermore, a reasonable linearity of the plot allows extraction of solubility data in the temperature range studied.

### 3.3.6

#### Oiling-Out

Oiling-out is the occurrence of a liquid–liquid phase separation during crystallization from solution. It is caused by a miscibility gap in liquid state, as illustrated in Figures 3.27 and 3.28 for an arbitrary binary system of components A and B (where B can be a solvent). A miscibility gap in liquid state is frequently observed when an organic compound (with hydrophobic properties) is mixed with water, or vice versa, a salt of an organic component (with hydrophilic properties) is added to an organic hydrophobic solvent. A miscibility gap can occur under stable equilibrium conditions, and thus is represented in the equilibrium phase diagram, or might characterize metastable equilibria. Therefore, the knowledge of the phase diagram of the particular system is essential (i) to identify the presence of a miscibility gap in liquid state and the corresponding liquid–liquid phase boundary and (ii) to derive possible existence regions of metastable miscibility gaps.

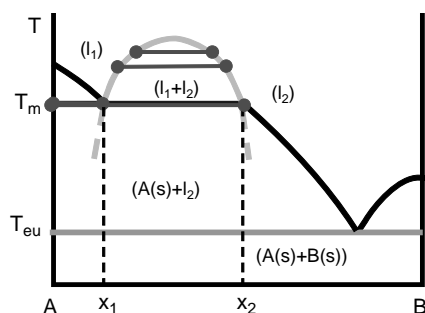


**Figure 3.27** Miscibility gap in liquid state and monotectic phase transition in a binary system. When cooling a liquid of a composition between  $x_1$  and  $x_2$  and reaching the phase boundary of the miscibility gap, a second liquid phase appears. On further cooling, the compositions of the two liquid phases  $l_1$  and  $l_2$  alter along the phase boundary of the miscibility

gap indicated by tie lines. At  $T_m$ , a third phase, solid A, is formed. This three-phase invariant is called monotectic invariant, and the corresponding temperature  $T_m$  monotectic temperature. The dashed lines extrapolating the phase boundary of the miscibility gap indicate metastable equilibria that may impair a particular separation process.

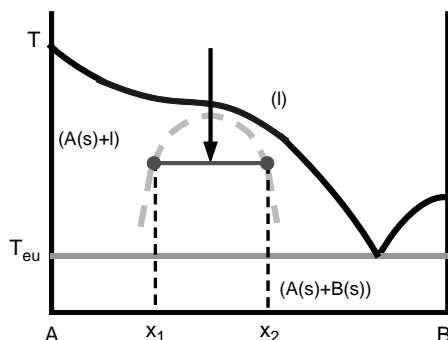


**Figure 3.28** Metastable miscibility gap. In case that liquid–liquid demixing occurs only on supercooling, the miscibility gap is located below the liquidus curve. If the phase boundary of the miscibility gap is closely related to the metastable zone (here of A), the liquid–liquid phase separation may be favored before

nucleation is initiated. This might be attributed to a “low” nucleation rate that is at least lower than that required to form a new liquid phase. The two liquid phases differ in their composition (specified by the tie line) and nucleation may occur in both phases.

With regard to the latter, several examples have been reported where liquid–liquid phase separation was observed prior to crystallization [13]. A reasonable explanation is the existence of a metastable miscibility gap (located below the solubility curve of the solute) which is passed when nucleation starts. This situation is illustrated in Figure 3.28. Oiling-out, in particular when unexpected, that is, in metastable conditions, is undesired in industrial applications. The high supersaturation present at the onset of nucleation can lead to very small particles, subsequent agglomeration, low purity of the crystals obtained, and the formation of unwanted polymorphs. In consequence, the crystallization and subsequent downstream processes are difficult to control.

Besides high levels of supersaturation, the following reaction conditions may promote oiling-out in crystallization:

- less or no seeds,
- too quick generation of supersaturation,
- high levels of impurities,
- presence of crystallization inhibitors, and
- insufficient agitation resulting in high local supersaturations.

Essential factors to limit or prevent oiling-out are controlled supersaturation and efficient seeding strategies.

In case of a stable miscibility gap in the phase diagram, one can check if it is reasonable to work at conditions outside the liquid–liquid phase boundary (e.g., right from the miscibility gap in Figure 3.27). If not, different solvents might have to be considered.

More practical aspects are addressed in Ref. [14]. A very interesting case of oiling-out for an API intermediate has recently been published in Ref. [15].

## 3.3.7

**Ternary Solution Equilibria: Case of Enantiomers**

As already indicated in Section 3.1.4, there are numerous cases where a ternary system, that is, a system comprising three phases (one being a solvent), has to be considered. Examples are a single impurity in a solute–solution system, the separation of diastereomeric salts or the two enantiomers of a chiral system, and the application of two solvents (where often the solute is highly soluble in one and only slightly soluble in the other (e.g., antisolvent crystallization)). Both the separation of diastereomeric salts and the separation of enantiomers refer to chiral separation as an important issue in pharmaceutical, agrochemical, and fine chemical industries such as the production of flavor and fragrance chemicals. In these industries, the request for pure enantiomers instead of the racemates (containing the enantiomers in an 1:1 ratio as mostly provided from chemical synthesis) is steadily increasing. In this chapter, the ternary system of the two enantiomers and a solvent will be considered as an example of ternary solution equilibria.

Figure 3.29 presents the relation between the binary melt phase diagrams and an isothermal slice of the ternary solubility phase diagrams (introduced in Section 3.1.4). Since the two enantiomers of a chiral system have same melting points and melting enthalpies, their melt phase diagrams are symmetrical to the 1:1 (i.e., racemic) composition. The same applies to the solubility diagrams of the enantiomers as shown in Figure 3.29. Therefore, in general only one half of the phase diagram has to be measured.

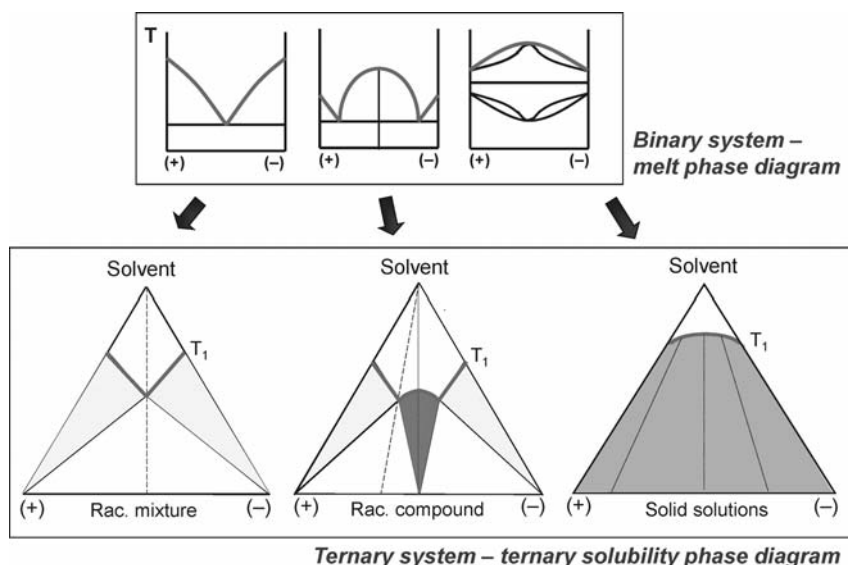


**Figure 3.29** The relation of binary melt phase diagrams and ternary solubility phase diagrams of enantiomers. The latter are represented as isothermal slices at an

arbitrary temperature  $T_1$ . Bold lines mark related liquidus (saturation) lines, (+) and (–) denote the two enantiomers.

Shown are the three main types of systems characterized by a simple eutectic (i.e. a 1:1 mixture is a racemic mixture or conglomerate), an intermediate compound (the so-called racemic compound), and solid solutions (here with complete miscibility in solid state). As can be seen, the shape of the solubility isotherms in the ternary system is clearly related to the liquidus curves in the binary system. The light gray areas in the ternary phase diagrams represent the existence regions of the appropriate enantiomers, where in equilibrium the pure enantiomer as solid phase can be crystallized. The dark gray area below the solubility isotherm of the racemic compound corresponds to the existence region of this intermediate compound, that is, the racemic compound is the solid phase crystallizing from solutions of compositions in that region. The two-phase regions are separated by a three-phase region, where a pure enantiomer can only be crystallized under kinetically driven, out-of-equilibrium conditions. As indicated by tie lines, for solid solution systems always a solid solution is the solid phase in equilibrium with a liquid phase of particular composition.

What is not considered here is partial miscibility in solid state also occurring in chiral systems. How this is represented in a ternary solubility phase diagram is shown in Section 7.2.

For a simple eutectic and a racemic compound-forming system in Figure 3.30, the measured ternary phase diagrams of the amino acid threonine and the fine chemical mandelic acid, both in water as solvent, are exemplarily shown. The diagrams contain equilibrium data measured in isothermal experiments as described in Section 3.3.5.2. Different temperatures were applied. All solubilities are related to the solid phases given, no solvate was found. Most points measured refer to

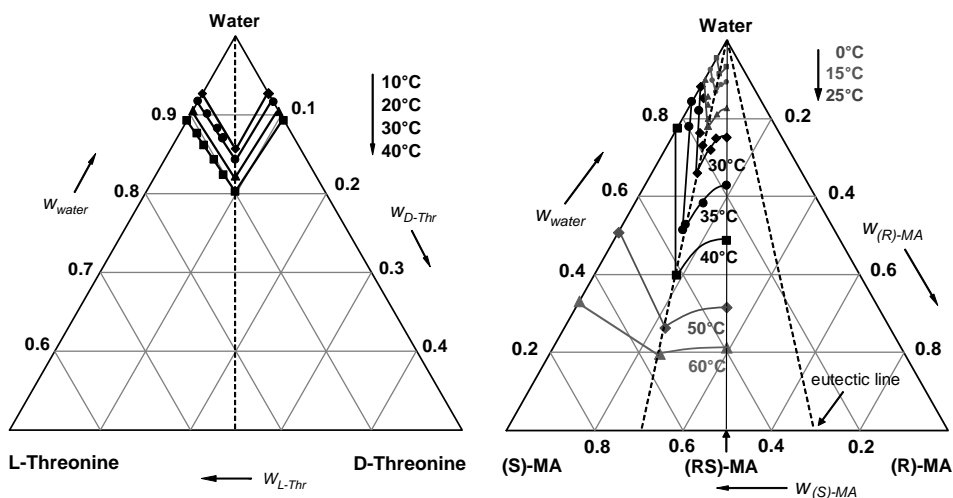


**Figure 3.30** Ternary solubility phase diagrams of the threonine and mandelic acid (MA) enantiomers in water. Shown are solubility isotherms at different temperatures. Due to low

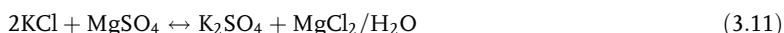
solubilities in the threonine/water system, only the upper part of the phase diagram is depicted (axes in weight fractions).

an excess of one of the enantiomers (L-threonine and (S)-mandelic acid, respectively). For mixtures containing the counter-enantiomer in excess, only some data have been determined to confirm the symmetry in the diagrams. In both systems, solubility increases with temperature. The mandelic acid enantiomers are less soluble than the racemic compound. The eutectic composition in the chiral mandelic acid system is found at mol fractions of about 0.3 and 0.7 respectively. The so-called “eutectic line”, where the solution is saturated on both (S)- and (RS)-mandelic acid, is linear, which is not necessarily the case for other systems. On that line in the ternary (polythermal) system, the system has one degree of freedom that could be the composition variable resulting in a curved shape.

### 3.3.8

#### Quaternary Systems: Case of Reciprocal Salt Pairs

As already introduced in Section 3.1.4, the reciprocal salt pairs represent industrially relevant examples of quaternary systems. They play an important role in the production of inorganic salts via the so-called reciprocal conversion in water. Industrial applications are the manufacture of  $K_2SO_4$  and  $Na_2CO_3$  on the basis of mined potash ores according to the following reactions:



In principle, what is done in reciprocal conversion is an exchange of anions and cations between the salt pairs. The underlying heterogeneous equilibria at a certain temperature can be represented in a square phase diagram as derived in Section 3.1.4.

In Figure 3.31a, the schematic phase diagram for a reciprocal conversion is shown. Both the reaction products (e.g., AY and BX) and the educts (AX and BY, respectively) stand vis-à-vis to each other and occupy the four corners of the phase diagram. The regions denoted as AY, BY, AX, and BX characterize the existence regions of the particular salts, where they can be crystallized as pure substances AY, BY, AX, and BX. Along the lines  $P_1-P_3$  or  $P_1-P_4$ , two solid phases coexist in equilibrium, AY and BY or BY and BX. The points  $P_1$  and  $P_2$  are three-salt points where in equilibrium three solid phases coexist; at  $P_1$  the phases AY, BY, and BX and at point  $P_2$  the phases AY, AX, and BX coexist. The dashed line connecting the educts AX and BY represents mixtures of the two salts. This line crosses the existence region of salt AY, which should be considered as desired reaction product of the reciprocal conversion here. To receive AY in solid state with high yield, salt BX must exist in the corresponding solution preferably in maximum concentration. When mixing the salts AX and BY at a ratio that corresponds to composition M, solid product AY and a saturated solution of composition  $P_2$  result. Quantification can be done via the lever rule.

For application purposes, the reciprocal conversion according to Equation 3.12 shall be discussed in more detail. The conversion of sodium chloride with



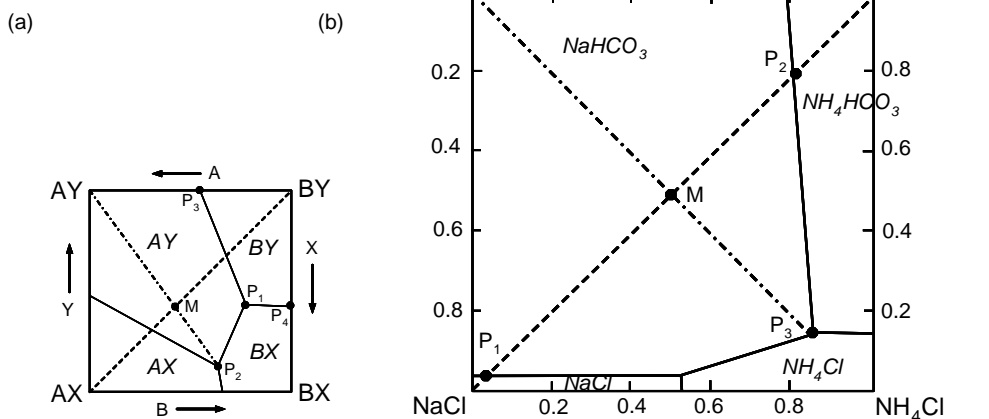


**Figure 3.31** Phase diagrams of reciprocal salt pairs. (a) Schematic phase diagram of an arbitrary reciprocal salt pair and reciprocal conversion (see also Figure 3.6b). (b) Heterogeneous equilibria in the system of the reciprocal salt pair  $\text{NaCl} + \text{NH}_4\text{HCO}_3$  at  $30^\circ\text{C}$ . On the ordinate and the abscissa of the phase diagram, the amount of each salt is given as a

molar fraction of the total salt content in the solution. Thus, the diagram does not represent absolute solubilities but the percentages of the salts in the entire salt content of the solution. The corners represent the pure salts or a solution of a single salt, while the corresponding marked regions specify the existence regions of the particular salt (figure from Ref. [16]).

ammonium hydrogencarbonate in aqueous solution to sodium hydrogencarbonate as desired product is the fundamental reaction of the famous ammonia–soda process that is principally based on the low solubility of  $\text{NaHCO}_3$ . The process includes several steps, where a saturated solution of  $\text{NaCl}$  in water is further saturated with ammonia and the desired  $\text{NaHCO}_3$  is precipitated by the introduction of  $\text{CO}_2$ . The conversion process is basically determined by the solubilities of the individual salts in the presence of the other components of the reciprocal salt pairs. Figure 3.31b shows the phase diagram of the reciprocal salt pair  $\text{NaCl}$  and  $\text{NH}_4\text{HCO}_3$  exemplified by the  $30^\circ\text{C}$  isotherm. Due to the low solubility of  $\text{NaHCO}_3$ , the corresponding existence region is comparatively large. On adding  $\text{NH}_4\text{HCO}_3$  (in reality by introducing ammonia and  $\text{CO}_2$ ) to a solution of  $\text{NaCl}$ , the composition of the mixture moves from the  $\text{NaCl}$  corner toward the  $\text{NH}_4\text{HCO}_3$  corner. In equilibrium, all mixtures of a composition between points  $P_1$  and  $P_2$  provide the desired  $\text{NaHCO}_3$  as solid phase. For the ammonia–soda process, the three-salt point  $P_3$ , where  $\text{NaHCO}_3$ ,  $\text{NH}_4\text{HCO}_3$ , and  $\text{NH}_4\text{Cl}$  coexist as solid phases, is of special importance. At this point, the concentration of  $\text{NH}_4\text{Cl}$  in the solution is highest within the entire range facilitating maximum yield for solid  $\text{NaHCO}_3$ . Thus, when mixing  $\text{NaCl}$  and  $\text{NH}_4\text{HCO}_3$  (solutions) at a ratio that corresponds to point  $M$ , solid  $\text{NaHCO}_3$  is precipitated at highest yield. The saturated solution in equilibrium has composition  $P_3$ . Application of the lever rule provides the amounts of the solid product and the respective liquid phase. Nevertheless, in reality, it is recommended not to reach point  $P_3$  exactly in order to avoid coprecipitation of  $\text{NH}_4\text{HCO}_3$  and

$\text{NH}_4\text{Cl}$  contaminating the desired  $\text{NaHCO}_3$ . Thus, an end point that is as close as possible to  $P_3$  but within the  $\text{NaHCO}_3$  existence region is considered to be optimal.

### Acknowledgment

I would like to thank Prof. Gérard Coquerel, University of Rouen, for inspiring the research work on solid-liquid equilibria and numerous valuable discussions on related issues.

### References

- Mullin, J.W. (1997) *Crystallization*, Butterworth-Heinemann, Oxford.
- Predel, B., Hoch, M., and Pool, M. (2004) *Phase Diagrams and Heterogeneous Equilibria: A Practical Introduction*, Springer, Berlin.
- Zernike, J. (1955) *Chemical Phase Theory*, Kluwer, Djakarta.
- Ricci, J.E. (1966) *The Phase Rule and Heterogeneous Equilibrium*, Dover Publications, Inc., New York.
- Garside, J., Davey, R.J., and Jones, A.G. (eds) (1991) *Advances in Industrial Crystallization*, Butterworth-Heinemann, Oxford.
- Wunderlich, B. (1990) *Thermal Analysis*, Academic Press, Boston.
- Urbanus, J., Roelands, C.P.M., Verdoes, D., Jansens, P.J., and ter Horst, J. (2010) *Cryst. Growth Des.*, **10**, 1171–1179.
- Emons, H.-H. et al. (1984) *Lehrbuch der Technischen Chemie*, Deutscher Verlag für Grundstoffindustrie, Leipzig.
- Mohan, R., Lorenz, H., and Myerson, A.S. (2002) *Ind. Eng. Chem. Res.*, **41**, 4854–4862.
- Sapoundjiev, D., Lorenz, H., and Seidel-Morgenstern, A. (2005) *Thermochim. Acta*, **436**, 1–9.
- Chen, C.-C. and Mathias, P.M. (2002) *AIChE J.*, **48**, 194–200.
- Frank, T.C., Downey, J.R., and Gupta, S.K. (1999) *Chem. Eng. Progress*, **95**, 41–61.
- Bonnett, P.E., Carpenter, K.J., Dawson, S., and Davey, R.J. (2003) *Chem. Commun.*, 698–699.
- Tung, H.-H., Paul, E.L., Midler, M., and MaCauley, J.A. (2009) *Crystallization of Organic Compounds-An Industrial Perspective*, John Wiley & Sons, Inc., Hoboken, New Jersey.
- Codan, L., Bähler, M.U., and Mazzotti, M. (2010) *Cryst. Growth Des.*, **10**, 4005–4013.
- Emons, H.-H. et al. (1983) *Technische Anorganische Chemie*, Deutscher Verlag für Grundstoffindustrie, Leipzig.
- Beckmann, W. and Lorenz, H. (2006) *Chem. Eng. Technol.*, **29**, 226–232.

### Further Reading

- Gmehling, J. and Kolbe, B. (1993) *Thermodynamik*, Wiley-VCH Verlag GmbH, Weinheim.
- Hefter, G.T. and Tomkins, R.P.T. (2003) *The Experimental Determination of Solubilities*, John Wiley & Sons, Inc., New York.
- Heinz, A. (1989) *Technologie der Mineralsalzverarbeitung*, Deutscher Verlag für Grundstoffindustrie, Leipzig.
- Jacques, J., Collet, A., and Wilen, S.H. (1994) *Enantiomers, Racemates, and Resolutions*, Krieger, Malabar.
- Prausnitz, J.M., Lichtenthaler, R.N., and de Azevedo, E.G. (1986) *Molecular Thermodynamics of Fluid-Phase Equilibria*, Prentice Hall, Englewood-Cliffs, NJ.
- Reich, R. (1993) *Thermodynamik*, Wiley-VCH Verlag GmbH, Weinheim.
- Walas, S.M. (1985) *Phase Equilibria in Chemical Engineering*, Butterworth, Boston.
- Yalkowsky, S.H. (1999) *Solubility and Solubilization in Aqueous Media*, American Chemical Society, Washington D.C.

## 4

### **Agglomeration during Crystallization**

*Wolfgang Beckmann*

The formation of agglomerates is observed for all stages of solid-state processes, particularly if small particles are involved. It occurs and influences the processes from particle generation to the drying of the crop and finally to its storage and use. The term agglomerates is understood to encompass both the formation of loosely bound aggregates that easily disintegrate and the agglomerates that are tightly bound by solid bridges and that only disintegrate under brute force. Here, the most important processes for agglomeration and their dependence on process conditions will be discussed. Some techniques to prevent agglomeration and to support agglomeration will also be mentioned.

#### 4.1

##### **Mechanisms and Kinetics of Agglomeration**

##### 4.1.1

###### **Process of Agglomeration**

For agglomeration to occur, two particles have to collide and the attractive forces between the two particles have to exceed the force resulting from the inertia of the particles to disintegrate again. The particles hit, tumble and either disintegrate or agglomerate. This first binding has to be fast. For particles in a shear flow field, the process is schematically shown in Figure 4.1.

Repulsive forces between particles hindering agglomeration are, for example, electrostatic forces (Figure 4.2). The surface charge is often called zeta potential and can be measured. The surface charge can be influenced by a number of parameters, such as pH, pI, or additives. Figure 4.3 schematically shows such a dependence. The variation of the solution pH effectively changes the surface charge and thereby the tendency for agglomeration. A low charge will often support agglomeration, while a higher surface charge often hinders agglomeration by hindering the first contacts.

Depending on the size of the primary particles of the agglomerates, different force regimes are necessary. While intermolecular forces suffice to bind very small

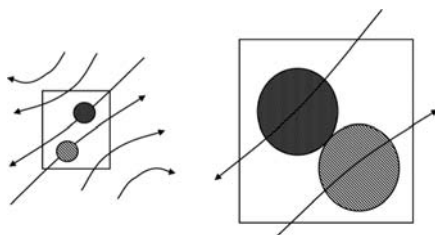


**Figure 4.1** Schematic of the steps involved in agglomeration, shown for two particles in a shear field in a suspension. Two particles have to collide, overcoming repulsive forces (a). The

first binding forces have to overcome the inertial forces that would otherwise lead to disintegration [1].

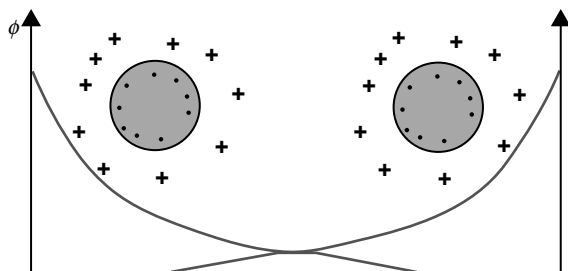


**Figure 4.2** Repulsive forces between equally charged particles. For agglomeration, this force has to be overcome.

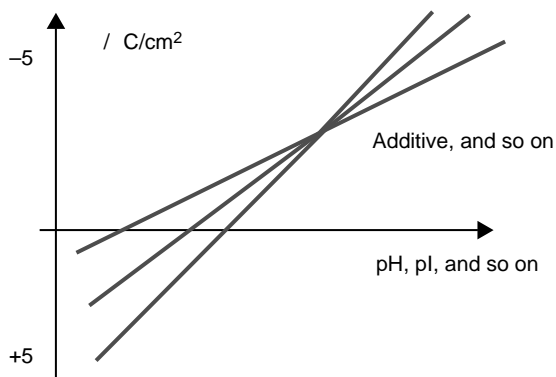


**Figure 4.3** Dependence of the surface charge as a function of pH, ionic strength, or concentration of additives.

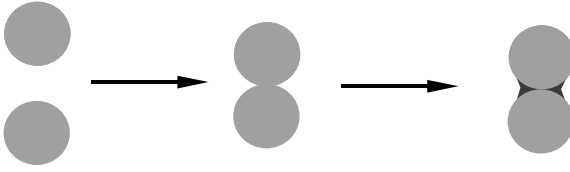


**Figure 4.4** Formation of solid bridges between particles. For these to be formed, a supersaturation is necessary,  $\sigma > 0$ . The cementation can occur during growth – the higher the supersaturation, the more likely the cementation – as well as during drying by depositing residual amounts of solid. The solid bridge between the particles is relatively rigid.

particles in agglomerates, liquid or solid bridges are necessary to bind larger particles. For the formation of solid bridges between particles, a supersaturation is necessary. This can occur during growth – the higher the supersaturation, the more likely the cementation – as well as during drying by depositing residual amounts of solid (Figure 4.4).

#### 4.1.2

##### Kinetics of Agglomeration

The kinetics of agglomeration can be understood as a quasi-bimolecular reaction. If only particles of one size are concerned, the kinetics can be described by Equation 4.1, with  $N$  as density of these particles. Here,  $\alpha$  denotes the efficiency of the bimolecular collisions:

$$-\dot{N} = \alpha \cdot \beta \cdot N^2. \quad (4.1)$$

The agglomeration kernel  $\beta$  depends on the mechanism of agglomeration and on the particle size (Figure 4.5). For small particles, the Brownian motion due to fluctuations in the solution suffices for an effective agglomeration; this is called orthokinetic agglomeration. For larger particles, a velocity gradient in the mother phase is necessary for particles to collide and thus to agglomerate, this is the perikinetic agglomeration.

Using Equation 4.1, the half time for agglomeration can be calculated,  $t_{1/2} = 1 / \alpha \beta N_0$ . Using the values for the agglomeration kernel in Figure 4.5, the half time for agglomeration of a slurry of particles with a size of  $5 \mu\text{m}$  and a suspension density of  $50 \text{ g/l}$  was calculated. As  $N_0 = 10^{15} \text{ m}^{-3}$  and  $\beta = 5 \times 10^{-17} \text{ m}^3/\text{s}$ , the half time is obtained as  $t_{1/2} \approx 30 \text{ s}$ . From Figure 4.6, it is apparent that the size has doubled within  $60 \text{ s}$ , which roughly corresponds to the value estimated.

## 4.2

### Parameters Influencing Agglomeration

The agglomeration is most effective for small particles, while large particles hardly agglomerate. Figure 4.6 shows the development in particle size for a slurry of primary particles of  $\approx 5 \mu\text{m}$  size. The agglomeration nearly ceases for agglomerates exceeding  $50\text{--}100 \mu\text{m}$ .

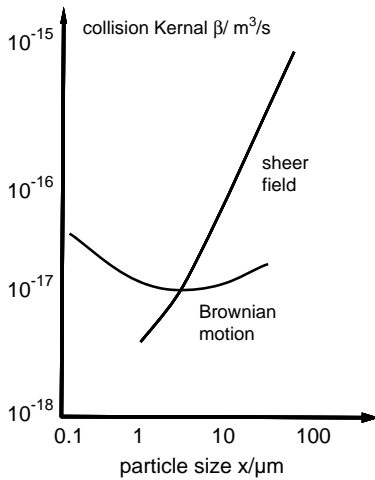
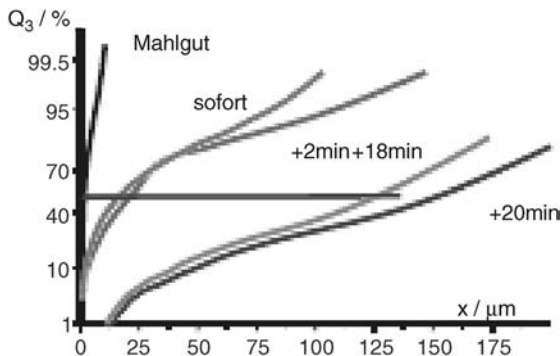


**Figure 4.5** Value of the agglomeration kernel as a function of particle size. Depending on the particle size, different mechanisms of agglomeration are active. For small particles,

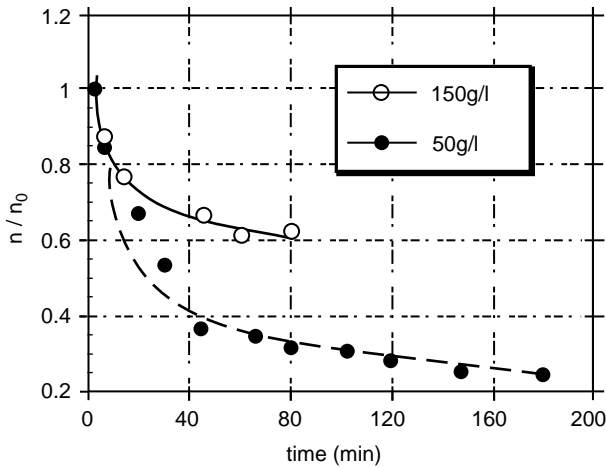
$r < 1 \mu\text{m}$ , the Brownian molecular motion is sufficient to result in collisions, while for larger particles,  $r > 1 \mu\text{m}$ , the gradient in the flow is necessary.

The agglomeration is shown to depend on the particle density (Equation 4.1). This is evident, for example, in the decrease in particle density as a function of agglomeration time, as shown in Figure 4.7.

The competition between agglomeration and desagglomeration becomes evident from Figure 4.8. The particle size of a seed for the Bayer process is given as a function of suspension density. Initially, the degree of agglomeration follows Equation 4.1 and increases with suspension density. Beyond a certain suspension density, the collisions to disintegrate agglomerates become dominant.



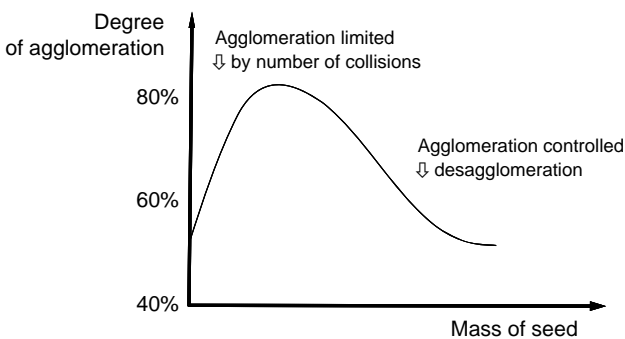
**Figure 4.6** Increase in mass referred to particle size of a suspension of particles  $5 \mu\text{m}$  in diameter. The increase in particle size is initially fast, but ceases for particles larger than  $100 \mu\text{m}$ .



**Figure 4.7** Decrease in particle density, that is, increase in degree of agglomeration, as a function of time for a sugar of two different suspension densities.

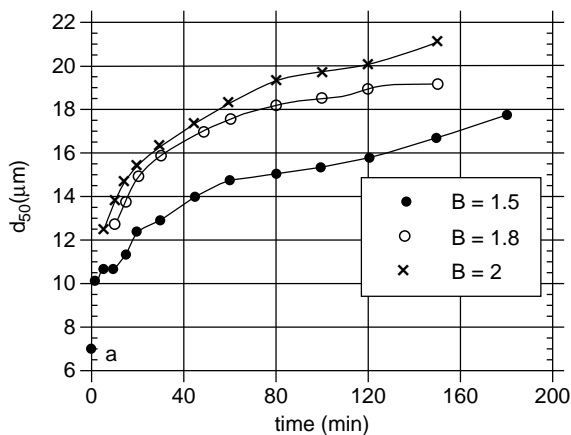
The influence of supersaturation on the agglomeration is shown in Figure 4.9, where the mean diameter of the agglomerates is plotted as a function of time for three different supersaturations. The higher the supersaturation during agglomeration, the stronger the binding between the agglomerating particles.

Figure 4.10 shows the mean particle size of agglomerates as a function of time for three different degrees of agitation of the suspension. The trend toward smaller diameters, lesser degree of agglomeration, increases with increasing intensity of mixing, which can be attributed to an increasing desagglomeration at high degrees of mixing.



**Figure 4.8** Particle size of a seed for the Bayer process as a function of suspension density. Initially, the degree of agglomeration follows Equation 4.1 and increases with suspension

density. Beyond a certain suspension density, the collisions to disintegrate agglomerates become dominant.



**Figure 4.9** Increase in agglomerate size with time for three different supersaturations.

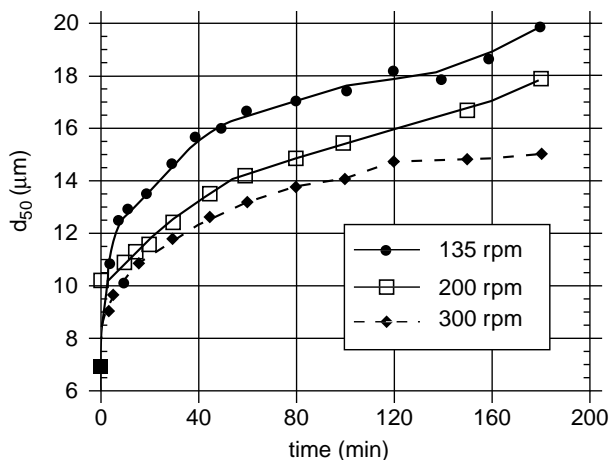


**Figure 4.10** Mean particle size of agglomerates as a function of time from three different power inputs during agglomeration.

### 4.3

#### Agglomeration during Crystallization

##### 4.3.1

##### Agglomeration during Crystallization

Agglomeration can occur at any stage of the crystallization process. Namely precipitations are prone to generate agglomerated crop, as small particles are generated and the supersaturation is high. It is thus advisable to check for each crystallization if agglomerated or separated primary particles are formed. As is shown in Figure 4.11, heavily agglomerated crystals can also be obtained in a seeded



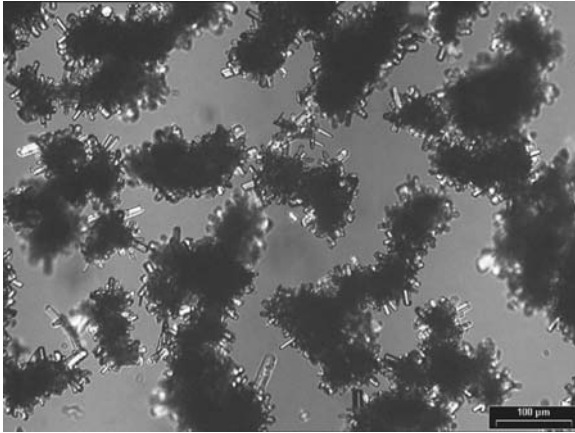


**Figure 4.11** Agglomeration during a seeded crystallization where the seeds were micrometer-sized particles with  $d_{50} \approx 3 \mu\text{m}$ . The size of the primary particles in the

agglomerates scales with the amount of seed used, while the agglomeration is independent of the seeding and thus cannot be controlled.

crystallization, for example, when the seed size is too small. In the case shown, the seeds were micrometer-sized particles with  $d_{50} \approx 3 \mu\text{m}$ . The size of the primary particles in the product agglomerates scales with the amount of seed used (cf. Chapter 9 and 10), while the agglomeration is independent of the seeding and thus cannot be controlled.

Even when the crop appears at first sight to be composed of separated primary particles, a closer inspection might prove otherwise. Figure 4.12 shows the particle size distribution as determined by laser diffraction and by sieve analysis to be in good agreement. However, sieving larger amounts (1 kg scale) leaves about 2% of oversized particles on the 1mm sieve. These particles are agglomerates. Note that such small fractions are difficult to detect by laser diffraction.

Finally, a microscopic inspection of the sieved residues of  $<1 \text{ mm}$  also shows agglomeration in the size fractions of  $500 \mu\text{m} < x < 1000 \mu\text{m}$  (Figure 4.13). Note that the fraction of particles in this size range is also  $\approx 3\text{--}5\%$  only.

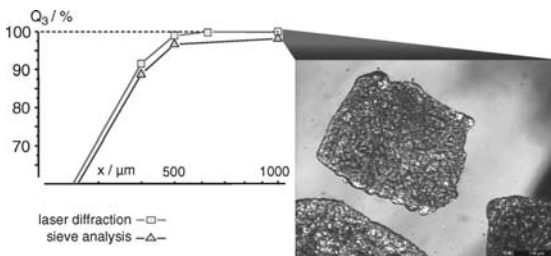


**Figure 4.12** Comparison of the particle size distribution as determined by laser diffraction and sieve analysis. The agreement is good. However, the sieving of a larger amount shows a fraction of approximately 2% of agglomerates  $>1 \text{ mm}$  in size.

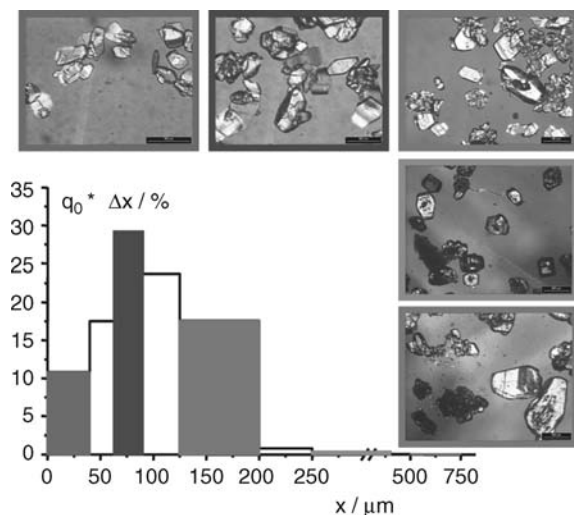


**Figure 4.13** Microscopic images of five sieve fractions of the sieve analysis shown. For sieve fractions >500  $\mu\text{m}$ , agglomerates can be seen.

For the measurement of particle size of agglomerates, the technique of dispersion of the sample is essential. Figure 4.14 shows the results of a particle size distribution for needlelike primary particles that are heavily agglomerated. A dry dispersion disintegrates the agglomerates partially, while somewhat surprisingly, the dispersion in suspension does not succeed in disintegrating the agglomerates sufficiently. For suspension the dispersion is sometimes aided by applying ultrasound to the suspension and observing the development in particle size distribution.

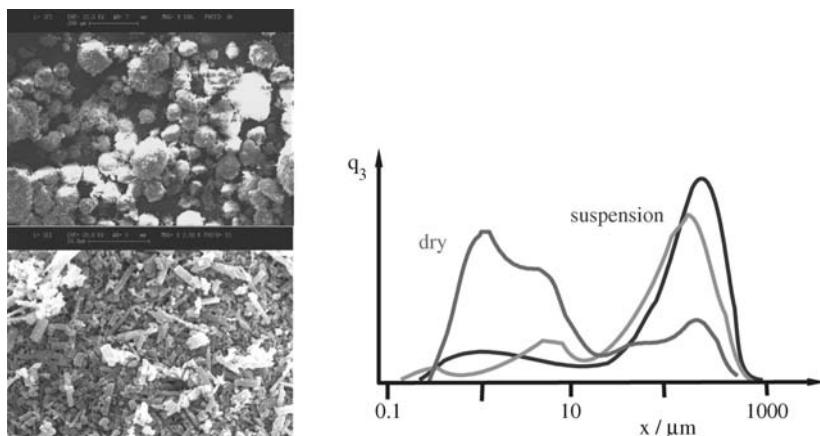


**Figure 4.14** Measurement of particle size distribution for heavily agglomerated needlelike primary particles. Depending on the technique for dispersion dry as in suspension, either the size of the agglomerates or a convolution of primary particles and agglomerates is found.

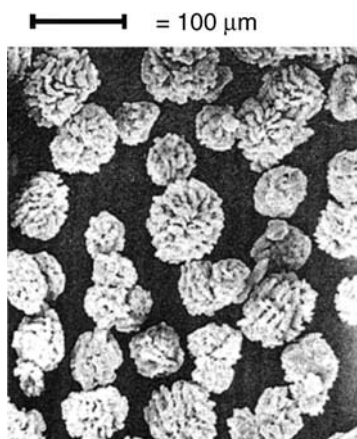


**Figure 4.15** Spherical agglomerates of paracetamol obtained by controlled crystallization. Note the even distribution of the size of the agglomerates.

It is a good advice to visually inspect the crop under a microscope and to supplement the wording measurements of the particle size by microscopic images.

#### 4.3.2

##### **Spherical Agglomeration**

Spherical agglomeration of paracetamol can be taken as an example for the controlled use of agglomeration for product design. Paracetamol in the registered solid-state form is difficult to tablet via direct compression. By forming agglomerates, this hurdle can be overcome. These agglomerates do have an even distribution of the size of the agglomerates (Figure 4.15).

The spherical agglomerates are obtained by drowning-out the paracetamol from THF with a mixture of hexane and trichloromethane in the presence of water as binding liquid. The water is not miscible with any of the solvents, so it will wet the paracetamol by forming a film on the surface. The hardness of the agglomerates is supported by building solid bridges.

Binding liquids can also be used for the reversible agglomeration to improve the filterability of small particles. The larger agglomerates usually filter better than small isolated particles. By using a binding liquid that can easily be evaporated, the agglomeration can be designed to be reversible, e.g. during the drying process.

#### 4.4

##### **Mechanical Properties of Agglomerates**

The mechanical properties of agglomerates are an indication of the mechanism of their formation and can also give an indication of the behavior of the agglomerates in their further processing.

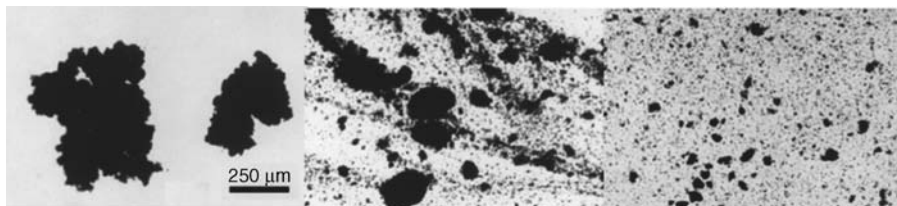


**Figure 4.16** Qualitative assessment of the hardness of agglomerates by placing the objects under oil between a microscope slide and a cover glass and applying gentle and increasing force. Weak agglomerates will disintegrate easily, which can easily be observed [2].

The hardness or resistance to disintegration of agglomerates can qualitatively be assessed by placing the objects under oil between a microscope slide and a cover glass and applying gentle force. Weak agglomerates will disintegrate easily, which can easily be observed (Figure 4.16).

## References

- 1 Brunsteiner, M., Jones, A.G., Pratola, F., Price, S.L., and Simons, S.J.R. (2005) Toward a molecular understanding of crystal agglomeration. *Cryst. Growth Des.*, **5** (1), 3–16.
- 2 Nichols, G., Bryard, S., Bloxham, M.J., Botterill, J., Dawson, N.J., Dennis, A., Diart, V., North, N.C., and Sherwood, J.D. (2002) A review of the terms agglomerate and aggregate with a recommendation for nomenclature used in powder and particle characterization. *J. Pharm. Sci.*, **91**, 2103–2109.

## Further Reading

- Alander, E.M., Uusi-Penttilä, M.S., and Rasmuson, A.C. (2004) Agglomeration of paracetamol during crystallization in pure and mixed solvents. *Ind. Eng. Chem. Res.*, **43** (2), 629–637.
- Pietsch, W. (2002) *Agglomeration*, Wiley–VCH Verlag GmbH.
- Tados, Th.F. (1987) *Solid/Liquid Dispersions*, Academic Press.

## 5

# Polymorphism of Crystalline Systems

Rolf Hilfiker

## 5.1

### Introduction and Definitions

The majority of organic and inorganic compounds can exist in different solid-state forms. The solid-state form can either possess long-range order, in which case it is called “crystalline,” or it can possess no order or only short-range order (extending over a distance of a few multiples of the diameter of the building unit), in which case it is called “amorphous.” If two crystalline solids have the same chemical composition, but different spatial arrangement of the constituents, they are commonly called “polymorphs.” This definition was conceived by McCrone [1]: “The polymorphism of any element or compound is its ability to crystallize as more than one distinct crystal species” and is the most widely used one and will also be applied throughout this chapter. Of practical importance are the solvates (sometimes called pseudopolymorphs) where solvent molecules are incorporated in the crystal lattice in a stoichiometric or nonstoichiometric way. Hydrates, where the solvent is water, are also of particular practical interest. This definition is schematically depicted in Figure 5.1. Figure 5.2 shows the spatial arrangement of the molecules in three polymorphs of benzamide [2] as derived from crystal structure determination. It is important to note, however, that other definitions for the term “polymorph” are also used. In particular, the definition used in the ICH (International Conference on Harmonisation) guidelines is a lot broader and includes the amorphous form as well as hydrates and solvates in the definition of “polymorph” [3].

The importance, implications, and investigation of polymorphism are described in-depth in several recent monographs and edited books [4–8].

It is imperative to clearly distinguish the term *polymorphism* from the term *morphology*. Polymorphism refers to the crystal structure, while morphology describes the macroscopic shape of a crystal (equant (cube), lath, needle, flake, column, and plate) [9]. The same polymorph can be easily crystallized in different morphologies; however, different polymorphs can also have the same morphology. In other words, polymorphism and morphology are independent of each other.

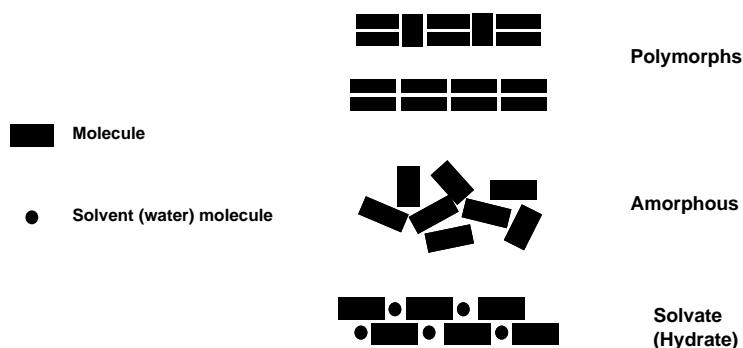


**Figure 5.1** Schematic depiction of polymorphs, solvates, and the amorphous form. (adapted from Ref. [7])

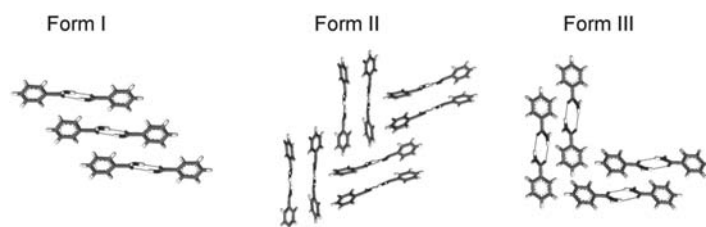


**Figure 5.2** Structure of three polymorphs (forms I, II, and III) of benzamide. (adapted from Ref. [2])

## 5.2

### Occurrence and Properties of Polymorphs and Solvates

Polymorphism is very common in connection with both organic and inorganic substances. Literature values for the prevalence of polymorphs, solvates, and hydrates for drug substances of small organic molecules (molecular weight <1000 g/mol) vary. Figure 5.3a shows the statistical evaluation of entries in the European Pharmacopeia with regard to solid-state information [10] and Figure 5.3b is the result of 180 focused polymorph screens carried out at a contract research organization (CRO) [11]. It is not surprising that the prevalence of different solid-state forms found in the European Pharmacopeia is lower than in the recently carried out polymorph screens (see Section 5.6), since some of the active pharmaceutical ingredients (API) in the Pharmacopeia have been discovered a long time ago, when polymorph screens were not always carried out thoroughly. But the data clearly show that the prevalence of substances that can exist in various solid-state forms is high and that if considerable effort is put into polymorph screening, several solid-state forms will be discovered for the vast majority (>85%) of substances.

Since the free energy of different polymorphs of the same substance is different (see Section 5.3), all physicochemical properties of two different polymorphs will be different, that is, solubility, melting point, density, hardness, refractive index, chemical and physical stability, heat capacity, hygroscopicity, and so on. Solvates

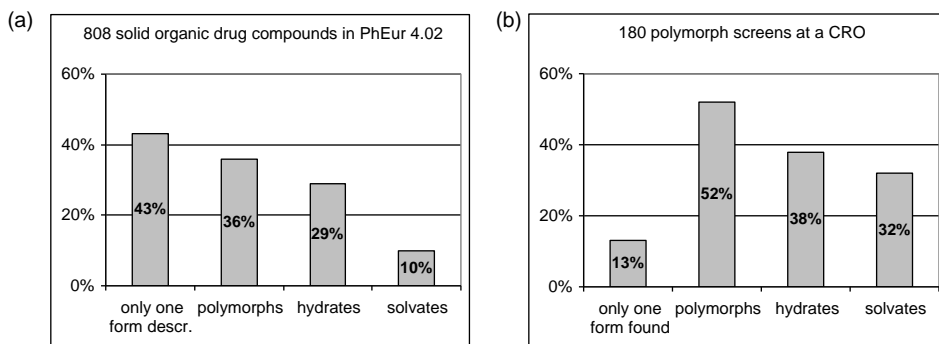


**Figure 5.3** Frequency of occurrence of solid-state forms of organic molecules. (a) A statistical evaluation of information on APIs on the market. (b) The result of 180 focused polymorph screens.

and hydrates – having a different chemical composition – generally differ even more in their properties. While solvates are rarely used in the finished product, many hydrates are used as the final form in the drug product. The difference in physical properties implies that the solid-state form of a product is of crucial importance for many different industries such as the pharmaceutical, animal health, agrochemical, fine chemical, or food industry. In the pharmaceutical, animal health, and agrochemical industries, the solubility of a solid is often the most important solid-state property since it can influence the bioavailability of a compound. But other properties (melting point, stability, compactibility, etc.) can also play an important role. In the food industry, the polymorphic form may impact taste (only one particular polymorph of cacao butter has the desired properties for chocolate). In the pigment industry, the color is affected by the solid-state form; the power of explosives crucially depends on the density of the solid; different polymorphs of dyes or additives can affect their photostability, and so on. For all these reasons, it is essential to identify all relevant solid-state forms of a substance, to determine their properties, to select the optimal form, and to ensure that this form can be produced reproducibly and that it does not undergo undesired conversions during its lifetime.

Another important aspect of solid-state forms is intellectual property issues [6]. Often the discovery of new solid-state forms with improved properties can lead to patents being granted and can therefore create important economic benefits.

### 5.3

#### Thermodynamics of Polymorphs of Solid-State Forms

##### 5.3.1

##### Basics

If different polymorphs can exist, their relative stability has to be determined, since it is vital to know whether a transformation from a less stable to a more stable form

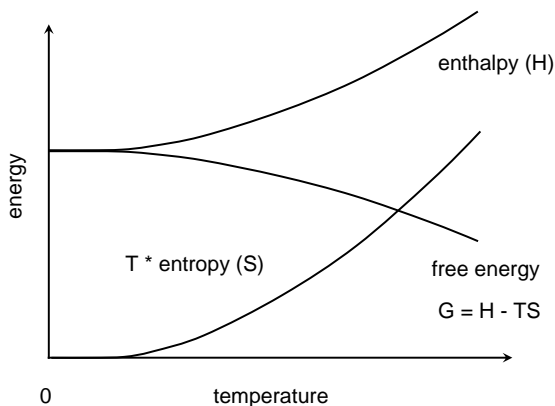


**Figure 5.4** Temperature dependence of enthalpy, free energy, and  $T^*$  entropy.

could occur during processing or storage. The stability of a substance is determined by its free energy. The temperature dependence of the basic thermodynamic state functions enthalpy ( $H$ ), entropy ( $S$ ), and Gibbs free energy ( $G$ ) is given by Equations 5.1–5.3; here,  $c_{p,m}$  is the molar heat capacity at constant pressure,  $T$  is the absolute temperature,  $H^0$  is the enthalpy at 0 K, and  $S^0$  is the entropy at 0 K. According to the third law of thermodynamics,  $S^0$  is zero for a perfect crystal.

$$H(T) = H^0 + \int_0^T c_{p,m}(T) dT. \quad (5.1)$$

$$S(T) = S^0 + \int_0^T \frac{c_{p,m}(T)}{T} dT. \quad (5.2)$$

$$G(T) = H(T) - T \cdot S(T). \quad (5.3)$$

The temperature dependence of  $H$ ,  $TS$ , and  $G$  of any solid is depicted schematically in Figure 5.4.

### 5.3.2

#### Energy–Temperature Diagrams

There is no universally recognized system for the nomenclature of polymorphs. They are often labeled with Arabic (1, 2, 3, . . .) or Roman (I, II, III, IV, . . .) numerals, lowercase or uppercase Roman letters (a, b, c, . . . or A, B, C, . . .) or lowercase Greek letters ( $\alpha$ ,  $\beta$ ,  $\gamma$ , . . .), or by names descriptive of properties (red form, low-temperature polymorph, metastable modification, etc.). If polymorphs are described by Roman numerals, it is a common convention to label the polymorph with the highest melting point with I, the one with the second highest with II, and so on. This notation will be used in this chapter.



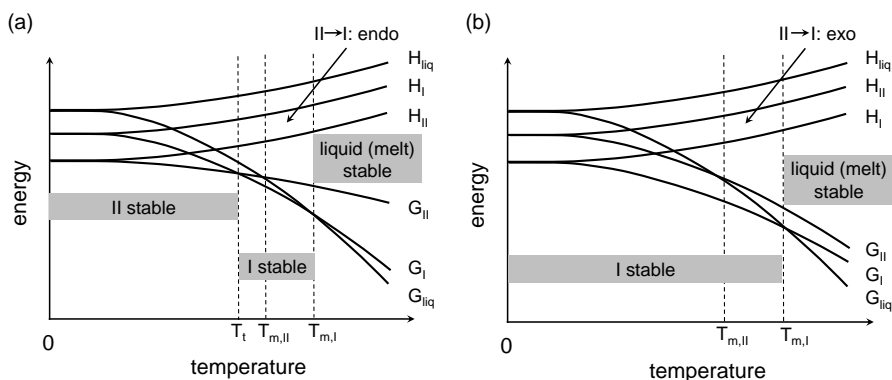


**Figure 5.5** Qualitative energy–temperature diagram for an enantiotropic (a) and a monotropic (b) system. Also indicated are the temperature regions of the stable forms.

Using Equations 5.1–5.3, enthalpy and free energy of two different polymorphs and the corresponding liquid phase (melt) can be plotted as a function of temperature. The phase with the lowest free energy ( $G$ ) at any temperature is always the thermodynamically stable one at that particular temperature. Therefore, the melting points of polymorph I and polymorph II ( $T_{m,I}$  and  $T_{m,II}$ ) are defined by the intersection points of the free energy of the respective polymorphs ( $G_I$  and  $G_{II}$ ) with the free energy of the liquid ( $G_{liq}$ ).

Two different situations are possible:

- i) The free energy lines of polymorphs I and II do intersect at a temperature below the melting point of polymorph II (Figure 5.5a).
- ii) The free energy lines of polymorphs I and II do not intersect at a temperature that is lower than the melting point of polymorph II (Figure 5.5b).

If (i) is the case, the system of polymorphs I and II is called an enantiotropic system. In such a situation, polymorph II is the thermodynamically stable form from 0 K to the transition temperature ( $T_t$ ) and polymorph I is the stable form from the transition temperature to its melting point ( $T_{m,I}$ ). In situation (ii), the system of polymorphs I and II is called a monotropic system. Here, form I is the stable form at all temperatures below its melting point. Obviously, it is of very large practical importance if a system is monotropic or enantiotropic and what the transition temperature is in an enantiotropic system. If, for example, the transition temperature is 40 °C and the low-temperature form is chosen for development, it has to be ascertained that a form conversion to the high-temperature form will not occur during processing steps or storage where higher temperatures may occur. It will also impact the design of the crystallization process. If crystallization starts at temperatures above the transition temperature, it must be ensured that the metastable form nucleates first if the stable form at room temperature is the target and if a phase transformation during the crystallization process is to be avoided, which is generally the case (see Chapter 10).

Equations 5.1–5.3 are difficult to apply directly in a practical way, since integration starts at 0 K where properties of the materials are very difficult to measure. However, Equations 5.1–5.3 can be transformed so that the free energy difference between melt and solid can be described by easily accessible parameters by expressing the difference between the free energy of the solid and the melt and by starting the integration at the melting point, where the free energy difference between liquid and solid is zero. In this way, Equation 5.4 is obtained:

$$(G_I - G_{\text{liq}})(T) = H_I - H_{\text{liq}} + \int_{T_m}^T \{c_{P,m,I}(T) - c_{P,m,\text{liq}}(T)\} dT - T \left\{ \frac{H_I - H_{\text{liq}}}{T_{m,I}} + \int_{T_m}^T \frac{c_{P,m,I}(T) - c_{P,m,\text{liq}}(T)}{T} dT \right\}. \quad (5.4)$$

If it is further assumed that the heat capacity differences between solid and liquid are zero in the temperature range of interest, which is often a fair approximation, Equation 5.5 follows, where  $\Delta H_{\text{melt},I}$  ( $= H_{\text{liq}} - H_I$ ) is the melting enthalpy of polymorph I:

$$G_I - G_{\text{liq}} \approx -\{\Delta H_{\text{melt},I}/T_{m,I}\}(T_{m,I} - T). \quad (5.5)$$

Using experimentally determined values of melting temperature and enthalpy (see Section 5.5.1 and Chapter 8.2.2), Equation 5.5 now allows a convenient quantitative depiction of energy temperature diagrams (Figure 5.6). This permits, for example, calculation of the ratio of the solubilities of the polymorphs at any temperature (see Section 5.3.3).

### 5.3.3

#### Rules to Predict Thermodynamic Relationships

Given the practical relevance of the relative thermodynamic relationship of various solid-state forms, rules have been developed to predict the relative thermodynamic stability of polymorphs and whether the relationship between polymorphs is monotropic or enantiotropic. First rules were developed by Tammann in 1926

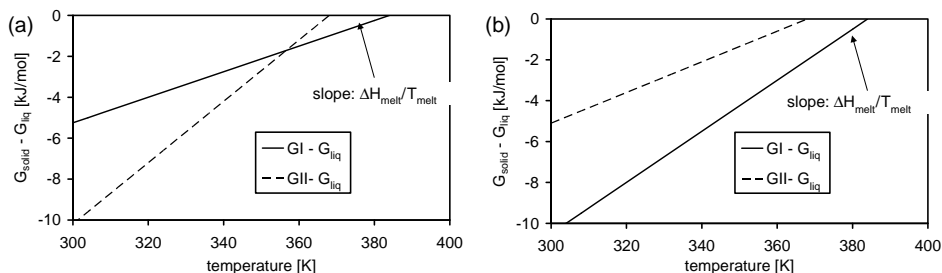


**Figure 5.6** Quantitative energy–temperature diagram for an enantiotropic (a) and a monotropic (b) system.

**Table 5.1** Burger–Ramberger rules.

	Enantiotropic systems	Monotropic systems
Definition	I stable @ $T_t \leq T \leq T_{m,I}$ II stable @ $0 \leq T \leq T_t$	I stable @ $0 \leq T \leq T_{m,I}$ II never stable
Consequence of definition	Transition II $\rightarrow$ I reversible  Solubility of I higher than solubility of II @ $0 \leq T \leq T_t$	Transition II $\rightarrow$ I irreversible  Solubility of I always lower than solubility of II
Rule 1	Transition II to I endothermic	Transition II to I exothermic
Rule 2	$\Delta H_{\text{melt},I} < \Delta H_{\text{melt},II}$	$\Delta H_{\text{melt},I} > \Delta H_{\text{melt},II}$
Rule 3	$c_{P,m,I} > c_{P,m,II}$	$c_{P,m,I} < c_{P,m,II}$
Rule 4	Density(II) > density (I) @ 0 K	Density(II) < density (I) @ 0 K

[12], which were later extended by Burger and Ramberger [13]. The well-known Burger–Ramberger rules are summarized in Table 5.1.

It can be seen that Rules 1 and 2 follow directly from Figures 5.5 and 5.6 and are thus universally valid as long as the heat capacity differences between solid and liquid are zero in the relevant temperature range. Rules 3 and 4 are known to fail sometimes and can be applied with much less confidence than the others.

If melting points and melting enthalpies can be measured accurately, the transition temperature can be estimated by Equation 5.6, which can be derived from Equation 5.5:

$$T_t = \frac{T_{m,I} \cdot T_{m,II} \cdot (\Delta H_{\text{melt},II} - \Delta H_{\text{melt},I})}{T_{m,I} \cdot \Delta H_{\text{melt},II} - T_{m,II} \cdot \Delta H_{\text{melt},I}}. \quad (5.6)$$

Typically, melting points and melting enthalpies are determined by differential scanning calorimetry (DSC). In some cases it may be difficult to determine melting point and melting enthalpy of polymorph II, since the transition to polymorph I might happen too fast during the heating process. Such a transition would be accompanied by the transition enthalpy  $\Delta H_{\text{melt},II} - \Delta H_{\text{melt},I}$ , which would then allow calculation of the melting enthalpy of polymorph II, together with the determined melting enthalpy of polymorph I, but it would still not allow calculation of  $T_t$ , since  $T_{m,I}$  is unknown (see also Section 8.2.2.1). In such a situation,  $T_t$  would have to be determined by other methods as described in Section 5.5.

## 5.4

### Thermodynamics of Hydrates

Hydrates are of large practical importance because water is ubiquitous in the atmosphere and, as mentioned in Section 5.2, the probability that a certain compound can crystallize as a hydrate is large. Both stoichiometric and non-stoichiometric hydrates are known. In the first case, the ratio between the number of water molecules and the number of compound molecules in the crystal is well

defined and constant over a certain range of water activities. The water molecules are located at specific positions in the crystal lattice, as schematically depicted in Figure 5.1. Nonstoichiometric hydrates, however, contain a water amount that can continuously vary within a certain range when the water activity of the environment of the crystal is varied. In such cases, the water molecules often reside within channels, larger voids, or in layers of the crystal lattice [14]. It should be noted that a compound may form multiple stoichiometric hydrates, e.g. a mono, sesqui, di, hemipenta and trihydrate (see Chapter 8.2.3.2).

While the thermodynamic properties of nonsolvated forms depend only on temperature and pressure, the free energy of hydrates (and solvates) is influenced by the activity of the water (or solvent) in the environment. Formation of a stoichiometric hydrate with  $n$  molecules of water per compound molecule can be described by Equation 5.7:



From the mass law of action, the equilibrium constant  $K_h$  can be expressed by Equation 5.8, where  $a[A(\text{solid})]_{\text{eq}}$ ,  $a[\text{H}_2\text{O}]_{\text{eq}}$ , and  $a[A \cdot n\text{H}_2\text{O}]_{\text{eq}}$  are the activities of  $A$ , water, and the hydrate  $A \cdot n\text{H}_2\text{O}$ , respectively, at the equilibrium:

$$K_h = \frac{a[A \cdot n\text{H}_2\text{O}]_{\text{eq}}}{a[A]_{\text{eq}} \cdot a[\text{H}_2\text{O}]_{\text{eq}}^n} \quad (5.8)$$

Since the activities of solids are 1, Equation 5.8 simplifies to Equation 5.9 with the corresponding free energy for hydrate formation  $\Delta G_h^0$ :

$$K_h = a[\text{H}_2\text{O}]_{\text{eq}}^{-n} \quad (5.9)$$

$$\Delta G_h^0 = -RT \ln(K_h) \quad (5.10)$$

It follows from Equation 5.9 that there is one precise water activity where hydrate and anhydrate are in equilibrium. At lower water activities, the anhydrate is stable and above the hydrate it is the thermodynamically stable form. Knowledge of this critical water activity is of great importance in order to be able to decide which form is the preferred one. If, for example, only one hydrate can be formed and the critical water activity for hydrate formation is 0.1 (which corresponds to 10% relative humidity), the hydrate may be a very appropriate form for development, as it will be the thermodynamically stable one at ambient humidities. The critical water activity is also important for the design of a stable crystallization process, since it has to be ensured that the water activity of the solution or suspension stays either below or above this value depending on whether the hydrate or the anhydrate should be produced.

Knowing  $K_h$ , the free energy difference between hydrate and anhydrate,  $\Delta G_h$ , can be calculated as a function of water activity using Equation 5.11:

$$\Delta G_h = \Delta G_h^0 + RT \ln \{a[\text{H}_2\text{O}]^{-n}\} \quad (5.11)$$

In Figure 5.7, the free energy of the dihydrate of carbamazepine is plotted as a function of the water activity of the environment. The critical water activity of 0.6 was determined by suspension equilibration experiments, as described in Section 5.5.2.

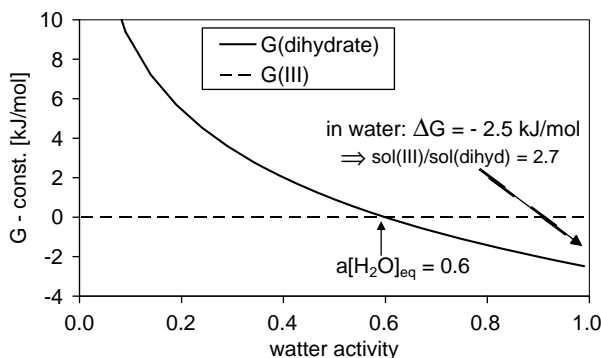


**Figure 5.7** Free energy of carbamazepine form III and dihydrate as a function of water activity at 25 °C.

From this,  $K_h = 2.8$  is obtained by Equation 5.9, and  $\Delta G_h^0 = -2.5$  kJ/mol by Equation 5.10. The solubility ratio of the dihydrate and anhydrate (form III) in water can be calculated using Equation 5.12:

$$\Delta G_h = \Delta G_h^0 = RT \ln \frac{\text{solubility of dihydrate in water}}{\text{solubility of form III in water}} \quad (5.12)$$

The critical water activity for hydrate formation will also depend on temperature, of course, and will increase with increasing temperature in agreement with Le Chatelier's principle as hydrate formation is generally exothermic. Knowledge of these values can again be essential for the design of a stable crystallization process of the desired form. The corresponding behavior of carbamazepine is plotted in Figure 5.8.

A practically very useful method to investigate hydrates is dynamic vapor sorption (DVS) (see Section 8.2.3.2). It provides information on the water sorption behavior of substances, and while it is less suited than slurry experiments to obtain thermodynamic parameters of hydrates, it provides very valuable kinetic information.

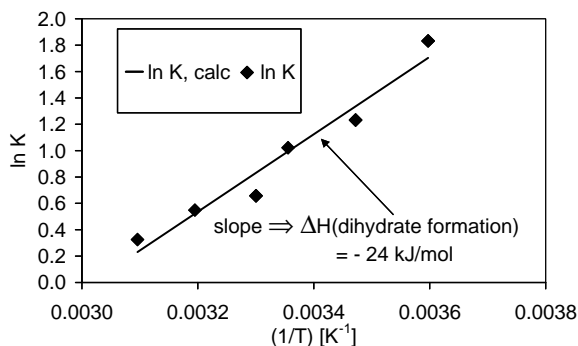


**Figure 5.8** Temperature dependence of  $K_h = a[\text{H}_2\text{O}]_{\text{eq}}^{-2}$  of carbamazepine dihydrate formation from form III. From the slope of the line, the enthalpy of dihydrate formation can be calculated using the van't Hoff equation as  $-24$  kJ/mol.

## 5.5

### Experimental Techniques to Elucidate Thermodynamics

#### 5.5.1

##### DSC

Several techniques are available in order to experimentally determine the thermodynamic properties of solids. As outlined in Sections 5.3.2 and 5.3.3, DSC data allow a very convenient and fast prediction of the relative thermodynamic relationship of various polymorphs. DSC, however, is not universally applicable, since compounds may decompose close to the melting point, making it impossible to determine accurate values of melting point and melting enthalpy. Also, it may not be possible to determine melting point and melting enthalpy of the form with the lower melting point if the solid–solid conversion to the higher melting form is too fast. Very fast DSC techniques (hyper DSC) can help in such a case. Finally, even if melting point and melting enthalpies can be determined, they will only allow an estimate of the transition temperature according to Equation 5.6, since for an accurate determination, knowledge of the heat capacities of all forms is also necessary.

#### 5.5.2

##### Suspension Equilibration

One of the most useful and unambiguous methods to assess the relative stability of two or more forms is suspension equilibration or slurry experiments. If a mixture of two forms is slurried in a solvent at a constant temperature for a long enough period of time, only two outcomes are possible:

- i) only one of the two forms, or
- ii) a third, new, form

will be found at the end of the experiment. (The only exception is when the temperature *exactly* corresponds to the transition temperature of an enantiotropic system. Then, a mixture of two forms will result.) In the first case, one has proof that the prevailing form is thermodynamically more stable than all other forms slurried; and in the second case, either a new, even more stable, polymorph has been discovered or a solvate with the solvent that was used was formed. Therefore, solvents that may form solvates with the compound of interest are not suitable for such suspension equilibration experiments. From the polymorph screening that is generally performed prior to evaluating the thermodynamic stability of forms, it is known which solvents will not form solvates with the compound of interest. It is also advisable to choose a solvent, where the compound has a reasonably high solubility; otherwise, the kinetics of the transformation can be very slow.

The slurry technique can also be used to determine the critical water activity of hydrate formation. If a mixture of hydrate and anhydrate is slurried in a solvent/-water mixture of known water activity, the hydrate has to convert to the anhydrate when the water activity of the solvent is below the critical water activity of hydrate

formation or vice versa. During that conversion, the hydrate will of course release water to the solvent, which will increase its water activity. If large enough amounts of hydrate and anhydrate are used in the slurry, it will lead to the increase of the water activity during the slurry equilibration up to the critical water activity and the end result will therefore be a thermodynamically stable mixture of hydrate and anhydrate. Determination of the water content of the solvent and knowledge of the relationship between water activity and water content of that solvent/water mixture will then immediately allow the calculation of the critical water activity for hydrate formation.

Suspension equilibration experiments have the advantage of delivering an unambiguous answer about the relative thermodynamic stability at a particular temperature, but the disadvantage is that they provide information only on the sign of the free energy difference and not on its magnitude, that is, they reveal which form is more stable but not how much more stable. So, in order to determine the transition temperature, a series of suspension equilibrations at different temperatures have to be carried out, and the higher the desired precision of the transition temperature, the more the experiments necessary.

### 5.5.3

#### Solubility Measurements

The solubility of form  $X$  of a compound  $A$  is defined as the state where the free energy of the solid ( $G_{\text{solid}}(A^x)$ ) is equal to the free energy of the solution ( $G_{\text{solution}}(A)_X$ ) (Equation 5.13), which can then be expanded to Equation 5.14, considering that the activity of the solid is defined as 1 (see also Chapter 3):

$$G_{\text{solid}}(A^x) = G_{\text{solution}}(A)_X \quad (5.13)$$

$$G_{\text{solid}}^0(A^x) = G_{\text{solution}}^0(A) + RT \ln a[A]_X \quad (5.14)$$

$G_{\text{solid}}^0(A^x)$  and  $G_{\text{solution}}^0(A)$  are the standard free energies of  $A$  in the solid state and  $A$  in solution, and  $a[A]_X$  is the activity of form  $X$  of  $A$  in the solution. Obviously,  $G_{\text{solution}}^0(A)$  is not affected by the solid-state form of  $A$ . The activity of  $A$  in solution is given by Equation 5.15, where  $f(A)$  is the activity coefficient and  $c[A]$  is the concentration of a saturated solution of  $A$ :

$$a[A] = f(A) \times c[A] \quad (5.15)$$

If the solubility of  $A$  in a particular solvent is not very large,  $f(A)$  will be close to 1, and Equation 5.16 is obtained:

$$G_{\text{solid}}^0(A^x) \approx G_{\text{solution}}^0(A) + RT \ln c[A]_X \quad (5.16)$$

Thus, measuring the solubility of two forms (e.g., form I and form II) of compound  $A$  in a certain solvent immediately allows the quantitative calculation of the free energy difference of these two forms by Equation 5.17. It is also clear from the equation that while the solubilities of the various forms will be very different in different solvents, the ratio of the solubility of two forms will be the same in every

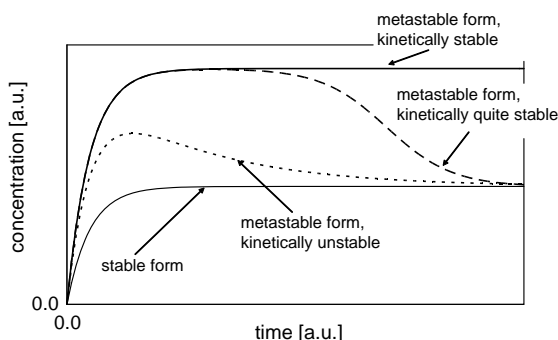


**Figure 5.9** Concentration of various forms as a function of time.

solvent as long as the activity coefficient is close to 1:

$$G_{\text{solid}}^0(A^I) - G_{\text{solid}}^0(A^{II}) \approx RT \ln \{c[A]_I / c[A]_{II}\}. \quad (5.17)$$

Determination of the solubility difference at a few temperatures and plotting the free energy difference versus temperature then allows the determination of the transition temperature.

In some cases, the experimental determination of the solubility of metastable forms may, however, be difficult. The solubility behavior of various forms is schematically depicted in Figure 5.9.

The concentration of the stable form will approach its equilibrium value asymptotically as a function of time. If the solubility of a metastable form is measured, the form will ultimately convert to the stable form and the concentration will drop to the corresponding value of the stable form. Depending on the kinetic stability of the metastable form, different types of behavior can be observed, as schematically depicted in Figure 5.9. If the metastable form is kinetically very unstable, determination of its true solubility may be impossible. Switching to another solvent may help in such a case. Since conversion of the metastable form to the stable form may occur during such a solubility measurement, it is important to (i) measure the time dependence of the solubility and to (ii) determine the solid-state form of the solid residue at the end of the experiment in order to prove that the form has not converted during the measurement.

Experimentally determined solubility ratios of polymorphs and solvates can vary in a broad range. A comprehensive compilation of published values can be found in Ref. [15]. It shows that the solubility ratios of polymorphs are often between 1 and 2.

#### 5.5.4

#### Other Methods

A number of other methods are available to elucidate the thermodynamic relationship between polymorphs. Solution calorimetry, for example, can be used to determine the enthalpy difference of two forms ( $H_{\text{solid}}^0(A^I) - H_{\text{solid}}^0(A^{II})$ ), since the enthalpy difference is equal to the difference of the heats of dissolution.



Together with the determination of  $G_{\text{solid}}^0(A^I) - G_{\text{solid}}^0(A^{II})$  by solubility measurements at one particular temperature ( $T_0$ ), this will allow calculation of the entropy difference ( $S_{\text{solid}}^0(A^I) - S_{\text{solid}}^0(A^{II})$ ) using Equation 5.18.

$$G_{\text{solid}}^0(A^I) - G_{\text{solid}}^0(A^{II}) = H_{\text{solid}}^0(A^I) - H_{\text{solid}}^0(A^{II}) - T^* \{S_{\text{solid}}^0(A^I) - S_{\text{solid}}^0(A^{II})\} \quad (5.18)$$

Equation 5.18 can then be used to calculate the free energy difference and the solubility ratio as a function of temperature as long as the difference of the heat capacities of the two polymorphs is small.

More exotic methods that give direct information on free energy are, for example, vapor pressure measurements [16], but they are limited to substances that have a reasonably large vapor pressure.

## 5.6

### Formation of Various Polymorphs and Solid-State Forms-Polymorph Screens

#### 5.6.1

##### Principles

Different polymorphic forms can be obtained when the crystallization conditions are changed. This can be explained by Ostwald's rule of stages, which states that "When leaving a given state and in transforming to another state, the state which is sought out is not the thermodynamically stable one, but the state nearest in stability to the original state." [17]. The rule implies that during a crystallization process, several forms may crystallize in sequence starting from the least stable form and ending up in the stable form. Or, in other words, if a very fast crystallization method, such as rapid precipitation, is applied, one is likely to obtain a metastable form, while a very slow crystallization process, such as a slow cooling or slurry ripening, would yield the stable form. But true to its name, Ostwald's rule of stages is a rule and not a law, and many violations of this rule have been reported. Nevertheless, it is a useful concept for the design of polymorphism screens. In Figure 5.10, the formation of different polymorphs is

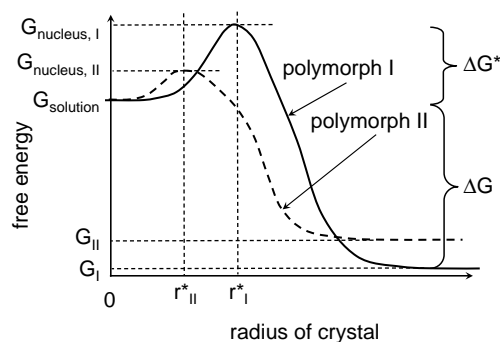


**Figure 5.10** Energy barriers for polymorph crystallization.

explained in a mechanistic way. In a supersaturated solution, where the free energy of the solid is lower than that of the solution, spontaneous nucleation can occur. The free energy of a nucleus is the sum of a volume and a surface free energy term. The surface free energy term is positive, since the interfacial tension between nucleus and solvent is positive, and the volume free energy term is negative in a supersaturated solution. For very small clusters, the surface free energy term dominates, but its relative contribution becomes smaller as the cluster grows. Therefore, the molar free energy of a nucleus with radius  $r$  first increases with increasing nucleus size until a certain critical size ( $r^*$ ) is reached, and then decreases until the bulk value is reached (see also Chapter 2.2). Crystallization can only occur if the free energy difference ( $\Delta G^* = G_{\text{nucleus}} - G_{\text{solution}}$ ) is overcome, so in the end the free energy of crystallization ( $\Delta G = G_{\text{I,II}} - G_{\text{solution}}$ ) is gained. Obviously, a polymorph with a small  $\Delta G^*$  is now the kinetically favored form, while a polymorph with a large  $\Delta G$  is the thermodynamically favored form. Ostwald's rule of stages implies that a small  $\Delta G$  leads to a small  $\Delta G^*$ . This is reasonable if we assume that in a metastable form, the molecules are arranged in the crystal lattice in a way similar to that in the solution, thus requiring a small energy barrier for their rearrangement; the stable form may require other conformations and arrangements of the molecules, which can only be achieved by overcoming a larger energy barrier. The solvent or environment used in the crystallization experiment will also influence  $\Delta G^*$ , because different solvents will have different adsorption energies to the surface of the nucleus, leading to different interfacial tensions and thus different surface energy contributions. As the surfaces of different polymorphs have different properties, this contribution will depend on the polymorph. A particular solvent X may stabilize the nucleus of polymorph A and destabilize the nucleus of polymorph B, while solvent Y may destabilize the nucleus of polymorph A and stabilize the nucleus of polymorph B. This will lead to preferential crystallization of polymorph A in solvent X and polymorph B in solvent Y. Therefore, the solvent may change the *propensity for the formation* of one polymorph or the other. The *relative thermodynamic stability* of polymorphs of non-solvated forms, on the other hand, is independent of the solvent it is formed in, since the solvent can only contribute to the surface free energy of the crystal; and while the surface free energy is an important contribution to the total free energy of nuclei which are less than a few nanometers in diameter, the surface free energy is negligible compared to the bulk free energy if the crystal size is larger than some 100 nm. The formation and stability of solvates, however, are influenced by the choice of solvent. This is another reason why various solvents should be used in a polymorph screen.

Therefore, in order to find all possible polymorphs and solvates, a very large number of crystallization methods in a very large number of diverse environments have to be carried out. Of course, one can never be sure that one has found all relevant polymorphs unless one carries out an infinite number of experiments. This essentially paraphrases McCrone's famous statement, "It is at least this author's opinion that every compound has different polymorphic forms and that, in general, the number of forms known for a given compound is proportional to the time and money spent in research on that compound" [1]. Depending on the target of the polymorph screen, for example, only identifying the thermodynamically stable form or finding as many forms as possible, different screening strategies have to be chosen.

It may also be difficult to reproduce the crystallization of a metastable form and there are accounts of the so-called “disappearing polymorphs,” that is, forms that could be obtained at some stage but not reproduced later. Since nucleation is a stochastic process, it is possible that two crystallization experiments that are performed in exactly the same way may lead to a different outcome. But if conditions are chosen properly and any potential seeds of other forms are carefully removed, it should always be possible to reproduce any form if a large enough number of experiments are performed.

### 5.6.2

#### Crystallization Methods and Choice of Solvent

Classical crystallization methods have been reviewed by Guillory [18] and are listed in Table 5.2. Depending on the method, various degrees of freedom are possible. They include type of solvent or solvent mixture, cooling profile, temperature at start, temperature at end, concentration, pressure, humidity, surface-to-volume ratio, vessel type, and material of surface. Furthermore, many crystallization experiments are influenced by the initial solid-state form that is used (i.e., polymorph, solvate, hydrate, or the amorphous form) as this can affect the solubility and hence the degree of supersaturation.

The choice of solvent is of particular importance. First, it has to be chosen such that the solubility is in a suitable range for the selected type of crystallization experiment (reasonably high solubility for cooling experiments, very low solubility in solvents used for precipitation, etc.). Second, it is important to use solvents with *diverse* physical properties in order to explore the whole parameter space of possible environments. In addition to molecular solvent–solute interactions, bulk properties of solvents such as viscosity may play a role. Gu *et al.* [19] examined 96 solvents in terms of 8 relevant solvent properties: hydrogen bond acceptor propensity, hydrogen bond donor propensity, polarity/dipolarity, dipole moment, dielectric constant, viscosity, surface tension, and cohesive energy density (calculated from the heat of vaporization). Based on all 8 properties, the 96 solvents were sorted into 15 groups

**Table 5.2** Classical crystallization methods.

	Method
(i)	Crystallization by cooling a solution
(ii)	Evaporation
(iii)	Precipitation
(iv)	Vapor diffusion
(v)	Suspension equilibration (often also called “slurry ripening”)
(vi)	Crystallization from the melt
(vii)	Heat-induced transformations
(viii)	Sublimation
(ix)	Desolvation of solvates
(x)	Salting out
(xi)	pH change
(xii)	Lyophilization

according to their statistical similarity. Some groups contain only 1 solvent (e.g., water), some several (e.g., *N*-methyl-2-pyrrolidone, dimethylformamide, dimethylacetamide, and dimethylsulfoxide), while others contain up to 16, which then allow choosing a solvent with a suitable solubility for the particular substance and type of crystallization experiment as described above. Molecules with the same functional groups were often grouped together as one would intuitively assume. In a thorough polymorphism screen, crystallizations using at least one solvent of each group should be carried out, so that the whole spectrum of solvent properties is used in the crystallization experiments.

### 5.6.3

#### Types of Polymorph Screens

According to ICH guidelines [3], a polymorph screen has to be carried out in order to get regulatory approval for pharmaceutical products. However, there is no guideline given on how such a screen should be performed. It certainly makes sense to proceed along a well-structured and standardized way, while recognizing that the procedure has to be tailored with respect to the substance that is investigated. An approach that is not adapted to the substance is prone to be inefficient and to overlook relevant forms. The procedure used should also be tunable to permit various degrees of thoroughness in the search for all relevant polymorphs since at an early stage in development, a smaller screening might make economical sense, while at a later stage, one wants to be highly confident that all relevant solid-state forms have been found. A polymorph screen in a preclinical phase may have the target to identify the form which is likely to be chosen for development (that is the thermodynamically stable polymorph or a hydrate) with a confidence level of 70% to 90%, while a polymorph screen in an advanced clinical phase should identify all relevant polymorphs with a confidence level > 99%.

In essence, a polymorph screen should at least contain the following elements:

- Characterization of the starting material by methods such as powder or single-crystal X-ray diffraction, DSC, thermogravimetry–Fourier transform infrared (TG–FTIR) or thermogravimetry–mass spectroscopy (TG–MS), DVS, Raman or infrared (IR), magic angle spinning (MAS) nuclear magnetic resonance (NMR), solubility measurements, microscopy, and high-performance liquid chromatography (HPLC) (purity).
- If the substance does not degrade at the melting point, hot-stage microscopy or hot-stage Raman microscopy can be a very efficient way for creating other polymorphs [20].
- Crystallization experiments from solution, using several techniques (e.g., (i), (ii), (iii), and (v) in Table 5.1) with a variety of solvents and solvent mixtures. Due to the practical relevance of hydrates, water and water/solvent mixtures should always be included. Suspension equilibration and slow cooling experiments play a particular role in finding the thermodynamically stable form, which is often the most important aim of a polymorph screen.

- All new forms have to be characterized by the methods used to characterize the starting material and their thermodynamic relationships (see Sections 5.3 and 5.4) have to be elucidated.
- Optionally, other techniques such as desolvation of solvates and mechanical stress (pressure and grinding) are necessary to get the information needed for processing and manufacturing steps.

Since many crystallizations have to be performed in such a polymorph screen, a reliable classical polymorphism screening can be rather time-consuming. In addition, substance amounts on the order of 5–10 g are typically needed to carry out such a study. This can be a limiting factor in some cases. Therefore, a definite need for automation and miniaturization exists in order to perform crystallizations in a high-throughput format. When designing such a system, it is critical to incorporate the best practices developed earlier and not to choose particular crystallization methods just because they can be easily automated. Even if experiments can be performed quickly and in parallel, they should still be designed carefully and adapted to the properties of the substance investigated. In particular, the choice of solvents and solvent mixtures should normally be different for every substance, taking into account solubilities, possible chemical reactions, and specific solvent–solute interactions.

High-throughput polymorphism screening systems have been developed by research foundations [21], large pharma companies [22–24], and companies specialized in solid-state research and development [25–29].

## 5.7

### Selection of Optimal Form for Development

As stated in Section 5.1, all solid-state properties of different polymorphs will be different. Which of these parameters is of special importance for a particular type of industry and a particular application can vary. While color is probably the most important parameter of a pigment, taste and “feel” are decisive for foods, density for explosives, solubility, processability and stability in the pharmaceutical industry, and so on. In any case, it is imperative for all industries that all possible forms are known and characterized, since the unexpected appearance of a new form may have very serious consequences. An example for that is the well-known “Norvir Case” [30], where the thermodynamically stable form was found only long after the product was on the market. Subsequently, the original metastable form could not be produced anymore and a new formulation for the product had to be developed [31] causing very high costs.

The selection process consists of determining all properties that are important for the product, such as stability, solubility and dissolution rate, hygroscopicity, melting point, ease of preparation, compressibility, and manufacturability of each solid-state form that has been discovered. Each property can then be graded, for example, from “bad” to “good” on a scale of 1–10. Finally, one can assign a weight factor to each property, depending on whether it is of high or little importance for the final product performance. These weight factors will depend very much on substance and

application. The overall score of each form would then be the sum of the product of scores and weight factors, and the form with the highest score would be chosen for development. A simpler approach could also consist of listing the properties of the various solid forms in descending order of importance for the final product in a table, and grading the respective property of each form with a color code green for “good”, yellow for “acceptable” or red for “unacceptable”. A look the color scheme of the various forms would then quickly show which one is the preferred form.

In the pharmaceutical industry, often stability is the overriding factor; so, in most cases, the stable polymorph or a hydrate will be chosen for development. As outlined in Section 5.3, the stable form has the normally undesired property of being the least soluble one, but that is often considered a smaller problem than the potential conversion of a metastable form to the stable form during storage. If hydrates exist, the decision becomes more difficult, since the thermodynamic stability then depends on humidity. Knowledge of the critical water activity, the kinetics of conversion, the conditions of use, and so on are then crucial in order to be able to select the optimal form.

### Symbols

$c$	concentration
$c_p$	heat capacity at constant pressure
$f$	activity coefficient
$G$	free energy
$H$	enthalpy
$K$	equilibrium constant
$R$	universal gas constant
$S$	entropy
$T$	temperature

### Acknowledgments

We acknowledge J. Thun and M. Szelagiewicz for providing valuable comments, data, and figures.

### References

- 1 McCrone, W.C. (1965) *Phys. Chem. Org. Solid State*, **2**, 725–767.
- 2 Thun, J., Seyfarth, L., Butterhof, C., Senker, J., Dinnebier, R.E., and Breu, J. (2009) *Cryst. Growth Des.*, **9**, 2435–2441.
- 3 International Conference on Harmonisation of Technical Requirements for Registration of Pharmaceuticals for Human Use (1999), ICH Harmonised Tripartite Guideline. Q6A Specifications: Test Procedures and Acceptance Criteria for New Drug Substances and New Drug Products: Chemical Substances ([www.ich.org](http://www.ich.org)).
- 4 Brittain, H.G. (1999) *Polymorphism in Pharmaceutical Solids*, Marcel Dekker, Inc., New York.
- 5 Byrn, S.R., Pfeiffer, R., and Stowell, J.G. (1999) *Solid State Chemistry of Drugs*, 2nd edn, SSCI Inc., West Lafayette, IN.

- 6 Bernstein, J. (2002) *Polymorphism in Molecular Crystals*, Oxford Science Publications, Oxford.
- 7 Hilfiker, R. (2006) *Polymorphism in the Pharmaceutical Industry*, Wiley-VCH Verlag GmbH, Weinheim.
- 8 Brittain, H.G. (2009) *Polymorphism in Pharmaceutical Solids*, 2nd edn, Informa Healthcare, New York.
- 9 Nichols, G. (2006) in *Polymorphism in the Pharmaceutical Industry* (ed. R. Hilfiker), Wiley-VCH Verlag GmbH, Weinheim, p. 191.
- 10 Griesser, U.J. (2006) in *Polymorphism in the Pharmaceutical Industry* (ed. R. Hilfiker), Wiley-VCH Verlag GmbH, Weinheim, p. 220.
- 11 Stahly, G.P. (2004) Paper presented at 22nd SCI Process Development Symposium. Cambridge, December 2004.
- 12 Tammann, G.H.J.A. (1926) *The States of Aggregation* (translation by F.F. Mehl), Constable & Co., Ltd., London.
- 13 Burger, A. and Ramberger, R. (1979) *Mikrochim. Acta*, **2**, 273–316.
- 14 Morris, K.R. (1999) in *Polymorphism in Pharmaceutical Solids* (ed. H.G. Brittain), Marcel Dekker, Inc., New York, pp. 125–181.
- 15 Pudipeddi, M. and Serajuddin, A.T.M. (2005) *J. Pharm. Sci.*, **94**, 929–939.
- 16 Griesser, U.J., Szelagiewicz, M., Hofmeier, U.C., Pitt, C., and Cianferani, S. (1999) *J. Therm. Anal. Calorim.*, **57**, 45–60.
- 17 Ostwald, W. (1897) *Z. Phys. Chem.*, **22**, 289–330.
- 18 Guillory, J.K. (1999) in *Polymorphism in Pharmaceutical Solids* (ed. H.G. Brittain), Marcel Dekker, Inc., New York, pp. 125–181.
- 19 Gu, C.-H., Li, H., Gandhi, R.B., and Raghavan, K. (2004) *Int. J. Pharm.*, **283**, 117–125.
- 20 Szelagiewicz, M., Marcolli, C., Cianferani, S., Hard, A.P., Vit, A., Burkhard, A., von Raumer, M., Hofmeier, U.C., Zilian, A., Francotte, E., and Schenker, R. (1999) *J. Therm. Anal. Calorim.*, **57**, 23–43.
- 21 Maier, W.-F., Klein, J., Lehmann, C., and Schmidt, H.W. (1999) Kombinatorisches Verfahren zur Herstellung und Charakterisierung von kristallinen und amorphen Materialbibliotheken im Mikrogramm-Massstab, Offenlegungsschrift DE 198 22 077 A1.
- 22 Balbach, S. and Korn, C. (2004) *Int. J. Pharm.*, **275**, 1–12.
- 23 Storey, R., Docherty, R., Higginson, P., Dallman, C., Gilmore, C., Barr, G., and Dong, W. (2004) *Crystallogr. Rev.*, **10**, 45–56.
- 24 Carlton, D.L., Dhingra, O.P., and Waters, P.W. (1972) High throughput crystal form screening workstation and method of use, Patent No. WO 00/67872.
- 25 Morissette, S.L., Almarsson, Ö., Peterson, M.L., Remenar, J.F., Read, M.J., Lemmo, A. V., Ellis, S., Cima, M.J., and Gardner, C.R. (2004) *Adv. Drug Deliv. Rev.*, **56**, 275–300.
- 26 Gardner, C.R., Walsh, C.T., and Almarsson, Ö. (2004) *Nat. Rev.*, **3**, 926–934.
- 27 Van Langevelde, A. and Blomsma, E. (2002) *Acta Crystallogr.*, **A58** (Suppl.), C9.
- 28 Desrosiers, P., Carlson, E., Chandler, W., Chau, H., Cong, P., Doolen, R., Freitag, C., Lin, S., Masui, C., Wu, E., Crevier, T., Mullins, D., Song, L., Lou, R., Zhan, J., Tangkilisan, A., Ung, Q., and Phan, K. (2002) *Acta Crystallogr.*, **A58** (Suppl.), C9.
- 29 Hilfiker, R., Berghausen, J., Blatter, F., Burkhard, A., De Paul, S.M., Freiermuth, B., Geoffroy, A., Hofmeier, U., Marcolli, C., Siebenhaar, B., Szelagiewicz, M., Vit, A., and von Raumer, M. (2003) *J. Therm. Anal. Calorim.*, **73**, 429–440.
- 30 Chemburkar, S.R., Bauer, J., Deming, K., Spiwek, H., Patel, K., Morris, J., Henry, R., Spanton, S., Dziki, W., Porter, W., Quick, J., Bauer, P., Donaubauer, J., Narayanan, B.A., Soldani, M., Riley, D., and McFarland, K. (2000) *Org. Process Res. Dev.*, **4**, 413–417.
- 31 In agreement with the statement in Section 5.6.1, about 2 years later the original form could be produced again: Bauer, J., Spanton, R., Henry, R., Quick, J., Dziki, W., Porter, W., and Morris, J. (2001) *Pharm. Res.*, **18**, 859–866.

## 6

### The Influence of Additives and Impurities on Crystallization

*Christiane Schmidt, Matthew J. Jones, and Joachim Ulrich*

Crystallization is governed by the usual thermodynamic variables of temperature, composition, and pressure. It is common to describe the thermodynamics in terms of dominant chemical species present, which in the majority of crystallization processes are the material to be crystallized and a small number of solvents. For all real systems, a further influence has to be taken into account, that is, of impurities. These are present in every system, in varying amounts. These impurities can have an effect on the solubility or melting point of the material to be crystallized, if small. The presence of additional components in the solution is often more noticeable in their effect upon the kinetics of crystallization and more specifically on growth rates of crystals. For the sake of clarity, “additive” is used as a collective noun for any minor component in a given system, whether this “additive” is in fact an impurity stemming from the raw materials employed or a by-product from the reaction stages required to manufacture the final product, or a true additive supplied to the system to achieve a specific effect. It is noted that the word impurity is even more widely used, as solvent or solvent mixture can also act as additives.

#### 6.1

##### Influence of Additives and Impurities on Crystallization

The discussion on characteristic crystallization processes center first on the properties of the material to be crystallized (in the case of melt crystallization) or on those of the solution from which a given component is to be crystallized. However, any real system is not entirely pure and does contain any number of impurities at concentrations that may vary from barely detectable traces to significant concentrations.

##### 6.1.1

###### Solubility

As the solubility of a given substance in a given solvent depends upon the composition of the system, the solubility will change with the presence of additional



chemical species. Currently, it is not possible to predict the precise effect an additional component will have, but experience shows that the solubility of a substance generally increases in the presence of additives.

#### 6.1.1.1 Common Ion Effect

One exception is the so-called common ion effect observed in electrolyte solutions. Here, the solubility product governs the solubility behavior (Equations 6.1 and 6.2):



$$K_L = [A]^m [B]^n. \quad (6.2)$$

The presence of a second electrolyte sharing a common ion with the dominant species will reduce the solubility. The solubility product  $K_L$  is a constant, and any increase in the concentration of one or the other component reduces the concentration of the counterion. As a result, the apparent solubility of the salt is decreasing.

#### 6.1.1.2 Thermodynamic Basis of Solubility and the Influence of Additives

In an ideal solution, the solubility of a solute in a given solvent is governed by the temperature of fusion of the solute and the enthalpy of fusion:

$$\ln [c = (\Delta H_m)/(RT_m)(1 - T_m/T)], \quad (6.3)$$

where  $c$  is the solubility of the solute at temperature  $T$ ,  $T_m$  and  $\Delta H_m$  are the temperature and enthalpy of fusion, respectively, and  $R$  is the ideal gas constant. For real systems, the enthalpy of fusion is replaced by the enthalpy of dissolution.

Strong interactions between different components in a solution will lead to observable deviations from ideal behavior [1–3]. In the literature, analysis of such deviations is often carried out based upon empirical equations rather than taking a stringent thermodynamic approach.

Some points are often neglected. This includes, for example, the uptake of traces of gases in the solvent (e.g., oxygen or water), which can dramatically change the solubility. Such a phenomenon might occur slowly over time depending on the ambient conditions and can lead on the first glance to surprising and unexplainable results.

#### 6.1.1.3 Complex Formation

The formation of molecular complexes in solution may lead to an apparent increase in solubility. It is important to be aware that this increase is a manifestation of the fact that the molecular complexes formed must be treated as chemical entities that are distinct from the actual solute under investigation, as having properties such as solubility different from that of the solute.

Figure 6.1 shows an increase of solubility with increasing concentration of electrolytes. The example shows an increase in the solubility of silver chloride ( $\text{AgCl}$ ) at increasing concentrations of added electrolytes (here  $\text{NaNO}_3$  and  $\text{CaCl}_2$ ).

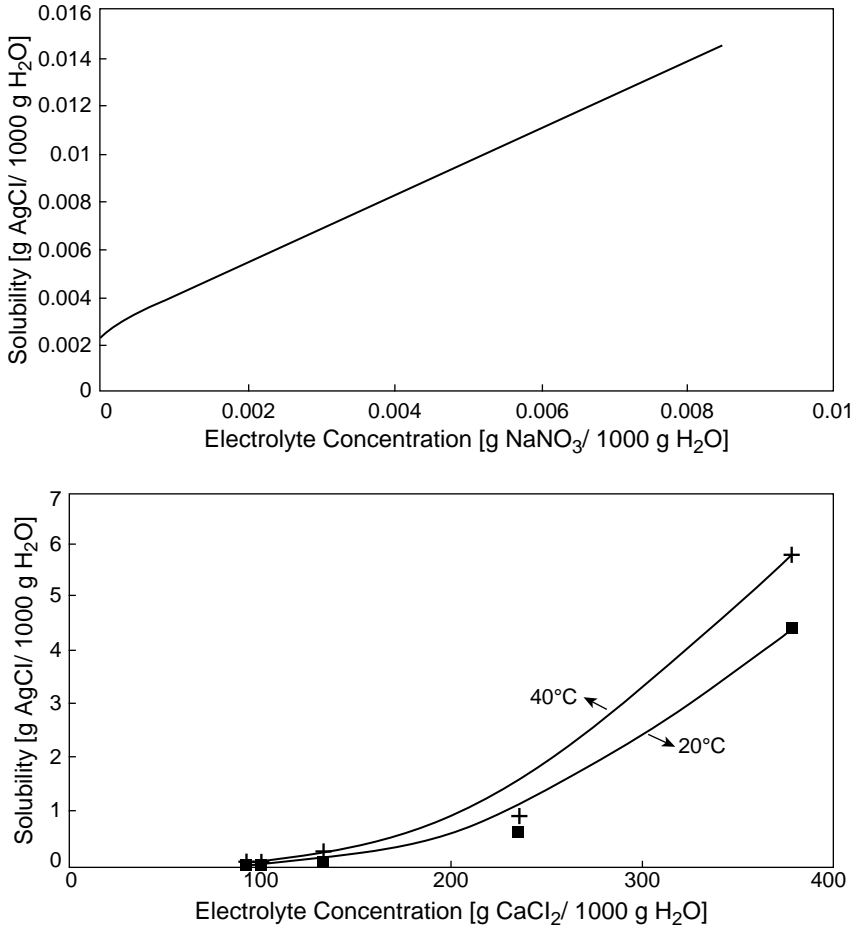


**Figure 6.1** Solubility of AgCl in aqueous solution of NaNO<sub>3</sub> and CaCl<sub>2</sub> [4,5].

### 6.1.2

#### Rate of Nucleation and Crystal Growth

##### 6.1.2.1 Nucleation Rates

The presence of foreign species in a solution may increase or decrease the nucleation rate of the crystallizing substance. Both effects can be understood in terms of classical nucleation theory, where the nucleation rate is given by

$$J = J_0 \exp \left( -C_S \frac{\gamma_n^3 V_{\text{mol}}^2}{k^3 T^3 (\ln S)^2} \right). \quad (6.4)$$

$J_0$  is a pre-exponential factor, the shape factor  $C_S$  accounts for the geometry of the nucleus,  $\gamma_n$  is the interfacial energy of the nucleus with respect to the solvent,  $V_{\text{mol}}$  is

the molecular volume,  $k$  the Boltzmann constant,  $T$  is the temperature, and  $S$  is the relative supersaturation.

The presence of additives may increase or decrease the interfacial energy, which will result in a respective increase or decrease of the nucleation rate. Nývlt and Ulrich [6] commented upon the similarity between adsorption isotherms and the behavior of nucleation rate with additive concentration, suggesting a link between nucleation rate and adsorption. The consequence of such a link should be an increase of nucleation rate as the adsorption of an additive on a surface is expected to decrease the interfacial energy [7]. However, a decrease in nucleation rate is frequently observed in the presence of additional components and it is likely that blocking action by the additive at the surface of a cluster of molecules inhibiting their growth may be the cause of this effect. Although this is a reasonable explanation, experimental evidence is lacking.

Additives may also affect the equilibrium solubility of a solute and thereby modify the supersaturation, which in turn results in a change in nucleation rate [8].

Any decrease in nucleation rate leads to an increase in the metastable zone width [9] and the induction time, both of which can be measured using suitable techniques, for example, ultrasonic probe [10]. Figure 6.2 illustrates the impact of  $\text{Fe}^{3+}$  on the metastable zone width of ammonium sulfate; the width increases from 1 K to more than 4 K.

The induction time  $t_{\text{ind}}$  is the inverse of the nucleation rate. Classical nucleation theory requires that a plot of  $\ln(t_{\text{ind}})$  against  $1/(T^3 \ln(S)^2)$  is a straight line, the slope

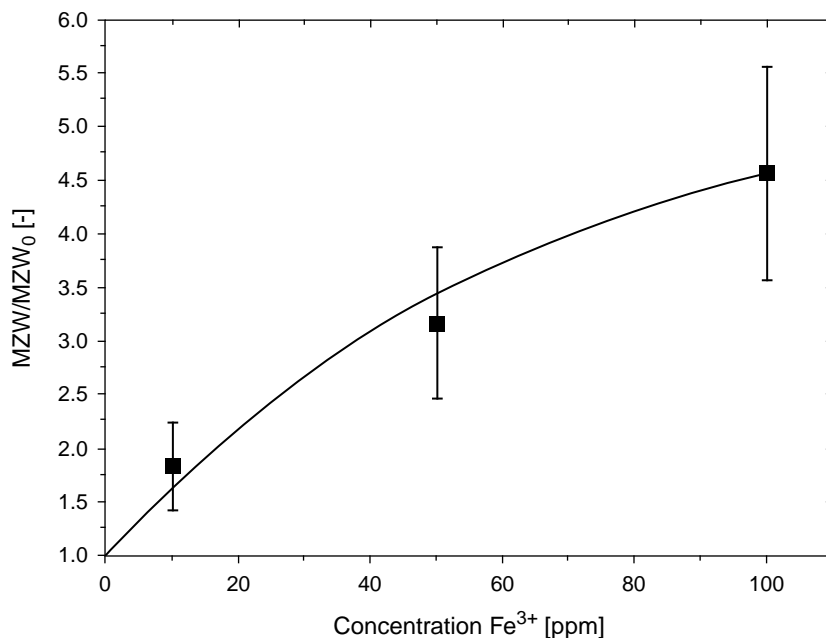


**Figure 6.2** Influence of  $\text{Fe}_3^{+}$  on the normalized growth rates of ammonium sulfate at pH 4 [11].

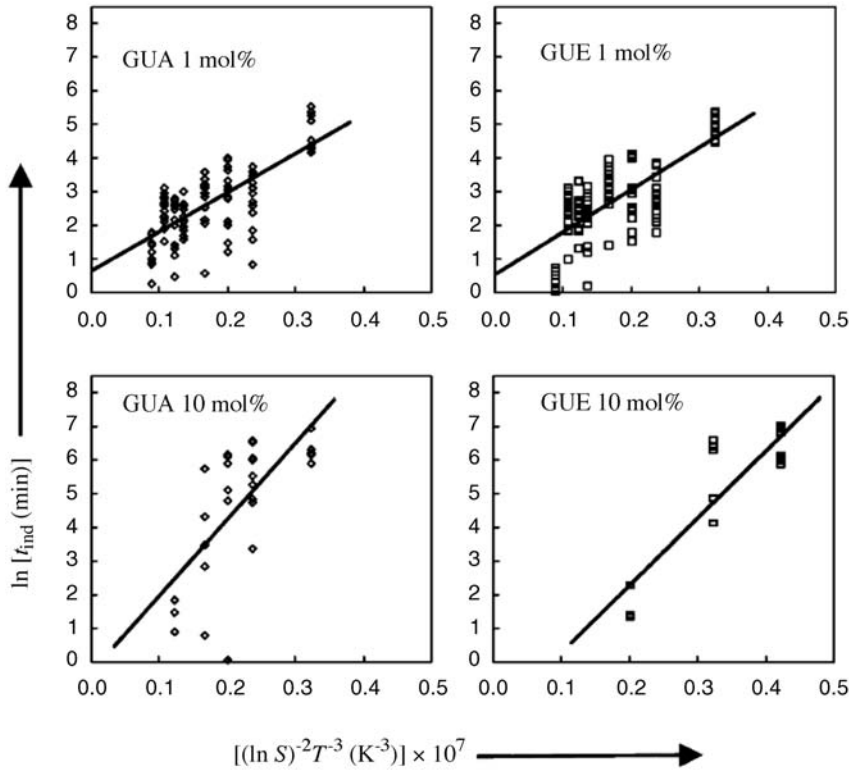


**Figure 6.3** Data of the induction time for the nucleation of vanillin in 2-propanol/water in the presence of various additives and regressions (solid lines) based on the method of least squares [12].

of which is proportional to the interfacial energy of the nucleus. This is illustrated in Figure 6.3 for the induction time of the nucleation for vanillin in 2-propanol/water in the presence of various additives.

Inhibition of nucleation has been investigated for a range of different crystallization phenomena, most notably for calcium carbonate crystallization with the aim of preventing fouling [8,13,14], crystallization of calcium oxalate with a view to understanding possible mechanisms for preventing urolithiasis (kidney stone formation) [15,16], crystallization of salts from well waters (prevention of well blockage in oil and gas exploitation [17], and sea water desalination [18].

Antinozzi *et al.* [19] studied the inhibition of calcium oxalate in the presence of citrate ions. It is worth emphasizing that these authors were very careful to ensure that the addition of citrate ions in the form of calcium citrate did not influence the concentration of the calcium ions in the solution. In taking this approach, they could ensure that the observed effects can be correlated with the citrate concentrations alone and avoid any additional common ion effects.

Lowered crystal growth rates are observed in the presence of calcium–citrate complex and citrate ions. Due to the action of citrate on specific crystal faces, the ions

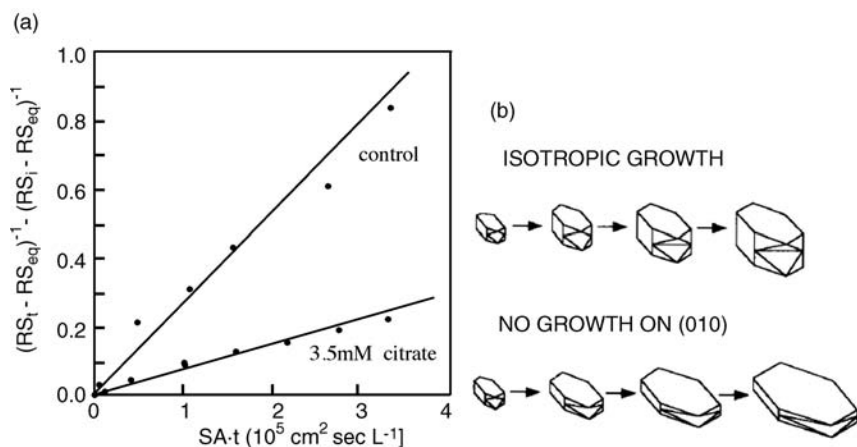


**Figure 6.4** (a) Determination of the crystal growth rates of COM crystals: reference and reduced growth rates in the presence of citrate. (b) Isotropic growth of the control sample (top) and inhibited growth in the presence of citrate (bottom) [19].

have a growth rate-modifying impact and, as a consequence, morphological changes of the crystals are observed. Figure 6.4 presents the corresponding effect on the normalized growth rates of calcium oxalate monohydrate (COM) in the presence of citrate and the morphological changes.

Pino-Garcia and Rasmuson [12] investigated the influence of additives of similar chemical structure on the crystallization of vanillin (Figure 6.5). With few exceptions, a reduction in interfacial energy was derived from nucleation data. In this paper, the authors also used molecular modeling in an attempt to rationalize the experimental observations, as will be discussed in more detail subsequently.

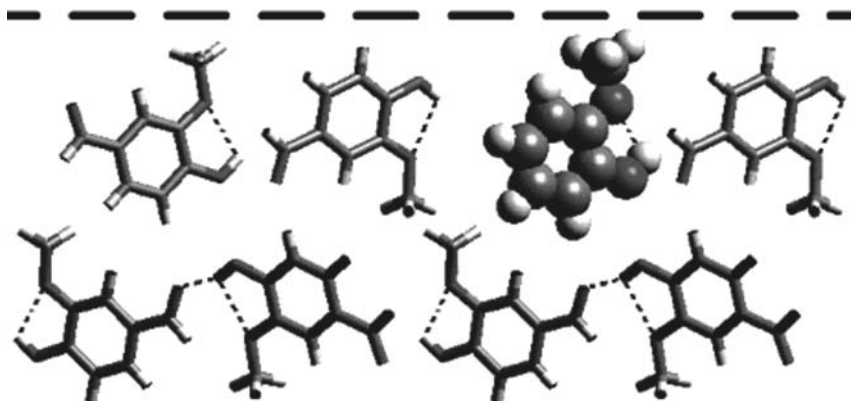


**Figure 6.5** Illustration of the differences in the molecules employed as additives compared to vanillin: View along the face  $\{001\}$  of vanillin showing an additive (guaiacol (GUA)) in the crystal lattice using the lattice integration approach [12].

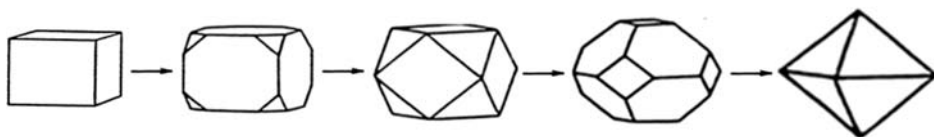


**Figure 6.6** Additive inhibited growth of a crystal [20].

The presence of additives affects the parameters supersaturation and interfacial energy. It is found that additives at high concentrations and at a high supersaturation do lower the induction time. The interfacial energy is estimated for various vanillin–additive systems. Lowering the interfacial energy was found for the additives acetovanillone, ethyl vanillin, 4-hydroxyacetophenone, and vanillic acid. Modeling aimed to examine the conditions of a growing surface. Using the surface adsorption and the lattice integration method, respectively, an additive is identified as nucleation modifier for vanillin.

#### 6.1.2.2 Crystal Growth Rates

Crystal growth rates can be expressed in a number of different ways. For the purpose of characterizing the growth kinetics in a manner that is relevant to the design of a crystallization process, it is convenient to express growth rates in terms of mass deposition rates or overall growth rates:

$$G = \frac{dm}{dt}. \quad (6.5)$$

$$R = \frac{dL}{dt}. \quad (6.6)$$

Both of these quantities can be expressed in terms of the respective face growth rates of the individual crystal faces.

The change of (relative) face growth rates affects the crystal morphology. Figure 6.6 represents a qualitative change of the morphology due to the action of additives.

The investigations conducted by Ulrich and coworkers [11] revealed the impact of  $\text{Fe}^{3+}$  ions on the (overall) crystal growth rates. An increasing amount of  $\text{Fe}^{3+}$  ions reduces crystal growth rates dramatically, as seen in Figure 6.7.

The presence of different impurities and the pH value [21] have strong impact on the crystal growth rates (Figure 6.8). It is differentiated between the thermodynamic and the kinetic effects. In the first case, impurities change the equilibrium saturation concentration; in the latter case, the impurities change the kinetics and hence the crystal growth rates. The combination of thermodynamic and kinetic effects is observed when the impurities affect the solubility, the metastable zone width, and the crystal growth rates. This is illustrated in Figure 6.9. See Ref. [22] for further reading.

The presence of impurity does not necessarily have an impact on the crystallization process, it can be inert (as seen in Figure 6.10 for NaCl in the presence of

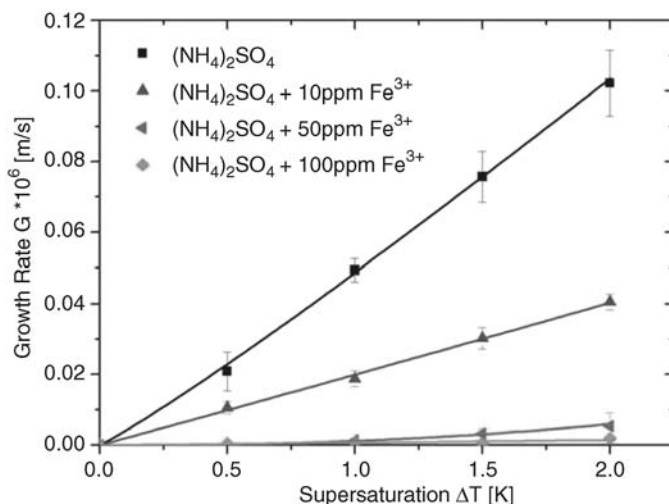


**Figure 6.7** Influence of  $\text{Fe}_3^+$  on the growth rate of ammonium sulfate at pH 4 and temperature level 30 °C [11].

$\text{CuSO}_4 \cdot 5\text{H}_2\text{O}$ ). It can, however, slow down the kinetic process up to a no growth (Figure 6.7), can modify the thermodynamics (shift the solubility as seen in Figure 6.9), and can have an impact on the morphology (via affecting a selective face) (Figure 6.6).

In order to understand and make use of the phenomena of different growth rates of crystal faces in the presence of additives, computational methods can be employed. Established routine methods are employed to calculate the morphology

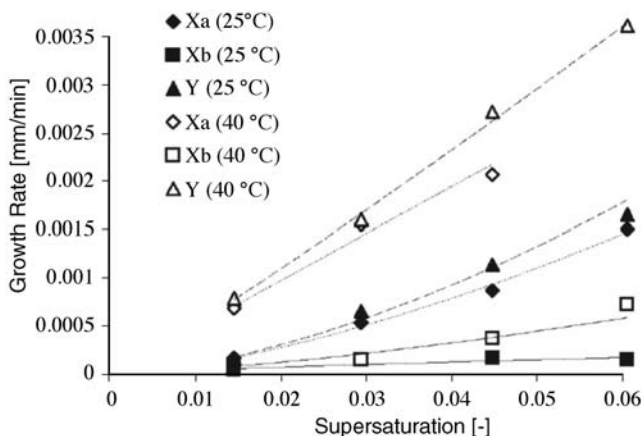


**Figure 6.8** The average growth rate value of a paracetamol single crystal as a function of supersaturation at 25 °C and 40 °C measured for the different growth directions (Xa, Xb, and Y) [23].

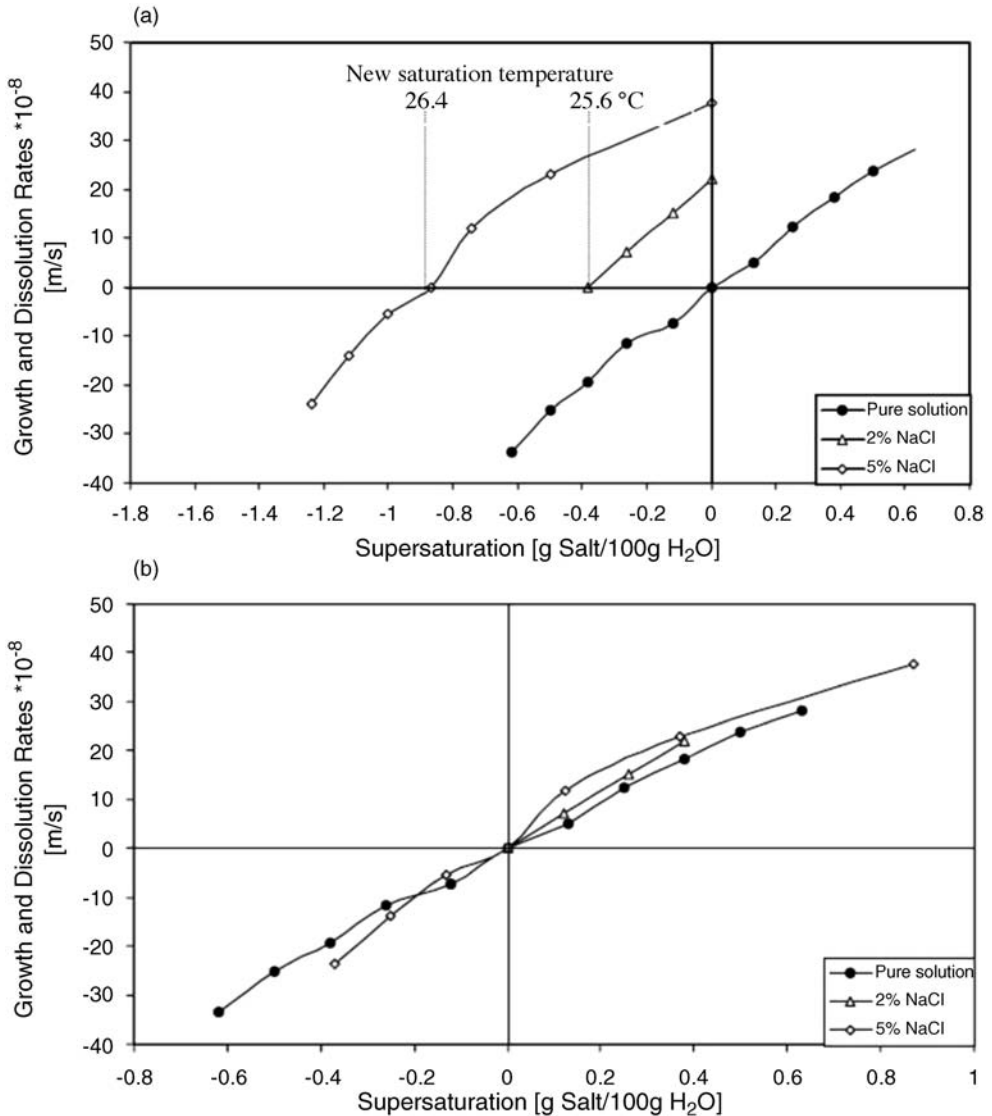


**Figure 6.9** Growth and dissolution rates of epsomite in the presence of NaCl. (a) Thermodynamic effect. (b) After correction of the supersaturation: kinetic effect [22].

of the pure crystal and the corresponding face growth rates. These methods form the base for further steps that aim to predict the face growth rates and the crystal morphology in the presence of additives. Molecular modeling and the concept of tailor-made additives are helpful tools and will be discussed in the following section.



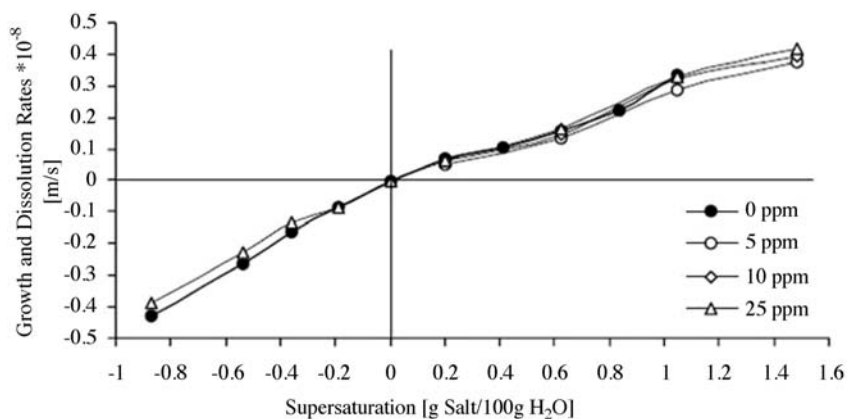


**Figure 6.10** Growth and dissolution rates of NaCl in the presence of  $\text{CuSO}_4 \cdot 5\text{H}_2\text{O}$  [22].

### 6.1.3

#### Habit Modification

The term crystal habit is used to describe the geometric appearance of the crystal. Related to the relative width and length and the number of the crystal faces, the habit can be, for example, acicular, tabular, or striated. The term morphology describes the number of all possible combinations of crystal faces. Thus, two crystals of an identical morphology may have different habits.

The crystal shape depends on the relative growth rate of the crystal faces. Major impact on the face growth rate is due to the effect of impurities (desired, for example, additives, and undesired) as well as solvents.

Depending on the species of the impurity, the molecule may selectively incorporate into the crystal lattice and may block or inhibit the growth of the face. Docherty and coworkers [24,25] classify additives as disruptive or blocker-type molecules (see Section 4.4). The disruptive effect of an additive is presented in Figure 6.11. It is seen that one part of the molecule can incorporate into the crystal lattice (due to the structural similarity), whereas one part of the molecule is significantly different in structure. The adsorption of the new growth layer will be disturbed here, since incorporation of the structural different moiety of the molecules is not possible. The disruptive effect has impact on the growth rate of the face.

The inhibited growth of a crystal surface and the thus caused change of the crystal habit are illustrated in Figure 6.12. The adsorption of the impurity causes the blockage of a crystal surface 1, which reduces the face growth rate. As a consequence, the surface 1 remains visible on the crystal. The growth rate of surface 2 is not affected. Figure 6.12 shows that in the presence of the impurity, surface 1 becomes larger on the crystal, whereas surface 2 grows without hindrances and, therefore, becomes smaller. This is referred to as morphological importance (MI) of a crystal surface. The morphological importance of a face is

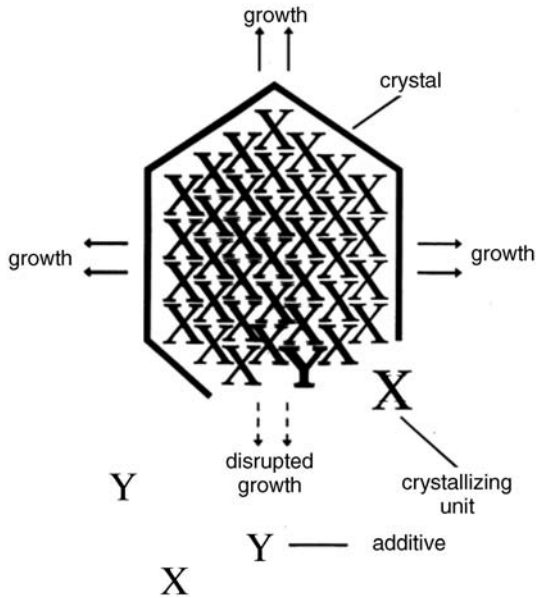


Figure 6.11 Additives: disruptive effect [26].

inversely proportional to the corresponding face growth rate:

$$MI_{hkl} \propto R_{hkl}. \quad (6.7)$$

An overview of additives acting as habit modifier for sodium chloride is given in Table 6.1. More information on habit-modifying agents for other substances is found in Ref. [6].

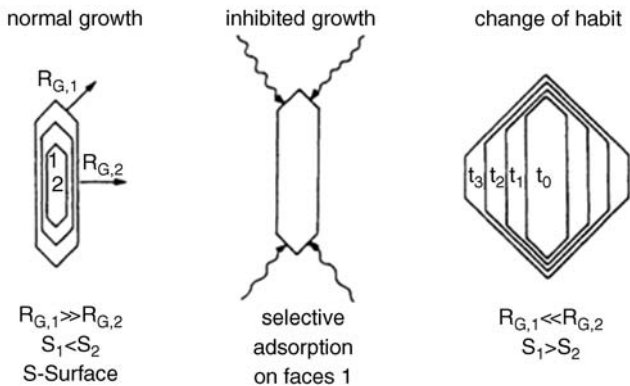


Figure 6.12 Generalization of the growth rate and the surface area when growth is inhibited [27].

**Table 6.1** Habit-modifying agents for sodium chloride [28].

Additive	Crystal change
Inorganic	
Manganous sulfate	
Manganous chloride	Octahedra
Cadmium chloride	Octahedra
Zinc chloride	Octahedra
Magnesium chloride	(110)
Bismuth chloride	Pyramidal and starlike
Complex cyanide	Dendritic, octahedral, and so on
Organic	
Urea	Octahedra
Glycine	Rhombic dodecahedra
Formamide	Octahedra
Nitrilotriacetic acid	Octahedra
Copolymers of vinyl acetate and maleic anhydride	Hollow-faced cubes
Polyvinyl acetate	Needles
Cysteine	Octahedra
Creatinine	Octahedra
Papaine	Octahedra
Monosodium glutamate	Octahedra
Sodium hexametaphosphate	Octahedra
Sodium hexametaphosphate plus an aluminum salt	Tetrikaidecahedra
Polyvinyl alcohol	Needles

## 6.2

### Influence of Impurities: Modeling

The various influences of impurities and additives on crystal growth phenomena can be best understood in terms of their influence on habit. Following, the need arises for a tool to model these influences on a molecular level. This molecular model can then be used to predict the effect of additives, which in the end results in tailoring additives to facilitate the goals of a crystallization process.

#### 6.2.1

##### Calculating Crystal Habit

For the shape of a crystal, the equilibrium and growth form have to be distinguished. The equilibrium form follows from the Wulff construction, while the growth form is determined by the relative growth rates of the different faces.

Several methods exist to calculate relative growth rates. The earliest and simplest of these was initially proposed by Bravais [29] and Friedel [30] and later extended by Donnay and Harker [31]. Known as the Bravais–Friedel–Donnay–Harker (BFDH) model, it states that the growth rate of a given crystallographic face with Miller indices  $(hkl)$  is proportional to the inverse of the interplanar distance  $d_{hkl}$  between

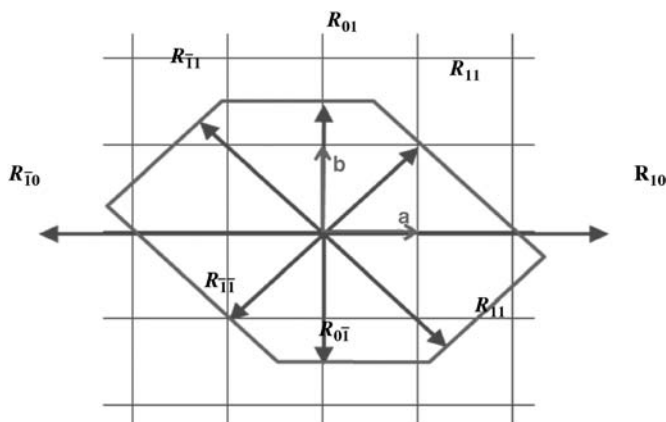


**Figure 6.13** Construction of the crystal habit using the calculated growth rates. The (relative) growth rates are plotted from the origin of the lattice as vectors with magnitudes proportional to the calculated relative rates and normal to the respective lattice planes. The smallest closed polygon joining the end points of the

rate vectors and with edges normal to the vectors represents the crystal habit. In this example, the end points growth rate vectors for the symmetry equivalent (10) and (−10) faces lie outside the smallest possible polygon. These faces are fast growing and are therefore not expressed in the crystal habit.

symmetry equivalent lattice planes:

$$R \propto \frac{1}{d_{hkl}}. \quad (6.8)$$

This model is purely geometric and does not require any knowledge of the crystal structure of the solid, merely the unit cell dimensions need to be known. The smaller the interplanar distance, the larger the relative growth rate, and as the low index faces are those with the largest interplanar distances, it is these that are expressed in the crystal habit.

Relative growth rates are straightforward to calculate using the BFDH model. The crystal habit can be constructed using the Wulff construction. Figure 6.13 illustrates the Wulff construction using a two-dimensional representation. The calculated growth rates are plotted from a central point normal to the respective crystallographic face. The smallest, closed, circumscribing polygon connecting end points of the vectors representing the growth rates generate the BFDH crystal habit.

Since the BFDH model is purely geometric and takes no account of the crystal structure, it cannot account for specific strong and directional interactions such as hydrogen bonding between distinct molecules.

#### 6.2.1.1 Surface Energy Model

The attachment energy model first published by Hartman and Perdok in 1955 [32] specifically accounts for the intermolecular interactions in the crystals when calculating relative growth rates. The growth rate of a crystal face is proportional to the attachment energy, which in turn can be calculated from the lattice energy

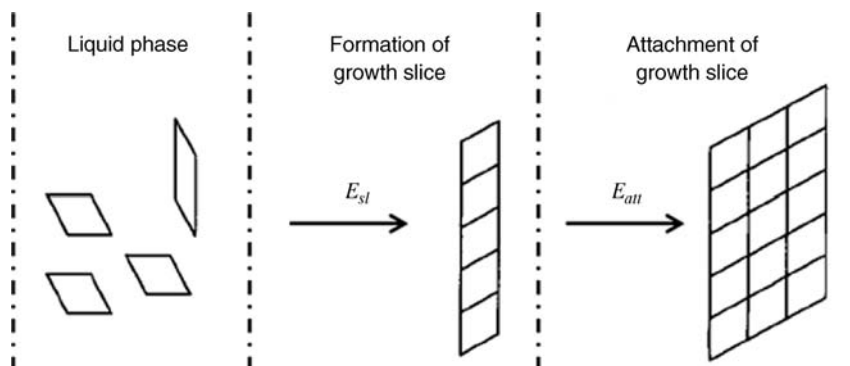


**Figure 6.14** Illustration of the formation of a growth slice from the liquid phase and attachment of the growth slice to a crystal surface [3,33].

defined as the energy required to bring a growth slice from an infinite distance to attach to a given crystal face. The sum of the attachment energy  $E_{att}$  and the slice energy  $E_{sl}$  – an energy required to generate the growth slice – is the lattice energy  $E_{lat}$  of the crystal:

$$E_{lat} = E_{sl} + E_{att}. \quad (6.9)$$

$$R \propto E_{att}. \quad (6.10)$$

The lattice energy is defined as the sum of all intermolecular interactions in the crystal and can be calculated rapidly using molecular mechanics. Using a suitable definition of the nature of the growth slice, the slice energy can also be calculated using molecular mechanics approaches and the attachment energy is then simply the difference between the slice energy and the lattice energy. The corresponding scheme is presented in Figure 6.14.

Although the attachment energy model accounts for the intermolecular interactions in the crystal, it does not account for any external influences such as solvent or impurity effects [34].

### 6.2.2

#### Molecular Modeling

Energy calculations for periodic crystals can be carried out by atom–atom method first developed by Kitaigorodsky *et al.* [35,36]. Here, all interactions within a given molecule as well as between distinct molecules are calculated by pairwise summation of all interactions between all pairs of atoms within a given system. It is, of course, impractical to calculate all possible interactions in an infinite system, but thankfully most interactions decay rapidly with increasing distance of the atoms and as a result it is necessary to calculate interactions only within a given radius around a central atom. In order to calculate the lattice energy, slice energy, and ultimately the attachment energy, a suitable expression for the intermolecular interactions has to be found. Molecular mechanics provides a

recipe for calculating the energy of molecules and assemblies of molecules based upon classical mechanics. The potential energy of a system is determined by the pairwise addition of all atom–atom interactions within the system and the resulting energy function is known as a force field. Over the past decades, a large number of different force fields have been developed, all of which have common features [37].

- a) A force field contains energy terms representing bonded (intramolecular) and nonbonded (both intra- and intermolecular) interactions.
- b) Each energy term contains parameters representing the strength of the interaction (force constants) and an expectation value for the particular interaction (i.e., standard bond length, standard bond angle, etc.).

At a minimum, a force field energy equation will account for valence (or bonded) interactions, such as bond stretch, bond angle, and bend and torsional energies, as well as nonbonded interactions via potential energy terms for dispersive (van der Waals) and electrostatic (Coulomb) interactions (Equation 6.12):

$$\begin{aligned}
 V(r) = & \sum_{\text{bonds}} \frac{k_i}{2} (l_i - l_{i,0})^2 + \sum_{\text{angles}} \frac{k_i}{2} (\theta_i - \theta_{i,0})^2 + \sum_{\text{torsions}} \frac{V_n}{2} (1 + \cos(n\omega - \gamma)) \\
 & + \cdots + \sum_{i=1}^N \sum_{j=i+1}^N \left( 4\epsilon_{ij} \left[ \left( \frac{\sigma_{ij}}{r_{ij}} \right)^{12} - \left( \frac{\sigma_{ij}}{r_{ij}} \right)^6 \right] + \frac{q_i q_j}{4\pi\epsilon_0 r_{ij}} \right).
 \end{aligned}
 \tag{6.11}$$

Here, the bond stretch and angle bend terms are represented by simple harmonic approximations each with their respective force constant  $k_i$  and an energy contribution that is proportional to the square of the deviation of the bond length or angle from the respective expectation values. The torsional term has a well-defined well depth  $V_n$  and discrete maxima and minima governed by the geometry of the torsion.

As a result of the definition of the lattice energy, the important terms for the calculation of the lattice energy are the dispersive van der Waals term and the coulomb term. In those cases where intermolecular hydrogen bonds exist and these are explicitly considered in the force field, these interactions would also be taken into account.

The electrostatic (coulomb) interactions take a special place in any force field expression. One major difference between the coulombic and all other interactions is the slow decay of the energy term with distance due to the  $1/r$  dependence. This results in practical issues when calculating these energy contributions, as much longer cutoff distances are required to ensure that the energy term is represented accurately in the total energy. An alternative method that calculates coulombic interactions in reciprocal space (Ewald summation) is preferable to direct space calculations due to faster convergence.

The precise functional form of the force field is empirical and is chosen not only with a view to giving a reasonable representation of the molecular geometry or energy but also with a consideration of the computational effort required to

compute the individual terms. This is especially important when working with large assemblies of molecules where a large number of atom–atom interactions must be calculated. The force field parameters, that is, force constants and expectation values, can be derived either from experimental data or from quantum mechanical calculations.

Several commercial and freely available modeling programs exist (such as CERIUS2 [38], MaterialsStudio 4.0 [39], and HABIT95 [40,41]), which frequently offer the use of different force fields. Experience shows that for the purpose of lattice energy calculations, the choice of force field is often not critical.

### 6.2.3

#### Modeling of Additives

Industrial crystallization processes rarely involve pure materials, but are rather used as purification process to achieve purified material and are often conducted from melt or solution. The presence of any other molecules but the crystalline material (substrate) frequently causes significant changes in the crystalline morphology [42–45]. Components denoted as additives or impurities predominantly occur in small amounts, whereas a solvent is represented by a large number of molecules in a mixed system. Here, the modeling procedure conducted for morphology prediction in the presence of additives is described.

Berkovitch-Yellin [46] introduces a simple approach for the morphology prediction in the presence of additives. Herein, the additive molecule is build into the unit cell to replace each of the host molecules stepwise. The structure of the polar surfaces is analyzed and the mappings of the corresponding electrostatic potentials are employed to determine the solvent effect. The method supplies accurate results and considers the solvent and the additive effect, respectively. Nonetheless, it is lacking the implementation of the concentration of solute, solvent, and potential additives in the solution.

Bennema *et al.* [47] introduce a modeling concept for the prediction of crystal morphology grown in the presence of additives, which is based on the knowledge of the internal crystal structure. The method employs the theory of the roughening temperature [48]. Preliminary investigations on the solid–liquid interface revealed an intensive structuring of molecules in the interfacial fluid phase and none in the bulk fluid phase [49].

By means of the approach presented by Liu and Bennema [50,51], the habit-controlling factors and the relative growth rate are related via the crystal growth mechanism. The PBC theory as well as the interfacial structure analysis forms the basis of the approach.

Investigations of Docherty and coworkers [24,25] aimed to model the effect of tailor-made additives. Disruptive and blocking additives disturb the local symmetry of the crystal. In terms of the presented approach, the molecules in the central crystal unit cell are stepwise replaced by an additive molecule, and the surrounding unit cells consist of host molecules (build-in). The obtained slice and attachment energies in presence of the additive are averaged. The attachment energy in

presence of additives and without additives is then compared. A second method is assuming the additive incorporation of an outer growth slice, and thus is not in the central unit cell. Here, the obtained slice energies in presence of the additive are averaged and the incorporation energy is calculated. The results are presented for disruptive tailor-made additives [24]. The presence of blocking tailor-made additives is modeled via the vacancy approach [25].

Myerson and Jang [52] developed an approach to reveal additives as possible growth inhibitors according to the binding energy difference. The method is based on the implementation of an additive molecule onto a crystal surface. Subsequently, by means of the binding energy, an interaction energy between the additive and the surface is obtained. The larger the absolute value of the binding energy, the stronger the interaction between the molecule and the corresponding face.

Despite the high accuracy of some methods in modeling the effect of additives on crystal morphology, the main drawback is the large amount of manual steps and time-consuming analysis required for a proper prediction. Furthermore, some of the aforementioned methods are very complex and difficult to handle for untrained users. Nonetheless, the presented investigations and findings provide with a good base for the development of approaches for morphology prediction. Simple approaches such as the build-in [53–55] and the surface docking [56] (illustrated in Figure 6.15) are deduced from the fundamental findings of these preliminary achievements. These methods are approaching the attachment energy via the building-in of additives [53,54,57], use of the PBC, and build-in coupled [55] or docking molecules on the surface [56]. All these methods estimate the attachment energy in the presence of additives based on the binding energy differences between the additive and the solute molecule on the crystalline surface. In addition, the latter method (surface docking) is successfully applied for the presence of various solvents [58,59]. However, these methods fail in considering supersaturation and concentration.

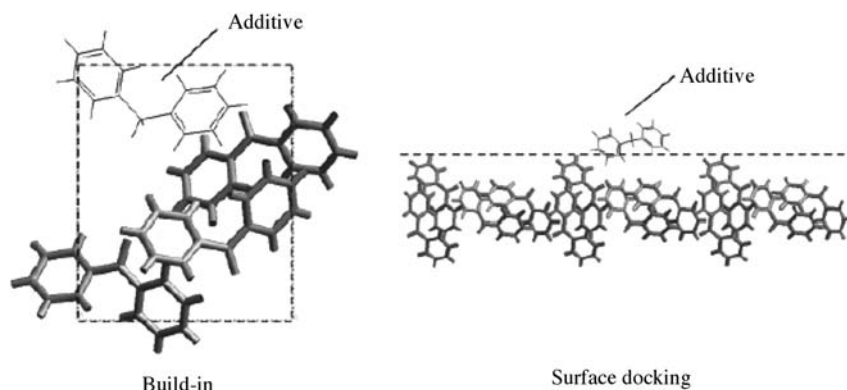


**Figure 6.15** Description of the build-in and the surface docking approaches [60].



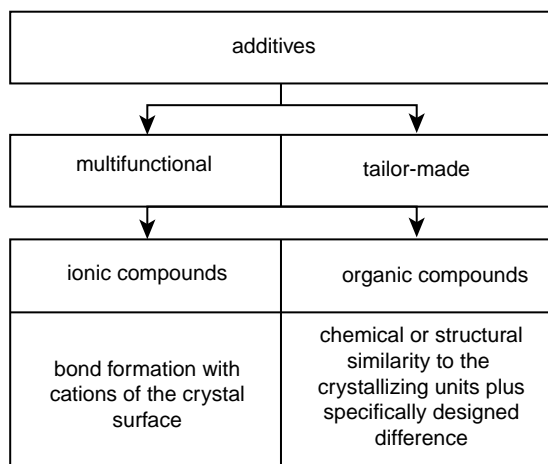


**Figure 6.16** Classification of additives (according to Refs [61,62]).

### 6.3

#### Tailor-Made Additives

The selective incorporation of additive molecules into a crystal surface is promoted if the molecular structure is similar to the structure of the crystalline host molecules. These are so-called designer impurities and the molecules are referred to as tailor-made additives [3]. A general classification of additives is given in Figure 6.16.

The focus of the investigations of Leiserowitz and coworkers [63] is on the tailor-made additives that disrupt or block crystal growth depending on the molecular structure. Berkovitch-Yellin *et al.* [64] suggested the presence of a polar axis within the crystal and therefore a selective incorporation of tailor-made additives at specific faces. Due to the additive's nature, a significant change of the face growth rates and hence the morphology is induced.

Here, controlled morphological changes can be induced, which can have strong impact on productivity and product quality in crystallization processes. Thus, tailor-made additives receive high industrial attention. As a result, a wide range of research is conducted to theoretically predict the effect of these molecules on the crystal morphology.

### 6.4

#### Modeling the Influence of Solvents

Numerous investigations aim to model the effect of solvents on the crystal morphology. A selection of those that are commonly referred to is presented in the following section. In addition, it can be traced by means of the scheme given in Figure 6.17.

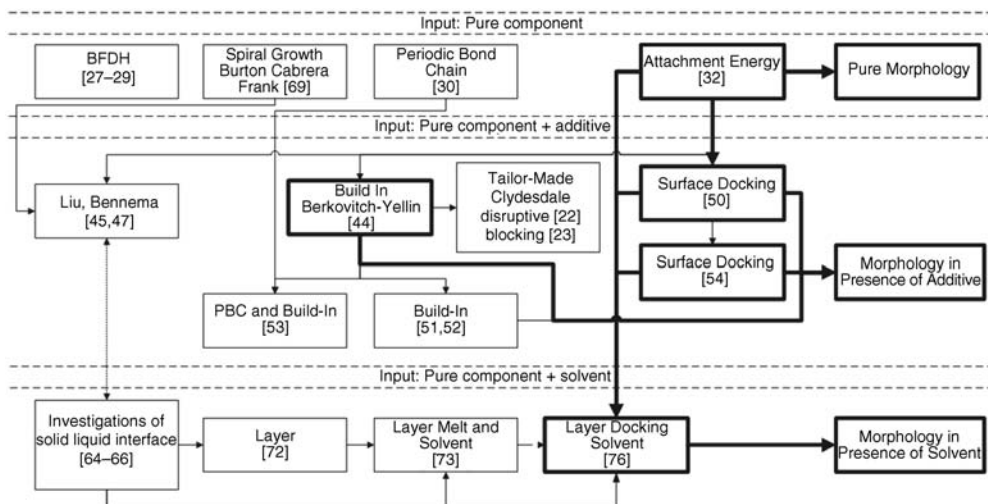


Figure 6.17 Tracing of modeling approaches [65].

Boek *et al.* [66,67] conducted molecular dynamics (MD) investigations on the solid–liquid interface for the pure solvent [66] and the corresponding investigations on the clustering of water in the solution are presented [67]. Subsequently, a saturated solution consisting of solute and solvent molecules is modeled in molecules dynamics for the solid–liquid investigations [68]. A detailed study is presented with plenty of information on a simple application in MD, since clear instructions are given in the corresponding publications.

The approach of Winn and Docherty [69] aims to predict the morphology of solution-grown crystals based on the properties of pure components. The crystal structure, the internal energy of the solid, and the surface free energy of the solvent are required to employ the method. It considers the 2D nucleation (birth and spread model) [70], spiral growth according to Burton *et al.* [71], and the occurrence of surface roughening. The provided concept aims to predict the morphology of crystals in the presence of solvents without an intensive molecular dynamics simulation of the liquid phase. Solely, a computational procedure for the calculation of the attachment energy for the pure crystal is carried out, while subsequent steps proceed manually as described by Winn and Docherty [69]. Further works [72,73] improved the predicted results for the presence of polar solvents. The drawback of intensive computation on the liquid side was eliminated and the method proceeds fast.

A drawback of the aforementioned approaches for modeling the additive effect is the missing implementation of concentration. In the above section, methods of modeling the solvent and the solution impact on the crystal morphology are introduced. Further intensive MD studies conducted by Ulrich and coworkers [56,59,74–77] considered the solid–liquid interface in the crystal growth process. Herein, based on the method of Boek *et al.* [66–68], a modeling of the effect of a

solution on the crystal morphology was conducted. The derived data enabled to estimate the attachment energy in the presence of solvents [76].

A manual on how to use the modeling approaches and which data and software need to be available in order to obtain the desired prediction is presented in the annex of Ref. [78].

## References

- 1 Prausnitz, J.M., Lichtenthaler, R.M., and de Azevedo, E.G. (1973) *Molecular Thermodynamics of Fluid-Phase Equilibria*, 3rd edn, Prentice-Hall, Eaglewood Cliffs, NJ.
- 2 Eidelman, N., Azoury, R., and Sarig, S. (1986) Reversal of trends in impurity effects on crystallization parameters. *J. Cryst. Growth*, **74**, 1–9.
- 3 Myerson, A.S. (2001) *Handbook of Industrial Crystallization*, Butterworth-Heinemann, Oxford, UK.
- 4 Linke, W.R. and Seidell, A. (1958) *Solubilities: Inorganic and Metal–Organic Compounds*, Vol. I, American Chemical Society, Washington, D.C..
- 5 Linke, W.R. and Seidell, A. (1965) *Solubilities: Inorganic and Metal–Organic Compounds*, Vol. II, American Chemical Society, Washington, D.C..
- 6 Nývlt, J. and Ulrich, J. (1995) *Admixtures in Crystallization*, Wiley–VCH Verlag GmbH, Weinheim.
- 7 Babic-Ivancic, V., Füredi-Milhofer, H., Purgaric, B., Brnicevic, N., and Despotovic, Z. (1985) Precipitation of calcium oxalates from high ionic strength solutions: III. The influence of reactant concentrations on the properties of the precipitates. *J. Cryst. Growth*, **71**, 655–663.
- 8 Mersmann, A. (2001) *Crystallization Technology Handbook*, Marcel Dekker, New York.
- 9 Mersmann, A. and Bartosch, K. (1998) How to predict the metastable zone width. *J. Cryst. Growth*, **183**, 240–250.
- 10 Pertig, D., Buchfink, R., Petersen, S., Stelzer, T., and Ulrich, J. (2011) Inline analyzing of industrial crystallization processes by an innovative ultrasonic probe technique. *Chem. Eng. Technol.*, **34**, 639–646.
- 11 Buchfink, R., Schmidt, C., and Ulrich, J. (2011)  $\text{Fe}_3^{+}$  as an example of the effect of trivalent additives on the crystallization of inorganic compounds, here ammonium sulfate. *CrystEngComm*, **13**, 1118–1122.
- 12 Pino-García, O. and Rasmuson, A.C. (2004) Influence of additives on nucleation of vanillin: experiments and introductory molecular simulations. *Cryst. Growth Des.*, **4**, 1025–1037.
- 13 Kavanagh, A.B., Rayment, T., Price, T.J. (1990) Inhibitor Effects on Calcite Growth at low Supersaturations. in *J. Chem. Soc., Faraday Trans* **86**, 965–972.
- 14 Tomson, M.B. (1983) Effect of precipitation inhibitors on calcium carbonate scale formation. *J. Cryst. Growth*, **62**, 106–112.
- 15 Giannimaras, E.K. and Koutsoukos, P.G. (1988) Precipitation of calcium carbonate in aqueous solutions in the presence of oxalate anions. *Langmuir*, **4**, 855–861.
- 16 Sarig, S., Raphael, M., and Ron, A. (1973) Calcium oxalate crystallization from inhibited solutions. *Israel J. Chem.*, **11**, 635–643.
- 17 Amjad, Z. (1987) Kinetic study of the seeded growth of calcium carbonate in the presence of benzenepolycarboxylic acids. *Langmuir*, **3**, 224–228.
- 18 Omar, W., Chen, J., and Ulrich, J. (2010) Reduction of seawater scale forming potential using the fluidized bed crystallization technology. *Desalination*, **250**, 95–100.
- 19 Antinozzi, P.A., Brown, C.M., and Purich, D.L. (1992) Calcium oxalate monohydrate crystallization: citrate inhibition of nucleation and growth steps. *J. Cryst. Growth*, **125**, 215–222.
- 20 Mullin, J.W. (2001) *Crystallization*, Butterworth-Heinemann, Oxford, UK.
- 21 Mohameed, H.A. and Ulrich, J. (1996) Influence of the pH-value on the growth and dissolution rate of potassium chloride. *Cryst. Res. Technol.*, **31** (2), 27–31.

- 22 Al-Jiabbouri, S., Strege, C., and Ulrich, J. (2002) Crystallization kinetics of epsomite influenced by pH-value and impurities. *J. Cryst. Growth*, **236**, 400–406.
- 23 Omar, W., Al-Sayed, S., Sultan, A. and Ulrich, J. (2008) Growth rate of single acetaminophen crystals in supersaturated aqueous solution under different operating conditions. **43**, 22–27.
- 24 Clydesdale, G., Roberts, K.J., and Docherty, R. (1994) Modeling the morphology of molecular crystals in the presence of disruptive tailor-made additives. *J. Cryst. Growth*, **135**, 331–340.
- 25 Clydesdale, G., Roberts, K.J., Lewtas, K., and Docherty, R. (1994) Modeling the morphology of molecular crystals in the presence of blocking tailor-made additives. *J. Cryst. Growth*, **141**, 443–450.
- 26 Ulrich, J. and Niehörster, S. (1994) Maßgeschneidert und multifunktionell. *Chem. Ind.*, **11**, 46–47.
- 27 Weissbuch, I., Shimon, L.J.W., Landau, E.M., Popovitz-Biro, R., Berkovitch-Yellin, Z., Addadi, L., Lahav, M., and Leiserowitz, L. (1986) "Tailormade" auxiliaries for nucleation, growth and dissolution of organic crystals. *Pure Appl. Chem.*, **58**, 947–954.
- 28 Ulrich, J. (2004) Fremdstoffbeeinflussung in der Kristallisation, in *Kristallisation in der Industriellen Praxis* (ed. G. Hofmann), Wiley-VCH Verlag GmbH, Weinheim, pp. 131–147.
- 29 Bravais, A. (1866) *Etudes Crystallographiques*, Gauthier-Villars, Paris, France.
- 30 Friedel, M.G. (1907) Etudes Sur la Loi de Bravais. *Bull. Soc. Franc. Mineral.*, **30**, 326–455.
- 31 Donnay, J.D. and Harker, D. (1937) A new law for crystal morphology extending the law of bravais. *Am. Mineral.*, **22**, 446–467.
- 32 Hartman, P. and Perdok, W.G. (1955) On the relations between structure and morphology of crystals I, II and III. *Acta Crystallogr.*, **8**, 49–52, 521–524, 525–529.
- 33 Docherty, R. and Meenan, P. (1999) The study of organic materials using computational chemistry, in *Molecular Modeling Applications in Crystallization* (ed. A.S. Myerson), Cambridge University Press, New York, pp. 106–165.
- 34 Hartman, P. and Bennema, P. (1980) The attachment energy as a habit controlling factor I–III. *J. Cryst. Growth*, **49**, 145–156, 157–165, 166–170.
- 35 Kitaigorodsky, A.I. (1955) *Organic Chemical Crystals*, Consultants Bureau, New York.
- 36 Kitaigorodsky, A.I., Mirskaya, K.V., and Tobvis, A.B. (1968) Lattice energy of crystalline benzene in the atom–atom approximation. *Soviet Phys. Crystallogr.*, **13**, 176–180.
- 37 Leach, A.R. (2001) *Molecular Modeling: Principles and Applications*, Pearson Education Ltd., Essex, UK.
- 38 Molecular Simulations Inc. (1999) CERIU2 Software, San Diego, CA.
- 39 Accelrys Software Inc. (2005) MaterialsStudio 4.0, San Diego, CA.
- 40 Clydesdale, G., Roberts, K.J., and Docherty, R. (1991) HABIT: a program for predicting the morphology of molecular crystals. *Comp. Phys. Commun.*, **64**, 311–328.
- 41 Clydesdale, G., Roberts, K.J., and Docherty, R. (1996) HABIT95: a program for predicting the morphology of molecular crystals when mediated by the growth environment, in *Crystal Growth of Organic Materials* (eds A.S. Myerson, D. Green, and P. Meenan), American Chemical Society, Washington DC, pp. 43–52.
- 42 Bunyan, J.M.E., Shankland, N., and Sheen, D.B. (1991) Solvent effects on the morphology of ibuprofen. *AIChE Symp. Ser.*, **87**, 44–57.
- 43 Davey, R.J. (1976) Effect of impurity adsorption on the kinetics of crystal growth. *J. Cryst. Growth*, **34**, 109–119.
- 44 Davey, R.J., Mullin, J.W., and Whiting, M.J.L. (1982) Habit modification of succinic acid crystals grown from different solvents. *J. Cryst. Growth*, **58**, 304–312.
- 45 Wireko, F.C., Shimon, L.J.W., Frolov, F., Berkovitch-Yellin, Z., Lahav, M., and Leiserowitz, L. (1987) Effect of solvent on the growth of organic crystals: 1. The riddle of  $\alpha$ -resorcinol. *J. Phys. Chem.*, **91**, 474–481.
- 46 Berkovitch-Yellin, Z. (1985) Toward an *ab initio* derivation of crystal morphology. *J. Am. Chem. Soc.*, **107**, 3111–3122.
- 47 Bennema, P., Liu, X.Y., Lewtas, K., Tack, R.D., Rijpkema, J.J.M., and Roberts, K.J. (1992) Morphology of orthorhombic long

- chain normal alkenes: theory and observations. *J. Cryst. Growth*, **121**, 679–696.
- 48 Jackson, J.A. (1958) Mechanism of growth, in *Liquid Materials and Solidification*, American Society for Metals, Cleveland, OH, pp. 174–186.
  - 49 Liu, X.Y. and Bennema, P. (1992) The equilibrium state of solid–liquid interfaces of aliphatic compounds. *J. Chem. Phys.*, **97**, 3600–3609.
  - 50 Liu, X.Y. and Bennema, P. (1996) Theoretical consideration of the growth morphology of crystals. *Phys. Rev. B*, **53**, 2314–2325.
  - 51 Liu, X.Y. and Bennema, P. (1996) Prediction of the growth morphology of crystals. *J. Cryst. Growth*, **166**, 117–123.
  - 52 Myerson, A.S. and Jang, S.M. (1995) A comparison of binding energy and metastable zone width for adipic acid with various additives. *J. Cryst. Growth*, **156**, 459–466.
  - 53 Niehörster, S. and Ulrich, J. (1995) Designing morphology by a simple approach. *Cryst. Res. Technol.*, **30**, 389–395.
  - 54 Mattos, M.V.C., Niehörster, S., Wangnick, K., and Ulrich, J. (1996) Comparison between theoretical and experimental habit modification of crystalline stabilizers for foods. Proceedings of 13th International Symposium on Industrial Crystallization (ISIC) 1996 (eds B. Biscans and N. Gabas), Toulouse, France, pp. 19–24.
  - 55 Schmiech, P. and Ulrich, J. (2004) Improvement of a model for the crystal habit prediction by use of PBC-vectors. *Chem. Eng. Technol.*, **27**, 733–736.
  - 56 Lu, J.J. and Ulrich, J. (2004) Improved understanding of molecular modelling: the importance of additive incorporation. *J. Cryst. Growth*, **270**, 203–210.
  - 57 Niehörster, S., Mattos, M., and Ulrich, J. (1996) An approach to design the habit of organic crystals: modeling and verification. Proceedings of 13<sup>th</sup> International Symposium on Industrial Crystallization (ISIC) 1996 (eds B. Biscans and N. Gabas), Toulouse, France, pp. 25–30.
  - 58 Schmidt, C., Yürüdü, C., Wachsmuth, A., and Ulrich, J. (2011) Modeling the morphology of benzoic acid crystals grown from aqueous solution. *CrystEngComm*, **13**, 1159–1169.
  - 59 Schmidt, C. and Ulrich, J. (2011) Morphology prediction of benzoic acid crystals: thermostats. *Chem. Eng. Technol.*, **34**, 563–570.
  - 60 Lu, J.J. and Ulrich, J. (2005) Influence of supersaturation on crystal morphology: experimental and theoretical study. *Cryst. Res. Technol.*, **40**, 839–846.
  - 61 van Rosmalen, G.M., Witkamp, G.J., and Vreugd, C.H. (1987) Additive and impurity effects in crystallization processes, in *Proceedings of the 10th International Symposium on Industrial Crystallization (ISIC) 1987* (eds J. Nývlt and S. Žáček), Elsevier, New York, pp. 15–20.
  - 62 van der Leerden, M.C., van Rosmalen, G. M., Vreugd, C.H., and Witkamp, G.J. (1989) Einfluss von Additiven und Verunreinigungen auf Kristallisationsprozesse. *Chem. Ing. Tech.*, **61**, 385–395.
  - 63 Addadi, L., Berkovitch-Yellin, Z., Domb, N., Gati, E., Lahav, M., and Leiserowitz, L. (1982) Resolution of conglomerates by stereoselective habit modifications. *Nature*, **296**, 21–26.
  - 64 Berkovitch-Yellin, Z., Addadi, L., Idelson, M., Lahav, M., and Leiserowitz, L. (1982) Absolute configuration of chiral polar crystals. *Nature*, **296**, 27–34.
  - 65 Schmidt, C. and Ulrich, J. (2011) Molecular modeling: scientific toy or industrial tool. Proceedings of the 20th Nisshin Engineering Particle Technology International Seminar (NEPTIS), 2011 (ed. K. Higashitani), Otsu, Japan, pp. 1–10.
  - 66 Boek, E.S., Briels, W.J., van Erden, J., and Feil, D. (1992) Molecular-dynamics simulations of interfaces between water and crystalline urea. *J. Phys. Chem.*, **96**, 7010–7018.
  - 67 Boek, E.S. and Briels, W.J. (1993) Molecular dynamics simulations of aqueous urea solutions: study of dimer stability and solution structure, and calculation of the total nitrogen radial distribution function  $G_N(r)$ . *J. Chem. Phys.*, **98**, 1422–1427.
  - 68 Boek, E.S., Briels, W.J., and Feil, D. (1994) Interfaces between a saturated urea

- solution and crystalline urea: a molecular dynamics study. *J. Phys. Chem.*, **98**, 1674–1681.
- 69 Winn, D. and Docherty, M.F. (1998) A new technique for predicting the shape of solution-grown organic crystals. *AIChE J.*, **44**, 2501–2514.
- 70 Ohara, M. and Reid, R.C. (1973) *Modeling Crystal Growth Rates from Solution*, Prentice-Hall, Eaglewood Cliffs, NJ.
- 71 Burton, W.K., Cabrera, N., and Frank, F.C. (1951) The growth of crystals and the equilibrium structure of their surfaces. *Phil. Trans. R. Soc. Lond.*, **A243**, 299–358.
- 72 Winn, D. and Docherty, M.F. (2000) Modeling crystal shapes of organic materials grown from solution. *AIChE J.*, **47**, 1359–1377.
- 73 Winn, D. and Docherty, M.F. (2002) Predicting shape of organic crystals grown from polar solvents. *Chem. Eng. Sci.*, **57**, 1805–1813.
- 74 Fiebig, A., Jones, M.J., and Ulrich, J. (2007) Predicting the effect of impurity adsorption on crystal morphology. *Cryst. Growth Des.*, **7**, 1623–1627.
- 75 Yürüdü, C., Jones, M.J., and Ulrich, J. (2012) Modeling of diffusion for crystal growth. *Soft Mater.*, **10**, 257–284.
- 76 Schmidt, C. and Ulrich, J. (2011) Predicting crystal habits grown from aqueous multi-component solutions: method of computation involving multiple solvents, in *Proceedings of the 18th International Workshop on Industrial Crystallization (BIWIC), 2011* (eds S.S. Kadam, S.A. Kulkarni, and J.H.T. Horst), Delft University of Technology, Delft, Netherlands, pp. 278–283.
- 77 Schmidt, C. and Ulrich, J. (2011) Crystal habit prediction including the liquid as well as the solid side, in *Proceedings of the 18th International Symposium on Industrial Crystallization (ISIC), 2011* (ed. M. Mazzotti), AIDIC, Milan, Italy, pp. 96–97.
- 78 Schmidt, C. (2012) Predicting crystal morphology grown from aqueous solution. PhD thesis. Martin-Luther-Universität Halle-Wittenberg.

## 7

### Purification by Crystallization

*Heike Lorenz and Wolfgang Beckmann*

Crystallization can be regarded as a process to separate the target compound from a complex matrix of starting materials or from a reaction mixture containing coproducts or by-products. This separation is generally accompanied by a depletion of impurities present in the starting material; crystallization entails a purification of the target compound. The rejection of impurities by the growing crystal is highly specific with respect to both the target molecule and the impurity to be depleted. This depletion is due to the fact that the fit of most impurity molecules into the lattice of the target molecule is energetically less favorable than the inclusion of the target molecule. This leads to a net rejection of the impurities. In this sense, purification can be regarded as molecular recognition.

The purification effect can be limited or decreased by a finite solubility of the impurity in the target crystal and also by kinetic effects such as fast growth conditions whereby the rejection becomes incomplete. Most detrimental to the purification is the incomplete removal of the mother phase from the isolated crop.

#### 7.1

##### Introduction

The separation of a target compound from a complex mixture of starting materials or from a reaction mixture is generally accompanied by a purification of the target compound. Thus, in principle, separation and purification are equivalent terms: purification is commonly used to indicate a content of the impurity to be much below the content of the target compound. Thus, purification is a rather special case of separation. In this context, it is often distinguished between macro- and microimpurities, where the first refers to an impurity content of the same order of magnitude or one order lower than the content of the target compound. On the contrary, microimpurities refer to contents of at least two orders of magnitude lower than that of the target component. This differentiation is useful, since micro- and macroimpurities may affect the crystallization process differently.

While microimpurities in particular have an impact on phenomena at the crystal–liquid interface, large impurity contents may influence the solubility and driving force of crystallization (degree of supersaturation), the physical and chemical properties of the solution and of the crystalline product (particle size and particle size distribution, purity), and the phenomena at the crystal–liquid interface.

It has been discussed in Chapter 2.1.5 that a crystal in equilibrium with its mother phase tends to acquire the form with the least free enthalpy, *inter alia*, by maximizing the intermolecular interactions. Due to the structural differences between the impurity and target molecule, almost any impurity molecule will have a different interaction enthalpy in the crystal lattice than the target molecule. Typically, the enthalpic term for the interaction will increase by replacing a target molecule by a foreign molecule. This is equivalent to the reversible rejection of additives by a growing interface, as discussed in Chapter 6. However, cases are known where the interaction enthalpy is not drastically changed by the incorporation of the impurity into the crystal lattice of the target component. This leads to a finite solubility in the solid state leading to a partial or complete miscibility in the solid state (Chapter 3).

The efficiency of the rejection of impurities can be decreased by kinetic effects of the growing interface, that is, when the desorption of impurity molecules from the interface is not fast enough so that the impurity molecules become kinetically incorporated. In addition, any depletion of impurities must be accompanied by a transport of this impurity molecule from the interface into the bulk of the mother phase; this transport can also become a limiting factor for the purification.

Besides this molecular incorporation of impurities into the lattice either by a finite solubility or kinetic incorporation, impurities can also be incorporated into the growing crystal in three-dimensional defects, as liquid inclusions (Figure 7.1 right).

In addition, impurities can be incorporated into the crop via mother liquor entrapped between crystals and mother liquor adhering to the crystal surface

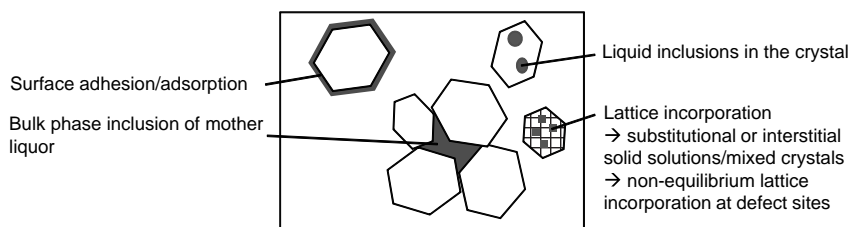


**Figure 7.1** Location of impurities in a crystalline product after solid–liquid separation. The growing crystal itself can incorporate impurities either in the lattice on a molecular level or as three-dimensional faults, liquid

inclusions (right). In addition, the crop can contain impurities via mother liquor, either adsorbed on the crystals or entrapped between crystals (left).



**Table 7.1** Incorporation mechanisms of impurities and potential purification methods (based on Ref. [1]).

Phenomena	Physical properties	Purification methods
Adhesion to the surface	Interfacial tension and viscosity	Washing and centrifuge
Macroscale inclusion	Surface irregularity	Crushing, reslurrying, and washing
Microscale inclusion	Step behavior	Sweating, reslurrying
Lattice incorporation	Resemblance of molecular shapes	Sweating, fractional crystallization

(Figure 7.1 left). Though in principle the removal of the mother phase is straightforward, incomplete removal is the most important source of impurities in technical crystallizations.

All but the formation of solid solutions are kinetically controlled processes that can be modified by the crystallization conditions. The formation of a solid solution is a thermodynamically controlled process. The physical properties responsible for the different types of impurity incorporation are summarized in Table 7.1. Also given are typical methods to remove the impurities incorporated via the different mechanisms.

The total amount of impurities in the crystalline product,  $m_{\text{Imp}}$ , is the sum of all potential impurities as depicted in Figure 7.1, that is, the contributions of the surface adsorption,  $m_1$ , of bulk phase inclusion of mother liquor,  $m_2$ , the liquid inclusions in the crystal,  $m_3$ , and the lattice incorporation,  $m_4$  (Equation 7.1):

$$m_{\text{Imp}} = m_1 + m_2 + m_3 + m_4. \quad (7.1)$$

In the following, the incorporation of impurities into the crystal lattice and the crystalline crop via adsorption and bulk phase inclusion of mother liquor will be discussed in detail.

## 7.2

### Mechanisms of Impurity Incorporation and Purification

The incorporation of impurities into the lattice by the formation of partial or complete solid solutions cannot be influenced by process conditions. In this respect, this is the limit of the purification effect attainable. Contrarily, the incorporation of impurities by 3D inclusion or adhesion to mother liquor in or onto the crop can be influenced by modifying the growth, that is, crystallization conditions or the workup conditions in downstream processes. In the case of partial or complete solid solutions, the purification of a single-step crystallization is limited, higher purities can be obtained by fractional crystallization techniques.

## 7.2.1

## Solubility in the Solid State

Solid solutions of the impurity and the target compound can be formed via two different mechanisms that are regarded as limiting cases. Either the impurity molecules occupy sites in-between host molecules, forming so-called interstitial mixed crystals, or the impurity (guest) molecules replace the molecules of the target compound (host) forming so-called substitutional mixed crystals.

The formation of solid solutions requires a certain resemblance of the molecular shapes and sizes. According to Matsuoka [1], about 14% of the organic systems exhibit (partial or even full) miscibility in the solid state in the binary melt phase diagrams (Figure 3.7). Thus, the formation of mixed crystals is not rare. However, the number of such phase diagrams published is sparse, partly due to the fact that the solubilities in solid state might be low and therefore difficult to detect. In addition, achieving equilibrium conditions in solid state transformations is only very slow, as the mobility of molecules in the solid state is very low, making the determination difficult. Extensive information on the topic is given in Refs [2,3].

In case of partial miscibility of the target product and the impurity, the maximal achievable purity of the crystallization product ( $P$ ) is determined by the binary phase diagram of  $P$  and the impurity (Imp). A crystallization under carefully controlled conditions will only provide a crystalline product of very high purity when the target compound and the impurity are completely immiscible in solid state as shown in Figure 7.2a. It is possible to achieve purification of materials that are free of impurities at the ppm level. In case of miscibility of the target molecule and the impurity a partial purification is only achieved, that is, several purification steps are required to gain highly pure  $P$ . It is shown in Figure 7.2b that starting with an initial impurity content of  $x_{\text{Imp}} = x_0$ , after a first purification step  $x_{\text{Imp},s}$  remains. Clearly, the location of the tie line determines the degree of purification and the product yield (according to the lever rule).

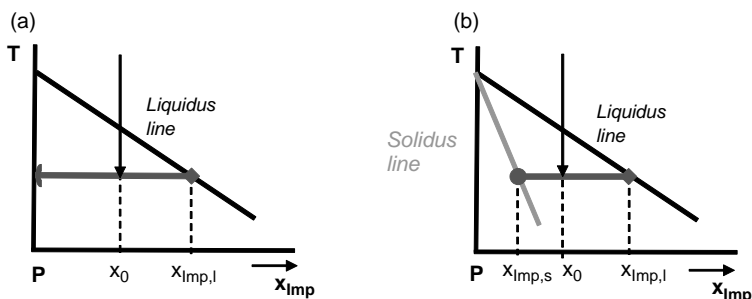


**Figure 7.2** Illustration of the phase behavior for immiscibility (a) and miscibility (b) in the solid state. The figures only show the part of the phase diagram close to the target compound

( $P$ , target product; Imp, impurity). The  $x$ -axis is given in mol fractions  $x$ . The tie line specifies the composition of the solid phase in equilibrium with the liquid phase.

The incorporation of similarly shaped guest components into the lattice of a host component can be quantified by a distribution coefficient,  $k_{eq}$ , equal to the ratio of the impurity content in the solid phase,  $x_{Imp,s}$ , to that in the liquid phase,  $x_{Imp,l}$  (with  $x$  in mol fractions), supposing both phases are in equilibrium at a given temperature. The so-defined coefficient is called thermodynamic distribution (or segregation) coefficient (Equation 7.2):

$$k_{eq} = x_{Imp,s}/x_{Imp,l}. \quad (7.2)$$

The thermodynamic distribution coefficient is only a constant in the region close to the target component, that is, at ideal dilution with respect to the impurity (solidus and liquidus lines are linear). For values of  $k_{eq}$  equal to unity, no purification is achieved; for  $k_{eq}$  less than unity, a purification can be obtained with highest purity for  $k_{eq}$  close to zero.

### 7.2.2

#### Fractional Crystallization

Successive purification steps using the solid phases separated after each step lead to a stepwise purification, a process called fractional crystallization. It differs from simple repeated recrystallization; in fractional crystallization procedures, both the crystals obtained and the mother liquor are repeatedly fractionated. Usually two or more compounds shall be separated with the objective of isolating each as pure substance. In case that the target compound and the impurity form solid solutions, elaborate fractionation schemes may be necessary to finally provide pure substances. The procedure is best illustrated by means of the binary phase diagram. Figure 7.3 shows the phase diagram of a model system exhibiting full miscibility in the solid state.

Assuming a melt having an initial composition  $x_0$  is cooled down to a temperature  $T_0$ , it splits along the tie line into a solid phase of composition  $x_{Imp,s1}$  and a liquid phase of composition  $x_{Imp,l1}$ . This liquid phase is enriched with the impurity, while in the solid phase (consisting of mixed crystals of composition  $x_{Imp,s1}$ ) the impurity is depleted, that is, a first partial purification has been achieved. The solid phase is separated from the liquid phase and subjected to a next purification (melt/recrystallization) step. A melt of this solid cooled down to a temperature  $T_1$ , in equilibrium again splits into a new liquid phase and a solid, that has a higher purity compared to the first step ( $x_{Imp,s2} < x_{Imp,s1}$ ). In equilibrium between melt and mixed crystals, the melt is always enriched with the component having the lower melting temperature, while the mixed crystals are enriched with the component having the higher melting temperature (Konovalov' rule). Each further purification step increases the purity of the target compound, as seen in Figure 7.3.

A phase diagram showing complete miscibility in the solid state is known, for example, for the binary systems of phenanthrene and anthracene or naphthalene and  $\beta$ -naphthol.

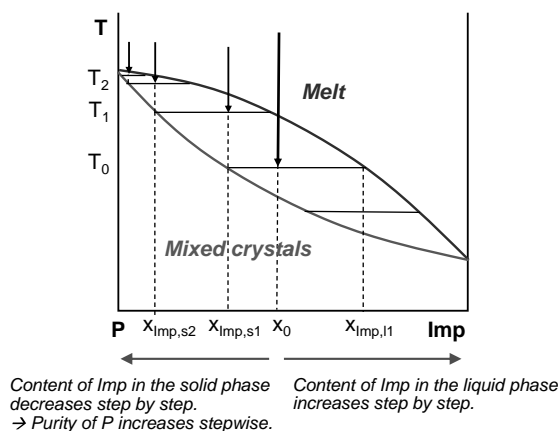


**Figure 7.3** Phase diagram of a target compound ( $P$ ) and an impurity ( $Imp$ ), a system characterized by full miscibility in the solid state. Thus,  $P$  and  $Imp$  form a so-called continuous series of mixed crystals covering the entire concentration range in the phase

diagram. The segments of the tie line left and right to the appropriate start composition determine the amount of liquid and solid phases provided as a result of the purification step performed.

### 7.2.3

#### Inclusion and Surface Adsorption of Impurities

The thermodynamic distribution coefficient  $k_{eq}$  characterizes the maximum purity achievable by crystallization; it is a substance-specific parameter. Under real process conditions, the amount of impurities incorporated in the crystallized material usually exceeds the amount predicted from thermodynamics. This arises from different factors related to nonequilibrium, that is, kinetically controlled growth processes that commonly occur in technical crystallization processes.

From a mother phase containing both target and impurity molecules, both types of building blocks will adsorb on the growing crystal surface. The rejection of the impurities requires the replacement of an impurity molecule by a target molecule, the latter being more strongly bound. A fast growth will inevitably lead to a kinetic incorporation of some impurity molecules.

Further, a growing crystal surface rejecting impurity molecules will lead to an increased concentration of the impurities at the crystal interface (Figure 7.4). The increase in concentration is directly proportional to the growth rate and also depends on the level of impurities in the bulk phase and the depletion; for a high concentration of impurities in the bulk phase, the increase can be considerable. The level of impurity concentration is reduced by diffusion and convection in the bulk phase. Thus, both the growth kinetics and the mixing influence the impurity level.

In real crystallization processes (e.g., in industrial-scale crystallizers), the level of impurities incorporated in the target product is often strongly related to

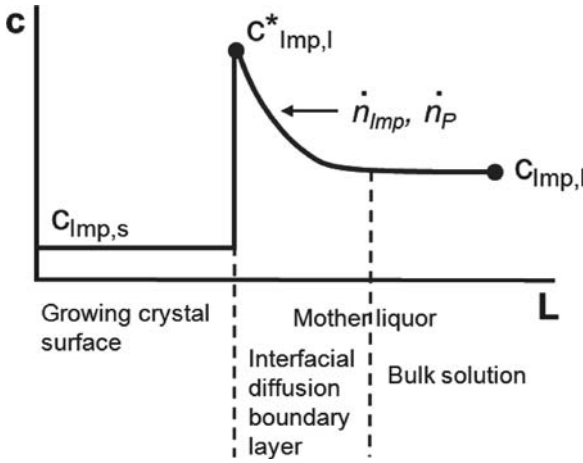


**Figure 7.4** Impurity concentration at the interface between a (planar) growing crystal surface and the liquid solution phase ( $L$ , distance parameter;  $c$ , concentration;  $C^*_{imp,l}$ , concentration of impurities at the s–l interface).

The rejection of impurities by the growing crystal leads to an enrichment of the impurities at the interface that is decreased by both diffusion and convection.

crystallization kinetics. It is obvious that with growth rates normally applied to achieve a sufficient productivity, the tendency of e.g. inclusions of mother liquor in the crystal rises resulting in a higher impurity capture. Typical growth rates in technical crystallization processes are between 10 and 100 nm/s. For comparison, growth rates of molecular crystals of organic compounds are a factor of 10 slower than those of ionic crystals of inorganic salts.

$$k_{eff} = x_{imp,s}/x_{imp,l} \quad (7.3)$$

To account for deviation from thermodynamics, under real conditions an effective distribution coefficient  $k_{eff}$  is defined (Equation 7.3). The equation is similar to Equation 7.2, but the effective distribution coefficient results from parameters measured under real crystallization conditions. That is, the parameters  $x_{imp,s}$  as the impurity content in the solid phase and  $x_{imp,l}$  as the impurity content in the liquid phase are values obtained from the separation process performed. In contrast, the parameters in Equation 7.2 are directly related to the phase diagram. Thus, the effective distribution coefficient also comprises the influence of the crystallization kinetics, in particular the crystal growth rate and mass transfer limitations.

Burton *et al.* [4, 5] introduced an expression that quantitatively relates the effective distribution coefficient  $k_{eff}$  to the thermodynamic distribution coefficient  $k_{eq}$  (Equation 7.4):

$$k_{eff} = \frac{k_{eq}}{k_{eq} + (1 - k_{eq}) \cdot e^{-(G/k_d)}}, \quad (7.4)$$

where  $G$  is the crystal growth rate and  $k_d$  is the mass transfer coefficient. The latter can be defined as

$$k_d = \frac{D}{\delta}, \quad (7.5)$$

where  $D$  is the diffusion coefficient and  $\delta$  is the thickness of the interfacial boundary layer.

According to Equation 7.4, pure crystals, i.e.,  $k_{\text{eff}}$  close to 0, are obtained at low growth rates and high mass transfer, that is, at a thin interfacial boundary layer. This sets the conditions for an optimized process aiming at a highly pure solid product.

Sometimes in industrial processes the so-called progress of purification  $pp$  is used instead of the distribution coefficient. It is defined as the ratio of the impurity content in the solid phase,  $x_{\text{Imp},s}$ , to that in the initial solution,  $x_{\text{Imp},0}$  (Equation 7.6), having the advantage that just the impurity content in the solid phase must be followed:

$$pp = x_{\text{Imp},s} / x_{\text{Imp},0}. \quad (7.6)$$

The objective of process development in industrial crystallization is the minimization of the kinetically determined part of the impurities in the target product to achieve a purity as high as possible. The factors influencing the final product purity relate to the process conditions comprising both crystallization and downstream processes.

In the following section, the possibilities of affecting the impurity uptake of the product by modification of the process conditions will be considered in detail.

#### 7.2.4

##### Influence of Crystallization Conditions

As already stated, the crystallization conditions have a significant influence on the product purity achieved. For example, the crystallization conditions that control the growth rate particularly affect the content of impurities originating from liquid inclusions and lattice incorporation.

In the following sections, the impacts of product yield, crystallization rate and technique, solvent applied, and mixing will be discussed. Selected examples will illustrate particular cases.

##### 7.2.4.1 Product Yield

When lattice integration due to a partial or complete miscibility in the solid state is the dominant mechanism of impurity incorporation, the impurity content in the crystalline product increases with the yield. This can be easily verified on the basis of the phase diagram (Figure 7.5a). Assuming equilibrium conditions (i.e., slow crystallization), the concentration of the impurity incorporated in the target compound steadily increases with progressing crystallization (arrow at the solidus line) and reaches a maximum value close to the eutectic temperature. Simultaneously, the

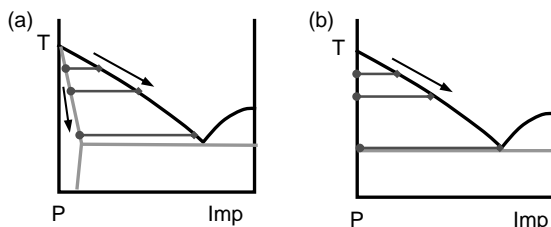


**Figure 7.5** Phase diagram of a target product (P) and an impurity (Imp) showing partial miscibility (a) and immiscibility (b) at solid state. With progressing crystallization, the content of the impurity in the mixed crystal increases and is maximal close to the eutectic composition. In case of immiscibility, first crystals of the impurity appear when the mother liquor reaches eutectic composition. The same

holds for the case of partial miscibility. When the mother liquor reaches eutectic composition, crystals of the impurity are formed as a new solid phase in addition to the mixed crystals (which are saturated with Imp at this point). Thus, a crystallization process must urgently be stopped before reaching the eutectic composition/temperature to avoid a purity drop in the product.

impurity concentration in the mother liquor continuously increases toward the eutectic composition. In practice, this can lead to an uneven distribution of the impurity within the crystals. In fact, the impurity content in the outer layer of the crystals increases, while the average content of the impurity in the crystals increases only slightly. This behavior is due to the fact that at the low temperatures, crystallization from solution is usually performed, the mobility of molecules in the solid state is extremely low. The concentration gradient of the impurity within the crystal can be described by a so-called “onionskin” model (formation of multilayer crystals).

The fact that the impurity concentration in the mother liquor steadily increases with progressing crystallization of the target component also holds for immiscibility of the target substance and the impurity involved (Figure 7.5b). Thus, with increasing yield, the crystallization of the (pure) target compound occurs from a more and more impurity-enriched solution. The growth of the target crystals entails a depletion of the target molecules at the crystal–solution interface and an enrichment of the impurity molecules (Figure 7.4).

Figure 7.6 illustrates the influence of yield on product purity on the basis of a system with an effective distribution coefficient of  $\approx 0.2$ . Shown is the depletion behavior of a certain impurity for different crystallizations. From the figure, one could simplify that for a yield of  $< 80\text{--}90\%$ , the purification is of same level within the limit of the high dispersion in the data and deteriorates drastically above that yield.

#### 7.2.4.2 Crystallization Technique and Rate of Crystallization

Equation 7.4 describing the effective distribution coefficient contains the crystal growth rate  $G$  and the mass transfer coefficient  $k_d$  characterized by the diffusion coefficient in the liquid  $D$  and the thickness of the interfacial diffusion boundary

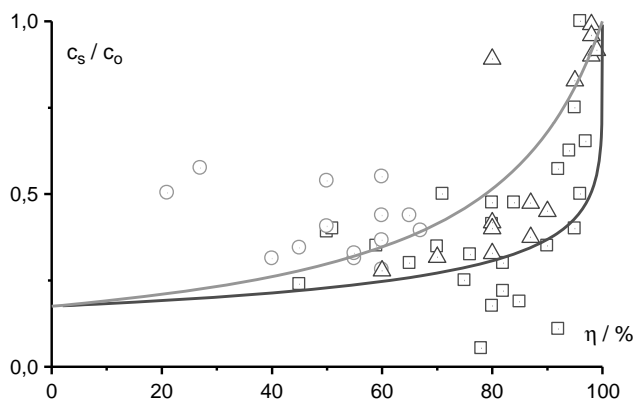


**Figure 7.6** Depletion behavior of a certain impurity for a cooling crystallization from different solvents. The data are given as a function of the yield and referred to the starting concentration of the impurity,  $c_0$ . The scatter in

the data is considerable but typical. The symbols differentiate different solvents and crystallization techniques. The solid lines follow the onionskin model with an effective distribution coefficient of 0.2 and 0.5.

layer,  $\delta$ . As the crystal growth rate decreases, the effective distribution coefficient decreases as well and thus a higher product purity can be obtained. The growth rate directly relates to supersaturation, which accordingly should be kept at moderate levels to avoid primary nucleation on the one hand and to ensure a moderate growth rate on the other. Seeding generally prevents from undesired nucleation. The seed amount must exceed a critical quantity (normally 0.1–1 wt%) and the seeds should be of good quality with regard to purity, surface properties, and crystal size. Details of the seeding process are discussed in Chapter 10.

The influence of the growth rate on the purification potential of melt crystallization has been studied by König and Schreiner [6] comparing different crystallization techniques, namely, suspension crystallization, layer crystallization, and a total solidification. In Figure 7.7, the results are presented. For suspension crystallization with slow growth rates between 0.01 and 0.3 kg/(h m<sup>2</sup>), low effective distribution coefficients between 0.2 and 0.4 and, thus, high product purities are found. The layer crystallization experiments at growth rates between 1 and 100 kg/(h m<sup>2</sup>) clearly demonstrate the decreasing product purity with increasing growth rate. The fast solidification process does not allow any purification, no separation is obtained.

As a further example, referring to crystallization from solution, in Figure 7.8 the depletion behavior of three different impurities for a slow and fast drowning-out crystallization of the drug Abecarnil are compared. Not surprisingly, the purification during the slow crystallization is superior to that of the precipitation. This effect is found for all impurities, although most pronounced for the impurity (B).



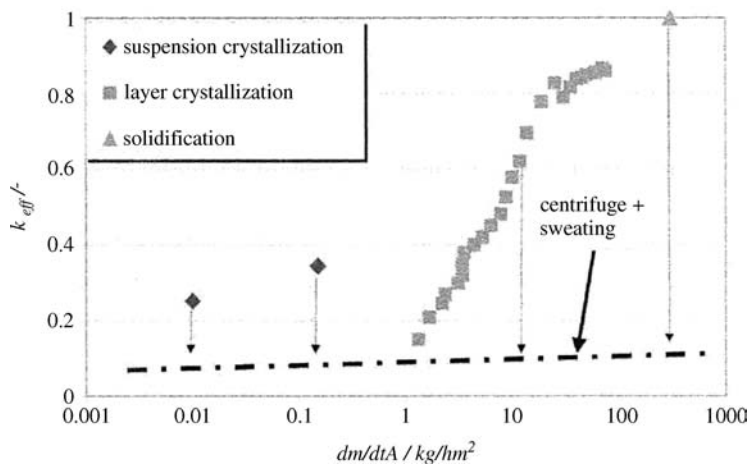


**Figure 7.7** Effective distribution coefficient as function of growth rate ( $dm/dtA$ ) for different crystallization techniques. The system studied was a mixture of 80 wt% diphenyl and 20 wt% naphthalene. Symbols indicate downstream

processing only by draining; the dash-point line shows the results after treating the crystallization product in a heated centrifuge by centrifugation and sweating (reproduced with permission from Ref. [6]).

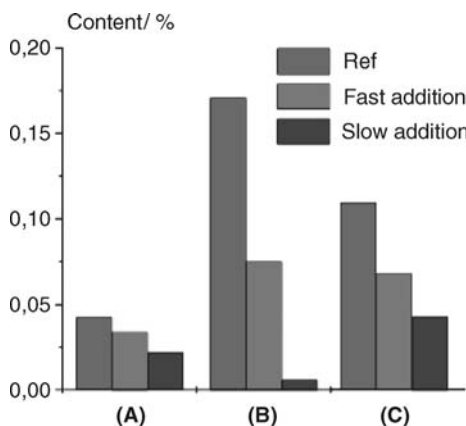


**Figure 7.8** Purification of Abecarnil for a fast and slow drowning-out crystallization to a yield of 60%. Given is the depletion behavior of three different impurities (A), (B), and (C).

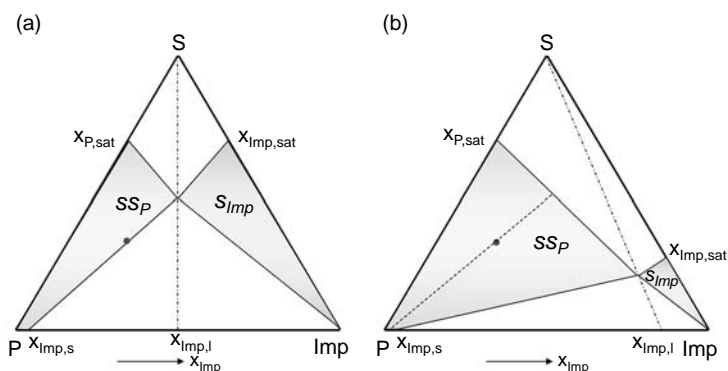
#### 7.2.4.3 Solvent Applied

The solvent in solution crystallization can have different effects on product purity. First, the solvent can be incorporated as an impurity, whether as part of the mother liquor (liquid inclusions and surface adsorption), or incorporated in the lattice of the target compound as a new solvate phase.

Furthermore, the selection of the solvent is a crucial issue in purification of substances forming solid solutions with the impurity involved. The temperature dependence of solubility of both the impurity and the target compound in the solvent plays a significant role in the purification result. Generally, a better purification is achieved, the higher the solubility of the impurity relative to the target component over the likely range of the crystallization temperature. Givand *et al.* [7] explicitly depict such a behavior for the purification of isoleucine from aqueous solutions containing leucine as impurity. A broader study of Givand *et al.* [8] involving also valine confirms the important impact of the ratio of the target compound solubility to that of the impurity. The selection of a solvent or solvent mixture that favorably affects the lattice integration of the impurity in the target product is an essential step to improve the purification result.

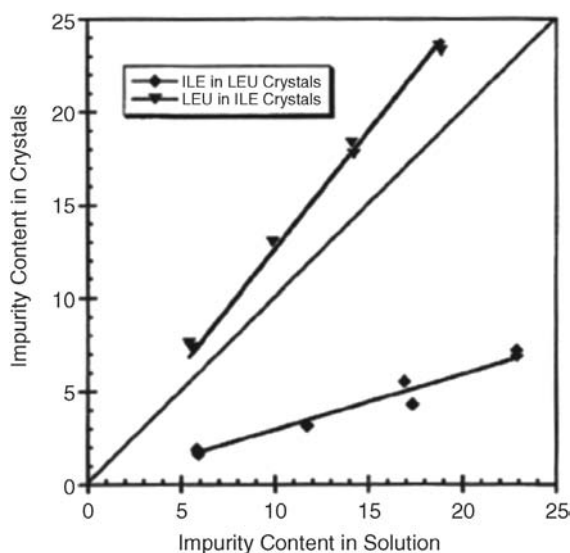
This can be illustrated in the corresponding ternary solubility phase diagram of the target compound  $P$  and the impurity  $\text{Imp}$  in a solvent  $S$  (Figure 7.9). As can be seen, the region where mixed crystals of  $P$  can be gained ( $ss_P$ ) is much bigger for a system with higher solubility of  $\text{Imp}$  (as shown in Figure 7.9b) than for comparable solubilities (Figure 7.9a). According to the different locations of the tie lines in this region, the purity of  $P$  crystallized from a solution of same composition, dot in Figure 7.9, is improved for a solvent with higher solubility of  $\text{Imp}$ .

Figure 7.10 shows the results depicted by Givand *et al.* [7]. It can be seen that the leucine content in isoleucine crystals is greater than that in the equilibrium mother liquor and, on the other hand, the isoleucine content in leucine crystals is significantly



**Figure 7.9** Ternary solubility phase diagrams of a target compound  $P$  and an impurity  $\text{Imp}$  in a solvent  $S$  at a given temperature. Shown is a solubility isotherm at a given temperature  $T$  in case of comparable solubilities of  $P$  and  $\text{Imp}$  ( $x_{P,\text{sat}} \sim x_{\text{Imp},\text{sat}}$ ) (a) and a solubility of  $\text{Imp}$  much higher than that of  $P$  ( $x_{P,\text{sat}} \ll x_{\text{Imp},\text{sat}}$ ) (b). The maximum solubility of  $\text{Imp}$  in  $P$  in the solid state is given as  $x_{\text{Imp},s}$ . A mixed crystal of that composition is called  $\text{Imp}$ -saturated mixed

crystal of  $P$ . An initial solution of a composition in the region  $ss_P$  in equilibrium splits into a solid phase and a mother liquor according to the appropriate tie line. A solution of same composition (dot in (a) and (b)) allows an increased purity of  $P$  when selecting a solvent with high solubility of  $\text{Imp}$  as illustrated in (b) (axes in mol fractions,  $x$ ;  $ss_P$  and  $s_{\text{Imp}}$  are the existence regions of  $\text{Imp}$ -rich mixed crystals of  $P$  and  $\text{Imp}$  as solid phase, respectively).



**Figure 7.10** Impurity content of L-isoleucine and L-leucine crystals with the particular other component. (triangles/upper line: leucine in isoleucine; diamonds/lower line: isoleucine in leucine) (compositions in mol%, temperature 25 °C). (reproduced with permission from Ref. [7])

lower than that in the equilibrium mother liquor. Since isoleucine has a higher solubility in water than leucine, the tendency of leucine to contaminate isoleucine crystals is greater than the tendency of isoleucine to contaminate leucine crystals.

As a further example, the influence of the solvent on the depletion behavior of a particular impurity during crystallization, as reported by Koch *et al.* [9] for a derivative of Ascomycin, is shown in Table 7.2.

The 19-epimer of the compound has a very low depletion behavior in a number of solvents. Starting from an initial content of 7.1%, the crystallization from methanol or acetone did not entail any purification, while ethylacetate, propanol, or THF

**Table 7.2** Depletion behavior of a certain impurity, the 19-epimer of an Ascomycin derivative, for the crystallization from different solvents.

Solvent	Concentration/ (g/ml solvent)	Yield/%	Final concentration of 19-epimer/%
Ethylacetate	1 : 10	>99	2.1
Acetone	1 : 13	>99	7.8
MTBE/ethylacetate (1 : 1)	1 : 13	>99	0.8
MTBE	1 : 34	92	1.0
THF	1 : 4	>99	4.7
Methanol	1 : 4	99	8.3
Propanol	1 : 4	97	3.6

The initial concentration of the impurity is 7.1%.

entailed a mediocre purification. However, a mixture of MTBE and ethylacetate resulted in a 10-fold depletion at a high yield.

Finally, as the depletion behavior is molecular recognition by the crystal lattice and more specifically by the growing surface, and as the solvent can influence the solid-state form crystallizing (being it either different polymorphs or solvates) as well as the habit of the crystals, the choice of the solvent is of importance.

#### 7.2.4.4 Mixing

Mixing is an important issue in crystallization processes, since it significantly affects the mass transfer rate of both the solute target molecules to the growing crystal surface and the impurity molecules away from the crystal surface, and thus has an impact on the product purity. For a mother liquor not ideally mixed, the increasing concentration of the impurity with progressing crystallization of the target compound leads to a higher level of the impurity at the crystal–solution interface that causes an effective distribution coefficient higher than the equilibrium one. The influence of mixing depends on both the size of the crystals and the mixing intensity. As mixing intensity increases, the mass transfer rate increases and the film thickness (i.e., thickness of the interfacial diffusion boundary layer between the growing crystal surface and the bulk solution) decreases (cf. Figure 7.4). At a certain limit, diffusion processes are so fast that the growth rate is primarily limited by resistances of surface integration (surface reaction/integration control). Then, the influence of mixing on incorporation of impurities by nonequilibrium mechanisms is minimized; for systems showing partial miscibility of the target compound and the impurity, the impurity incorporation is limited to the thermodynamic (miscibility) value. Very small crystals ( $\sim 10\text{--}20\text{ }\mu\text{m}$ ) are usually not significantly affected by mixing issues since the film thickness is comparatively tight due to the higher surface area per mass of crystals.

In case of enantiomers where the counter-enantiomer (as impurity) can reach the same content as the target enantiomer, insufficient mixing may have a dramatic effect on the purification process. Beilles *et al.* [10] and Gervais *et al.* [11] have shown for a case where no stirring was applied to a certain racemate resolution by preferential crystallization that some kind of epitaxial growth occurred leading to alternating layers of the two enantiomers in the crystals formed. As a result, no resolution could be achieved (Figure 7.11).

Mixing can be provided by application of an agitator in a stirred tank reactor or a fluidized bed or forced circulation-type crystallizer. A variety of impellers of different geometry, for larger vessels also equipped with several turbines, are available. An extended discussion of mixing in crystallization is found in Chapter 13.

#### 7.2.5

##### Downstream Processes

In the following section, important downstream processes as solid–liquid separation, washing, and reslurrying are discussed briefly with respect to their impact on final product purity.

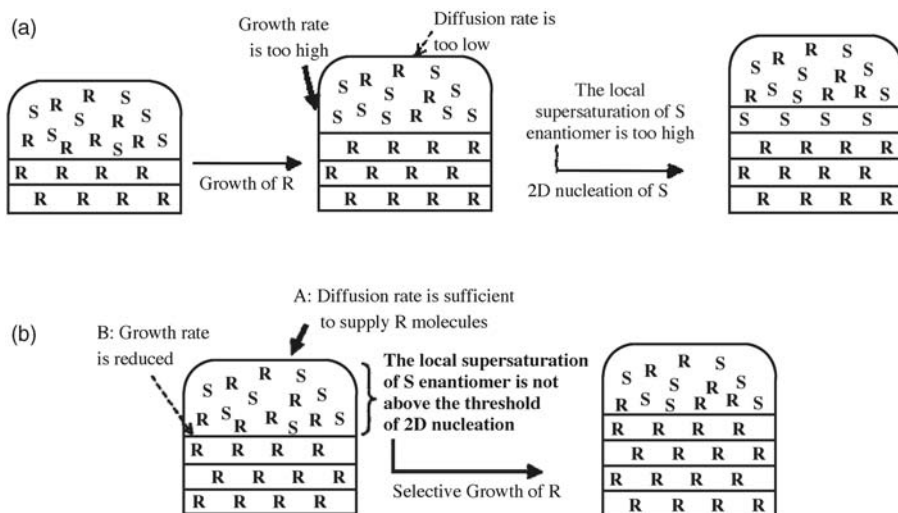


**Figure 7.11** Influence of stirring on preferential crystallization from a racemic solution: (a) lamellar epitaxy occurring without stirring; (b) sufficient stirring (A) and/or a lower

supersaturation (B) facilitate preferential crystallization of one enantiomer (reproduced with permission from Ref. [11]).

### 7.2.5.1 Solid–Liquid Separation and Sweating

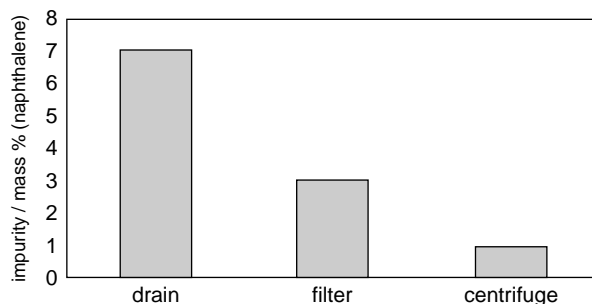
The process of solid–liquid separation controls the content of impurities via the quantity of mother liquor left in the solid. This refers to impurities being adsorbed on the crystal surface or entrapped between crystals. Obviously, the more efficient the solid–liquid separation, the lower the content of mother liquor remaining in the solid product and the higher the purity achievable by this process step.

Generally, there are different techniques to separate the solid phase, the crystals, from the mother liquor. In most cases, pressure filtration or centrifugation is used; sedimentation rather rarely. Furthermore, different technical equipment are available to apply the individual techniques for solid–liquid separation. A major characteristic of these techniques is the residual moisture content, which directly determines the amount of impurity in the solid separated.

As shown in Table 7.3, the residual moisture content decreases significantly from sedimentation to filtration, with best results for centrifugation, where still 4–8% residual moisture remain in the product. These data stem from experiences of the potash industry, a very optimistic case in particular with regard to the filtration results. Since the quality of filtration also depends on particle properties (size and shape), the residual moisture content can vary in a wide range. For example, there are also references to residual moisture contents between 30% and 50% for nutsche or pressure filters. For highly disperse materials such as  $\text{Al}(\text{OH})_3$  or  $\text{Fe}(\text{OH})_3$  the residual moisture content can reach 70–90%.

**Table 7.3** Residual moisture content as provided by different techniques of solid–liquid separation (experiences from potash manufacture) [12].

	Residual moisture content related to the solid (wt%)
Sedimentation	20–40
Filtration	8–18
Centrifugation	4–8

**Figure 7.12** Impurity content as a result of suspension (melt) crystallization of diphenyl from 80% diphenyl/20% naphthalene mixtures and application of different solid–liquid separation techniques (reproduced with permission from Ref. [6]).

In Figure 7.12, results of studies performed by König and Schreiner [6] on the purification potential of solid–liquid separation by draining, filtration, and centrifugation are presented.

The impurity content decreases clearly from about 7 wt% for simple draining to 3 wt% for filtration and below 1 wt% for centrifugation. Further improvement was achieved by sweating (partial melting) and washing in the centrifuge reaching a purity of 99.8 wt%.

A similar trend follows from Figure 7.7, where a considerable drop in the effective distribution coefficient is observed when using centrifugation combined with sweating instead of simple draining. The sweating process is targeted at improving the purification efficiency by depletion of impurities originating from liquid inclusions in the crystalline material. It is a common purification step in melt crystallization that allows substantial improvement of the final product purity. For more information, refer to Chapters 14 and 16 dealing with crystallization from the melt.

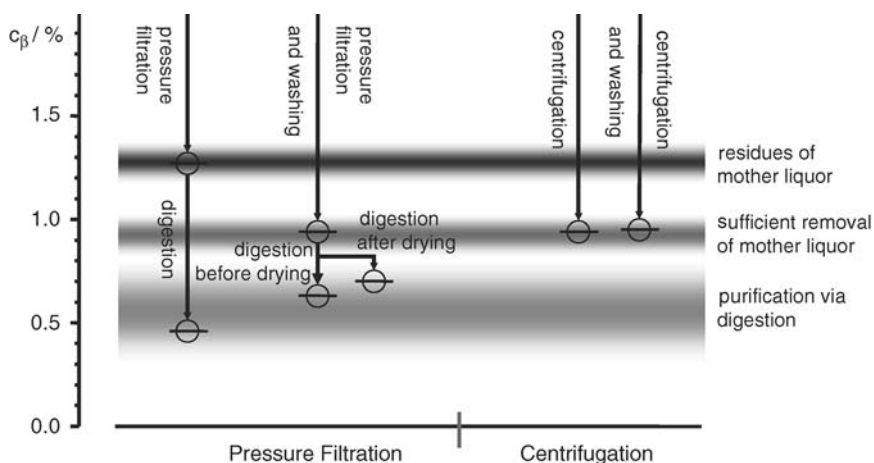
#### 7.2.5.2 Reslurrying and Washing

Reslurrying and washing the crystalline product are aimed at a further removal of impurities that remained after solid–liquid separation. In fact, a further depletion of impurities originating from bulk phase inclusion of mother liquor, surface adhesion to the crystals, and also liquid inclusions in the crystals can be achieved

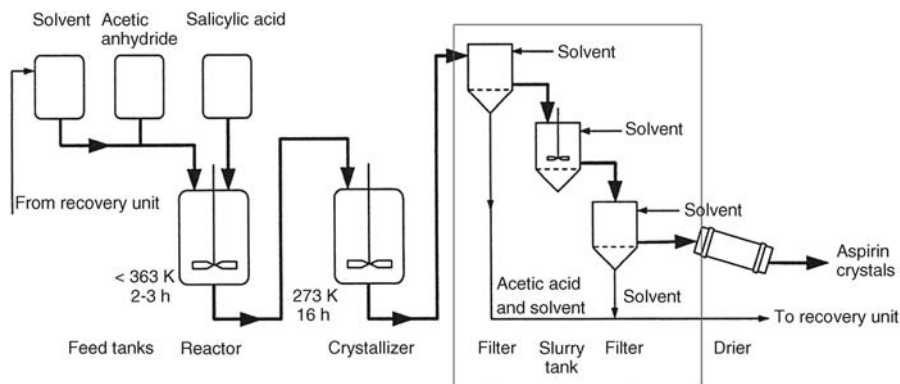
(Table 7.1). Reslurrying the crystals (the filter cake) by addition of solvent and (vigorous) stirring the suspension over a sufficient period of time entails breaking up of crystal agglomerates that entrap mother liquor and also facilitates breakage of crystals associated with release of mother liquor embedded inside the crystal. Therefore, reslurrying is usually more efficient than ordinary washing. Often washing is done in combination with solid–liquid separation, for example, using a filter centrifuge or a wash column. However, when washing on a filter, channeling may occur and not all crystals may get in contact with the solvent. Repeated washing with small amounts of solvent is more effective than fewer washing with the same total volume of solvent. In an industrial environment, the decreasing crystal yield connected with each washing step is an important issue to be considered.

Figure 7.13 shows the depletion of a certain impurity in a crystalline product using different downstream processes, such as pressure filtration, pressure filtration together with washing, both also combined with reslurrying (digestion), centrifugation and centrifugation together with washing. As already stated in Section 7.2.5.1, centrifugation leads to a more efficient depletion of impurities than filtration. Furthermore, reslurrying the filter cake allows further purification meeting the purity requirements for the given product.

Exemplarily, for a typical fine chemical manufacturing process, the simplified process scheme of the aspirin production is presented in Figure 7.14. Acetylsalicylic acid as produced by reaction of salicylic acid and acetic anhydride in a batch reactor is subjected to a cooling crystallization. The resulting suspension is transferred to a filter to remove the solvent and acetic acid formed as by-product. After washing with solvent, the product crystals are reslurried and filtered again.



**Figure 7.13** Depletion behavior of an impurity  $\beta$  using different downstream processes separately and combined with each other. The starting material had a content of 14.2% Beta that was enriched to 29.1% in the mother liquor.



**Figure 7.14** Simplified process scheme of aspirin production. The downstream purification processes consisting of solid–liquid separation, reslurrying, and washing steps are framed for indication. (Reproduced with permission from Ref. [13].)

Following a further washing step, the crystalline product is dried and sent to final formulation steps. The solvent and unconverted anhydride are recycled to the reactor.

#### 7.2.6

##### Workflow to “Manage” Impurities in Process Development

In development of a new manufacturing process, studying and minimization, that is management of the impurities, is an important issue since the purity of the final product has to meet the purity specifications defined. Therefore, the influence of the crystallization conditions and the downstream processing techniques on product purity have to be studied. This issue has been addressed in Ref. [14], which will be used here to suggest a workflow for impurity management in process development.

The tasks that have to be handled are as follows:

- 1) Study of SLE
- 2) Study of inclusion behavior
- 3) Study of washing and deliquoring behavior
  - a) Determination of filter cake properties
  - b) Determination of washing efficiency
  - c) Determination of moisture (solvent) content
- 4) Conceptual process design

Figure 7.15 illustrates the implementation and iterative fulfillment of the particular tasks in an integrated crystallization and downstream process development. The workflow shown facilitates the design of a manufacturing process that provides the target product at desired purity.



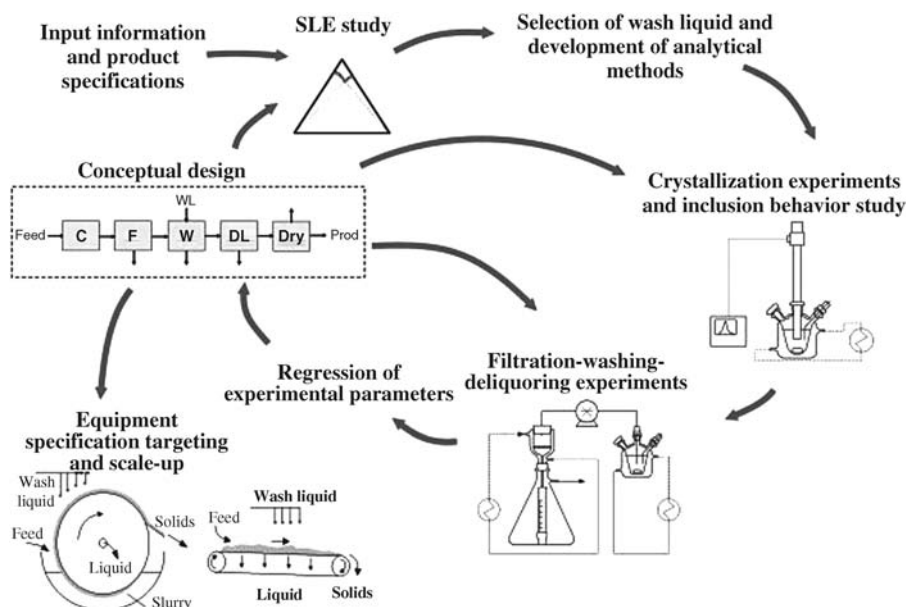


**Figure 7.15** Workflow diagram for an integrated crystallization and downstream process development (reproduced with permission from Ref. [14]).

## References

- 1 Matsuoka, M. (1991) Developments in melt crystallization, in *Advances in Industrial Crystallization* (eds J. Garside, R.J. Davey, and A.G. Jones), Butterworth-Heinemann, London, pp. 229–244.
- 2 Predel, B., Hoch, M., and Pool, M. (2004) *Phase Diagrams and Heterogeneous Equilibria: A Practical Introduction*, Springer, Berlin-Heidelberg.
- 3 Predel, B. (1982) *Heterogene Gleichgewichte: Grundlagen und Anwendungen*, Steinkopff Verlag, Darmstadt.
- 4 Burton, J.A., Prim, R.C., and Slichter, W.P. (1953) The distribution of solute in crystals grown from the melt: part I. *J. Chem. Phys.*, **21**, 1987–1991.
- 5 Burton, J.A., Kolb, E.D., Slichter, W.P., and Struthers, J.D. (1953) Distribution of solute in crystals grown from the melt: part II. *J. Chem. Phys.*, **21**, 1991–1996.
- 6 König, A. and Schreiner, A. (2001) Purification potential of melt crystallisation. *Powder Technol.*, **121**, 88–92.
- 7 Givand, J.C., Teja, A.S., and Rousseau, R.W. (2001) Effect of relative solubility on amino acid crystal purity. *AIChE J.*, **47**, 2705–2712.
- 8 Givand, J., Chang, B.-K., Teja, A.S., and Rousseau, R.W. (2002) Distribution of isomorphous amino acids between a crystal phase and an aqueous solution. *Ind. Eng. Chem. Res.*, **41**, 1873–1876.
- 9 Koch, G., Jeck, R., Hartmann, O., and Küsters, E. (2001) Selective synthesis of a new Ascomycin rearrangement product (SDZ ASD732) on a pilot plant scale. *Org. Process Res. Dev.*, **5**, 211–215.
- 10 Beilles, S., Cardinael, P., Ndzié, E., Petit, S., and Coquerel, G. (2001) Preferential crystallization and comparative crystal growth study between pure enantiomer and racemic mixture of a chiral molecule: 5-ethyl-5-methylhydantoin. *Chem. Eng. Sci.*, **56**, 2281–2294.
- 11 Gervais, C., Beilles, S., Cardinael, P., Petit, S., and Coquerel, G. (2002) Oscillating crystallization in solution between (+)- and

- (–)-5-ethyl-5-methylhydantoin under the influence of stirring. *J. Phys. Chem. B*, **106**, 646–652.
- 12 Heinz, A. (1989) *Technologie der Mineralsalzverarbeitung*, Deutscher Verlag für Grundstoffindustrie, Leipzig.
- 13 Moulijn, J.A., Makkee, M., and Diepen, A. V. (2001) *Chemical Process Technology*, John Wiley & Sons, Inc., Chichester.
- 14 Cheng, Y.S., Lam, K.W., Ng, K.M., and Wibowo, C. (2010) Workflow for managing impurities in an integrated crystallization process. *AIChE J.*, **56**, 633–649.

### Further Reading

- Jacques, J., Collet, A., and Wilen, S.H. (1994) *Enantiomers, Racemates, and Resolutions*, Krieger, Malabar.
- Kitaigorodsky, A.I. (1984) *Mixed Crystals*, *Springer Series in Solid-State Sciences* 33, Springer, Berlin.
- Myerson, A.S. (2002) *Handbook of Industrial Crystallization*, Butterworth-Heinemann, Boston.
- Ulrich, J. and Glade, H. (eds) (2003) *Melt Crystallization*, Shaker Verlag, Aachen.

## 8

# Characterization of Crystalline Products

*Rolf Hilfiker*

### 8.1

#### Introduction

Any product obtained from a chemical process has to be characterized. If the product is a solid, an even larger set of characterization data is required than that required for a liquid or a gas. Liquids and gases are homogeneous on a molecular level and therefore the properties of the bulk are identical to the properties of any volume element larger than a few molecules. A solid can be inhomogeneous, so the properties of any volume element may be different from each other. If products from crystallization processes are considered, the product no doubt should be homogeneous on a medium scale, but it will still be necessary to determine both the intrinsic properties of the solid and the particle shape, particle size, and particle size distribution in addition to the mechanical properties of the solid such as powder flow properties.

A large variety of methods are necessary to characterize a solid in depth and a number of texts are available that describe these techniques in detail. The scope of this chapter is to give a brief overview of the most important techniques, highlighting which method can provide what type of information about the properties of the solid. Solubility and its measurement are discussed in Chapter 3 and will not be treated here, although this property is one of the most important characteristics of a solid, providing, for example, direct information on its free energy (see Chapter 5).

### 8.2

#### Characterization of Intrinsic Properties of a Solid

A solid of a certain composition can often exist in different solid forms (see Chapter 5). Characterization of such a form can be viewed from different angles, since polymorphs can be regarded either as distinct phases or as distinct crystal structures and all the analytical methods for the solid state depend on these considerations. Threlfall [1] characterized this situation: “Until around 1950, polymorphism was regarded exclusively as a thermodynamic issue, i.e. polymorphs are different solid phases of a compound. This was inevitable, because few

structures of polymorphs had been determined. In the past 50 years, polymorphism has been increasingly regarded as exclusively a structural phenomenon i.e. polymorphs are different molecular packings. This is unsurprising, given the aversion of most students to thermodynamics! But, it is both! The phase aspects (solubility, thermal stability) are generally the most significant in respect of technical behavior in any application. It is sensible to bear this duality in mind.”

### 8.2.1

#### Crystal Structure

Several methods are suitable to characterize the crystal structure of a solid, such as single-crystal X-ray diffraction, X-ray powder diffraction (XRPD), Raman, infrared (IR), near infrared (NIR), terahertz (THz), and solid-state NMR (ssNMR) spectroscopy [2–5]. Each method has its advantages and disadvantages. The most widely used ones will be described in some more detail.

While single-crystal X-ray diffraction provides the ultimate characterization of the crystal structure, its practical usefulness, particularly as a method for quality control, is limited by the fact that single crystals are needed for this technique, and that it provides information only on that particular single crystal that might not be representative of the whole sample, and that it is time-consuming. All these restrictions do not apply for X-ray powder diffraction, where a certain amount of powder is irradiated giving an averaged pattern. This makes it one of the most widely used methods for polymorph characterization.

##### 8.2.1.1 X-Ray Powder Diffraction (XRPD)

The underlying principle of both single-crystal X-ray diffraction and XRPD is Bragg's law (Equation 8.1), which describes the relationship between the angle for constructive interference ( $\Theta$ ), layer spacing ( $d$ ), wavelength ( $\lambda$ ), and order of the interference ( $n$ ):

$$n \cdot \lambda = 2 d \sin (\Theta). \quad (8.1)$$

In XRPD, the sample exposed to the X-ray beam is a powder and if the particles are randomly oriented, all crystal planes in the crystal lattice will be suitably oriented with respect to the X-ray beam and give rise to constructive interference at the respective angle (Figure 8.1). Therefore, a pattern of the form depicted in Figure 8.2 will be obtained. Different polymorphs will have different crystal plane spacings and

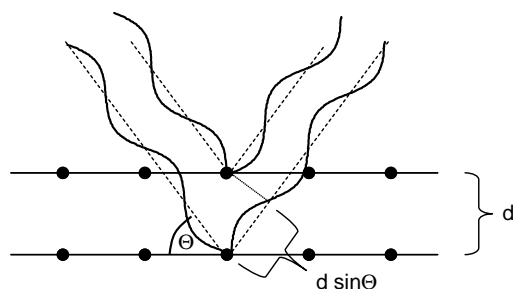


**Figure 8.1** Principle of Bragg's law: constructive interference when the path difference is  $\lambda$  or multiples of  $\lambda$ .

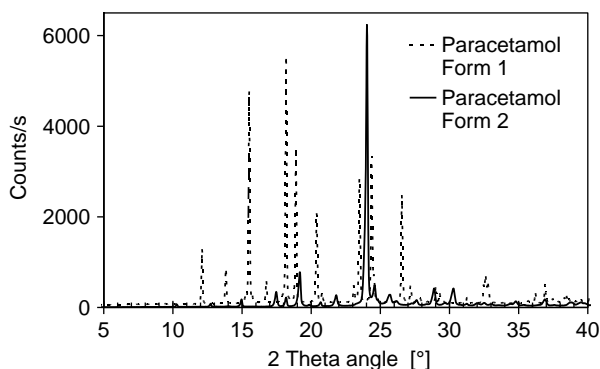


**Figure 8.2** XRPD of paracetamol form 1 (broken line) and form 2 (solid line).

will therefore lead to a different XRPD. Rare exceptions exist, where the differences are so small that they may not be discernible using standard instrumentation.

A practical problem with XRPD can be the so-called preferential orientation. If the particles are nonspherical (e.g., plates or needles) and are not randomly oriented, some lines in the XRPD may become greatly attenuated or even disappear. When comparing XRPDs of various samples, good sample preparation is therefore essential. Orientation effects, for example, can be reduced by gentle grinding of the substance. Investigating the sample by optical microscopy may also be very helpful to see if the particles are preferentially oriented. When a sample is ground, care must be taken that the solid form is not changed due to the grinding. The absence of such changes can be confirmed if the positions of the lines in the XRPD diagram are not shifted by the grinding if the intensity of the grinding is varied.

Due to the principle of XRPD, the method will lead to strong constructive interference if the spacing of crystal planes is constant over an extended distance. It is therefore sensitive to long-range order. In contrast to XRPD, vibrational and NMR spectroscopy is essentially sensitive to the immediate environment of the molecule.

#### 8.2.1.2 Vibrational Spectroscopy (Raman, IR, NIR, THz)

Vibrational spectra are mainly governed by vibrations within the molecule. But since these vibrations are influenced by the environment of the molecule and hence the crystal packing, they will also differ for different polymorphs of the same molecule. The differences will in general not be as obvious as for XRPD, but nevertheless the specificity of spectroscopic and diffraction methods with respect to the differentiation of polymorphs is similar. Figure 8.3 a shows the Raman spectra of the same two polymorphs of paracetamol, as given in Figure 8.2. While the spectra look essentially similar, clear line shifts, for example, can be observed between 1700 and 1200  $\text{cm}^{-1}$  (Figure 8.3b). In some cases, such as isomorphous solvates (solvates which are identical in structure, except that different solvents occupy a certain lattice space), the specificity of IR and Raman is often superior to XRPD.

Raman and IR are complementary methods. They differ in their selection rules (change of dipole moment or polarizability during the vibration) and in practical aspects. The main advantages of Raman compared to IR are as follows:

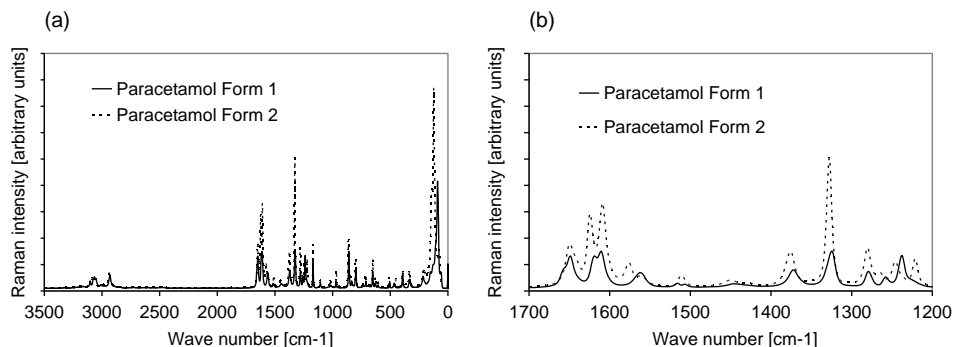


**Figure 8.3** Raman spectrum of paracetamol form 1 (solid line) and form 2 (broken line). (a) Whole spectrum. (b) Section of Raman spectrum where differences between form 1 and form 2 are most obvious.

- No sample preparation necessary (IR often uses KBr pellets; modern ATR-IR also eliminates sample preparation).
- In general, narrower bands.
- Raman microscopy needs less sample preparation and has a better resolution than IR microscopy.
- Raman spectroscopy can easily be applied for online monitoring (Section 8.5.2).
- Low frequencies more readily attainable; this is the range of lattice vibrations, where the difference between polymorphs is often very pronounced.
- Can measure through glass/quartz containers.
- Little interference from water (weak Raman scatterer).
- Hydrogen bonding shows up weakly.

The main advantages of IR are as follows:

- More widely available.
- Cheaper instruments.
- Hydrogen bonding shows up strongly.
- No problems with samples that exhibit fluorescence.

NIR spectra are due to overtone and combination bands, mostly of OH, NH, and CH stretching vibrations. They are generally less specific with respect to polymorphs than IR or Raman spectra, but may offer practical advantages due to sample preparation and wide availability for online monitoring.

Terahertz spectroscopy accesses the wave number region approximately between 2 and 100  $\text{cm}^{-1}$ , that is, even lower wave numbers than Raman spectroscopy. This is a region where differences between polymorphs may be very large, which makes it a powerful method for differentiating polymorphs. The technique however is still expensive and not widely available.

#### 8.2.1.3 Solid-State NMR (ssNMR)

Nuclear magnetic resonance (NMR) spectroscopy is one of the most important methods for determining the structure of molecules in solution. Recording NMR spectra of solids is technically more challenging and requires specialized equipment

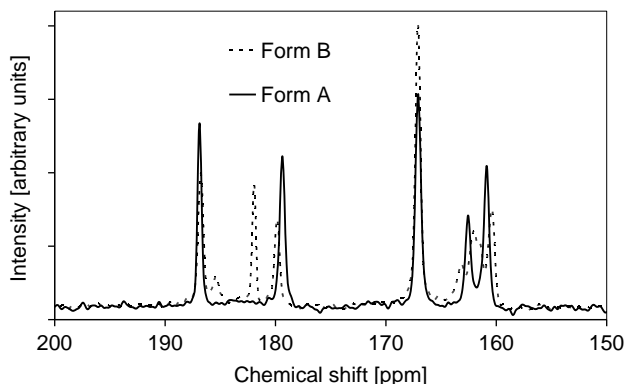


**Figure 8.4** Section of  $^{13}\text{C}$  MAS ssNMR spectra of two different polymorphs of an active pharmaceutical ingredient.

and techniques. One such technique is known as “magic angle spinning” and involves very fast rotation (often at rates of tens of kilohertz, that is, millions of revolutions per minute) of the sample about a specified angle ( $54.7^\circ$ ). Two other fundamental techniques involve the application of series of precisely timed, high-power radiofrequency pulses for purposes of spectral simplification (in the case of “dipolar decoupling”) or sensitivity enhancement (in the case of “cross-polarization”). These techniques can be combined in a variety of ways so that the spectral resolution of modern solid-state NMR (ssNMR) spectra currently approaches that of solution-state spectra. The wide range of both one- and two-dimensional NMR spectroscopic techniques known to the organic chemist can now, with appropriate modifications, be applied to solids.

Like IR and Raman spectra, solid-state NMR spectra are sensitive to local order and local properties, i.e. “chemical” information, whereas X-ray diffraction is sensitive to long-range order. As different polymorphs will also differ in their local crystal lattice packing and/or molecular conformation, they can generally be distinguished by ssNMR [6,7]. Figure 8.4 shows a section of the ssNMR spectra of two different polymorphs of an active pharmaceutical ingredient.

Solid-state NMR offers many advantages compared to other techniques:

- Chemical-specific ( $^{13}\text{C}$ ,  $^{19}\text{F}$ ,  $^1\text{H}$ ,  $^{31}\text{P}$ , etc.) structural information.
- Narrow, well-resolved bands (especially compared to NIR).
- Possibility of rigorous peak assignment (spectral editing, 2D methods) in many cases.
- Nondestructive sampling.
- Insensitivity to particle size effects.
- Applicability to both drug substances and formulated drug products.
- Quantitative (in principle) with limit of quantification (LOQ) as low as  $\sim 1\%$ .
- Suitable for studying solvation and desolvation, with both organic solvent “guest” molecules and solid “host” molecules being directly observable.
- Dynamical information on the nanosecond to second timescale can be derived, which may be useful to detect fast isomerizations.

However, the method also has the following disadvantages:

- Large sample sizes (up to ~300 mg) required.
- Time-consuming (more than 2 days required to obtain some spectra).
- Possible sample transformation under certain measurement conditions (fast sample spinning speeds, high-power radiofrequency pulses).
- Extensive calibration studies generally required for quantitation.
- Need for isotopic labeling to apply some methods.
- Lack of spatial resolution.
- Expensive.
- Requires specialized knowledge to both implement and evaluate experiments.

Solid-state NMR, therefore, is a very powerful tool for research and development, but is not particularly suitable as a routine technique for quality control.

### 8.2.2

#### Thermodynamic Properties

Thermal methods play a key role in both the identification and the characterization of solid forms. A thermal method can be defined as a method where the heat flow is measured as a function of an externally varied parameter. If this parameter is, for example, time and all other parameters are held constant, the method is called isothermal calorimetry. In solution calorimetry, a solid is dissolved in a particular solvent and the associated heat of dissolution is measured. Probably the most frequently used thermal technique is differential scanning calorimetry (DSC) [8], where temperature is varied and the associated heat flow is measured.

##### 8.2.2.1 Differential Scanning Calorimetry (DSC)

Two major types of DSC instruments are available on the market. The first one is the power compensation mode used in Perkin Elmer instruments. In this mode, sample and reference are kept at the same (changing) temperature and the power input that is needed to achieve this temperature is measured for both sample and reference. The second mode, which is used by the majority of DSC instrument providers, is called heat flux DSC. Here, the temperature difference between sample and reference is measured as a function of temperature, while both are heated or cooled in two compartments of one oven. The heat flow difference between sample and reference is then calculated from this temperature difference and the independently determined thermal resistance between sample and reference. Both methods yield essentially the same data:

$$dQ/dt = m \times c_p \times (dT/dt). \quad (8.2)$$

The heat flow  $dQ/dt$  is measured as a function of temperature when this temperature is changed at a certain rate  $dT/dt$ . Equation 8.2 relates the two quantities to  $c_p$ , the heat capacity at constant pressure, and  $m$ , the sample mass. In the absence of phase transitions, the DSC signal is proportional to the heat capacity of the sample. If the sample undergoes a first-order phase transition (e.g.,



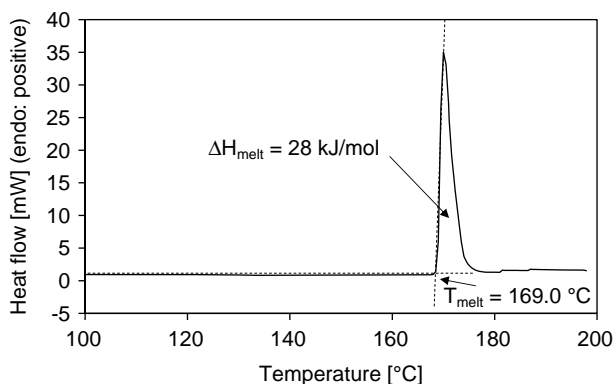


**Figure 8.5** DSC thermogram of paracetamol is determined to be 169.0 °C. From the area under the melting peak, a melting enthalpy of 28 kJ/mol is determined. By applying a tangent to the melting peak, the melting point

melting), the effective heat capacity of the system goes to infinity at the transition temperature due to the latent heat associated with that event. This leads to a peak in the DSC curve. If melting is the only event observed in a DSC scan, the melting point of that solid can be determined accurately by applying a tangent to the melting peak (Figure 8.5). The melting enthalpy can be determined from the area under the peak. Melting point and enthalpy are essential parameters to describe a solid form (cf. Section 5.4).

If a substance can exist in various polymorphs and the polymorph that is not thermodynamically stable at the melting temperature is subjected to a DSC scan, then either of the following occurs:

- i) The melting point and melting temperature of that polymorph may be observed.
- ii) The start of melting is immediately followed by recrystallization into the high-temperature form, which is then followed by melting of the high-temperature form.
- iii) A solid–solid transition from the metastable to the stable polymorph and subsequent melting of the stable polymorph may be observed.

Figure 8.6a and b shows cases (ii) and (iii) for two polymorphs of carbamazepine.

Whether a solid–solid transition as described in case (iii) above is observed or not depends on the moiety under investigation and on properties of the sample (such as particle size, crystal imperfections, small amounts of the other form, or residual solvent). In addition, it may also depend on instrument parameters: fast scanning rates favor melting/recrystallization, while solid–solid transitions are preferentially seen for slower scanning rates. In all three cases, DSC provides important information on the properties of the two forms. If melting temperatures and heats of fusion of both forms can be determined, it can be deduced from Burger–Ramberger rule 2 (see Section 5.4.3) whether the forms are monotropically or enantiotropically related and if a solid–solid transformation might be observed. Rule 1 provides the

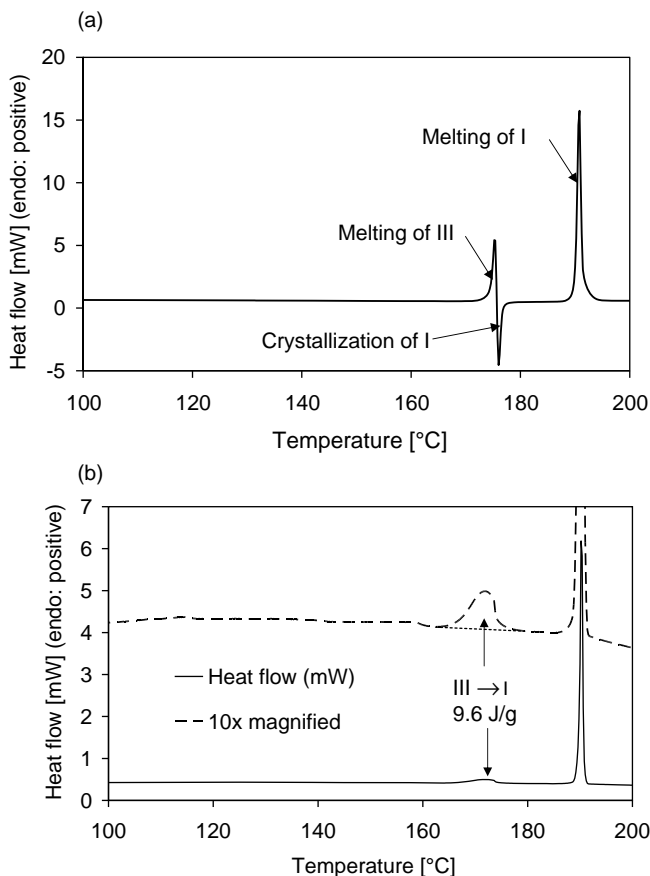


**Figure 8.6** (a) DSC thermogram of carbamazepine form III. Carbamazepine form III is the stable form at room temperature. At 175 °C, melting of form III is observed, which is immediately followed by (exothermic) recrystallization into form I. Form I is the thermodynamically stable form at temperatures above 118 °C. Form I and form III are therefore

enantiotropically related. At 190 °C, melting of form I is observed. Scanning rate was 10 K/min. (b) DSC thermogram of carbamazepine form III at a lower scanning rate of 2 K/min. Now an endothermic solid–solid transition of form III to form I at  $\approx 170$  °C is observed in accordance with the Burger–Ramberger rules (see Section 5.4.3). Subsequently, form I melts at 190 °C.

same answer in the other two cases. The corresponding temperature of a solid–solid transformation can vary from experiment to experiment according to the nature of the sample and in general will not correspond to the thermodynamic transition temperature of the two forms. For enantiotropic systems, it will be higher than the thermodynamic transition temperature; Figure 8.6b shows that the transition from form III to form I occurs at  $\approx 170$  °C, while the thermodynamic transition temperature is 118 °C. For monotropic systems, there is no thermodynamic transition temperature at all.

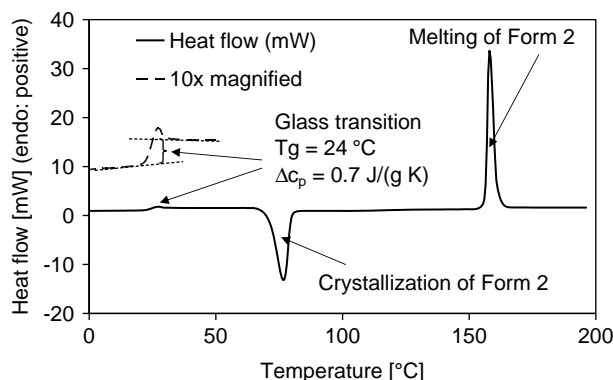


**Figure 8.7** DSC thermogram of amorphous paracetamol. At  $24^\circ\text{C}$ , the glass transition from the glassy to the rubbery state is observed by a change of the heat capacity of  $0.7 \text{ J/g/K}$ . At  $\approx 76^\circ\text{C}$ , the rubbery paracetamol crystallizes into the metastable form 2, which subsequently melts at  $156^\circ\text{C}$ .

Finally, DSC is also well suited for the characterization of amorphous forms. At the glass transition temperature, where the amorphous form converts from the glassy to the rubbery state, a jump in the heat capacity will be observed. It may also happen that the amorphous substance crystallizes when it becomes rubbery. This will manifest itself in the DSC by an exothermic heat of crystallization and subsequently the crystalline solid will melt (Figure 8.7).

#### 8.2.2.2 Isothermal Microcalorimetry

Isothermal microcalorimetry is a versatile method that can be used for diverse applications such as assessing chemical stability, heats of dissolution by solution calorimetry, and binding affinities by titration calorimetry. An important application of isothermal microcalorimetry related to characterization of solids is the determination of the amorphous content [9]. Typically, it is desired that the product of a crystallization process is 100% crystalline. If the crystallization process is carried out in a nonoptimized way, the resulting solid may contain amorphous fractions. One possible cause for this could be that the crystallization is carried out too fast. Also, processes following the crystallization process, such as drying or milling, may induce formation of amorphous fractions. In most instances such amorphous fractions are undesired, since they may reduce the chemical stability and change the dissolution characteristics of the product.

For a lot of compounds, it is possible to induce crystallization of amorphous fractions by subjecting the sample to humidity or solvent vapors, since adsorption of water or solvent in amorphous sections will reduce the glass transition temperature. By exposing samples to a controlled atmosphere in an isothermal microcalorimeter, the heat of crystallization can be measured and the amorphous content may be calculated after having performed a calibration of the system (Figure 8.8). In addition to finding conditions that are suitable to induce crystallization of the

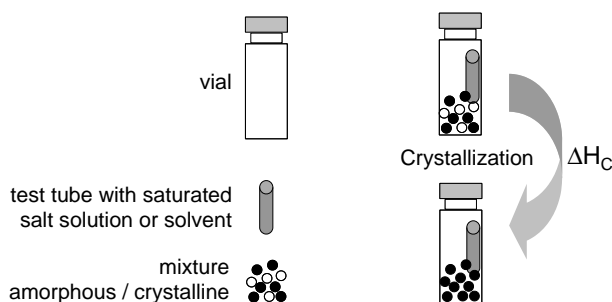


**Figure 8.8** Amorphous content by isothermal microcalorimetry. After having identified a suitable solvent, the substance is placed in the vial together with a small test tube filled with a salt solution or solvent to provide the appropriate humidity or solvent atmosphere. Crystallization of the amorphous fraction will then occur in the isothermal microcalorimeter.

amorphous fractions, it is necessary to optimize the conditions in such a way that the kinetics of the crystallization is suitable. The crystallization event should only start after about an hour so that the vial has sufficient time to equilibrate after it has been placed in the isothermal microcalorimeter, and the crystallization event should be completed after 5–10 h in order to be easily discernible from the background. Figure 8.9 a shows the thermal events observed in an isothermal microcalorimeter for a sample with a fraction of 0% and 0.5% amorphous material.

Figure 8.9b shows the respective calibration curve indicating the limit of detection for amorphous fractions in the solid.

Accurate determination of the amorphous content will allow optimization of process parameters to minimize amorphous content.

### 8.2.3

#### Composition

##### 8.2.3.1 Thermogravimetry (TG, TG-FTIR, and TG-MS)

Often substances may crystallize as solvates or hydrates. A very convenient way to assess if a solvate or hydrate has been obtained is thermogravimetry (TG). In such an instrument, the sample is heated in an open sample pan while its mass is measured. During the measurement, a weak nitrogen flow (in the order of 10 ml/min) is applied over the sample. When the solvent evaporates, a mass loss is detected. In case the solvent molecule is bound in the crystal lattice and is not just present on the surface of the particles, the mass loss typically occurs above the boiling point of the respective solvent. Even more useful are TG-FTIR or TG-MS instruments, where the nature of the emitted gas is determined by Fourier transform infrared (FTIR) or mass spectroscopy (MS) (Figure 8.10). This also allows the detection of thermal decomposition of the sample.

##### 8.2.3.2 Dynamic Vapor Sorption (DVS)

Dynamic vapor sorption (DVS) (sometimes also called gravimetric vapor sorption (GVS)) is a suitable method to investigate hydrate formation and hygroscopicity. In a

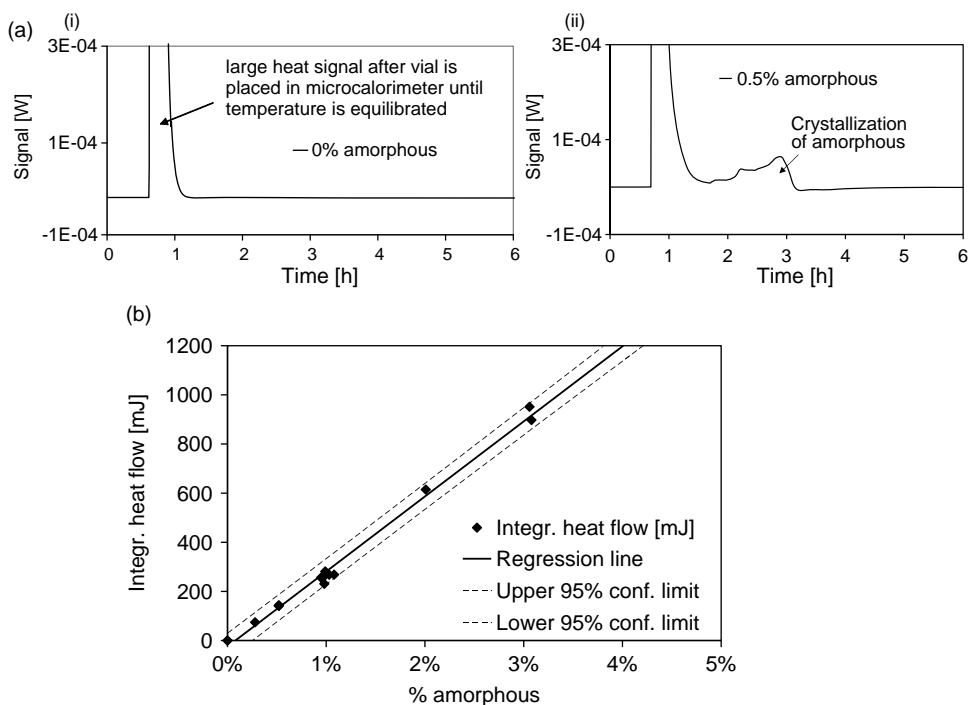


**Figure 8.9** (a) Signal in isothermal microcalorimeter of 100% crystalline (i) and 99.5% crystalline (ii) substance. (b) Regression line with 95% confidence limits to the measured heat flow

values of mixtures with varying amorphous content. From the linear regression analysis, it can be calculated that the limit of detection is 0.3% and the limit of quantification is 0.8%.

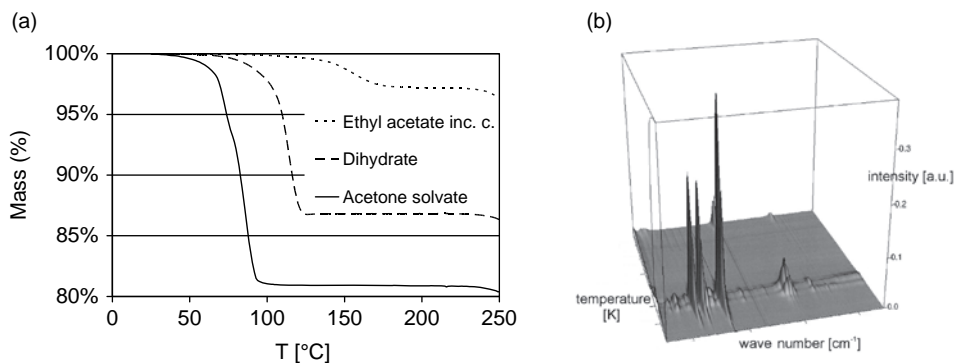


**Figure 8.10** TG-FTIR of three forms of carbamazepine. In part a, the TG curves of the dihydrate, the acetone solvate, and the ethyl acetate inclusion compound are depicted. The emitted gas is identified by FTIR; FTIR of gas phase of the acetone solvate is shown in part (b). The measured mass losses of the acetone solvate (19.1%) and the dihydrate (13.2%) correspond very well to the theoretical values of

19.7% and 13.2% and occur mainly above the corresponding boiling points of the liquids of 56 °C and 100 °C, respectively. The ethyl acetate solvate is a non-stoichiometric solvate, where the solvent molecules (about 0.1 solvent molecules per carbamazepine molecule) are very tightly bound in pores of the crystal lattice and are released only high above the boiling point of ethyl acetate (77.1 °C).

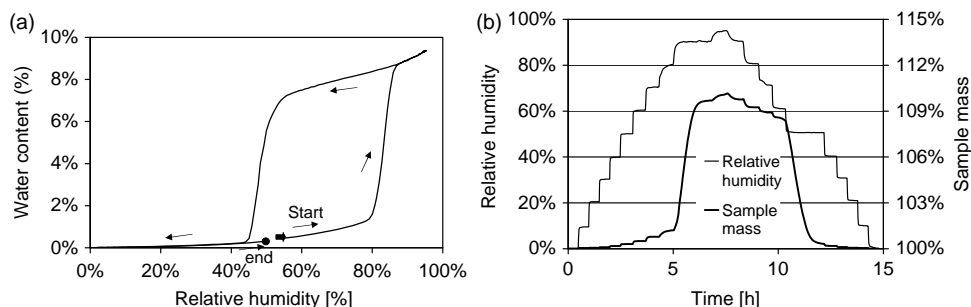


**Figure 8.11** Two ways of representing a DVS of a substance that can form a monohydrate. (a) The humidity is scanned continuously and the corresponding mass change is recorded. (b) The humidity is changed stepwise and after each humidity change, the humidity is held constant until the mass of the sample is constant.

DVS instrument, the mass of the sample is measured as a function of relative humidity (r.h.). Humidity is either changed continuously or stepwise and the mass of the sample is plotted as a function of humidity (or time). Figure 8.11 shows a typical DVS diagram of a substance that forms one hydrate. When humidity is increased from 0% to 95%, a sharp mass increase is observed at  $\approx 80\%$  r.h. From the magnitude of the mass increase, it can be calculated if a hemi, mono, sesqui, and so on hydrate is formed. When the humidity is decreased from 95% to 0%, a loss in mass is observed at  $\approx 50\%$  r.h. Such a hysteresis is typical for a substance that forms a stoichiometric hydrate and it is due to kinetic hindrance of hydration and dehydration. Some hydrates show extreme hystereses, such that hydration or dehydration may not be observed at all in a standard DVS experiment. Substances that form nonstoichiometric hydrates or that just adsorb surface water normally show a more continuous mass increase and decrease and almost no hysteresis. Substances that can form several hydrates may lead to complicated DVS traces (Figure 8.12).

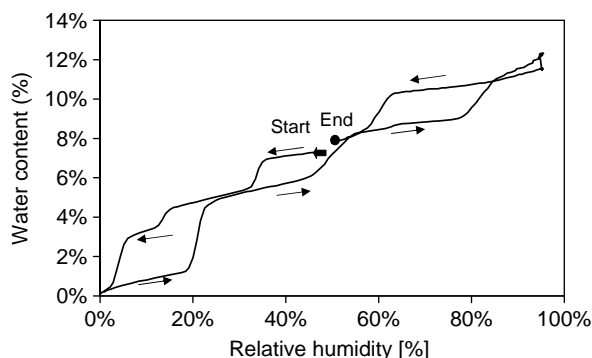


**Figure 8.12** Complicated DVS of a substance that can form an anhydrate, a mono, sesqui, di, hemipenta, and trihydrate.

### 8.3

#### Characterization of Particle Shape and Size

The quality of a solid product critically depends on its particle size, particle size distribution, and particle shape. Properties such as dissolution rate, bulk density, flowability, ease of formulation, and content uniformity of the final product can be influenced. Therefore, accurate particle size and shape determination is of paramount importance.

##### 8.3.1

#### Particle Size Distribution: Characteristic Values and Graphs

Particle size distributions can be represented in different ways. The two most commonly used distributions are the number distribution and the mass or volume distribution. Both these distributions can be displayed as a differential or cumulative distribution.

In the differential mass distribution or *probability density function* ( $q_3$ ), the area under the curve between  $d$  and  $d+\Delta d$  (or  $\ln d$  and  $\ln d+\Delta \ln d$  if the diameter is plotted on a logarithmic scale) is equal to the mass percentage of particles that have a diameter between  $d$  and  $d+\Delta d$ . The number 3 in  $q_3$  stands for volume, that is,  $d^3$ . In the *cumulative mass distribution function* ( $Q_3$ ), the value of  $Q_3$  at  $d$  is equal to the mass percentage of particles that have a diameter smaller than or equal to  $d$ . Both descriptions contain the same amount of information and depending on the question to be answered, one or the other representation may be more appropriate. In the number distributions  $q_0$  and  $Q_0$ , the number percentage of particles between  $d$  and  $d+\Delta d$  and the number of particles that have a diameter smaller than or equal to  $d$  are displayed. Note that in both cases, it is implicitly assumed that the particles are spherical. Often number distributions are given if the particles are counted (e.g., microscopy) and mass distributions are given when the particles are weighed (e.g., sieve analysis).

Figure 8.13 shows that  $q_3$  is shifted to larger diameters compared to  $q_0$ . The broader the distribution, the larger the shift.

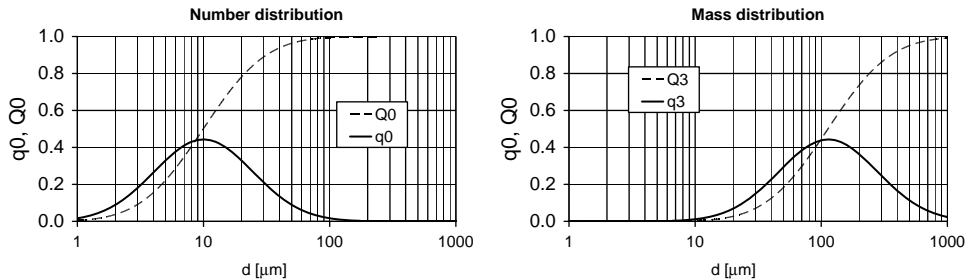


**Figure 8.13**  $q_0$  and  $Q_0$  (a) and  $q_3$  and  $Q_3$  (b) of the same distribution:  $\langle d \rangle_{\text{num}} = 15 \mu\text{m}$ ,  $\langle d \rangle_{\text{mass}} = 170 \mu\text{m}$ .

From the particle size distributions, the mean particle size can be calculated. The most commonly used averages are the number ( $\langle d \rangle_{\text{num}}$ ) and the mass ( $\langle d \rangle_{\text{mass}}$ ) average, respectively. The definition is given by Equations 8.3a and 8.3b. For broad distributions, the mass average diameter is quite larger than the number average. It is therefore important to state which mean diameter is meant. Finally, a particle size distribution can be characterized by their  $dN,x$  values, which are defined by Equation 8.3c:

$$\langle d \rangle_{\text{num}} = \frac{\int_0^{\infty} d \cdot N(d) dd}{\int_0^{\infty} N(d) dd} \quad (8.3a)$$

$$\langle d \rangle_{\text{mass}} = \frac{\int_0^{\infty} d \cdot d^3 \cdot N(d) dd}{\int_0^{\infty} d^3 \cdot N(d) dd} \quad (8.3b)$$

$$QN(dN,x) = \int_0^{dN,x} qN(x) dx = \frac{x}{100} \quad (8.3c)$$

In practice,  $N$  is often omitted and implicitly assumed as  $N = 3$ . Common characteristic values are the  $d_{10}$ ,  $d_{50}$ , and  $d_{90}$ . The value  $d_{10} = 5 \mu\text{m}$  according to Equation 8.3c means that  $10/100 = 10\%$  of the mass of the particles have a diameter of  $5 \mu\text{m}$  or less.

### 8.3.2

#### Overview of Available Methods

A number of methods are available to determine particle size distributions. An overview is given in Table 8.1. Depending on the size of the particles and the desired information, different methods may be optimal. For a comparison of the various methods.<sup>1)</sup>

**Table 8.1** Common methods to measure particle size.

Method	Size range ( $\mu\text{m}$ )
Sieving	>20
Optical microscopy	0.5–150
Electron microscopy	0.001–5
Sedimentation	0.01–50
Colter counter	1–200
Laser light diffraction (Fraunhofer diffraction)	1–1000
Quasi-elastic laser light scattering (photon correlation spectroscopy)	0.001–1

Adapted from Ref. [10].

1) [http://www.malvern.com/LabEng/technology/laser\\_diffraction/comparing\\_different\\_techniques.htm](http://www.malvern.com/LabEng/technology/laser_diffraction/comparing_different_techniques.htm).



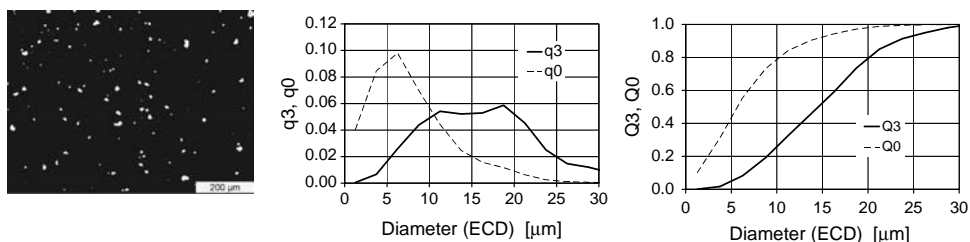


**Figure 8.14** Particle size distribution by microscopy (3597 particles were counted).

### 8.3.2.1 Microscopy

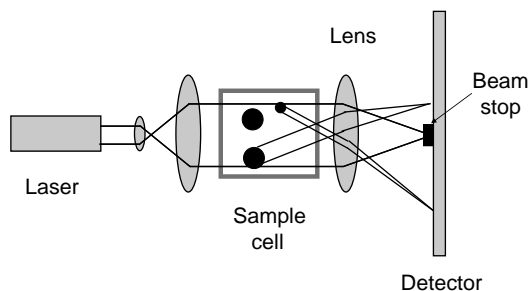
Microscopy provides the unique advantage that it can measure both particle shape and particle size. Its disadvantage is that compared to other methods, only a small number of particles are counted and that the result may therefore be accompanied by a large statistical error. Automatic image processing reduces this problem to some extent.

Figure 8.14 shows an example of particle size distribution determined by microscopy together with the determined differential and cumulative number and volume distributions. The diameter that is normally used in particle sizes determined by microscopy is the ECD (equivalent circle diameter) value, which is defined as the diameter of a circle that has the same area as the particle. Given the small dynamic range of particle size determinations by microscopy, the diameter is normally displayed on a linear rather than on a logarithmic scale. It can be seen again that  $q_3$  is significantly larger than  $q_0$ .

### 8.3.2.2 Laser Light Diffraction

The most frequently used method for particle size determination is laser light (Fraunhofer) diffraction. It has the advantages of a very large dynamic range in a size domain where most crystallization products exist, ease of use, excellent statistics, and speed. Modern instruments provide a dynamic range of particle size diameters between 0.2 and 2000  $\mu\text{m}$  when in the size range below 20  $\mu\text{m}$  corrections due to Mie scattering are applied.<sup>2)</sup> The method can be used for both dry powders and suspensions. The technique of laser light diffraction is based on the principle that particles that are illuminated by coherent light will scatter light at an angle that is directly related to their size. As the particle size decreases, the observed scattering angle increases. The principal set up of a Fraunhofer diffraction instrument is shown in Figure 8.15. The sample in the measuring cell is illuminated by an expanded parallel coherent and monochromatic laser beam. The light scattered by the particles in the cell is focused by a lens system on a position-sensitive detector. From the measured intensity distribution on the detector, the particle size

2) [http://www.malvern.com/LabEng/technology/laser\\_diffraction/mie\\_theory\\_fraunhofer.htm](http://www.malvern.com/LabEng/technology/laser_diffraction/mie_theory_fraunhofer.htm).



**Figure 8.15** Principle of Fraunhofer diffraction instrument.

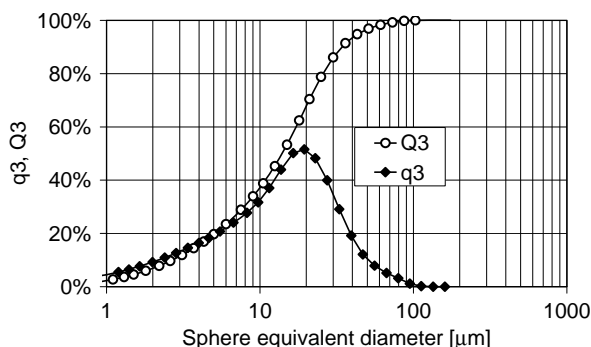


**Figure 8.16** Typical result of a particle size distribution obtained by laser light diffraction.

distribution can be calculated. The result obtained is the size distribution of equivalent spherical particles, that is, the result refers to a distribution of spherical particles that interact with the laser light in the same way as the sample consisting of nonspherical particles. Therefore, differences can occur in comparison to sieving, sedimentation, or other particle size distribution techniques. Typically, volume distributions ( $q_3$  and  $Q_3$ ) are given as results (Figure 8.16).

As with any physical measurement, sample preparation is of utmost importance. This is particularly true for particle size determinations. If the measurement is performed in suspension, dispersing aids may have to be added and ultrasound may have to be applied to ensure homogeneous dispersion. This may disrupt aggregates, which can be desired or undesired. In any case, it is highly advisable to observe the effects of sample preparation by additional methods such as microscopy. Guidelines for method development, instrument calibration, and acceptance criteria can be found in regulatory documents.<sup>3)</sup>

3) USP32-NF27 <429> Light Diffraction Measurement of Particle Size; European Pharmacopoeia EP 6.8 (2010) 2.9.31 Particle Size Analysis by Laser Light Diffraction.

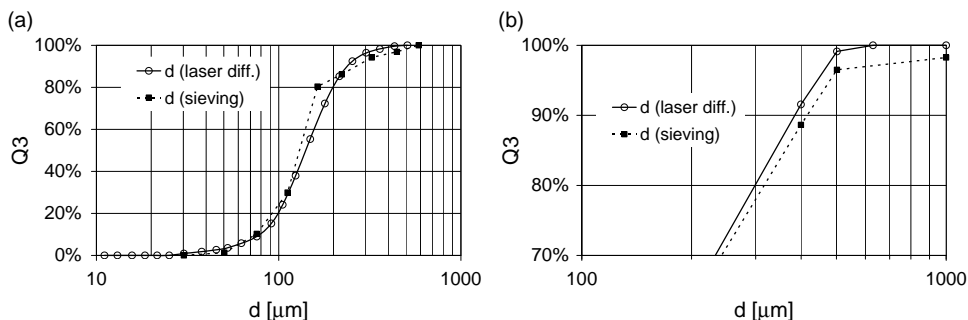


**Figure 8.17** Comparison of particle size distribution measurements by laser light diffraction and sieve analysis. In part (a), it can be seen that the overall agreement is very good. Part (b) shows the result of sieving of a very

large amount (1 kg) of crystals. Here, small deviations for large particle sizes can be observed, since a small percentage of large aggregates exists that is beyond the dynamic range of laser light diffraction.<sup>4)</sup>

### 8.3.2.3 Sieving

The most easily understood method of particle size determination is sieve analysis, where the powder is separated through sieves of different sizes. Accordingly, the PSD is defined in terms of discrete size ranges, for example, fraction of sample mass between 60 and 70  $\mu\text{m}$ . The sieves with the smallest holes are around 20  $\mu\text{m}$ ; therefore, sieve analysis accesses the size range larger than 20  $\mu\text{m}$ . It continues to be used for many measurements because of its simplicity, cheapness, and ease of interpretation. The simplest form of performing sieve analysis is shaking the sample on a stack of sieves of progressively smaller size until the weight stays constant in each sieve. Of course, the intensity with which the sieve is shaken may affect the measured particle size distribution as it may lead to the breaking up of aggregates. A reproducible mechanical shaker should be used.

For spherical particles, the measured particle size distribution by laser light diffraction and sieving may be very similar (Figure 8.17).

For rodlike particles, sieving essentially determines the diameter of the rod, whereas laser light diffraction determines the diameter of a sphere with same volume as the rod. Therefore, the result obtained by sieving will be smaller than that obtained by laser light diffraction. The opposite applies for platelike particles, where sieving measures the diameter of the plate.

## 8.4

### Powder Flow Properties

In addition to the microscopic properties of a solid product, its bulk properties are also of great practical importance. These properties include bulk density, tapped density,

4) Data obtained from Wolfgang Beckmann.

and flow properties. The aim is to predict the behavior of a powder during various manufacturing processes from powder flow properties determined in a standardized setup. Naturally, the predictive power of such a measurement can never be perfect, but it may provide a useful guidance. The practical value of a method can be gauged based on its predictability, reproducibility, sensitivity, and ease of use. The following are the most commonly used methods to characterize the powder flow.<sup>5)</sup>

- Hausner ratio or compressibility index,
- angle of repose,
- flow rate through an orifice, and
- powder rheometer/shear cell.

The Hausner ratio and compressibility index are calculated from the measured “bulk volume” or “poured volume” ( $V_0$ ) and “tapped volume” or “settled volume” ( $V_t$ ) and are defined by Equations 8.4a and 8.4b, respectively. The bulk volume can be determined by filling a known amount of powder in a graduated cylinder, while the tapped volume is obtained by mechanically tapping a measuring cylinder containing a powder sample in a controlled way.<sup>6)</sup> A Hausner ratio close to 1 or a low-compressibility index indicates good flow properties, while a Hausner index  $>1.35$  or a compressibility index  $>26\%$  would indicate poor flow properties. For a more detailed classification.<sup>5)</sup>

$$\text{Hausner ratio} = \frac{V_0}{V_t}. \quad (8.4a)$$

$$\text{Compressibility index} = 100\% \frac{V_0 - V_t}{V_0}. \quad (8.4b)$$

Various methods for the measurement of the angle of repose are used and both static and dynamic angles of repose can be determined. One way of evaluating the static angle of repose is letting the powder flow through a funnel on a flat surface allowing a cone of powder to be produced on the surface. During the formation of the cone, the funnel is moved in such a way that the distance between the top of the cone and the base of the funnel stays constant. The angle of repose ( $\alpha$ ) is defined by Equation 8.5. An angle of repose  $<30^\circ$  would point toward excellent powder flow properties, while an angle of  $>45^\circ$  would indicate poor flow properties:

$$\tan \alpha = \frac{2 \times \text{height of cone}}{\text{diameter of base of cone}}. \quad (8.5)$$

Measuring the flow rate through an orifice may be directly linked to the behavior during a manufacturing step, for example, the filling of a die with powder through a funnel, but the measured flow rates through orifices depend very much on the setup used (diameter and shape of orifice, type of container material, diameter and height of powder bed, etc.)

5) USP32-NF27 <1174> Powder Flow; European Pharmacopoeia EP 6.8 (2010) 2.9.36. Powder Flow; European Pharmacopoeia EP 6.8 (2010) 2.9.16. Flowability.

6) USP32-NF27 <616> Bulk Density and Tapped Density; European Pharmacopoeia EP 6.8 (2010) 2.9.34 Bulk Density and Tapped Density.

and therefore no universal scale is available for that property. If a defined setup is used, the measured flow rates of a series of different samples may correlate well with the behavior of the corresponding samples in a processing step on large scale.

The most fundamental powder properties can be determined in a powder rheometer [11]. Its principle of operation is similar to that of a rheometer for liquids, where the sample is placed in a shear cell and stress/strain relationships are measured. Design of a shear cell for a powder sample is more demanding than for a liquid sample, as an adequate contact between cell surface and powder need to be ensured. Accordingly, many shear cell configurations exist. While a powder rheometer provides very detailed information on powder properties, the interpretation of the data is also very demanding. A detailed discussion of this aspect is beyond the scope of this chapter.

## 8.5

### In-Process Characterization

In addition to the characterization of the product, the characterization of the system during the crystallization process may be very important as it may help to ensure a stable and controlled crystallization process leading to material of the desired quality. A number of methods have been adapted for online use. These include XRPD, IR, ultrasound absorption, and Fraunhofer diffraction. The most commonly and conveniently used ones are turbidity, NIR, Raman, FBRM<sup>®</sup> (focused beam reflectance measurement), and PVM<sup>®</sup> (particle vision measurement).

#### 8.5.1

##### Turbidity

Online determination of turbidity is probably the least expensive online tool, yet it can furnish a lot of information on the crystallization process. The simplest optical setup for turbidity probes is the one where the backscattered light is measured (other probes measure 90° or forward scattering). Turbidity measurements provide data on the concentration, size, and nature of undissolved, suspended particles present in a liquid phase. They are very well suited to determine the onset of spontaneous nucleation and thus the metastable zone widths or induction times (cf. Section 2.2.2), but they may even be sensitive to the polymorphic form obtained in a crystallization process. In Figure 8.18, the turbidity and the temperature of two crystallization processes are depicted. The particular substance can exist in two polymorphs (form 1, thermodynamically stable at all temperatures, and form 2). Form 1 is the desired form; in unseeded crystallization processes, form 2 is obtained. Therefore, seeded processes were carried out and the rate of cooling was varied. Figure 8.18a shows a process with slow cooling. The turbidity increases smoothly after addition of seeds and off-line measurements prove that the crystals are form 1 throughout the process. When a fast cooling is applied, however, the turbidity increase is not smooth indicating a mixture of form 1 and form 2. The notches in turbidity are caused by spontaneous nucleation of a

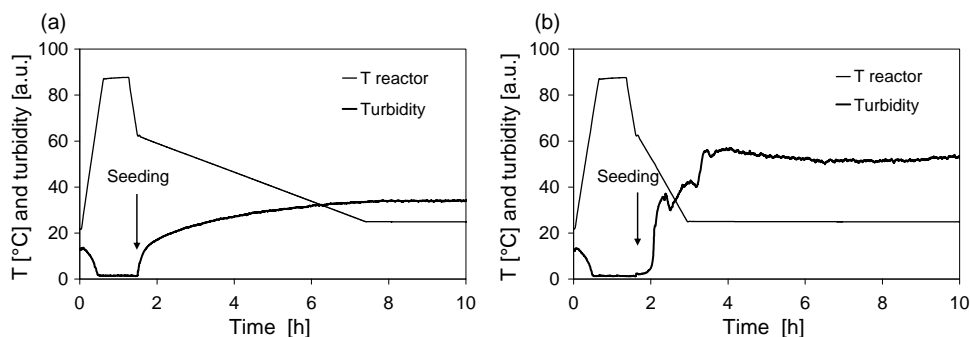


**Figure 8.18** Temperature profile (thin line) and turbidity (thick line) of a seeded crystallization process. (a) Slow cooling leads to a smooth increase in turbidity and production of pure form 1. (b) Fast cooling leads to spontaneous nucleation of the undesired form 2 and production of a mixture of form 1 and form 2. Form conversion and spontaneous nucleation lead to a fluctuation of the turbidity.

large number of form 2 particles and by the differences of light scattering properties of form 1 and form 2. The notions are confirmed by off-line measurements.

### 8.5.2

#### Raman

Online Raman immersion probes can be inserted in a crystallization vessel. An advantage of these probes is that they can be made intrinsically safe since they do not require any electrical connections, only light is transmitted via fiber-optic cables to and from the probe. The light used for Raman excitation is normally in the visible or NIR region; therefore, the probe may be connected to the detector with long fiber-optic cables and the detector can be located in a remote location. The obtained Raman spectra can be used to determine the polymorphic composition in a slurry of a compound that can exist in different solid forms. The measured Raman spectrum ( $R_m$ ) is related to the Raman spectra of the various possible solid forms ( $R_i$ ) by Equation 8.6 where  $c_i$  is the concentration of solid form  $i$  and  $s_i$  is the relative Raman scattering intensity of form  $i$ . The practical difficulty in determining the relative concentrations of the various solid forms in a slurry lies in  $s_i$ , since the relative Raman scattering intensity may also depend on particle size. Therefore, extensive calibrations are necessary before a real-time online quantification of the concentrations of the various solid forms in a crystallization process can be made.

$$R_m = \sum_i c_i s_i R_i. \quad (8.6)$$

Figure 8.19 shows such a determination. The particular substance can exist in three nonsolvated polymorphs (A, B, and C). C is the stable polymorph, B is less stable, and A is the least stable form. The aim was to convert A to B. This was achieved by seeding a slurry of A with B. Since it is known that C is the stable form, one has to ensure that the slurry process is stopped as soon as the conversion of A

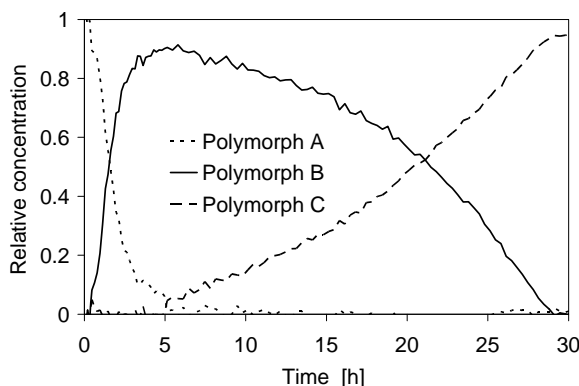


**Figure 8.19** Polymorph conversion monitored by Raman spectroscopy. A suspension of polymorph A (dotted line) is seeded at  $t = 0$  with the more stable polymorph B (solid line) that eventually converts to the thermodynamically stable polymorph C (broken line).

to B is almost complete or when the first traces of C are observed. Since it is very difficult to predict the speed of a slurry conversion as it, *inter alia*, depends on particle size, online determination of polymorph composition is mandatory in such a situation.

### 8.5.3

#### FBRM and PVM

FBRM is a real-time quantitative characterization of particle number and particle size in a suspension. An FBRM probe consists of a laser beam that is focused on a focal plane just outside the sapphire window of the probe [12]. The laser beam rotates at a fixed high speed while describing a circle. The diameter of this circle is 8 mm independent of the size of the probe and the speed of the laser beam is 2–8 m/s. When the laser beam hits a particle, light will be backscattered during the time period, while the laser beam focus is on the particle. These pulses of backscattered light are translated into chord lengths based on the simple calculation of the scan speed (velocity) multiplied by the pulse width (time). The method of chord length determination means that even monodisperse spherical particles will lead to a distribution of chord lengths, since the laser beam will intersect the sphere at various locations, that is, anywhere from the edge to the largest dimension, that is, the diameter. The measured distribution of chord lengths is therefore a convolution of particle shape and particle size distribution and normally cannot be directly compared with other particle size distributions (e.g., from the laser light diffraction method). Nevertheless, the chord length distribution is a “fingerprint” of the particle system, and provides statistics to detect and monitor rate and degree of changes in particle dimension in real time. In addition, the principle of measurement provides quantitative data on the number of particles in the suspension. This makes FBRM a highly suitable

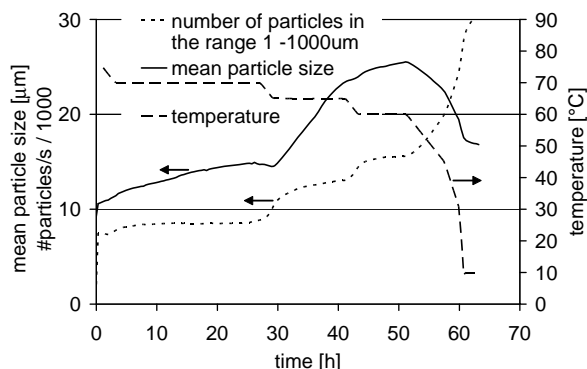


**Figure 8.20** A seeded crystallization process monitored by an FBRM probe. It can be seen that while the temperature is decreased slowly from 75 °C to 60 °C, the number of particles only increases moderately while the average particle size increases. Upon further decrease of

temperature, a rapid increase of particle number and a concomitant decrease of average particle size are observed. This indicates nucleation, which could be reduced by a slower temperature decrease.

method to monitor seeded crystallization processes, where generally the ideal situation would be that the seeds grow during the crystallization process and no new particles nucleate, that is, particle number should stay constant while particle size increases. Obviously, this ideal situation is hardly ever achieved, since stirring will normally lead to particle breakage and thus to an increase in particle number. Figure 8.20 shows typical traces of a seeded crystallization process with an FBRM probe. The observed behavior indicates how the process could be improved.

Since the measured chord length distribution is a convolution of particle shape and particle size as mentioned above, a change in particle shape during the crystallization process may be misinterpreted as a change in size. A method that allows direct observation of particle shape and to resolve these problems is PVM. PVM uses a high-resolution CCD camera and internal illumination source to obtain images in suspensions. A change in particle shape can therefore be directly observed. The method is suited to observe qualitative changes; the use of image analysis for quantitative information on particle size and number is limited to lower solid concentrations to prevent overlapping particles in the images.

### Acknowledgments

We wish to thank W. Beckmann for the data given in Figure 8.17 and acknowledge the help of F. Blatter, S. De Paul, A. Decker, H. Erni, K. Grosse-Sender, N. Martin, N. Matthes, S. Poux, K. Pulfer, J. Schoell, B. Siebenhaar, and M. Szelagiewicz for providing comments, data, and figures.



## References

- 1 Threlfall, T. (2007) *Training Course: Understanding Polymorphism & Crystallisation in the Pharmaceutical Industry*, Scientific Update, London.
- 2 Bernstein, J. (2002) *Polymorphism in Molecular Crystals*, Oxford Science Publications, Oxford.
- 3 Byrn, S.R., Pfeiffer, R., and Stowell, J.G. (1999) *Solid State Chemistry of Drugs*, 2nd edn, SSCI Inc., West Lafayette, IN.
- 4 (a) Zakrzewski, A.E. (2006) *Solid State Characterization of Pharmaceuticals*, Pergamon, Poland; (b) Brittain, H.G. (2009) *Polymorphism in Pharmaceutical Solids*, 2nd edn, Informa Healthcare, New York.
- 5 Hilfiker, R. (2006) *Polymorphism in the Pharmaceutical Industry*, Wiley-VCH Verlag GmbH, Weinheim.
- 6 Harris, R.K. (2006) NMR studies of organic polymorphs & solvates. *Analyst*, **131**, 351–373.
- 7 Gao, P. (1996) Determination of the composition of delavirdine mesylate polymorph and pseudopolymorph mixtures using <sup>13</sup>C CP/MAS NMR. *Pharm. Res.*, **7**, 1095–1104.
- 8 Höhne, G., Hemminger, W., and Flammersheim, H.-J. (1996) *Differential Scanning Calorimetry*, Springer, Berlin.
- 9 Ahmed, H., Buckton, G., and Rawlins, D.A. (1996) The use of isothermal microcalorimetry in the study of small degrees of amorphous content of a hydrophobic powder. *Int. J. Pharm.*, **130**, 195–201.
- 10 Wedd, M.W., Price, C.J., York, P., Maginn, S.J., and Mullin, J.W. (1993) The role of particle characterization in industrial crystallization. *Anal. Proc.*, **30**, 455–456.
- 11 Guerin, E., Tchoreloff, P., Leclerc, B., Tanguy, D., Deleuil, M., and Couarraze, G. (1999) Rheological characterization of pharmaceutical powders using tap testing, shear cell and mercury porosimeter. *Int. J. Pharm.*, **189**, 91–103.
- 12 Ruf, A., Worlitschek, J., and Mazzotti, M. (2000) Modeling and experimental analysis of PSD measurements through FBRM. *Part. Part. Syst. Char.*, **17**, 167–179.

## 9

# Basics of Industrial Crystallization from Solution

Wolfgang Beckmann

The development of an industrial crystallization process is driven by a variety of considerations, which will determine the details of the process realized. These considerations include properties of the moiety to be crystallized, the technique with which the supersaturation can be generated, product properties such as particle size, and finally the crystallization to be performed in a batch or in a continuous mode. This chapter summarizes these underlying principles.

## 9.1

### Generation of Supersaturation in a Crystallizer

The techniques to generate supersaturation and the path of the crystallization in the phase diagram are summarized in Figures 9.1, 9.2 and 9.3. Cooling is the most commonly used and the most easily controlled technique. However, it requires the solubility to have a sufficient dependence on temperature in order to achieve a sufficient yield.

Evaporation can be applied for all dependences of the solubility on temperature. However, as evaporative crystallizations are more difficult to control, this technique is mostly restricted to systems with a low dependence of the solubility on temperature.

A further and often used technique to induce supersaturation is the addition of an anti solvent (Figure 9.3). The solubility of the target compound decreases with the addition of an antisolvent. This technique is often used to drown-out organic compounds from an organic solvent such as acetone by the addition of water.

Finally, it is possible to generate a supersaturation by a pH shift (Figure 9.2). This technique is most often used to precipitate a free compound either from the water-soluble base by the addition of acid or by precipitating acid by the addition of a base.

Typical arrangements for the antisolvent, salt formation, and pH shift crystallizations are the batch and semibatch arrangements. All crystallizations involve the mixing of two reactants; this can occur, as shown in Figure 9.4, either via the mixing of two streams or by the addition of one component to the second residing in the vessel.

The path of the antisolvent and reactive crystallization in the phase diagram is characterized by the mixing line. Mixing schemes will be discussed in Chapter 12. It should be noted that an antisolvent or a pH shift crystallization can be run

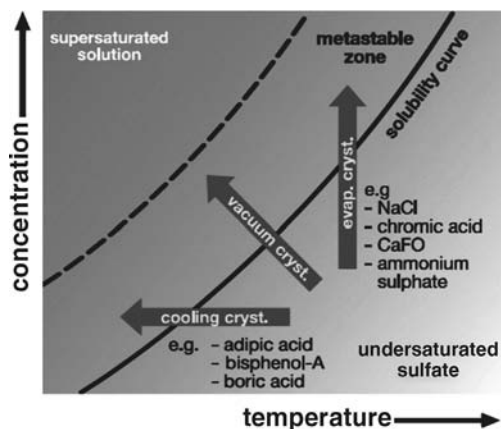


**Figure 9.1** Typical arrangements for the cooling and evaporative crystallizations and path of the crystallization in the temperature–concentration diagram.

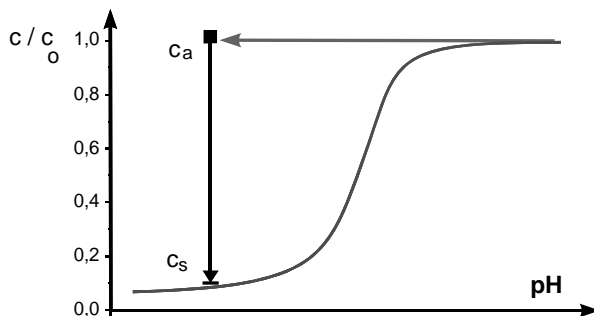


**Figure 9.2** Solubility curve of a compound precipitation by a shift in pH. This could be the case for a base soluble in water with the free compound insoluble in water.

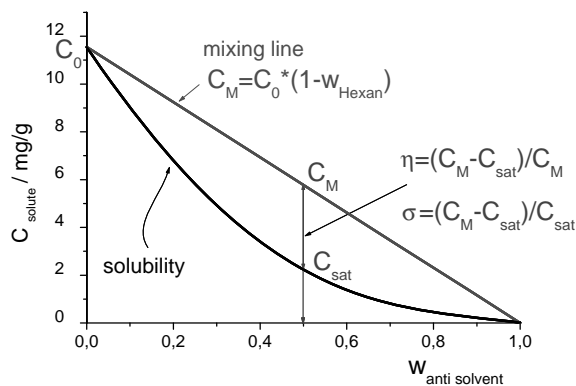


**Figure 9.3** Typical solubility curve for an antisolvent crystallization. The solubility of the target compound is given as a function of the fraction of antisolvent (here to the right). The solubility curve has a concave curvature, so that the straight mixing line leads to a supersaturation.

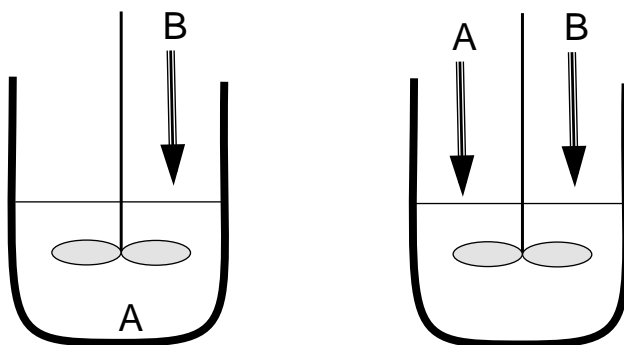


**Figure 9.4** Typical arrangements for the antisolvent, pH shift crystallization, and salt formation and their path in the phase diagram.

as both precipitation and crystallization, depending on the rate of addition and mixing. When the anti-solvent is rapidly introduced, a high supersaturation is generated, leading to the generation of a large number of nuclei. This in turn will generally lead to small particles. With the slow addition of anti-solvent it is possible to grow larger particles; by keeping the supersaturation low.

Drowning-out crystallizations and precipitations are prone to oiling-out, because of the use of solvent mixtures and the high supersaturations that can be realized. In Figure 9.5, the region of oil formation has been sketched for a drowning-out. The solubility and region of metastability are also shown. The domain for oil formation extends to the metastable zone. Thus, for the path depicted, oiling-out will occur for an unseeded crystallization. Thus, one straightforward solution for metastable oiling-out would be to seed the crystallization.

The homogeneity of the supersaturation in the crystallizer is excellent for a cooling crystallization. With sufficient mixing, the temperature gradient in the crystallizer is practically zero and confined to the adhering layer to the heat exchanger surface.

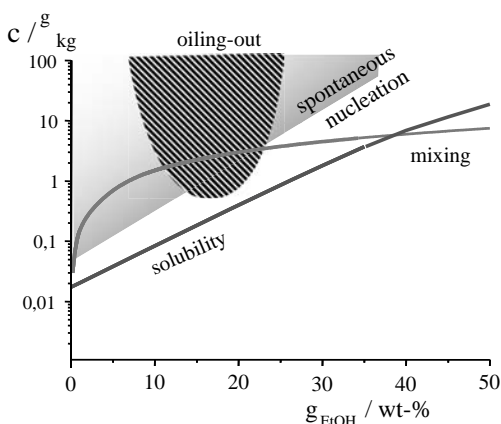


**Figure 9.5** Instable oiling-out during an antisolvent crystallization, the region for oiling-out intersects only the line of metastability. Note that the solubility follows a log-lin relationship, which renders the mixing line nonlinear.

For an evaporative crystallization, inhomogeneties exist in the boiling zone and at the solution/bubble interface. Finally, for an antisolvent or reactive crystallization, the macro- and micromixing in the zone of addition can lead to substantial inhomogeneties.

## 9.2

### Mass and Population Balance for Growth from Suspension

#### 9.2.1

##### Mass Balance

For crystallization from solutions, the mass and heat balance can be confined to the mass balance. The amount of heat liberated by crystallization as given by the heat of dissolution (cf. Chapter 3) is, except for cases with extremely high solute concentration crystallizations, small compared to the heat transfer through the vessel, even for large crystallizers with an unfavorable surface-to-volume ratio (equation 9.1):

$$V \frac{dc}{dt} - \frac{dV_{in}}{dt} c_{in} + \frac{dV_{out}}{dt} c_{out} + (\rho_s - c)A \times R = 0. \quad (9.1)$$

For evaporation crystallizations, the heat transfer is determined by the enthalpy of evaporation of the solvent (Equation 9.1). The general form of the mass balance is given in Equation 9.1. For a cooling crystallization, this reduces to Equation 9.2:

$$V \frac{dc}{dt} + \frac{dM}{dt} = 0. \quad (9.2)$$

with  $M$  as mass of crystals formed.

#### 9.2.2

##### Population Balance

Crystal growth in a batch or continuous crystallizer can be modeled by the population balance. The population of crystals in a crystallizer are the particles spread over the entire size range from  $L = 0$  to  $L$ .

The population of crystals in a crystallizer can be summarized by the moments of the population (Equation 9.3). The zeroth and the third moments describe the number of particles and the mass of crystals in the crystallizer:

$$\begin{array}{l|l} \text{number of particles} & M_0 = N = \int_0^{\infty} n \, dL \\ \vdots & \vdots \\ \text{mass of crystals} & M_3 = M = k_v \rho_c \int_0^{\infty} n L^3 \, dL \end{array} \quad (9.3)$$

$\rho_c$  and  $k_v$  are the crystal density and the shape factor, respectively, correlating length of a sphere to that of a crystal.

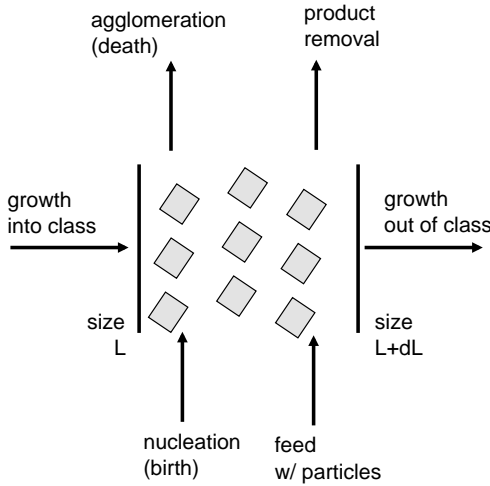


**Figure 9.6** Population, that is, number of particles per unit volume in size class  $L$  to  $L + dL$ . The number will change by growth into and out of the class, by agglomeration into and out of the class, and by nucleation. Finally, the product is removed. The feed usually is free of particles.

The number of particles in a size class, class  $L$  to  $L + dL$  (Figure 9.6), will change with the (i) growth of smaller particles into this size class and with the growth of particles out of this size class, (2) generation of particles of this size by nucleation and agglomeration, (3) loss of particles due to breakage and attrition, and (4) influx of particles and as well as by product removal.

The change in the population is described by a differential equation (Equation 9.4):

$$\begin{aligned} \text{Change of particle density, } \frac{\partial n}{\partial t} \text{ in class} = & - \frac{\frac{\partial n(dL/dt)}{\partial L}}{\text{growth into and out of the class}} \\ & - \frac{\frac{\partial \ln V}{\partial t}}{\text{change in volume}} + \frac{B(L)}{\text{nucleation and agglomeration into class}} - \frac{D(L)}{\text{attrition}} + \frac{\frac{Q}{V}n_i - \frac{n}{\tau}}{\text{in- and outflow of particles}}. \end{aligned} \quad (9.4)$$

For the growth term, the growth rate can depend on crystal size; as has been found experimentally. Some crystallization can be better described by assuming a size-dependent growth rate. However, in a first approximation, it can be set as constant, so that term simplifies to  $-R(\partial n / \partial L)$ .

The feed into the crystallizer is usually free of particles,  $-(Q/V)n_i = 0$ , and nucleation occurs only in the size class  $L = 0$ .

Neglecting agglomeration and breakage,  $B(L) = D(L) = 0$ , the population balance simplifies to Equation 9.5:

$$\frac{\partial n}{\partial t} = -R \frac{\partial n}{\partial L} - \frac{n}{\tau}. \quad (9.5)$$

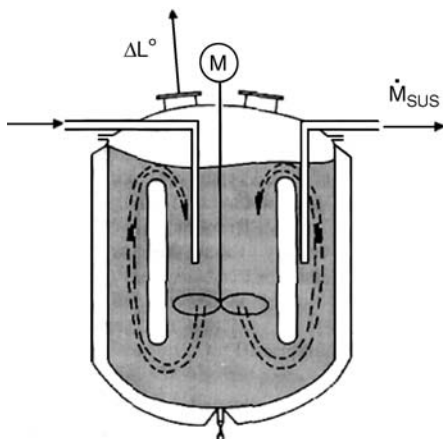


**Figure 9.7** Schematic of a MSMPR, a continuous crystallizer. The suspension is fed with fresh feed; the removal of product is isokinetic, the particle size distribution is that of the suspension. The supersaturation is typically generated by evaporation.

### 9.3

#### Operation of a Continuous Crystallizer: Basics

##### 9.3.1

##### Concept and Design of Continuous Crystallizers

The concept of a continuous crystallizer is abstracted by the MSMPR, mixed suspension, and mixed product removal reactor (Figure 9.7).

Fresh feed is fed into a well-mixed suspension, the removal of product is isokinetic, and the particle size distribution of the product stream is that of the suspension. The supersaturation is typically generated by evaporation.

##### 9.3.2

##### Mass Balance in a Continuous Crystallizer

The mass balance for the mass of solvent and solute over a continuously operated evaporation crystallizer is given by Equation 9.6:

$$\begin{aligned} 0 &= \dot{m}_{\text{in}} - \dot{m}_{\text{vapor}} - \dot{m}_{\text{out}} \\ 0 &= c_{\text{feed}} \dot{m}_{\text{in}} - \dot{m}_{\text{off}} (m_T + c) \end{aligned} \quad (9.6)$$

Thus, the feed stream is much greater than the product stream.

##### 9.3.3

##### Population Balance in a Continuous Crystallizer

The population in a continuous crystallizer is constant over time,  $\dot{n} = 0$ . By setting the growth rate independent of size, Equation 9.4 takes the form  $-(n/\tau) = R(dn/dL)$ .

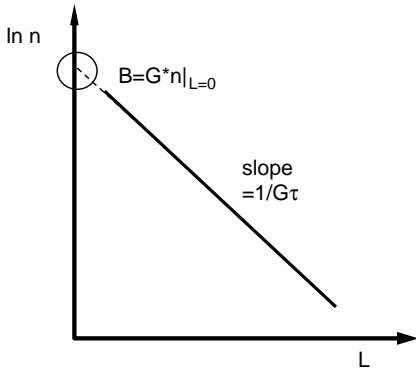


**Figure 9.8** Plot of  $n$  versus  $L$ . The slope corresponds to the growth rate  $R$ , while the intercept with the size axis is the amount of crystals leaving the size class  $L = 0$ , which corresponds to the nucleation rate.

Integrating from size  $L = 0$  to size  $L$  yields Equation 9.7:

$$\ln \frac{n}{n_0} = -\frac{L}{R\tau}. \quad (9.7)$$

A plot of  $\ln n$  versus size  $L$  should yield a straight line with the slope corresponding to the growth rate  $R$ . The intercept at  $L = 0$ ,  $n_0$ , is the number of crystals in this size class. Multiplying the number with the growth rate gives the number of particles leaving the size class  $L = 0$ , which is by definition nucleation rate  $B$  (Equation 9.8 and Figure 9.8):

$$B = n_0 \times R. \quad (9.8)$$

Customarily, the nucleation rate is plotted as a function of growth rate, both derived from Figure 9.8, for different process conditions (Figure 9.9).

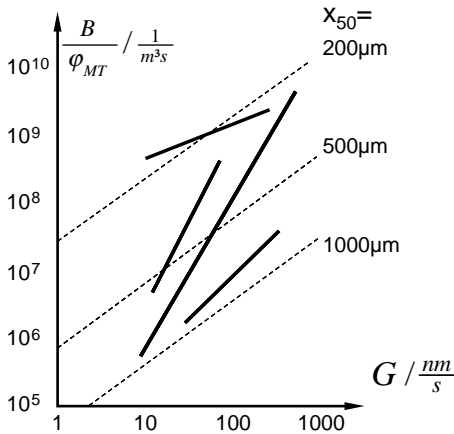


**Figure 9.9** Plot of the nucleation rate as a function of growth rates, both derived from plots of population densities vs. crystal size, such as in Figure 9.8. The nucleation rate is referred to as suspension density  $\varphi_T$ .



## 9.3.4

**Mean Particle Size**

The mean particle size obtained in a continuous crystallizer can be calculated from the moments of the particle size distribution (Equation 9.3),  $\bar{L} = (\int_0^\infty m_L L dL) / (\int_0^\infty m_L dL) = (\int_0^\infty n_L L^4 dL) / (\int_0^\infty n_L L^3 dL)$ . The mass of particles of size  $L$ ,  $m_L$ , can be calculated from Equation 9.7,  $m_L \propto L^3 n_L = L^3 n_0 e^{-(L/R\tau)}$ . This leads to the average size as given in Equation 9.9, where the mode, median, and mean particle size are given:

$$\begin{aligned}\bar{L} &= 3 \times \tau \times G \\ \bar{L} &= 3.67 \times \tau \times G. \\ \bar{L} &= 4 \times \tau \times G\end{aligned}\tag{9.9}$$

The growth rate cannot be manipulated directly, rather by changing the nucleation rate  $B$ , the surface in the crystallizer changes that determines how fast the supersaturation is decreased. This in turn will change the absolute concentration and thus supersaturation. Through the latter, the growth rate is modified. For a given nucleation and growth rate, the ensuing mean crystal size is also plotted in Figure 9.9.

## 9.3.5

**Secondary Nucleation**

A continuous crystallizer cannot be operated with spontaneous nucleation, as this would lead to instability in the particle size distribution (see Chapter 11 and Figure 11.11). Instead, nuclei are formed continuously by the collision of larger crystals resulting in small particles, which act as nuclei. As crystals of the substance crystallizing are responsible for nucleation, this nucleation is called secondary nucleation.

Two types of secondary nucleation are exemplified: collision breeding and surface breeding.

In the former, the crystals colliding with surfaces such as the stirrer will generate a number of smaller fragments (Figure 9.10). In the latter, surface fragments are spun off.

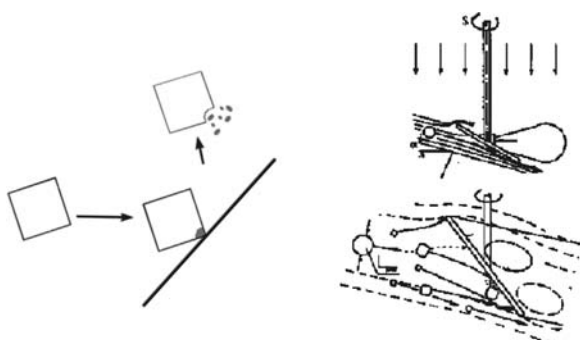


**Figure 9.10** Secondary nucleation by collisions of crystals with surfaces, that is, with the stirrer. The flow around the stirrer pushes the particles away. Depending on the shear flow, some particles will be hit by the stirrer. The strain

induced by the impact will be released by a fragmentation, and a number of smaller particles are formed that grow and thus increase the number density of particles.

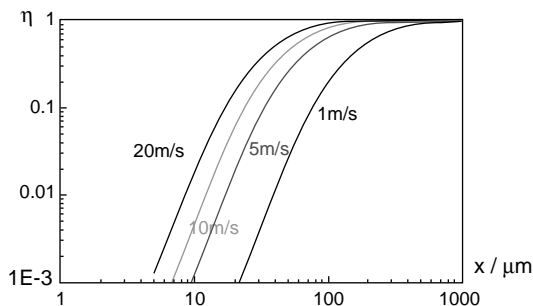


**Figure 9.11** Efficiency  $\eta$  of collisions as a function of particle size and for different relative velocities of suspended particles and stirrer blade. The efficiency only has appreciable values for particle sizes exceeding 50–100  $\mu\text{m}$ .

The strain in the crystals induced by the impact will lead to a partial fragmentation. The small fragments can grow and thus the particle density increases – nuclei are formed.

It is noted that the rate with which nuclei are formed suffices to crystallize a substance; however, sometimes the number of nuclei formed needs to be reduced, e.g. by fines dissolution (Chapter 11).

The efficiency of the collisions,  $\eta$ , is a function of the relative velocity of the suspended particles and the stirrer blade and thus of the particle size (Figure 9.11). The efficiency has appreciable values only for particle sizes exceeding 50–100  $\mu\text{m}$ . The calculations are for a difference in density between crystal and mother liquor of 0.5 g/ml and a viscosity of 1 mPa.s.

Due to the flow properties, the collisions between crystals and pump, crystals and vessel, crystals and crystals follow the ratio (crystal/pump) : (crystal/vessel) : (crystal/crystal)  $\approx$  1000 : 10 : 1. The surface hardness of the impeller does have an influence on the nucleation rate. A comparison of a steel and a plastic-lined impeller shows that harder surface leads to a much higher rate of secondary nucleation (Figure 9.12). This effect is most important when developing crystallizations in the laboratory.

The nucleation rate in a continuous crystallizer can be assessed by evaluating experimental data for the population balance (Figure 9.8 and Equation 9.7).

As the secondary nucleation is by collisions, its rate depends on the suspension density  $m_T$ , the power input  $\epsilon$  and the supersaturation  $\Delta c$ . Usually, a power law is used (Equation 9.10); typical values for the exponents are  $n = 1$ ,  $r = 1/2$ , and  $l = 1 - 2$ :

$$B \propto m_T^n \epsilon^r \Delta c^l. \quad (9.10)$$

The determination of the supersaturation in a continuous crystallizer is difficult, so data for the dependence are sparse (Figure 9.13). Usually the dependence is derived from a plot of nucleation and growth rate, as shown in Figure 9.8. As the growth rate typically depends linearly on supersaturation, the

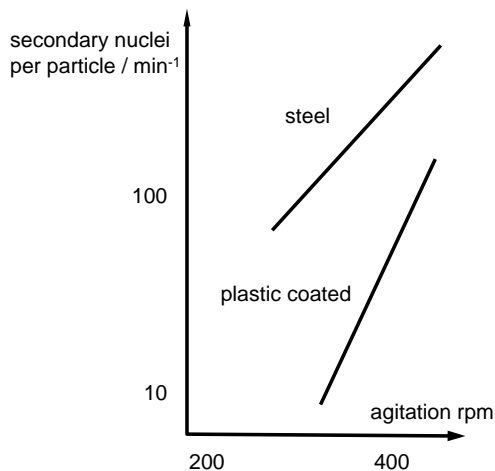


**Figure 9.12** Dependence of the rate of secondary nucleation on power input, here expressed as agitator speed. Two materials of the agitator are compared, a steel and a plastic impeller. The rate for the more rigid steel impeller is evident.

dependence of  $B$  on supersaturation can be assessed from the slope of the  $B$  versus  $G$  curve (Figure 9.9).

Thus, by secondary nucleation, crystals are generated at far lower supersaturations than that via primary nucleation, both homogeneous and heterogeneous

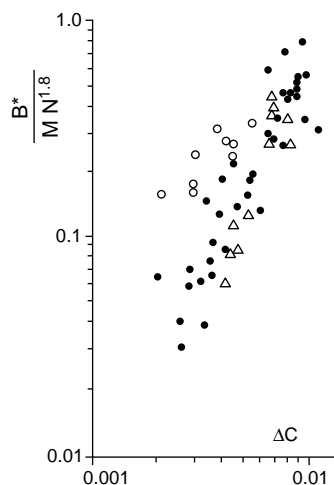


**Figure 9.13** Dependence of the rate of secondary nucleation on supersaturation in a continuous crystallizer.

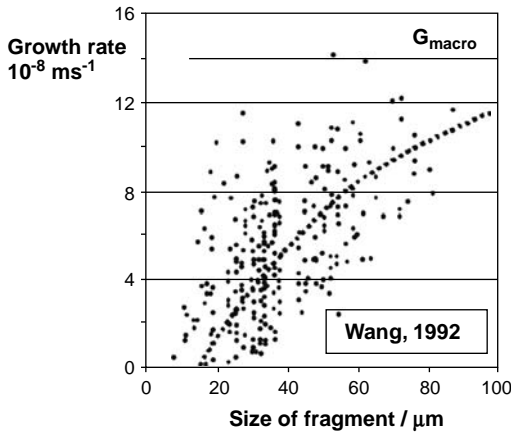


**Figure 9.14** Growth rate of small fragments of crystals after the process of secondary nucleation. The rate is compared with that of macroscopic crystals. Note the considerable dispersion in the rates Graph taken from Wang, PhD dissteration TU München.

primary nucleation. The prerequisite is that crystals of the solute are of a sufficient size and a sufficient power input is obtained by stirring or pumping.

When transferring processes relying on secondary nucleation from the laboratory to the plant, it should be noted, that the time between collisions changes, in a 1 l vessel,  $\tau = 1\text{--}10$  s, while in a 1 m<sup>3</sup> vessel, the time will increase by approximately one order of magnitude.

The growth rate of fragments/secondary nuclei immediately after their formation is found to be generally lower than that of a macroscopic unhurt crystal of the same species (Figure 9.14).

It is assumed that the strain induced in the crystals by the fragmentation process causes a higher solubility. An empirical relationship is given in Equation 9.11. The higher solubility causes slower growth and can even lead to the observation of the dissolution of small particles:

$$c_{\text{sat}}(L) = c_{\text{Perfect}} \exp \frac{1}{L} \frac{\Gamma_k}{RT}. \quad (9.11)$$

## 9.4

### Operation of a Batch Crystallizer: Basics

#### 9.4.1

#### Concept and Design of Batch Crystallizers

The concept of a batch crystallizer is shown in Figure 9.15. The vessel is charged with the starting solution. Next, the solution is supersaturated and nucleation induced, either via spontaneous nucleation or voluntarily, for example, by seeding. Details of the operation of a batch crystallizer are given in Chapter 10.

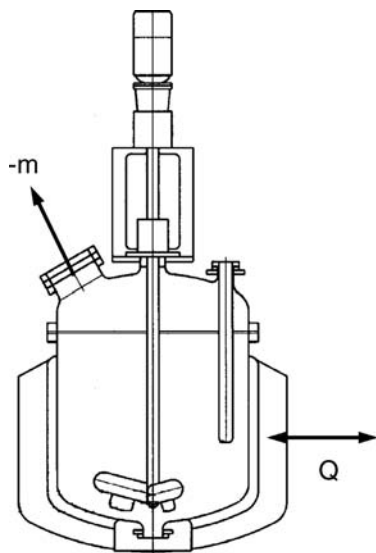


**Figure 9.15** Schematic of a batch crystallizer. The vessel is charged at the beginning of the batch with the starting solution. The supersaturation is generated either by cooling or

evaporation. The crystallization starts either by spontaneous nucleation or by seeding, and then it proceeds to the end of the batch. In many cases, the vessel is not equipped with baffles.

#### 9.4.2

##### Mass and Population Balance in a Batch Crystallizer

The mass balance in a batch crystallizer is given in Equation 9.12 and has two terms only. Concentration in the crystallizer will change with the mass deposited onto the crystals and by evaporation of solvent:

$$V \frac{dc}{dt} + \frac{dM}{dt} = 0. \quad (9.12)$$

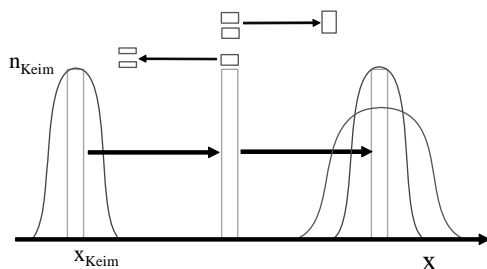


**Figure 9.16** Schematic of the development of a population of particles in a batch crystallizer. Except for agglomeration and breakage processes, the population will grow linearly.

Neglecting agglomeration and breakage, the population of particles in a batch crystallizer develops over time simply by the growth of the particles (Equation 9.13):

$$\frac{\partial n}{\partial t} + G \frac{\partial n}{\partial L} = 0. \quad (9.13)$$

Thus, an initially formed population of particles will develop linearly as shown in Figure 9.16.

The distribution of particle size will vary with agglomeration and breakage processes, which will occur in any type of crystallizer (cf. Chapter 4).

## 10

### Development of Batch Crystallizations

*Dierk Wieckhusen*

Batch crystallizations are used throughout the chemical industry to isolate a substance from the reaction broth and obtain particles with desired properties. At the same time, batch crystallization is a very versatile technique that can be adapted to the specific properties of the moiety and to the needs of product properties.

The underlying principles of the batch process are discussed that will lead to a stable and robust process.

#### 10.1

##### Setting Goals

Before any crystallization process is designed, the goals of the process and desired particle properties have to be defined. Table 10.1 lists some of these properties. One can distinguish goals that are directly influenced by the crystallization process such as yield, particle size, and/or particle size distribution (PSD) and properties that can be derived from these properties such as the bulk density. It is not always easy to predict the influence of primary particle properties on the derived ones: flowability, for example, is a very complex property that can depend on many primary particle properties such as shape, particle size, and particle size distribution or roughness. Some of these parameters can be influenced by the crystallization process, for example, particle size and particle size distribution, some are not that easy to control, for example, amorphous content and roughness, and others are more or less intrinsic and cannot be influenced by the process, for example, hardness and plasticity of the crystals.

Especially during scale-up, one has to focus on the most critical property for the foreseen downstream process such as the high purity of large crystals achieved by slow crystallization and only for a limited yield and neglect the others such as the particle size distribution that may be negatively affected by long stirring.

It is of utmost importance to have a close contact with the customers of the crystalline material to understand their needs, to define reasonable specifications, and on the one hand to meet their expectations and on the other hand to allow

**Table 10.1** Typical goals of the crystallization process.

Primary goals	Purity
Derived goals	Yield
	Particle size and PSD
	Particle shape
	Crystal form (polymorph, solvate)
	Downstream processing – filtration, drying behavior
	Flowability, bulk density, roughness, amorphous content, milling behavior
	Formulation behavior

The primary goals are related to particle properties that can be directly influenced by the crystallization process while the secondary goals are indirectly influenced by the crystallization process.

enough degrees of freedom to design an economic, robust, and scalable crystallization process.

## 10.2

### Crystallization of Organic Moieties

Most batch crystallization processes developed involve the crystallization of organic moieties, and, in most cases, the crystallization is from the reaction broth. This involves several tasks and constraints.

Organic molecules are prone to the formation of polymorphs and solvates (for details see Chapter 5). The main reason for this behavior is the large number of degrees of freedom within these molecules that allow the molecule to adopt a large variety of conformations and hence a large number of potential structures in a crystal lattice with or without solvent incorporation. Each of these new forms has a different crystal lattice and therefore most likely different lattice energy and solubility. Most important for the development of the crystallization process, each modification will have a different crystallization behavior.

A reaction broth will usually contain a great variety of by-products formed during the chemical synthesis. Most by-products are closely related to the desired molecule, for example, one part of the molecule may be same and maybe just one group is missing. If the missing group is the anchor for the next molecule in a crystal lattice, this by-product may be able to attach to the crystal with the correct structure, but it cannot act as an anchor for the next molecule – hence crystal growth is hindered at this crystal face. Knowing that good additives are able to significantly modify crystal shape or even stop further crystal growth or avoid nucleation at concentrations in the ppm range, it becomes clear that the large variety of impurities that can be seen in an HPLC pattern is a huge source of potent additives that may affect the crystallization process (see Chapter 6).

Organic molecules usually are much more sensitive toward reactions with solvents or degradation with temperature compared to inorganic materials. Each new salt that an organic base or acid is forming can be treated as a new chemical



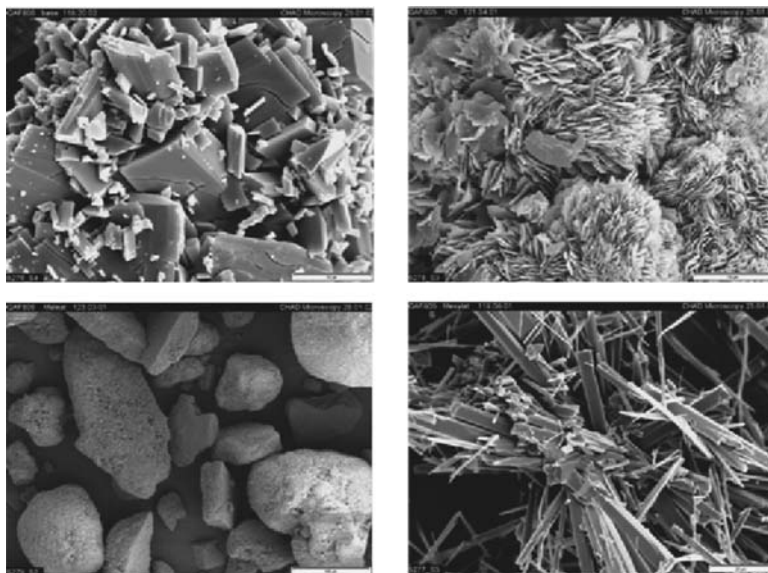


**Figure 10.1** Four different salts of the same drug substance (reproduced with permission from Chimia).

entity and hence requires totally new investigations regarding solubility and physicochemical behavior in order to define a robust crystallization process. Figure 10.1 shows the shape of four different salts of the same drug substance. Both the habit of the crystals and the size of the primary particles and the agglomerates differ vastly.

### 10.3

#### Generation of Supersaturation in Batch Crystallizations

In the majority of batch crystallizations, three ways to generate supersaturation are used. These will be discussed in order of their usage in some detail below.

##### 10.3.1

##### Cooling

Cooling crystallization is the preferred option for batch crystallizations as the temperature profile in a reactor can be easily controlled giving perfect control of the supersaturation profile. This curve gives information at which temperature the process has to be started in order to have a reasonable solute/solvent ratio and avoid unnecessary high dilution; on the other hand, the solubility at low temperatures fixes the yield that can be achieved with this process.

Typical cooling rates for organic moieties are on the order of 0.1–0.2 K/min. A rule of thumb classifies the cooling regimes as summarized in Table 10.2.

**Table 10.2** Classification of cooling rates for the growth of organic molecules in a batch crystallizer.

Classification	Cooling rate (K/h)
Slow	1–5
Realistic	5–10
Fast	10–15
Crash	>15

The only tricky point to keep in mind is the temperature at the inner crystallizer wall. Depending on the cooling rate, this temperature is somewhere between internal temperature and jacket temperature. If the jacket is too cold in order to reach high cooling rates, local supersaturation at the wall can become so high that nucleation occurs on the wall and thus the formation of crusts or in the solution close to the wall, which can broaden the particle size distribution obtained.

The maximum yield  $Y$  of a cooling crystallization is given by the starting concentration  $c_0$  and the equilibrium solubility at the final temperature,  $c_w$  (Equation 10.1):

$$Y = \frac{c_w - c_0}{c_0}. \quad (10.1)$$

Thus, for a sufficient yield to be obtained, the solubility has to change by at least a factor of 10–20 over an acceptable range in temperature. Typically, crystallizations will start about 5–10 K below the normal boiling point and will not be performed below  $-10$  to  $-20$  °C.

### 10.3.2

#### Use of Antisolvent

Antisolvents can be used in three ways: (1) to create supersaturation in an isothermal process, (2) to decrease the solubility at the end of a cooling crystallization to increase yield, and (3) simply to modify, to decrease the solubility of moiety.

In some cases, it is necessary to add antisolvent in order to increase the yield of the crystallization processes. There is a risk of spontaneous nucleation around the location of the addition of the antisolvent in the reactor because there supersaturation reaches its maximum values.

This may not be seen on small scale where the liquid stream coming into the solution is only a mm in diameter and will be rapidly mixed with the bulk, but on large scale streams of 10–20 mm may need significant amount of time to get mixed with the bulk and during this time locally high supersaturation may lead to precipitation of undefined material (regarding polymorph or solvate status and also regarding particle size distribution). Also, the formation of less stable polymorphs or solvates may be triggered due to this process.

In the light of these potential issues, it is advised to limit the addition of antisolvents whenever possible. In some cases, it is overseen that the antisolvent that is added to

decrease solubility at the same time increases the total dilution of the system and may compensate at least partially the benefit from the decrease in solubility. Often it can be beneficial to mix the solvent and antisolvent before adding the solute and in this way find a new solvent mix that has solubility properties that enable a cooling crystallization without any further antisolvent addition after the crystallization has started. Some of the drawbacks of antisolvent addition (e.g., high supersaturation at point of addition) can be partially mitigated if the antisolvent is added at a lower temperature after seeding and cooling when there is less solute remaining in the solvent and where there is a much higher surface area of crystals available that can consume the generated supersaturation faster than the few seed crystals at the beginning of the crystallization process. The antisolvent addition temperature should, however, not be too low in order to allow for good crystal growth kinetics and yield. In many cases, the addition of small amounts of antisolvent significantly increases the solubility of the solvent mix before the antisolvent characteristics are developed. In this case, the antisolvent helps as a solubility facilitator by building a bridge between areas of the molecule that do not interact with the initial solvent, but show affinity to parts of the antisolvent that itself is interacting with the solvent.

Drowning-out is a term sometimes used for fast antisolvent addition resulting in high supersaturations that lead to high nucleation rates. This variant is described in detail in Chapter 12.

### 10.3.3

#### Evaporation

Evaporative crystallization is a technique of choice for a moiety with a weak dependence of solubility on temperature. However, this technique has several drawbacks that should be regarded when using this technique.

- During batch distillation the liquid level in the vessel drops, which could lead to the formation of a crust. This crust is difficult to remove; in addition, the process conditions in this crust are not well defined – especially in the case of solvent mixtures, the solvent composition changes over time leading to the formation of multiple solvates. Wall encrustation can be limited by refraining from heating via the jacket and using only the latent heat of the batch for evaporation. In addition, encrustation can at least partially be overcome by keeping the level constant during distillation.
- In case solvent mixtures are used, the solvent composition changes over the process. In case different solvates are traversed, it may be difficult to obtain the desired particle properties. In some cases, the crop can undergo a solvent-mediated phase transformation, which could affect the particle integrity.

$$Y = \frac{V_{\omega} - V_0}{V_0}. \quad (10.2)$$

The maximum yield  $Y$  of an isothermal evaporative crystallization is given by the starting volume  $V_0$  and the final volume  $V_{\omega}$  (Equation 10.2). It is apparent that

acceptable yields can only be reached for high degrees of evaporation. Thus, in general, an evaporative crystallization step at elevated temperature is followed by a cooling step to increase yield.

## 10.4

### Initiation of Crystallization – Nucleation Phase

Basically, two possibilities to start crystallization exist: either spontaneous nucleation is initiated by increasing the supersaturation beyond the supersolubility curve or by seeding with crystals of the moiety to be crystallized within the metastable zone. Figure 10.2 shows a typical solubility curve of an organic moiety and its region of metastability. A cooling crystallization will start at point A and cross the solubility at point B. Without the addition of seed crystals, the system can be cooled to point C or D, before spontaneous nucleation occurs. The point of spontaneous nucleation will depend *inter alia* on the purity of the system and the rate at which the solution is cooled.

Conversely, seed crystals can be introduced shortly after the system has become supersaturated, but well before the border of the metastable zone has been reached. This seeding avoids effectively spontaneous nucleation.

This spontaneous nucleation has several drawbacks that are all about not actively controlling the crystallization process:

- Regarding polymorphism, the metastable forms are often obtained – forms that are prone to be lost during further processing if the stable form shows up (cf. Chapter 5), a form that is prone to be lost during the process. More important, the modification obtained can depend on (1) the solvent used and (2) the purity of the system. Thus, a change in solvent might not be possible, and a change in the purity of the system can have unpredictable effects.

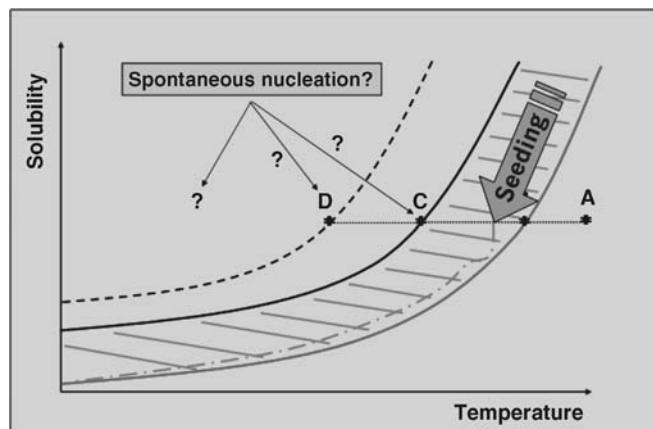


**Figure 10.2** Solubility curve (gray) and supersolubility curves (black). The point of seeding has to be well within the metastable zone to avoid any spontaneous nucleation.

- Regarding the particle size distribution, crystallizations with spontaneous nucleation exhibit a large variability. In addition, process conditions can also have an influence on the particle size.
- During the nucleation phase, the amount of material crystallizing instantaneously depends on the width of the metastable zone (cf. Chapter 2). This amount can be substantial: for organic moieties, sometimes more than 30–40% of the entire material will crystallize upon spontaneous nucleation. This material crystallizes at high supersaturations, which can have negative effects on the purification via crystallization.

Although the control on the crystallization process by spontaneous nucleation is limited, this nucleation process is often used throughout the industry.

## 10.5

### Seeded Batch Crystallizations

Seeding in batch crystallizations can have two major goals: (1) avoiding the usually high supersaturations for spontaneous nucleation and thus also the growth at high supersaturations immediately after nucleation and (2) controlling particle properties, namely, polymorphism and crystal size distribution. In both cases, the choice and preparation of the seed, the point of addition, and the relation between the amount used and the proceeding of the crystallization play a determining role for the success of the seeding.

Although in some cases heterogeneous seeding can be applied, the seeds in this chapter are understood as crystalline material of the solute to be crystallized. These are usually in milled form, both with respect to chemical purity and with respect to the solid-state form (polymorphism or solvate form).

Seeding a batch crystallization and thus avoiding spontaneous nucleation gives the possibility to achieve a number of important goals and at the same time makes it more robust:

- Due to the low supersaturation at which seeds are added, secondary nucleation rate can be kept very low if secondary nucleation occurs at all.
- No uncontrolled primary nucleation is possible – the outcome of spontaneous nucleation would vary depending on the supersaturation when it occurs.
- The formation of amorphous or partially amorphous phases can be avoided.
- The start of the crystallization process is very well defined and reproducible. For example, solvent composition or temperature is given, which define the stability region of enantiotropic or solvated forms.
- Seeding and low supersaturation minimize the chance of new – more stable – forms to nucleate (by keeping their supersaturation low as well).
- The desired polymorph or solvated form is added from the beginning as seed and thus other forms are less likely to occur, even if they are supersaturated or more stable.

- Particle size and particle size distribution are relatively easy to control.
- Very short development times are required.
- Process robustness is typically very high compared to non-seeded processes.

### 10.5.1

#### Seeding Strategy

Before a seeding process is designed, one should have clarity about the targets to be achieved in this process and potential hurdles that are likely to show up. For example, if a substance is prone to *polymorphic transformations* or forms a variety of different *solvates*, the first goal would be to circumvent the formation of such unwanted forms. In this case, a large amount of seeds of the desired form (i.e., a large active surface area) can be used to suppress unwanted forms as far as possible. If seeds are added to slightly supersaturated solutions in this case, the chance for unwanted forms to nucleate is minimized. Of course, active seed surface also means that the seeds are well dispersed. In this case, wet dispersion with high shear may be considered.

In other cases, *purity* may play a role – also here good seeding can keep supersaturation low and hence crystal growth rate low – which is in most cases a prerequisite for high-purity crystals. The usefulness of seeding is very obvious if a given *particle size* or particle size distribution has to be achieved. In this case, the mass balance shown below will help to obtain the desired size. This applies not only for the mean particle size, but also for the particle size distribution. In certain cases, it is desirable to have bimodal distributions (e.g., to ensure good flowability or to have different dissolution characteristics for sustained release) and then seeding with two or more different seed crystal size fractions can be performed. For narrow PSD, narrow seed size distributions are necessary, and for wide distributions wide PSD of seeds can be applied.

*Particle shape* can be manipulated if adequate seeds are used. If needle-like crystals are micronized to a compact shape and these particles are used in a large amount (e.g., 10% of the expected yields), the resulting product crystals are forced to have an aspect ratio of less than 10, even if they would grow only in the longitudinal direction.

In every case, seeding should be applied in a way to take away unnecessary degrees of freedom for the crystallization process and obtain the desired product in a reproducible way.

Usually it is very helpful if seed crystals are very well defined and specified – that is, milled to the desired PSD. In other cases – if former product crystals are used as seeds – in the long run the product particle size will become larger and larger, efficient seed surface area will accordingly become smaller, and the process will change and no longer deliver the desired product quality.

### 10.5.2

#### Designing a Seeding Process

Building up on the discussion in the previous chapter, seeding comprises the following steps.

### 10.5.2.1 Quality of Seeds

Based on these goals, the quality of the seeds has to be selected. Quality comprises the source of the seed material – for example, micronized or milled drug substance of a defined particle size distribution, the correct polymorph or solvate, high purity, and in some cases the right shape of the seed crystals.

### 10.5.2.2 Quantity of Seeds

Seeding should be done in such a way that as many seeds are added as required to provide enough crystal surface area to desupersaturate the solution in reasonable time (e.g., 20 min) without forcing crystal growth rate too much. In this way, high purities of the crystals can be obtained already at this stage of the crystallization process. Also, only these seeds should grow without giving nucleation events a chance to spoil the particle size distribution determined by the size and amount of the seed crystals. Further nucleation processes typically occur from secondary nucleation that heavily depends on supersaturation (see Chapter 9.3.5). Keeping supersaturation low by adding enough seeds and slowly generating further supersaturation, for example, by slow cooling combined with gentle mixing, the further breeding effects of the crystallizer can be minimized.

The easiest way to manipulate *particle size and particle size distribution* is by seeding. Often this power of seeding is underestimated or neglected. Instead, just a few seeds are added to the supersaturated solution in order to somehow start the crystallization process. By this “homeopathic” seeding, a lot of potential control over the crystallization process is given out of hand.

The particle size obtained by a seeded crystallization is determined by the amount of seeds and their particle size. The final size can be estimated by assuming that (1) the number of particles introduced as seed,  $n_{\text{seed}}$ , is constant and (2) all seed particles grow at the same rate. If the seed particle size is narrowly distributed around  $d_{\text{seed}}$ , the product particle size is given by Equation 10.3:

$$d_p = d_s \sqrt[3]{\frac{m_p}{\varphi m_s}}. \quad (10.3)$$

The assumption of a constant seed particle number heavily depends on the seed particle size: the smaller the seed particles, the more they are prone to agglomeration, and the introduction and the proceeding of the crystallization; the higher the power input, the more the particles are prone to breakage and secondary nucleation.

In general, for a 10-fold increase in particle size via seeding, 0.1% of seed is needed.

Figure 10.3 shows crystals obtained with different amounts of seeds (micronized substance with a mean diameter of around 3  $\mu\text{m}$ ). The grid lines have a distance of 100  $\mu\text{m}$ . It should be noted that in this case the crystal size obtained with spontaneous nucleation is larger than that obtained with seeding.

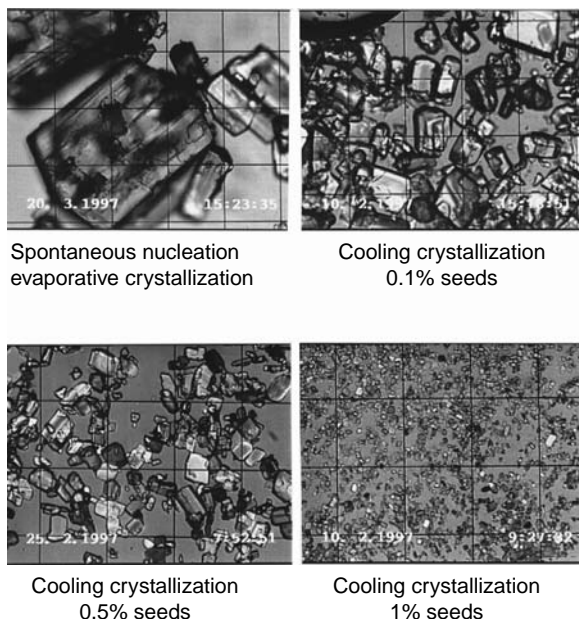


**Figure 10.3** Particle size as a result of varying seed amounts ( reproduced with permission from Chimia).

To gain good control over the crystallization process, typically 0.1–1% of seeds are added. In certain cases, where very small crystals are required or where shape has to be modulated, it may be necessary to add much more seeds. If, for example, needle-like crystals occur because the crystal preferentially grows in one direction, the addition of 10% cubic crystals would limit the length to width ratio to a maximum of 10! If very small seeds are available (e.g., 1  $\mu\text{m}$  cubes), and if again a large amount of seeds is used (again 10%), then very small product crystals can be expected – in this case around 2  $\mu\text{m}$  if they grow evenly in all 3 directions. Such small crystals may not be accessible in any other way, such as precipitation.

#### 10.5.2.3 Preparation of Seeds

The seed has to be introduced as well-dispersed particles. One should consider that storage of dry seeds, for example, in bags that are typically piled up in a storage room may in the long term lead to severe agglomeration inside these bags and if the user does not take care of this time consolidation, there may be a gradual loss of process control over time.

The best and safest way to prepare the seeds is to disperse them in the same solvent as used in the crystallizer. This dispersion can be achieved by sonication or high-shear mixing. Dispersing seeds has some more advantages: very fine material from the milling may be dissolved, distorted lattices may heal, amorphized surfaces may recrystallize, and desolvated solvates (during drying of the seed



material) may resolvate and become active for the solvate to be formed in crystallization.

#### 10.5.2.4 Supersaturation at the Start of Crystallization

The supersaturation before the addition of seeds should be adjusted according to the solubility curve and the supersolubility curve (cf. Figure 10.2). Typically, seeding at 4–5 K below saturation temperature is fine. Of course, the metastable zone width has to be considered here and the seeding point should be closer to the solubility curve than to the supersolubility curve. It should be kept in mind that the metastable zone width is not thermodynamically determined, but strongly depends on plant properties and process parameters, such as cooling rate. If the metastable zone width is very narrow, for the sake of process robustness temperature control has to be improved or even an inline measurement of the supersaturation (e.g., by NIR) may have to be used to detect supersaturation close to the solubility curve and to avoid spontaneous nucleation or unwanted dissolving of the seed crystals. In such cases, special care has to be taken that no crystals are present in the crystallizer from the previous batch.

#### 10.5.2.5 Holding Time After Seeding

Due to the high slope of the solubility curve at high temperatures, where seeding typically is taking place, a significant amount of solute can crystallize out after seeding until the solution has reached saturation. Therefore, enough time should be given to the still relatively small seed crystals to take up the supersaturation in the system before more supersaturation is generated. In lab trials, the time necessary can easily be found by watching the turbidity signal of the lab crystallizer – if this is reaching a constant value, further supersaturation may be generated. Typical holding times are at least 20–30 min.

## 10.6

### Crystallization Period

After nucleation, either spontaneous or via seeding, the bulk of the material has to be crystallized. This should be done in accordance to the solubility curve and the amount of crystal surface present in the crystallizer. In order to obtain a constant growth rate and thus a high purity during the whole crystallization process, it is beneficial to start with small supersaturation rate at the beginning and increase this rate as the overall crystal surface area grows. In the case of cooling crystallization, this means that cooling should ideally start slowly and the rate should be increased over time. If the temperature control system in the plant cannot follow programmed parabolic cooling, it is possible to approximate this curve by two or three linear cooling ramps as shown in Figure 10.4; the result will be virtually the same.

By keeping the supersaturation low during the whole crystallization process, the danger of secondary nucleation is reduced, which can be induced by the attrition of crystals with the stirrer, the reactor wall, or with themselves.

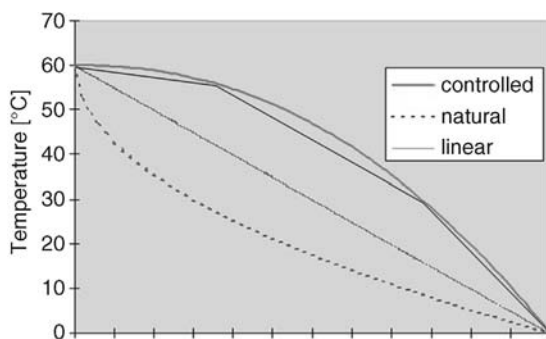


**Figure 10.4** Cooling variants: linear, natural, and controlled cooling. The controlled cooling profile can be approximated by two or three linear cooling profiles (three shown here).

After the final temperature or the degree of evaporation is reached, crystallization normally is not finished yet. Due to the low temperatures that are applied to obtain good yield, crystal growth rate becomes very slow. Therefore, it is necessary to stir the crystallizer for a few hours – typically overnight before the product can be harvested. Again, a turbidity signal gives a good indication when the process is finished. The yield obtained should be compared with the solubility and dilution given before filtration. For example, if dilution is 10-fold (i.e., 10 g of substance has been dissolved in 100 g solvent) and the final solubility before filtration, for example, at 0 °C is 1%, then the theoretical loss of material due to solubility in the mother liquor is 10% and the expected yield would be around 90%. In this way, it can be checked if equilibrium solubility and thus maximum yield is really obtained. If the achieved yield is still too low, crystallization kinetics especially at low temperature was too slow. In this case, it makes sense to slow down cooling rates or to increase holding time at final temperature. In rare cases, by-products can hinder crystallization and prevent the system to reach equilibrium. This is a reason to measure true solubilities by dissolving of crystals rather than by approaching the solubility equilibrium by cooling.

## 10.7

### Scale-Up Considerations

Generally batch crystallizations can be quite robust if designed the right way, however scale-up is not an easy task and several points have to be taken into consideration.

#### 10.7.1

##### Process Time – Rate of crystallization

During scale-up of a crystallization, each process time, time of cooling or time of addition of antisolvent, should be kept constant, although this rule might be limited by certain physical constraints.

The specific surface area of a crystallization reactor decreases with increasing size, while the volume grows with a power of 3 and the surface area for the cooling jacket

grows only with a power of 2 with reactor diameter. Regarding the scale-up of cooling processes with a given cooling rate, this means that on large scale one needs much lower jacket temperatures to obtain the same overall cooling rate as on small scale. This lower wall temperature can lead to incrustations or increased nucleation rates near or on the wall. This problem can of course be easily handled by decreasing the cooling rates; however, the resulting longer processing times may then be critical with respect to product throughput or the longer stirring may lead to increased abrasion that may not be acceptable.

For evaporative crystallizations, the surface area through which evaporation occurs also increases only with a power of 2 with the reactor diameter, again making it necessary to increase the process time to avoid high boiling rates.

In case the crystallization is induced by spontaneous nucleation, it is advisable to keep the cooling rate constant, so that the supersaturation at which nucleation occurs is kept constant.

The seeding process is easily scaled. In any case, it is advisable to use the same type of seed, for example, polymorph, type and size of comminution, and type of preparation. In this case, the amount of seed is kept constant. This can be seen from Figure 10.5, showing images of the crop and particle size distributions as the seeding process was scaled up from 1 l in the lab to the pilot plant and finally to production. The efficiency is constant; thus, the amount of seed per kg of product could be kept constant. For each scale, two crops are reproduced showing the dispersion in particle size obtained.

### 10.7.2

#### Stirring

Stirring is typically the most critical parameter in scale-up of crystallization processes, namely, for batch crystallizations. Two aspects have to be considered: (i) homogenization of the batch and mixing during the addition of antisolvent and (ii) the suspension of the crystals.

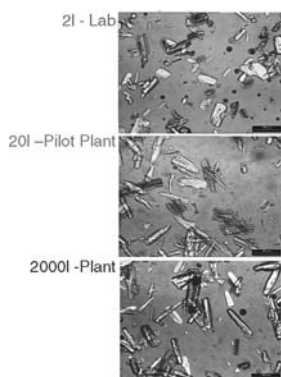


**Figure 10.5** Particles obtained with 0.1% seed in the lab and during scale-up from pilot plant to production.

**Table 10.3** Scale-up rules in a draft tube crystallizer.

Volume (l)	Pilot scale	Production scale		
	90	11 250		
Power input (kW)	1	125	3125	25
Power (V)	1	1	25	0.2
Stirrer speed, $n$	1	0.34	1	0.2
$D$ (stirrer)	1	5	5	5
$nD$ ( $\sim \nu$ )	1	1.7	5	1

Reproduced with permission from A. Myerson.

With respect to mixing during the addition of antisolvent, it is important to have a good understanding as to how sensitive the process is toward stirring effects. It pays off if the process is designed in a way that it is independent of addition rates, addition mode (spray ball, rake, or pipe), and position of addition (under or above liquid level) or turbulence. All these may be very critical if mixing (micro- or mesomixing) plays a decisive role, for example, in precipitations or sometimes also in crystallizations with antisolvent addition, if local supersaturation leads to additional nucleation.

Keeping the crystals well suspended by stirring is the other important aspect in scale-up, namely, for large crystals that are fast settling. Depending on difference of densities of the crystals and the mother liquor, typically settling becomes relevant above 100  $\mu\text{m}$  and critical above 200–300  $\mu\text{m}$ . Whereas it may be easy to keep these particles suspended on small scale, especially if high stirring rates and stirrers with good axial flow are used, it can be difficult to keep these suspended in a large industrial reactor – if power input per unit volume is kept constant (for good dispersion), tip speed on large scale automatically goes up if the same stirrer type is used. Table 10.3 shows the dependence of typical process parameters of a stirred tank reactor (propeller stirrer) on each other (adapted from Oldshue/Myerson, Ed. 1993).

If one parameter, for example, the power input per unit volume, is kept constant for small and large scales, the other parameters such as the tip speed of the stirrer will significantly increase 1.7-fold between the pilot and production scales. A higher tip speed can lead to increased particle attrition or even breakage.

Thus, keeping power input per unit volume constant for the sake of dispersion can result in crystal breakage. If specific power input is reduced, the crystals will settle and maybe clog the bottom outlet or fuse to large aggregates while sitting on the bottom of the crystallizer. In such cases, it may be necessary to change the stirrer type during scale-up. In this case, it is recommended to turn to a stirrer that generates higher axial flow. For example, if lab development were done with an impeller-type stirrer on the large scale, a pitched blade stirrer can be applied.

### 10.7.3

#### Operational Aspects

On production scale, crystallizations are often run in campaigns in which a certain number of crystallization batches is run in sequence without a thorough cleaning

after each batch. Crystals will remain in the crystallizing vessel and transfer lines and potentially become active as seeds. Crystals in the wet part of the reactor typically are dissolved during the transfer of the still undersaturated solution into the crystallizer and act as “autoseeds”.

The transfer of the suspension from the crystallizer to the separation unit can have a pronounced effect on the crop. Different to the usually gentle transfer in the lab, pumps are used that might exert high shear forces on the crystals. Large and brittle crystals are especially prone to breakage. Further, the peeling in automated centrifuges can be critical in this respect and the centrifuge speed has to be reduced significantly in order to avoid breakage at that stage.

To ensure the same washing efficiency on large scale as on lab scale, it is important to learn about the washing behavior of the filter cake. In case the filter cake tends to crack, this may be not critical on lab scale if the crack is closed, for example, with a spatula, but on large scale this happens to a much higher extent and the cracks may cause the wash to preferentially flow this way and the rest of the cake will not be washed properly.

## 10.8

### Manipulating Particle Shape

As stated in Chapter 2, crystals usually grow in a preferred orientation given by thermodynamic and/or kinetic constraints. Sometimes the “natural” shape is not favored in downstream processing and formulation; for example, platelets tend to filter poorly or they can have negative powder properties for micronization, and needles can break easily during handling or they can be bulky and hence require too large volumes in handling and formulation.

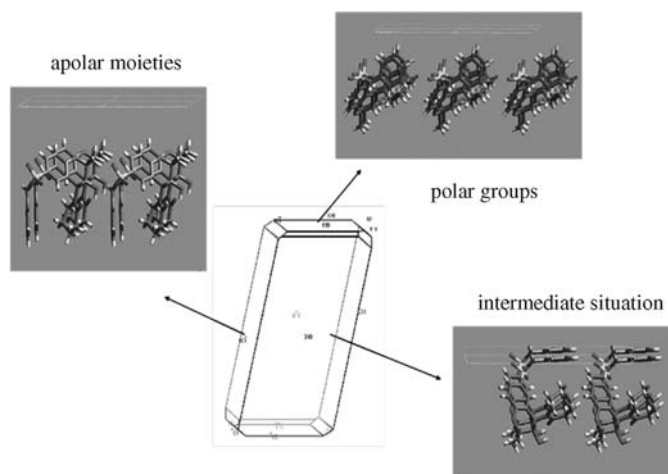


**Figure 10.6** Different polarities of crystal faces ( reproduced with permission from Chimia).

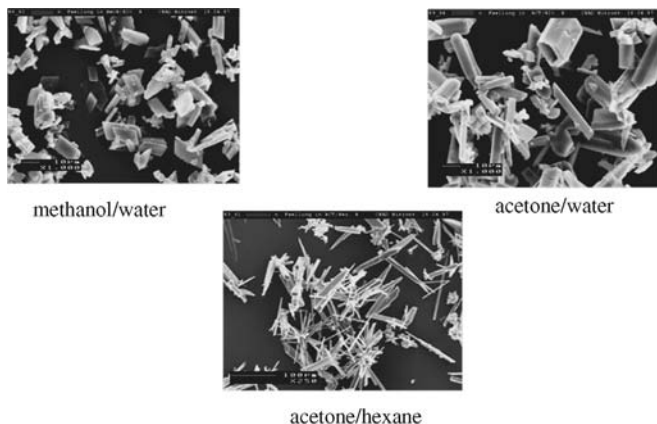


**Figure 10.7** Effect of solvent polarity on the shape of the crystals ( reproduced with permission from Chimia).

Therefore, it may become necessary to modify the natural shape in a way that it becomes more advantageous for the following steps. The habit may be modified by using additives (see Chapter 6). Here, changing or modifying the solvents is by far the easiest and most elegant way to achieve this effect. If the single crystal structure is known, the natural shape of a crystal can be modeled, for example, by attachment energy-based models and strategies for solvent selection for shape modification can be derived from the chemical surface structure of the crystal faces. In an example shown in Figure 10.6, the crystal structure reveals that polar groups are most pronounced at the tips of the elongated platelets. Polar solvents interacting preferentially with this crystal face can hinder the growth of this face and the crystal becomes more compact, while apolar solvent such as hexane inhibit lateral growth so that the crystals become more needle-like (Figure 10.7).

## 11

**Continuous Crystallization***Günter Hofmann and Christian Melches*

The first industrial crystallizers and crystallization processes came up about 150 years ago. The crystallization process became entirely independent of locations (e.g., solar ponds) or stationary energies and all product purities became educible. The further development led to different crystallizers adjusted to the respective crystallization processes and concentrated on the product quality aspect demanded by the market. Applying vacuum technology opened the possibility to choose operation apart from the atmospheric pressure and herewith the opportunity to precisely design the crystallization processes to the respective phase systems and the material properties. Today, these vacuum crystallization processes have become the common standard in the industrial continuous single mass crystallization from solutions.

While the unit operation evaporation, that is, the mass transfer from the liquid phase to the vapor phase, still possesses a direct connection with vacuum techniques, the connection of today's "single mass crystallization from solution" with vacuum techniques is only indirect. The techniques of vacuum cooling and vacuum evaporation are only the mostly used means for inducing the crystallization process. The reason for the dominant position of vacuum crystallization over classical surface cooling crystallization is the considerably reduced inclination to form incrustations. Vacuum crystallization is used in the low vacuum field down to 1 mbar. There are also applications in the overpressure field, although with increasing pressure the number of applications is reduced. In vacuum crystallization, one can find all the classical process control options used in the more familiar vacuum evaporation processes. However, an important difference to evaporation is the fact that the separation process is not concluded with the crystallization step. The suspension formed still has to be separated into crystal mass and mother liquor. Crystallization is therefore always associated with a mechanical separation process. The better this separation, the greater the purity of the crystallized masses.

The separation process is all the more complete, the more compactly the crystals are formed and the coarser they are when they become separated. The degree of separation also depends on the separation technology. Centrifugation is preferred, as the adhering mother liquor is less and washing is also less complicated. As centrifugation with pusher-type or worm/screen centrifuges is possible from a mean crystal size of approximately 0.2 mm, the success and cost effectiveness of the

crystallization substance separation process are also determined by the crystal size obtained and the crystal size distribution (CSD).

These parameters also influence the suitability of storage, freedom from dust, and strewability of the product. For example, ammonium sulfate, which is used as a straight fertilizer, has to be sufficiently coarsely crystallized so that when it is strewn it does not remain on the leaves of the plants. Other crystallized products have to be crystallized as finely as possible in order to positively influence their dissolving behavior. An important difference between vacuum evaporation and vacuum crystallization is the fact that in vacuum crystallization the supersaturated solution tends to induce incrustations on all solid surfaces. The design and layout of a vacuum crystallizer has to be adapted to this, otherwise the cost effectiveness of the process will be jeopardized by the lack of availability. Not all evaporator types can therefore be used in vacuum crystallization. Furthermore, the requirements placed on the granulometry and purity of the crystallized masses are also determined by consumer and market customs, and frequently also by the requirements of the follow-up processes.

All of the necessary design and layout techniques for the planning of crystallizers are derived from crystallization kinetics.

## 11.1

### Concept and Design of Continuous Crystallizers

#### 11.1.1

##### Importance of Secondary Nucleation

Provided that primary nucleation is reliably avoided by working within the metastable zone, the granulometry of the crystallized masses produced depends on the control of secondary nucleation. Secondary nucleation is therefore the most important control factor for the granulometry of crystallization processes.

The smaller the secondary nucleation, the more massive the individual crystal can become. For improved understanding of this process, an example is explained graphically in Figure 11.1. Here the supersaturation is set proportional to the production quantity.

For a produced quantity of 10 g, 10 crystals with a mass of 1 g each are produced from 10 crystal nuclei, while 10 000 crystal nuclei will lead to 10 000 crystals with a mass of only 1 mg each. As the supersaturation level cannot be increased above the metastable zone – otherwise the number of nuclei would increase spontaneously – it takes approximately 20 times longer (see time arrow) to incorporate the production quantity of 10 g in 10 crystals of 1 g each than to create 10 000 crystals of only 1 mg each.

In the case of the uncontrollable spontaneous nucleation with its tremendously higher nuclei production instead of secondary nucleation, the distribution of the production capacity to all of these nuclei will consequently lead to extremely fine crystals, difficult to separate from the impure mother liquor; that is, the targets for granulometry and purity will be entirely missed.



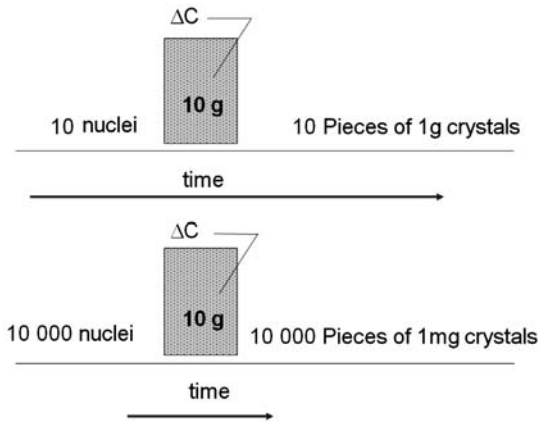


**Figure 11.1** Influence of number of nuclei formed on final particle size.

On this basis, it is possible to deduce the following two principles for the design and layout of crystallizers:

- At no location within a crystallizer may the supersaturation reach or exceed the limit of the metastable zone in order that primary nucleation is avoided and only secondary nucleation can occur during the crystallization process.
- The metastable zone width must, however, be exploited to a large extent in order that the crystal growth rate available is sufficient.

### 11.1.2

#### Control of Supersaturation

These two principles are the most important command variables in mass crystallization from solutions. Crystallizers in which these principles are taken into consideration will certainly function correctly. Building on this, various basic types of crystallizers have been developed with which the entire field of demands placed on grain size distributions and the mean crystal sizes can be fulfilled (Figure 11.2) [1].

Each of these basic types is aligned to a certain particle size range. The forced circulation (FC) crystallizer is used for the smaller particle sizes up to 0.8 mm, the draft tube baffle (DTB) crystallizer for the coarser particles up to 2.5 mm, and the Oslo-type crystallizer for even larger particle sizes. The volume of the crystallizers increases in Figure 11.2 from (c) to (a) reflecting the need to spend more retention time for crystal growth, if coarser crystals have to be produced. In order to allow the crystals become coarser by crystal growth during longer retention times, one has – in parallel – to carefully reduce the effective particle generation rate (secondary nucleation, attrition, and breakage) before the crystal growth can lead to larger particles.

The first to avoid in all these crystallizers is the primary (spontaneous) nucleation as only the secondary nucleation can be used to steer the nucleation rate via the energy input  $\varepsilon^r$  and thereby the particle sizes that shall be produced (see equation for

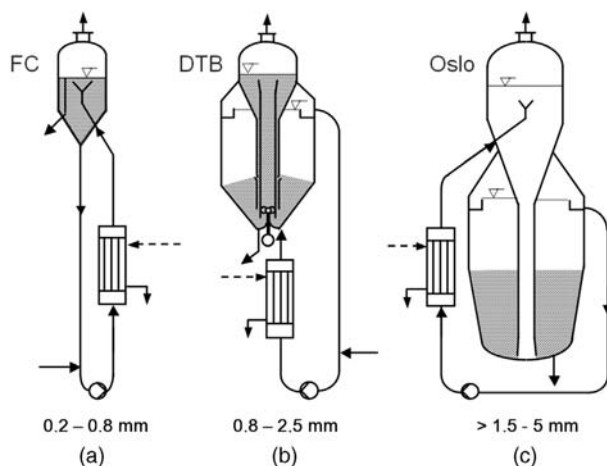


**Figure 11.2** Types of crystallizers: (a) FC crystallizer, (b) DTB crystallizer, and (c) Oslo crystallizer.

$B^0$  in Figure 11.5). Therefore, one aspect that they all have in common is the manner in which the level of supersaturation is controlled and kept within the metastable zone width to ensure the avoidance of the primary nucleation. This method, too, is independent of the respective crystallization process; hence, all of these basic designs can be used for all crystallization processes. How that is realized in the crystallizers exhibited in Figure 11.2 is described below.

Figure 11.3 shows the functional principle of this control method, using *vacuum cooling crystallization* as an example. Figure 11.3a shows a sketch of a FC crystallizer used for vacuum cooling crystallization. This is the simplest form of basic

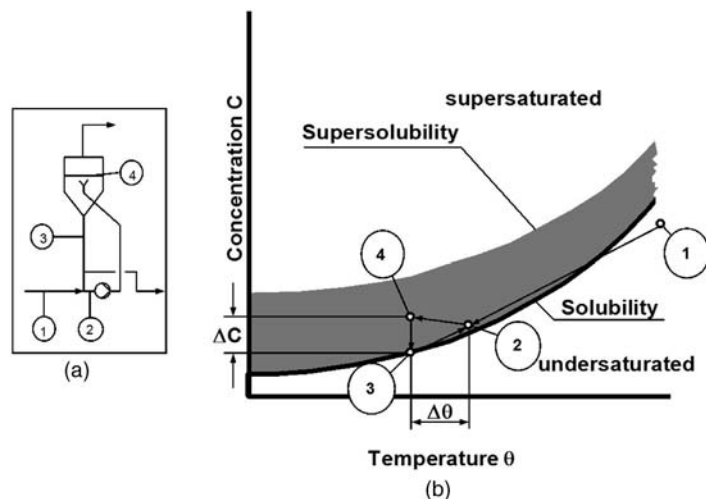


**Figure 11.3** (a) Control of the tip supersaturation. (b) The concentration at different points in the crystallizer is represented in the solubility diagram.

crystallizer design that has an external circulating line (cf. Figure 11.2). Due to the recirculation, the crystallized mass is suspended and the level of supersaturation adjusted at the same time. Figure 11.3b shows a sketch of a solubility system, whose clear temperature dependence is typical of vacuum cooling crystallization. The width of the (assumed) metastable zone is marked here in gray. The processes within the crystallizer in Figure 11.3a are reproduced in the solubility system in Figure 11.3b and the locations and processes allocated to one another in each case by means of figures.

The solution ③ in the crystallizer is mixed with the feed solution ①. In the case of vacuum cooling crystallization, this feed solution is hotter and more concentrated than the mother liquor. Thus, a mixed solution ②, is created that is also hotter and more concentrated. Depending on the position of the mixture line (always straight connection) in the respective solubility system, it is possible – as already indicated – that supersaturation is produced in the solution as a result of the mixing. The mixed solution is then conveyed to the liquor level by the recirculation pump. Above the level of the solution, the desired saturated vapor pressure of the solvent is maintained, which is controlled by means of a condensation device with downstream vacuum pump. When emitted from the central funnel of the recirculation line, the superheated solution now begins to boil ④, as it is superheated with respect to the vapor pressure above the level of the solution. As a consequence, the solution starts to boil adiabatically, dropping its temperature down to the temperature that corresponds to the saturated steam pressure in the vapor chamber. Due to the cooling process and the simultaneous removal of solvent, supersaturation is formed, as shown in the solubility system by the section between points ③ and ④. The supersaturation  $\Delta c$  created is dissipated on the suspended crystals by means of crystal growth, and the next cycle begins when point ③ is reached.

In this example, it is assumed that desupersaturation is complete when point ③ is again reached. For this case, it is clear that the level of the supersaturation produced at the level of the solution depends on the recirculation flow rate. High recirculation flow rates reduce the supersaturation produced there (dilution), while low recirculation flow rates increase it. The recirculation flow rate, adjusted to the production output, is therefore the most important design parameter in industrial crystallizers. Where the production outputs are the same, this parameter is equal for all crystallizer designs. The required recirculation flow rate depends on the metastable zone width. If this is not known, it has to be determined beforehand by means of measurements. In practice, half of the metastable zone width is used for determining the required recirculation flow rate. Therefore,

$$\Delta c = 0.5 \Delta c_{\text{met}}, \quad \frac{dV}{dt} = \frac{dP/dt}{\Delta c},$$

where  $dV/dt$  is the recirculation flow rate in  $\text{m}^3/\text{h}$ ,  $dP/dt$  is the production output in  $\text{kg}/\text{h}$ , and  $\Delta c_{\text{met}}$  is the metastable zone width in  $\text{kg}/\text{m}^3$  or  $\text{g}/\text{l}$ . As a result, the performance of the crystallizer laid out in this way is restricted to  $dP/dt$  if primary nucleation is to be excluded. As the metastable zone widths usually have a spread of just a few  $\text{g}/\text{l}$ , large recirculation flow rates are necessary. The recirculation flow rate

for a permitted supersaturation of maximum 1 g/l is already 1000 m<sup>3</sup>/h for only 1 t/h crystal production rate. These high recirculation rates are best achieved by axial flow pumps.

For the purpose of simplification, the assumption has been made in Figure 11.3 that the time for a recirculation process is sufficient to reduce the supersaturation down to negligible levels. This reduction in supersaturation is, however, a function of the mean mass deposition rate *and* the growing crystal surface area present [2]:

$$\frac{dm}{dt} = k_g A \Delta c^g \propto -\frac{d(\Delta c)}{dt}.$$

Here  $dm/dt$  denotes the mean mass deposition rate,  $A$  is the surface of the suspended crystals,  $\Delta c$  is the supersaturation, and  $k_g$  is the proportionality constant. From this relationship, it is evident that the desupersaturation rate  $-d(\Delta c)/dt$  depends on the crystal surface available. Where the crystal growth rate is slow or the crystal surface available is small, it is possible that the time for a recirculation cycle is not sufficient to allow negligible supersaturation to occur before the new supersaturation is produced. This is shown in Figure 11.4. The selected example is again vacuum cooling crystallization. After the creation of supersaturation ① at the level of the solution, the supersaturation is degraded on the crystals that have been carried along. Through the cyclical sequence of the generation of supersaturation and desupersaturation (as a result of crystal growth), the sawtooth curve shown, which is typical of this process, is created.

The smaller the active crystal surface available, the slower the mass deposition rate  $dm/dt$ , and the larger the supersaturation remaining after each recirculation cycle. The point ④, in Figures 11.3 and 11.4 moves up, if crystal growth does not desupersaturate to  $\Delta c \rightarrow 0$ . As this residual supersaturation is added to the newly created supersaturation, it is certainly possible that the metastable zone width will be

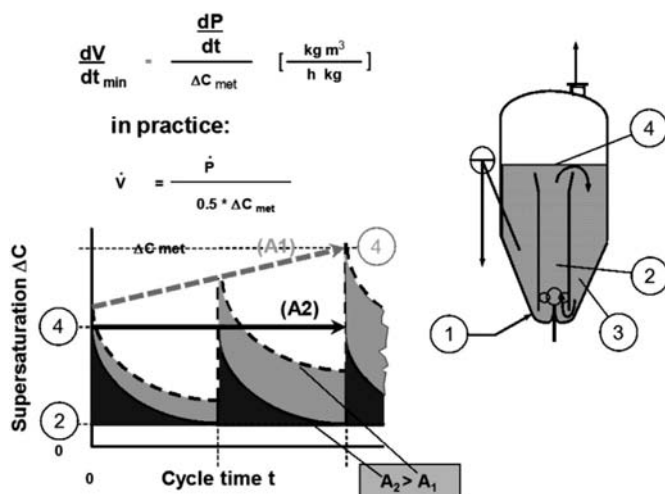


Figure 11.4 Desupersaturation as a function of crystal surface area.

exceeded and primary nucleation will occur. In addition to the “correct” recirculation flow rate, when the crystallizer is being designed attention must also be paid to the sufficient availability of crystal surface (function of suspension density), in order that primary nucleation can be reliably prevented.

This is mainly of importance where the mass balance resulting from the crystallization process would produce values that were too low for the suspension density. In this case, special measures have to be taken, as explained below. In general, suspension densities of between 15 and 25% by mass are sufficient in order to achieve an adequate desupersaturation rate.

With these measures and specifications relating to the level of supersaturation and suspended crystallized mass, it is generally possible to obtain sufficiently granular (coarse enough) crystallized masses, so that separation with centrifuges can be performed.

### 11.1.3

#### Adjustment of the Granulometry – Mean Crystal Size and Crystal Size Distribution

At this point, however, after having avoided the formation of spontaneous nucleation in these types of crystallizers, the question arises as to which measures remain in order to design the crystallizers for producing coarser crystals. The solution is clearly shown in the two kinetic relationships for crystal growth rate  $dm/dt$  and secondary nucleation rate  $B^0$ , which describe the crystallization process, though the specifications described above mean that the majority of the variables are now fixed by agreement. These fixed variables are circled in Figure 11.5. The remaining means available for controlling the granulometry are the proportionality constant  $k_g$  and the specific energy input  $\varepsilon$ .

As described in this book, secondary nucleation is a function of the mechanical energy input  $\varepsilon^r$  (see also Figure 11.5). This is introduced by the circulation pump.

$$\frac{dm}{dt} = \textcircled{k_g} * A * \Delta C^m = - \frac{d(\Delta C)}{dt}$$

$$B_0 = k_N * \textcircled{\varepsilon^r} * m_T^l * \Delta C^n$$

$$\Delta C = 0.4 - 0.6 \Delta C_{\text{met}}$$

$$m_T = 10 - 30 \text{ wt\% crystals in suspension}$$

$$k_G = f(T, \dots) \quad \text{Target: } T \text{ high}$$

$$\varepsilon^r = \text{specific energy input}$$

$$T = \text{crystallization temperature}$$

Figure 11.5 Importance of energy input.

The blades of the impeller pass this on to the suspension in the form of kinetic energy, whereby the acceleration process causes direct collisions between the blades of the impeller and the suspended crystals. The strength of these collisions increases with the increasing mass of the individual crystal, with the increasing difference in the specific densities of the crystal and mother liquor (mass inertia effect), and with the tip speed (circumferential velocity) of the impeller (see Section 11.1.4), while the quantity of collisions increases with the suspension density  $m_T$ .

In addition to the direct collisions of the crystals with the rotor blades, there are also consequential collisions between the crystals and the walls of the crystallizer or its components, or even collisions between the crystals themselves. The energies involved in these collisions are lower and the resulting secondary nucleation of secondary importance; however, they are also a function of the energy input via the circulation pump. The relationship of these attrition mechanisms to one another may be imagined as

$$\frac{\text{Crystal}}{\text{Crystal}} \bigg/ \frac{\text{Crystal}}{\text{Wall}} \bigg/ \frac{\text{Crystal}}{\text{Impeller}} = 1/10/1000.$$

The largest source of attrition and nucleation is the collisions between the suspended particles and the blades of the circulation pump.

The less energy that has to be expended for the recirculation process, the fewer crystal nuclei will be produced. The nucleation frequency is therefore the key to producing different crystal sizes (compare Figure 11.1). The designs of crystallizers also differ from one another mainly with respect to the specific amount of energy  $\varepsilon$ , which has to be expended for the recirculation process. For the different types of crystallizers, these specific energy inputs vary from around 10 W/kg for the FC types down to 0.1–1 W/kg for the DTB types and to below 0.1 W/kg for the fluidized bed crystallizers.

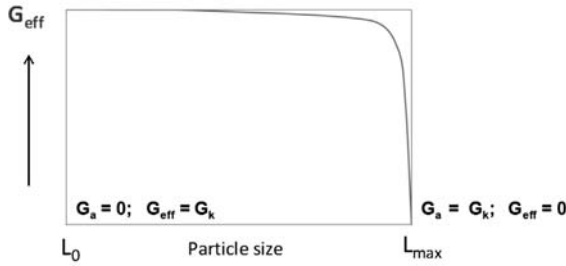
The crystal retention time  $\tau$  also has an influence on the crystal size. Of course, longer crystal retention times will be required, if coarser crystals are to be obtained. The population balance consequently defines a linear relation between the mean particle size  $L_{50}$  and the average retention time  $\tau$  (Figure 11.6).

However, in crystallizers that are used in everyday situations exactly the opposite may occur [3,4], as illustrated in Figure 11.6. The reason for this is the so-called attrition rate  $G_a$ , which counteracts the kinetic crystal growth rate  $G_k$ . While  $G_k$  depends exclusively on the supersaturation  $\Delta c$ ,  $G_a$  is a function of the crystal size  $L$ . From this follows an effective crystal growth rate  $G_{\text{eff}}$ , resulting from the difference between  $G_k$  and  $G_a$ ; for example, for the crystal size  $L$  the attrition rate  $G_a$  becomes equal to  $G_k$  and  $G_{\text{eff}}$  becomes zero, instead of the ideal kinetic crystal growth rate  $G_k$ . Longer retention times can therefore certainly result in smaller crystals – other than expected.

In fact, reality shows that the increase of the average retention time  $\tau$  leads to different results in the basic types of crystallizers. The dotted lines in Figure 11.7 show the typical deviation from the linear dependence of growth on the average retention time in DTB and FC crystallizers. Only products from the Oslo-type crystallizer with its suspension not in contact with the impeller pump follow the

**Attrition:**

$$G_{\text{eff}}(L, \Delta C) = G_k(\Delta C) - G_a(L)$$

**Retention time  $\tau$ :**

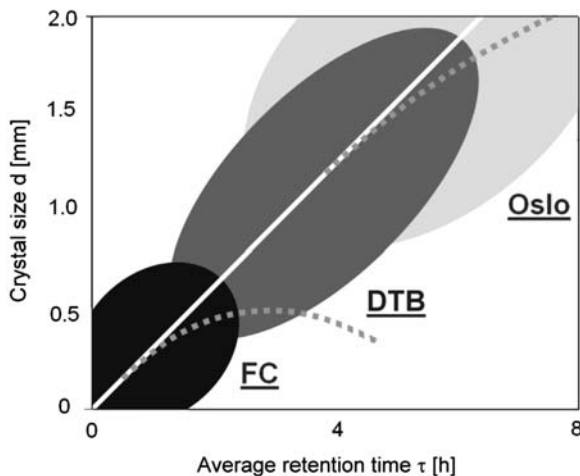
$$G_k \text{ or } \frac{dL}{dt} = \frac{1}{\rho} \cdot \frac{\beta}{3\alpha} \cdot \frac{1}{A} \cdot \frac{dm}{dt}$$

$$L_{50} = 3 G_k \tau \text{ (Population balance)}$$

**Figure 11.6** Retention time and attrition.

ideal function – at least for particle sizes of industrial interest. The improved results from the DTB and Oslo crystallizers are the consequences of measures taken to minimize secondary nucleation and attrition in these types.

Whereas the FC-type crystallizer is designed to safely avoid spontaneous nucleation only, additional measures and tools are integrated in the larger DTB and Oslo crystallizers to make their retention time longer leading to coarser crystals.

**Figure 11.7** Dependence of crystal size  $d$  on the average retention time in nonideal crystallizers [4].

## 11.1.4

**Energy Input and Retention Time**

In the growth types of crystallizers, DTB and Oslo-type, these interrelationships have all been taken into account. In the designs intended to produce coarser granularity via the longer retention times, these measures are taken in order to keep the energy input into the suspension smaller than that in the FC crystallizer with its short retention time. For this reason, the crystallizer designs differ from one another mainly with respect to the layout and location of the circulation pumps (whether these are inserted in the suspension or in clarified solution; cf. Figure 11.2).

In summary, crystals increase

- with a lower specific input of energy – that is, a lower mechanical load on the crystallized mass and low secondary nucleation rate;
- with an increase in the crystal retention time.

A further influencing factor is the level at which this energy is applied. Pumps with small impellers have to be operated at faster rates, that is, higher tip speeds of the impeller, in order to achieve the same recirculation rate as pumps with large impellers. The resulting higher tip speeds of the smaller impellers result in higher energy collisions, with the increased production of secondary nuclei, than is the case with the large pumps with lower tip speeds. This influences the selection of the circulation pumps in the following way:

For the power consumption  $N$  of a circulation pump – and therefore for the specific energy input  $\varepsilon$  (specific with respect to the suspension volume) – the following applies:

$$\frac{dN}{dt} = \frac{(dV/dt)\rho g H}{\eta},$$

$$\varepsilon = \frac{(dV/dt)\rho g H}{\eta} \frac{1}{V_{\text{cryst}Q}}.$$

Here  $\rho$  represents the specific density of the suspension or solution,  $g$  denotes the gravitational acceleration,  $H$  is the delivery head,  $\eta$  is the efficiency of the pump, and  $V_{\text{cryst}Q}$  is the filling volume of the crystallizer. As in all crystallizer designs the recirculation flow rate  $dV/dt$  is responsible for controlling the level of supersaturation, it can be directly seen from the equation that the specific energy input – without changing the recirculation flow rate – can be reduced by lowering the level of the system resistance  $H$ . This has been implemented, for example, in the DTB crystallizer (cf. Figure 11.2), where the heat exchanger – the main cause of a loss of pressure during recirculation of the suspension – has been transferred to an external circuit. As a consequence of this measure, the specific energy input to the inside recirculation – controlling the tip supersaturation – is lower. Due to the lower level of secondary nucleation, coarser crystals can be obtained because the frequency of nucleation and attrition are reduced.



Furthermore, the diameter of the circulation pump plays a role. As the pressure drop in the system is now lower, a pump with a larger impeller that rotates more slowly can be used. According to the equation for the power consumption  $N$ , there is a connection between the impeller diameter  $D$  and the impeller speed  $n$ :

$$\varepsilon \sim n^3 D^5 \frac{1}{V_{\text{crystQ}}}.$$

From this it can be deduced that when the rotating speed is reduced, that is, the tip speed is lowered, and there is a simultaneous increase in the size of the pump impeller, the energy of the collisions with the crystals also decreases. Consequently, the secondary nucleation frequency is lower and the mean crystal size increases.

Pumps with larger impeller diameters (i.e., lower tip speeds and therefore lower nucleation rate) are used in DTB crystallizers in order to produce coarser crystallized masses.

If crystallization is only used for separating substances, it is sufficient to create crystallized masses that can be readily separated. In such cases, a normal elbow-type circulation pump can be used, as is the case in the forced circulation crystallizers (Figure 11.2a). If coarser crystals are to be produced, a circulation pump that rotates more slowly will have to be used and the pressure drop of the system reduced. This is the case in the so-called DTB crystallizers (Figure 11.2b) that are equipped with an internal draft tube propeller pump. It is not unusual for these pumps to have a diameter of  $>1$  m up to about 2.5 m, with significantly lower tip speeds in comparison to the external pumps in the FC crystallizers (approximately 8–12 m/s instead of 16–20 m/s). In the case of evaporative crystallization, this crystallizer design offers the above-mentioned advantage that the system resistance  $H$  for the internal circulation pump is reduced and therefore the required specific energy input is considerably lower. Fewer nuclei are produced and the crystals become coarser.

DTB crystallizers also have an external recirculation loop that is necessary, for example, to introduce heat into the system by means of a heat exchanger. As a rule, the resulting heating of the recirculated solution leads to a high level of under-saturation for the crystallized substance. However, as the external recirculation loop in this DTB crystallizer is operated with solution clarified by sedimentation, this has a considerable influence on the crystallization process in this type of crystallizer.

This external recirculation loop is operated with a solution that has been clarified, that is, from which crystals have been removed. This is performed in order to prevent secondary nucleation in the external recirculation loop, which now has the higher resistance level due to the heat exchanger used there. If no crystals are suspended in this external loop, it is not possible for the circulation pump used there to produce secondary nuclei. However, the statement that this solution is free of crystals is only partially correct. In fact, in the clarification zone of a DTB crystallizer, the main mass of the crystals has indeed been separated out of the solution by sedimentation, but the finer crystals (fines) and the crystal nuclei with settling rates greater than upstream velocities are not separated out. The sum total of these

particles is entirely negligible with respect to mass, but not with respect to numbers. The particles are too small, however, to be able to produce any secondary nuclei.

As a result of being heated up in the heat exchanger, the solution becomes undersaturated in most of the cases and these particles dissolve. This process is referred to as “fines dissolving.” Such fines dissolving is equivalent to a corresponding reduction in nucleation frequency. The crystallized mass becomes coarser. In DTB crystallizers, it is therefore possible without any further measure to obtain medium crystal sizes of up to 2.5 mm – and larger. The minority of substances with inverse solubilities, such as the monohydrates of some transition element sulfates, cannot take advantage of such fines dissolving due to the missing undersaturation possibility. Contrary to fines dissolving, there is even the danger to form supersaturation on the heater surface with the consequence of scaling. Those substances are difficult to be produced as granular qualities by crystallization at all.

Such kind of restriction is also given in the case of missing density differences between the solids and the mother liquor, that is, in cases where sedimentation cannot be used to produce clarified solutions for the fines dissolving loop, or if high viscosities are hindering the sedimentation.

DTB and fluidized bed crystallizers are usually operated with fines dissolving. The strong effect of fines dissolving on the mean crystal size that can be achieved is demonstrated in Figure 11.8 with the example of the DTB crystallizer for the production of potassium chloride. In this example, the clear liquor overflow of the crystallizer amounts to  $500 \text{ m}^3/\text{h}$  and still contains  $0.3 \text{ g/l}$  of fines. If it is assumed that all of these crystals were to have a particle size of  $0.1 \text{ mm}$ , the  $500 \text{ m}^3/\text{h}$  overflow would contain  $10^{11}$  crystal particles. During the same period, the crystallizer creates product crystals at a rate of  $10\,000 \text{ kg/h}$  with a mean crystal size of  $1.25 \text{ mm}$ . Again assuming that all product crystals are of the same size, the product stream contains far fewer crystals than the clear liquor overflow:  $5 \times 10^9$ . This shows very clearly the influence that fines removal has on the mean crystal size.

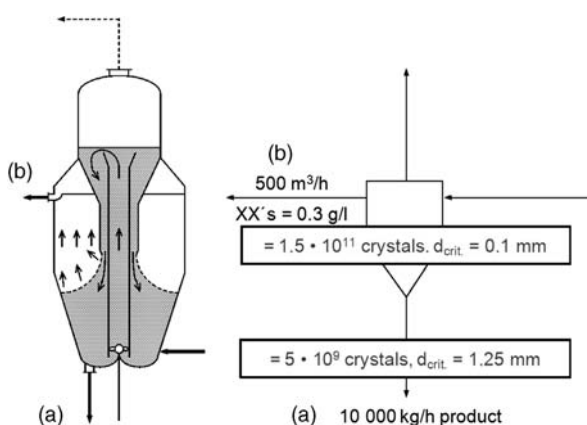


**Figure 11.8** Effect of the fines removal (fines dissolving).

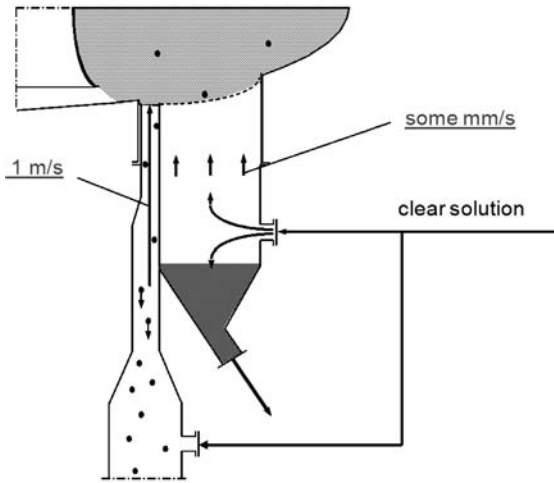


**Figure 11.9** Classified product removal via elutriation leg.

One disadvantage of fines removal is the associated deterioration in the uniformity (cf. Figures 11.22–11.23) of crystal size distribution (see Section 11.2.5). For this reason, DTB and Oslo crystallizers (synonyms for fluidized bed crystallizers) very often incorporate elutriation legs, with which the product can be classified while being removed. For this there are special construction designs available with which incrustation fragments can also be captured separately, which as a result cannot enter the product path (Figure 11.9).

FC and DTB crystallizers belong to the group of suspension crystallizers. In this design category, a suspension is recirculated. If mean crystal sizes  $>2.5$  mm are to be obtained, the circulation pump must not be used in the suspension anymore. This is the case in the fluidized bed crystallizers. In this design category, only clarified solution is recirculated (Figure 11.2c). With the recirculated solution, the crystals are protectively held in suspension as a fluidized bed in part of the crystallizer specifically designed for this purpose – the suspension vessel. The mean crystal sizes can thus reach several millimeters in this design category.

#### 11.1.5

##### **Which Type of Crystallizer to Select?**

Among all these crystallizers that crystallizer has to be selected that is the most economical for achieving the requested average particle size. As a summary from the above, the available crystallizers can be subdivided into three main classes with different potentials in regard to particle sizes:

- FC crystallizers: 0.2–0.8 mm.
- DTB crystallizers: 0.8–2.5 mm.
- Oslo crystallizers: 1.5–5 mm.

All these crystallizers are equipped with a forced circulation loop that serves to keep the supersaturation within the metastable zone, that is, serves to avoid spontaneous nucleation.

For the production of coarser particles, additional effects have to be used. These are as follows:

- i) Reduction of the impeller pump tip speed to the minimum level hydraulically possible (FC and DTB).
- ii) Reduction of the specific energy input to the suspension via the impeller pump to the minimum, for example, by separating the tasks: control of the tip supersaturation internally and heat input to a clarified solution (mostly free of crystals) externally, which requires already a bigger crystallizer volume (DTB), that is, extended retention time, strongly reduced energy input to the suspension, elevated fines dissolving, and possibility to remove suspension classified.
- iii) Elimination of the strongest energy input source (that to suspension in direct contact with the impeller pump) by keeping the suspension concentrated in a fluidized bed and recirculating only clarified solution for the control of the heat input and the control of the tip supersaturation; requiring the biggest volume of all due to the entire clarification of the recirculation rate needed to control the tip supersaturation (Oslo-type), that is, longest retention time, minimum energy input, maximum fines dissolving, and classified product removal.

After the preselection of the crystallizer type according to its performance potential, additional measures, in particular the impeller tip speed, classification, and fines dissolving, are the adjustment tools needed to set the selected crystallizer operation to the given crystal size target.

Due to their easier operation and their more compact design, the suspension-type crystallizers are selected wherever possible: the FC crystallizers for all applications with moderate claims toward particle sizes (90% of all crystallizers worldwide are of FC-type) and the DTB crystallizers for all applications up to a  $d'$  (RRSB distribution) of 2.5 mm (about 8%). The rest of the applications above the  $d'$  of 2.5 mm use the Oslo-type crystallizer (about 2%).

Whereas the fines dissolving is a strong tool to correct the effects of secondary nucleation, attrition, and breakage toward larger particle diameters, it also has one negative effect on the steady-state operation of the DTB and Oslo crystallizers: most of the time it is too strong. Unfortunately, its intensity is difficult to control.

#### 11.1.6

##### Seeding of DTB and Oslo Crystallizers

Additional measures are required to continuously produce these coarse crystallized masses [5]. This applies to both basic types of coarse grain crystallizers, the DTB and the fluidized bed crystallizer. It is indeed observed that in the case of coarse grain crystallizers with fines dissolving the mean crystal size of the discharged product can become subject to cyclical fluctuations beyond an average crystal size of about 2 mm. This results from the fact that the effective nucleation  $B_{\text{eff}}$ , which is the sum total of

the secondary nucleation frequency  $B^0$  and the opposing dissolution of fine crystals  $B_{FA}$ , is too low or even negative:

$$B_{\text{eff}} = B^0 - B_{FA}.$$

In DTB and Oslo-type crystallizers, the dissolution of fine crystals  $B_{FA}$  is large compared to the low level of secondary nucleation  $B^0$ .  $B_{\text{eff}}$  is very small as a result, as almost all nuclei fall victim to the dissolution of fine crystals in the outer loop. As a consequence, the crystallizer contains increasingly fewer crystals, which become increasingly coarse, until with increasing crystal size the amount of suspended crystal surface available is too low to degrade the supersaturation during each recirculation cycle. The ascending supersaturation finally penetrates the metastable zone width. Primary nucleation occurs and the entire process begins again. A typical sawtooth curve is produced for the coarse grain fractions obtained [5]. Figure 11.10 shows ammonium sulfate crystals produced by such cyclical behavior from large-scale production. The increase in the crystal size can be clearly seen, as can the sudden occurrence of a second finer number fraction that has been created by primary nucleation.

This behavior of the coarse grain crystallizers is undesirable because the sales returns for the coarse crystallized masses often exceed by a multiple the yields for finally crystallized masses at the fines end of such a cyclical fluctuation. Through

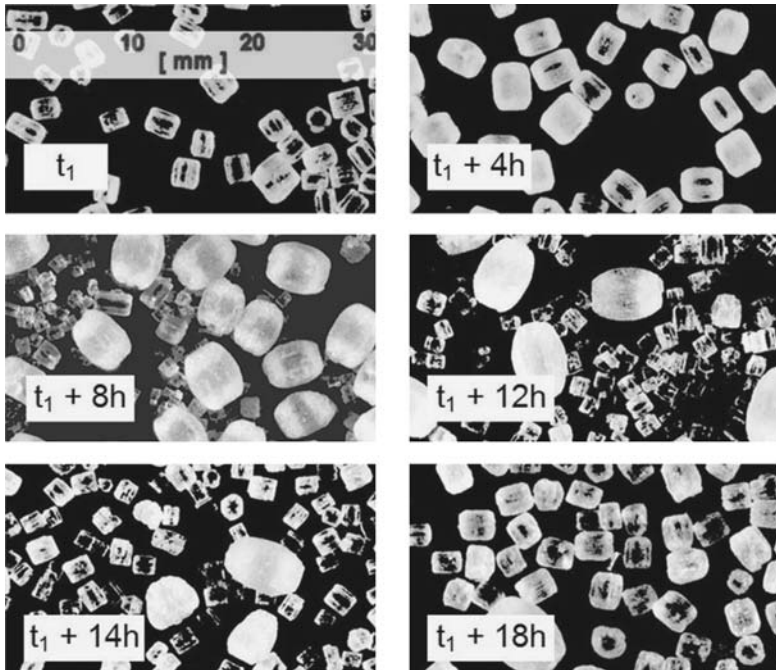


**Figure 11.10** Unseeded DTB – granular ammonium sulfate. One cycle from fine to granular and back to fine is shown.

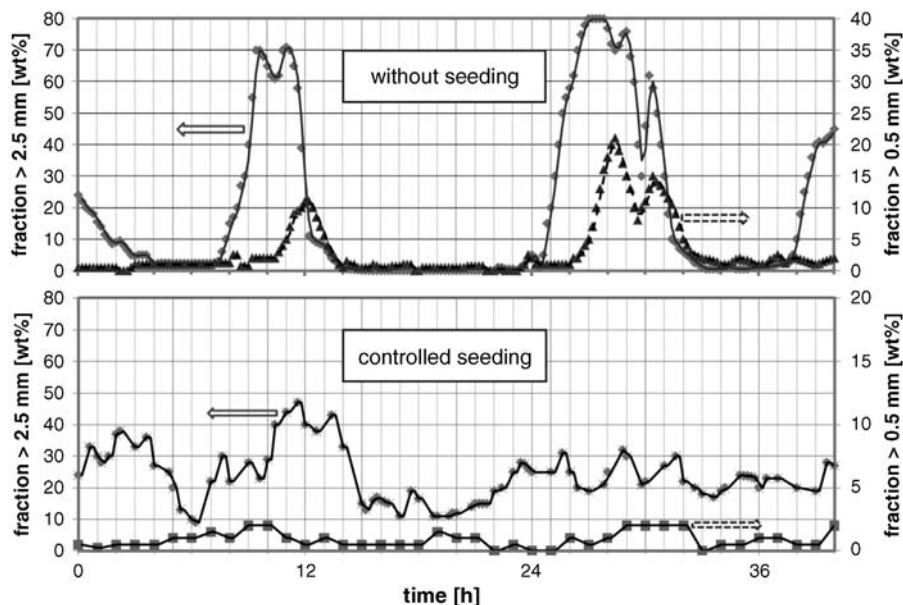


**Figure 11.11** Effect of seeding (DTB – granular ammonium sulfate).

measured controlled introduction of finer crystals (seeding), it is possible to stop the fluctuation in the mean grain size (Figure 11.11). However, these seed crystals have to be large enough to ensure that they cannot enter the external recirculation process (settling rate > upstream velocity). These are usually seed particles with mean crystal sizes >1 mm. The introduction of the seed crystals is performed as a rule using the concentration of a certain fine fraction of the suspended crystallized mass, which is kept constant as a result of the seeding.

## 11.2

### Various Continuous Crystallizers

Within every model category there are various designs, which are adapted to the specific individual applications.

#### 11.2.1

##### FC Group

Figure 11.12 shows the different designs of the simple FC group; depending on the crystallization process such FC crystallizers can be used for (vacuum cooling crystallization or vacuum evaporative crystallization), one can find the typical FC ④, and ⑤ with and without a tube and shell heat exchanger. These are the simple stirred tank ①, the draft tube (DT) crystallizer ②, and the FC crystallizer (④, ⑤).

The suspension is recirculated by stirrers or circulation pumps and the supersaturation created within the suspension. The stirred tank ① is suitable for vacuum cooling crystallization. The disadvantage of this design is the absence of directed flow recirculation, as only a simple, but inexpensive stirrer is used. This means that the maximum supersaturation is not fully under control, which is why this design should only be used for systems with large metastable zones.

The draft tube crystallizer ② (the difference of the DTB crystallizer to the DT crystallizer is the baffle for the clear liquor overflow to the external recirculation) is equipped with a draft tube propeller pump instead of a stirrer. This provides full control of the maximum supersaturation. This design is used in vacuum cooling crystallization for larger production outputs. Also, the so-called horizontal crystallizer ③ is used exclusively for vacuum cooling crystallization. It features several crystallizer stages that are connected in series in a single vacuum vessel in order to save space and costs. Such multistage vacuum cooling crystallization is found in applications in which the vapors are colder than the condensation possibilities allow and which for this reason initially have to be raised to a sufficiently high temperature and pressure level by means of vapor recompression (thermocompression). The more cooling stages can be carried out, the less energy is required to compress the vapors to the respective condensation conditions (Figure 11.12). (The worst-case scenario with the highest consumption of steam is the single-stage design, in which the entire quantity of vapors has to be increased in temperature and pressure to the condensation level by means of thermocompression.)

The disadvantage of this design is the unfavorable geometry of the chambers for the suspension process. Sedimentation is unavoidable over the long term, which results in incrustations. The maximum realizable operation periods are approximately 1 week. Its use is therefore limited today to companies where production stops running at weekends. If longer operating times are planned, a few draft tube crystallizers are connected in sequence today instead of the horizontal crystallizer and if necessary the condensation carried out on cooling brines, which are recooled using ammonia cooling units.

Use of the FC crystallizer ④ is preferred for evaporative crystallization. The directed and controlled recirculation is carried out with an axial flow pump (elbow-type). This design can also be used for vacuum cooling crystallization, so that then the heat exchanger is no longer required (⑤). The use of this version is recommended if due to the lack of barometric cover in the draft tube crystallizer the incoming solution would boil out of the feed-in point.

In these simple crystallizers, the crystal content of the suspension can be determined directly from the mass balance. Higher suspension densities can only be adjusted if parallel to the suspension discharge clear liquor is also removed. This is necessary when the mass balance shows suspension densities (crystal surface area) that are not sufficient for the desupersaturation (Figure 11.25). In this case, it is possible to install clarification surfaces even in these simple crystallizers. If this is carried out with the draft tube crystallizer, the result is a typical crystallizer of the DTB group as already pointed out above.

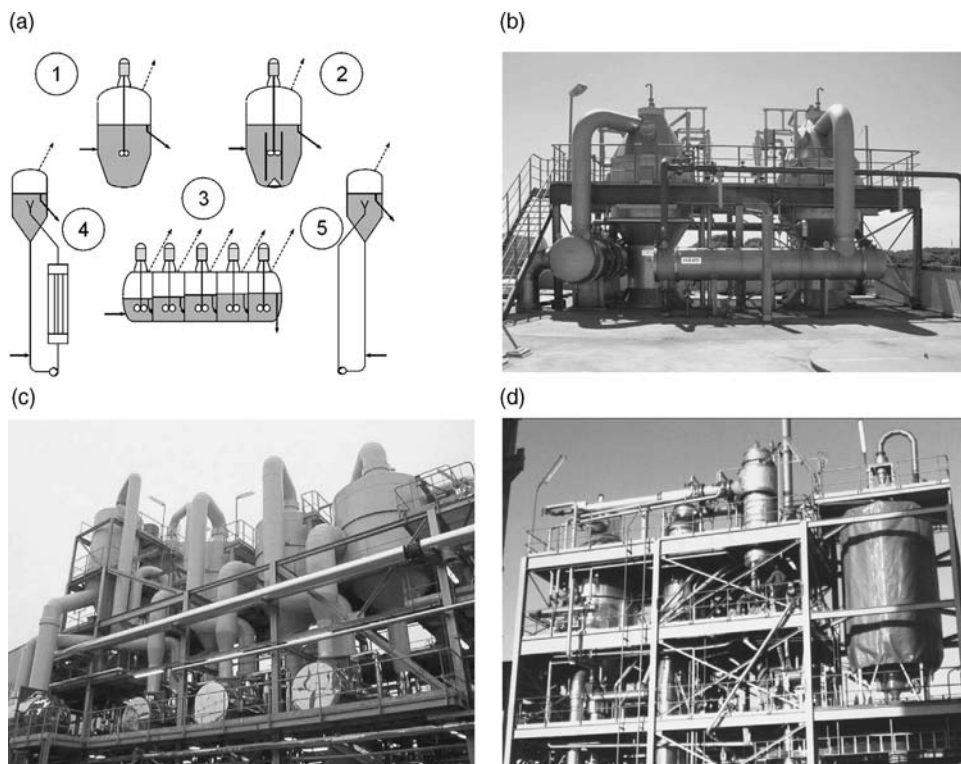


**Figure 11.12** (a) Group of FC crystallizers. (b) FC crystallizers in the food industries. (c) FC crystallizers in vinasse concentration ( $K_2SO_4$  crystallization). (d) FC crystallizers (vacuum evaporation) for  $Na_2SO_4$ .

### 11.2.2

#### DTB Group

The DTB crystallizers (Figure 11.13), whose eponymous representative has already been introduced, show three different representatives. In the subcategory DP crystallizer [6], the propeller of the circulation pump is divided into two sections. The section located within the draft tube creates an upstream, while the section found outside the draft tube, which is bordered by the partition of the clarification section, creates a downstream. The external and internal sections are adapted to one another and ideally produce exactly the same degree of recirculation. In this manner, it is possible to use very low tip speeds for the desired recirculation flow rate.

In the Messo turbulence crystallizer, a secondary circulation loop (see vortex) – driven by the primary circulation loop – is created in the outer suspension section. This secondary circulation loop serves the purpose of sorting out the coarser crystals from the inner draft tube recirculation process, concentrating them in an outer



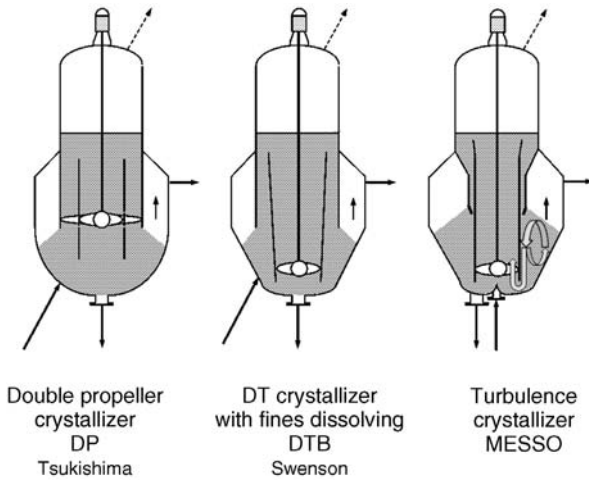


**Figure 11.13** DTB group crystallizers.

vortex and thereby removing these coarser crystals from the influence of the circulation pump for the purpose of further growth. In this way, the product crystals can be preclassified. With all DTB crystallizers, this classification during removal, which serves the purpose of improving the uniformity of the particle size distribution, can be achieved by adding an elutriation leg. Typical products that are produced by means of this category of crystallizers are ammonium sulfate and potassium chloride, which must be readily strewable as compound fertilizers or which are added as already coarse particles to mixed fertilizers.

Figures 11.14 and 11.15 show DTB crystallizers in two plants for the crystallization of potash fertilizers.

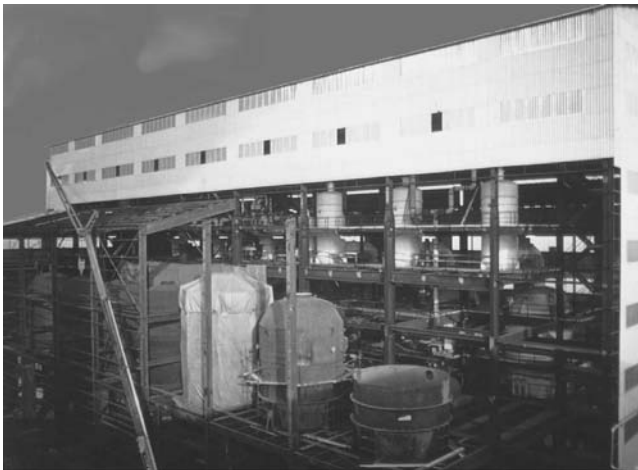


**Figure 11.14** DTB crystallizers in the potash industries (vacuum cooling crystallization).



**Figure 11.15** Plant with DTB crystallizer in the fertilizer industries.

### 11.2.3

#### Group of Fluidized Bed Crystallizers

The best-known representative of the group of fluidized bed crystallizers is the “Oslo crystallizer” [7]. Today, there are two known versions (Figure 11.16). The original design was developed in the 1920s by a firm called Krystal A/S in Oslo, which explains the name. This design is susceptible to malfunctions in the case of products that tend to produce incrustations, as falling crusts can block the annular gap at the entrance to the fluidized bed. In the case of the crystallization of sodium chloride,

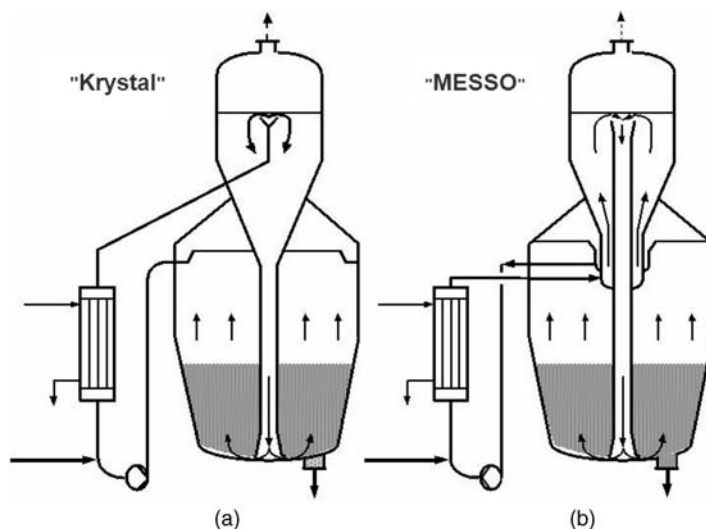


**Figure 11.16** Fluidized bed crystallizers of (a) Krystal and (b) Messo types.



**Figure 11.17** Fluidized bed crystallizer for chromic acid (made up of titanium).

the incrustations in the evaporation chamber of the “Krystal” crystallizer become so thick after just 3 days that they fall down and block this annular gap. The fluidized bed collapses and the blockage can only be removed by thorough cleaning that takes several days without any production at all.

The more modern design (“Messo”) has been specially designed to overcome this problem [8]. By reversing the direction of flow in the inflow area of the evaporation section, in this modified design the solution that has been superheated by the heat exchanger and is therefore undersaturated is passed over the conical surface that was previously susceptible to incrustations, before the supersaturation is created by means of the boiling process. As a result, no incrustations can form on the conical surface and the possibility of malfunctions is excluded. In this manner, it is possible to achieve operation periods of several weeks.

Figures 11.17 and 11.18 show fluidized bed crystallizers for the crystallization of chromic acid and sodium sulfate.

#### 11.2.4

##### Comments on Population Balance and Modeling

While the population balance [9] forms the basis for the design and control of crystal sizes and crystal size distributions in continuous crystallizers, there is hardly any direct application in practice. The main reason for this is the poor transferability of the measured (apparatus-specific) proportionality constant  $k_r$  (from  $B^0 = k_r M^j G^i$ ) in the following equation, presented here for the simple MSMPR [10], to the large-scale plant that is to be planned:

$$P_c = 2k_v \rho G^{i-1} k_r M^j L_D^4 / 27.$$

Case I: MSMPR,  $j = 1$ ,  $i > 1$ ,  $P_c \equiv M$ ;  $L_D = [27 / (2k_v k_r \rho G^{i-1})]$ .

Case II: MSMPR,  $j = 1$ ,  $i = 1$ ,  $P_c \equiv M$ ;  $L_D = [27 / (2k_v k_r \rho)]$ .

Case III: MSMPR,  $j \neq 1$ ,  $i \neq 1$ ,  $P_c \equiv M$ ;  $L_D = [27 M^{i-1} / (2k_v k_r \rho G^{i-1})]$ .



**Figure 11.18** Fluidized bed crystallizer (12 m diameter) for granular sodium sulfate.

In the equations, according to Larson and Garside [10],  $j$  denotes the exponent for the suspension density  $M$ ,  $i$  is the quotient of the exponents  $m$  (for the supersaturation  $s$  at the nucleation rate  $B^0$ ) and  $n$  (for the supersaturation  $s$  at the crystal growth rate  $G$ ),  $L_D$  is the dominant particle size of the population balance,  $k_v$  is the volume shape factor for the crystallized mass produced, and  $k_r$  is the quotient of the proportionality constants  $k_N$  of the secondary nucleation rate  $B^0$  and  $k_g^{m/n}$  of the crystal growth rate  $G$ .

All three characteristic variables  $i$ ,  $j$ , and  $k_r$  depend on the specific solubility system with its various and changing impurities (this refers to additives at the lowest concentrations).

While in the ideal world the exponents  $i$  and  $j$  are not functions of the temperature or the stirring/recirculation (i.e., energy input), the speed constant  $k_r$  is dependent on them. In  $k_r$ , there are therefore apparatus-specific properties such as size, energy input, levels of efficiency, and so on, which change significantly within the framework of the scale-up and cannot be transferred on a one-to-one basis.

Furthermore, the MSMPR approach

$$\ln n/n_0 = -L/G\tau$$

only applies strictly to an ideal crystallizer (stirred tank reactor) with homogeneously distributed supersaturation, without crystal breakage, attrition, and agglomeration, and only for the case of isokinetic suspension withdrawal. Although these are frequently equated with FC crystallizers without the dissolution of fine crystals and

without classification, the approach and reality differ considerably here and make the respective population balance more complicated.

Both the merely specific validity of the measurement results from pilot trials and the deviations from reality of an MSMR from the FC concept lead to an unsatisfactory correlation of the results between trials and large-scale plants that are not better than the current fact that at least the mean crystal size produced in the laboratory in a small glass reactor from original solution can reliably be obtained in the large-scale FC crystallizers without the need for further measures.

An even greater problem is the quantitative application of the population balance in the coarse grain crystallizers of DTB and fluidized bed design, which due to the cyclical behavior described above are almost impossible to describe with the MSCPR (mixed suspension classified product removal) and CSCPR (classified suspension classified product removal) approaches.

The effort involved is therefore disproportionate to the benefits achieved [11] and for the plant constructors is anyway outside the time horizon available to them when designing the crystallizers.

For the plant constructors, the benefit of the population balance is mainly derived from the transparency of the interplay of the kinetic variables of nucleation rate and crystal growth rate, the mean retention time, the fines dissolving, and the classification of product crystals during withdrawal with respect to the resulting mean particle size of the crystallization process. Here, reference is made to the publications, such as that of Toyokura and Sakai [12].

### 11.2.5

#### **Manipulation of Crystal Size Distributions**

Due to the difficulty of transferring the results of measurements of the population balance to the large-scale installation, in the field of crystallization plant construction it has so far not been reasonable to carry out any simulation of crystallization results (crystal size, crystal size distribution) for industrial-scale planning. On the other hand, it is certainly possible to imagine simulations of the operational behavior of large-scale crystallizers for overload or partial load conditions on the basis of the population balance.

The fact that the population balance is clearly able to determine the influences on particle size distribution is shown, for example, by the effects produced by the fines dissolution and the classification of product during withdrawal.

The use of fines dissolution, as shown in Figures 11.19 and 11.20, results according to the population balance in an increase in the share of coarse crystals in the crystallized mass, while the uniformity of the crystallized mass produced deteriorates in the process (Figure 11.19a and line (1) in Figure 11.20). DTB crystallizers with fine crystal dissolution, but without classification, precisely display this effect. As a rule, therefore, DTB and fluidized bed crystallizers with classified product removal are used, which again corrects the effect of reduced uniformity (Figure 11.19b and line (2) in Figure 11.20; see also Figure 11.21).

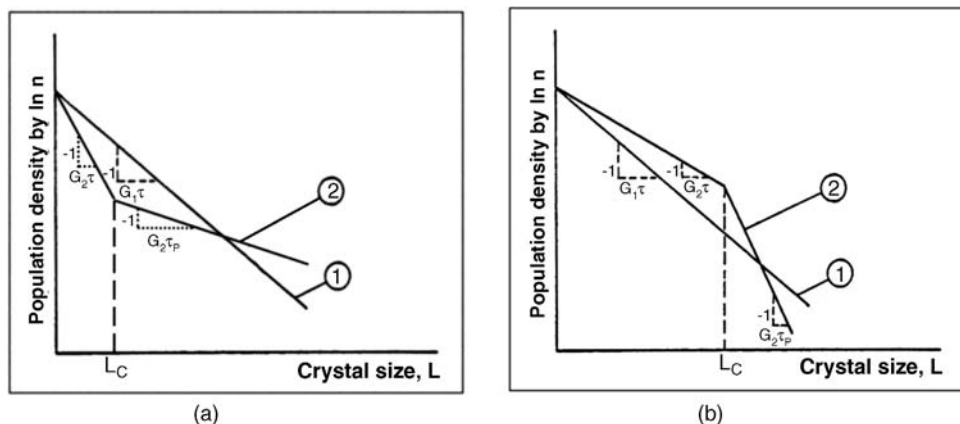


**Figure 11.19** Typical behavior of crystallizers with fines removal (a) or classification (b);  $\tau_p$  is retention time of product crystals.

### 11.3

#### Periphery

As mentioned above, the crystallization process is not yet complete with the crystallization itself. The suspension produced first has to be separated, while the crystals still have to be dried and packaged. The vapors released have to be condensed and the noncondensable gases extracted from the system by means of a vacuum pump. Figure 11.22 shows a simplified flowchart of the principle, using vacuum evaporation crystallization as an example.

In place of the FC crystallizer shown, any other type of crystallizer can also be used. Even multistage systems or systems with thermocompression (TVR) or with

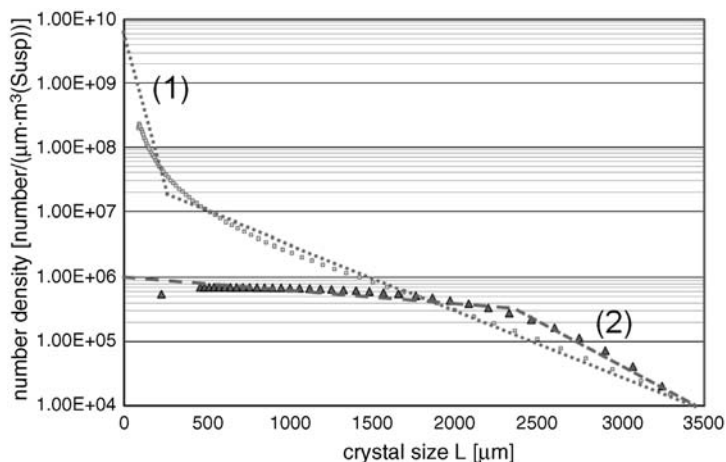


**Figure 11.20** CSD in DTB with fines removal (1) and with classified product removal (2).

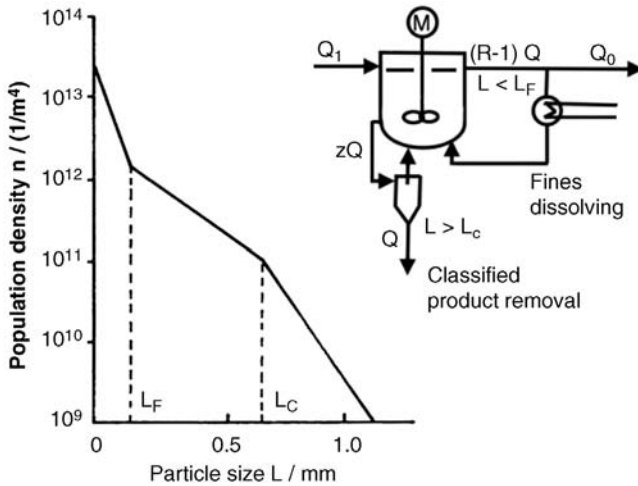


Figure 11.21 Typical CSD from DTB with fines dissolution and classified product removal.

mechanical vapor recompression (MVR) can be used here. In the illustrated example, the vapors of the (last) crystallizer stage are condensed on a surface condenser (indirect condensation) and removed from the process. The condensate is mostly reused as process water. If there is no requirement for process water, a mixing condenser (direct condensation) may be used. Here, for the system shown in the flowchart, the noncondensable gases are removed from the system with a two-stage steam jet vacuum pump with auxiliary condensation. In the case of pressures  $>70$  mbar, liquid ring pumps are also economical. Combinations of steam jet

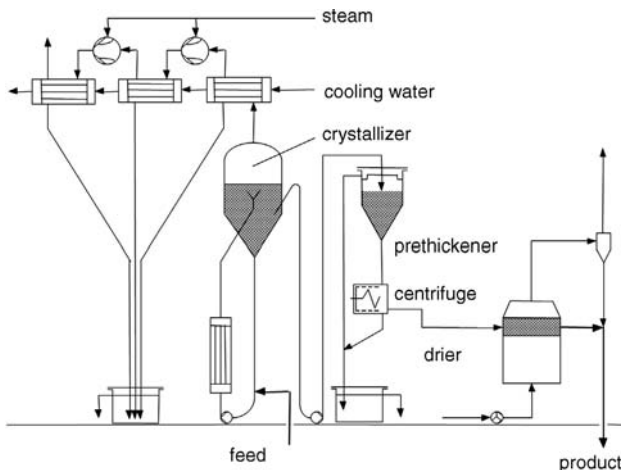


Figure 11.22 Simplified flowchart of a simple crystallization plant.

vacuum pumps and liquid ring pumps are also used. If work has to be carried out at very low temperatures and the vapors are colder than the cooling water, the above-mentioned thermocompression is frequently used before the condenser, that is, a steam ejector, in order to compress the vapors up to a higher pressure (= higher temperature for condensation) and thereby enable condensation with normal cooling water.

The suspension produced can be removed from the crystallizer through the overflow. If this is not possible for overriding reasons, the feed solution can also be added in a feed-controlled manner to the liquid level in the crystallizer.

The concentration of the suspension density in the crystallizer is still too low for separating in a centrifuge. As mentioned in this chapter, the standard suspension densities in the crystallizers are 15–25% by mass, while centrifuges only begin to work ideally from a level of 50–60%. For this reason, the suspensions are initially preconcentrated in static prethickeners or in hydrocyclones. The tail flow from this equipment is either removed from the process or partly returned to the crystallizer if dilution of the suspension that is being produced is required. In any case, part of the mother liquor has to be removed from the process in order to discharge the impurities that must not be contained in the crystallized mass from the process.

The underflow of the suspension is passed freely to the centrifuge. Depending on the crystal size distribution, there is a choice of at least four different types of centrifuges (Figure 11.23). The sieve decanter and the peeler-type centrifuge are selected for the separation of finer products. The pusher-type centrifuge or the sieve/worm centrifuges are used for coarser products. While the pusher-type

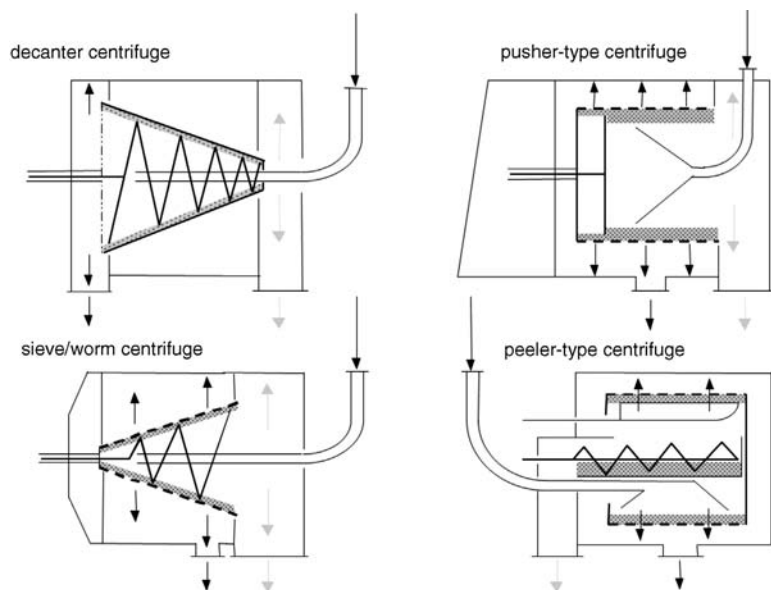


**Figure 11.23** Centrifuges used in crystallization processes.



centrifuge in the two-stage version is particularly recommended where intensive washing is required, the sieve/worm centrifuge is used if the feed concentration of the suspension can fluctuate for process technology reasons. The final drying of the crystallized mass that is still moist from the centrifuge is mostly carried out in flash dryers or fluidized bed dryers.

## 11.4

### Special Features of the Process

The crystallization processes are given designations that indicate the method of creating the supersaturation. Supersaturation can be created in solutions by various measures: vacuum evaporation crystallization, for example, when vacuum evaporation is the means used to create the supersaturation, or cooling crystallization (vacuum cooling crystallization or surface cooling crystallization) if the supersaturation is created by cooling. The principle is shown in Figure 11.24. In the case of solubility functions that are not dependent on the temperature – or only slightly so – solvent removal is selected, while in cases where there is considerable temperature dependence the chosen process is the cooling method, which is mostly more favorable with respect to the amount of energy used. In addition, there are other important factors that influence the selection of the process. The most important of these are presented below.

#### 11.4.1

##### Surface Cooling Crystallization

Continuous surface cooling crystallization is not a modern process. In this method, the supersaturation is created using the surface of a heat exchanger. As soon as this surface is covered by incrustations, the production output is directly affected. The

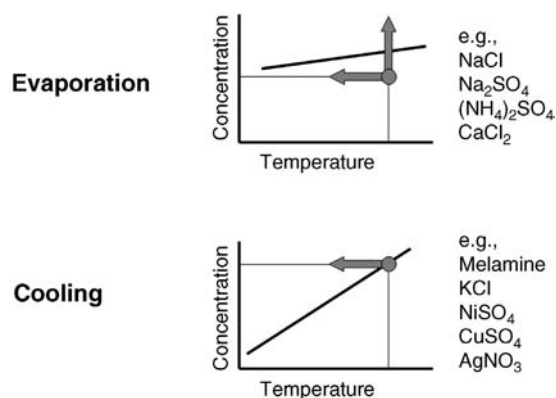


Figure 11.24 Typical examples to generate supersaturation.

probability of this is very high, as the highest supersaturation in the crystallizer takes place directly on the surface of the heat exchanger. The operating times between the requisite cleaning periods are therefore significantly shorter than those of vacuum crystallization processes. The tendency to develop incrustations can be reduced somewhat by means of large (and expensive) heat exchanger surfaces. As a result, the supersaturation directly on the cooling surface is reduced in size and the rate of incrustation growth slowed.

Surface cooling crystallization can be used for discontinuous processes without the need for any further measure, as the incrustations are dissolved again at the beginning of each new batch. In continuous processes today, surface cooling crystallization is only used where the vacuum methods become uneconomical, for example, when the vapor pressures of the solvent are too low. This is mainly the case with solvents with a high boiling point, for example, phenol. For aqueous solutions today, surface cooling crystallization is only used if the boiling point elevation is so great that vacuum crystallization is uneconomical due to the pressures being too low.

#### 11.4.2

##### **Vacuum Cooling Crystallization**

Due to the disadvantage mentioned above, vacuum cooling crystallization is the preferred cooling method for the continuous process. Cooling is carried out on a liquid surface whose process function cannot be disturbed by incrustations. This makes it possible to achieve long operation periods. Vacuum cooling only becomes uneconomical if cooling down to very low temperatures is required. However, as long as the vapor temperatures are not below the freezing point of the solvent concerned, vacuum cooling – for example, through the use of cold water or coolants with high boiling point elevations – is always the more economical alternative due to the longer service life in comparison to surface cooling crystallization. Frequently, processes are found in which the existing surface cooling crystallization at low temperatures could be replaced by vacuum cooling crystallization at a higher temperature. This may be the case when the upstream process task is only the balance-related ejection of impurities and does not relate to the process yield. Instead of cooling a small quantity down to low temperatures, in these cases a larger quantity can also be treated at moderate temperatures and then the more favorable vacuum cooling crystallization is used.

#### 11.4.3

##### **Vacuum Evaporation Crystallization**

Unlike vacuum cooling crystallization, this method does not depend on the concentration and temperature of the feed solution. Additional heat can be introduced by means of a heat exchanger and thus undersaturated solutions treated in a crystallizer. Furthermore, the concentration factor of the mother liquor can be selected; that is, the quantity of solvent to be evaporated is adjustable to the requirements of the mass balance. The mass balance is based on the corresponding

solubility system and must ensure that only the desired substance is crystallized out of the mother liquor. The permitted concentration of impurities in the mother liquor is to be geared on the one hand to the properties of the solubility system. On the other hand, the impurities of the product resulting from the adhering mother liquors have to be taken into account. As is the case with vacuum cooling crystallization, in evaporative crystallization there are no particular incrustation problems. Only in conjunction with the relatively rare inverse solubilities do supersaturations occur on the surface of the heat exchanger. This is the case, for example, during the crystallization of gypsum. This is remedied by means of seeding and limiting the temperature differences using the heat exchanger, as in surface cooling crystallization. Higher flow speeds and higher suspension densities can also help. Overall, the problems should be considered to be small. Particular attention should be paid to the falling incrustations from the evaporation chamber, as these can block the heat exchanger from below. Such incrustations of the evaporator section can be reduced by polishing the vessel walls. The energy carrier used in evaporative crystallization is steam or recompressed vapors. In order to save operating costs, the plants used in evaporative crystallization are frequently designed as multiple-effect evaporator systems. Here the first stage works near to atmospheric pressure and the last stage under such a vacuum that the vapors can be condensed on cooling water without any additional measure.

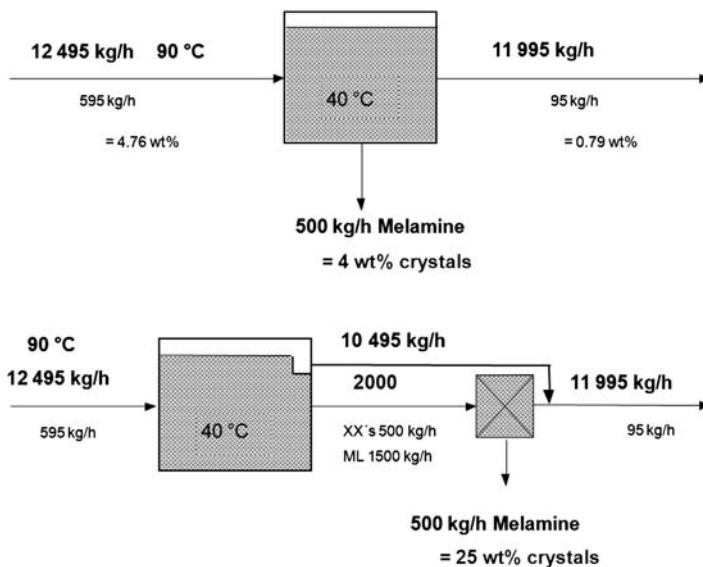


Figure 11.25 Method to increase suspension density.

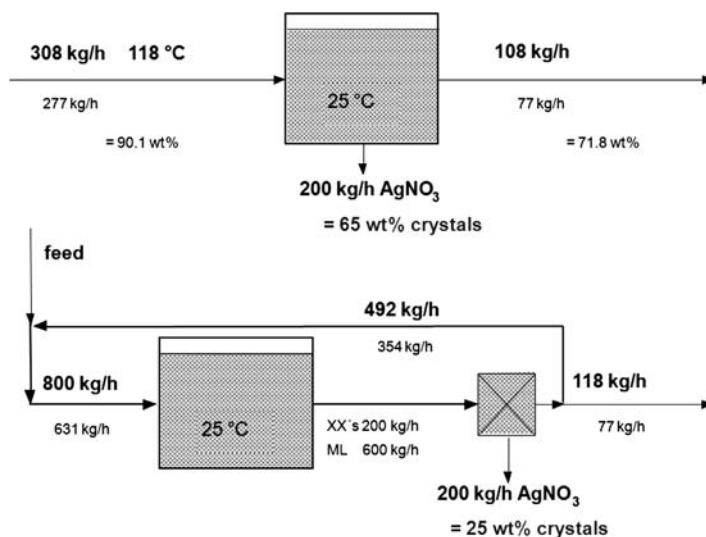


Figure 11.26 Method to decrease suspension density.

## 11.5

### Adjustment of Suspension Densities

As described above, crystallizers are operated with suspension densities of between 15 and 25% by mass. Suspension densities lower than 15% by mass increase the risk of primary nucleation and the probability of incrustations, while suspension densities greater than 25% by mass cause a greater attrition and increase the probability of deposits.

The only exception to this is the Oslo crystallizer, which due to the system properties can also be operated at higher suspension densities. It is not unusual for the mass balances, however, to show suspension densities that are below the limit of 15% by mass. This can be easily remedied by the installation of a clear liquor outlet (Figure 11.25). The suspension in the crystallizer is concentrated as a result. Figure 11.26 shows the opposite measure, which is necessary when the suspension density is too high. In this case, the suspension is diluted by returning mother liquor (centrifuged filtrate).

In the second case, attention has to be paid to secondary effects. The recirculation of mother liquor is of course only possible if after the separation of the crystals there is still enough mother liquor remaining, which is not always the case, particularly with viscous mother liquors. It should also be ensured that before recirculation, all crystal nuclei and crystals are removed by heating or the addition of solvent. Otherwise, the crystal size distribution of the crystallizer will deteriorate.

## References

- 1 Wöhlk, W. and Hofmann, G. (1985) Bauarten von Kristallisatoren. *Chem. Ing. Tech.*, **3**, 322-327.
- 2 Mullin, J.W. (1993) *Crystallisation*, 3rd edn, Butterworth-Heinemann, Oxford.
- 3 Mersmann, A. (1995) *Crystallization*, Marcel Dekker, New York.
- 4 Pohlisch, J. (1987) *Einfluss von mechanischer Beeinflussung und Abrieb auf die Korngrößenverteilung in Kühlungskristallisatoren*. Dissertation, Technische Universität München.
- 5 Widua, J., Hofmann, G., Wang, S., and Wöhlk, W. (2000) *Zyklische Korngrößenschwankungen in Massenkristallisatoren*, in Vortrag zur FA Kristallisation in Strasbourg 2000, Chemie-Technik 8/2000, Hüthig-Verlag, Heidelberg.
- 6 Tatsui, K. (1966) Klassifizierender Kristallisor DE-AS 1 519 915 (to Tsukishima Kikai Co. Ltd., Tokyo).
- 7 Bamforth, A.W. (1965) *Industrial Crystallisation*, Leonard Hill, London.
- 8 Hofmann, G. (1983) *Ein Oslo-Kristallisor für lange Reisezeiten*, Vortrag zur GVC-FA Kristallisation, Deggendorf, Bayern.
- 9 Randolph, A. and Larson, M.A. (1971) *The Theory of Particulate Processes*, Academic Press, New York.
- 10 Larson, M.A. and Garside, J. (1973) Crystallizer design techniques using the population balance. *Chem. Eng.*, **274**, 318-328.
- 11 Wöhlk, W., Hofmann, G., and de Jong, J. (1991) Die Kristallisationstheorie in der Praxis. *Chem. Ing. Tech.*, **63**, 293-297.
- 12 Toyokura, K. and Sakai, H. (1995) Design chart and industrial application. *J. Chem. Eng. Jpn.*, **28**, 361-371.

## 12

### Precipitation

*Wolfgang Beckmann*

Precipitations are characterized by a high supersaturation during the nucleation phase, entailing a large number of nuclei. Consequently, the amount of solute that can grow onto the crystallites will decrease with increasing nucleation rate, which ultimately leads to small particles, generally below a value of  $\approx 10 \mu\text{m}$ . This high supersaturation can only be achieved for a low solubility of the product, which is also a characteristic for precipitation. In order to achieve the high supersaturation, special schemes can be used. A consequence of the high supersaturation and nucleation rates is an increase in crystal imperfections; up to the occurrence of amorphous phases.

#### 12.1

##### Precipitation from Solution by Mixing Two Streams

##### 12.1.1

##### Devices and Mixing Schemes

The precipitation by mixing two streams, during a solvent or pH shift, or by mixing two salts can be carried out in a number of arrangements. The most commonly used, though not optimal, configuration is the semi-batch arrangement using a vessel containing the first component and adding, feeding, the second stream under a more or less vigorous stirring (Figure 12.1, geometry D). At the point of addition, the supersaturation is relatively high, leading to moderately small crystals. Feeding both streams into the mother liquor, the local supersaturations can be decreased (geometries C, B, and A). On the other hand, mixing the two streams in a nozzle, the local supersaturations can be increased substantially (geometry E).

The supersaturation in a precipitation is highly disperse: it varies along the axis of the mixing and with time. For the mixing schemes B and E depicted in Figure 12.1, the profile of the supersaturation is shown in Figure 12.2. The T-mixer has a very pronounced maximum in the supersaturation, leading to locally very high supersaturations and thus small particles, while in the semi-batch arrangement, the supersaturations are lower, leading to larger particles. The lower supersaturation also entails a longer induction time, and a longer presiding supersaturation.

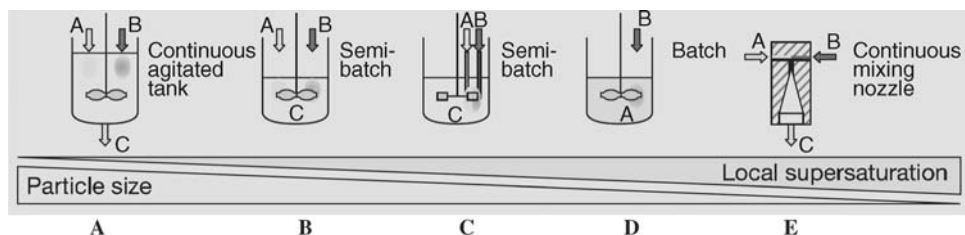


**Figure 12.1** Geometries for the addition of components in a drowning-out or pH-shift precipitation. Depending on the local supersaturation, either large crystals (left) or smaller particles (right) are obtained. The local supersaturation is a function of intensity of mixing.

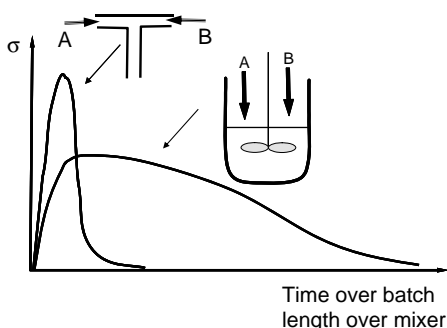


**Figure 12.2** Profile of the supersaturation as a function of time for the mixing schemes B and E depicted in Figure 12.1.

The geometry of the T-mixer, for example, as shown in Figure 12.1, can be improved to increase the efficiency of mixing by modifying the geometry of the mixing chamber and the outlet. Various geometries have been proposed. The closed geometry of the T-mixer bears the danger of clogging. Free-flowing impinging jet geometries might be used; Figure 12.3 shows two of the more commonly discussed geometries.

The efficiency of mixing can be increased by subjecting the mixing zone to a sonication or by using an Ultra-Turrax.

It should be emphasized that though the geometry of mixing will influence the supersaturation and nucleation rate and consequently the particle size; the absolute particle size obtained will highly depend on the system crystallized.

## 12.2

### Semi-Batch Precipitations

The most commonly used mode of operation for precipitations in the life science and specialty chemicals field is the semi-batch operation, the fed-batch (geometry D in Figure 12.1). One of the two solutions is present in a stirred tank vessel and the other solution is added. The goal of these precipitations is often not the (fine) particle size but rather the fact that no alternative and more gentle crystallization technique is available.

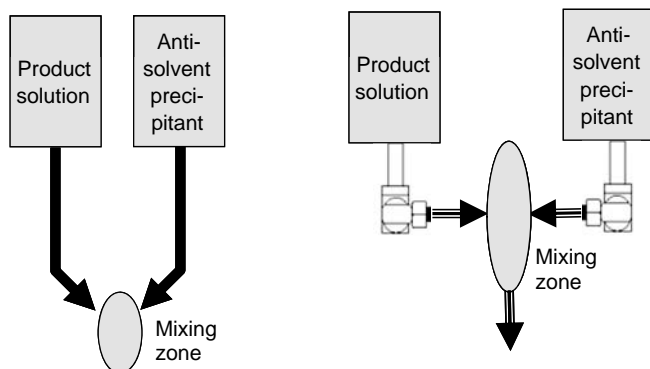


**Figure 12.3** (a and b) Design examples of impinging jet mixing devices, where the two streams are not confined.

Two modes of operation are possible for drowning-out and pH-shift operations: either the antisolvent is added to the solution of the target molecule (the classical operation) or the solution of the target molecule is added to the antisolvent (also called inverse drowning-out). The path in the solubility diagram is schematically shown in Figure 12.4. Depending on the nature of the droplets, these contain either

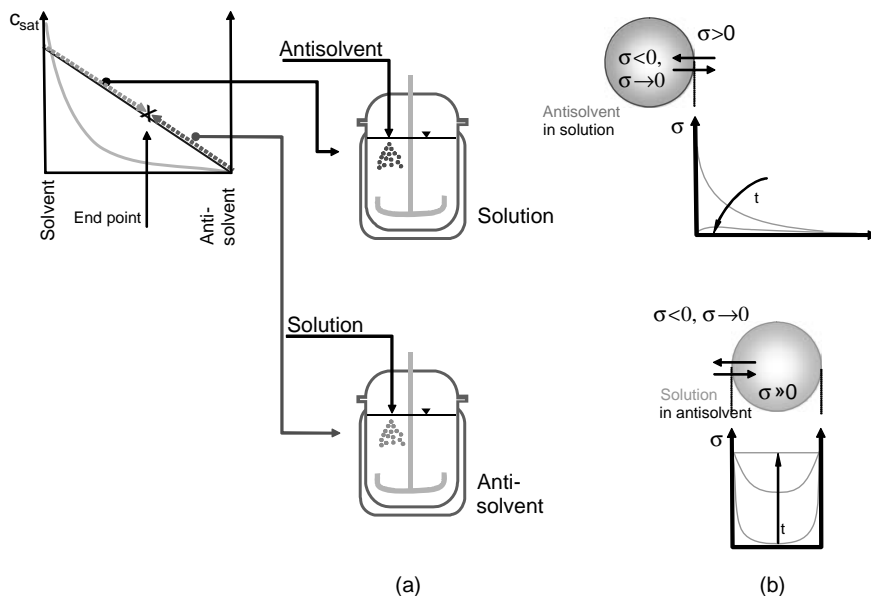


**Figure 12.4** (a) Path of a classical and an inverse drowning-out crystallization in the solubility diagram and (b) mixing of solution and antisolvent on the droplet level. The diffusion of anti-solvent from the droplets of anti-solvent into

the bulk of the solvent-phase is much slower, entailing much lower supersaturations, that the diffusion of anti-solvent from a bulk-phase of anti-solvent into the small droplets of solution, top and bottom right.



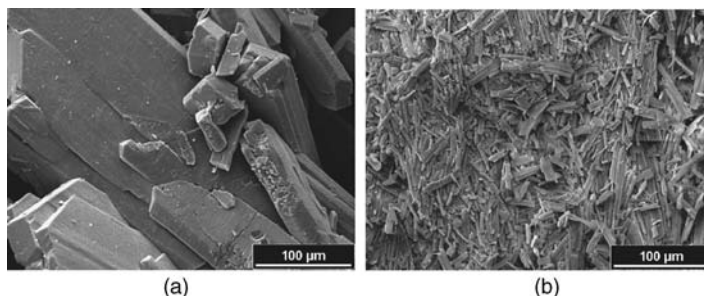


**Figure 12.5** Comparison of the product from a drowning-out precipitation using methanol as antisolvent. (a) The antisolvent is dosed into the solution of the active, leading to large crystals. (b) The addition of the solution of the active into an antisolvent leads to small particles. Note that the small primary particles are heavily agglomerated.

solution or solvent; the diffusion process leads to relatively low supersaturation in the bulk of the mother phase for the classical drowning-out and relatively high supersaturations in the droplets containing the target molecule in the case of the inverse process.

Products of the two modes of operation are shown in Figure 12.5. If the antisolvent is added to the solution of the active, relatively well-developed particles are obtained. The size will depend on the speed of the dosing; however, the effects of variations in the dosing scheme are mostly minute.

If the solution is dosed into the antisolvent, the local supersaturations are far higher, leading to smaller primary particles. The size is on the order of 10 μm. Note also that the habit changes to elongated particles. It is also evident from Figure 12.5 that the primary particles are heavily agglomerated into larger agglomerates with a size on the order of the primary particles from the classical drowning-out.

### 12.3

#### Model of Mixing during Precipitation

The mixing process can be envisaged as follows. To describe the mixing process during precipitation, processes on different scales have to be distinguished (Figure 12.6). First, the two streams are coarsely mixed forming eddies, the so-called macromixing. In a vessel with a mechanical stirring element, the processes are on the “meter” scale and the mixing time is inversely proportional to the stirring rate:  $t_{macro} \propto 1/n$ . The large eddies break down, and mesomixing occurs followed by the micromixing. Finally, the fluid engulfs small eddies and molecular diffusion takes over (micromixing). All scales have to be treated in the model.

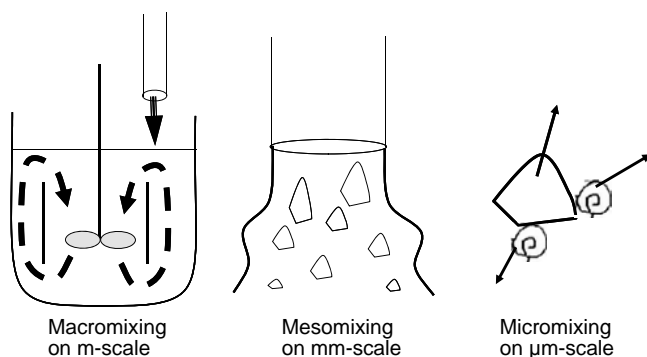


**Figure 12.6** Different length and timescales for the mixing of two fluid streams. The precipitation process is governed by both the mixing on the large scale (macromixing) and the processes on the molecular level, when the mixing is nearly complete.

## 12.4

### Precipitations Using Supercritical Fluids

Several techniques have been proposed using supercritical fluids for precipitations. The main advantage is the lower viscosity of supercritical fluids compared to classical fluids, which facilitates mixing and thus higher supersaturations can be achieved. Due to its ready availability, negligible toxicity, and convenient critical point of 32 °C and 100 bar, carbon dioxide is used in most cases as a supercritical fluid.

The supercritical or near-critical carbon dioxide is used as a solvent, as the solubility of most organic compounds is substantial near the critical point and decreases readily with decreasing pressure. On the other hand, near-critical carbon dioxide can also be used as antisolvent, as the critical fluid can dissolve to substantial amounts in organic solvents. At the same time, the solubility of organic compounds in the organic solvent is substantially decreased.

In the RESS process, the rapid expansion of supercritical solutions, the target compound is dissolved in the supercritical solvent, that is, in supercritical carbon dioxide. Due to the apolar nature of the solvent, the solubility is limited; nevertheless, the pressures of up to 300 bar allow for a solution of sometimes >2% at 50 °C. These solutions are rapidly expanded to subcritical conditions, that is, often ambient pressures. The cooling due to the adiabatic expansion limits the pressure ratio. As mentioned earlier, the solubility decreases with falling pressure, leading to a supersaturation and subsequently nucleation and growth of crystals. The expansion itself can be carried out very fast; thus, very small crystalline particles are formed. In the case of benzoic acid, a mean particle size on the order of 100 nm can be achieved (Figure 12.7).

Organic solvents are known to dissolve considerable amounts of carbon dioxide when pressurized to near- or supercritical conditions. Concurrently, the solubility of

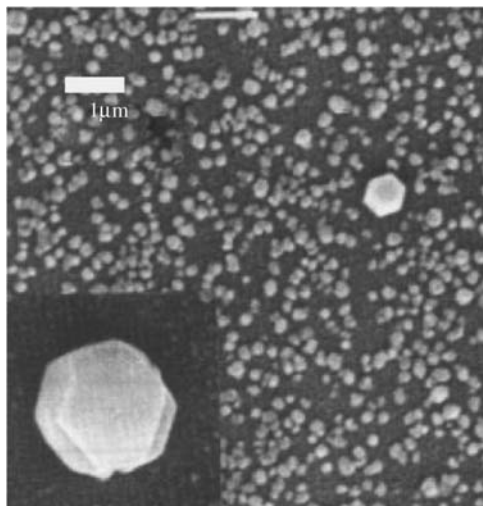


**Figure 12.7** Particles of benzoic acid precipitated using the RESS process with supercritical carbon dioxide as solvent. Courtesy of A. König, Erlangen.

an organic solute in the solvent will decrease accordingly. When the organic solution is rapidly pressurized (Figure 12.8), the precipitation of fine particles occurs.

The precipitations can be regarded as an antisolvent crystallization (Figure 12.9). It is noted that carbon dioxide behaves nearly similar to hexane regarding the modification of solubility and antisolvent.

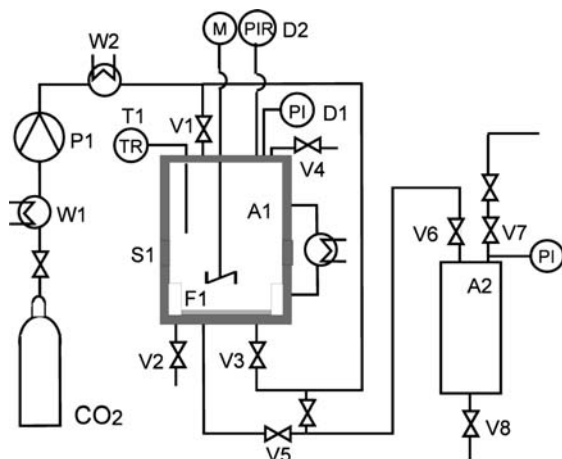


**Figure 12.8** Process of an antisolvent precipitation of a solution of an organic solute in an organic solvent using near-critical or supercritical carbon dioxide. A solution of

critical carbon dioxide in the active or solution of active in an organic solvent is prepared and rapidly expanded into a second vessel. The precipitated solid is collected in the latter.

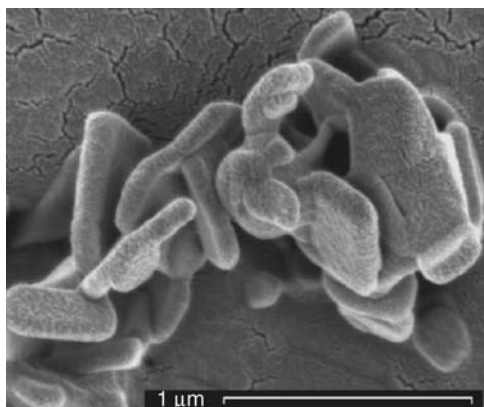


**Figure 12.9** Crystals of an active compound crystallized by an antisolvent crystallization using supercritical carbon dioxide. In the case shown, an inverse drowning-out mixing scheme was used, leading to small particles.

## 12.5

### Crystal Issues

#### 12.5.1

#### Polymorphism of Precipitates

The modification obtained in precipitations can only be controlled by the variation in the process conditions. It has been shown for the precipitations of a certain active by using supercritical carbon dioxide as antisolvent in the SEDS process that the domains of occurrence of individual polymorphs can clearly be distinguished. Figure 12.10 shows the influence of the amount of antisolvent and temperature. At least five different domains can be distinguished, in which different modifications of the moiety are observed. However, the effects leading to different modifications are kinetic effects. The response of the system to certain conditions can depend on less well controlled conditions such as the impurity content. Further, the borderlines between the domains are by no means sharp. In addition, by no way all modifications might be accessible, namely, the thermodynamically stable form might be inaccessible, see also chapter 5.

Due to the high supersaturation during precipitation, a number of highly metastable states occur. Metastable oiling-out has already been mentioned. Such oils can easily be mistaken for crystals, so that a solid–liquid separation results in a loss of the batch, which on a later inspection will be crystalline.

Further, gels might be formed; Figure 12.11 shows the result of a pH-shift precipitation on an organic acid. The gel agglomerates into large, fist-sized lumps. In this case, the gel will crystallize over tens of minutes into very well developed crystals also having an excellent filterability. It is interesting to note that the concentration of solute in the solution surrounding the gel-like lumps is well

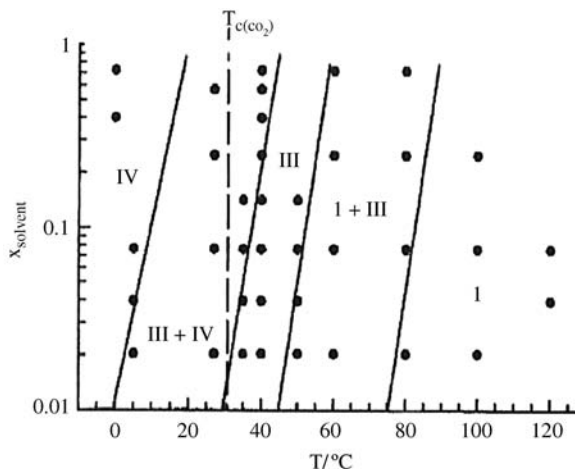


**Figure 12.10** Domains of occurrence of the polymorphs I, I + III, III, III + IV, and IV of a certain organic compound during the precipitation using supercritical carbon dioxide as antisolvent. Graph adopted from P York.



**Figure 12.11** Gel formation during a precipitation in a batch crystallizer. Fist-sized lumps are formed.

above the saturation concentration of the crystalline state, underlining the metastable nature of the gel.

Such gel phases have also been observed for the precipitation of salts (Figure 12.12). Depending on the precipitation conditions, the gel state can be short-lived for low supersaturations and low absolute concentrations or results in an amorphous solid product for high supersaturations and high concentrations.

If an oil is found, this might not recrystallize completely, which can lead to lollypop-like structures, where crystals are embedded into solidified oils (Figure 12.13). It is noted that strategies exist to avoid it.

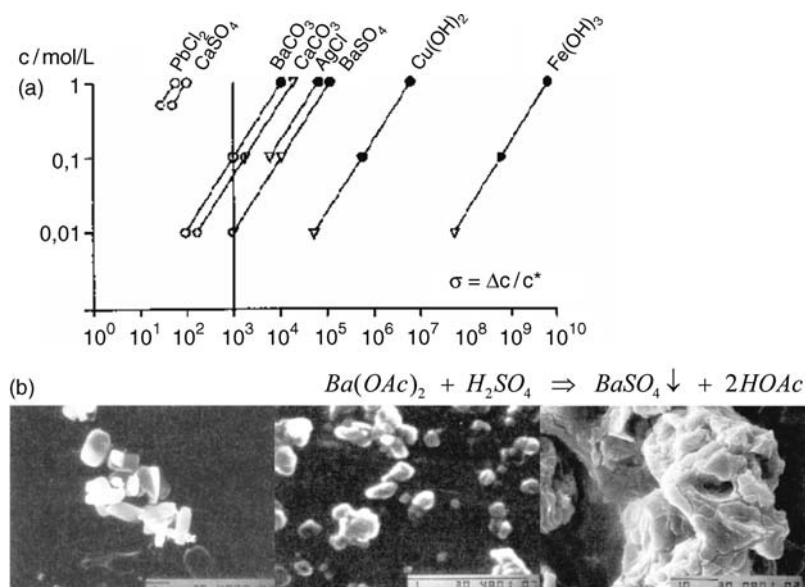


**Figure 12.12** (a) Formation of crystalline end products (○), gel-like intermediates (▽), and gel-like end products (●), during the precipitation of various salts with different solubilities and for concentrations of 0.01, 0.1,

and 1 mol/l. Different regions can be distinguished. (b) The gel-like solid state generated during such a precipitation is shown for the formation of barium sulfate. Graph according to Goesele.

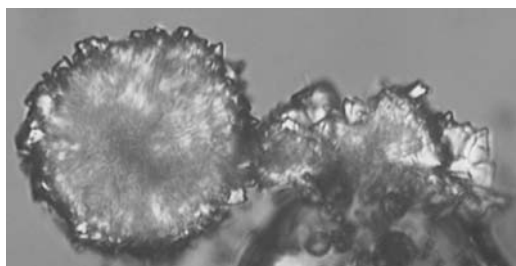


**Figure 12.13** Formation of lollypop-like structures for the crystallization of system prone to oiling-out. The structures show crystals lumped up in solidified oil droplets.

### 12.5.2

#### Crystal Perfection

Due to the very fast processes in precipitations, the crystal perfection can deteriorate considerably. This can be seen, for example, in a peak broadening in the XRPD diffractogram. However, a peak broadening is also to be expected for small crystal sizes.

Figure 12.14 shows the diffractograms of the precipitation of aluminum hydroxide by a pH-shift reaction. With increasing supersaturation, the (200) peak of the Boehmit modification first broadens and finally vanishes.

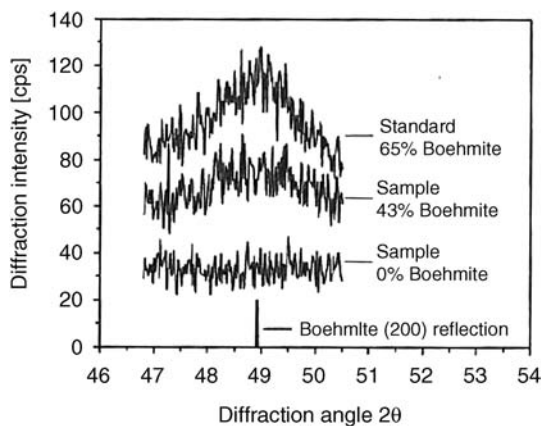


**Figure 12.14** Peak broadening for the precipitation of aluminum hydroxide by a pH shift. The broadening is determined both by the small crystal size and by the imperfection in the lattice.

### 12.5.3

#### **Agglomeration**

Due to the high particle density and high supersaturation during precipitations, the collision frequency of particles and their binding due to cementation lead to a high degree of agglomeration. The sticking efficiency can be reduced by using surfactants.

It should be stressed that the conditions for precipitation can only influence the size of the primary particles. The size of the agglomerates will mainly depend on other conditions of the process, such as the shear field generated by mixing.

## 12.6

### **Particle Size as a Function of Operating Conditions**

The variability in an isothermal antisolvent precipitation can best be described in a triangular solubility diagram (Figure 12.15). The tie line for a certain concentration of the active in the organic solvent and the tie line for a certain mixing ratio of the solvent and antisolvent are shown. The intersection of both lines defines the supersaturation at ideal mixing. By varying the solute concentration and the ratio of solvent and antisolvent, different supersaturation can be realized; Table 12.1 exemplifies typical values.

Note that these supersaturations are nominal values under the assumption that complete mixing has been achieved before nucleation occurs. Using the conditions listed in Table 12.1, experiments have been carried out and the particle size has been assessed. Part of the data is shown in Figure 12.16. Note that the size of the primary particles is given, as this is the only size that can be influenced.

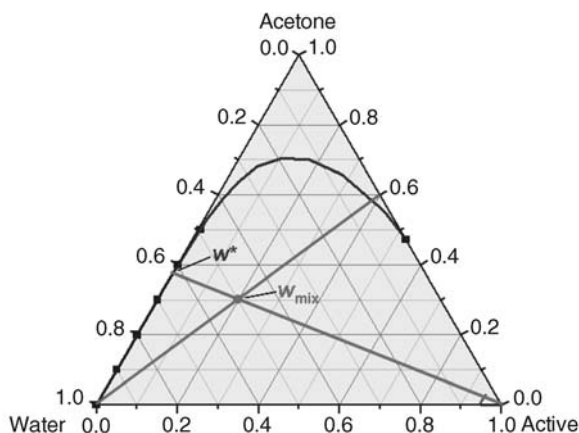


**Figure 12.15** Path of an isothermal antisolvent precipitation in a triangular solubility diagram. The tie line for a certain concentration of the active in the organic solvent and the tie line for a certain mixing ratio of the solvent and antisolvent are shown. The intersection of both lines defines the supersaturation at ideal mixing.

**Table 12.1** Supersaturations at complete, ideal mixing in an antisolvent precipitation for the system shown in Figure 12.15.

Mixing ratio	Concentration of solute in solvent (%)	Supersaturation ratio, $c/c_{\text{sat}}$
3 : 1	30	850
	40	1310
	50	1960
	60	3000
1 : 1	40	300
2 : 1		600
3 : 1		1310
5 : 1		1490
6 : 1		1525

Values are given for different starting concentrations of the solute in the solvent and mixing ratios of solvent and antisolvent.

Though the supersaturation varies by one order of magnitude, the final particle size distribution varies only by a factor of  $\approx 3$ .

Finally, the influence of the intensity of mixing in a T-mixing device on the particle size has been qualitatively assessed. Again, the influence of the intensity of mixing is clearly seen; however, the variability in the size obtained is only a factor of 3–5.



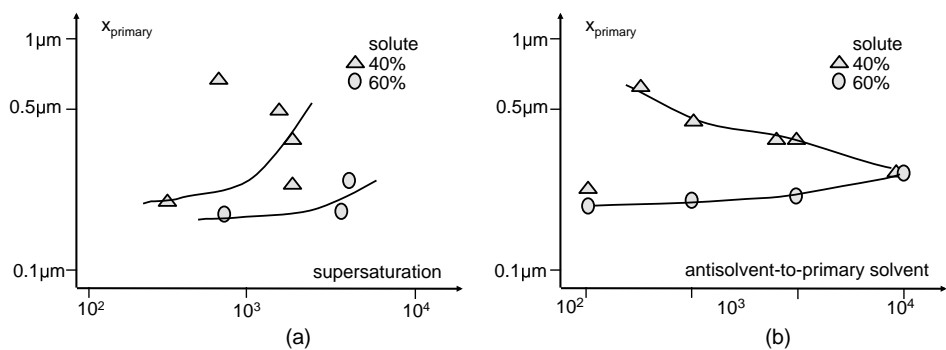


**Figure 12.16** Variability in the particle size distribution of an antisolvent precipitation with varying supersaturation (a) and mixing ratios of solvent and antisolvent (b).

## 13

### Mixing in Crystallization Processes

Bernd Nienhaus

Mixing or agitation in a crystallization process from suspension is a critical success factor. Especially during scale-up of a crystallization process, special attention has to be paid when choosing a suitable mixing system. To find a systematic approach, first the mixing tasks that are special about the process and the mixing tasks that dominate the process have to be defined. In addition, the influence of mixing on other significant process parameters in crystallization cannot be neglected. The challenge is – based on these considerations – to develop a suitable or even an optimum setup of a vessel, agitator, impeller, baffles, dosing points, draw-off points, and so on.

Typical mixing tasks that will be found in any crystallization or precipitation process are *blending*, that is, the adjustment of concentration or temperature differences over the total volume of the vessel, *suspension*, that is, lifting off the bottom and/or homogeneous distribution of solids in the solvent, and *heat transfer*, that is, acceleration of heat exchange between the vessel content and the heating/cooling media. At first, we will have a closer look at the basic mixing tasks in batch and continuous crystallization processes. Then, we will have a look at the mixing tasks and their dominating correlations in more detail together with a look at their influences among one another.

#### 13.1

##### Mixing in Batch and Continuous Crystallization Processes

Batch crystallization is frequently applied for recrystallization or purification of specialty chemicals, intermediates, or APIs. In small to medium vessels (0.1–20 m<sup>3</sup>), various products or specifications are manufactured, typically in multipurpose plants. Preferably, in these kinds of processes, precipitation or cooling crystallization is applied. A batch crystallizer used in a multipurpose plant as well as the corresponding mixing system has to be flexible. Such a flexible setup, for example, should be able to guarantee high flow velocities close to the wall to provide a good heat transfer – e.g. to be able to apply different cooling strategies. Together with this, the setup must be suitable for suspending the crystals or solids generated from the corresponding process step. At the same time, it should be able to deliver short blend

times for a homogeneous solution as well as for a heterogeneous suspension – maybe at very different filling levels and maybe for very different ranges of viscosities or solids concentrations.

Especially during a fast precipitation process, a short blend time is of an outstanding importance, as nucleation and growth processes compared to cooling crystallization are very fast. Here, insufficient blending together with dead zones may have a dramatic and disadvantageous impact on product quality. The objective for such a process must be to find a suitable impeller system to prevent these effects and therefore to prevent uncontrolled particle formation.

In continuous crystallizers, supersaturation is predominantly generated by vacuum or evaporation. Here, very large vessels are commonly applied to manufacture dedicated products such as inorganic salts as well as organic base chemicals or intermediates such as terephthalic acid (PTA). The detailed mixing tasks differ significantly if compared to batch operation. Continuously running crystallizers have to provide a constant product quality. In the majority of the cases, this means a constant purity combined with a constant and well-controlled particle size distribution is desired. With such a constant crystallization product quality, the consecutive process steps such as solid–liquid separation and drying can be optimized and smoothly operated as well.

For this purpose, during design and scale-up of such a crystallizer the generation of a homogeneous suspension is most critical. At the same time, too high local energy input has to be avoided as crystals can be destroyed and production of fines has to be prevented. In addition to this, stationary conditions and constant product quality are also positively influenced by a well-considered positioning of feed and draw-off points.



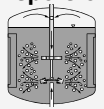

Regarding continuous mass crystallization processes in general, it is important to carefully select a high-efficient product-sensitive impeller system that fits to the corresponding mixing tasks of the process. Here, the shaft power has to be transferred into power available for suspending the solids in a most efficient way. Together with this, any dead zone, that is, any severe inhomogeneity of solids distribution or even scaling, endangers continuous operation and - together with this - constant product quality.

## 13.2

### **Basic Mixing Tasks – Mixing Tasks in Crystallization**

The wide variety in the requirements that exist, such as extremely large vessels, mastery of very high viscosities, or minimizing operating costs, means that many different types of agitator impeller and vessel internals are used in practice. The basic mixing tasks encountered in practice can be divided into four categories (Figure 13.1):

- blending;
- suspension;
- dispersion (liquid–liquid and gas–liquid);
- heat transfer.

	Requirement	Parameters
<b>Blending</b> 	blend time and degree of homogeneity ; flow velocity ; surface entrainment or agglomeration ; prevent air entrainment	Flow characteristic (Newtonian / non-Newtonian)
<b>Suspension</b> 	homogeneous suspension or off-bottom suspension sufficient ; restarting in settled sediment	particle size ; solids concentration ; liquid and solids density
<b>Dispersion</b> 	required conversion or mass transfer ; gassing rate ; superficial gas velocity ; mass transfer coefficient ; local / global specific power input	required stoichiometric excess of reacting gas
<b>Heat transfer</b> 	temperature difference at process start / end ; required heating / cooling time ; local / global heat transfer coefficient	specific heat capacity and heat conductivity of the product

**Figure 13.1** Basic mixing tasks.

Every mixing task is governed by laws, which must be known for the scientific design of the agitator. Complex mixing tasks involve two or more of these mixing categories simultaneously. In these cases, special attention must be paid to the dominant mixing category.

Agitators or agitation systems usually have to fulfill a combination of the following objectives during crystallization:

- short blend times, such that zones of high local supersaturation will be avoided;
- homogeneous off-bottom suspension of the crystals to provide uniform growth conditions;
- gentle treatment of the crystallized material to prevent uncontrolled nucleation, which would cause the particle size distribution to be shifted toward the fines range;
- high wall velocities to prevent scaling;
- high heat transfer to make it possible to operate with low temperature differences between product and cooling surface.

### 13.3

#### Impellers and Agitation Systems

In mixing technology, a wide variety of impellers are encountered that differ from one another essentially in their main field of application. Their diversity of shape can

be traced back to just a few basic designs, the dimensions and nomenclature of which are standardized in DIN 28131. Fundamentally, they can be differentiated by the following features:

- Primary direction of induced flow: axial, radial, or tangential.
- Ratio of impeller diameter to vessel diameter.
- Peripheral speed at the impeller tip.
- Viscosity range of application, or, correspondingly.
- Flow range: laminar or turbulent.

In practice, it has proven expedient to classify impellers according to the primary direction of the induced flow, even though in parts of the vessel an axial flow necessarily gives rise to radial flow and, vice versa, a primarily radial flow also causes an axial flow.

In recent decades, there has been an ongoing optimization process for conventional impellers in terms of their process, mechanical, and application-related properties. The result of this development means that there is a wide range of agitator impellers that can satisfy a wide diversity of mixing requirements.

### 13.3.1

#### **General Overview and Selection Criteria**

Since every impeller creates tangential flow, in addition to the desired axial or radial flow, by transmitting its rotating motion to the liquid, the flow in stirred vessels is three-dimensional. The flow pattern is also greatly influenced by the internals at the vessel wall, whose number and shape must therefore be taken into consideration.

The rest of this section is a comparative appraisal of the flow characteristics of commonly used impeller systems (Figure 13.2) [1].

### 13.3.2

#### **Axial Impellers**







##### 13.3.2.1 **Propeller**

The axial impeller typically used for low- to medium-viscosity media is the propeller, preferably with three blades. This versatile impeller type is especially suitable for blending and suspension duties.

The flow pattern shows the liquid being drawn in axially and discharged in a focused jet in the turbulent flow range. The axial flow from the impeller - which quite commonly is pumping downwards - is diverted at the bottom of the vessel and then rises adjacent to the vessel wall up to the surface. Acceleration of the liquid takes place at the level of the propeller.

##### 13.3.2.2 **Pitched Blade Turbine**

A fairly similar flow pattern is produced by the four-bladed pitched turbine with its blades set at a 45° angle. The radial component, however, is already more evident with this design.

Impeller	Geometrical Environment	Position	Primary Flow	Common Range of Operation			Mixing Tasks
				$D/T$ $u_{tip}$ [m/s] Flow regime	Re number Ne	Power number $\eta$ [Pa s]	
Propeller	 $H/T = 1.0$ $D/T = 0.33$ $h_b/T = 0.33$ $\alpha = 25^\circ$ 3-bladed	Centric with internals - Excentric without internals	Axial in the turbulent regime	0.1 – 0.5 3–15	$Re > 10^3$ turbulent	3-bladed: $Ne = 0.35$	Blending solid-liquid / liquid-liquid Suspension Heat transfer
Pitched Blade Turbine	 $H/T = 1.0$ $D/T = 0.3 - 0.4$ $h_b/T = 0.17 - 0.34$ $\alpha = 45^\circ$ 4-bladed	Centric with internals - Excentric without internals	Axial with radial components	0.2 – 0.5 2–6	$Re > 10^3$ turbulent	4-bladed: $Ne = 0.6$ 6-bladed: $Ne = 1.2$	Blending solid-liquid / liquid-liquid Suspension Heat transfer
Disc Turbine	 $H/T = 1.0$ $D/T = 0.33$ $h_b/T = 0.33$ 6-bladed	Centric with internals	Radial	0.2 – 0.5 2–6	$Re > 10^3$ transition turbulent	6-bladed: $Ne = 5.5$	Dispersion liquid-liquid / gas-liquid (Blending) Heat transfer
Curved Impeller	 $H/T = 1.0$ $D/T = 0.57$ $h_b/T = 0.05-0.1$ 3-bladed	Centric with internals	Radial	0.4 – 0.7 6–12	$Re > 10^3$ turbulent	3-bladed: $Ne = 0.7$ with flat baffles $Ne = 0.5$ with finger baffles	Blending solid-liquid / liquid-liquid Heat transfer
EKATO Isojet	 $H/T = 1.0$ $D/T = 0.2 - 0.5$ $h_b/T = 0.2 - 0.3$ 2-bladed	Centric or excentric with or without internals	Axial	0.05 – 0.5 3–15	$Re > 10^3$ turbulent		Blending solid-liquid / liquid-liquid Suspension Heat transfer
EKATO Viscoprop	 $H/T = 1.0$ $D/T = 0.4 - 0.7$ $h_b/T = 0.2$ $\alpha = 25^\circ - 53^\circ$ 2 or 4-bladed	Centric or excentric with or without internals	Axial	0.3 – 0.7 2–10	$Re > 10^3$ turbulent		Blending solid-liquid / liquid-liquid Suspension Heat transfer



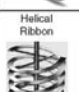


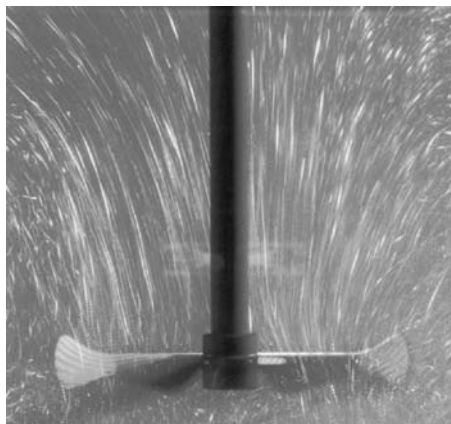
Impeller	Geometrical Environment	Position	Primary Flow	Common Range of Operation			Mixing Tasks
				$D/T$ $u_{tip}$ [m/s] Flow regime	Re number Ne	Viscosity $\eta$ [Pa s]	
EKATO Intermig	 $H/T = 1.0$ $D/T = 0.7$ $h_b/T = 0.22$ 2-bladed	Centric	Axial / radial	0.5 – 0.95 1–9	turbulent: $D/T < 0.7$ laminar: $D/T > 0.7$	$Ne = 0.35$ one stage $\eta < 40$	Blending Suspension (Surface Gassing) Heat Transfer
Anchor	 $H/T = 1.0$ $D/T = 0.96$ $h_b/T = 0.025$ 2-bladed	Centric	Tangential	0.9 – 0.99 < 2	$Re > 10^3$ transition turbulent	$Ne = 0.2 - 2.0$ $\eta < 20$	Heat Transfer Variations: Finger Type Grid Type Blade Type
Helical Ribbon	 $H/T = 1.0$ $D/T = 0.96$ $h_b/T = 0.01$ $s/D = 0.5$	Centric No internals possible (!)	Axial	0.9 – 0.99 < 2	$Re > 20$ laminar	$Ne > 40$ $\eta < 50$	Blending in viscous media designs with single or double helix
EKATO Paravisc	 $H/T = 1.0$ $D/T = 0.9 - 0.98$ $h_b/T = 0.01 - 0.03$ 2-bladed	Centric	Axial	0.9 – 0.98 < 2.5	$Re > 20$ laminar	$Ne$ strongly depends on design model and $D/T$ ratio $\eta < 200$	Blending in viscous media Suspension Heat Transfer
Dissolver	 $H/T = 1.0$ $D/T = 0.375$ $h_b/T = 0.375$ 2 x 36 teeth	Centric with and without internals	Radial	0.2 – 0.5 8–30	$Re > 10^3$ turbulent	for $Re > 10^3$ : $Ne = 0.1$ for $Re = 10^3$ : $Ne = 0.5$ $\eta < 20$	Dispersion liquid-liquid / solid-liquid often used in combination with axial pumping impellers

Figure 13.2 Characteristics of common impeller systems.

Its field of application is broader than that of the propeller, as it can cope with viscosities up to 20 000 Pa s, making it suitable for laminar as well as turbulent flow ranges. There are more effective axial working impellers, for example, the Isojet impeller shown in Figure 13.3.



**Figure 13.3** Isojet visualized with the light section process.

### 13.3.2.3 Helical Ribbon Impeller

The helical ribbon impeller is suitable for blending highly viscous media. It comprises a spiral strip attached to the central shaft by supporting struts, as shown in Figure 13.2. In contrast to the propeller, this impeller induces axial flow not by a pressure differential but by positive displacement in the laminar flow range.

With a diameter ratio of 0.9–0.98, the helical ribbon belongs to the close-clearance category of impellers.

## 13.3.3

### Radial Impellers

The primary flow produced by radial impellers is directed radially outward towards the vessel wall, where it is then diverted upward and downward. Two ring vortices are therefore formed, thus giving an axial flow to the impeller from above and below.

#### 13.3.3.1 Flat Blade Disk Turbine

A typical form of the radial flow impeller is the flat blade disk turbine, its typical flow pattern being illustrated in Figure 13.4.

Six rectangular blades are mounted symmetrically around the circumference of a horizontal carrier disk and perpendicular to it, as shown in Figure 13.2. The flat blade disk turbine is used especially on gassing duties because of its good dispersing effect. Under certain conditions, it can also be used for other mixing duties.

The actual mixing effect is predominantly in the shear zone of the radial emerging jet.

#### 13.3.3.2 Disperser Disk

Another typical radial flow impeller is the disperser disk, also known as the toothed disk or dissolver disk. The EKATO MIZER disk belongs to this category, and consists

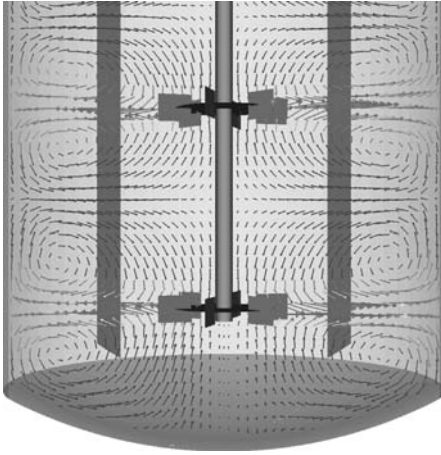


**Figure 13.4** Flat blade disk turbine, two stages, flow pattern visualized by CFD.

of a disk carrying tooth-shaped elements perpendicular to it around its circumference (Figure 13.2).

It is suitable for mixing duties requiring high shear gradients, such as emulsifying, size reduction of solids, or wet grinding. The high shear forces that are necessary are achieved by high peripheral speeds. With high-viscosity media, an additional axial flow impeller is fitted to ensure an adequate circulation rate in the vessel.

#### 13.3.4

##### **Tangential Impellers**

A typical example of this type is the anchor impeller. In general, this consists essentially of two blades parallel to the agitator shaft and connected to the shaft by a U-shaped blade that closely follows the contour of the vessel bottom, as shown in Figure 13.2.

This close-clearance impeller has a diameter ratio of 0.9–0.98. Its main duty consists essentially of minimizing the highly viscous boundary layer clinging to the vessel wall, thus improving the heat transfer.

Older designs, that is, finger, frame, blade, and paddle impellers, some of which are still in widespread use, have similar characteristics compared to the impellers shown in Figure 13.2.

#### 13.4

##### **Power Consumption of an Impeller System [2]**

The generation of a three-dimensional flow pattern inside a vessel together with the corresponding energy dissipation and shear stress of course is linked to a certain



power consumption of the impeller system. The power consumption is derived from resisting power following from the relative velocity between the impeller and the surrounding liquid:

$$F_R = \xi \frac{\rho}{2} u^2 A. \quad (13.1)$$

Generally, the resisting power is made up of inertial forces and internal friction. As the relative velocity due to the complex flow pattern cannot be exactly derived, the proportional tip speed

$$u \sim u_{tip} = \pi n D \quad (13.2)$$

is used to describe the resisting power. The surface  $A$  is the projection screen typical for the impeller and is put on a level with the circular surface covered by the impeller. Therefore, the resulting forces acting on the impeller can be derived from

$$F_R \sim \rho n^2 D^4. \quad (13.3)$$

Together with this, for the resulting power the following relationship is valid:

$$P = F_R u \sim \rho n^2 D^4 n D \sim \rho n^3 D^5. \quad (13.4)$$

To calculate the impeller power or shaft power brought into the system, the following equation is widely used:

$$P = Ne \rho n^3 D^5. \quad (13.5)$$

The dimensionless power number  $Ne$  basically is a function of geometry of the impeller system. Besides this fact, it is also dependent on the Reynolds number of the impeller:

$$Re = n D^2 / \nu. \quad (13.6)$$

The dependence of the power number  $Ne$  on the Reynolds number  $Re$  is the so-called power characteristic of the impeller system. This very important correlation has to be determined experimentally for any impeller together with its surrounding geometry. As the capability of numerical methods is steadily increasing, there will be alternative methods in the future to calculate the power characteristics [2]. In Figure 13.5, the power characteristics for some different impeller systems are shown. The resulting curves can be divided into three regimes:

- a) In the *laminar regime* ( $Re < 10$ , only for close to the wall working impellers  $Re < 100$ ), the influence of inertial forces is eliminated by the influence of internal frictional forces. Therefore, it can be noted that

$$Ne = \text{const}_1 Re^{-1}. \quad (13.7)$$

In this regime, usually no baffles are needed.

- b) In the *turbulent regime*, there is no longer an influence of the internal friction; the forces acting on the impeller mainly are inertial forces. Therefore,

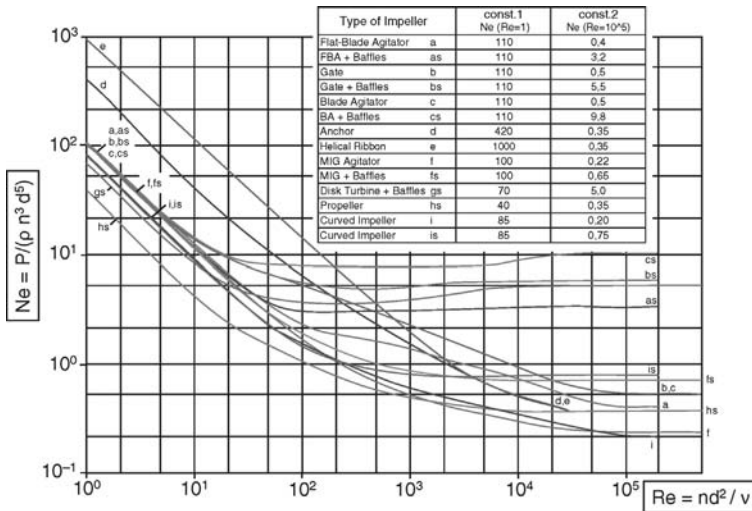


Figure 13.5 Simplified power characteristics for selected impellers.

$$Ne = \text{const}_2. \quad (13.8)$$

The absolute value of the power number  $Ne$  here can be derived only from the impeller and from the surrounding geometry. Baffles are generally needed and increase the shaft power up to a factor of 10 compared to an unbaffled system.

- c) In the *transition regime* that can be found between laminar and turbulent regimes, with increasing Reynolds number the internal friction more and more decreases. At the same time, the influence of the inertial forces increases.

For the determination of the power number  $Ne$  following Equations 13.7 or 13.8, the corresponding constants  $\text{const}_1$  and  $\text{const}_2$  can be taken from the connected table (Figure 13.5).

When using any power characteristic, it has to be mentioned that only geometrically similar systems are regarded. In any other case, important parameters resulting from a special geometry might not be taken into account, leading to wrong results. In reality, the influences of geometrical modifications are complex and hardly investigated. Nevertheless, some trends can be derived from experimental results.

#### 13.4.1

##### Diameter Ratio

For propeller-type impellers, there is an almost constant power number in the region of  $0.2 < D < 0.5$ . In contrast to this, for the disk turbine the power number decreases in the same range by about 20% with increasing diameter.

## 13.4.2

**Bottom Clearance**

Usually impellers are installed in the lower part of a vessel. When axial impellers are chosen, the power number increases with decreasing bottom clearance due to the flow deflection at the vessel bottom. When radial impellers are used, the power number decreases with decreasing bottom clearance as there is no recirculation below the impeller.

## 13.4.3

**Filling Level**

The influence on power number is high for blade-type impellers. For pitched blade turbines or propellers,  $Ne$  is constant for filling levels  $H/T > 0.8$ .

## 13.4.4

**Multistage Impellers**

In thin and tall vessels ( $H/T > 1$ ), multistage impeller systems are commonly used. The resulting shaft power is highly influenced by the clearance  $\Delta h$  between the impeller stages. In fully baffled systems and for  $\Delta h > 1.2$ , the power for the single stages can be summed up. When multiphase systems are agitated, the power consumption can extremely differ from the one-phase system (see Section 13.6).

## 13.5

**Blending**

The objective of any mixing action is to achieve a homogeneity that is required for the process throughout a defined volume, for example, the volume of a stirred vessel or any other apparatus used for crystallization. Concentration and/or temperature gradients arise through feeding in product, mass transfer, chemical reactions, or by supplying or removing heat. These situations can occur in single-phase and multiphase systems.

## 13.5.1

**Degree of Homogeneity**

The degree of homogeneity  $M(t)$  is given by the change in concentration of a tracer from  $c_a$  to  $c(t)$  with time:

$$M(t) = \frac{c_a - c(t)}{c_a - c_\infty}, \quad (13.9)$$

where  $c_\infty$  is the concentration after an infinite period of time. The same relation holds when the blend time is determined by temperature measurements, in which

case the concentration  $c$  is replaced by the temperature  $T$ . It is normal to aim for a degree of homogeneity of 0.95 when investigating blend times.

Blend time measurements described by different authors can only be compared after they have been converted to the same degree of homogeneity. As the fluctuations in concentration decline exponentially, the blend time can be converted as follows:

$$\theta_x = \theta_{95} \frac{\ln(1-x)}{\ln(0.05)}. \quad (13.10)$$

### 13.5.2

#### Turbulent Blending

Extensive basic research by many authors together with measurements taken in industrial vessels has shown that the blend time characteristic  $n\theta$  is a constant for stirred vessels fitted with baffles. This applies generally for turbulent flow regimes, but also for laminar flow induced by positive displacement impeller systems (Figure 13.6). The numerical value of this constant depends mainly on the type of impeller and the diameter ratio.

Mersmann [3] evaluated the measurement results of various authors and determined a demarcation line for favorable conditions. It is characterized by the following relation:

$$\frac{P\theta^3}{\rho d_1^5} = 300 \quad (\text{turbulent}). \quad (13.11)$$

In dimensionless form, the equation becomes

$$n\theta = 6.7 \left[ \frac{d_2}{d_1} \right]^{-5/3} Ne^{-1/3}. \quad (13.12)$$

EKATO's own measurements show that this equation forms a good basis for design calculations for impellers with larger diameter ratios ( $d_2/d_1 > 0.5$ ). The following

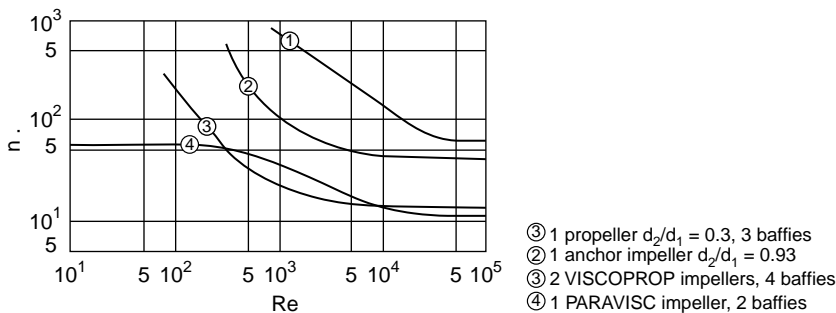


Figure 13.6 Blend time characteristics.

relation for agitator impellers pumping mainly axially, with diameter ratios in the range 0.1–0.5, is suitable for calculating the blend time to an accuracy of  $\pm 10\%$  if a 95% degree of homogeneity is to be achieved:

$$n\theta = 5.5 \left[ \frac{d_1}{d_2} \right]^2 N\epsilon^{-1/3}. \quad (13.13)$$

This equation only applies for  $h_1/d_1 = 1$  and single-stage impellers.

### 13.5.3

#### Significance of Circulation Rate

The circulation characteristic of impellers is used for comparison purposes, especially in the English-speaking world, for assessing the performance of agitator impellers. The blend time is then derived from the number of times it is necessary to circulate the vessel contents to achieve homogeneity:

$$\Theta = z \frac{V}{q}. \quad (13.14)$$

The empirical value  $z = 4$  is often used for the number of times the vessel contents are circulated.

### 13.5.4

#### Laminar Blending

To achieve a defined blending result, it is a prerequisite that the entire volume of the vessel is involved in the laminar flow. The Reynolds number calculated with the impeller diameter represents only an inadequate description of the flow conditions in the entire vessel, particularly in the case of impellers with small zones of agitation. The dimensionless blend time in  $n\theta$  for these impellers therefore starts to increase at a point where the reducing Reynolds number theoretically still indicates turbulent flow (see Figure 13.6, propeller  $D/T = 0.3$ ).

The anchor agitator has an impeller with a large blade area and only achieves a mixing effect in the annular space adjacent to the vessel wall. The zone around the agitator shaft, however, is poorly mixed, so that at values of  $Re < 200$  no satisfactory homogeneity can be achieved. Moreover, there is almost no axial blending, resulting in very poor blend times and large difficulties with surface entrainment.

Multiple impeller systems with a large diameter ratio, such as Viscoprop impellers arranged one above another, are suitable for  $Re > 50$ .

With high viscosities, encountered in crystallization processes leading to high solids concentrations or treating non-Newtonian suspensions (up to 1000 Pa s), only positive displacement impellers such as the Paravisc or helical ribbon agitators can ensure a sufficient degree of homogeneity. Even at extremely low Reynolds numbers, a circulating flow throughout the entire process space is achieved. At Schmidt numbers  $Sc > 10^4$  and viscosities  $\nu > 5 \times 10^{-3} \text{ m}^2/\text{s}$ , the

macroblend time in the laminar range can, according to Geisler [4], be estimated from the relation

$$\theta \approx 1000(\nu/\bar{\varepsilon})^{1/2}. \quad (13.15)$$

In contrast to turbulent mixing, in the laminar range the microblend time is identical with the macroblend time. In the laminar range  $Ne \sim Re^{-1}$ , that is,  $Ne \cdot Re = \text{const}$  applies in the laminar zone (see Equation 13.5), when scaling up with  $P/V = \text{const}$ . The same rotational frequency  $n$  must be used on a commercial scale as on a model scale. This also means, however, that the same blend time is achieved on both scales, and is therefore in agreement with Equation 13.15.

## 13.6

### Suspending

Suspending of solids is the basic mixing task for any agitated crystallization process. Technical applications cover a wide range of various suspending tasks. Particle size distribution, viscosity of the solvent, and the density difference between solids and solution mainly influence the settling behavior of a suspension. The settling rates of particles are found mostly between 0.001 and 0.1 m/s, while the solids content of the suspension can go up to values of 50 wt% [2].

Slow sedimentation of particles will occur, for example, in an activated sludge or in fine particle catalyst suspensions. For those kinds of systems, a homogeneous distribution of solids is characteristic. Here, the liftoff from the vessel bottom as well as the state of a homogeneous suspension can be achieved with a comparably low power input or only slight movement of the liquid. On the other hand, at higher solids concentrations a pseudoplastic flow characteristic of the suspension can occur. As an example, concentrations of only 6% of fibrous material – typically known from paper industry – can lead to this non-Newtonian behavior. Frequently observed in suspensions with high solids concentrations is a Bingham plastic behavior. In this case, if a certain amount of shear is not introduced by agitation, the system behaves like an elastic solid body or a gel.

In this chapter, solid/liquid systems are treated, where the particle size and the density difference between both phases are large enough and at the same time the liquid viscosity is low enough. Due to gravitation and presumably also due to inertial forces generated by the flow scheme in those systems, both phases tend to separate. The power needed to lift the particles off the bottom and keep them homogeneously suspended has to be introduced by the agitator.

#### 13.6.1

#### Suspending Criteria and Different States of Suspension

For a given agitated suspension, we discriminate between various states that are shown schematically in Figure 13.7, where the degrees of suspension “on-bottom motion,” “off-bottom suspension,” and “visually uniform suspension” are illustrated.

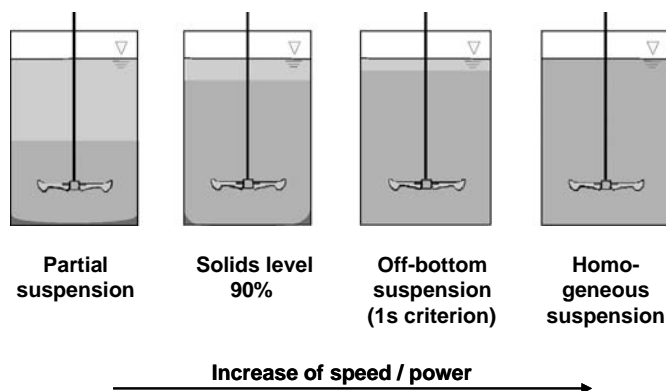


**Figure 13.7** Various states of suspension.

With “on-bottom motion” although most of the solids are in motion, large clear (i.e., particle-free) zones can occur in the upper part of the vessel. Temporary deposits of solids are tolerated underneath the impeller and in the corners.

“Off-bottom suspension” defines a condition in which individual particles never come to rest for longer than a second at the bottom of the vessel. Zwietering was the first to work with this visual suspension criterion. He determined minimum shaft speeds  $n_{js}$  ( $js$  = just suspended) at which this condition first occurs. The off-bottom suspension point can be determined by methods such as the ultrasonic Doppler anemometer, which do not, however, take into account the uniformity of distribution in the vessel. This means that particularly with particles with high settling velocities, even when the criteria “on-bottom motion” and “off-bottom suspension” are fulfilled, there are often clear zones near to the liquid surface containing no particles. In these cases, a further assessment process is employed, the so-called “layer thickness criterion,” at which the layer of particles in suspension has reached 90% of the height of the liquid.

In contrast, “visually uniform suspensions” have no large clear zones. In this condition, settling of the coarser particles can still occur, if, for example, there is a wide range of particle sizes, even though the fine particle fraction is already held in suspension near the liquid surface. If “visually uniform suspension” is used as the sole criterion, the shaft speed required to achieve it can therefore be higher or less than that for “off-bottom suspension.”

For the more demanding suspension duties, for example, continuously operated equipment with an overflow of the suspension, a “uniform suspension” is required. To achieve this, both the “1 s criterion” at the bottom of the vessel and the “visually uniform suspension” criterion must be fulfilled.

The ideal case of a “homogeneous suspension” can only be reached if the settling velocity of the particles approaches a value of zero. As a rule for a standard crystallization process, normally local differences in solids concentration cannot be avoided.

For characterizing the homogeneity of a suspension, usually the deviation of the local solids concentration from the average solids concentration is used. As a value for the distribution quality, the variance

$$\sigma^2 = \frac{1}{k} \sum_{j=1}^k \left( \frac{\varphi_{vj}}{\varphi_v} - 1 \right)^2 \quad (13.16)$$

or the variation coefficient  $\sigma$  is used. In this correlation,  $k$  is the number of different measuring positions. For a homogeneous suspension, the variance value  $\sigma^2 = 0$  is obtained.

In literature for the characterization of a suspension, mainly the above-mentioned criteria are found. This leads to the question, which is the link to the corresponding shaft speeds and to the corresponding power for suspending. Figure 13.8 illustrates for various solids concentrations how the solids level changes with shaft speed [5]. In addition, the shaft speeds are given at which the “1 s criterion” is just fulfilled. Obviously, to fulfill the “90% solids level criterion,” higher shaft speeds are required than for the “1 s criterion.”

At the same time, it is obvious that with reduced solids concentrations it becomes easier to reach a certain solids level in the vessel. From experimental work of other authors, it can be derived that under certain circumstances the “90% solids level criterion” had been fulfilled, but with a certain amount of solid material still remaining on the bottom of the vessel.

Generally, the comparison of shaft speeds determined from both criteria is not consistent and can only be derived qualitatively. The same conclusions can be drawn from comparisons of a certain distribution quality with the solids level. The corresponding correlations given in the literature are only valid for certain systems or regimes and therefore cannot be generally used.

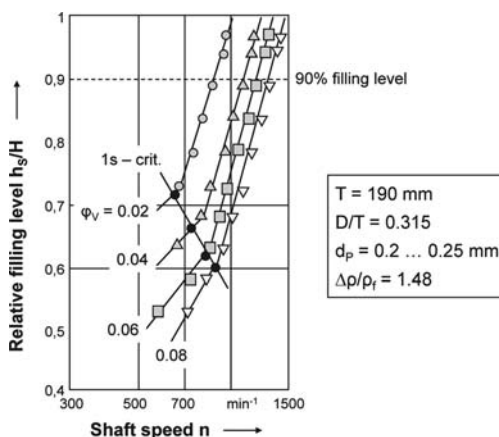


Figure 13.8 Solids level versus shaft speed for various solids concentrations.



### 13.6.2

#### Power Requirement for the Suspension of Solids

At higher Reynolds numbers ( $>10^4$ ), the impeller causes high flow velocities, which leads to the effect that solid particles with higher densities than the liquid are driven outward due to centrifugal forces. Due to this phenomenon, the flow pattern around the impeller as well as the power number  $Ne$  does not differ from one-phase operation, as long as the solids concentration remains smaller than 10 wt%.

For higher solids contents, the situation is not as simple. Figure 13.9 shows the power number  $Ne$  versus Reynolds number  $Re$  for solid volume concentrations between 0 and 0.29. The higher the solids concentration, the earlier the impeller acts within the suspended phase. Especially at low shaft speeds or Reynolds numbers, the solids concentration around the impeller is much higher than the average, as the particles are not completely suspended. With increasing shaft speed, the solids concentration around the impeller decreases – together with that the power number also decreases. As soon as the impeller runs clear, the power number of the one-phase system will nearly be reached. Due to the fact that not all of the solids have been lifted off the bottom at this point, for a further increase in shaft speed the power number rises again. Roughly correlating with the state of “off-bottom suspension,” the power required correlates with the density difference between solids and solution.

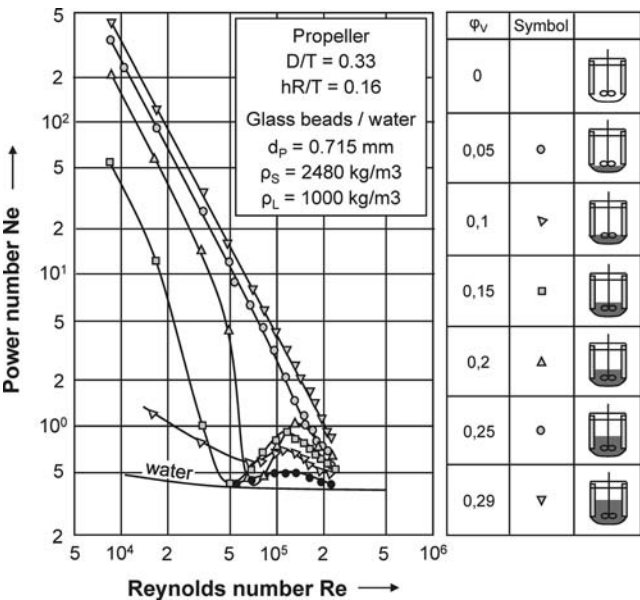


Figure 13.9 Power number  $Ne$  versus Reynolds number  $Re$  for various solids concentrations [6].

## 13.6.3

**Models and Mechanisms for the Suspension of Solids**

Suspension of solids can be divided into two main tasks:

- lifting the particles off the vessel bottom;
- keeping the particles suspended.

Despite that for these phenomena there are numerous models and theoretical approaches, there is no basic agreement to be found. The main difference between the models is based on the prediction of the power input necessary for large vessels, where significant points differ from one approach to another [7,8]. The reason for this is that there are only few data from large vessels and that measurement methods in this case are not so easy to apply.

The following mechanisms have been taken into account for lifting off the particles and therefore to describe the state of “off-bottom suspension”:

- The liftoff of the particles results from the forces resulting from resistance forces provided by the liquid flow profile close to the vessel bottom, which have to be larger than gravity forces diminished by buoyancy, to provide a particle liftoff (Figure 13.10) [1]. An important prerequisite for describing this effect is the knowledge of the velocity profile close to the vessel wall.
- The second model is based on turbulence theory [9]. Following this theory, particles lift off due to interaction with eddies occurring close to the wall. So the kinetic energy of the eddies is partially transferred into potential energy of the particles. As a consequence, they rise up from the bottom and are entrained by the continuous flow profile. A basic difficulty in this model is the unknown influence of solids concentration, particle size, and viscosity on the intensity of turbulence close to the vessel wall.

In order to keep the particles suspended and reach an “off-bottom suspension,” there are two different models:

- It is assumed that the power for suspending the particles results from the power necessary to keep the particles away from the bottom together with the power

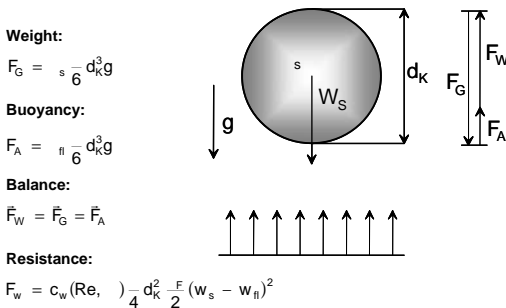


**Figure 13.10** Scheme of settling and suspending forces on the particles.

necessary to keep up the continuous flow profile [10]. But frequently the power for keeping up the continuous flow – which at the same time is not easy to be determined – is neglected compared to the effect of settling. This may lead to a failure in the description especially for low particle concentrations when the settling power is low.

- b) The settling velocity of the particles and the medium flow velocity upward in the opposite direction are equalized. Here the determination of the upflow velocity turns out to be difficult. It is hard to determine for pure liquids already and the published circulation numbers [11] significantly shift with solids concentration.

#### 13.6.4

#### Determination of the Shaft Speed Necessary for Suspending

Again very different approaches can be found in this field, delivering various models for correlation or calculation. The reasons for this are

- a) the very hard availability of solids with a defined form but different physical properties at the same time for experiments beyond laboratory scale;
- b) the different measurement methods used during the experiments;
- c) the different choice and interpretation of suspending criteria (Figure 13.7).

Nevertheless, some general conclusions can be drawn, concerning the following parameters that have to be considered:

- 1) Physical parameters of liquid and solid:
  - liquid density;
  - liquid viscosity;
  - solids density;
  - particle size;
  - particle size distribution;
  - particle shape.
- 2) Overall solids concentration.
- 3) Geometry:
  - type of impeller;
  - bottom clearance of agitator;
  - diameter ratio of impeller to vessel  $D/T$ ;
  - height of liquid level;
  - one- or multi-stage impeller.
- 4) Scale.

Among the models for calculation of the shaft speed needed for suspension, the equation of Zwietering [12] is based on numerous experimental results. The shaft speed necessary to reach a state where the particles are just suspended ( $n_{js}$ ) can be correlated as follows:

$$n_{js} = S \nu^{0.1} d_p^{0.2} \left( \frac{\Delta \rho}{\rho_f} \right)^{0.5} B^{0.13} D^{-0.85}. \quad (13.17)$$

In this equation,  $S$  is a dimensionless constant and characterizes the influence of agitator type together with the geometrical situation  $D/T$  and  $H/T$ . This equation can be chosen for calculations on small scale, if no special geometries have to be considered. Even when keeping up with these requirements, still deviations from experimental data larger than 20% can occur.

In the case of the distribution of solids all over the vessel, there is also a multitude of correlations, all of them based on the settling velocity of a single particle  $w_s$  or of the particles in collective  $w_{ss}$ . This settling velocity is described in relation to a circulation flow velocity inside the vessel.

According to [13], the minimum circulation flow velocity can be calculated as

$$w_{f,\min} \sim \sqrt[3]{\frac{\Delta\rho}{\rho_f} g T \varphi_v w_{ss}}. \quad (13.18)$$

With this correlation, the power demand for fulfilling the 90% solids level criterion

$$P_{90\%} = Ne \rho n_{90\%}^3 d^5 \quad (13.19)$$

related to the sinking velocity of the particles in collective

$$P_{set} = \Delta\rho g \varphi_v w_{ss} \frac{\pi}{4} T^3 \quad (13.20)$$

can be calculated as

$$\frac{P_{90\%}}{P_{set}} \frac{D}{T} = C_1 + \frac{C_2}{D w_{f,\min} / \nu^{3/4}}, \quad (13.21)$$

where  $C_1$  and  $C_2$  have to be determined for the corresponding geometry.

Independent of the regarded state of suspension or criterion, the following can be stated to the impact of significant parameters.

#### 13.6.4.1 Physical Parameters of Liquids and Solids

Particle size in the state of a complete suspension has only a slight impact on shaft speed (Equation 13.17). When the solids level criterion is applied at lower particle sizes, there is a more significant dependence. Changes in viscosity are of a minor relevance as soon as they occur in a range  $<100$  mPa s. Hence, for the density the following correlation to shaft speed is found:

$$n \sim \left( \frac{\Delta\rho}{\rho_f} \right)^{x_1} \quad \text{with } 0.4 \leq x_1 \leq 0.7. \quad (13.22)$$

#### 13.6.4.2 Solids Concentration

The solids fraction only slightly influences the necessary shaft speed for suspension, as shown in Equation 13.17 and in Figure 13.8. When applying the 90% solids level criterion, the influence is more significant. The viscosity behavior of the suspension usually remains Newtonian up to a fraction range of 0.25–0.3.

### 13.6.4.3 Geometry

There is a very high dependence on diameter ratio  $D/T$ . Independent of the state of suspension, the following is obtained:

$$n \sim \left(\frac{D}{T}\right)^{-x_2} \quad \text{with } 0.9 \leq x_2 \leq 1.5. \quad (13.23)$$

In practice, a diameter ratio  $D/T$  of 0.3–0.4 is frequently chosen due to being close to the energetic optimum [1].

The most important impact on the power input necessary for suspension comes from the impeller type. Axially working impellers are the most economic tools for suspending. A comparison of a Viscoprop impeller with a Rushton turbine shows that the Viscoprop impeller is able to reach the same result with less than 1/3 of the energy consumption. It has to be considered that for shear-sensitive particles such as needle- or plate-shaped crystals the power input is of less importance than particle exposure to the local specific energy dissipation rate.

Multistage agitation systems do not lead to a reduction of the necessary shaft speed for suspending, but the power input increases with the number of stages.

### 13.6.5

#### Distribution of Solids

The radial distribution of solids in a vessel turns out to be nearly uniform. In contrast to this, significant differences occur regarding the profile over the height of the vessel as Figure 13.11 shows. This distribution is characterized by a concentration maximum just above the stirrer. This is valid for radial as well as axial pumping organs. Above the maximum, there is a significant decrease in solids concentration, with a pronounced solids level.

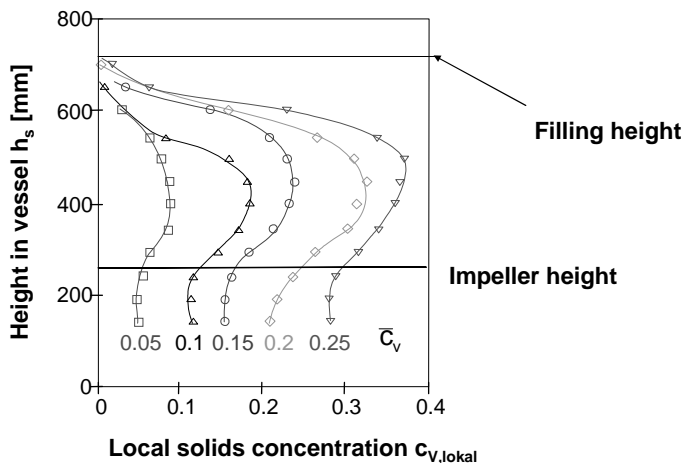


Figure 13.11 Local solids concentrations over the vessel height.

With increasing shaft speed, the concentration profile homogenizes. Nevertheless, a complete suspension with a completely homogeneous solids distribution cannot be reached in reality.

For the operation of agitators in a continuous crystallization process, this means that the draw-off point for the particle suspension has to be chosen carefully. To reach conditions close to an ideal mixed tank reactor, the combination of agitation and draw-off has to guarantee a constant solids concentration and together with that a stable particle size distribution.

### 13.6.6

#### Influence on Mass Transfer

For the crystallization process, mass transfer from the liquid phase to the solid phase is of great importance. The influence of the complete suspension for mass transfer is illustrated in Figure 13.12.

### 13.6.7

#### Influence on Blend Times

As soon as solids appear in the stirred vessel, they have a significant influence on blend time. The correlations known from one-phase operation lose their validity in the presence of a solid phase [14]. In Figure 13.13, the influence of solids concentration is visualized when dealing with solids concentrations larger than  $x_s = 0.1$ . Results are presented for both cases, one-phase and two-phase media. As

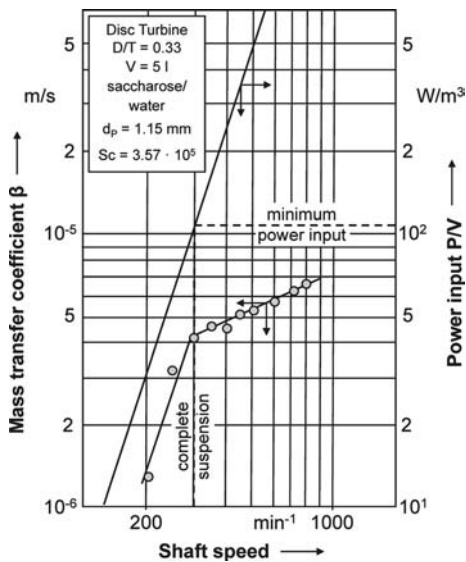


Figure 13.12 Dependence of mass transfer coefficient on power input and shaft speed.

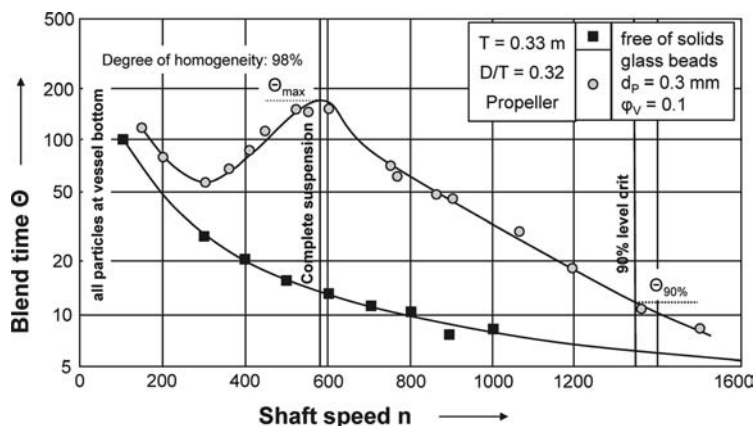


Figure 13.13 Influence of a solid phase on blend times.

soon as particles lift off the vessel bottom, the blend time increases significantly compared to only liquid-phase operation. The maximum blend time that is found at complete suspension can be up to 10 times longer than that for the corresponding case with only a liquid phase. Especially in the clear liquid on top of the solids level, blend time increases dramatically. But as soon as the 90% solids level criterion is fulfilled, both blend times differ only by a factor of 2.

The above-described effect is caused by the power needed for suspending the particles not being available for keeping up the continuous flow. As this flow is slowed down, the blend time consecutively increases. As it has been found in experimental investigations [15], micromixing processes are not influenced as long as the solids content in the vessel does not increase above  $x_s = 0.05$ .

### 13.7

#### Scale-Up of a Crystallization Process

If similarity theory is applied correctly, the dimensionless numbers and characteristics that are determined are independent of the scale. This makes it possible, by using appropriate scale-up rules, to specify the operating parameters for industrial-scale systems from the results of tests carried out on models. Computational fluid dynamics (CFD) can be used to visualize the impeller system at its full scale, thus contributing to solving scale-up problems.

As in practice “complete similarity” can hardly ever be achieved, scale-up procedures must nearly always confine the analysis to those aspects that are of more importance for the process. The set of graphs shown in the “Penney diagram” (Figure 13.14), in which each straight line represents a scale-up criterion, illustrates the problems involved.

The cubic scale factor  $\mu^3$  is used to convert the ratio of the power per unit volume from the industrial scale to the model scale. Each of the straight lines results from a combination of the power equation with different scale-up criteria. Taking the

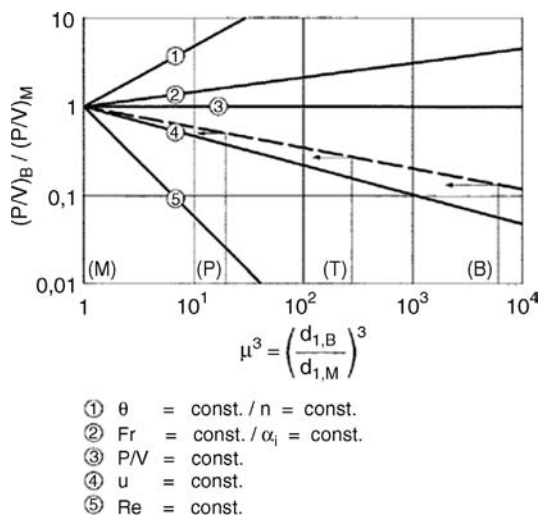


Figure 13.14 Penney diagram.

criterion for a constant blend time ( $\theta = \text{const}$ ) as example, this is described for the zone of turbulent flow.

In a similar way, all the other straight lines can be determined by combining the power equation with other elements such as the Froude number ( $Fr \propto n^2 d_2$ ), the Nusselt equation ( $\alpha_i \propto d_2^{1/3} \propto n^{2/3}$ ), the Reynolds number ( $Re \propto n d_2^2$ ), and so on.

### 13.7.1

#### Model Tests

If a pertinent criterion for a scale-up cannot be arrived at empirically or on the basis of “theoretical considerations,” in particular inferences by analogy, it is necessary to carry out agitator tests on at least two scales in order to determine the relation  $P/V = \mu^x$ . The following table gives typical vessel sizes, the corresponding data in each case being plotted on the Penney diagram (Figure 13.14).

Table 13.1 Compilation of different scale-up criteria for suspending.

$\theta = \text{const}$	Specified scale-up criterion
$n\theta = \text{const}$	Rule from the blend time characteristic; see Section 13.5
$n = \text{const}$	Consequence of the conditions 1 and 2 above
$P = Ne\rho n^3 d_2^5$	Power equation
$P \propto n^3 d_2^5$	Same agitator system on model and industrial scales: $Ne = \text{const}$ ; same product: $= \text{const}$
$P/V \propto n^3 d_2^2$	Since $V \propto d_2^3$
$P/V \propto d_2^2 \sim \mu^2$	Consequence of 3 above



## 13.7.2

**“Scale-Up” Rules**

For many years, the pivotal criterion for scale-up to industrial dimensions was the relation  $P/V = \text{const}$ . As can be seen from the Penney diagram, this unavoidably violates all the other criteria. This is particularly noticeable with the criteria  $\alpha_i = \text{const}$  and  $\theta = \text{const}$ , since maintaining the power per unit volume at a constant value on an industrial scale results in a worse heat transfer and a considerably longer blend time. For scale-up, the “key criteria” must always be considered, that is, the minimum number of criteria that must be satisfied on both scales. In all cases, however, an adequate degree of compliance with geometric similarity is mandatory, since by convention all system dimensions relate to *one* characteristic parameter (impeller diameter  $D$ ) when calculating the dimensionless numbers. The following essential remarks apply to the various basic mixing tasks.

## 13.7.3

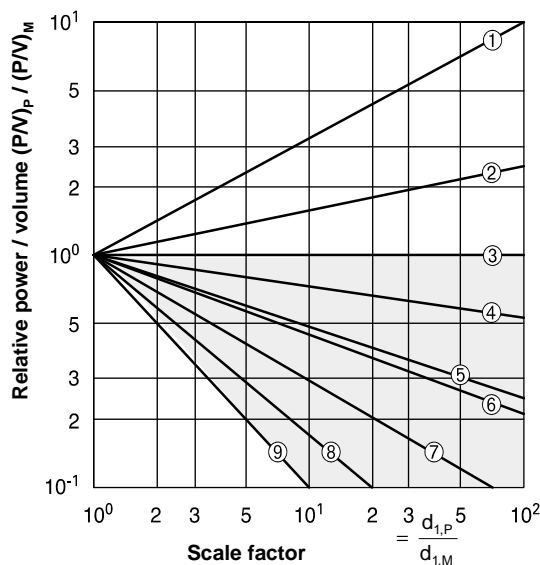
**Blending**

From the Penney diagram, it can be seen that for  $\theta = \text{const}$  it is necessary to increase the power input per unit volume by  $\mu^2$ . The effective power input therefore for a scale-up of  $\mu = 10$  is increased by a factor of  $10^5$ ! Following this rule to the letter would result in agitator systems with astronomical prices and alarming operating costs. In practice, however, it is nearly always unnecessary to apply this criterion, if the considerably longer batch times on an industrial scale are compared with the blend time necessitated by the process itself. If, for example, an increase in the blend time on industrial scale by a factor of 5 times that on a model scale can be tolerated, the required power input is only  $1/125$  of that which would have been necessary had the  $\theta = \text{const}$  rule been rigorously applied. In practice, the operating data for the industrial scale system are determined on the basis of the process specifications and the blend time is calculated using the blend time characteristic (see Section 13.5). If shorter blend times are necessary for particular reasons, appropriate measures may be taken (e.g., increased shaft speed, impeller systems suitable to improve blending) to achieve this.

## 13.7.4

**Suspension**

With suspending duties, the criteria for the scale-up of operating data from the model scale to an industrial scale are strongly dependent on the product involved (Figure 13.15) [1]. If particles with a high hindered settling velocity (large particles at a low concentration by volume and with a much higher density than the liquid) must be held in suspension, a criterion close to  $P/V = \text{const}$  must be selected. If, however, the hindered settling velocity is low (high concentration by volume, small particle diameter, low differential density), a criterion approximating to  $\mu = \text{const}$  can be considered as reasonable. Depending on the duty concerned,



①	Voigt, Mersmann, 1995	$d_k/d_2 > 3 \cdot 10^{-2}$	$P/V \sim d_1^{-1/2}$
②	Pavluschenka, Kostin, Matveev		$P/V \sim d_1^{-0.2}$
③	Kneule, 1983	$\mu > 10$	$P/V = \text{const.}$
③	Voigt, Mersmann, 1995	$d_k/d_2 < 1 \cdot 10^{-3}$	$P/V = \text{const.}$
③	Weisman, Efferding, Zlokarnik, Judat	$d_k/d_2 > 3 \cdot 10^{-2}$	$P/V = \text{const.}$
③	Kraume, Zehner, 1995	$Re_{ref} \geq 10^5$ *)	$P/V = \text{const.}$
③	Geisler, Buurmann, Mersmann; 1993	$d_k/d_2 < 3 \cdot 10^{-5}$	$P/V = \text{const.}$
④	Langhans, Liepe, Weißgräber, Eienkel		$P/V \sim d_1^{-0.13}$
⑤	Eienkel, 1979	$Re = 10^3 - 10^6$	$P/V \sim d_1^{-1/3}$
⑥	Eienkel, 1995	$\frac{w_{SS} \cdot d_k}{v} < 2 \cdot 10^3$	$P/V \sim d_1^{-0.38}$
⑦	Zwietering		$P/V \sim d_1^{-0.55}$
⑧	Müller, Todtenhaupt	$d_k/d_2 > 3 \cdot 10^{-2}$	$P/V \sim d_1^{-0.75}$
⑨	Kraume, Zehner, 1995	$Re_{ref} \leq 10^4$ *)	$P/V \sim d_1^{-1}$ $u = \text{const.}$
⑨	Geisler, Buurmann, Mersmann; 1993	$d_k/d_2 > 3 \cdot 10^{-4}$	$P/V \sim d_1^{-1}$ $u = \text{const.}$

$$*) Re_{ref} = \frac{d_1}{v} \cdot \left( \frac{\Delta p}{\rho_l} \cdot g \cdot d_1 \cdot c_v \cdot w_{SS} \right)^{1/3}$$

Figure 13.15 Scale-up criteria for suspending following various authors.

therefore, a broad spectrum of criterion from  $\mu = \text{const}$  to  $P/V = \text{const}$  may be relevant. There are therefore large differences in the power inputs required on an industrial scale.

Today, there is no reliable knowledge of the relationship available on this subject, and therefore no “design equations” based on the operating data and physical properties. It is only the accurate knowledge of the efficacy of the various agitator systems and rheology of the individual media based on results from model, pilot-scale, and industrial-scale systems that makes it possible to select the optimum scale-up rules to be applied. If relevant operational experience is not available, an extensive series of tests in vessels of different sizes must be carried out for the duty concerned.

### 13.7.5

#### Dispersing

With this process the main objective is to produce the same interfacial areas per unit volume on both scales, in order to achieve the same mass transfer. The analysis based on turbulence theory has been confirmed by the knowledge gained in practice in the form of the scale-up criterion  $P/V = \text{const}$ . This applies to dispersing processes in liquid/liquid and gas/liquid systems. Because of the numerous factors that influence the process (e.g., coalescence properties, physical properties of mixtures, anomalous flow characteristics, static pressure, etc.), substantial

deviations from the theoretical results occur on scale-up. It is therefore extremely rare that a reliable prediction of the mass transfer coefficients achievable on an industrial scale can be made.

#### 13.7.6

##### Heat Transfer

It is normal practice only to check out the heat transfer coefficient of the agitator system under consideration at its full-scale dimensions.

If the value of  $\alpha_i$  that is determined is insufficiently high, this can be improved by increasing the agitator power or - more efficiently - by providing additional heat transfer surfaces. For duties that require the vessel contents to be cooled an optimization problem arises, since although increasing the power per unit volume increases the film coefficient  $\alpha_i$ , this also means that the increased energy input from the agitator requires additional heat to be removed. Values of  $\alpha_i$  can be calculated using the heat transfer characteristic given in [1].

During scale-up, it must be taken into account that the vessel volume increases proportionately to the cube of the scale-up factor while the vessel surface area available for heat transfer increases in proportion to its square. If the scale-up is performed with a criterion "less" than  $\alpha_i = \text{const}$  due to process constraints ( $P/V \propto \mu^{0.5}$ ), the heat transfer capability is diminished not only due to the higher heat flux per unit area but also by the lower values of  $\alpha_i$ .

#### 13.7.7

##### Special Scale-Up Considerations

Once the process parameters and the rules for scale-up from the model dimensions have been determined by tests at various scales, the next step is to calculate the power rating for the industrial-scale system with the aid of the power characteristic. For Newtonian liquids this is no problem, in total contrast to non-Newtonian media, where the effective viscosity is always a function of agitator shaft speed [4].

A particular problem that frequently arises with suspension duties in very large stirred vessels with several side-entry agitators installed below the liquid surface is that on scale-up the volume increases in proportion to the cube of the linear scale-up factor whereas the surface area increases in proportion to its square. If the arrangement of the impellers found to give a certain rotary flow pattern for optimum suspension of the suspended solids at the model scale is retained at the industrial scale, a fundamentally different flow pattern would result that is totally unsuitable for suspension purposes. Particular account must be taken here of the fact that the secondary flow patterns in the large vessel are scale dependent on account of changed ratio of inertial to frictional forces. Other scale-up criteria derived from considerations of a theoretical free jet are required to achieve an optimum suspension of the particles.

On suspension duties in abrasive media, the anticipated erosion problem places a limit on the impeller tip speed. In this case, the properties of the agitated medium and the materials of construction place limits on the general applicability of the  $P/V = \mu^x$  scale-up rules.

A physical limit on the use of the  $P/V = \mu^x$  rule where  $x < 0$  occurs on suspension duties when from a certain scale-up factor  $\mu$  upward the agitator power input would in theory be less than the settling power of the solid particles. This cannot be the case when the energy balance is considered. An experienced agitator manufacturer has, however, sufficient practical data on agitated media, vessel size, and geometry to determine the lowest possible impeller tip speed.

On suspension duties, attention must also be paid to the fact that during plant shutdown the sediment buildup in large vessels is considerably higher, more densely compacted, and, depending on the medium involved, can also “set.” This means that restarting the system is much more problematic than on a pilot scale. In addition, the settling times depend on the scale involved.

### 13.7.8

#### Summary

The “traditional” recommendation for scale-up  $P/V = \text{const}$  must in many cases be regarded on account of the foregoing considerations as either insufficient or too conservative. It is a generalization that is inadequate to cover many areas of process technology.

An accurate knowledge of the product systems and the relevant process and agitator fundamentals nowadays enables “precision-made” scale-up rules to be used confidently with a minimum of effort.

The numerical simulation of flow, concentration, and temperature profiles can contribute to the solution of scale-up problems.

#### References

- 1 EKATO – The Book, Firmenschrift der EKATO Misch- und Rührtechnik, Schopfheim, 2012.
- 2 Matthias Kraume (Ed.) (2003) *Mischen und Rühren*, Wiley VCH, Weinheim.
- 3 Mersmann, A., Eienkel, W.D., and Käppel, N. (1975) Auslegung und Maßstabsvergrößerung von Rührapparaten, *Cem. Ing. Tech.*, 47, 23.
- 4 Geisler, Krebs, and Forschner (1994) Local turbulent shear stress in stirred vessels and its significance for different mixing tasks, 8th European Conference on Mixing, Cambridge (UK).
- 5 Eienkel, W.D. and Mersmann, A. (1977) Erforderliche Drehzahl zum Suspendieren in Rührwerken. *Verfahrenstechnik* 11.
- 6 Niesmak, G. (1982) Feststoffverteilung und Leistungsbedarf gerührter Suspensionen. Dissertation, TU Braunschweig.
- 7 Kipke, K. (1983) Anfahren aus abgesetzten Suspensionen. *Chem. Ing. Tech.*, 55.
- 8 Kraume, M. and Zehner, P. (1988) Suspendieren im Rührbehälter – Vergleich unterschiedlicher Berechnungsgleichungen. *Chem. Ing. Tech.*, 60.

- 9 Mersmann, A. and Werner, F. (1994) Theoretical approach to minimum stirrer speed in suspensions. 8<sup>th</sup> Conference on Mixing, Cambridge, IChemE Symposium, Series 136.
- 10 Eienkel, W.D. (1979) Beschreibung der fluiddynamischen Vorgänge beim Suspendieren im Rührwerk. VDI Forschungsheft Nr. 595.
- 11 Voit, H. and Mersmann, A. (1985) Allgemeine Aussagen zur Mindestdrehzahl beim Suspendieren. *Chem. Ing. Tech.*, 57.
- 12 Zwietering, T.N. (1958) Suspending of solid particles in liquids, *Chem. Eng. Sci.*, 8.
- 13 Kraume, M. and Zehner, P. (1995) Konzept zur Maßstabsübertragung beim Suspendieren im Rührbehälter. *Chem. Ing. Tech.*, 57.
- 14 Kraume, M. (1992) Mixing times in stirred suspensions *Chem. Eng. Technol.*, 15.
- 15 Guidardson, P. *et al.* (1995) Study of micro-mixing in a solid-liquid suspension in a stirred reactor. AIChE Symp. Series No. 305, Vol. 91.

## 14

### Downstream Processes

*Dierk Wieckhusen and Wolfgang Beckmann*

The unit operations of solid–liquid separation and of drying are closely linked to crystallization. A solid–liquid separation process can best be improved by changes in the habit and particle size distribution obtained in the crystallization step. The same holds for the drying process. Furthermore, both the solid–liquid separation and the drying step can have a pronounced influence on the crop, with respect to chemical purity, crystal size and degree of agglomeration, and solid-state form. Thus, crystallization and the downstream processes have a mutual interference.

#### 14.1

##### Transfer of Suspension and Filter Cake

During the transfer of the suspension from the crystallizer to the nutsche or centrifuge shear forces may have an impact on large, brittle crystals, especially if centrifugal pumps are used instead of pressure in the crystallizer. Also, the peeling in automated centrifuges can be critical in this respect and then centrifuge speed has to be reduced significantly in order to avoid breakage at that stage.

These effects are difficult to model, so a sampling scheme for the suspension from the crystallizer and after solid–liquid separation and drying is advisable.

#### 14.2

##### Solid–Liquid Separation

Depending on the task of the separation process, a large number of different types of equipment for the solid–liquid separation are available. Criteria for the selection are, *inter alia*, the filtration properties of the crop and the size of the particles, the suspension density, and the mode of operation, batchwise or continuous. Two main types of solid–liquid separations can be distinguished, cake forming filtration under pressure and centrifugation. In both cases, the crystals form a filter cake on a medium through which the mother liquor has to pass. The resistance is the rate-limiting step for the filtration and the characteristic property of the suspension.

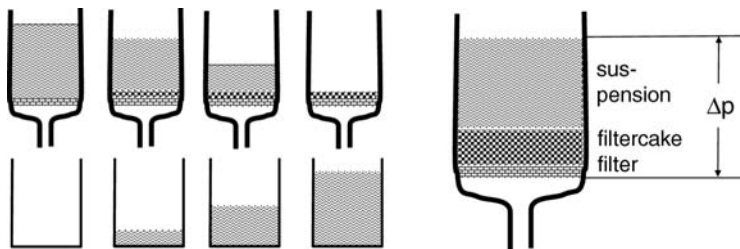


**Figure 14.1** Cake forming filtration of a suspension. The suspension is assumed to settle very slowly so that the cake is formed proportional to the amount of suspension filtered. The driving force for filtration is the pressure drop  $\Delta p$  over filter cake and filter cloth.

For suspensions with a low solid content, a thickening of the suspension, for example, in a hydrocyclone, can be advantageous. Some centrifuges need high suspension densities to work properly. In cases where the filter resistance of a suspension is high, a thickening can reduce the filtration time considerably.

#### 14.2.1

##### Cake Forming Filtration

The cake forming filtration in a nutsche type of apparatus is schematically shown in Figure 14.1. In case that the suspension does not sediment during the filtration, the height of the filter cake increases with the amount of volume filtered. The amount of mother liquor filtered is given by Equation 14.1. Integrating Equation 14.1 between  $V = 0$  at  $t = 0$  to  $V$  at  $t$  leads to Equation 14.2:

$$\frac{dV}{dt} = A \frac{1}{h} \frac{1}{\alpha} \Delta p \frac{1}{\eta} + \frac{1}{\beta}. \quad (14.1)$$

$\Delta p$  is the presser drop over the filter cake;  $h$  is the height of the filter cake and  $\eta$  the viscosity of the mother liquor. The characteristic properties  $\alpha$  and  $\beta$  are the resistance of the filter cake and of the filter cloth to the flow of mother liquor, respectively. It is the  $\alpha$ -value that characterizes the filterability of the crop.

Note that the filtration time quadratically increases with the suspension volume to be filtered; that is, doubling the amount of suspension will increase the filtration time by a factor of 4.

$$\frac{\mu \alpha V^2}{A} + \frac{\mu \beta V}{A} = \Delta p \cdot t. \quad (14.2)$$

By rearrangement Equation 14.3 is obtained. Plotting  $t/V$  versus  $V$  yields a straight line with a slope corresponding to  $\alpha$  and an intercept corresponding to  $\beta$  (Figure 14.4).

$$\frac{t}{V} = \frac{1}{\Delta p} \left( \frac{\mu \alpha}{A} V + \frac{\mu \beta}{A} \right). \quad (14.3)$$

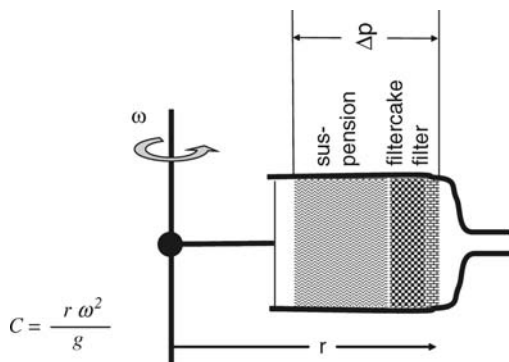


**Figure 14.2** Filtration in a centrifugal field. A close relationship exists in the pressure filtration, the only difference being the forced sedimentation in the centrifugal field. The entire amount of mother phase has to filter through the entire filter cake.

The permeability of filter cakes, as described by  $\alpha$ , can depend on pressure applied, the filter cake can be compressible, resulting in an increasing resistance with the pressure applied.

#### 14.2.2

##### Centrifugation

The most prominent difference between a nutsche and a centrifuge lies in the forced sedimentation of the filter cake (Figure 14.2). The entire mother liquor has to pass through the filter cake. The pressure drop over the filter cake is given by the height of the liquid above the filter cake and the centrifugal acceleration  $c \times h$ . At  $c = 2000g$ , a liquid height of 5 cm will result in a pressure of  $\Delta p = 10$  bar. This is the same order of magnitude as realized in pressure filtrations.

$$\dot{V} = \frac{1}{K} \cdot \frac{\varepsilon}{(1 - \varepsilon)^2} \cdot \frac{\Delta p \cdot dp^2}{\eta \cdot h} \cdot A. \quad (14.4)$$

Opposed to the pressure (or vacuum) filtration, the suspension immediately forced sediments so that the entire amount of mother phase has to filter through the entire filter cake. The filtration Equation 14.1 can be integrated to yield Equation 14.4.

#### 14.2.3

##### Characterization of Filterability in the Laboratory

The filterability of a suspension should be characterized as early as possible. For a first characterization, the resistance of the filter medium can be set as zero, that is,  $\beta = 0$ . In this case, the resistance  $\alpha$  is given by Equation 14.5.

$$\alpha = t \cdot \Delta p \cdot \frac{2/\eta}{m_T} \left( \frac{A}{V} \right)^2. \quad (14.5)$$



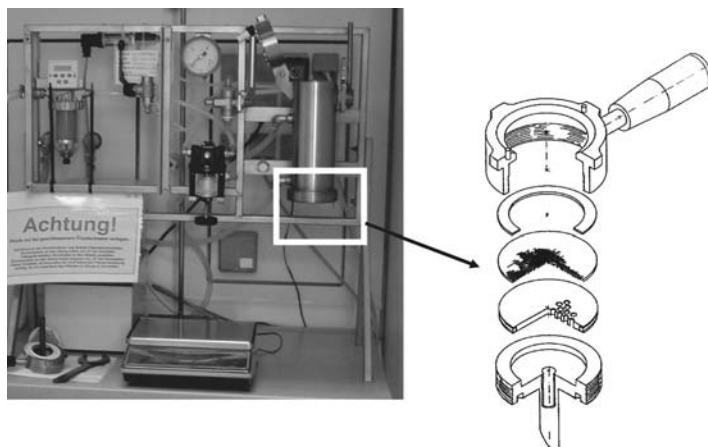


**Figure 14.3** Commercial pressure filtration apparatus and data acquisition unit to assess the full filtration curve following the VDI Richtlinie 2762. The media holder allows the testing of a large variety of filter media.

The parameters in the equations can, for example, be determined by a suction filtration, measuring the time  $t$  necessary to filter a certain volume  $V$  via a filter with the area  $A$ . The pressure drop is given by the difference between atmospheric pressure and the vacuum applied.

The filtration curve can be assessed by using a filtration apparatus as, for example, described in the VDI Richtlinie 2762. The filtered volume is determined as a function of time, allowing the calculation of both the resistance of the filter cake and the filtration media using Equation 14.3. The apparatus allows the testing of a variety of filter media (Figure 14.3).

The filter cake resistance typically ranges from  $10^{10} \text{ m}^{-2} < \alpha < 10^{16} \text{ m}^{-2}$ . For mother liquors with a viscosity in the vicinity of water, a resistance of  $\alpha \approx 10^{10} \text{ m}^{-2}$  can be regarded as an excellent filterability, values of  $10^{13} \text{ m}^{-2} < \alpha < 10^{14} \text{ m}^{-2}$  are borderline depending on the efficiency required and values of  $10^{16} \text{ m}^{-2} < \alpha$  can be regarded as insufficient. Note, that the cake height in these experiments should be at least on the order of 10 to 20 mm.

#### 14.2.4

##### Improving Filterability

The filterability of a filter cake can best be improved by changing the properties of the crystals. By plotting the filtered volume  $V$  as a function of time in the form  $t/V$  versus  $V$  (Equation 14.3) different cases, lab and plant, as well as different crystallizations can be compared.

As an example, the filterability of a certain moiety crystallized in the plant and lab and under different conditions is plotted in Figure 14.4. In the upper curves, the difficulties encountered in the plant are scaled down; nevertheless, the reduced curves are comparable. In the following, the crystallization was changed

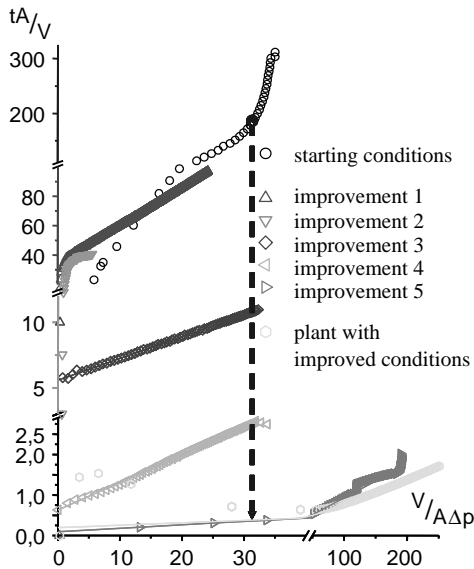


**Figure 14.4** Plot of the filtered volume  $V$  as a function of time in the form  $t/V$  versus  $V$  (Equation 14.3). Different cases, lab and plant, as well as different crystallizations are

compared. Note that by reducing the volumes of mother liquor by the area of the filter unit, different scales can be compared.

in several steps, whereby the filter cake resistance is successively reduced, until the product having the lowest resistance, lowest curve, is obtained. Upon transfer to the plant, a comparable curve is obtained. Note that by reducing the volumes of mother liquor by the area of the filter unit, different scales can be compared.

In certain cases, filter aids can be used to improve the filterability of a suspension. These filter aids are normally added to the suspension prior to filtration and thereby improve the permeability of the filter cake. It is also possible to put a layer of these aids onto the filter medium.

Particle shape and particle size are often linked to the permeability of the filter. Figure 14.5 shows such a clear-cut example. However, cases of large plate-like crystals are known that still have an acceptable filterability. Thus, a determination of the filter resistance is highly recommended.

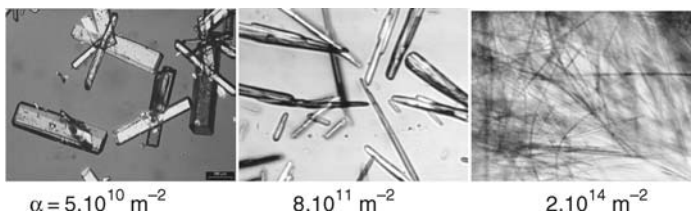


**Figure 14.5** Influence of particle size and shape on the permeability of the filter cake.

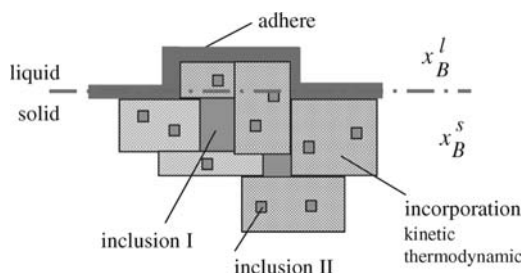


**Figure 14.6** Different mechanisms of impurity inclusion in crops. The impurities can form a complete or partial solid solution, can form inclusion within the crystals and between agglomerated crystals, and finally can adhere to the surface of the crystals. Only adhering impurities and inclusions I are accessible to the washing process.

#### 14.2.5

#### Washing

Impurities are partially or completely rejected during the crystallization process, depending on the kinetic and thermodynamic phase diagrams and whether a partial or complete solid solution is formed or not (cf. Chapter 7). These are impurities that are incorporated into the crystal. In addition, impurities are carried by inclusion of mother liquor between crystals, as the so-called Zwickelflüssigkeit. Finally, the crystals are covered by an adhering layer of mother liquor (Figure 14.6).

For the washing process, only the adhering mother liquor and the mother liquor included between agglomerated crystals are accessible to the washing process. It is important to note that the amount of mother liquor and washing liquor retained by the filter cake and that is carrying impurities into the finished material carrying impurities and to be treated in the washing operation differs between a nutsche and a centrifuge. The moisture content after nutsche will be on the order of 40–60%, while after centrifugation 10–20% residual moisture is typical. Two types of washing, displacement and dilution washing, have to be distinguished, the latter being either on the apparatus or as digestion.

The decrease in impurity level in the filter cake for a displacement washing is shown in Figure 14.7 as a function of the amount of washing liquid used. The amount of washing liquid is referenced to the filter cake volume. Usually, the impurity content drops considerably after 1.5 volumes of washing liquid per volume of filter cake.

### 14.3

#### Drying

A large variety of equipment for drying is available. The selection criteria are beyond the scope of this book. However, in general, agitated dryers and static dryers have to be differentiated, namely, due to their different potential effects on the crop. In the following, drying aspects related to the properties of the crop are discussed.

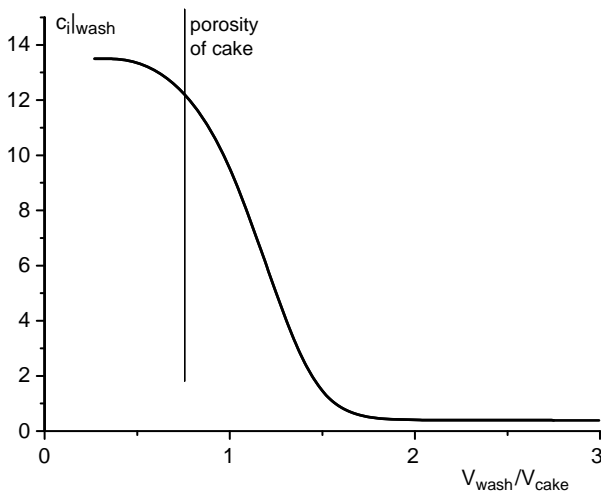


**Figure 14.7** Decrease in impurity content of the filter cake with the amount of washing liquid used for a displacement washing. The amount is referenced to the filter cake volume. Typically, 1.5 filter cake volumes suffice to remove impurities stemming from adhering mother phase.

#### 14.3.1

##### Phases of the Drying Process

Three phases of the drying process are distinguished: I, II, and III. In phases I and II, the mother liquor, first as bulk and second as adhering liquid, is evaporated. This evaporation occurs at the temperature and pressure close to the equilibrium vapor pressure of the mother phase (see Figure 14.8).

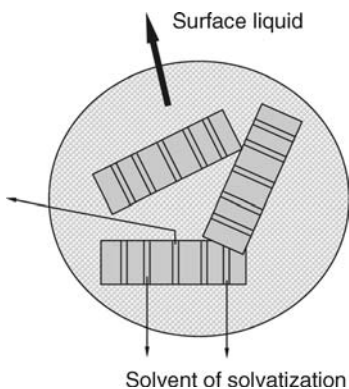


**Figure 14.8** Schematic representation of the liquids evaporated, dried in the drying phases I–III. In phases I and II, surrounding and adhering liquid is removed via evaporation.

In phase III, bound liquid such as solvents bound as solvates or water bound as hydrate is removed.

In the third phase, bound liquids, that is, solvates bound in solvates or water bound in hydrates, are removed, the drying is discussed in detail below.

### 14.3.2

#### Drying of Hydrates and Solvates

For the drying of systems that can form hydrates or solvates, two tasks can be differentiated: (i) removal of the solvent and (ii) keeping the level of solvatization or drying to a certain state of solvatization.

The removal of the solvent of solvatization requires pressure conditions lower than the equilibrium vapor pressure relationship. Furthermore, it is kinetically limited by diffusion of the solvent through the crystals, often through channels on the molecular scale. Moreover, the solvent can be located at isolated lattice sites, necessitating a reconstruction of the lattice.

For the hydrate of caffeine, that crystallizes in elongated platelets it was shown that the drying of this hydrate proceeds from the end faces of the platelets into the crystal. The direction is identical with the channels in which the water molecules are located in the crystal.

The drying of solvates and hydrates is often very destructive, that is, the starting crystals appear nice and transparent, while the product after the drying appears nontransparent. This effect is also sometimes used to comminute the crop.

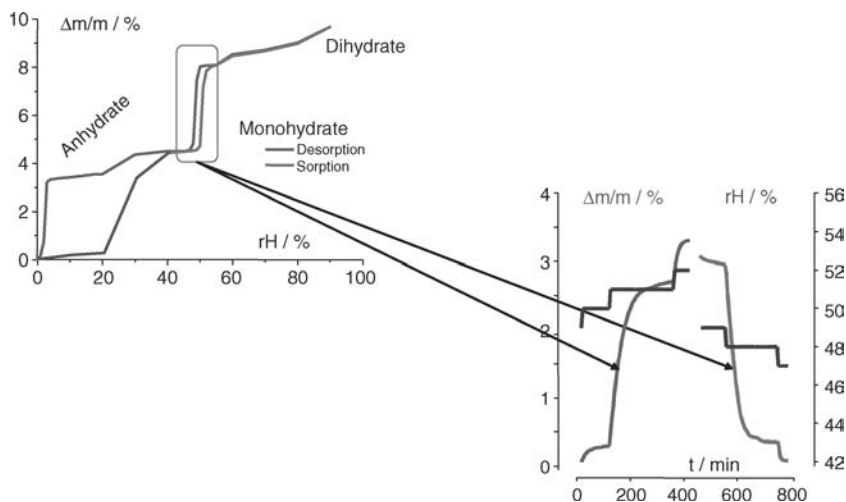


**Figure 14.09** Results of a DVS measurement of the uptake and loss of water as a function of relative humidity. The system exemplified can exist as anhydrate and also as a monohydrate and dihydrate. Note the large hysteresis

between the anhydrate and monohydrate. Between the monohydrate and dihydrate, the hysteresis is close to nonexistence and the kinetics of the uptake and loss of water are fast (right part).

The kinetics of desolvatization can best be discussed in a  $\Delta m/m$  versus RH diagram (Figure 14.9). Depending on the system and even on the stage of hydration, large hystereses of typically several tens of percentage in relative humidity are observed, indicating a high driving force necessary for removing the solvent.

When a certain hydration state is required, the stability regime of this solvate can be deduced from Figure 14.9. In the specific case depicted, the monohydrate is thermodynamically stable at least between 20 and 40% RH. However, the loss of water of the monohydrate to the anhydrate occurs only at a relative humidity of <5%. Thus, to obtain the anhydrate, the relative humidity must be below 5%, which can be difficult to reach by technical vacuum pumps, so purging the humid atmosphere, for example, with nitrogen might be advisable.

The arguments for hydrates also hold for solvates, the only difference being the typically higher vapor pressures of organic solvents.

The kinetics of desolvatization can depend on the solvent of solvatization. For a system forming both a solvate and a hydrate as well as an anhydrate, it has been observed that the solvate does not easily desolvate upon drying, while the hydrate is easily dried to anhydrous. Finally, as the change of solvatization from the solvate to the hydrate is also fast, the process of drying is best carried out via a resolvatization to the hydrate and subsequently drying of the hydrate (cf. Figure 14.10).

On the other hand, if the monohydrate is required, the drying can be done either at a relative humidity above 0%, which is difficult to control, or by using a purge gas with controlled humidity (Figure 14.11). If the drying is under reduced pressure, the relative humidity of the purge gas before being introduced into the dryer can be calculated as  $RH|_p = (1013 \text{ mbar}/p)RH|_{1013 \text{ mbar}}$ .

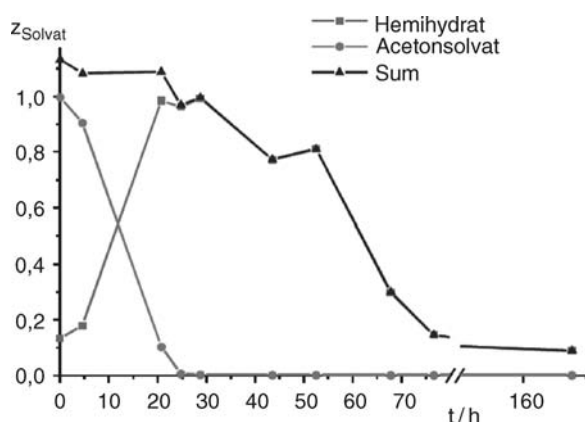


**Figure 14.10** Drying of a solvate to the anhydrate via an intermediate resolvatization to the hydrate, which dries much faster. After the change in solvation state, the drying starts at 40 h.

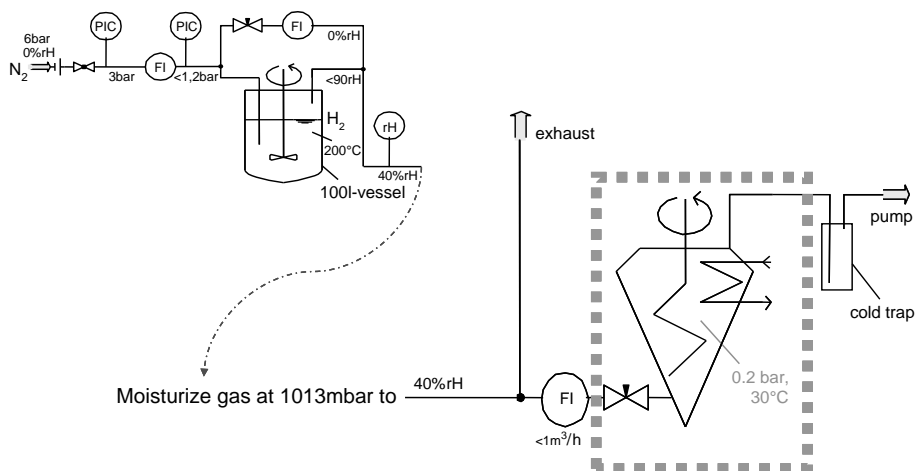


**Figure 14.11** Humidification of the purge gas to actively control the hydrate state of a hydrate during drying.

### 14.3.3

#### Characterizing the Drying Behavior in the Laboratory

The kinetics of the drying process can be assessed in the laboratory by a thermobalance (Figure 14.12). It allows monitoring the weight loss of a sample over time while varying temperature as well as pressure. This directly corresponds to the process foreseen on a larger scale in an industrial dryer. It is possible to characterize the drying behavior with a few grams of wet cake.

The sample is heated in vacuum and the mass loss is recorded. Figure 14.13 shows such a trace. The free mother liquor is evaporating at a pressure of 100 mbar, while a pressure of  $\leq 10$  mbar is required in the final drying stage.

The results can be used to assess the vacuum necessary to achieve a certain solvatization state. However, it must be emphasized that the drying characteristic obtained is due to kinetic effects.

### 14.3.4

#### Amorphization during Drying

A partial or complete amorphization can occur during drying, either via a desolvatization or by a mechanical action.

It has been observed in many cases that the thermal desolvatization results in a partial or complete amorphization. It should be noted that this process does not need to be upscalable.

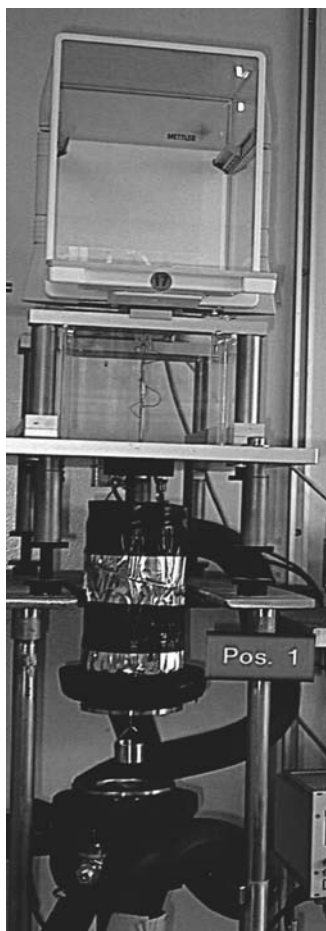


**Figure 14.12** Thermobalance to assess the drying behavior of a sample in the laboratory. The filter cake is placed on a balance in a heatable vacuum chamber suspended at a balance.

The mechanical action in a nutsche type of dryer has been observed to lead to a partial amorphization.

#### 14.3.5

##### **Effect of Drying on the Particle Size Distribution**

Static and agitated dryers can have an influence on the particle size distribution of the product.



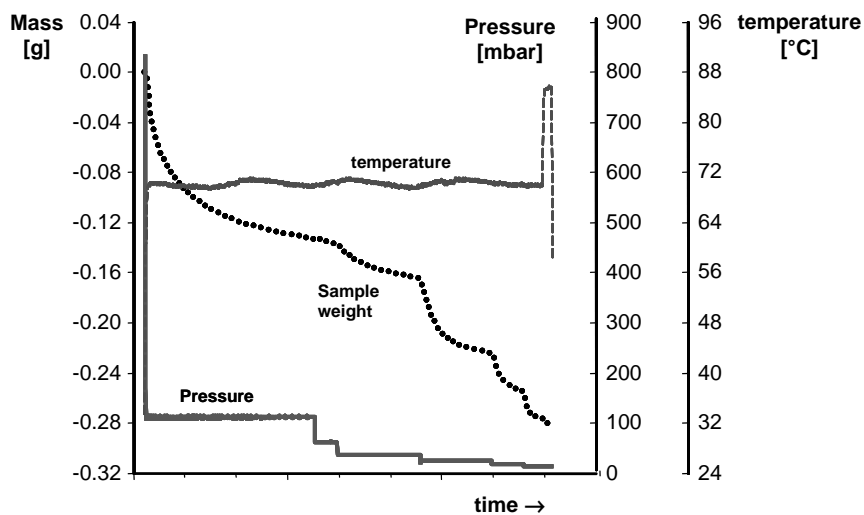


**Figure 14.13** Result of a thermobalance experiment. As a function of time, the loss in mass is recorded. Note that the pressure is ramped with time, while the temperature is kept constant.

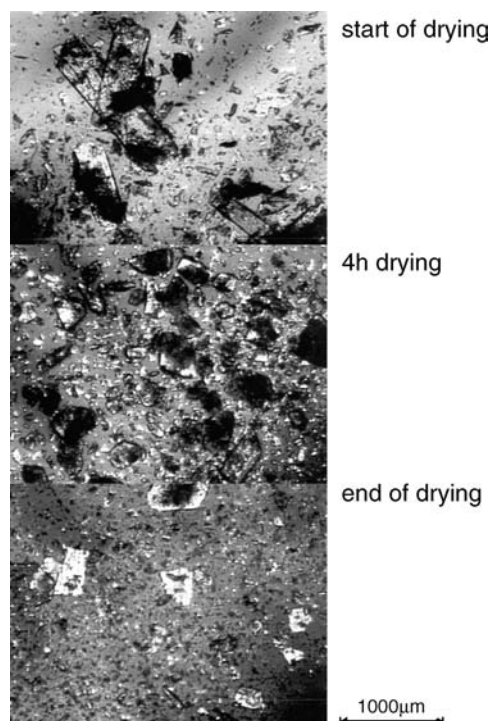


**Figure 14.14** Micrographs of a crop at the start of the drying process through 19 h drying in an agitated dryer. The crystals grown are thin and fragile platelets, see article in the topmost micrograph. The comminuting effect is evident.

In static dryers (tray drier), particles can agglomerate, especially if adhering mother liquor or wash contains dissolved matter that can form solid bridges during drying. For small particles, the liquid bridges can be strong enough to bring these particles into close contact leading to strong Van der Waals interactions that will remain after drying. The crystallization of residual amounts of solute in the liquid will also cement the agglomerates. In these cases, deagglomeration or delumping may be necessary to obtain the desired product.

In agitated dryers, the movement of the drying bed can lead to abrasion that can have an effect on the particle size distribution of the dried material. Especially if the cake is still wet, mechanical forces, for example, in a paddle dryer or in a stirred nutsche dryer can be large. Besides abrasion, breakage can occur. Figure 14.14 shows micrographs for the development of a crop from the start of the drying to the end after 19 h in a shovel dryer. The starting material is comprised of large, thin platelets that turn out to be fragile and that are comminuted to a size on the order of 10–20  $\mu\text{m}$ .

On the other hand, the movement in agitated dryers can also lead to the formation of agglomerates of considerable size (Figure 14.15).

It is thus important to understand whether and when stirring needs to be applied in an agitated dryer. In many cases, the latent heat in the wet filter cake can be used to remove most of the solvent just by pulling vacuum without stirring. Toward the end of drying when the filter cake gets really cold, mechanical stirring is necessary to bring in the heat for the evaporation of the remaining solvent.

A prediction of the stress to be expected in large-scale dryers is extremely difficult. Small-scale nutsches are available, while paddle dryers have to be custom-made, one example is shown in Figure 14.16.



**Figure 14.15** Formation of agglomerates of considerable size in an agitated dryer.

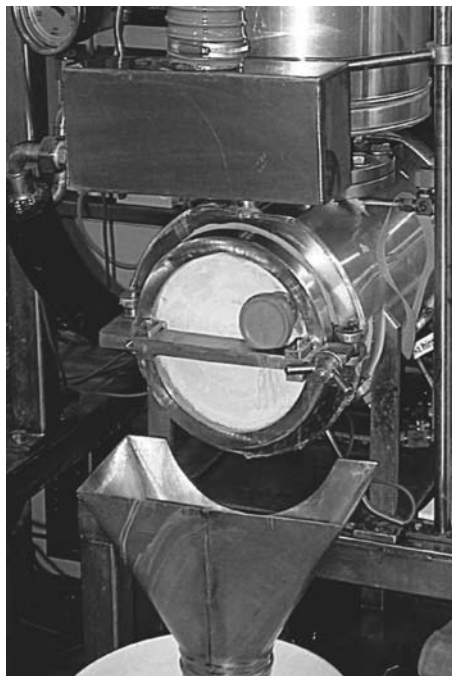


**Figure 14.16** Shovel dryer for lab-scale experiments with a volume of 1 l.

The scale-up of the mechanical stress especially in paddle dryers is currently not possible because the bed height on large scale can only be mimicked by larger stirrer tip speed on small scale leading to a somewhat similar “shear stress.”

## References

- 1 Rushton, A., Ward, A.S., and Holdich, R.G. (1996) Solid–liquid filtration and separation technology, VCH Wiley.
- 2 Krisher, O. and Kröll, K. (1956) Trocknungstechnik, Springer, volume 1.

## 15

### Melt Crystallization

*Joachim Ulrich and Torsten Stelzer*

#### 15.1

##### Characteristics of Melt Crystallization

Melt crystallization is an important separation, purification, and concentration technique used in the chemical, pharmaceutical, and food industries. Crystallization from melt is a very powerful separation process for the purification of organic compounds up to very high purities of 99.99%. Hence, the objectives of melt crystallization (purity, separation, or concentration) are quite often different compared to crystallization from solution (purity and defined crystal size distribution).

In the following chapters, the basics concerning melt crystallization will be introduced. Examples of plants for melt crystallization are provided in Chapter 16.

##### 15.1.1

###### Definitions

In crystallization processes, two expressions are often used: crystallization from solution and crystallization from melt. A solution is a homogeneous mixture of more than one species. A melt most correctly refers to a pure molten solid, for example, molten silicon. Unfortunately, the term melt is used in a more general way to describe solutions of materials that are usually solid at room temperature.

The phase diagrams (for a diagram see Chapter 3) give the melting point curve or plane for the full range of concentrations possible of a binary or more component system.

The solubility diagrams (for a diagram see Chapter 3) are usually plotted with exchanged axis of temperature and concentration. Furthermore, solubility diagrams give only a limited section of concentrations. Hence, there is no difference between a solution and a melt when looking at the phase diagram. How can one differentiate between the two expressions melt and solution as they are used today?

It was suggested by Ulrich *et al.* [1] that whenever the expression “solution” is used the mass transfer effects should dominate a process. Whenever a process of liquid–solid phase change is dominated by the heat transfer, it should be called “melt” crystallization. An additional explanation could be found in the different growth

rates. Crystal growth rates within solution crystallization processes are in most cases in the range of  $10^{-7}$  to  $10^{-9}$  m/s. However, in melt crystallization the growth rates can often be about  $10^{-6}$  m/s and in extreme cases up to  $10^{-4}$  m/s and still lead to highly pure products. This allows the economical use of technologies such as solid layer melt crystallization (see Section 15.2.1).

### 15.1.2

#### Benefits of Melt Crystallization

Melt crystallization can have advantages and features that establish it as an alternative separation technique compared to other thermal unit operations in chemical engineering.

One major advantage of melt crystallization becomes obvious when comparing the energy required for the phase change of melt crystallization (solid/liquid) to distillation (liquid/vapor) or evaporation crystallization processes in solution crystallization. In melt crystallization, only about 1/3 to 1/7 of the energy compared to distillation or evaporation crystallization is required. A further point in this context is that most known organic chemicals have melting points in a range where low-level waste heat from other processes can be used. The last point becomes more clear when looking at Figure 15.1. The shown data are based on the data available on the chemistry database of Merck (Germany) in 1999. The numbers of substances are plotted versus their melting points.

About 60% of the substances examined have melting points between 0 and 210 °C. Therefore, the much lower level in temperature and the clear smaller

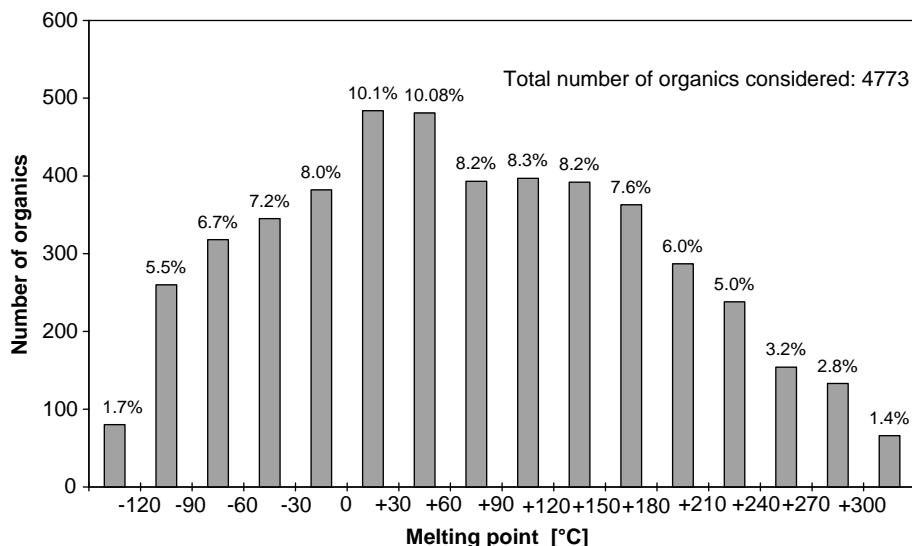


**Figure 15.1** Distribution of melting points according to Ulrich, Glade, and Lu based on the chemistry database of Merck, Germany, in 1999 [2].

differences in phase change energy are the benefits in comparison to evaporation processes. The moderate temperature level shows obvious advantages when heat-sensitive substances (e.g., foods, polymers, or pharmaceuticals) are processed (requirement is thermal stability (no decomposition) or at least a slow enough decomposition at the melting point). In the case of materials such as wastewaters from electroplating processes, a too high temperature can lead to chemical reactions and accelerated corrosion. Hence, treatment with crystallization (low temperature level) instead of distillation would be reasonable. Another example for heat-sensitive substances, besides the purification and separation, is the concentration of fresh juice to reduce the volume by freezing out the water (called freeze concentration). The advantage of the freeze concentration technology compared to the evaporation technology (the most common method for liquid food concentration) is, among others, the nondegrading of thermally fragile components such as aroma as well as the vitamins due to the low process temperatures.

The above-mentioned advantages of the melt crystallization processes concerning the temperature level of the product component do not exist if the comparison is made to the crystallization from solutions, because the product is crystallized in solution at temperatures lower than its melting point. However, the solvent has to be separated (evaporated), usually in larger amounts, and is often to be treated as impurity. Hence, melt crystallization does not need any additional substance compared to extraction or solution crystallization. Therefore, no wastewater will be produced and no other chemical (solvent) has to be reprocessed. The capital and energy costs for solvent recycling can represent a major portion of a product isolation process utilizing solution crystallization.

The high selectivity of melt crystallization processes is a further very important fact and can lead to an almost pure product within one separation step if the mixture to be separated is eutectic in nature (see Chapter 3). 54.3% of all known two-compound organic mixtures for which phase diagrams could be found (1486 in International Critical Tables 1927–1930) are eutectic (see Figure 3.7). Furthermore, 31.6% of the phase diagrams belong to the group of molecule-forming compounds and systems with peritectic and eutectic points. Only 14.1% of all investigated substances belong to the group of solid solution-forming substances (over a part or the total range of composition). In solid solutions, the separation has to be done step by step, as in distillation processes. The number of steps is determined by the phase diagram (slopes of the solidus and the liquidus lines as well as by the distance between these two lines) and the required purity of the product. As a result, complete product recovery is also possible for solid solution-type systems, although such processes are more complicated, because the number of required steps increases rapidly as recovery approaches unity.

Further advantages of melt crystallization are the smaller volume of the liquid compared to the vapor phase. A smaller volume requires less space or less construction work, which means less capital costs. These advantages are sometimes lost if the process of crystallization and remelting is very slow. Therefore, the residence time in the apparatus is high. The nonexistence of a vapor phase, however,

also leads to a better control concerning safety, for example, leakages and collection of lost product. Totally closed equipments lead to a high environmental safety.

## 15.2

### Processes of Melt Crystallization

Concepts of plants can be divided into solid layer and suspension crystallization. Furthermore, these two techniques can be split into continuous and batchwise as well as into static and dynamic (stagnant or flowing melt) operating modes. A detailed overview of the different designs of existing and commercially available plants in solid layer as well as suspension crystallization is provided in Chapter 16. In the Sections 15.2.1 and 15.2.2, the basics of solid layer and suspension crystallization are discussed.

#### 15.2.1

##### Solid Layer Crystallization

Solid layer crystallization is a process in which the growth of a crystal layer takes place perpendicular to a cooled surface into the bulk of a melt (so-called mother liquid). The phase change is used as the basis for the separation of the feed mixture. Such a phase separation is possible due to different equilibrium concentrations of the solid and liquid phases of the mixture (see Chapter 3). The driving force for the crystal growth is the temperature difference between the equilibrium temperature of the melt (the bulk) in front of the solid layer and the temperature of the cooled surface (see Figure 15.2).

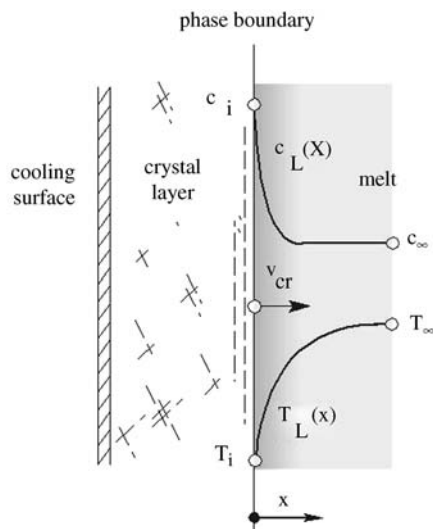


**Figure 15.2** Temperature and concentration profile in front of the solid layer (according to Ref. [3]).

The latent heat of crystallization is transported through the solid crystal layer and the cooled surface. Therefore, almost any crystal growth rate is theoretically achievable. However, in real processes the increase in thickness of the solid layer on the cooled surface requires a permanent reduction in temperature to preserve the same growth rate and, therefore, to maintain the same driving force due to the increase of the crystal coat. Otherwise, the productivity decreases with increasing solid layer thickness. Nevertheless, the crystal growth rates (layer growth rates) are adjustable by the driving force that is well controllable by the temperature difference through the cooled wall.

The higher the selected crystal growth rate, the more impurities will be enriched at the interface (melt/crystal layer). Hence, a concentration gradient is composed of an additional driving force. These effects are called constitutional supercooling. The tendency of dendritic crystal growth advances with increasing constitutional supercooling and lowers the quality of the purification by enhancing the incorporation impurities. This phenomenon is accepted within a certain defined small limit to obtain the required yields. It is an optimization problem between dendritic crystal growth and the purity on the one hand and the yield on the other hand. Therefore, the growth rates can be as high as the desired purity of the crystal layer allows it. There is no limit by the width of the metastable zone as in suspension crystallization, because in solid layer crystallization the bulk melt is always higher in temperature than the melting point. The specific mass transfer surface area (interface melt/crystal) is, however, lower ( $<10^2 \text{ m}^2/\text{m}^3$ ) in solid layer crystallization compared to suspension crystallization ( $10^4 \text{ m}^2/\text{m}^3$ ). This is a weak point in solid layer processes compared to suspension processes, since the surface area is a limiting factor for mass transfer processes or the investment costs, respectively.

Subsequent to the crystallization step and draining of the residue melt, the desired product is obtained by remelting the crystal coat (incrustation) and is collected in a tank (liquid). Hence, solid layer processes have no problems of incrustation compared to suspension processes. Rather the incrustations (solid layer) are the product and the waste and the concentrated residual melt is in this case the product. Furthermore, no problems caused by slurry handling can appear, because there are no slurries. All product handling takes place in the liquid stage of product. The solid/liquid separation is easily performed by gravity and draining of the residual melt. Unfortunately, a film of melt with residual composition remains on the crystal coat and reduces the quality (purity) of the product. This film, or at least the most of it, however, can be removed by postcrystallization treatments such as sweating or washing (see Section 15.3). Figure 15.3 demonstrates a principle flow diagram showing all liquid streams and all possible procedural steps in a solid layer process.

A further advantage of solid layer crystallization is that, besides pumps, no moving parts are needed in such processes, since only liquids are transported. A weak point of solid layer crystallization processes is the batchwise or quasicontinuous operating mode. This is different from most suspension crystallization processes that are continuous.



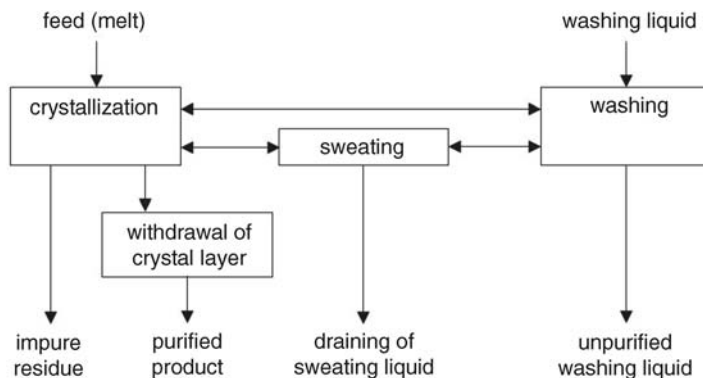


**Figure 15.3** Principle flow diagram of solid layer processes (according to Ref. [4]).

### 15.2.2

#### Suspension Crystallization

Contrary to solid layer crystallization, the solid product in suspension crystallization is present as crystals freely suspended in the melt. The suspension crystallization is often initiated on cooled surfaces, as in solid layer crystallization, but the crystals are periodically scraped off. Most of the crystal growth occurs on the crystals suspended in the melt (see Chapter 16 Figures 16.9 and 16.10). Thus, the crystal surface area available for growth is the total surface area of a very large number of crystals. It is not limited as in the solid layer process by the surface area of heat transfer. The specific surface area of mass transfer in suspension crystallization amounts to approximately  $10^4 \text{ m}^2/\text{m}^3$  and is about two orders of magnitude higher compared to solid layer crystallization ( $<10^2 \text{ m}^2/\text{m}^3$ ). However, contrary to solid layer crystallization, suspension processes require additional slurry handling. Furthermore, problems caused by incrustations appear. In suspension crystallization, the incrustations are not the product and hence are unwanted! Therefore, an enhanced risk of clogging is definitely a weak point in suspension crystallization compared to solid layer crystallization. On the other hand, in principle no additional energy costs are needed to remelt the crystals as in solid layer crystallization. Moreover, suspension crystallization can operate efficiently only with one continuous crystallization step for desired highly pure products since low growth rates can be applied. However, an almost complete solid/liquid separation is required to obtain the full benefit of the promising features of suspension crystallization. Hence, the complete separation of crystals from the residual melt is at least as important as the growth of pure crystals, which aims at an ultrapure product or a concentrated residue (e.g., fruit juice). The importance of the solid/liquid separation can be illustrated by the fact that even a small portion of residual melt can deteriorate the product purity dramatically. The adherence of 1% of residual melt containing 40 wt% of the main compound to the crystals that are 99.99 wt% pure implies that the final product purity will decrease to 99.4 wt%. Here, a second set of problems occurs when preparing the final product. The very pure crystals must be separated from the highly contaminated residual

**Table 15.1** Comparison of solid layer and suspension crystallization [5].

Feature	Solid layer crystallization	Suspension crystallization
apparatus	no moving parts, besides pumps	moving parts, especially scrapers
operating mode	batchwise	continuous (predominantly)
temperature of melt	above, but close to solidification temperature	below solidification temperature
melt flow rate	large	small
heat withdrawal	through crystal layer	through the melt
crystal growth rates	large, $10^{-5}$ – $10^{-7}$ m/s	small, $10^{-7}$ – $10^{-8}$ m/s
relative interface	small, $10$ – $10^2$ m <sup>2</sup> /m <sup>3</sup>	large, $10^4$ m <sup>2</sup> /m <sup>3</sup>
melt/crystal transportation of product	no problems, all liquid	problems due to suspensions
solid/liquid separation	easy, just draining	difficult
encrustation problems	no	yes
scale-up	easy	difficult

melt. This requires unit operations such as filtration and centrifugation or post-crystallization treatments such as washing or sweating (see Section 15.3). The wash columns can significantly improve the process, as they are able to reach purities of >99.9 wt% compared to the other unit operations. However, the additional procedural steps are costly, need energy, or limit the overall production capacity. Hence, the quality of purification by suspension crystallization depends on solid/liquid separation after the crystallization step (crystal growth).

Finally, and very importantly, there are limitations in many of the suspension techniques due to high viscosities of the melts and very small differences in the densities between the melt and the crystals. These limitations are important when the processes depend on natural settling velocities of the solids within the melts.

The main features of the solid layer and suspension crystallization techniques are summarized in Table 15.1.

Solid layer- and suspension-based crystallization processes are used for the treatment of many different substances on lab as well as on industrial scale. Both techniques have positive and limiting features. Consequently, the arguments have to be weighed in each individual case. There is not the one best technology, but in each case according to the boundary conditions and the product specification the one or the other technique could be the better choice.

### 15.3

#### Postcrystallization Treatments

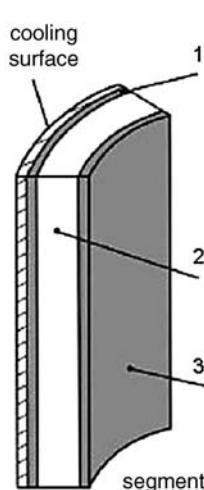
Due to above-mentioned adhering or captured liquid inclusions of the residual melt at the crystals after the solid/liquid separation, additional purification steps are

necessary to obtain the desired purity. These steps are either further costly crystallization steps or additional postcrystallization treatments. Hence, the purification is the final result of different procedural steps, including crystallization in one or more stages, the solid/liquid separation, and/or additional postcrystallization treatments such as sweating and washing. Therefore, it is important to have information available on the purification potential of the integral processes as well as of the different procedural steps. In suspension crystallization, the crystals are always surrounded by impure melt. In solid layer crystallization, however, the melt is only in front of the layer. It is, therefore, more easy to explain the three mechanisms of the incorporation of impurities using the solid layer process, but the same mechanisms exist in suspension crystallization as well:

- 1) nucleation (initiation step) on cooled surface;
- 2) crystallization (solid layer growth) perpendicular to the cooled surface;
- 3) end of crystallization (draining of the residual melt).

Figure 15.4 shows the different possible origins of impurity incorporation in or on the solid layer as well as measures to reduce or even to prevent them. Along with this information, the potential of the postcrystallization treatments to partially or fully avoid or reduce inclusions is listed.

Figure 15.4 shows that impurities caused by nucleation and crystal growth can be reduced to a minimum by controlling the process parameters of crystallization. Additional postcrystallization treatments such as sweating or washing can even improve the purity to the same extent as can be reached just by a crystallization step.



mechanisms of impurity incorporation	operation measures to prevent impurities in the crystal product	additional purifying measures
1. high impurity concentration due to nucleation at high supercooling	- nucleation by controlled temperature and flow conditions - controlled seeding - mechanically induced nucleation (shock waves ultrasonic vibration or cavitation)	sweating
2. impurities in the crystal layer on account of high crystal growth rates	"criterion of purity" relates the maximum allowable growth rate for the production of a pure layer to the relevant set of flow conditions	sweating
3. impurities due to adherence of contaminated residual melt at the end of the process	minimized and smooth crystal layer surface to reduce the wettable area	sweating, washing

segment of crystal layer

**Figure 15.4** Mechanisms of impurity incorporation in a crystal layer as well as measures to prevent it and additional purification measures (postcrystallization treatments) [6,7].

However, a crystallization step is more costly compared to postcrystallization treatments and hence the latter can be the better alternative instead of an additional crystallization step to obtain the desired purity.

### 15.3.1

#### Sweating

The postcrystallization treatment sweating is a temperature-induced purification step. After the crystallization process, the temperature of the cooled surface is raised close to the melting point of the pure component (about 1–2 K below). As a consequence, the impurities adhering to the crystal coat and those contained in pores of the crystalline material remelt (partially diluted with pure material). The remolten impure material flows out of the pores and finally drains under the influence of gravity. During the sweating process, a product loss of about 10% is accompanied.

The important part of the purification effect by sweating is that liquid inclusions have a lower melting point and solidification point compared to the more pure material. As a consequence, at temperatures where the product compound is still solid, the impurity-rich areas are liquid or become liquid and will, therefore, leave off the crystal coat. This process is supported by the decrease in viscosity due to the higher temperature. The purification effect by sweating is shown in Figure 15.5 by the distribution coefficient. A distribution coefficient of zero means here a perfect purification, whereas a coefficient of 1 means no purification at all.

The effect of sweating can be seen in Figure 15.5 by a decrease of the distribution coefficient from about 0.4 to 0.2 at a growth rate of about  $0.3 \times 10^{-6}$  m/s, as well as from about 0.6 to 0.3 at a growth rate of about  $1.7 \times 10^{-6}$  m/s. Therefore, sweating can even reach in individual cases the same purification as by an additional (a second) crystallization step [8,10]. The results shown in Figure 15.5 were obtained

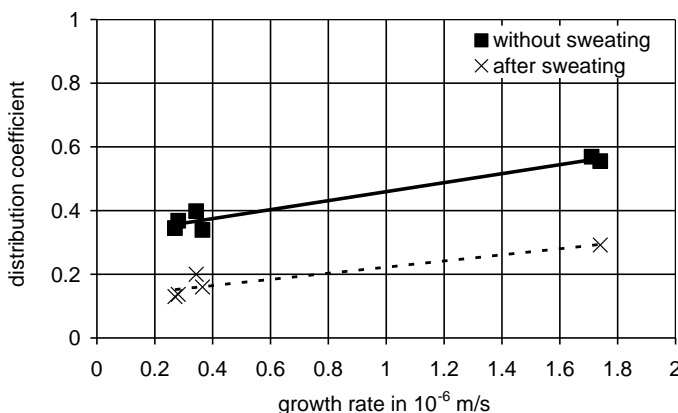


**Figure 15.5** Purification effect of crystallization and sweating of a crystal layer process considering crystal growth rates (feed mixture: methacrylic acid/water) [7–9].

for the static mode of solid layer crystallization. The efficiency of sweating for the dynamic mode of solid layer crystallization, however, is in general reduced compared to the static mode. An overview of the static and dynamic modes of solid layer crystallization plants is provided in Chapter 16.

As rule of thumb, it can be stated that the purification step sweating is more suitable for the static mode compared to the dynamic mode, because the achieved improvements in distribution coefficient are less than those for static mode. This rule depends, of course, on the mixture (the substances) used. In summary, the possible advantages of sweating are [7,9]

- additional purification in the same range as crystallization step;
- much shorter retention time of the process (about 1/3 to 1/9 of a crystallization step);
- less energy consumption compared to a crystallization step, because there is no phase transition energy required and the product has to be remolten anyway;
- about 10% product loss, which should be compared to a yield of a crystallization step that in most cases is about 80% of the maximum achievable (see position of the eutectic point).

### 15.3.2

#### **Washing**

The second postcrystallization treatment washing can be divided into rinsing and diffusion washing. In rinsing, the highly contaminated residual melt adhering at the crystals or crystal coat is substituted with a film of a more pure rinsing or washing liquid. The washing liquid consists of pure desired product or a purer mixture (e.g., feed mixture) compared to the residual melt. In the case of pure product, a small amount of purified product is needed and will be contaminated again to purify the crystal coat. The rinsing takes place within only a few seconds and is driven by mechanical forces (pushing away impure product and substituting it by a pure one).

Diffusion washing effectively operates in the range of about 15–20 min. The washing liquid causes a liquid/liquid diffusion of impurities from the pores of the crystalline material into the washing liquid. In order to avoid crystallization of the washing liquid onto the crystals or crystal layer, it must be superheated. Therefore, the diffusion washing is always, at least to some extent, accompanied by sweating, which increases the efficiency of the purification effect. All three phenomena, rinsing, diffusion, and sweating, are involved in the so-called diffusion washing, since rinsing also takes place when draining the washing liquid. The washing liquid has to be purified and accounts for about 10% by mass. The diffusion washing is other than the two further postcrystallization steps also a concentration-driven process. In summary, the possible advantages of washing (rinsing and diffusion washing) are [7]

- additional purification;
- much shorter retention times (rinsing few seconds, diffusion washing 15–20 min) compared to a further crystallization step (several hours);

- less energy consumption compared to a crystallization step (just pumps and temperature control);
- no additional contamination by solvents;
- just pure product or feed is used, which has to be repurified;
- it accounts for about 10% of product loss, which should be compared, however, to a yield of a crystallization step that in most cases is about only 80%.

### 15.3.3

#### Choices

The choice of postcrystallization treatment depends on the system to be purified and varies from case to case. Sweating is easy to operate and needs no additional equipment. It is always worth trying if the crystalline coat is not slipping off when getting warmer by its own weight. Washing is probably more efficient, but needs modification of the equipment. Furthermore, in the case of diffusion washing, extremely precise temperature control is needed. Otherwise, too much remelting or crystallization of the washing liquid takes place. Both are required only in small amounts.

All postcrystallization treatments described and discussed above on the basis of the layer technique can and are also used in suspension crystallization processes [11]. The crystals grown in suspension crystallization processes are almost pure, because the incorporation of impurities by kinetic effects and the inclusion of residual melt due to unstable growth morphologies are negligible when the appropriate growth rates and mixing regimes are applied. The final purity of product based on suspension crystallization depends on the performance of the solid/liquid separation. Consequently, additional washing (rinsing) of the crystals with a relatively pure washing liquid is required to achieve a highly purified product. Washing on filters or in centrifuges is possible but difficult, because the temperature of the washing liquid needs to be controlled precisely. Otherwise, the washing liquid will crystallize on the crystals or lead to caking of the crystals (filter/centrifuge cake) or partially melt the crystals and hence remelt the product. Furthermore, the washing liquid gets contaminated with impurities and needs to be reprocessed. Wash columns combine solid/liquid separation and washing in one apparatus in which the temperature can be controlled rather precisely. Therefore, in wash columns some of the above-mentioned problems do not explicitly arise.

### 15.3.4

#### Wash Columns

Wash columns can be distinguished into gravity and forced transport columns, which can be differentiated into mechanical and hydraulic operating modes. In Figure 15.6, for instance, a mechanical wash column is shown.

The principal operating mode of a wash column is as follows. A slurry of crystals and melt is created in the crystallizer and is fed into the wash column and the residual melt leaves through a filter, which causes a compaction of crystals into the so-called packed

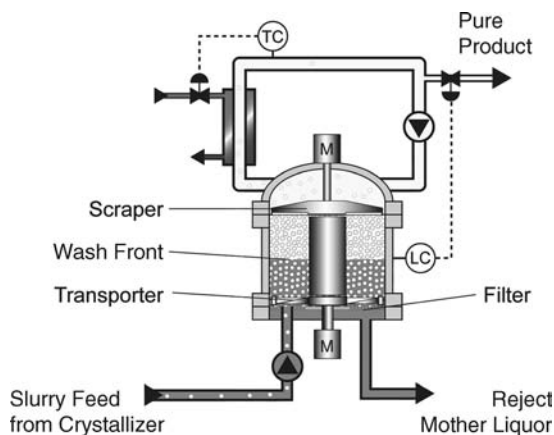


**Figure 15.6** Principle of a mechanical wash column (reproduced with permission from GEA Messo PT).

bed. This bed is forced through the wash column by solid floating (if the density is lower than the residual melt, for example, ice) or settling (if the density is higher than the residual melt, in general) and pressure as transport mechanism. The packed bed is scrapped off by rotating scrappers at the end (here, at the top) of the column. Thereafter, the scrapped off crystals are fluidized in a reslurry section by recirculated molten product and fed in an external heat exchanger. After melting the crystals, the obtained melt is split into two streams. The largest portion is removed as product and the other portion of pure molten product is forced back into the porous packed crystal bed. At this point, it has to be stated that no additional energy is required for the wash column. The crystals have to be molten anyway in order to obtain the desired product. This can be compared with the necessary condensation of the high-boiling compound in distillation in order to obtain the desired product.

Due to crystals passing the reslurry section, they will be washed countercurrently with the molten pure product. The washing liquid (pure molten product) crystallizes on the surface of the crystals as soon as it contacts the colder crystals (due to impurities, generally 5–20 K colder) from the unwashed part of the bed. Therefore, only minor amount of pure product of the washing liquid is lost to the filtrate. This horizontally extending zone across the crystal bed is called wash front. The position of the wash front that indicates the occurrence of purification is in some cases visible by a color shift (e.g., freeze concentration of fruit juice). Alternatively, the position can be determined by measuring the temperature in the column. A sharp temperature difference is the indicator. A good overview of wash columns is given, for instance, by Arkenbout [12].

In summary, postcrystallization treatments are shorter in time and, if efficient, have higher yields and less energy consumption than additional costly crystallization steps. It is, therefore, of utmost importance to know the potential of the post-crystallization treatments before evaluating melt crystallization as an alternative to other thermal separation, purification, or concentration processes.

## 15.4

### Laboratory Techniques

This section presents simple laboratory techniques that can be used to screen the potential of melt crystallization as a purification or concentration technique for chemicals, pharmaceuticals, and foods. These substances will be in most of the cases of organic nature, but the described techniques are suitable for water or other inorganic substances and metals as well.

#### 15.4.1

##### Bottle Test

The simplest approach to investigate the potential of melt crystallization is the so-called bottle test. The feed mixture (molten or has to be molten) is filled in a glass bottle or flask. Thereafter, the flask is cooled slowly in a temperature-controlled bath or is allowed to cool at ambient conditions or, if necessary, in a freezer. Only a part *not* all has to be solidified! Quite often, already a color shift clearly indicates a separation. However, to determine the quality of the purification, for instance by distribution coefficient, the residual melt has to be separated from the crystallized portion by decanting. Finally, the solid, the residual melt, and the feed material can be analyzed to decide whether melt crystallization is suitable as purification technique or not. The advantage of the bottle test is that it is quite simple. Only lab equipment is required to obtain the desired answer concerning the feasibility of melt crystallization. In case the result is positive, everything is clear. If the result, however, is not positive, a more detailed examination technique is required, for example, the cold finger experiment.

#### 15.4.2

##### Cold Finger Experiments

A further simple, but very efficient and powerful technique to obtain important information especially on the purification by melt crystallization is the so-called cold finger experiment. Compared to the bottle test, more but simple lab equipment is required for this setup. Figure 15.7 shows the essential parts of a cold finger apparatus allowing a static operating mode.

The so-called “cold finger” is just an internally cooled at the bottom end closed tube. The size of the beaker is determined by the volume of melt required (0.2–5 L) to obtain the desired information. The temperature difference between melt and the cold finger surface or the crystal coat (later in the crystallization process) can be controlled by the thermostat of the cold finger. Hence, the driving force in solid layer crystallization that determines the growth rate of the solid layer and consequently the maximum achievable purity is adjustable. Therefore, the important parameter growth rate (as fast as possible, but avoiding inclusions of impure melt that means avoiding constitutional supercooling as much as possible) to



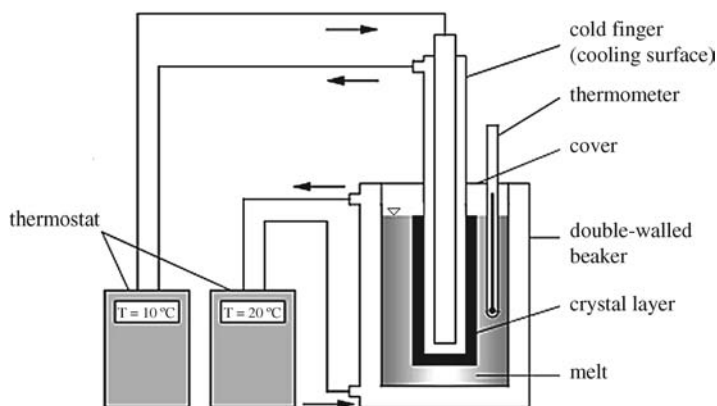


**Figure 15.7** Cold finger apparatus (static) (according to Ref. [13]; see also Refs [4, 14]).

design a solid layer crystallizer can be investigated with the cold finger experiment. It is, however, very important to use the same material for the cold finger as will be used for the cooled surface in the industrial plant. Other materials might show a different behavior concerning nucleation (no nucleation, poor nucleation, or even better nucleation).

The achieved purity can be analyzed by taking samples from the solid layer, the residual melt, and the feed. After experiments with the original feed mixture, experiments with highly enriched impurities (enriched compared to the feed mixture) can show the limits concerning achievable purity and yield (how good remains the separation with increasing impurity concentration). Moreover, the cold finger setup is also suitable for investigating the influence of the above-mentioned postcrystallization treatments. In the case of sweating, the cold finger has just to be placed in a different beaker or the residual melt has to be decanted. By heating the cold finger, the optimal sweating temperature (about the melting temperature of the pure product) and sweating time (about 15–20 min) can be determined. In rinsing the solid layer, it will be stripped from the adhering residue melt and will be substituted by a film of more pure washing liquid after solid/liquid separation. Diffusion washing can be carried out with the described equipment as well. This can be done by dipping the cold finger with the solid layer in pure product or feed and taking it out after a certain residence time. During rinsing and diffusion washing, it has to be guaranteed that the washing liquid does not crystallize on the solid layer by controlling the temperature of the cold finger as well as of the washing and rinsing liquid in order to prevent melt down of the crystal layer.

The dynamic operating mode of the solid layer crystallization (see Chapter 16) can be tested quite realistically with the shown cold finger equipment, too. However, several modifications of the setup are required, for instance, a circulating loop of the melt has to be installed in order to create a falling film from the top of the cold finger (see, for example, Refs [4,14]).

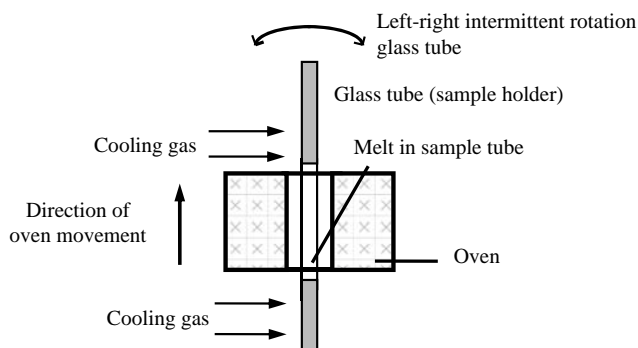


**Figure 15.8** Schematic diagram of a single oven zone melter [14].

### 15.4.3

#### Zone Melting

Zone melting is a multistage melt crystallization technique based on a repeated formation of solid layers, however, in a continuous mode. Repeated layer formation is necessary in order to get high purity. Hence, the aim of zone melting is to determine whether the required level of purity can be attained using crystallization from the melt. In the semiconductor industry, for instance,  $>99.99\%$  purity can be obtained by zone melting even in industrial applications. Therefore, zone melting is first of all more important in semiconductor industry compared to “classical” melt crystallization of commodities. Nevertheless, the technique can be used if it is available. However, zone melting is a costly technique compared to the above-mentioned techniques that are more simple and less costly. Figure 15.8 shows the schematic principle of zone melting.

The experimental procedure is as follows. First, the glass tube has to be filled with the sample material and is placed on a shaft. The shaft permits a practically instantaneous reversal of rotation direction (clockwise and counterclockwise) that is followed by very rapid acceleration to the maximum number of revolutions. The purpose is to get an effective mixing in the liquid phase. The glass tube is moved downward with a linear rate through an electrical oven. The material is molten inside the glass tube when entering the oven. Above and below the oven, a cooling zone (of gas) is led around the glass tube. This cools down the melt until the material recrystallizes. The procedure can be repeated several times. Due to the material in the bottom end of the glass tube, sample becomes purer after every cycle, while the impurities are forced to the top end of the glass tube. Subsequent to the zone melting experiment, the glass tube can be cut into several pieces in order to analyze the samples concerning the feasibility of melt crystallization for the purification of the investigated material.

## References

- 1 Ulrich, J., Özügüz, Y., and Stepanski, M. (1988) *Chem. Ing. Tech.*, **60**, 481–483.
- 2 Ulrich, J. (2003) *Melt Crystallization – Fundamentals, Equipment and Applications* (eds J. Ulrich and H. Glade), Shaker, Aachen, pp. 1–6.
- 3 Neumann, M. (1996) Vergleich statischer und dynamischer Schichtkristallisation und das Reinigungspotential der Diffusionswäsche. Ph.D. thesis, Universität Bremen, Papierflieger, Clausthal-Zellerfeld.
- 4 Özügüz, Y. (1992) Zur Schichtkristallisation als Schmelzkristallisationsverfahren. Ph.D. thesis, Universität Bremen, Fortschrittsberichte VDI, Reihe 3, Nr. 271, VDI Verlag, Düsseldorf.
- 5 Ulrich, J. (2002) *Kirk-Othmer Encyclopedia of Chemical Technology*, vol. 8 (eds R.E. Kirk and D.F. Othmer), Wiley-VCH Verlag GmbH, Weinheim, pp. 95–147.
- 6 Scholz, R. (1993) Die Schichtkristallisation als thermisches Trennverfahren. Ph.D. thesis, Universität Bremen, Fortschrittsberichte VDI, Reihe 3, Nr. 347, VDI Verlag, Düsseldorf.
- 7 Ulrich, J. (2006) *Fluidverfahrenstechnik – Grundlagen, Methodik, Technik, Praxis* (ed. R. Goedecke), Wiley-VCH Verlag GmbH, Weinheim, pp. 1131–1196.
- 8 Delannoy, C., Ulrich, J., and Fauconet, M. (1993) Laboratory tests on an organic acid as a basis for scale-up calculations, in *Proceedings of 12th ISIC*, vol. 1 (ed. Z.H. Rojkowski), pp. 49–54.
- 9 Ulrich, J. and Bülau, H.C. (2002) *Handbook of Industrial Crystallization*, 2nd edn (ed. A.S. Myerson), Butterworth–Heinemann, Boston, MA, pp. 161–179.
- 10 Ulrich, J. and Özügüz, Y. (1989) *Chem. Ing. Tech.*, **61**, 76–77.
- 11 Poschmann, M. (1996) Zur Suspensionskristallisation organischer Schmelzen und Nachbehandlung der Kristalle durch Schwitzen und Waschen. Ph.D. thesis, Universität Bremen, Shaker Verlag, Aachen.
- 12 Arkenbout, G.J. (1995) *Melt Crystallization Technology*, Technomic Publishing Company Inc., Lancaster.
- 13 Haasner, T. (2002) Beeinflussung der Keimbildung in der Schichtkristallisation durch gezielte Oberflächenmodifikation. Ph.D. thesis, Martin-Luther-Universität Halle-Wittenberg, Fortschrittsberichte VDI, Reihe 3, Nr. 759, VDI Verlag, Düsseldorf.
- 14 Glade, H. and Ulrich, J. (2003) *Melt Crystallization – Fundamentals, Equipment and Applications* (eds J. Ulrich and H. Glade), Shaker, Aachen, pp. 129–165.
- 15 Ulrich, J., Hünken, I., Fischer, O., and König, A. (1992) *Chem. Ing. Tech.*, **64**, 842–844.

## 16

### Examples of Realized Continuous Crystallization Processes

*Günter Hofmann and Christian Melches*

#### 16.1

##### Choosing the Drain Point in Process Design

A crystallization process has to be designed to meet a number of requirements, for example, particle properties such as particle size and purity. As concerns the purification, a continuously operated crystallization has to deal with the accumulation of impurities in the mother liquor. The drain point for these impurities has to be carefully chosen. It is one of the most underestimated aspect of the process design activity and the source of many errors. Moreover, the process yield is strongly connected with the planning of the process drain points, as is the specific energy consumption and, thus, the success of the process. However, the separation attribute of the unit operation crystallization may not be the best available and one should remain open for competing alternatives. That could be recommendable, for example, in cases of solid solutions, especially with distribution coefficients close to 1, which are not feasible to separate by crystallization at all.

In most of the cases, lab tests are already sufficient to balance the process design ideas against each other, and besides this function these tests are used to provide all the substance properties needed for the mass and heat balance and the dimensioning of the plant. Only in more complicated processes, additional piloting work may be required.

The impurities have to be drawn off the process as concentrated as possible by setting the appropriate drain points for impurities in order to keep product losses minimum (Figure 16.1). It requires a full understanding of the respective phase system. The more the phasesystem is known in detail, the better the chances for the optimal process design. A good strategy can be to configure the process following the point targets, that is, following the product purity and the optimal process yield. It may, therefore, be a good solution to configure one part of the process to safely get the desired product purity, whereas configure the second part to maximize the process yield.

Such a strategy is particularly suitable for the isolation of products from fermentation broths. Those processes are called crop processes. There are two crops at least: the first crop provides the desired product quality and the second

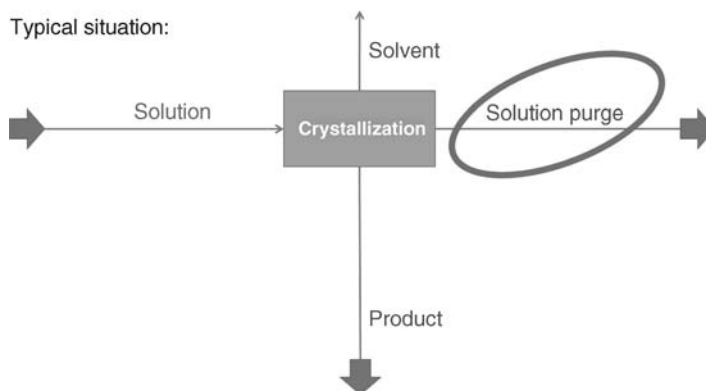


**Figure 16.1** Drain point for impurities in a continuously operated crystallizer.

crop is configured to maximize the yield (Figure 16.2). The crystal mass from the second crop has, of course, a much lower purity and its particle size is smaller most of the time. The lower purity is a consequence of the larger quantity of adherent mother liquor, which might be caused by the finer crystal mass and higher solution viscosity or even by the cocrystallization of impurities, and the crystals cannot be brought to the market. Therefore, the usual way is to redissolve the crystal mass from the second crop in the feed solution sent to the first crop and to recrystallize this part again without any more product loss than caused by the mother liquor purged from the second crop. In this way, the first crop can be defined as the process stage for product purity, whereas the second crop becomes the process stage for the process yield.

There are many possibilities to optimize this crop concept for the respective case. For instance, the crystallization in the second crop – if the phase system and the frame conditions allow – can be executed at a lower temperature to minimize the product losses (to be balanced against energy costs). In some of the cases, however, the concentration of impurities or the viscosity may already be too high to still realize the desired product purity within the first crop. In such cases, one can regard the

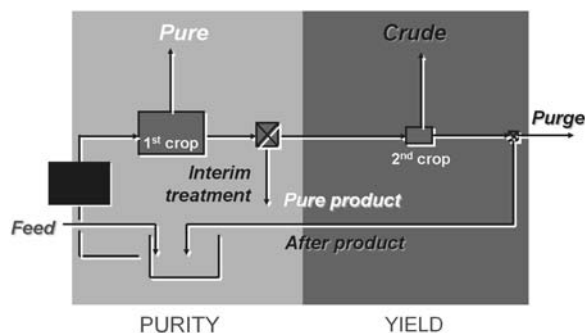


**Figure 16.2** Drain point in a crop system crystallization scheme.

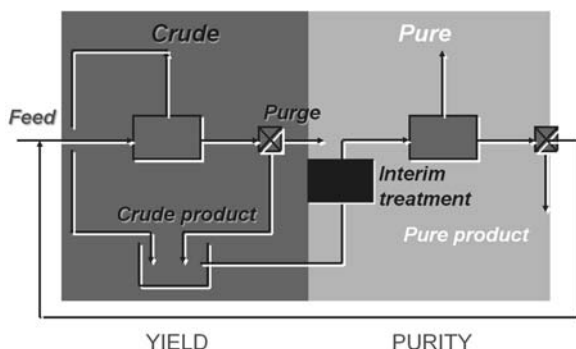


**Figure 16.3** Drain point in a recrystallization principle.

recrystallization as the comparative of the crop system (Figure 16.3). Contrary to the crop system, the first stage here is used to achieve the maximized process yield, that is, the process purge is withdrawn from here. The recovered crystal mass (the crude crystal mass) does not meet the quality requirement and, therefore, is redissolved again in solvent (e.g., water) and is recrystallized in the subsequently following second process stage. This stage now has the task to crystallize the crystal mass reaching the product requirement. This is realized by concentrating the impurities only to such an extent that the product purity can safely be reached by washing the crystal mass during separation (e.g., in a two-stage pusher-type centrifuge). The resulting mother liquor is returned to the first stage of the recrystallization process and used again to recover the crude quality. The disadvantage of the recrystallization principle compared to the crop system is the entire redissolution of the crude crystal mass. It leads to elevated energy consumption and requires bigger crystallizers compared to the crop system, where the second crop takes over only the mother liquor from the first crop.

In these process alternatives that are completely dedicated to the unit operation crystallization, one can find remarkably often, though, some other unit operations used to intensify the crystallization in separating components and to make the entire process more feasible (process intensification). Best examples are the discoloration with activated carbon or the use of a washing thickener for replacing the mother liquor (Figure 16.4). In the case of washing thickener, one uses the countercurrent washing principle to treat the suspension of the crystals from second crop with the purest solution available in this system, which is the feed solution. Even a solution prepared by redissolution of product could be taken.

This leads to the replacement of the impure mother liquor by the wash solution, before the suspension becomes separated on the centrifuge. It has the advantage that the mother liquor in the crude crystallization, respectively the second crop, can be more concentrated; that is, higher yields can be realized. Even solid impurities can be separated, if their settling rates are smaller than those of the product crystals. This is, for example, the case in the recrystallization of table salt from solar salt or in the case of the direct evaporative crystallization from solar pond concentrates, where

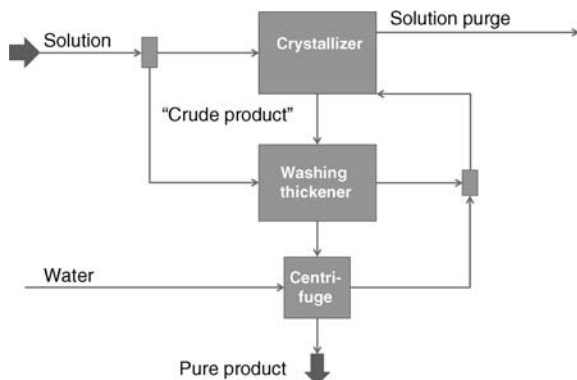


**Figure 16.4** Purification by countercurrent washing and using a washing thickener.

a solid  $\text{CaSO}_4$  modification has to be separated from the table salt. For the back-flushed particles one has to design a drain point, which can be the process purge, if the particles are kept suspended.

Intragranular impurities, however, cannot be taken away by countercurrent washing. Solid solutions ( $\text{KCl}/\text{KBr}$ ) or enclosed foreign crystal matter (nanocrystals) are typical examples. Inclusions of mother liquor or of suspensions in intragranular or intergranular caverns can also not be removed by simple washing. The avoidance of solid solution remains the field of some other unit operations, such as debromination, whereas the intra- or intergranular impurities, depending on their kind, can be minimized by further purification using crystallization or by applying precipitation (like the brine purification in the rock salt-based solution before salt crystallization) before the crystallization step.

The design of drain points is brought to the extreme in the case of the so-called ZLD (zero liquid discharge) plants. As the name suggests, in such cases there is not any liquid purge permitted anymore. Hence, impurities can only be taken off either with the crystal mass in the adherent mother liquor after separation as dissolved impurity or as cocrystallized substances. Most of the time, the crystal mass recovered this way has to be wasted and the crystallization cannot be considered for separation of the compounds anymore (Figure 16.5). The plant is forced to cocrystallize – up to a lot of substances – at their invariant point in their relevant solubility systems.

Sometimes that is even a bigger challenge to the designer of the crystallization plant than to design a plant for product purity. Invariant points are good for a lot of surprises, such as high supersaturations initiating incrustations, sudden inversion of the temperature dependence of a solute solubility leading to unexpected heater incrustations where undersaturations are expected, and so on. The first rule in the design of crystallization plants is, therefore, to avoid operating on invariant points. Here, there is no other chance. Here, the attribute of components separation has to be replaced by the task of simply and safely maintaining the plant in operation, despite the missing process purge.

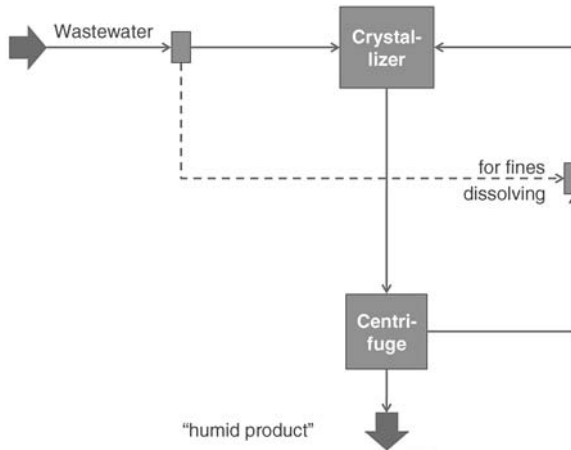


**Figure 16.5** Drain point for impurities in a zero liquid discharge crystallization via residual mother liquor in the solid.

To a special degree, the plant operation in these cases is jeopardized by unexpected material properties of the mother liquors, because the very high concentration factors bring those impurities to light that nobody is able to predict. Nevertheless, these cases of applications are becoming more and more common in the wastewater market.

The problem becomes transparent using the example of wastewater from a flue gas scrubber system in a waste-fired power plant (Figure 16.6). A seemingly

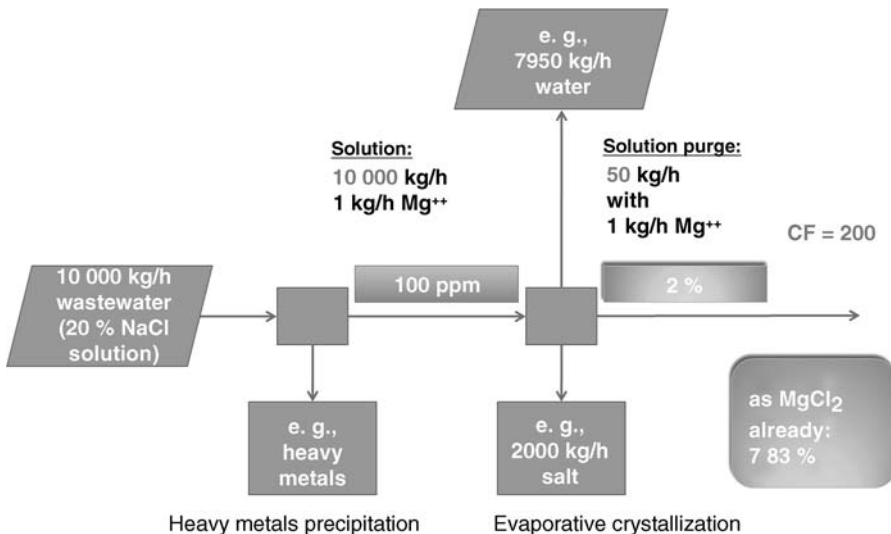


**Figure 16.6** Effect of underestimated "traces" of highly soluble compounds.



modest and perhaps not noted impurity concentration of only 100 ppm  $\text{Mg}^{2+}$  in the feed solution becomes a major component in the mother liquor, simply due to its high solubility. Assuming the “mother liquor purge” to be only the adherent mother liquor of about 5 wt%, the  $\text{Mg}^{2+}$  concentration in the mother liquor gets up to 2 wt%. Assuming chlorides are present, it amounts to 7.8 wt%  $\text{MgCl}_2$ , which might cause significant changes in the mother liquor properties compared to the original plant design. This may happen or not, depending on the waste material that has been incinerated. If the crystallization plant were not designed for such incidents, these would easily lead to capacity reductions or even to total malfunction.

## 16.2

### Example Crop Crystallization for Organic Compounds

#### 16.2.1

##### Fields of Application for the Crop Principle

A typical field of the above-described crop crystallization is the recovery of products generated by fermentation or enzymatic processes. Typical products to be recovered from their fermentation broths either by crop crystallization or by re-crystallization are the essential amino acids, the water-soluble vitamins, and their primary products, such as the ketogulonic acid, the hydroxyl carbonic acids, and dicarbonic acids, or their salts (Figure 16.7).

In most of the cases, the separation task of the crystallization process is supported by some unit operations applied in front of the crystallization part, for example, the separation of the mycelium by flocculation and filtration, which may be a precipitation of the fermented product as insoluble salt (e.g., calcium citrate) from the deeply colored and heavily polluted fermentation broth, the treatment with activated carbon to reduce color, and so on. The majority of the

*by fermentation, e.g.:*

Essential amino acids	Lysine, threonine, glutamic acid, methionine
Vitamins	Ascorbic acid, ketogulonic acid, salts, $\beta$ -carotene, astaxanthin
Hydroxy carbonic acids	Citric acid (gypsum-free process), malic acid, tartaric acid
Dicarbonic acids	Fumaric acid, succinic acid

**Figure 16.7** Typical products from fermentation broths.

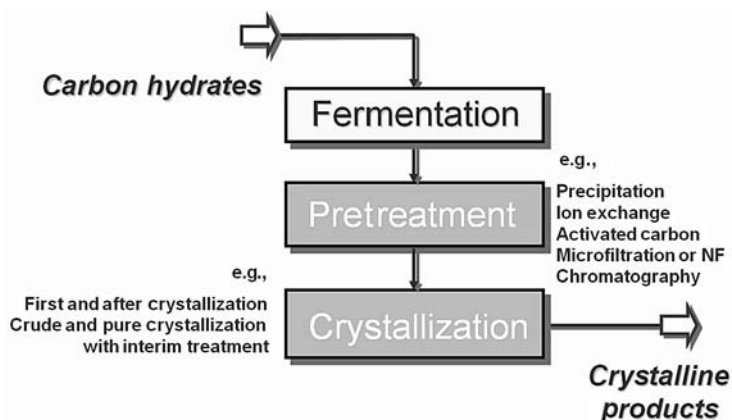


**Figure 16.8** Typical concept to separate carbohydrates from fermentation broths.

applications are crop systems. Recrystallization is reserved for the more difficult cases (Figure 16.8).

#### 16.2.2

##### Definition of Task

In the example described in Figure 16.9, the feed solution is a fermentation broth containing the product A, derivatives of product A, and numerous impurities (educts, neutral salts, and decomposition products), most of which are colored. The feed stream is about 19 t/h and the temperature is around 25 °C.

From this feed solution, we need to recover 4250 kg/h of a white product A with a purity of >99.5%, corresponding to a yield of >90% (Figure 16.10). There is no special request for the average particle size.

<b>Feed capacity</b>	18 600	kg/h
<b>Feed composition</b>		
Product A	25	mass%
Others	6.3	mass%
Water	rest	
<b>Temperature</b>	35	°C
<b>Density</b>	1150	kg/m <sup>3</sup>
<b>Viscosity</b>	3	mPa s

**Figure 16.9** Definition of feed stream.

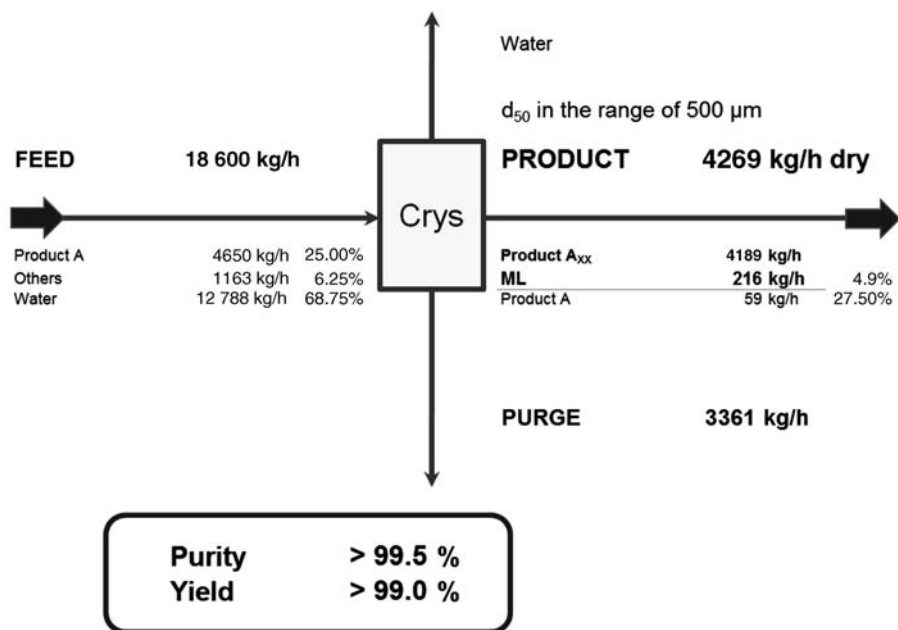


Figure 16.10 Definition of task.

## 16.2.3

**Selection of the Process Design**

The process is generally designed on the basis of a bench-scale development study, here executed on working with a representative spread of *original* fermentation broths. The main task of the performed bench-scale tests is to decide for the process technology, that is, between crop system and recrystallization, but at the same time to collect all the needed chemophysical properties needed for the design, for example, thermal decomposition rate, the solubility system, boiling point elevations, desupersaturation rate as a function of suspension density, densities of solution and suspensions, composition of the solutions, viscosities of solution and suspensions, and so on.

The crop system, the first to be investigated because of its superior economy, can prove here its ability to recover the product A at the desired yield and quality. Therefore, the recrystallization process alternative need not be applied.

The first decision to be made is the operating temperature for the crystallization process. The results of the corresponding investigation are shown in Figure 16.11. The data are typical for this kind of fermentation broths. From the figure it can easily be seen that the operating temperature of 100 °C causes an unacceptable and fast decomposition compared to the operating temperature of 60 °C. This is indicated (typically by photometry) by the generation of new compounds over the time of exposition.

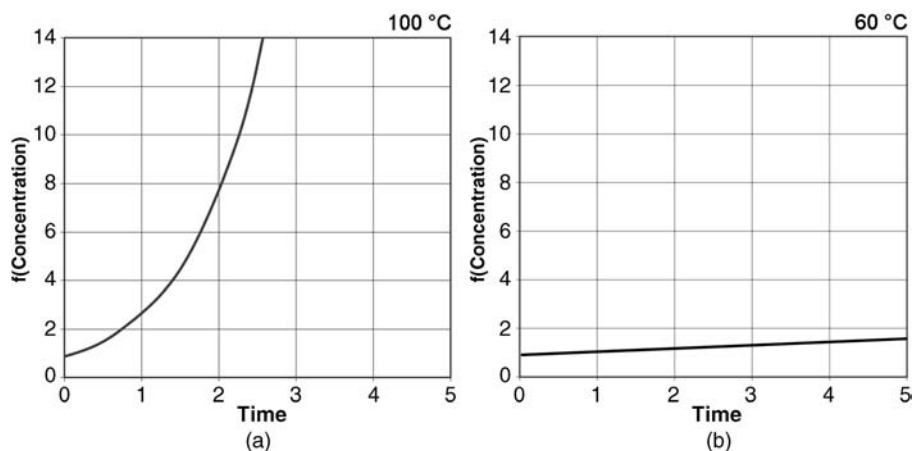


Figure 16.11 Decomposition at 100 °C (a) and at 60 °C (b).

The next step is to understand the solubility system within the field of interest. Figure 16.12 shows the findings. It can be seen that the concentration of product A is depressed by the increase of impurities' concentration. Coprecipitation is not observed. This behavior has the advantage of limiting the product losses due to the unavoidable process purge.

The design is now made on the basis of the solubility curve and the information gathered around boiling point elevations, viscosities, desupersaturation rates, and so on. Based on these findings, the crop system is proven to achieve the desired purity of >99.5% under the targeted yield of at least 90% as the mass balance in Figure 16.13 demonstrates.

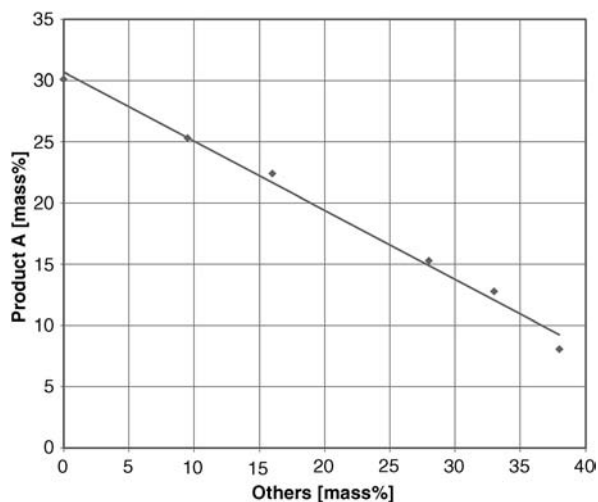
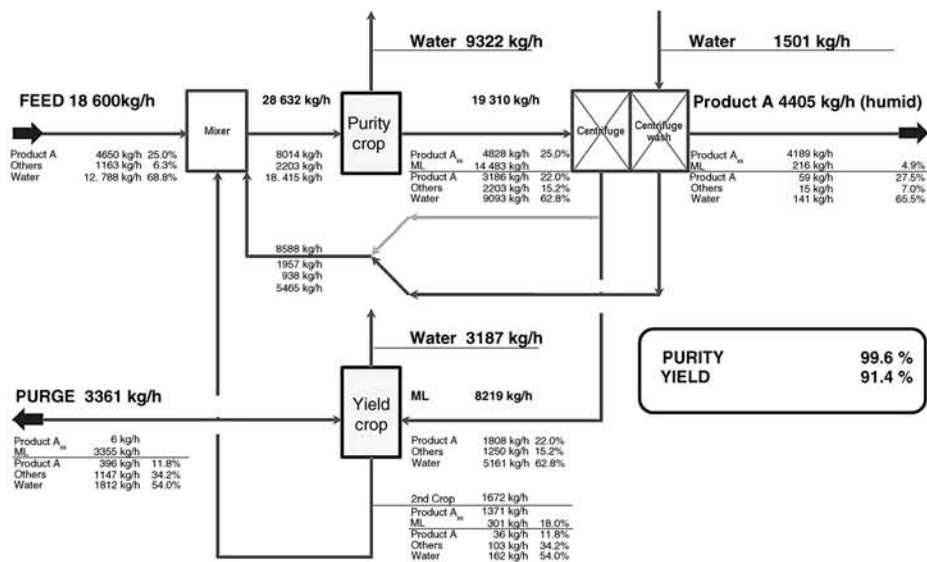
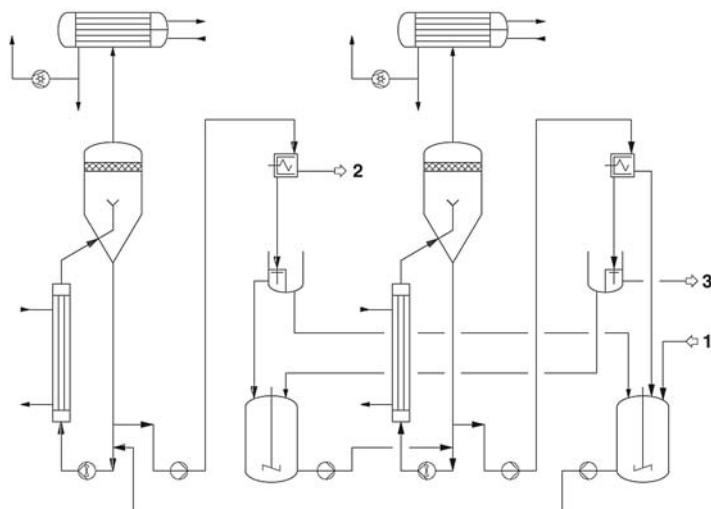


Figure 16.12 Solubility system of product A–others–H<sub>2</sub>O.



**Figure 16.13** Mass balance for the crop system crystallization of product A.



**Figure 16.14** Simplified PFD for the crop system crystallization of product A. 1: Feed liquor; 2: product; 3: purge liquor.

In the majority of the recoveries of organics from fermentation broths, the typical characteristic of those crop system recoveries is the viscosity increase with increasing concentration factors. Typically, this sets the limits for the yield figure. With higher viscosities, the resulting particle sizes get smaller and more difficult to separate effectively; hence, the separation becomes the major bottleneck and is eventually the yield limiting factor. Washing can rarely be realized, with the exception of the dilution effect only that is given by the injection water to the suspension immediately before the separation to ease the suspension flow.

The corresponding plant here consists of two FC-type crystallizers (Figure 16.14). The crystallizer on the left-hand side is operated as the first crop stage and the crystallizer on the right-hand side produces the second crop quality.

The feed stream, for example, the prefiltered, decolorized, and preconcentrated fermentation broth, enters the storage tank on the right-hand side by level control. This tank also receives the second crop filter cake from the centrifuge that mostly is a filter decanter or a filter. The second crop crystals are redissolved in the feed liquor, which is withdrawn slightly undersaturated from the preconcentration step for this purpose, before being sent to the first crop stage for crystallization of the product A. The feed flow follows the liquor level in the crystallizer. If required for other applications, this solution could be further treated for purification purposes (e.g., sent through an activated carbon station for intense decolorization).

The first crop concentrates the mixed feed to such a degree following the above mass balance that the product can safely reach the purity demand. Therefore, the concentration factor must be monitored and controlled by keeping constant one certain and selective physical property that changes with concentration. Those properties usually are viscosity, boiling point elevation, density, and so on. The control action is pointed out below.

During the concentration, the crystallization of the product A takes place. The suspension produced is withdrawn continuously, keeping constant the suspension density within this crystallizer at a sufficient value, for example, at 20 mass%. The suspension density is monitored, for example, by radiometric measurement. The suspension is separated on the centrifuge that preferably is of pusher-type to allow best washing efficiencies.

The centrate is collected in an intermediate receiver tank. This tank receives the centrate in its always filled chamber with overflow to the second chamber. The solution from the second chamber is guided to the feed mixing tank on the right-hand side and returned to the first crop crystallizer. From the filled chamber some solution is continuously withdrawn and collected in the receiver tank in front of the second crop crystallizer. The mass flow of this withdrawal decides on the concentration factor that is already described above.

The second crop crystallizer is then fed with the solution collected in the receiver tank keeping constant the liquor level in the second crop crystallizer. Hence, the liquor level in that receiver tank varies over the time and must be kept in range by setting the heating steam supply to the second crop system accordingly from time to time.

The second crop crystallizer now has to concentrate the solution to the impurity level given by the mass balance in Figure 16.13, in order to reach the yield demand. The crystallization is again designed following the rules for the design of crystallizers described above. The slurry is again withdrawn to keep the suspension density constant and given to the separation station. The separated crystal cake is redissolved in the feed stream, as already described above, whereas the mother liquor is completely returned to the receiver tank in front of the second crop crystallizer.

Before being returned to the receiver tank, the purge liquor is separated by controlled withdrawal following the same principle as described for the identical tank after the first crop crystallizer. This purge liquor is withdrawn to keep constant the impurity level in the second crop crystallizer, following a selective physical property as also described for the first crop crystallizer above, here controlling the process yield demand.

Crystallization plants such as these are typical for the downstream processing after fermentation processes. The above concept consumes about 12.5 t/h of either saturated heating steam under atmospheric pressure or vacuum steam (vapor of, for example, minimum 85 °C). The cooling water consumption is 500 m<sup>3</sup>/h and the electrical demand is about 280 kWh/h effective. Figure 16.15 shows a typical setup of such a crop crystallization system.

## 16.3

### Example Crystallization of Table Salt

#### 16.3.1

##### Introduction

The unit operation crystallization belongs to the oldest technologies used by humans. Quite a number of early civilizations were formed in coastal areas with



**Figure 16.15** Typical arrangement of a crop crystallizer system.

natural solar ponds that provided an adequate supply of the essential salt (e.g., Roman salt pans). Due to the simple process technology and the free energy supply, the solar ponds are still used today for the recovery of salt. Despite the need for huge space, the large number of workers, and the only limited purity of the solar salt, the plenty sunshine as the free-of-charge energy resource for the concentration of the seawater prevails all these disadvantages.

Sea salt consists of quite large single crystals randomly grown together. Inclusions of mother liquor inside the crystals or between the grown-together crystals, as well as gypsum as cocrystals, are reasons for the limited purity of around 98 wt%.

In many cases, therefore, salt from solar ponds is processed downstream by some purification steps. These are, for example, a combined grinding and washing process or even the complete recrystallization by the evaporative vacuum crystallization. A modern alternative is the combination of the energy-saving solar pond concentration with industrial crystallization. In such cases, the seawater



concentration is still affected by solar technology with sunshine free of charge, whereas the crystallization step is replaced by the evaporative vacuum crystallization technology.

In order to make negligible any dilution by rainfall, the final solar pond brine is collected in 10 m deep tanks, before the brine is eventually used as feed stream for the crystallization plant constantly all over the year. The clear advantage of this alternative is the improvement in regard to salt quality and particle size distribution (uniformity and particle size as well) that helps to approach a more general market than before.

### 16.3.2

#### Performance Requirements

The example used below is a typical task definition and was realized in 1980–1982 in Croatia. A salt plant has to be designed for a production capacity of 9 t/h table salt. A part of that quantity (2.5 t/h) shall be recovered as granular salt with an average particle size  $d' > 2$  mm, whereas the rest (6.5 t/h) shall be produced as PDV (pure dried vacuum) salt with a mean particle size of around 0.4 mm. The purity of the vacuum salt had to be minimum 99.7% NaCl.

Energy is provided in the form of steam saturated at 10 bar. Cooling water will be seawater with a feed-in temperature of maximum 25 °C.

The solar pond brine to be used is foreseen to be provided with a sodium chloride content (minimum–maximum) of 20–22 wt% (Figure 16.16). This solution is saturated with gypsum and contains, among others, magnesium chloride and magnesium sulfate, besides a minor concentration of potassium chloride.

### 16.3.3

#### Process Design

Due to the higher concentrations of Ca and Mg in those solar pond brines, brine purification (easing the task to achieve product purity) cannot be considered. The high consumptions of soda ash, calcined soda, and calcium chloride (or lime milk and hydrochloric acid), and the disposal costs for the filter cakes including the additional investment costs cannot reach feasibility. In this case and for this concept,

NaCl	wt-%	21.57
KCl	wt-%	0.63
MgCl <sub>2</sub>	wt-%	2.62
MgSO <sub>4</sub>	wt-%	1.82
CaSO <sub>4</sub>	wt-%	0.14
H <sub>2</sub> O	wt-%	73.2

**Figure 16.16** Typical composition of solar pond brine.

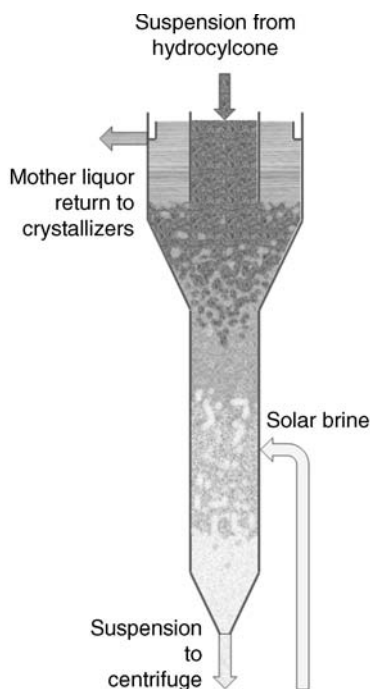


**Figure 16.17** Washing thickener device.

the task has to be fulfilled by the crystallization process on its own, only assisted by the downstream steps such as particle classification and washing. A counter-currently operated washing thickener is selected to provide this assistance (Figure 16.17).

$\text{CaSO}_4$  crystals, automatically cocrystallized with the sodium chloride crystals but significantly smaller than these, are separated from salt by countercurrent washing with a carrier solution. This way of separation takes advantage of the lower settling rates of the smaller gypsum crystals. The purest salt solution available in that ambience, for example, the solar pond feed brine, is taken as the carrier solution. This solution has only limited dissolving capacity for salt and leaves the crystal size unaffected, but replaces the significantly more impure mother liquor from the crystallization process and separates the gypsum particles.

Whereas the impurities leave the washing thickener with its overflow, the so treated solution reaches the centrifugation already prepurified before the final separation takes place. Though this treatment cannot replace a complete brine purification that provides up to  $>99.9\%$  NaCl, it avoids the chemical and other side costs and allows purities safely above the required  $99.7\%$  NaCl.

A quadruple-effect evaporative crystallization is chosen as the adequate process (Figure 16.18). Whereas FC-type crystallizers are selected for the production of PDV salt with the desired average particle size of around  $0.4\text{ mm}$ , a Messo Oslo-type crystallizer is chosen to produce the granular salt with the average particle size of

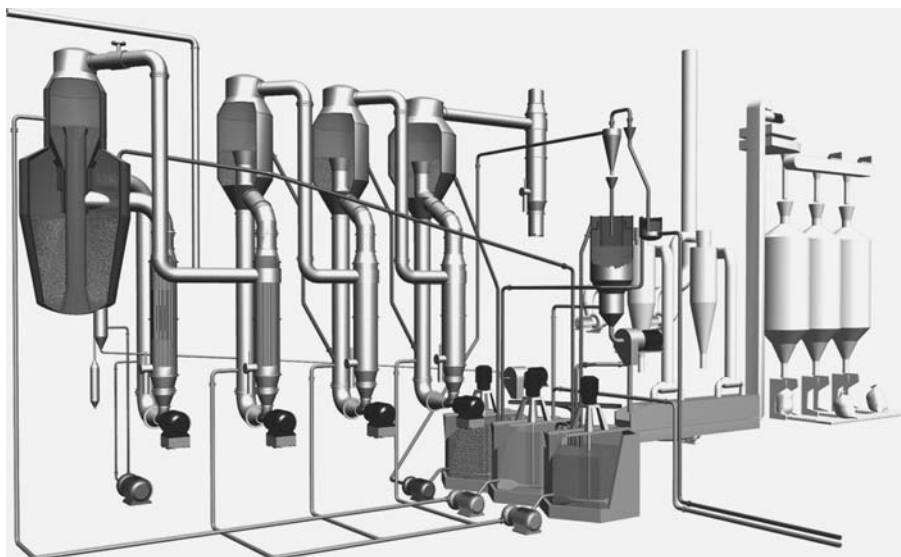


**Figure 16.18** Quadruple-effect evaporative crystallization plant with vacuum salt and granular salt production.

above 2 mm (see Chapter 11.1). The Messo Oslo-type crystallizer is selected to realize sufficiently long runtimes of several weeks between the necessary washouts that are not possible to achieve with fluidized bed crystallizers in use for salt.

In order to reach the desired particle size of 0.4 mm, decisions by experience have to be made. The salt retention times for the three FC-type crystallizers are set to 1.5 h each (span width for FCs: 0.5–2 h), the tip speeds of the impeller pumps to 14 m/s, and the tip supersaturation to maximum 1 g/l. Longer retention times do not have significant effect on the particle size, whereas lower tip speeds of the impeller pumps and lower tip supersaturations again lead to higher specific energy inputs per crystallizer.

The question of the salt retention time for the Oslo-type crystallizer can be left open until the start-up. The need to clarify the entire recirculation completely leads to a crystallizer diameter allowing any retention time between more than 10 h and lower than 20 h (easily achievable just by decreasing or increasing the crystal bed mass inside the crystallizer by simply opening or closing the salt withdrawal for a longer time).

Measures against cycling are not foreseen as the customer desires to get various sieve cuts of granular salt for different market approaches.

Considering cogeneration as not attractive for single plant, the multiple-effect evaporative crystallization is selected against a single-effect unit with mechanical vapor recompression. The latter would require reliable supply with electrical energy not existent in that certain location (at that time). Four thermal stages are selected to keep all stages in the moderate pressure/temperature field between 50 mbar and atmospheric pressure, being a feasible solution regarding the material of construction, the investment, and the specific steam consumption.

The Messo Oslo crystallizer is positioned as the first stage to take advantage of the high crystal growth rates at the high stage temperature. Moreover, taking into account the longer washout time needed for the Oslo-type crystallizer, the first position makes it easy to operate the FC crystallizers as triple-effect system separately, if, for example, a collapse of salt bed interrupts the Oslo operation for longer. Therefore, the plant is designed with a separate steam supply to the first FC effect, in order to allow the undisturbed production of the PDV salt, until the Oslo operation is restarted.

### 16.3.4

## Description of the Plant Function

The salt plant is fed with brine from the solar pond produced in the same way as earlier. However, unlike before, the brine is only concentrated near to saturation. Sodium chloride is not brought to crystallization in the fields anymore. By using the former crystallization fields instead also for brine concentration the solar pond capacity can be increased significantly.

The feed point of the concentrated brine is the receiver tank B (Figure 16.19). The only crystallizer fed from here is the Oslo crystallizer. While the concentrated brine in this receiver is still undersaturated, the Oslo crystallizer can be fed with crystal-free solution all the time – the absolute precondition for the granular production in the Oslo-type crystallizer.

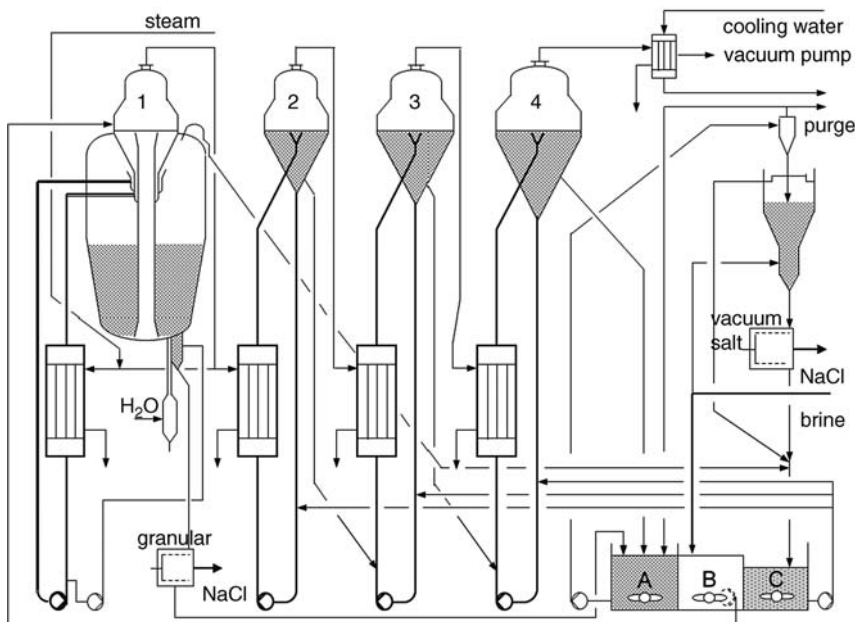


**Figure 16.19** Process flow sketch of the four-effect evaporative crystallization plant with vacuum salt and granular salt production.

Via the special salt elutriation leg, the granular salt is withdrawn from the crystallizer. Separated from the centrifugation of the PDV salt, this separation of the granular salt is effected on a pusher-type centrifuge, which is operated at low rotation speed to avoid breakage of these sensitive granular crystals.

Washing of the granular salt is not required because the amount of adherent mother liquor is negligibly small. This is also valid for the contamination with gypsum particles, which are simply slipping through the open sieve of the centrifuge basket.

The feed brine not taken to feed the Oslo-type crystallizer leaves the receiver tank B to receiver tank C by overflow. The fines-containing centrates and the hydrocyclone overflows from the separation stations are collected in the receiver tank C, too, where the still existing undersaturation redissolves the fines, before the resulting mixture is fed in parallel to the FC-type crystallizers.

The feed in parallel has the advantage of the perfect control of the suspension density dependent on the needs of the crystallization process, for example, to 20 wt% in every stage. A feed flow in series, instead, would lead to increasing suspension densities over the stages, increasing in line with the increasing concentration factors from stage to stage. Hence, a perfect suspension density in the first FC stage would have the consequence of a much too high suspension density in the last stage and vice versa.

The withdrawal of suspension is organized at first by overflow from stage to stage, and then finally to the agitated receiver tank A. This way also the sensible heats of the suspensions are used in multiple ways, thus still contributing to the heat economy of the process.

The receiver tank A is used as storage tank between the crystallization and the separation unit. The advantage of the storage tank in this position is the consequential independence of the crystallization unit and the separation. Disturbances in the one do not automatically lead to disturbances in the other. From here the separation station is served with suspension. It consists of the hydrocyclone, the washing thickener, and the centrifuge.

The hydrocyclone thickens the suspension from the 20 wt% existent in the crystallizers to some 50–60 wt%, before the suspension is sent to the centrifuge separation. The overflow liquor of the hydrocyclone is the point of the highest concentration of impurities in the process. It also contains suspended solid gypsum that is not separated by the hydrocyclone because of its fine particle size. Due to the fact that the gypsum is treated as solution, the amount of gypsum brought to the underflow is only some 10% of the amount present in the suspension from the crystallizers to the hydrocyclone. This can be regarded as the first significant purification before centrifugation.

Some of the hydrocyclone overflow is purged to balance the impurities, that is, to set the impurity concentration in the process to a constant level. This is executed by collecting the solution in an intermediate tank that is divided into two parts. One compartment is entirely filled and overflows into the other part, from where the solution is returned to the receiver tank B. From the filled compartment, the purge liquor is taken off back to the solar ponds, controlling the impurity level in the crystallizer stage 4.

This purge liquor contains, among others, the fine gypsum particles, besides the still dissolved magnesium chloride and magnesium sulfate. The purge stream is set constant at the rate needed to avoid any cocrystallization besides that of gypsum.

The task of the subsequently following washing thickener is to purify the suspension, that is, to reduce the concentration of gypsum particles and to replace the impure mother liquor against the feed brine from the solar pond as already described above. The washing thickener underflow, a purified and still concentrated suspension, is finally separated on the pusher-type centrifuge.

Preferably, the pusher-type centrifuge has two stages. The first stage is used to separate the solution from the crystal mass, and the second to wash the separated filter cake. In this way, the washing becomes significantly more effective. This is due to the washing only after the complete separation of the mother liquor (here solar pond brine) and due to the complete reformation of the filter cake before the washing.

Eventually, the crystal mass having still residual moisture of some 2% is unified with the filter cake of granular salt from the low-speed centrifuge. The mixed crystal mass is then dried in a fluidized bed drier to below 0.1%  $\text{H}_2\text{O}$ .

The dried salt is elevated to a sieving station via a bucket elevator. The sieving station separates the PDV salt from the granular salt again and the granular salt into various fractions according to the needs of the customer. The PDV salt and the granular fractions are collected in their respective silos from where packing is executed.

## 16.4 Results

Since its start-up, this plant produced 2.5 t/h granular salt and 6.5 t/h PDV salt. The hourly consumption of feed brine was 60 t. The PDV salt had a mean particle size of 0.42 mm (Figure 16.20), which remained approximately constant over all operational fluctuations. The purity reached 99.76%, calculated as  $100\% - \% \text{SO}_4 -$

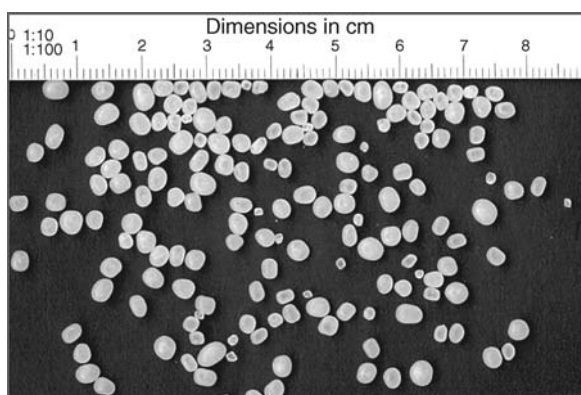


**Figure 16.20** Granular sodium chloride from the Oslo-type crystallizer. Note the rounding of the crystals due to attrition.

%Mg – %Ca. The Oslo-type crystallizer was able to produce an average particle size of above 2 mm, fluctuating between 1.8 and 3.5 mm. The period between two maxima was 2 days. While with increasing length of the operation the fluctuation became dampened, the uniformity of the salt bed was reduced.

The Messo Oslo-type crystallizer reached runtimes of around 3 weeks between washouts without any disturbance from scaling. This was a breakthrough in the Oslo crystallizer history for salt crystallization and the approved consequence of the inversion of the internal recirculation. The process required about 11 t/h of heating steam and evaporated 34 t of water per hour.

Besides a maintenance period of 1 month during the wintertime, the plant could be operated during the entire year.

## 17

### Design Examples of Melt Crystallization

*Joachim Ulrich and Torsten Stelzer*

#### 17.1

##### Concepts of Melt Crystallization

The basics of melt crystallization are provided in Chapter 15. Here, the concepts of plants and/or existing and commercially available equipment are shown. As mentioned in Chapter 15, the concepts of plants can be divided into two lines of technology: solid layer crystallization and suspension crystallization. Furthermore, in industrial applications these two techniques are split into continuous and batchwise as well as into static and dynamic (stagnant or flowing melt) operating modes. A detailed overview of the different techniques and apparatuses in solid layer as well as suspension crystallization is provided in the Sections 17.1.1 and 17.1.2.

##### 17.1.1

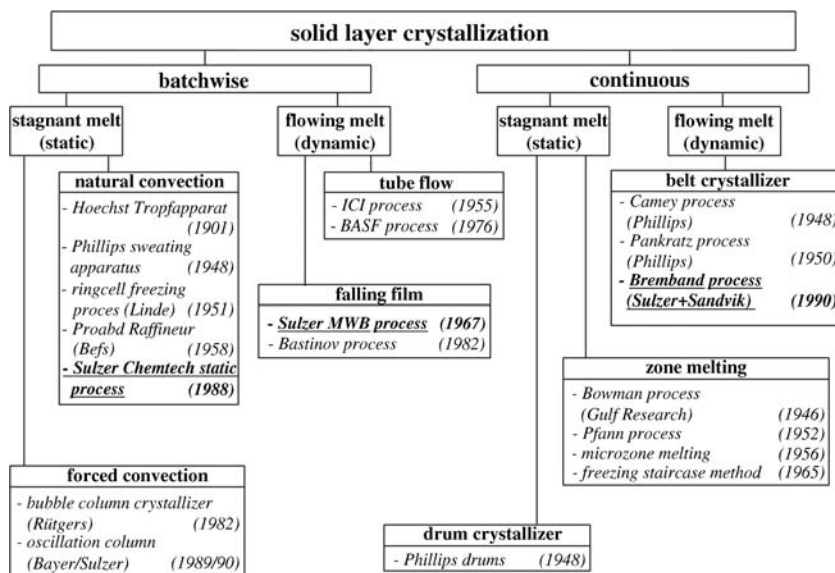
##### Solid Layer Crystallization

Figure 17.1 shows the most discussed technologies of solid layer crystallization from several providers (see, for example, Ref. [1]). The highlighted examples of equipment in Figure 17.1 will be discussed in detail.

The first group of commercially available equipment is based on the “Hoechst Tropfapparat” (sweating apparatus) patented more than 100 years ago. It is a solid layer equipment of the batch type with stagnant melts (only natural convection). These crystallizers are commercially available, for example, as the Proabd type (Befs) using tubes and as the static plate crystallizer from Sulzer Chemtech Ltd (see Figure 17.2). Both crystallizers feature cooled surfaces for crystallization of the melt.

The cooled surface for the crystal growth of the solid layer is provided in the static plate crystallizer of Sulzer Chemtech Ltd by plates that are located in the stagnant melt. The melt feedstock is progressively crystallized by cooling the heat transfer surface. As the crystallization proceeds, the remaining melt becomes more and more impure. The crystallization process needs about 2–30 h. Subsequently, the remaining residual melt is allowed to drain by opening a valve at the bottom of the apparatus. A film of melt with residual composition, however, remains unfortunately on the crystal coat. This





**Figure 17.1** Equipment of solid layer crystallization. (according to Ref. [1]).

film, or at least most of it, can and needs to be removed by postcrystallization treatments such as sweating (hence Hoechst Tropfapparat) or washing (see Section 15.3) in order to achieve higher purities. Subsequently, the final product is obtained by melting the crystal coat and collecting it in a different tank than the residue.

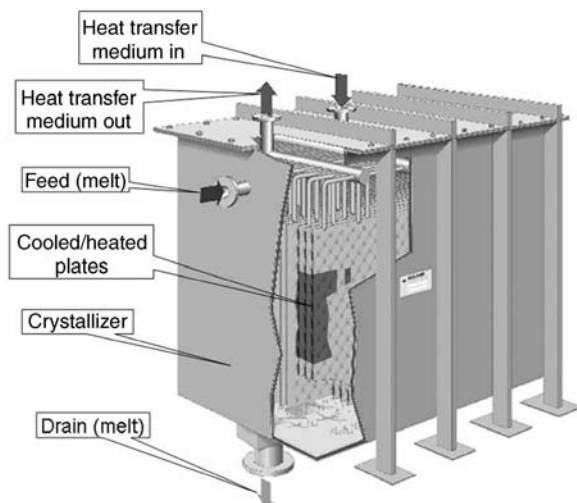


**Figure 17.2** Static plate crystallizer of Sulzer Chemtech Ltd. (reproduced with permission from Sulzer Chemtech Ltd).

Both the Hoechst Tropfapparat and the Proabd are tube bundle crystallization equipment run in the same way, as mentioned above. In principle, every plate or tube bundle heat exchanger can be used as static solid layer crystallizer; however, a few special geometrical considerations have to be obeyed.

This technique has a high operating safety due to the simple assembly (no moving parts) and no additional solid/liquid separation. However, the space–time yield of this technique is relatively small. The reason is that the heat and mass transfer are forced just by conduction and diffusion, respectively, and are supported only by natural convection. Hence, only very slow crystal growth rates lead to high purities. Due to these facts, large volumes of crystallizers are required to achieve high yields with the stagnant batchwise technique. The efficiency of solid layer crystallization processes can be enhanced by mechanisms that improve the heat and mass transfer on the one hand and by continuous operating mode on the other hand.

The second considered group of batchwise solid layer techniques consists of those with moving (forced circulation) melts, which counts to the dynamic operating mode. The flowing melt improves the heat and mass transfer, reducing the boundary layer thickness and, therefore, the possibility of constitutional supercooling. Here, for instance, the Sulzer MWB process (falling film), nowadays called Sulzer falling film process (Figure 17.3), of Sulzer Chemtech Ltd needs to be mentioned.

In this process, the crystallization takes place on the inside of a tube that is cooled from the outside. These tubes are assembled as bundles of up to 1600 tubes. The diameter is up to 70 mm and the length is up to 12–18 m. This process features, as indicated by its name, a falling film on the inside of the tubes for the melt and outside for cooling fluid. The melt coming from a feed tank is continuously circulated (pumped) through the tubes until the crystal coat at the surface reaches the desired thickness, that is, until the required percentage of product from the feed

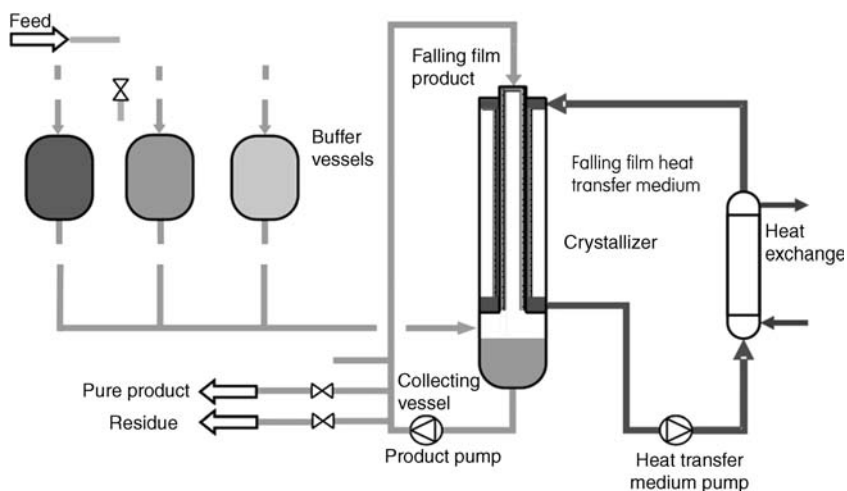


**Figure 17.3** Flow diagram of a falling film crystallizer (Sulzer MWB process). (reproduced with permission from Sulzer Chemtech Ltd).

is crystallized. Thereafter, as mentioned above, the residual melt is drained and postcrystallization treatments (for instance, in the form of sweating, see Section 15.3.1) can be conducted to remove the film of residue. Finally, the product is recovered by melting the crystal coat and collecting it in a different tank than the residue. Two more processes (ICI and BASF), besides the Sulzer falling film process, need to be mentioned. The important difference to the Sulzer falling film process is that the ICI and BASF processes have no falling film but rather the spaces in the tubes are completely filled by the melt. The cooling fluid on the outside of the tubes also does not run as falling film. Hence, the ICI and BASF processes are in the subdivision tube flow and not falling film like the Sulzer falling film process.

Furthermore, in case the resulting purity after one cycle is not enough, a staging is easily possible. Each stage after another can be conducted in the same crystallizer just by storing the products of different purities in different tanks. The dynamic processes without the multistage operating mode achieve higher purities compared to the static processes. This is shown in Figure 17.4 by means of lower distribution coefficients (for definition see, for example, Section 15.3.1) for dynamic operating mode compared to the static process. The results provided in Figure 17.4 are for the feed mixture of methacrylic acid/water [2].

Only for quite small growth rates the static processes are able to get the same purification (distribution coefficient) as the dynamic operating mode plants, however, with higher growth rates [3].

These above-mentioned dynamic operating mode plants have, besides pumps, no moving parts and produce the product in liquid form. The scale-up of the plants is quite easy, just by adding tubes or a new apparatus of tubes. Acrylic acid, benzoic acid, bisphenol A, and naphthalene are few examples of materials which are purified with such a dynamic solid layer operating mode (Sulzer falling film process).

However, the disadvantage of the processes discussed so far is that these processes just run in batchwise or semi-batchwise operating mode.

Therefore, in the third group of processes the continuously operating ones are considered, for example, belt crystallizer. The advantages of these processes are no dead time through filling and draining of the equipment as well as no waste

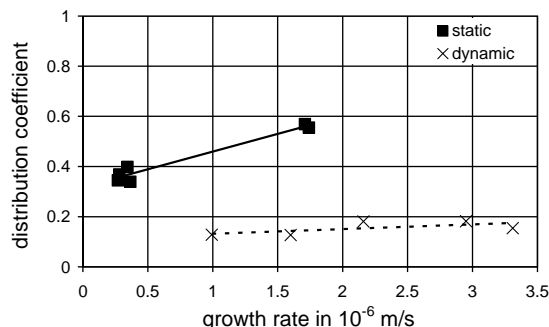


**Figure 17.4** Purification effect of crystallization of a crystal layer process in static and dynamic operating modes considering crystal growth rates (feed mixture: methacrylic acid/water) [2].

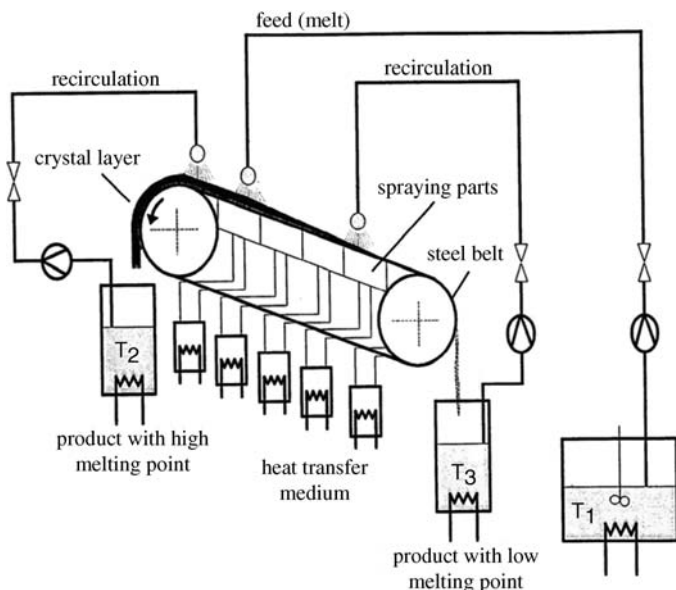


**Figure 17.5** The Bremband process. (according to Ref. [4]).

of energy by cooling and heating of the heat transfer medium and the equipment. Here, for instance, the drum flaker process of Phillips (static) as well as the Bremband process of Sulzer Chemtech Ltd and Sandvik Process Systems (Figure 17.5) need to be mentioned.

The crystallization takes place on a conveyor belt. This belt is positioned at an angle and is temperature controlled from the bottom side. The feed is distributed onto the belt in the upper third, where it crystallizes. The crystallized material is transported to the upper end of the steel belt while the residue flows down over the already crystallized product and keeps crystallizing there with the same growth rate due to the adjusted cooling profile by the different cooling zones. This is like in the Sulzer falling film equipment. By using different cooling or heating zones on the bottom side of the belt and different positioning of the recirculation of the product, postcrystallization treatments (see Section 15.3) are simultaneously possible in the same apparatus [5]. The advantage of this process is the continuously countercurrent flow operating mode in order to enhance the purification. The energy consumption of the Bremband process is less per cycle compared to, for example, the Sulzer falling film process and the purification features 1.5 times the effect of one falling film stage. Once the process is started, there is no nucleation problem since a crystal front is always available.

More detailed information on the introduced design examples of solid layer crystallization plants is, in general, industrial secret and hence not published. The authors will provide here design examples based on cold finger experiments (see Section 15.4.2) by Neumann [3]. These experiments are representative for solid layer crystallization techniques and are helpful to understand the topic concerning

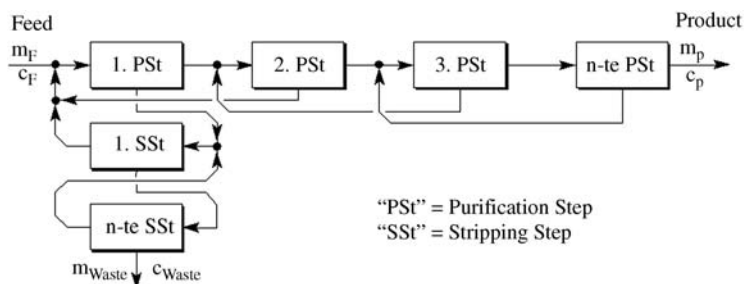


**Figure 17.6** Principle of multistage solid layer crystallization plant. (according to Ref. [3]).

product purity as well as yield and number of crystallization steps. Neumann [3] developed a simulation procedure in order to configure solid layer crystallization plants (static as well as dynamic operating mode). This simulation procedure was based on experimentally determined distribution coefficients. The experiments were carried out with the cold finger setup [3]. By using the above-mentioned simulation procedure, the user is able to design/configure the plant for each individual case, if the distribution coefficients are known. Otherwise, the coefficients can be determined with the cold finger setup.

Here, the results of Neumann [3] are shown. The starting point for the dimensioning of the plant concepts was a mixture of 90 wt% caprolactam and 10 wt% cyclohexanone. The feed mass amount was 1000 kg. The aim was purification of caprolactam to at least 99 wt% (1 wt% cyclohexanone) and a yield of 62%. Due to the demands of high product quality and coincident quantity in general, multistage crystallization plants are required. Such plants consist of a combination of purification steps (PSt) and stripping steps (SSt). This principle is similar to that of distillation. The purification step increases the purity and the stripping step enhances the yield. The principle of such multistage crystallization is to feed the residual melt from the purification or stripping step ( $n$ ) to one of the previous purification or stripping steps (here,  $n - 1$ ). In Figure 17.6, the principle of a multistage solid layer crystallization plant is shown.

By means of the simulation software, several concepts of plants were analyzed. The results are summarized in Table 17.1.

In Table 17.1, it can be seen that the concept of the static solid layer crystallization without postcrystallization treatments leads to the desired purity. The yield, however,

**Table 17.1** Results of several concepts of solid layer crystallization plants [3].

Concept	Configuration	Yield (%)	Purity (wt%)	Conclusion
Static	3 PSt + 2 SSt	38	99.0	Not satisfied
Static with sweating	3 PSt + 2 SSt	68	99.0	Fulfilled
Static with diffusion washing	2 PSt + 1 SSt	73	99.0	Fulfilled
Dynamic	2 PSt + 1 SSt	72	99.0	Fulfilled
Dynamic with sweating	2 PSt + 1 SSt	75	99.0	Fulfilled
Dynamic with diffusion washing	2 PSt	74	99.0	Fulfilled

does not match the target value of 62%. Hence, this plant concept is not recommendable. All the other concepts shown in Table 17.1 fulfill the target values of purity and yield. Moreover, it is obvious that by means of the dynamic operating mode in general, one purification step and one stripping step can be saved compared to the static operating mode of a solid layer crystallization plant. As mentioned above, the heat and mass transfer are improved by forced circulation of the melt (dynamic). Since the required space for the plant is smaller, the investment costs are lower.

### 17.1.2

#### Suspension Crystallization

Suspension crystallization is capable of producing very pure crystals mostly in a continuous operating mode, which is an advantage compared to the most batch solid layer crystallization processes. Another positive feature compared to solid layer crystallization is the better purification per process step and hence a less number of process steps usually with respect to crystallization. Therefore, suspension crystallization plants need in principle less energy compared to solid layer processes. Whether the investment costs of such plants are smaller as well depends on the complexity of the moving parts in suspension plant concepts compared to solid layer concepts (no moving parts, except pumps).

Figure 17.7 shows the most discussed equipment or concepts in suspension crystallization from several providers (see, for example, Ref. [1]). The highlighted examples of equipment in Figure 17.7 will be discussed in detail.

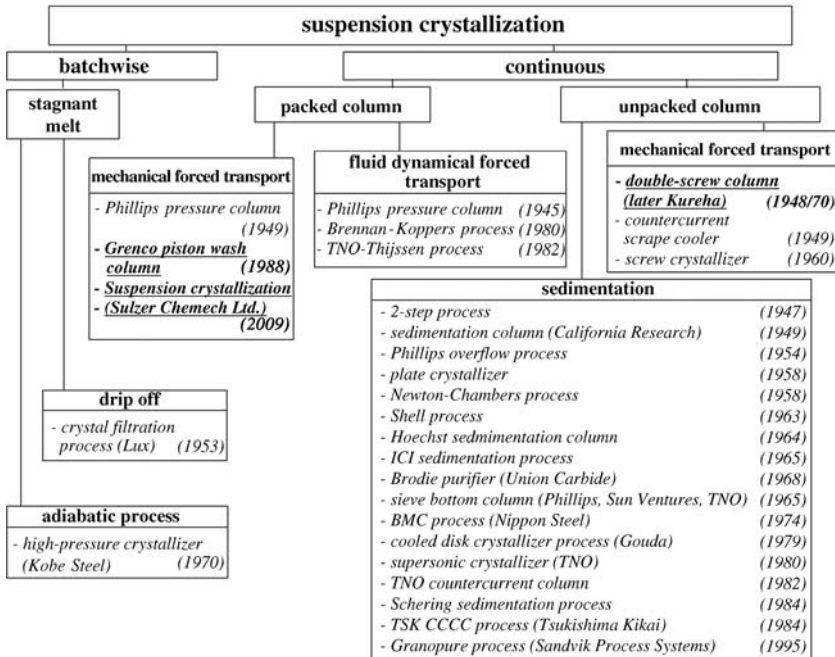
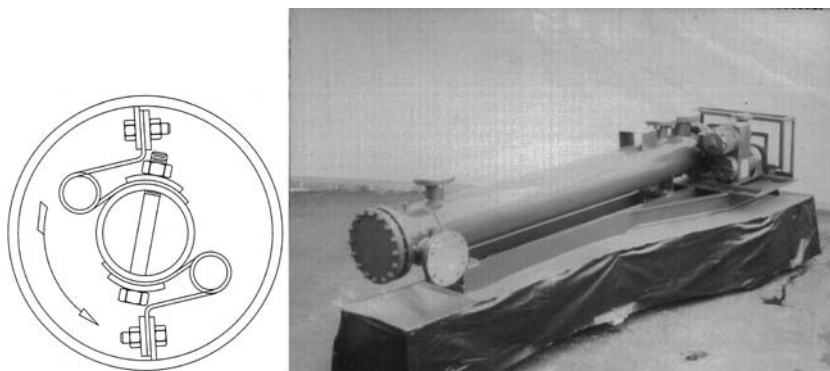


Figure 17.7 Equipment of suspension crystallization. (according to Ref. [1]).



**Figure 17.8** Scraped surface heat exchanger with rotating scrapers (Armstrong-Chemtec Group).

The suspension processes are usually initiated on cooled surfaces, as in solid layer crystallization, and the crystals are periodically scraped off, and most of the crystal growth occurs on the crystals suspended in the melt. The melt gets supercooled at the scraped cooler wall. The supercooled melt is mixed by the scraper into the bulk of the melt and provides the growth potential. Thus, the crystal surface area available for growth is the total surface area of a very large number of crystals and is not limited to the cooled surface area as in solid layer crystallization. The crystal growth rate can be much lower (therefore, much purer crystals) and still have the same yield. The specific mass transfer surface area in suspension crystallization amounts to approximately  $10^4 \text{ m}^2/\text{m}^{-3}$ . Commercially available so-called scraped surface heat exchangers (Figure 17.8) are quite frequently used to generate the initial crystals.

Other manufacturers (for instance, GMF Gouda), besides Armstrong-Chemtec Group, need to be mentioned in this field. This type of equipment provides cooled surfaces for crystallization of melts. Rotating scrapers or disks scrape the crystals off the cooled surfaces and transport those crystals to the growth vessel (see Figure 17.9).

As the name growth vessel suggests, the created crystals (in the cooled surface crystallizers) have time to increase in size (grow) in the vessel. Furthermore, the crystals are kept evenly suspended within the vessel by an agitator. Therefore, it is named suspension crystallization. As can be seen in Figure 17.9, the crystal suspension is continuously circulated through the crystallizer and the growth vessel. Hence, continuously new crystals are generated on the one hand and on the other hand the mature crystal suspension (suspension with desired crystal size) is continuously discharged out of the growth vessel to further postcrystallization treatments (see Section 15.3). Here, for instance, a wash column is shown in the principle process flow diagram in Figure 17.9. Due to continuous creation and discharge of crystals, the suspension density is kept almost constant. A similar design of suspension crystallization, as mentioned above, by Sulzer Chemtech Ltd (the former Freeze Tec B.V.), is provided by GEA Messo PT (the former Gresco and later Niro PT), just without a separate growth vessel (see Figure 17.10).

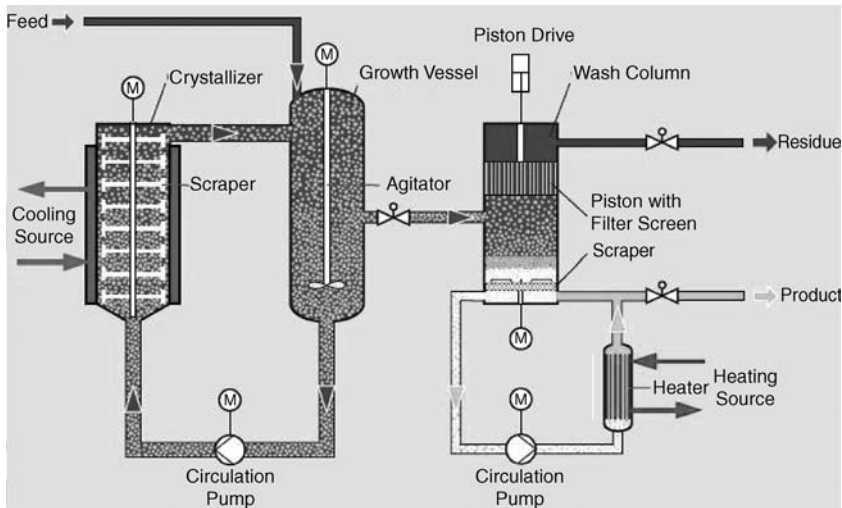


**Figure 17.9** Principle process flow diagram of a suspension crystallization process. (reproduced with permission from Sulzer Chemtech Ltd).

There are numerous examples of purified materials by the above-mentioned two types of suspension crystallization process designs; some of them are acetic acid, caprolactam, methacrylic acid, and phenol. The two discussed suspension crystallization concepts, shown in the Figures 17.9 and 17.10, count to the continuous packed column with mechanical forced transport.

Another design concept of a suspension crystallization process (unpacked column) that deserves mention is the double-screw column, nowadays called Kureha double-screw purifier or KCP column (see Figure 17.11) [6].

In a KCP column, the crystals are transported by a double-screw conveyor from the bottom to the top of the column (mechanical forced transport). At the top of the column, the crystals are molten (molten product). Some part of the molten product

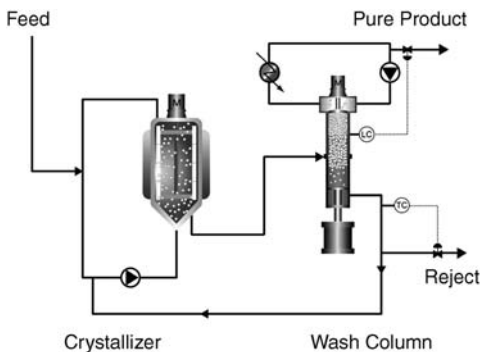


**Figure 17.10** Principle process flow diagram of a suspension crystallization process without growth vessel. (reproduced with permission from GEA Messo PT).



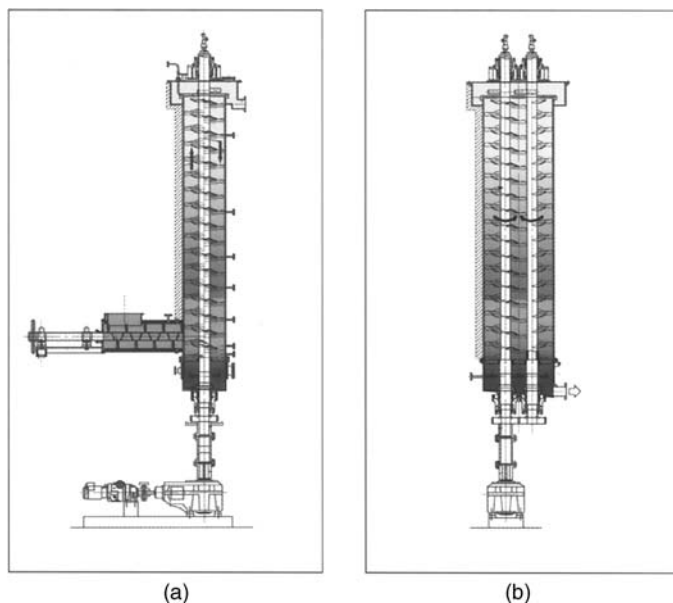


**Figure 17.11** (a and b) Two-side view of KCP column with the crystal suspension transported by double-screw conveyor [7].

is used as reflux. The reflux washes the crystals while moving in countercurrent direction just like in a wash column (see Section 15.3.4). Hence, the KCP column is a wash melt column. At the bottom, some of the highly concentrated residue is taken out. The KCP column is a proven design concept in Japan with about 20 applications, for instance, *p*-dichlorobenzene. The process is described in more detail, for example, by Rittner and Steiner [8].

As mentioned for solid layer crystallization, the authors would like to provide more detailed information on suspension crystallization plants, too. However, this information is, in general, industrial secret and hence not published.

## 17.2

### Outlook

The number of applications of melt crystallization (solid layer as well as suspension) is continuously growing. This development is supported by the fact that in the future a paradigm shift is arising in terms of the design of chemical, pharmaceutical, and food processes, which means away from single plants toward to the so-called hybrid processes. Hybrid processes mean a combination of several separation techniques, for example, distillation and crystallization, in order to enhance the throughput, the heat and mass transfer, and the reaction rates. Hybrid processes are a subset of the so-called process intensification techniques. Process intensification paves the way

for reducing the size of plants. Therefore, the paradigm shift leads to a more green chemistry and engineering that enables sustainable development. Furthermore, process intensification results in lower investment and operating costs. The important thing is, however, that melt crystallization is in that respect a part of process intensification. An example of a hybrid process consisting of distillation and melt suspension crystallization is the purification of 4,4'-diphenylmethane diisocyanate [9].

## References

- 1 Özüguz, Y. (1992) Zur Schichtkristallisation als Schmelzkristallisationsverfahren. Ph.D. thesis, Universität Bremen, Fortschrittsberichte VDI, Reihe 3, Nr. 271, VDI Verlag, Düsseldorf.
- 2 Delannoy, C., Ulrich, J., Fauconet, M. (1993) Laboratory tests on an organic acid as a basis for a scale up operation, in proceedings, Vol. 2, 12th Symposium on Industrial Crystallization, Warsaw/Poland, 21–23 Sept. 1993 (ed. Z.H. Rojkowski), pp. 1-049–1-054.
- 3 Neumann, M. (1996) Vergleich statischer und dynamischer Schichtkristallisation und das Reinigungspotential der Diffusionswäsche. Ph.D. thesis, Universität Bremen, Papierflieger, Clausthal-Zellerfeld.
- 4 Hünken, I. and Ulrich, J. (1993) *Chem. Ing. Tech.*, **65**, 91–102.
- 5 Ulrich, J., Hünken, I., Fischer, O., and König, A. (1992) *Chem. Ing. Tech.*, **64**, 842–844.
- 6 Yamada, J., Shimizu, C., and Saitoh, S. (1982) Purification of organic chemicals by Kureha continuous crystal purifier. Proceedings of 8th ISIC (eds S.J. Jancic and E.J.de Jong), pp. 265–270.
- 7 Ulrich, J. (2006) *Fluidverfahrenstechnik – Grundlagen, Methodik, Technik, Praxis* (ed. R. Goedecke), Wiley-VCH Verlag GmbH, Weinheim, pp. 1131–1196.
- 8 Rittner, S. and Steiner, R. (1985) *Chem. Ing. Tech.*, **57**, 91–102.
- 9 Dette, S.S. (2010) *Chem. Tech.*, **39**.

## Index

### **a**

additives 4, 75, 76, 87, 106, 114

- classification 122
- disruptive effect 114, 115
- effect on crystallization (*See* impurities)
- inhibited growth of crystal 111
- modeling 120
- tailor-made 122

adsorption

- energies 98
- impurity 114, 134
- isotherms 108
- surface 111

agglomerates 4, 75–77, 83, 177, 195, 244

- during crystallization 80–83
- disintegrate 78, 79
- kinetics 77
- mechanical properties 83, 84
- parameters influencing 77–80
- particle size 80, 82
- qualitative assessment of hardness 84
- spherical 83
- steps involved in 76

aggregation 19, 38, 75

agitation 69, 79, 247, 249, 258, 259, 266

ammonium sulfate

- growth rate 112
- normalized growth rates 108

amorphization 284, 285

amorphous 85, 86, 99

- crystallization of fraction 157
- paracetamol, DSC thermogram 157
- solid product 242

anisotropy 15

antisolvent

- drawbacks of addition 191
- use 190, 191

antisolvent crystallization 61, 174

- crystals of an active compound crystallized by 241
- precipitations 240
- solubility curve 174

ascomycin derivative 19-epimer

- depletion behavior of impurity 141

aspirin production process scheme 145

atom–atom interactions 119

attachment energy 117, 118, 120, 121, 123

- based models and strategies for solvent selection for 202

axial impellers 250

- helical ribbon impeller 252
- pitched blade turbine 250–252
- propeller 250

### **b**

BASF-process 328

batch crystallizations 4, 188, 193, 198, 199, 247

- crystallization period 197, 198
- generation of supersaturation in 189–192
  - – cooling 189, 190
  - – evaporation 191, 192
  - – use of antisolvent 190, 191
- initiation, nucleation phase 192, 193
- manipulating particle shape 201, 202
- mixing 247
- organic moieties crystallization 188, 189
- scale-up considerations 198–201
- seeded batch crystallizations 193–197 (*See also* seeding)

batch crystallizer

- concept and design 183, 184
- mass and population balance 184, 185
- schematic presentation 184

batch process, principles 187

binary system 36–38

- phase rule 36

blending 247, 256–259

- degree of homogeneity 256, 257
  - influence on blend times 267, 268
  - laminar blending 258, 259
  - significance of circulation rate 258
  - significance of microblend time 259
  - turbulent blending 257, 258
  - bottle test 301
  - Bragg's law 150
  - Bravais–Friedel–Donnay–Harker (BFDH) model 116, 117
  - Burger–Ramberger rules 91, 155
- C**
- cake forming filtration 276–277
  - carbamazepine
    - DSC thermogram 156
    - TG-FTIR 158
  - carbon atoms
    - hexagonal symmetry 1
    - two face-centered cubic lattices 1
  - carbon crystallizing modifications 2
  - centrifugation 277
  - classical nucleation theory 107, 108
  - Clausius–Clapeyron equation 40
  - cold finger apparatus 302
  - collision breeding 180
  - common ion effect 106
  - computational fluid dynamics (CFD) 268
  - contact angle 20
  - continuous crystallizers 176, 178, 180, 204
    - adjustment of granulometry 209–211
    - centrifuges used, in crystallization processes 228, 229
    - concept and design 178, 204
    - crystallization processes 247
    - mixing 247, 248
    - crystallizer selection 215, 216
    - crystal size distributions, manipulation 225–226
    - DTB group crystallizers 220–222
    - energy input
      - importance of 209
      - and retention time 212–215
    - FC group crystallizers 218–220
    - features of process 229–232
    - group of fluidized bed crystallizers 222, 223
    - mass balance in 176
    - mean particle size 180
    - nucleation rate in 179, 180
    - operation
      - concept and design 183, 184
      - mass balance in 176
      - mean particle size 180
      - population balance 176–178
      - secondary nucleation 180–183
    - periphery 226–229
    - population balance 178, 179
    - and modeling 223–225
    - retention time, and attrition 211
    - secondary nucleation 180–183
    - importance 204, 205
    - seeding of draft tube (DTB) and Oslo crystallizers 216–218
    - simple crystallization plant, flowchart 227
    - supersaturation, control of 205–209
    - surface cooling crystallization 229, 230
    - suspension densities, adjustment of 232
    - vacuum cooling crystallization 230, 231
    - vacuum evaporation crystallization 230–232
  - cooling crystallization 21, 22, 54, 61, 138, 145, 175, 176, 189–192, 196, 203, 247, 248
  - Coulomb interactions 119
  - crop crystallization, for organic compounds 310
    - definition of task 311, 312
    - fields of application, for crop principle 310, 311
    - selection of process design 312–316
  - crystal lattice 7
    - building blocks and symmetries 7–9
    - lattice defects 12–14
    - Miller indices to describe crystal faces 11, 12
    - unit cell 9–11
  - crystalline products, annual production of 5
  - crystalline products characterization 149
    - in-process characterization 167–170
      - FBRM and PVM 169, 170
      - Raman 168, 169
      - turbidity 167, 168
    - particle shape and size 161–165
    - laser light diffraction 163, 164
    - microscopy 163
    - particle size distribution, characteristic values and graphs 161, 162
    - powder flow properties 165–167
    - sieving 165
    - solid intrinsic properties 149–160
      - composition 158–160
      - crystal structure 150–154
      - differential scanning calorimetry (DSC) 154–157
      - dynamic vapor sorption (DVS) 158–160
      - isothermal microcalorimetry 157, 158
      - solid-state NMR (ssNMR) 152–154
      - thermogravimetry (TG) 158
      - thermodynamic properties 154–158
      - vibrational spectroscopy 151, 152
      - x-ray powder diffraction (XRPD) 150, 151

- crystalline state, determine product properties 4
  - crystallization of table salt 316–318
    - description of plant function 321–323
    - performance requirements 318
    - process design 318–321
    - results 323, 324
  - crystallization period 197, 198
  - crystallization processes 134, 135, 149, 167, 193, 196, 197, 199
    - typical goals 188
  - crystallization product 132, 139, 248
  - crystals
    - additive inhibited growth 111
    - crystal face, description of 12
    - cubic crystal with three lowest-indexed faces 27
    - faces polarities 201
    - growth rates 24
      - determination 110
    - habit, construction 117
    - lollipop-like structures 243
    - needle-like crystals 17, 194
    - perfection 243
    - rock sugar 2
    - size (*See* crystal size)
  - crystal size 98, 180, 193, 203, 205, 210, 213, 215, 217, 223, 225, 244, 319, 332
    - distribution (CSD) 204, 209, 226, 227
    - increase in 217
    - manipulation of distributions 225, 226
  - CSD. *See* crystal size, distribution
  - cumulative mass distribution function 161
- d**
- degree of evaporation 198
  - degree of supersaturation 99, 130
  - degrees of freedom 36, 37, 42, 99, 188, 194
  - designer impurities 122
  - diamond 1
    - crystals 1
    - lattice arrangements 3
  - diastereomeric system 50–53
  - differential scanning calorimetry (DSC) 91, 154–157
    - heat flux 154
  - diffusion 24, 32
    - coefficient 136, 137
    - processes 142
    - washing 298
  - discharge of crystals 216, 332
  - dispersion 23
  - dissolution 14
  - distribution coefficient 133, 135, 137, 138
  - downstream processes 142–146, 187, 201, 275
    - cake forming filtration of suspension 276
    - drying 280
      - amorphization during drying 284, 285
      - drying behavior, characterization 284
      - effect on particle size distribution 285–288
      - of hydrates and solvates 282, 283
      - phases of 281, 282
      - reslurrying and washing 144–146
    - solid–liquid separation 275, 276
    - solid–liquid separation and sweating 143, 144
    - transfer of suspension 275
    - washing 280, 281
    - workflow diagram 147
  - draft tube crystallizer, scale-up rules in 200
  - drain point in process design 305
    - in crop system crystallization scheme 306
    - for impurities
      - in a continuously operated crystallizer 306
      - in zero liquid discharge crystallization 309
    - in recrystallization principle 307
  - drowning-out crystallizations 175
  - drying 77, 83, 157, 197, 229, 248, 280
    - amorphization during drying 284, 285
    - drying behavior, characterization 284
    - effect on particle size distribution 285–288
    - of hydrates and solvates 282, 283
    - phases of 281, 282
  - dynamic vapor sorption (DVS) 93, 158–160
- e**
- effective distribution coefficient 139, 142, 144
  - electrolytes 61, 106, 107
  - energy barriers, for polymorph crystallization 97
  - enthalpy 88
    - of condensation 18
    - for creation of new interface 18
    - of crystallization 26
    - melting 41, 47
  - enthalpy of fusion 106
  - entropy 88
  - epsomite growth, and dissolution rates 113
  - equilibrium 14, 35
    - construction 15
    - solid–liquid equilibria 37, 40
    - solution 38, 39
  - equivalent circle diameter (ECD) value 163
  - eutectic temperature 37
  - evaporation 4, 49, 64, 191, 192
    - drawbacks 191
  - evaporative crystallizations 191, 199
  - Ewald summation 119

**f**

- faces F, S, and K 25
- falling film crystallizer 327
- fatty acid 4
- FBRM probe 169, 170
- feed stream 178, 311, 315, 316, 318
- fermentation broths
  - separate carbohydrates from 311
  - typical products from 310
- filterability
  - improvement 278–280
  - in laboratory, characterization 277, 278
- flat F faces 25
- flow
  - ability 187, 188, 194
  - axial 200, 250, 252, 253
  - continuous flow profile 263, 264
  - dimensionless flow rate 258
  - feed flow in series 322
  - free-flowing product 4
  - heat flow 52, 66, 154–157, 159, 161
  - melt 327
  - pattern 262
  - powder flow properties 165, 166
  - process flow diagram 332, 333
  - radial 250
  - recirculation flow rate 207, 212, 220
  - turbulent flow regimes 250, 257
- fluidized bed crystallizers 222–224
- force field 119
- fractional crystallization 53, 131, 133, 134
- fragmentation process 183
- fragments/secondary nuclei 183
- Fraunhofer diffraction instrument 163, 167
  - principle 164
- free energy 15, 86, 88–90, 92, 93, 95–98, 123, 317

**g**

- Gibbs free energy 88
- graphite 1
  - lattice arrangements 3
- growth 14
  - average growth rate value of a paracetamol 112
  - crystal growth rates 111–114
  - dependence of growth rate on supersaturation 28, 31
  - depend exponentially on supersaturation 28
  - and dissolution rates
    - of epsomite 113
    - of NaCl 114
  - 2D nucleation 28
  - of face as perpendicular displacement 30

- ideal crystals 27, 28
- influence of  $\text{Fe}^{3+}$  on growth rate of ammonium sulfate 108
- organic molecules, classification of cooling rates in 190
- rate of crystal face 25
- real crystals 28–31
- at screw dislocation 29
- slice formation 118
- spirals 29

**h**

- habit-modifying agents 115
- Hausner ratio 166
- heat
  - conductivity, of mother phase 32
  - liberated by crystallization 32
  - transfer 32, 176, 247, 249, 272, 289, 294
- heterogeneous seeding 193
- homeopathic seeding 195
- humidification 284
- humidity 4

**i**

- impellers 249, 250
  - characteristics of common impeller systems 251
  - computational fluid dynamics (CFD) 268
  - impeller-type stirrer 200
  - Isojet 251
  - power consumption 253–255
    - bottom clearance 256
    - diameter ratio 255
    - filling level 256
    - multistage impellers 256
- impurities
  - concentration 135
  - contents
    - of L-isoleucine and L-leucine crystals 141
    - as a result of suspension (melt) crystallization of 144
  - incorporation, and purification mechanisms 131–147
    - crystallization conditions influence 135–142
    - crystallization technique, and rate of crystallization 137–139
    - downstream processes 142–146
    - fractional crystallization 133, 134
    - impurities, inclusion and surface adsorption 134–136
    - mixing 142
    - process development, workflow to “manage” impurities 146, 147
    - product yield 136, 137

- solubility in solid state 132, 133
- solvent applied 139–142
- influence on crystallization
- crystal growth rates 111–114
- habit modification 114–116
- nucleation rates 107–111
- solubility 105–107
- location 130
- management workflow 146
- incorporation energy 121
- induction time 23
- industrial crystallization
  - equipment used in 5
  - from solution 173
- influence of impurities, on modeling
  - additives modeling 120–122
  - calculating crystal habit 116–118
  - molecular modeling 118–120
  - surface energy model 117, 118
- integrated crystallization 147
- interaction energy 26
- interaction enthalpy 130
- interfacial kinetics 33
- interstitial mixed crystals 132
- isothermal evaporative crystallization 191
- isothermal microcalorimeter 157, 158

## **k**

- K-face 27
- kinetics
  - agglomeration 77
  - crystallization 135, 198
  - dissolution 63, 65, 66
  - effects 111
  - for good crystal growth 191
  - interfacial 33
  - transformation 94
- kink positions 26
- Kirchhoff relation 40
- Kononow' rule 133
- Krystal crystallizer 223

## **l**

- lab crystallizer 197
- laser beam 169
- laser light diffraction 163
- lattices
  - of closely packed spheres 11
  - constants and angles for crystal systems, relation 10
  - construction of 2D lattice 8
  - cubic
  - indices of three lowest indexed faces 12
  - sodium chloride 2

- defects 12–14
- energy 118
- definition 119
- formation of twin in fcc lattice 14
- integration method 111
- lattice defects ordered by dimensionality 13
- sssmodel for closest packing of spheres 9
- two-dimensional lattice 10
- unit cell as smallest building block 10
- vacancy and interstitial atoms 13
- L-leucine crystals
  - impurity content 141
- limit of quantification (LOQ) 153
- liquid homogeneous mixture 38
- liquid–liquid demixing 35
- low-compressibility index 166

## **m**

- macroimpurities 129
- magic angle spinning 153
- mass
  - balance 176, 178, 230, 232, 313–316
  - changes 46
  - crystallization 5, 35, 205, 248
  - flux 32
  - through bulk of mother face 32
  - transfer 267, 271, 293, 294, 327, 331, 334
  - coefficient 136
  - by diffusion 32
  - limitations 135
  - rate 142
- transport 33
- mean crystal size 209
- mechanical vapor recompression (MVR) 227
- mechanical wash column 300
- melt crystallization
  - benefits 290–292
  - characteristics 289
  - definitions 289, 290
  - laboratory techniques 301
  - bottle test 301
  - cold finger experiments 301, 302
  - zone melting 303
  - postcrystallization treatments 295–299
  - processes 292
  - solid layer crystallization 292–294
  - suspension crystallization 294, 295
- melts 157
  - crystallization 4, 105, 291, 292, 325, 332
  - enthalpy 40, 51, 57, 91, 94, 155
  - at eutectic temperature 37, 50
  - phase diagrams 44
  - measurement 46–50
  - types, and occurrence 44, 45

- phase equilibria 46
  - zone 303
  - Messo turbulence crystallizer 220
  - metastability 23, 175, 192
  - metastable zone 22, 23
  - microimpurities 129
  - microscopy 46, 100, 162, 163
    - optical microscopy 151
    - particle size distribution by 163, 164
    - Raman microscopy 100, 152
  - Miller indices 116
    - to describe crystal faces 11, 12
  - mixing
    - blending 256
    - in crystallization processes 142
    - devices 237
    - enthalpy of 41
    - impellers and agitation systems 249
    - micromixing processes 268
    - modifying geometry 236
    - optimal 64
    - precipitation 235
    - tasks in crystallization 248
    - categories 248, 249
    - two fluid streams 239
  - models
    - for derivation, rate of displacement 30
    - growth via 2D surface nuclei 28
    - influence of impurities 116
    - lattice model of closest-packed spheres 11
    - and mechanisms for suspension of solids 263, 264
    - mixing during precipitation 238
    - modeling approaches, tracing 123
    - modeling of additives 120
    - model tests 269
    - molecular modeling 113, 118
    - population balance and 223–225
    - predictive models 67
    - surface energy model 117
    - tracing of modeling approaches 123
  - molecular complexes formation 106
  - molecular dynamics (MD) investigations 123
  - molecular mechanics approaches 118
  - monotropic systems 156
  - morphologies, crystals 16
  - MSMPR
    - continuous crystallizer 178
    - equations 224, 225
- n**
- nanocrystals 308
  - nomenclature 88, 250
  - nonmiscibility, phase behavior 132
  - nucleation 193, 195
    - of citric acid 24
    - correction factor 20
    - of crystals 17
    - metastable zone and induction time 20–25
    - primary nucleation 18–20
    - droplet with size  $r$  from a supersaturated vapor phase 18
    - 2D nucleation 19, 25, 27, 28, 123
    - primary, categories 20
    - qualitative dependence on 19
    - rate 19, 179
    - plot of 179
- o**
- onionskin model 137
  - optical microscopy 151
  - organic moieties crystallization 188, 189
  - organic solvents 22, 23, 58, 153, 173, 239, 240, 244, 245
  - Oslo crystallizers 216–218, 321
  - Ostwald's law of stages 25
- p**
- paracetamol
    - average growth rate value 112
    - DSC thermogram 155
    - polymorphs 151
    - Raman spectrum 152
    - XRPD 151
  - particles
    - of benzoic acid precipitated using 240
    - coarser 216, 260
    - production of 216
    - density 79
    - diameter 161
    - equally charged 76
    - formation of solid bridges 77
    - gypsum 319, 323
    - mass 78, 180
    - nonspherical 164
    - overlapping 170
    - platelike 165
    - rodlike 165
    - seed 195, 218
    - size (*See* particle size)
    - spherical 165, 169
  - particle size
    - agglomerates 80
    - average 318, 319, 324
    - crystallization process 225
    - determinations 163, 165, 169, 180, 187, 194, 195, 199, 245, 249



- distributions 4, 162, 163, 165, 178, 187, 188, 194, 199, 267
  - characteristic values and graphs 161, 162
  - laser light diffraction 164
  - measurements, comparison 165
  - microscopy 163
  - as function of operating conditions 244–246
  - of seed 79
  - for Bayer process 79
  - PBC theory 120, 121
  - phase diagrams
    - binary 38, 39
    - informative value 36
    - liquidus curve 39–41
    - quantification 38
    - quaternary systems 43, 44
    - target compound 134
    - target product 137
    - temperature–concentration diagram 37
    - ternary solubility phase diagrams 35
    - ternary systems 42–44
  - phases 36
    - coexist in equilibrium 37
    - diagrams (*See* phase diagrams)
    - rule universally valid for 37
    - in binary system 36–38
    - transitions 41, 45–49, 57–60, 64, 154, 298
  - polar solvents 123, 202
  - polymorphic transformations 59, 194
  - polymorphism 5, 85
    - of precipitates 241–243
  - polymorphs 4, 35, 37
    - C13 MAS ssNMR spectra section 153
    - conversion 169
    - disappearing 99
    - domains of occurrence 242
    - formation 97
    - choice of solvent 99
    - crystallization methods 99
    - principles 97–99
    - properties 86
    - selection of optimal form for development 101, 102
    - of solid-state forms (*See* thermodynamics)
    - types of screens 100, 101
  - postcrystallization treatments 295–297, 302, 329, 332
    - choice, depend on 299
    - sweating 297, 298
    - wash columns 299, 300
    - washing 298, 299
  - precipitations 235
    - antisolvent precipitation 240
    - variability in particle size distribution 246
    - gel formation during 242
    - model of mixing during 238, 239
    - semi-batch precipitations 236–238
    - from solution by mixing two streams 235
    - devices and mixing schemes 235, 236
    - triangular solubility diagram 245
    - using supercritical fluids 239–241
  - pre-exponential factor 107
  - preferential orientation 151
  - probability density function 161
  - programmed parabolic cooling 197
  - purification process 120, 328
    - abecarnil purification 138
    - by countercurrent washing and 308
    - of crystallization, crystal layer process in 328
    - by enhancing incorporation impurities 293
    - impurity incorporation, and purification mechanisms (*See* impurities)
    - temperature-induced (*See* sweating)
- q**
- quadruple-effect evaporative crystallization 319, 320
  - quartzite crystals 1
  - quaternary systems 35
    - phase diagrams 42–44
    - reciprocal salt pairs 72–74
- r**
- radial impellers 252
    - actual mixing effect 252
    - disperser disk 252–253
    - flat blade disk turbine 253
  - Raman spectroscopy 168
    - advantages 151, 152
  - rapid expansion of supercritical solutions 239
  - repulsive forces 76
- s**
- scale-up of crystallization process 268, 269
    - blending 270
    - constant blend time 269
    - cubic scale factor 268
    - dispersing 271, 272
    - heat transfer 272
    - manipulating particle shape 201, 202
    - model tests 269
    - operational aspects 200, 201
    - Penney diagram 270
    - process time – speed of crystallization 198, 199
    - scale-up rules 270
    - special scale-up considerations 272, 273
    - stirring 199, 200

- suspension 270, 271
- Schröder–van Laar equation 41
- screw dislocation 14
- secondary nucleation 180
  - dependence of rate 182
- sedimentation 219
- seeding 81, 199
  - in batch crystallizations 193
  - with crystals 192
  - designing process 194–197
    - holding time after seeding 197
    - preparation of seeds 196, 197
    - quality of seeds 195
    - quantity of seeds 195, 196
    - supersaturation at start of crystallization 197
  - of DTB and Oslo crystallizers 216
  - heterogeneous 193
  - strategies 69, 194
- segregation coefficient. *See* thermodynamics, distribution coefficient
- semi-batch precipitations 236–238
- S-faces 27
- shear cell 167
- sieving 165
- simple harmonic approximations 119
- single-crystal x-ray diffraction 150
- single oven zone melter 303
- size. *See* particle size, crystal size
- slurry process 168
- sodium chloride 2
  - growth and dissolution rates 114
  - habit-modifying agents 116
- solar ponds 3
  - brine composition 318
- solidification process 138
- solid layer crystallization 325–331
  - Bremsband process 329
  - equipment 326
  - results, of plant 330
- solid–liquid equilibria (SLE) 35, 37
  - data in ternary system 61
  - thermodynamic description of 39–41
- solid–liquid interface 120, 123
- solid–liquid separation 143, 144, 275
- solid–solid transition 155
- solid-state NMR (ssNMR) 152–154
  - advantages 153
  - disadvantages 154
- solubility 39, 105–107
  - for antisolvent crystallization 174
  - citric acid in water 24
  - common ion effect 106
  - complex formation 106
  - curves of inorganic and organic substances 55, 192
    - influence of solvents and impurities 60–62
    - inorganic substances 55–57
    - organic substances 57, 58
    - solvates, polymorphs, and cocrystals 58–60
  - influence of additives and 105, 106
  - measurement, and corroboration 62
    - equilibrium conditions 63, 64
    - excess method 64, 65
    - oiling-out 68–70
    - polythermal measurements 65–67
    - prediction and correlation of solubilities 67, 68
    - quaternary systems 72–74
    - ternary solution equilibria 70–72, 140
  - silver chloride (AgCl) 106, 107
  - in solid state 132
  - thermodynamic basis 106 (*See also* thermodynamics)
- solution equilibria 35, 53
  - solubility, and concentration units 53, 54
- solution-grown crystals 123
- solvates 86, 87
- solvents
  - methods, and choice of solvent 99, 100
  - polarity (*See* polar solvents)
  - solvents, modeling the influence 122–124
- spontaneous nucleation 17, 21, 98, 180, 183
  - drawbacks 192
- static plate crystallizer 326
- stirred tank reactor 142
- stirrer blade 181
- stirring 199, 200
  - influence 143
- supercritical carbon dioxide 240
- supersaturations 28, 32, 197, 236, 244, 245
  - control of 205–209
  - critical 28
  - dependence of growth rate on
    - regimes identification 31
  - generation 189–192
    - cooling 189, 190
    - evaporation 191, 192
    - use of antisolvent 190, 191
  - generation in crystallizer 173–176
  - homogeneity 175
  - necessary for transport 32
  - during precipitation 241, 244
- surface charge 76
- surface cooling crystallization 230, 231
- surface docking approaches 121
- surface energy model 117, 118
- surface tension 15

surfactants 244  
 suspending of solids, for agitated crystallization 247, 259  
 – criteria and different states, of suspension 259–261  
 – determination of shaft speed 264–266  
 – distribution of solids 266, 267  
 – geometry 266  
 – influence on blend times 267, 268  
 – influence on mass transfer 267  
 – physical parameters 265  
 – solids concentration 265  
 – influence of solid phase on blend times 268  
 – models and mechanisms 263, 264  
 – power requirement 262  
 – scheme of settling, and suspending forces on 263  
 – solids level vs. shaft speed for various solids concentrations 261  
 – various states of suspension 260  
 suspension crystallization 331–334  
 – equipment 331  
 – KCP column 333, 334  
 – process flow diagram 333  
 – scraped surface heat exchangers 332  
 sweating 144, 297, 298, 326, 328, 330

## t

tailor-made additives 113, 122  
 tangential impellers 253  
 task, definition 311, 312  
 temperatures 5, 24, 38  
 – and concentration profile 292  
 – degradation with 188  
 – dependence of  
 – enthalpy, free energy, and entropy 88  
 – saturation activity (*See* solubility)  
 – energy–temperature diagrams 88  
 – eutectic 50, 51, 53  
 – fusion of solute and 106  
 – glass transition temperature 157  
 – liquidus temperature 48  
 – measurements 256, 300  
 – melting 50  
 – phase transition temperature 56, 58  
 – quantitative energy–temperature 90  
 – in square phase diagram 72  
 – temperature–concentration diagram 174  
 – transition temperature 89, 94–96  
 – weak solubility–temperature relationship 61  
 terahertz spectroscopy 152  
 terephthalic acid (PTA) 248  
 ternary solubility phase diagram 140

ternary system  
 – phase rule 42  
 – SLE and temperature dependence in 43  
 – solute–solution system 70  
 – of threonine enantiomers 37  
 thermocompression 219, 228  
 thermodynamics  
 – description of solid-liquid equilibria (SLE) 39–41  
 – distribution coefficient 133, 134  
 – experimental techniques to elucidate 94  
 – DSC techniques 94  
 – enthalpy difference, of two forms 96  
 – solubility measurements 95, 96  
 – suspension equilibration 94, 95  
 – vapor pressure measurements 97  
 – of hydrates 91–93  
 – of polymorphs of solid-state forms 87, 88  
 – energy–temperature diagrams 88–90  
 – rules to predict thermodynamic relationships 90, 91  
 – properties  
 – thermodynamically controlled process 131  
 thermogravimetry (TG) 158  
 T-mixing device 245  
 transport phenomena 28, 32, 33  
 turbidity measurements 167, 168

## u

ultrasonic probe 108  
 underestimated “traces” of highly soluble compounds, effect of 309  
 UNIFAC (Universal Functional group Activity Coefficient) 67  
 units  
 – crystallizing 122  
 – growth 26  
 – packing 8  
 unseeded crystallization 167, 175  
 urolithiasis prevention mechanisms 109

## v

vacancy approach 121  
 vacuum crystallization 3, 203, 204  
 – cooling 206–208, 218–221, 229–231  
 – evaporation 204, 317, 318  
 van der Waals forces 8  
 vanillin  
 – crystallization 110  
 – nucleation induction time 109  
 velocity, of spreading 30  
 vibrational spectroscopy 151, 152  
 viscosity 24, 131, 239, 259, 265, 272, 306, 315  
 volume defects 14

**w**

washing 280, 281, 298, 299

waste-fired power plant 309

**x**

x-ray powder diffraction (XRPD) 150, 151

**z**

ZLD (zero liquid discharge) plants 308, 309

– drain point 309

zone melting 303

zone width 20

– metastable 21, 22, 65, 108, 111, 167, 197, 205